

Pertanika Journal of  
**SCIENCE &  
TECHNOLOGY**

**JST**

**VOL. 25 (S) APR. 2017**

*A special issue devoted to*  
**Advances in Science & Technology Research**

Guest Editors  
**Aidah Jumahat, Hadariah Bahron & Chen Ai Hong**



**PERTANIKA**  
JOURNALS

**A scientific journal published by Universiti Putra Malaysia Press**

## *Journal of Science & Technology*

### About the Journal

#### Overview

Pertanika Journal of Science & Technology (JST) is the official journal of Universiti Putra Malaysia published by UPM Press. It is an open-access online scientific journal which is free of charge. It publishes the scientific outputs. It neither accepts nor commissions third party content.

Recognized internationally as the leading peer-reviewed interdisciplinary journal devoted to the publication of original papers, it serves as a forum for practical approaches to improving quality in issues pertaining to science and engineering and its related fields.

JST is a **quarterly** (January, April, July and October) periodical that considers for publication original articles as per its scope. The journal publishes in **English** and it is open to authors around the world regardless of the nationality.

The Journal is available world-wide.

#### Aims and scope

Pertanika Journal of Science and Technology aims to provide a forum for high quality research related to science and engineering research. Areas relevant to the scope of the journal include: bioinformatics, bioscience, biotechnology and bio-molecular sciences, chemistry, computer science, ecology, engineering, engineering design, environmental control and management, mathematics and statistics, medicine and health sciences, nanotechnology, physics, safety and emergency management, and related fields of study.

#### History

Pertanika was founded in 1978. A decision was made in 1992 to streamline Pertanika into three journals as Journal of Tropical Agricultural Science, Journal of Science & Technology, and Journal of Social Sciences & Humanities to meet the need for specialised journals in areas of study aligned with the interdisciplinary strengths of the university.

After almost 25 years, as an interdisciplinary Journal of Science & Technology, the revamped journal now focuses on research in science and engineering and its related fields.

#### Goal of *Pertanika*

Our goal is to bring the highest quality research to the widest possible audience.

#### Quality

We aim for excellence, sustained by a responsible and professional approach to journal publishing. Submissions are guaranteed to receive a decision within 14 weeks. The elapsed time from submission to publication for the articles averages 5-6 months.

#### Abstracting and indexing of *Pertanika*

Pertanika is almost **40 years old**; this accumulated knowledge has resulted in Pertanika JST being abstracted and indexed in **SCOPUS** (Elsevier), Clarivate Analytics [*formerly known as Thomson (ISI)*] **Web of Science™ Core Collection** Emerging Sources Citation Index (ESCI). Web of Knowledge [BIOSIS & CAB Abstracts], **EBSCO** and EBSCOhost, **DOAJ**, **ERA**, **Google Scholar**, **TIB**, **MyCite**, Islamic World Science Citation Center (ISC), ASEAN Citation Index (ACI), **Cabell's Directories** & Journal Guide.

### Future vision

We are continuously improving access to our journal archives, content, and research services. We have the drive to realise exciting new horizons that will benefit not only the academic community, but society itself.

### Citing journal articles

The abbreviation for Pertanika Journal of Science & Technology is *Pertanika J. Sci. Technol.*

### Publication policy

Pertanika policy prohibits an author from submitting the same manuscript for concurrent consideration by two or more publications. It prohibits as well publication of any manuscript that has already been published either in whole or substantial part elsewhere. It also does not permit publication of manuscript that has been published in full in Proceedings.

### Code of Ethics

The Pertanika Journals and Universiti Putra Malaysia takes seriously the responsibility of all of its journal publications to reflect the highest in publication ethics. Thus all journals and journal editors are expected to abide by the Journal's codes of ethics. Refer to Pertanika's **Code of Ethics** for full details, or visit the Journal's web link at [http://www.pertanika.upm.edu.my/code\\_of\\_ethics.php](http://www.pertanika.upm.edu.my/code_of_ethics.php)

### International Standard Serial Number (ISSN)

An ISSN is an 8-digit code used to identify periodicals such as journals of all kinds and on all media—print and electronic. All Pertanika journals have ISSN as well as an e-ISSN.

Journal of Science & Technology: ISSN 0128-7680 (*Print*); ISSN 2231-8526 (*Online*).

### Lag time

A decision on acceptance or rejection of a manuscript is reached in 3 to 4 months (average 14 weeks). The elapsed time from submission to publication for the articles averages 5-6 months.

### Authorship

Authors are not permitted to add or remove any names from the authorship provided at the time of initial submission without the consent of the Journal's Chief Executive Editor.

### Manuscript preparation

Refer to Pertanika's **INSTRUCTIONS TO AUTHORS** at the back of this journal.

Most scientific papers are prepared according to a format called IMRAD. The term represents the first letters of the words **I**ntroduction, **M**aterials and **M**ethods, **R**esults, **A**nd, **D**iscussion. IMRAD is simply a more 'defined' version of the "IBC" [Introduction, Body, Conclusion] format used for all academic writing. IMRAD indicates a pattern or format rather than a complete list of headings or components of research papers; the missing parts of a paper are: *Title, Authors, Keywords, Abstract, Conclusions, and References*. Additionally, some papers include Acknowledgments and Appendices.

The *Introduction* explains the scope and objective of the study in the light of current knowledge on the subject; the *Materials and Methods* describes how the study was conducted; the *Results* section reports what was found in the study; and the *Discussion* section explains meaning and significance of the results and provides suggestions for future directions of research. The manuscript must be prepared according to the Journal's **INSTRUCTIONS TO AUTHORS**.

### Editorial process

Authors are notified with an acknowledgement containing a *Manuscript ID* on receipt of a manuscript, and upon the editorial decision regarding publication.

Pertanika follows a **double-blind peer-review** process. Manuscripts deemed suitable for publication are usually sent to reviewers. Authors are encouraged to suggest names of at least three potential reviewers at the time of submission of their manuscript to Pertanika, but the editors will make the final choice. The editors are not, however, bound by these suggestions.

Notification of the editorial decision is usually provided within ten to fourteen weeks from the receipt of manuscript. Publication of solicited manuscripts is not guaranteed. In most cases, manuscripts are accepted conditionally, pending an author's revision of the material.

As articles are double-blind reviewed, material that might identify authorship of the paper should be placed only on page 2 as described in the first-4 page format in Pertanika's **INSTRUCTIONS TO AUTHORS** given at the back of this journal.

### The Journal's peer-review

In the peer-review process, three referees independently evaluate the scientific quality of the submitted manuscripts.

Peer reviewers are experts chosen by journal editors to provide written assessment of the **strengths** and **weaknesses** of written research, with the aim of improving the reporting of research and identifying the most appropriate and highest quality material for the journal.

### Operating and review process

What happens to a manuscript once it is submitted to *Pertanika*? Typically, there are seven steps to the editorial review process:

1. The Journal's chief executive editor and the editorial board examine the paper to determine whether it is appropriate for the journal and should be reviewed. If not appropriate, the manuscript is rejected outright and the author is informed.
2. The chief executive editor sends the article-identifying information having been removed, to three reviewers. Typically, one of these is from the Journal's editorial board. Others are specialists in the subject matter represented by the article. The chief executive editor asks them to complete the review in three weeks.

Comments to authors are about the appropriateness and adequacy of the theoretical or conceptual framework, literature review, method, results and discussion, and conclusions. Reviewers often include suggestions for strengthening of the manuscript. Comments to the editor are in the nature of the significance of the work and its potential contribution to the literature.

3. The chief executive editor, in consultation with the editor-in-chief, examines the reviews and decides whether to reject the manuscript, invite the author(s) to revise and resubmit the manuscript, or seek additional reviews. Final acceptance or rejection rests with the Editor-in-Chief, who reserves the right to refuse any material for publication. In rare instances, the manuscript is accepted with almost no revision. Almost without exception, reviewers' comments (to the author) are forwarded to the author. If a revision is indicated, the editor provides guidelines for attending to the reviewers' suggestions and perhaps additional advice about revising the manuscript.

4. The authors decide whether and how to address the reviewers' comments and criticisms and the editor's concerns. The authors return a revised version of the paper to the chief executive editor along with specific information describing how they have answered' the concerns of the reviewers and the editor, usually in a tabular form. The author(s) may also submit a rebuttal if there is a need especially when the author disagrees with certain comments provided by reviewer(s).
5. The chief executive editor sends the revised paper out for re-review. Typically, at least one of the original reviewers will be asked to examine the article.
6. When the reviewers have completed their work, the chief executive editor in consultation with the editorial board and the editor-in-chief examine their comments and decide whether the paper is ready to be published, needs another round of revisions, or should be rejected.
7. If the decision is to accept, an acceptance letter is sent to all the author(s), the paper is sent to the Press. The article should appear in print in approximately three months.

The Publisher ensures that the paper adheres to the correct style (in-text citations, the reference list, and tables are typical areas of concern, clarity, and grammar). The authors are asked to respond to any minor queries by the Publisher. Following these corrections, page proofs are mailed to the corresponding authors for their final approval. At this point, **only essential changes are accepted**. Finally, the article appears in the pages of the Journal and is posted on-line.



Pertanika Journal of  
**SCIENCE &  
TECHNOLOGY**

*A special issue devoted to*  
Advances in Science & Technology Research

**Vol. 25 (S) Apr. 2017**  
(Special Edition)

Guest Editors  
**Aidah Jumahat, Hadariah Bahron & Chen Ai Hong**

A scientific journal published by Universiti Putra Malaysia Press





## EDITOR-IN-CHIEF

**Mohd Adzir Mahdi**

*Physics, Optical Communications*

## CHIEF EXECUTIVE EDITOR

**Nayan Deep S. Kanwal**

*Environmental Issues – Landscape  
Plant Modelling Applications*

## UNIVERSITY PUBLICATIONS COMMITTEE

**Husaini Omar, Chair**

## EDITORIAL STAFF

### Journal Officers:

Kanagamalar Silvarajoo, *ScholarOne*

Tee Syin-Ying, *ScholarOne*

### Editorial Assistants:

Zulinaardawati Kamarudin

Florence Jiyom

Ummi Fairuz Hanapi

### COPY EDITORS

Doreen Dillah

Crescentia Morais

Pooja Terasha Stanslas

### PRODUCTION STAFF

#### Pre-press Officers:

Kanagamalar Silvarajoo

Nur Farrah Dila Ismail

#### Layout & Typeset:

Wong Wai Mann

### WEBMASTER

Mohd Nazri Othman

### PUBLICITY & PRESS RELEASE

Magdalene Pokar (*ResearchSEA*)

Florence Jiyom

### EDITORIAL OFFICE

#### JOURNAL DIVISION

Office of the Deputy Vice Chancellor (R&I)

1<sup>st</sup> Floor, IDEA Tower II

UPM-MTDC Technology Centre

Universiti Putra Malaysia

43400 Serdang, Selangor Malaysia.

Gen Enq.: +603 8947 1622 | 1616

E-mail: [executive\\_editor.pertanika@upm.my](mailto:executive_editor.pertanika@upm.my)

URL: [www.journals-td.upm.edu.my](http://www.journals-td.upm.edu.my)

#### PUBLISHER

Kamariah Mohd Saidin

UPM Press

Universiti Putra Malaysia

43400 UPM, Serdang, Selangor, Malaysia.

Tel: +603 8946 8855, 8946 8854

Fax: +603 8941 6172

E-mail: [penerbit@putra.upm.edu.my](mailto:penerbit@putra.upm.edu.my)

URL: <http://penerbit.upm.edu.my>

## EDITORIAL BOARD

2015-2017

### Abdul Halim Shaari

*Superconductivity and Magnetism,  
Universiti Putra Malaysia, Malaysia.*

### Adem Kilicman

*Mathematical Sciences,  
Universiti Putra Malaysia, Malaysia.*

### Ahmad Makmom Abdullah

*Ecophysiology and Air Pollution  
Modelling, Universiti Putra Malaysia,  
Malaysia.*

### Ali A. Moosavi-Movahedi

*Biophysical Chemistry,  
University of Tehran, Tehran, Iran.*

### Amu Therwath

*Oncology, Molecular Biology,  
Université Paris, France.*

### Angelina Chin

*Mathematics, Group Theory and  
Generalisations, Ring Theory,  
University of Malaya, Malaysia.*

### Bassim H. Hameed

*Chemical Engineering: Reaction  
Engineering, Environmental Catalysis  
& Adsorption,  
Universiti Sains Malaysia, Malaysia.*

### Biswa Mohan Biswal

*Medical, Clinical Oncology, Radiotherapy,  
Universiti Sains Malaysia, Malaysia.*

### Christopher G. Jesudason

*Mathematical Chemistry, Molecular  
Dynamics Simulations, Thermodynamics  
and General Physical Theory,  
University of Malaya, Malaysia.*

### Hari M. Srivastava

*Mathematics and Statistics,  
University of Victoria, Canada.*

### Ivan D. Rukhlenko

*Nonlinear Optics, Silicon Photonics,  
Plasmonics and Nanotechnology,  
Monash University, Australia.*

### Kaniraj R. Shenbaga

*Geotechnical Engineering,  
Universiti Malaysia Sarawak, Malaysia.*

### Kanury Rao

*Senior Scientist & Head, Immunology  
Group, International Center for Genetic  
Engineering and Biotechnology,  
Immunology, Infectious Disease Biology  
and System Biology, International Centre  
for Genetic Engineering & Biotechnology,  
New Delhi, India.*

### Karen Ann Crouse

*Chemistry, Material Chemistry, Metal  
Complexes – Synthesis, Reactivity,  
Bioactivity, Universiti Putra Malaysia,  
Malaysia.*

### Ki-Hyung Kim

*Computer and Wireless Sensor Networks,  
AIOU University, Korea.*

### Kunnawee Kanitpong

*Transportation Engineering-Road  
Traffic Safety, Highway Materials  
and Construction, Asian Institute of  
Technology, Thailand.*

### Megat Mohd Hamdan

**Megat Ahmad**  
*Mechanical and Manufacturing  
Engineering, Universiti Pertahanan  
Nasional Malaysia, Malaysia.*

### Miralini Kandiah

*Public Health Nutrition, Nutritional  
Epidemiology, UCSJ University, Malaysia.*

### Mohamed Othman

*Communication Technology and  
Network, Scientific Computing,  
Universiti Putra Malaysia, Malaysia.*

### Mohd. Ali Hassan

*Bioprocess Engineering, Environmental  
Biotechnology, Universiti Putra Malaysia,  
Malaysia.*

### Mohd Sapuan Salit

*Concurrent Engineering and Composite  
Materials, Universiti Putra Malaysia,  
Malaysia.*

### Narongrit Sombatsompop

*Engineering & Technology: Materials  
and Polymer Research, King Mongkut's  
University of Technology Thonburi  
(KMUTT), Thailand.*

### Prakash C. Sinha

*Physical Oceanography, Mathematical  
Modelling, Fluid Mechanics, Numerical  
Techniques, Universiti Malaysia  
Terengganu, Malaysia.*

### Rajinder Singh

*Biotechnology, Biomolecular Sciences,  
Molecular Markers/ Genetic Mapping,  
Malaysia Palm Oil Board, Kajang,  
Malaysia.*

### Renuganth Varatharajoo

*Engineering, Space System,  
Universiti Putra Malaysia, Malaysia.*

### Riyanto T. Bambang

*Electrical Engineering, Control, Intelligent  
Systems & Robotics, Bandung Institute of  
Technology, Indonesia.*

### Sabira Khatun

*Engineering, Computer Systems  
& Software Engineering, Applied  
Mathematics, Universiti Malaysia  
Pahang, Malaysia.*

### Shiv Dutt Gupta

*Director, IHMR, Health Management,  
Public Health, Epidemiology, Chronic  
and Non-communicable Diseases,  
Indian Institute of Health Management  
Research, India.*

### Suan-Choo Cheah

*Biotechnology, Plant Molecular Biology,  
Asiatic Centre for Genome Technology  
(ACGT), Kuala Lumpur, Malaysia.*

### Wagar Asrar

*Engineering, Computational Fluid  
Dynamics, Experimental Aerodynamics,  
International Islamic University,  
Malaysia.*

### Wing Keong Ng

*Aquaculture, Aquatic Animal Nutrition,  
Aqua Feed Technology, Universiti Sains  
Malaysia, Malaysia.*

### Yudi Samyudia

*Chemical Engineering, Advanced  
Process Engineering, Curtin University of  
Technology, Malaysia.*

## INTERNATIONAL ADVISORY BOARD

2017-2019

### Adarsh Sandhu

*Editorial Consultant for Nature  
Nanotechnology and Contributing  
Writer for Nature Photonics, Physics,  
Magnetoresistive Semiconducting  
Magnetic Field Sensors, Nano-Bio-  
Magnetism, Magnetic Particle Colloids,  
Point of Care Diagnostics, Medical  
Physics, Scanning Hall Probe Microscopy,  
Synthesis and Application of Graphene,  
Electronics-inspired Interdisciplinary  
Research Institute (EIIRIS), Toyohashi  
University of Technology, Japan.*

### Graham Megson

*Computer Science, The University of  
Westminster, U.K.*

### Kuan-Chong Ting

*Agricultural and Biological Engineering,  
University of Illinois at  
Urbana-Champaign, USA.*

### Malin Premaratne

*Advanced Computing and Simulation,  
Monash University, Australia.*

### Mohammed Ismail Elnaggar

*Electrical Engineering, Ohio State  
University, USA.*

### Peter G. Alderson

*Bioscience, The University of Nottingham,  
Malaysia Campus.*

### Peter J. Heggs

*Chemical Engineering,  
University of Leeds, U.K.*

### Ravi Prakash

*Vice Chancellor, JUIT, Mechanical  
Engineering, Machine Design, Biomedical  
and Materials Science, Jaypee University  
of Information Technology, India.*

### Said S.E.H. Elnashaie

*Environmental and Sustainable  
Engineering, Penn. State University at  
Harrisburg, USA.*

### Suhash Chandra Dutta Roy

*Electrical Engineering, Indian Institute of  
Technology (IIT) Delhi, India.*

### Vijay Arora

*Quantum and Nano-Engineering  
Processes, Wilkes University, USA.*

### Yi Li

*Chemistry, Photochemical Studies,  
Organic Compounds, Chemical  
Engineering, Chinese Academy of  
Sciences, Beijing, China.*

## ABSTRACTING/INDEXING

*Pertanika* is now over 40 years old; this accumulated knowledge has resulted the journals being indexed in abstracted in SCOPUS (Elsevier), Web of Science Core Collection (formerly ISI) [ESCI, BIOSIS & CAB Abstracts], EBSCO & EBSCOhost, ERA, DOAJ, AGRICOLA (National Agric. Library, USA), Cabell's Directories, Google Scholar, MyAIS, Islamic World Science Citation Center (ISC), ASEAN Citation Index (ACI) & Rubriq (Journal Guide).



The publisher of *Pertanika* will not be responsible for the statements made by the authors in any articles published in the journal. Under no circumstances will the publisher of this publication be liable for any loss or damage caused by your reliance on the advice, opinion or information obtained either explicitly or implied through the contents of this publication.

All rights of reproduction are reserved in respect of all papers, articles, illustrations, etc., published in *Pertanika*. *Pertanika* provides free access to the full text of research articles for anyone, web-wide. It does not charge either its authors or author-institution for refereeing/publishing outgoing articles or user-institution for accessing incoming articles.

No material published in *Pertanika* may be reproduced or stored on microfilm or in electronic, optical or magnetic form without the written authorization of the Publisher.

Copyright © 2017 Universiti Putra Malaysia Press. All Rights Reserved.



## Preface

We are very pleased to present this special issue (2<sup>nd</sup> volume) of *Pertanika Journal of Science and Technology (JST)*, which is a compilation of selected papers presented at the 3<sup>rd</sup> International Conference on Science and Social Research (CSSR2016). CSSR2016 was held on the 6<sup>th</sup> – 7<sup>th</sup> December 2016 in Putrajaya, Malaysia. With the theme, “Waves of Interdisciplinary Research”, the conference covers multi-disciplinary research areas from science and technology to social sciences and humanities. The conference track was divided into three major areas: Track 1: Engineering, Science, & Technology; Track 2: Clinical & Health sciences; and Track 3: Arts, Humanities & Social Sciences. All full papers submitted to CSSR2016 were subjected to a rigorous peer reviewing process to ensure quality and consistency in contents before the papers were accepted for presentation. A total of 188 full papers in Track 1 (Engineering, Science, & Technology) and Track 2 (Clinical & Health sciences) were presented during the conference, 33 of which were accepted for publication in this special issue (2<sup>nd</sup> volume).

The theme of the special issue is “Advances in Science and Technology Research”. In line with this theme, research areas of the full papers, which are included in this issue, cover chemistry, clinical sciences, medical biochemistry, environmental sciences, biotechnology, analytical chemistry, pharmacology, electrochemical materials, nanocomposites, nanotechnology, wastewater treatment, materials processing, composite materials, hydrology, information system, electrical engineering, image processing, applied statistics and power engineering, biomass energy, solar energy, thermal and fluid mechanics, wear and tribology, metals and alloys, plastics, polymers, building physic, urban environment and artificial intelligence.

We would like to thank all the contributors, as well as the reviewers, for their commitment and patience, which made this special issue Volume 2 JST-CSSR2016 a success. It is hoped that this publication would encourage researchers from around the world to be more active in publishing their research output, particularly good quality science and technology papers, that would be useful for academics and practitioners alike. Special thanks to the Chief Executive Editor of UPM Journals, Dr. Nayan Kanwal, and all staff of the Journal Division, for their guidance and continuous support in making this issue feasible. This has certainly motivated us to be more prolific and thrive better in the future.

### **Guest Editors:**

Aidah Jumahat (*Assoc. Prof. Dr.*)

Hadariah Bahron (*Prof. Dr.*)

Chen Ai Hong (*Prof. Dr.*)

**April 2017**



**Pertanika Journal of Science & Technology**  
**Vol. 25 (S) Apr. 2017**

**Contents**

**Advances in Science and Technology Research**

- Serological and Molecular Detection of RhD DEL Phenotype in National Blood Centre, Malaysia 1  
*Safura Ramli, Evana Kamarudin and Mazura Bahari*
- Seasonal Temporal Distribution of Forecasted Wind Speed Data in Langkawi, Malaysia 7  
*Siti Noratiqah Mohamad Deros, Arnis Asmat and Shattri Mansor*
- Isolation and Characterisation of Filamentous Fungi from Animal Agricultural Farm Soil 19  
*Muhammad Shukri Senwan, Muhd Fauzi Safian, Zainon Mohd Noor and Zaidah Zainal Ariffin*
- Electrodeposition of Copper Coating on 304 Stainless Steel Substrate: Physicochemical Properties and Antibacterial Activity 29  
*Nik Norziehana Che Isa, Yusairie Mohd, Mohammad Hafizuddin Mohd Zaki and Sharifah Aminah Syed Mohamad*
- Enhancement of Oxidative DNA Damage and Alteration of p53, Bax, and Bcl-2 Protein Expressions Following Low Dose Radiation Exposure 41  
*Wan Mazlina Md Saad, Mohd Khairul Amran Mohammad, Muhamad Idham Mohamed and Hairil Rashmizal Abdul Razak*
- Microbial Fuel Cell's Performance of Original and Deoxygenated Palm Oil Mill Effluent in 3 Different Stages of Fermentation Process 53  
*Khairul Baqir Alkhair Khairul Amin, Oskar Hasdinor Hassan, Sharifah Aminah Syed Mohamed, Yap Kian Chung Andrew, Zulkifli Ab. Rahman, Hazlini Mohamad Ameran, Nurul Khamsatul Akma Kamaruzaman, Tunku Ishak Tunku Kudin, Ab. Malik Marwan Ali, Mohd Zu Azhan Yahya and Muhammad Haikal Zainal*
- Optimising Processing Conditions of PLA Nanocomposites Using Response Surface Methodology 63  
*Norazura Ibrahim, Margaret Jollands and Rajarathinam Parthasarathy*
- Modified Spent Tea Leaves as Bioadsorbent for Methyl Orange Dye Removal 73  
*Lim Ying Pei, Amira Nadzirah Suhaidi, Siti Marziya Zulkifli, Syamil Hidayat Hassim, Devagi Kanakaraju and Lim Ying Chin*

A Study on the Formation of PVA/Kenaf Nanofibres via Electrospinning <i>Nor Dalila Nor Affandi, Mohd Rozi Ahmad, Sabiha Hanim Saleh, Muhammad Fairuz Remeli, Nur Hayati Humairah Nur Ikhwan Teo and Nurul Farihin Amran</i>	85
Flexural Properties of Random and Unidirectional Arenga Pinnata Fibre Reinforced Epoxy Composite <i>Muhamad Faris Syafiq Khalid, Aidah Jumahat, Zuraidah Salleh and Mohammad Jawaid</i>	93
Advection and Dispersion of Water Quality Constituents in Batu Ferringhi Penang <i>Muhammad Ilyas Ahmad Jamalluddin and Wei-Koon Lee</i>	103
Substituent Effect on Catalytic Activity of Palladium(II) Schiff Base Complexes for Sonogashira Reaction <i>Hadariah Bahron, Shahrul Nizam Ahmad, Amalina Mohd Tajuddin and Syed Illah Al-Yahya Syed Abdul Kadir</i>	115
Syntheses, Characterisation and Application of Palladium(II) Complexes as Catalysts in Heck Cross-Coupling Reaction <i>Amalina Mohd Tajuddin and Hadariah Bahron</i>	125
The Development of Personal Portable Wireless Range Extender for IEEE 802.11 <i>Norharyati Harum, Nur Atikah Mohd Yusof and Nurul Azma Zakaria</i>	137
Productivity Improvement in Automotive Component Company using Line Balancing <i>Muhammad Fikri Alif Dzulkarnain and Wan Emri Wan Abdul Rahaman</i>	147
Association between Marital Status and the Outcome of Teenage Pregnancy: A Retrospective Review in Year 2009-2012 in Hospital Ampang <i>Salleha Khalid and Muhammad Shamsir Mohd Aris</i>	159
Experimental Investigations on the Effects of Design Parameters on Single Slope Solar Still Evaporation Rate under Malaysian Conditions <i>Zainal Abidin Kamarul Baharin and Aishah Arinah Abdul Aziz</i>	169
Second-hand Smoke Exposure and Psychological Distress amongst Non- Smoking Pregnant Women in Malaysia <i>Siti Munira Yasin, Khairul Mizan Taib, Mohd Rodi Isa, Mohd Ariff Fadzil, Mohd Razilan Abdul Kadir and Saiful Farik Mat Yatim</i>	181

Perspective of a Smoke-free Home among Second-hand Smokers during Pregnancy: A Qualitative Study <i>Izzah Amira Mohd Asri, Nur Amirah Abd Rani, Zulfakhri Dzulkifli, Muhamad Ilmam Muhamad Jamil, Mohd Shahril Ahmad Saman and Siti Munira Yasin</i>	191
Effect of the Deposited Layer, Withdrawal Speed and Coated Length on Immobilised Bromothymol Blue in Polyaniline Sol Gel towards pH Sensing Sensitivity <i>Norliza Othman, Uzer Mohd Noor and Sukreen Hana Herman</i>	205
Analysis on the OTTV of Modern-Style Apartment Facades in Bandar Sri Permaisuri, Kuala Lumpur <i>Ahmad Sanusi Hassan and Muhammad Hafeez Abdul Nasir</i>	215
Synthesisation Temperature-Dependent Cytotoxicity of Bismuth Oxide Nanoparticles in Vitro <i>Nur Amirah Mohd Nor, Zanariah Mohd, Hairil Rashmizal Abdul Razak, Zolkapli Eshak and Wan Mazlina Md Saad</i>	227
Personality Prediction Based on Social Media Using Decision Tree Algorithm <i>Tan Lee Chee Yoong, Nor Rahayu Ngatirin and Zurinahni Zainol</i>	237
Implementation of a Fuzzy-Based Line Follower Robot using Arduino <i>Mohammad Safwan Mohamed Alias, Ya'akob Yusof and Nurul Muthmainnah Mohd Noor</i>	249
Ziegler-Nichols First Tuning Method for Air Blower PT326 <i>Mahanijah Md Kamal and Muhammad Hanihazaim Abd Halim</i>	259
Synthesis and Characterisation of Silica from Palm Oil Fuel Ash (POFA) Using Alkaline Fusion Method <i>Nur Athirah Adam, Alawi Sulaiman, Azhari Samsu Baharuddin, Mohd Noriznan Mokhtar, Zainuri Busu and Tengku Elida Tengku Zainal Mulok</i>	269
Effect of Upstream Building Configurations on Mean Wind Speed Ratio at Urban Pedestrian Level Using LES <i>Muhd Azhar Zainol, Azli Abd Razak, Nor Merlisa Ali, Qi Jie Kwong and Sheikh Ahmad Zaki</i>	277
Self-similarity Hurst Parameter Estimation with Rescaled Range Method on IP-based Campus Internet Traffic <i>Murizah Kassim, Noor Laili Ismail, Roslina Mohamad, Saiful Izwan Suliman and Mahamod Ismail</i>	287

A Pre-shared Diffie-Hellman Key Exchange Scheme for a Secure TFTP Protocol <i>Nur Nabila Mohamed, Mohd Anuar Mat Isa, Yusnani Mohd Yussoff and Habibah Hashim</i>	303
Effects of the Number of Nozzles on Acoustic Signals Produced by a Ranque-Hilsch Vortex Tube <i>Khairil Muhaimin Abd Rahman, Wirachman Wisnoe and Valliyappan David Natarajan</i>	315
Tooth Frame Axes and Centroid for Dental Occlusal System <i>Muhammad Azmi Ayub, Mohd Shafiq Azni and Nagham Al-Jaf</i>	325
An Analysis on Node Cloning Attacks Prevention Using Unique Hardware Identity in WSN <i>Norhafyza Marbukhari, Yusnani Mohd Yussoff, Murizah Kassim, Mohd Anuar Mat Isa and Habibah Hashim</i>	335
Effects of Environment and Fibre Architecture on Wear Properties of Nano-Filled Epoxy Polymer Composite <i>Aidah Jumahat, Anis Adilah Abu Talib, Eliya Farah Hana Mohd Kamal, Muhammad Tarmizi Sulaiman and Ahmad Syahrul Mohd Roslan</i>	345





## Serological and Molecular Detection of RhD DEL Phenotype in National Blood Centre, Malaysia

Safura Ramli, Evana Kamarudin and Mazura Bahari\*

*Department of Medical Laboratory Technology, Faculty of Health Sciences, Universiti Teknologi MARA (UiTM) Puncak Alam, 42300 Bandar Puncak Alam, Selangor, Malaysia*

### ABSTRACT

After ABO, Rhesus (Rh) is the second most clinically important blood group regarding transfusion and pregnancy induced alloimmunisation. RhD DEL is a subtype of variant RhD, which is difficult to determine in a routine blood bank, since it expresses an extremely low level of D antigens. Serologically, it can only be detected via adsorption-elution test. To date, there have been limited data available on the RhD DEL phenotype in Malaysia. Thus, this study was carried out to detect DEL phenotype among RhD negative donors in Malaysia. A total of 43 RhD-negative blood samples were collected from National Blood Centre, Malaysia. Rh phenotype for each sample was tested, followed by adsorption elution technique. Then, identification of DEL carrying RHD1227A allele was performed via SSP-PCR. Rh-phenotype identified were ccee (79.07%), Ccee (13.95%), 4.65% of ccEe phenotype and only 2.33% of CCee phenotype. One (2.3%) out of the 43 samples was identified as DEL phenotype carrying RHD1227A allele when tested using SSP-PCR, but none was identified from adsorption-elution. A larger sample size is recommended to determine the exact prevalence of DEL phenotype, as well as specificity and sensitivity between SSP-PCR as compared with the traditional adsorption elution technique.

*Keywords:* DEL phenotype, RHD1227A alleles, SSP-PCR

### ARTICLE INFO

*Article history:*

Received: 25 October 2016

Accepted: 17 March 2017

*E-mail addresses:*

[safura1754@puncakalam.uitm.edu.my](mailto:safura1754@puncakalam.uitm.edu.my) (Safura Ramli),

[evana@salam.uitm.edu.my](mailto:evana@salam.uitm.edu.my) (Evana Kamarudin),

[mazurabahari@puncakalam.uitm.edu.my](mailto:mazurabahari@puncakalam.uitm.edu.my) (Mazura Bahari)

\*Corresponding Author

### INTRODUCTION

After ABO, Rhesus (Rh) is the second most clinical important and immunogenic blood group in transfusion medicine. In 1940, the Rhesus system was discovered by Landsteiner and Wiener (as cited in Westhoff, 2007). The terms Rh positive or Rh negative are based on the foundation of the D antigen either its presence or not correspondingly. Rhesus proteins encoded by two genes, which are

RHD and RHCE, are located in a tail-to-tail direction towards the end of the short arm of chromosome 1 (p34–36) (Huang, 2009). RhD encodes D antigen, while RHCE encodes CE antigens in many arrangements such as ce, CE, Ce or cE. Meanwhile, RHD and RHCE are closely related, differing in 36 out of 417 amino acids (Le Van Kim, Colin, & Cartron, 2006). The complex genetic basis of the Rh blood group owes to their large number of antigens (Flegel, 2007).

Rhesus is the largest of all 30 known blood group systems with more than 50 antigens (Kappler-Gratias et al., 2014). Based on their molecular structure and phenotype, these RHD alleles are classified as weak D, partial D, and DEL. DEL, or formerly known as D-elute (Del), was first discovered in 1984 (Okubo et al., 1984). DEL is the most weakly expressed of D antigens. In general, 30 or less copies of the D antigen per RBCs are expressed by DEL phenotype compared with 1500 to 7000 sites for weak D, and 30,000 antigen sites for normal D (Li et al., 2009; Sandler et al., 2014; Wagner, Moulds, & Flegel, 2005). The sensitivity of conventional serological assays is impeded because of the weak expression of the DEL variant that can only be detected using adsorption and elution techniques (Gardener et al., 2012). DEL phenotypes arise from several mechanisms such as deletion, missense, or splice-site mutations. RHD1227A is the most frequent allele reported in Asia, and it also known as K409K alleles (Chen et al., 2004). The aim of this study is to observe the frequency of DEL phenotype among blood donors at the National Blood Centre.

## **MATERIALS AND METHODS**

### **Sample collection**

Forty-three leftover samples in Ethylenediaminetetraacetate (EDTA) tubes were collected from the National Blood Centre. Criteria for samples selection included phenotype as Rh negative and negative results for all the routine screenings for blood donors. This study was approved by the Medical Research and Ethics Committee (MREC) of Malaysia.

### **Rhesus Phenotyping**

The Rh phenotype was determined by testing patients' red blood cells with the five standard antisera. Serotyping for the RhD, RhC/c, and RhE/e antigens was performed using monoclonal anti-D, monoclonal anti-C, anti-c, anti-E, and anti-e antibodies (DiaCidel, DiaMed, Cressier, Switzerland).

### **Adsorption Elution Test**

For adsorption test, 1000 µl of red cells were incubated with 1000 µl of monoclonal anti-D for 1 hour at 37°C. The cells were washed six times, while elute was prepared using the heat elution technique.

### Genomic DNA Extraction

Genomic DNA was isolated from peripheral blood cells using the QIAamp DNA Blood Mini Kit (Qiagen, Hilden, Germany) following the manufacturer's instructions. Meanwhile, DNA concentration and purity were determined using Biophotometer (Eppendorf, USA)

### Detection of RHD 1227A Polymorphisms

RHD1227A allele analysis was performed based on the method described by Chen et al. (2004). A set of RHD1227A primers (forward primer: 5'-GATGACCAAGTTTTCTGGAAA-3', reverse primer: 5'-GTTCTGTACCCCGCATGTCAG-3') were used in amplifying 348 bp product. Meanwhile, growth hormone gene was used for internal control by using another set of primers (forward primer: 5'-GCCTCCCAACCATTCCTTA-3', reverse primer: 5'-TAGACGTTGCTGTCAGAGGC-3') to generate 629 bp fragments. PCR preparation was done using HotStarTaq Mastermix Kit (Qiagen, Hilden, Germany) according to the manufacturer's instructions. Total volumes of PCR reactions were 25 µl. Each reaction contains 12.5 µl HotStarTaq Master Mix, 2.5 µl of each primer, 1 µl template DNA and 1.5 µl RNase-free water. After initial denaturation for 15 minutes at 95°C, and the samples were subjected to 40 cycles of PCR in the My Cycler (Biorad, USA). Each cycle included 94°C for 30 seconds, 60°C for 30 seconds, and 72°C for 1 minute, followed by a final extension at 72°C for 10 minutes. The PCR products were separated by electrophoresis in a 2% agarose gel.

### RESULTS AND DISCUSSION

Table 1 summarises the serological results with anti-sera D, C, E, c and e. This resulted in four Rh phenotype patterns. Most samples, i.e. 34 out of 43 samples (79.07%), were identified having ccee phenotype. The incidence of serological phenotype Ccee was the second highest with six samples (13.95%). Then, two out of 43 samples (4.65%) were ccEe phenotype. Lastly, only one sample (2.33%) was detected as the CCee phenotype. Eluates prepared using heat elution from all the samples were tested for indirect antiglobulin tests. However, none of these eluates showed positive reactivity for DEL phenotype. All the 43 RhD negative samples were subjected to RHD1227A polymorphism by Specific Sequence Primer-Polymerase Chain Reaction (SSP-PCR). However, only one sample showed an amplified band of 348bp, which demonstrated the RHD1227A amplification.

Table 1  
Possible genotypes for the 43 RhD-negative samples and the Rh phenotype in several terminologies

Apparent Rh phenotypes	Possible genotype	Fisher Race terminology	Rosenfield terminology	Shorthand Notation	Incidence Number (N=43)	Percentage (%)
ccee	ddccee	dce/dce	Rh <sup>4,5</sup>	Rr	34	79.07
Ccee	ddCcee	dCe/dce	Rh <sup>2,4,5</sup>	r'r	6	13.95
ccEe	ddccEe	dcE/dce	Rh <sup>3,4,5</sup>	r''r	2	4.65
CCee	ddCCee	dCe/dCe	Rh <sup>2,5</sup>	r'r'	1	2.33

As indicated earlier, DEL is the weakest D positive phenotype that expresses trace amounts of D antigens. It is rare and can be detected serologically using adsorption-elution methods. However, this test is tedious and time-consuming to perform, and it is also not a practical test for screening a large number of samples. Currently, molecular technique has been used to replace the serological technique, which is the easiest and most specific to detect this phenotype. In Asian countries, molecular background of DEL has been intensively investigated since these countries are reported to have high prevalence of DEL phenotype (Gu et al., 2014; Li et al., 2009). Nonetheless, there are limited existing data on DEL phenotypes in Malaysia. Therefore, the objective of this study was to detect DEL phenotype in RhD-negative blood using the adsorption-elution technique and Sequence Primer–Polymerase Chain Reaction (SSP-PCR).

Based on the phenotyping test that had been done, the highest frequency of Rh phenotype was the ccee phenotype (79.09%), followed by the Ccee phenotype (13.93%), while 4.66% of the samples were the ccEe phenotype and the lowest phenotype detected was the CCee phenotype (2.33%). The finding of this study is consistent with other studies on the RhD negative phenotype in other countries, especially in East Asia such as China, Korea, Japan and Thailand, which showed ccee and Ccee phenotypes as the most prevalently reported in the RhD-negative samples (Chen et al., 2004; Moussa et al., 2012; Srijinda et al., 2012). Similarly, a previous study by Kyaw et al. (2014) also showed the same results and discovered the highest RhD negative was in Indians, followed by Malays and Chinese. Nonetheless, no information on the blood donor races was given in this study. The serological heat elution test for the 43 RhD negative samples yielded all negative results, indicating no DEL phenotype was detected. Failure to detect the DEL phenotype might be due to the use of leftover or blood samples and a low number of antigen present on the cells. Hemolysed blood samples reduced the ability of antigen D to be detected. All the samples were tested for the presence RHD1227A allele using the Specific Sequence Primer–Polymerase Chain Reaction (SSP-PCR). Separation of PCR products was done in 2% agarose gel. Data from the present study demonstrated that only one (2.33%) out of 43 samples was positive for DEL carrying RHD1227A allele. The positive sample had Rh phenotype of Ccee. This can be related with the statement that DEL individuals who have intact RHD gene expressed the Cc or CC phenotype but did not show the cc phenotype (Wang et al., 2005). Interestingly, approximately 9% of DEL phenotype was still associated with the ce phenotype (Shao et al., 2002). There were five others sample having the same Ccee phenotypes but not identified as positive for DEL. Even though those samples have the same Rh phenotype, their RH genotypes might be different. In fact, a study proposed that there might be discrepancies between Rh phenotyping and RH genotyping (Musa et al., 2014).

To date, at least 14 DEL phenotype alleles have been described. They are RHDIVS2-2A>G, RHD(A137E), RHD(W408R), RHD(L84P), RHD3G>A, RHD(R10W), RHD(L18P), RHD(Y401X), RD(X418L), RHD(delE×9), RHDIVS3+1G>A, RHDIVS5-38del4, RHD(M295I) and RHD1227A. In East Asia, most of the DEL phenotypes carried RHD1227A allele which can be used as a genetic marker for DEL detection (Gu et al., 2014). A study by Srijinda and colleagues on Thailand RhD-negative donors found that 48 out of 50 DEL samples positive for the adsorption-elution test were also positive for RHD1227 allele (Srijinda et al., 2012). In addition, 154 (96.25%) out of 160 samples that were typed as DEL by the adsorption-elution test have RHD1227A allele in China (Gu et al., 2014). Furthermore, one of the previous

studies in Taiwan discovered the exact same RHD1227A allele found in all 94 (100%) DEL individuals (Chen et al., 2004). It is crucial to note that the frequency of D-negative varies among different ethnic groups. In a multi-ethnic country such as Malaysia, it is important to understand D-negative phenotype distribution to estimate compatible blood unit availability and evaluate the risks of Haemolytic Transfusion Reaction (HTR) and Haemolytic Disease of Newborn (HDN).

## CONCLUSION AND RECOMMENDATIONS

Based on the results, one out of the 43 RhD negative samples was positive for DEL phenotype for the RHD1227A polymorphism analysis by SSP-PCR, but not for the heat elution test. In this study, the heat elution technique can be concluded as an ineffective method for detecting the DEL phenotype. The specificity and sensitivity of the molecular technique helped to overcome limitations of the serological study. Herein, a similar study using a bigger sample size or at a different part of the country may give a better outcome.

## ACKNOWLEDGEMENT

This work was supported by the Fundamental Research Grant Scheme (FRGS) by the Ministry of Education, Malaysia (600-RMI/FRGS 5/3 (26/2014)).

## REFERENCES

- Chen, J.-C., Lin, T.-M., Chen, Y. L., Wang, Y.-H., Jin, Y.-T., & Yue, C.-T. (2004). RHD 1227A is an important genetic marker for RhD(el) individuals. *American Journal of Clinical Pathology*, 122(2), 193–8. doi:10.1309/3XMF-2NV5-707T-JE7X
- Flegel, W. A. (2007). The genetics of the Rhesus blood group system. *Blood Transfusion = Trasfusione Del Sangue*, 5(2), 50–7. doi:10.2450/2007.0011-07
- Gardener, G. J., Legler, T. J., Hyett, J. A., Liew, Y. W., Flower, R. L., & Hyland, C. A. (2012). Anti-D in pregnant women with the RHD(IVS3+1G>A)-associated DEL phenotype. *Transfusion*, 52(September 2012), 2016–2019. doi:10.1111/j.1537-2995.2011.03538.x
- Gu, J., Wang, X.-D., Shao, C.-P., Wang, J., Sun, A.-Y., Huang, L.-H., & Pan, Z.-L. (2014). Molecular basis of DEL phenotype in the Chinese population. *BMC Medical Genetics*, 15(1), 54. doi:10.1186/1471-2350-15-54
- Huang, C.-H. (2009). *Transfusion Rhesus Gene Family and Blood Group Antigens — Molecular Aspects in Relation to Genomic Transfusion Medicine*, 52–55.
- Kappler-gratias, S., Auxerre, C., Dubeaux, I., Beolet, M., Ripaux, M., Penneç, P. Le, & Pham, B. (2014). of African origin TI er v iz i Sr l TI er v i Sr l. doi:10.2450/2013.0270-12
- Le Van Kim, C., Colin, Y., & Cartron, J. P. (2006). Rh proteins: key structural and functional components of the red cell membrane. *Blood Reviews*, 20(2), 93-110.
- Li, Q., Hou, L., Guo, Z.-H., Ye, L.-Y., Yue, D.-Q., & Zhu, Z.-Y. (2009). Molecular basis of the RHD gene in blood donors with DEL phenotypes in Shanghai. *Vox Sanguinis*, 97(2), 139–46. doi:10.1111/j.1423-0410.2009.01181.x

- Moussa, H., Tsochandaridis, M., Chakroun, T., Jridi, S., Abdelneji, B., Hmida, S., & Jemni-yacoub, S. (2012). Molecular background of D-negative phenotype in the Tunisian population, (March). doi:10.1111/j.1365-3148.2012.01142.x
- Musa, R. H., Hassan, A., Ayob, Y., & Yusoff, N. M. (2014). RH genotypes among Malaysian blood donors. *Asian Biomedicine*, 8(4), 499–504. doi:10.5372/1905-7415.0804.319
- Okubo, Y., Yamaguchi, H., Tomita, T., & Nagao, N. (1984). A D variant, Del. *Transfusion*, 24(6), 542. doi:10.1046/j.1537-2995.1984.24685066827.x
- Sandler, S. G., Roseff, S. D., Domen, R. E., Shaz, B., & Gottschall, J. L. (2014). Policies and procedures related to testing for weak d phenotypes and administration of Rh immune globulin: results and recommendations related to supplemental questions in the comprehensive transfusion medicine survey of the College of American Pathologists. *Archives of Pathology and Laboratory Medicine*, 138(5), 620–5. doi:10.5858/arpa.2013-0141-CP
- Shao, C. P., Maas, J. H., Su, Y. Q., Köhler, M., & Legler, T. J. (2002). Molecular background of Rh D-positive, D-negative, Del and weak D phenotypes in Chinese. *Vox Sanguinis*, 83(2), 156–161. doi:10.1046/j.1423-0410.2002.00192.x
- Srijinda, S., Suwanasophon, C., Visawapoka, U., & Pongsavee, M. (2012). RhC Phenotyping, Adsorption/Elution Test, and SSP-PCR: The Combined Test for D-Elute Phenotype Screening in Thai RhD-Negative Blood Donors. *ISRN Hematology*, 358316. doi:10.5402/2012/358316
- Wagner, F. F., Moulds, J. M., & Flegel, W. A. (2005). Genetic mechanisms of Rhesus box variation. *Transfusion*, 45(3), 338–344. doi:10.1111/j.1537-2995.2005.04339.x
- Westhoff, C. (2007). The Structure and Function of the Rh antigen. *Complex*, 44(1), 42–50.



## Seasonal Temporal Distribution of Forecasted Wind Speed Data in Langkawi, Malaysia

Siti Noratiqah Mohamad Deros<sup>1\*</sup>, Arnis Asmat<sup>1</sup> and Shattri Mansor<sup>2</sup>

<sup>1</sup>Faculty of Applied Sciences, Universiti Teknologi MARA UiTM, 40450 Shah Alam, Selangor, Malaysia

<sup>2</sup>Institut of Advance Technology, Universiti Putra Malaysia (UPM), 43400 Serdang, Selangor, Malaysia

### ABSTRACT

Temporal distribution of forecasted wind speed is important to assess wind capacity for wind-related technology purposes. Regional wind energy estimation needs the development of wind pattern to monitor and forecast temporal wind behaviour. Temporal wind in Malaysia mainly depends on monsoonal factor that circulates yearly and each monsoon derives distinct character of wind. This paper aims to develop a model of wind speed pattern from historical wind speed data. Then, the model was used to forecast 5-years seasonal wind speed and identify temporal distribution. Wind speed model development and forecast was performed by identifying the best combination of wind speed seasonal component using Seasonal Auto-regressive and Moving Average (SARIMA) model. Thus, three distribution models, Lognormal, Weibull and Gamma models, were exploited to further observe consistency using Kolmogorov-Smirnov goodness-of-fit test. The best fit model to represent seasonal wind distribution in each monsoon season at Pulau Langkawi, Malaysia, is Log-normal distribution (0.04679-0.108).

*Keywords:* Lognormal, SARIMA model, seasonal distribution, wind speed forecast

### INTRODUCTION

In Malaysia, wind mainly depends on four monsoon seasons that occur throughout the

year, where each monsoon brings unique and different wind behaviours (Jamaludin et al., 2010). Hence, wind studies in Malaysia involved determination of regional wind pattern including wind speed, wind distribution and wind direction (Daut et al., 2011), and for this purpose, long-term data of at least 10 years are needed (Noram et al., 2010). Most studies on wind emphasize annual wind data (Azami, Khadijah, Mahir, & Kamaruzzaman, 2009; Khadijah et al. 2009; Siti, Norizah, & Syafrudin, 2011) rather than

#### ARTICLE INFO

##### Article history:

Received: 25 October 2016

Accepted: 17 March 2017

##### E-mail addresses:

atiqahmohdderos@gmail.com (Siti Noratiqah Mohamad Deros),

arnisamat@gmail.com (Arnis Asmat),

shattri@gmail.com (Shattri Mansor)

\*Corresponding Author

seasonal data. Siti et al. (2011) grouped annual wind speed data in Malaysia into four distinct seasons depending on the wind direction blows of each season. In other hands, Khadijah et al. (2009) and Azami et al. (2009) studied 2 years wind speed distributions to estimate wind capacity of regional study area. Nonetheless, these studies failed to project seasonal properties that highly influence wind in Malaysia. Therefore, seasonal wind study needs long-term data in order to gain sufficient information on seasonal factor.

Wind studies mainly used wind speed measurement data that are retrieved using an anemometer while wind vane records wind direction and these datasets provide timely wind measurement in hourly, daily, and monthly periods (Juan et al., 2016). This has initiated the questions on the relationships between timely wind speed and extreme wind events and how the datasets explain the long-term wind trends. Limited wind study that considers temporal and long-term data to get enough seasonal properties causes the lacking of impactful monsoonal wind study. Wind studies conducted by several researchers include determination of the best fit model to represent temporal distribution of wind in one regional area. Wind speed distribution is an important study to observe the frequency of certain wind speeds occurred to assess the cumulative wind (Zaharim, Najid, Razali, & Sopian, 2009); Azami et al. (2009) studied Weibull and Lognormal distributions to fit the wind speed data. They found that the Weibull distribution is the best fit model as compared to the Lognormal distribution to describe the behaviour of annual wind speed data. Moreover, researchers discussed the Weibull (Wengang & Igor, 2016) and Rayleigh (Maina et al., 2016) distributions to describe the wind energy potential on the basis of 5-years hourly time series wind speed data. They concluded that the Weibull distribution provides a better fit to probability distributions as compared to the Rayleigh model. However, the use of annual wind data only projects a general distribution of wind speed, and thus neglects the wind speed seasonal properties and actual wind condition in one monsoon. For example, the northeast monsoon was recorded to have the highest wind speed among other monsoon seasons that bring together abundant rainfall and may cause hurricane (Noratiqah, Arnis, & Shattri, 2012). This explains the importance of seasonal wind distribution study and long-term trend to forecast future wind scenario.

Wind pattern development is an important study to monitor and forecast wind including any wind-related hazards such as tsunami and hurricane. Development of wind pattern allows the forecast of wind that helps in planning effective coastal structuring activity and deep-water fishing. Seasonal wind forecast can estimate seasonal wind pattern from different properties of wind speed, distribution, and direction. Seasonal pattern studies had been done by Zuhaimy and Khairil (2005) on potential wind energy, and Noratiqah, Arnis and Shattri (2012) on seasonal wind speed model by using Seasonal Auto-regressive and Integrated Moving Average (SARIMA) models to simulate seasonal properties. The model has the ability to recognise the unique pattern of monsoonal wind and formulate the trend in one model (Soebiyanto, Adimi, & Kiang, 2010) such as seasonal wind. The trend formulates and forecasts wind speed by using SARIMA that has a high correlation with actual wind measurement.

This study attempted to forecast wind speed from 2011-2015 by formulating the seasonal forecast model using 2000-2010 wind speed data. Thus, the seasonal distribution of forecasted wind was determined as the best model to represent the temporal wind distribution in each monsoon season. The distribution models tested in this study were Gamma, Lognormal and



Weibull models, whereby the best model was determined by using the Kolmogorov-Smirnov Goodness-of-fit test.

## METHOD

In this study, the 10-year data of wind speed recorded from 2000 to 2010 were provided by Malaysian Meteorological Department (MMD). The data were recorded from the anemometer devices installed at 10-meter tower from the ground. The anemometer station is located in Pulau Langkawi (6° 20 'N Latitude and 99° 44' E Longitude, 6.4 metres above the Mean Sea Level, MSL). The data format or unit is in meter per second (m/s) and grouped into Northeast monsoon, April Intermonsoon, Southwest monsoon and October Intermonsoon. The mean and standard deviation of the data of every season are tabulated in Table 1 to show the wind speed properties in each season.

Table 1  
*Seasonal mean and standard deviation of wind speed data from year 2000 to 2010*

Year	Northeast Monsoon		April Inter-monsoon		Southwest Monsoon		October Inter-monsoon	
	Mean	S.D	Mean	S.D	Mean	S.D	Mean	S.D
2000	2.87	0.96	2.16	0.47	2.55	1.39	2.76	2.06
2001	2.55	0.81	2.12	0.48	2.43	1.34	2.17	0.71
2002	3.49	1.13	2.45	0.39	2.61	1.10	2.16	0.40
2003	2.94	0.97	2.17	0.26	2.54	0.98	3.32	1.91
2004	3.16	1.01	2.19	0.24	2.48	1.42	2.31	1.09
2005	3.28	0.99	1.93	0.31	1.75	0.46	1.54	0.39
2006	2.18	0.93	1.62	0.25	1.75	0.50	1.76	0.47
2007	2.29	0.76	1.71	0.37	1.57	0.43	1.67	0.58
2008	2.34	0.85	1.70	0.25	1.59	0.35	1.63	0.29
2009	2.31	0.76	1.76	0.46	1.79	0.72	1.65	0.47
2010	2.45	0.73	1.77	0.25	1.64	0.40	1.74	0.51

Table 1 shows the highest and consistent wind speed blow during the northeast monsoon with the mean range of 2.18-3.49 m/s from 2000 to 2010. On the other hand, the wind speed in other monsoon period is constant at the range of 1.54-3.32 m/s. However, the wind speed decreases gradually each year and this may be due to the coastal structuring that introduces frictional force on wind (Michael, 2009).

This section further explains the wind speed model development that is used in wind speed forecast. The forecasted seasonal wind speed distribution analysis is elaborated further so as to determine the distribution model of wind in each monsoon season. Wind pattern forecast model chosen in this study is the Seasonal Auto-Regressive Integrated Moving Average (SARIMA) model, which was adapted from Zuhaimy and Khairil (2005) who used SARIMA to model and forecast the seasonal energy demand for daily basis and found that the SARIMA model produced demand forecast that highly correlates with the actual demand. On the contrary,

Caixia (2010) also modelled the seasonal wind pattern by using the Autoregressive and Moving Average (ARMA) model. However, the model developed is not flexible enough to explain the seasonal properties of wind. In this study, the seasonal wind speed model can be best developed by using SARIMA due to its flexibility to recognise the seasonal pattern of data.

The plot of monthly mean wind speed data was used to determine wind speed properties and seasonality factor in the data. The seasonality span,  $T$ , which is the time taken for data to repeat the pattern for the next period was also identified from the plot. According to Zuhaimi and Khairil (2005), the span was determined in month scale. Hence, the seasonality span in this study is  $T=12$  due to the circulation of all monsoons that takes 12-month period. Meanwhile, the Seasonal Autoregressive Integrated Moving Average (SARIMA) model comprises of four processes; identification, estimation, diagnostic checking and forecasting. The SARIMA model can be expressed in SARIMA  $(p,d,q) \times (P,D,Q)$  form. This model consists of non-seasonal and seasonal winds represented by degree,  $p$ ,  $q$ ,  $P$  and  $Q$ . Seasonal integration order is represented as  $D$ , while non-seasonal integration order is represented by  $d$ . In order to identify the SARIMA model of wind speed, Equation [1] is applied.

$$\Phi_P(L^S)\phi_p(L)\Delta_S^D\Delta^d y_t = \Theta_Q(L^S)\theta(L)\varepsilon_t \quad [1]$$

Parameter  $\Delta_S^D$  is defined as the seasonal difference  $(1-L^S)^D$ ,  $\Delta^d$  as the non-seasonal difference  $(1-L)^d$  and  $\Phi$  as the parameter for non-seasonal autoregressive (AR). Meanwhile,  $\phi$  is the seasonal autoregressive (SAR) parameter,  $\Theta$  is the parameter for seasonal moving average (SMA) and  $\theta$  is the parameter for non-seasonal moving average (MA). All the four parameters are the respective lag operator,  $L$  polynomials. The model was examined by using the penalty function criteria method based on two penalty function statistics, Akaike Information Criterion (AIC) and Schwarz/Bayesian Information Criterion (BIC) (Lee, Yoo, & Jin, 2007).

The five-year (2011-2015) wind speed forecast was implemented by using the SARIMA model developed. The forecast method was done by applying the out-of-sample method (Gokhan, 2011), in which the data were divided into two; 80% the in-sample dataset and 20% the out-of-sample dataset. The forecast horizon,  $h=5$  represents the 5-years wind speed distribution forecast. To test the reliability of the SARIMA model developed, Mean Absolute Error (MAE), Root Mean Squared Error (RMSE) and Mean Absolute Percentage Error were calculated. The smaller error value ( $<0.5$ ) shows a good data forecast.

The three distribution models (Gamma, Lognormal and Weibull distribution model) were chosen in this study based on the suitability with the wind speed data that are asymmetric, continuous and mostly positive outliers. The best-fit model had been tested on the seasonal forecasted wind speed data. Important forecasted wind speed parameter was used in this stage according to the distribution model requirement.

**Gamma Distribution**

A positive random variable X is said to be gamma distributed when it has the probability density, as shown in [2] below.

$$\rho(t) = \frac{\lambda^\alpha t^{\alpha-1}}{\Gamma(\alpha)} e^{-\lambda t}, t \geq 0 \tag{2}$$

where  $\alpha > 0$  is the shape parameter and  $\lambda > 0$  is the scale parameter. The symbol  $\Gamma(\alpha)$  denotes the complete gamma function. The gamma density always has only one maximum at  $t = (\alpha-1)/\lambda > 0$ , and then decreases to zero when  $t \rightarrow \infty$ .

$$Gamma, g(x) = \frac{x_i^\alpha}{\beta^\alpha \Gamma(\alpha)} \exp\left[-\frac{x_i}{\beta}\right] \tag{3}$$

where  $g(x)$  is the gamma probability distribution  $\alpha$  is the scale parameter, and  $\beta$  is the shape parameter. The random variable is denoted by  $x$  and the normalising factor is presented as  $\Gamma$ .

**Log-normal Distribution**

Log-normal distribution is the reference to normal distribution. A random variable is log-normally distributed if the logarithm of the random variable is normally distributed (Zaharim, 2009).

$$F(x) = \frac{1}{2} \left[ 1 + erf \left( \frac{\ln x - \mu}{\sigma \sqrt{2}} \right) \right] \tag{4}$$

Equation [4] shows the cumulative probability function of log-normal distribution. The mean,  $\mu$ , and standard deviation,  $\sigma$ , of the wind speed distribution are the normal random variables of  $\ln(x)$ , not the log-normal random for variable  $x$ .

$$Log - normal, l(x) = \frac{1}{x\sigma\sqrt{2\pi}} e^{-\frac{\ln x - \mu^2}{2\sigma^2}} \tag{5}$$

The log-normal probability distribution is denoted by  $l(x)$ ,  $\ln x$  is the random variable that is log-normally distributed with the mean ( $\mu$ ) and standard deviation ( $\sigma$ ).

**Weibull Distribution**

The Weibull cumulative distribution function is effectively used to total up the wind speed distribution in one seasonal period (Akpınar & Akpınar, 2004). In the graphical method to estimate the Weibull shape parameter,  $k$ , and Weibull scale parameter,  $c$ , the cumulative wind speed distribution is required. These parameters may be estimated by using linear regression of the cumulative Weibull distribution (Youm et al., 2005).

$$Weibull, h(x) = \frac{\beta}{\alpha} \left(\frac{x_i}{\alpha}\right)^{\beta-1} e^{-\left(\frac{x_i}{\alpha}\right)^\beta} \tag{6}$$

For the Weibull probability distribution Equation [6],  $h(x)$  involved the scale parameter ( $\alpha$ ) and shape parameter ( $\beta$ ) of the random variable  $x$ . However, those parameters used in the distinct model are derived from the basic descriptive statistics, especially mean and standard deviation of the variables. Thus, the model structure itself influences the fitness of the distribution instead of the data. The function of cumulative Weibull distribution is described in Equation [7] below.

$$F(v) = 1 - \exp\left(-\left(\frac{v}{c}\right)^k\right) \quad [7]$$

Equation [7] explains the percentage of time when the wind speed is equal to or lower than the wind speed. The shape parameter,  $k$ , is important to explain the site topology. For a given average speed, a lower value of  $k$  shows a greater variability of wind speed. It occurs due to low shape factor, which makes the wind speed range greater (Piazza et al., 2010). According to Shamshad et al. (2009), the higher value of scale parameter,  $c$ , indicates that the wind speed is higher, while the shape parameter,  $k$ , shows the wind stability. In other words, shape parameter,  $k$ , helps to observe the distribution, i.e. whether they are closely related to each other or not. Shape parameter may be ranked from 1 to 3, where it can be high, moderate and consistent wind variations, while scale parameter,  $c$ , explains how windy the study area is. Goodness of fit-test was applied to test the fitness of the three distributions by indicating the error of the distributions. A comparison with the original data sample was done using the Kolmogorov-Smirnov test in Equation [7] (Zaharim, 2009).

$$D = \min_{1 \leq i \leq N} \left( F(Y_i) - \frac{i-1}{N}, \frac{i}{N} - F(Y_i) \right) \quad [8]$$

The Kolmogorov-Smirnov test with the distribution function  $Y$ , which is the continuous distribution denoted by  $F(Y)$ , and the test statistic value were presented by  $D$ . The goodness of fit test model such as Kolmogorov-Smirnov test measures the gaps between the data sample and the distribution tested. The lower the test statistic value, the smaller the gap is ( $<0.5$ ), and the fitter the distribution tested.

## RESULTS AND DISCUSSION

This section is divided into two parts; the seasonal wind speed model development and forecast and the seasonal distribution model determination.

The monthly mean wind speed from 2000 to 2010 is 2.306 m/s, while the standard deviation is 0.657 m/s. The monthly mean used to plot the graph of wind speed versus month shows that the highest wind speed in Langkawi has various wind speed patterns in different times, respectively. This variation is influenced by the southwest monsoon that occurs in May to September, the transition between two monsoons in October, the northeast monsoon in November to Mac and the second inter-monsoon in April each year. As shown in Table 2, there are four possible SARIMA models that can represent the time series data of wind speed.

Table 2  
AIC and BIC values of the ARIMA model

SARIMA	AIC	BIC
(1,1,1)×(1,1,1)	0.703544	0.747660
(1,1,2)×(1,1,1)	0.707552	0.751668
(1,1,3)×(1,1,1)	0.275654	0.319770
(1,1,4)×(1,1,1)	0.702883	0.746999

However, AIC and BIC values, that work by controlling the possible error and fitting the measure using the maximum likelihood method, indicate that SARIMA (1,1,3)×(1,1,1) has the smallest value. Therefore, it is the fittest model to the data series.

The forecasting of seasonal wind speed data later was done using the SARIMA (1,1,3)×(1,1,1) model. Results of the forecasting data produced low error with 0.3186 root mean squared error (RMSE), 0.265 mean absolute errors (MAE) and 11.644% mean absolute percentage error (MAPE). This shows the accuracy of the SARIMA (1,1,3)×(1,1,1) model to represent the wind speed data. Figure 1 shows the plot of mean wind speed data versus 2002 to 2015 during the southwest monsoon. The forecasting started after the first period of the sample. Only 2002 and ahead of the forecast data were produced after the adjustment to get an accurate forecast. The forecasted data of the wind speed generated from the wind speed model developed are described in Figure 1.

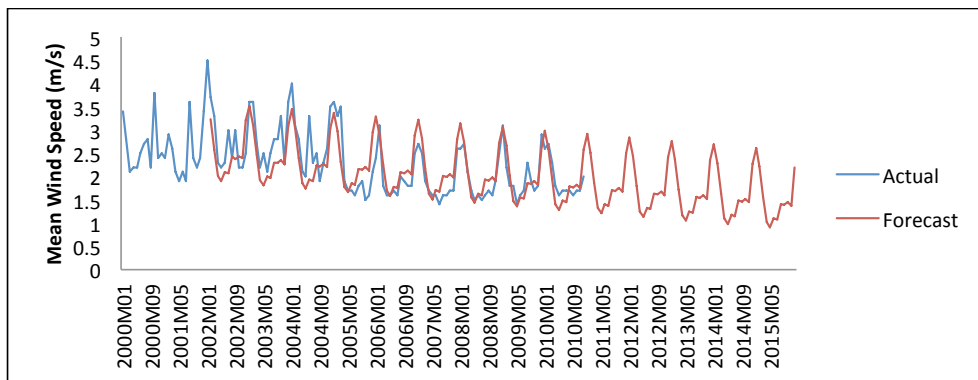


Figure 1. Actual vs. forecasted monthly wind speed data

As shown in Figure 1, there are temporal wind speed trend patterns of the actual and forecasted wind speed data. Figure 1 shows the forecasted wind speed that is represented by the red line, while the pattern of actual wind speed is represented by the blue line. The peak line shows the highest wind speed and it can be observed that wind speed is significantly high during the months of December, January and February of each year. Then, the wind speed gradually

decreases through the year, as can be observed from the plot. However, we can also observe that the highest wind speed of the consequence year is not as high as the wind speed of the previous year.

The descriptive statistics of seasonal wind speed forecasted is tabulated in Table 3. The highest mean wind speed is during the northeast monsoon, while the lowest is during the April Inter-monsoon. This is due to the fact that the distance travelled by wind from the Indian Ocean during the southwest monsoon introduced a higher friction force on wind (Michael, 2009).

Hence, in order to identify the distribution that satisfies the wind speed criteria, the Kolmogorov-Smirnov goodness-of-fit test was performed and the results are presented in Table 3. It can be observed that, of all season, the best fit distribution is the Log-normal distribution. Fit distribution should have (0.5) that indicates the small gap or difference between the distribution and original data sample.

Table 3  
*AIC and BIC values of the ARIMA model*

Seasonal	Kolmogorov-Smirnov Goodness-of-fit test		
	<i>Gamma</i>	<i>Log-normal</i>	<i>Weibull</i>
Northeast monsoon	0.04993	0.04679	0.06504
April inter-monsoon	0.07078	0.06997	0.084
Southwest monsoon	0.13875	0.108	0.17185
October inter-monsoon	0.13508	0.10165	0.14595

Table 3 shows that among three models tested, the Log-normal distribution model produced the lowest gap value among all the seasonal wind speed data in each monsoon season. This was followed by the Gamma distribution model and finally the least fit model for seasonal wind speed distribution is the Weibull model. Then, the distribution analysis performed by the Log-normal model shows that the Northeast monsoon is the season with the most fit data value (0.04679) compared to the Gamma (0.04993) and Weibull (0.06504) distribution models. This finding differs from the study by Eugene et al. (2011) who found that the wind speed is best represented by the Weibull distribution model. This may be due to the 10-minute mean wind speed data used that are more constant compared to the daily mean. In addition, the Weibull model has no ability to estimate extreme wind speed changes, the task that is best performed by the Lognormal distribution model (Burton et al., 2001).

The Lognormal distribution model projects the different mean and standard deviation of different monsoon seasons. This leads to the different frequencies and cumulative wind in an

individual monsoon. Based on the forecasted wind derived in the SARIMA and Lognormal distribution models, the seasonal wind speed can be expressed as in Figure 2 below.

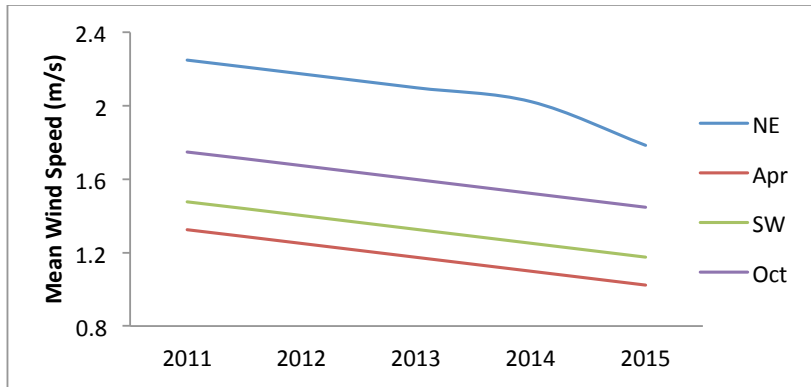


Figure 2. Seasonal Forecasted Mean Wind Speed (m/s) Distribution for 2011 to 2015

Figure 2 shows that the northeast (NE) monsoon acquires the highest mean wind speed with an average between 1.8 to 2.3 m/s, followed by October intermonsoon, Southwest monsoon and the lowest wind speed was estimated to be in April intermonsoon between 0.9 to 1.3 m/s. The monthly mean wind speed data explain the frequency and cumulative wind in one monsoon season, as summarised in Table 4.

Table 4  
Seasonal forecasted mean wind speed, standard deviation, the period and cumulative wind on each monsoon season

Monsoon	Mean, $\mu$ (m/s)	S. Deviation, $\sigma$	t (day)	Cumulative wind (m/s)
Northeast	2.458	0.348	755	9070.028
April intermonsoon	1.514	0.316	150	1673.145
Southwest	1.667	0.317	765	11923.645
October intermonsoon	1.938	0.316	155	1944.162

Wind speed distribution provides frequency and cumulative information of each monsoon season. Table 4 shows the cumulative wind speed provided in each monsoon season derived from seasonal mean wind speed and the period taken by each monsoon season. This shows that the northeast monsoon possesses a high mean wind speed, and also a high standard deviation value. This high standard deviation value means that the wind speed data in the northeast monsoon are not consistent and highly spread above or below the mean value. This is the main reason of the low cumulative wind speed derived during the northeast monsoon compared to the southwest monsoon that apparently has lower mean wind speed. The time period taken by the southwest monsoon that possesses 10 days longer than the northeast monsoon also contributes

to the higher cumulative wind speed produced during its season. The cumulative wind for the April and October intermonsoon highly depends on the mean wind speed and time period taken by each monsoon season. The consistent mean value, due to the low and equal standard deviation value, did not affect the cumulative wind of both intermonsos.

## CONCLUSION

Low goodness-of-fit test statistics value means the smaller the gaps among the data samples. The results of the three distribution models tested on the forecasted wind speed data show that the log-normal distribution model is the fittest model to represent wind speed distribution of all seasons. This is due to the lowest gap among the data samples distributed by the Lognormal distribution model in all the seasons.

Both mean and standard deviation of wind can help to determine the best location and appropriate wind-related technology devices to be installed. Cumulative wind is useful to estimate the amount of wind derived by each monsoon season for wind technology planning and design. Nevertheless, cumulative wind can also help in coastal structure observation and development.

## ACKNOWLEDGEMENTS

The authors gratefully acknowledge the support from Malaysian Meteorological Department (MMD) in providing the time series data and Ministry of Higher Education, Malaysia, for the financial support scholars under my Brain15 Programme. The authors would also like to thank the Institute of Research Management and Innovation (IRIM), Universiti Teknologi MARA, for the financial support under the BESTARI Research Grant no. 600-IRMI/DANA5/3/BESTARI (0012/2016).

## REFERENCES

- Azami, Z., Khadijah, S. N., Mahir, A. R., & Kamaruzzaman, S. (2009). Wind Speed Analysis in the East Coast of Malaysia. *European Journal of Scientific Research*, 32(2), 208-215.
- Burton, T., Sharpe, D., Jenkins, N., & Bossanyi, E. (2001). *Wind Energy Handbook*. Wiley.
- Daut, I., Irwanto, M., Irwan, Y. M., Gomesh, N., & Ahmad, N. S. (2011). Potential of Wind Speed for Wind Power Generation in Perlis, Northern Malaysia. *TELKOMNIKA* 9(3), 575-582.
- Eugene, C. M., Matthew L., Richard, M. V., & Laurie, G. B. (2011). Probability Distributions for Offshore Wind Speeds. *Energy Conversion and Management*, 52, 15-26.
- Gokhan, S. (2011). The Efficacy of SARIMA Models for Forecasting Inflation Rates in Developing Countries: The Case for Turkey. *International Research Journal of Finance and Economics*, (62), 111-142.
- Jamaludin, S., Sayang, M. D., Zawiah, W. Z. W., & Aziz, J. A. (2010). Trends in Peninsular Malaysia Rainfall Data during the Southwest Monsoon and Northeast Monsoon Seasons: 1975-2004. *Sains Malaysiana*, 39(4), 533-542.



- Juan, J. T., Janna, K. S., Ines, W., David, S., & Martin, K. (2016). Full-field Assessment of Wind Turbine near-wake Deviation in Relation to Yaw Misalignment. *European Academy of Wind Energy. Wind Energy Sci.*, 1, 41-53.
- Khadijah, S. N., Azami, Z., Mahir, A. R., Said, M. Z., Kamarulzaman, I., & Kamaruzzaman, S. (2009). Analyzing the East Coast Malaysia Wind Speed Data. *International Journal of Energy and Environment*, 3(2), 53-60.
- Lee, K., Yoo, S., & Jin, J. J. (2007). Neural Network Model vs. SARIMA Model in Forecasting Korean Stock Price Index (KOSPI). *Issues in Information System*, 8(2), 372-378.
- Maina, A. W., Kamau, J. N., Timonah, N., Nishizawa, Y., & Churchill, S. (2016). Wind Power Potential Analysis based on Different Methods Fitted in Weibull & Rayleigh Models for Wind Patterns in Juja & Nivasha. *International Journal of Innovative Research in Science, Engineering and Technology*, 4(1), 19-27.
- Malaysian Meteorological Department (MMD). *Monthly Weather Bulletin*. Retrieved from <http://www.met.gov.my>
- Michael, J. I. (2009). Why is the Wind Speed Decreasing? *Blue Hill Meteorological Observatory*, New York.
- Noram, I. R., Majid, T. A., Ali, M. I., Syamsyul, M. H. S., Hashim, M., & Zakaria, I. (2010). *Wind Related Disaster Risk Reduction in Malaysia*, Malaysia.
- Noratiqah, S. M. D., Arnis, A., & Shattri, M. (2012). Wind Power Estimation from Forecast Wind Data. *6<sup>th</sup> International Symposium on Advances in Science and Technology (SasTech)*. 24-25 March 2012, Kuala Lumpur, Malaysia.
- Noratiqah, S. M. D., Arnis, A., & Shattri, M. (2012). Seasonal Wind Speed Distribution Analysis in West Coast of Malaysia. *International Conference on Statistics in Science, Business and Engineering 2012 (ICSSBE2012)*, 201-205.
- Shamshad, A., Wan Hussin, W. M. A., Bawadi, M. A., & Mohd Sanusi, M. A. (2009). *Analysis of Wind Speed Variation and Estimation for Wind Power Generation in Malaysia*. Pulau Pinang, Malaysia.
- Siti, M. R. S., Norizah, M., & Syafrudin, M. (2011). The Evaluation of Wind Energy Potential in Peninsular Malaysia. *International Journal of Chemical and Environmental Engineering*, 2(4), 284-291.
- Soebiyanto, R. P., Adimi, F., & Kiang, R. K. (2010). Modeling and Predicting Seasonal Influenza Transmission in Warm Regions Using Climatological Parameters. *PLoS ONE*, 5(3).
- Wengang, M., & Igor, R. (2016). Estimation of Weibull Distribution for Wind Speed along Ship Routes. *Journal of Engineering for the Maritime Environment*. 1475690216653495.
- Zaharim, A., Najid, S. K., Razali, A. M., & Sopian, K. (2009, February). Analyzing Malaysian wind speed data using statistical distribution. In *Proceedings of the 4<sup>th</sup> IASME/WSEAS International conference on energy and environment, Cambridge, UK* (Vol. 2426, p. 360370).
- Zuhaimy, H. I., & Khairil, A. M. (2005). SARIMA Model for Forecasting Malaysian Electricity Generated. *Jabatan Matematik Universiti Teknologi Malaysia*, 21(2), 143-152.



## Isolation and Characterisation of Filamentous Fungi from Animal Agricultural Farm Soil

Muhammad Shukri Senwan<sup>1</sup>, Muhd Fauzi Safian<sup>2,3</sup>, Zainon Mohd Noor<sup>1</sup> and Zaidah Zainal Ariffin<sup>1,3\*</sup>

<sup>1</sup>School of Biology, Faculty of Applied Science, Universiti Teknologi MARA (UiTM), 40450 Shah Alam Selangor, Malaysia

<sup>2</sup>School of Chemistry, Faculty of Applied Science, Universiti Teknologi MARA (UiTM), 40450 Shah Alam Selangor, Malaysia

<sup>3</sup>Atta-ur-Rahman Institute for Natural Product Discovery, Universiti Teknologi MARA (UiTM) Puncak Alam, 42300 Bandar Puncak Alam, Selangor, Malaysia

### ABSTRACT

*Aspergillus* sp. is an extremely resilient species that can be found everywhere in the environment and is present abundantly in water and soil. The defining characteristic of *Aspergillus* sp. is their extensive hyphal network which enable them to survive anywhere, even in very harsh conditions. This study was carried out to isolate the filamentous fungi from peat soil of animal agricultural farm and characterise them based on their morphological and molecular characteristics. Growth rate of each isolated fungi was also evaluated in order to determine the period of maturity for each fungi. Soil samples were collected, weighed and then dissolved in sterile distilled water. The samples were serially diluted and spread onto potato dextrose agar (PDA) for isolation. Different isolated colonies that were morphologically different from each plate was purified and sub-cultured onto new media for macroscopic and microscopic identifications. For molecular identification, a conventional technique was used in genomic DNA extraction of filamentous fungi due to their thick cell wall and presence of surface proteins protecting the fungus. These characteristics make it difficult to harvest the genomic DNA. Polymerase chain reaction (PCR) was carried out using internal transcribed spacer primers; *ITS1* (forward) and *ITS4* (reverse).

The morphological identification and molecular technique showed that majority of these isolated fungi are *Aspergillus* sp.

### ARTICLE INFO

#### Article history:

Received: 25 October 2016

Accepted: 17 March 2017

#### E-mail addresses:

muhammadshukrisenwan@yahoo.com (Muhammad Shukri Senwan),

mohdf956@salam.uitm.edu.my (Muhd Fauzi Safian),

drzainonmn@salam.uitm.edu.my (Zainon Mohd Noor),

drzaidah@salam.uitm.edu.my (Zaidah Zainal Ariffin)

\*Corresponding Author

**Keywords:** *Aspergillus* sp., filamentous fungi, internal transcribed spacer, macroscopic and molecular identifications, polymerase chain reaction

## **INTRODUCTION**

Malaysia, comprising the regions of Peninsular Malaysia, Sabah and Sarawak, is covered with vast areas of peatland. Peatland is known as all lands on peat soil. This area plays an important role in preserving water supply, and providing nutrients for the trees and other resources to communities. Other than these, it also provides nutrients for soil micro flora. This study focuses on peatlands under crop or husbandry category in which the peatland areas are used for agricultural activities. In general, peat soil contains high carbon content which includes both organic and inorganic carbon. Organic carbon and water content in soil act as sources of nutrients for most soil fungi (Rudiyanto, Minasny, & Setiawan, 2016; Moore et al., 2013; Page et al., 2004; Drenovsky et al., 2004).

Animal agricultural farm is categorised under the crop and husbandry category. Most animal agricultural farm soils are contaminated with hazardous chemical compounds such as hormones and antibiotics (Kumar et al., 2005). These compounds are used on livestock to increase productivity rate and reduce diseases. Disposal of animal wastes on the soil contaminates the surrounding. Only around 30% of ingested compounds will remain in livestock's system, while the remaining is excreted back into the environment (Kumar et al., 2005; Gersema & Helling, 1986; Gavalchin & Katz, 1994). The compounds in animal waste are scattered on animal agricultural farm area, thus affecting the soil composition (Gavalchin & Katz, 1994). These contaminations also cause the emergence of antimicrobial resistance in terrestrial environment. The usage of antimicrobial compounds has led bacteria to develop resistance towards antibiotics used (Nordenberg, 1998; Bebell & Muiru, 2014). The emergence of antibiotic-resistant bacteria in the environment will create problems for antibiotic therapy in human and animal in the future (Tollefson & Karp, 2004; Lees & Aliabadi, 2002).

Filamentous fungi are the major decomposers in peat soil environment where their extensive hyphal networks enable them to use available nutrients dispersed in vast areas of the land. Other characteristics that are advantageous for such fungi to thrive in these lands are their high growth rate and thick cell wall, which protect them from their predators. Some filamentous fungi produce antibacterial compounds and are able to degrade certain types of chemical (Shukri et al., 2015). This study was carried out to isolate the filamentous fungi from peat soil of animal agricultural farm and characterise them based on their morphological and molecular characteristics.

## **METHOD**

### **Sample Collection**

Soil samples were collected from animal agricultural farm at MJ Fatonah Sdn. Bhd., Kuala Selangor. The samples were collected from various locations with different livestock. The soil samples were taken from a depth of 1-10 cm from the surface and stored in biohazard plastic bags. Then, the samples were brought back to the laboratory for further study.

### **Isolation and Purification of Fungi**

One gram of soil was collected from each sample and dissolved in 10 mL sterile distilled water. The mixture was serially diluted up to four times of tenfold dilution factor. 100  $\mu$ L of each dilution was taken out and spread onto the potato dextrose agar (PDA) containing 50 mg/mL chloramphenicol to prevent any growth of bacteria and saprophytic fungi. Each PDA plate was incubated at 28°C. After three days, a colony of fungus was collected and transferred into new sterile PDA using a sterile needle in order to get a pure culture. Then, each plate was incubated for 3-14 days at 28°C. The growth rate of each fungal isolates was obtained by measuring the diameter of respective fungal colonies.

### **Morphological Characteristics of Fungi**

At day 3 of incubation, macroscopic identification was carried out by observing the colour and texture of each fungal colony through the naked eyes. For microscopic identification, adhesive tape method was used to observe the reproductive system of each fungal isolate. A drop of methylene blue was added onto the glass slide. The sample was collected using transparent adhesive tape on the culture and transferred onto glass slide for observation under light microscope (Olympus CX21) by using 400 $\times$  magnification.

### **Genomic DNA Extraction of Isolated Fungi**

The technique for DNA extraction was performed using a conventional method. This method was designed to disrupt fungal cell wall through heating and rapid cooling. About 100  $\mu$ L of  $1 \times 10^6$  cfu/mL fungal spores suspension was inoculated onto PDA, followed by two days of incubation at 28°C. After the incubation period, approximately 5 mL of sterile distilled water was added onto the plate, followed by a collection of fungal spores and mycelia. This step was carried out gently using an inoculating loop or a sterile pipette tip to prevent any agar debris in the fungal and mycelia collection. About 1 mL of the spores and mycelia collected was respectively transferred into the microcentrifuge tube, followed by centrifugation at 14,000 rpm for 1 minute. The supernatant was removed carefully to avoid any dislodged to the pellet. After that, 1 mL of phosphate buffer saline (PBS) was mixed with the pellet. 25  $\mu$ L of spore suspension containing PBS was transferred into a PCR tube. Then, 25  $\mu$ L of sterile distilled water was added to dilute the spore suspension to 1:1 dilution.

Thermocycler MJ Mini Personal Thermal Cycler from BIO RAD was set at certain conditions: initial denaturation (95°C, 5 minutes), denaturation (95°C, 5 minutes) and rapid cooling (4°C, 10 minutes). Next, the nucleic acid was either stored at -20°C, or directly used for PCR amplification.

**Molecular identification of isolated fungi.** Briefly, ITS1 primer (5'-TCC GTA GGT GAA CCT TGC GG-3') and ITS4 primer (5'-TCC TCC GCT TAT TGA TAT GC-3') were used for a total of 25 µL reaction. The PCR reaction was carried out by using MJ Mini Personal Thermal Cycler from BIO RAD. The PCR mix contained template DNA, 10 µM of each primer (AIT biotech), 10x standard buffer (New England BioLabs), 10 mM dNTP mix (New England BioLabs) and 1.25U of *taq* DNA polymerase (New England BioLabs). The PCR conditions were set at: i) initial denaturation (95°C, 30 seconds), (ii) 35 cycles of denaturation(95°C, 30 seconds), (iii) annealing (45°C, 60 seconds), (iv) extension (68°C, 60 seconds), and followed by (v) another final extension (68°C, 60 seconds).

About 2 µl of each PCR product was electrophoresised in 1% agarose gel (BIO RAD). The samples were sent to AIT Biotech, Singapore, for sequencing. By using BioEdit software, the sequences were cleaned and sequence alignment was carried out using BLAST, NCBI.

## RESULTS AND DISCUSSION

### Morphological Identification of Fungal Isolates

A total of seven filamentous fungi were isolated from the peat soil of animal agricultural farms. Based on the morphological and molecular identification, only one sample was identified as *Eupenicillium* sp., while the remaining samples were identified as *Aspergillus* sp. The low pH level of peat soil, which ranged from 2 to 4, and the non-selective characteristics of *Aspergillus* sp. are the reasons for the abundance of *Aspergillus* sp. (Sarmah, Meyer, & Boxall, 2006). *Aspergillus* sp. can survive in a variety of substrates including animal remains which may contain excess contaminants from animal agricultural activities such as antibiotics and hormones. It can also survive in a very large range of temperatures and humidity (Krijgsheld et al., 2013).

The presence of *Aspergillus* sp. in the peat soil acts as a natural decomposer of animal remains in the farm (Song et al., 2010). Some of them are categorised under mycotoxin-producing fungi such as *A. fumigatus* (gliotoxin, fumagilin), *Aspergillus terreus* (citreoviridin) and *A. versicolor* (cyclopiazonic acid) (Manshor et al., 2012). Even though the use of these mycotoxins in decomposition process is hazardous to organic materials, it does not show any significant effect on humans and animals (Tamiya et al., 2015). As a saprotroph, *A. terreus* is widely found on decaying organic matter as it has important roles in carbon and nitrogen cycles (Haines, 1995; Pitt, 1994). The surface colour is cinnamon brown and the reverse area is tan or yellow (Latge, 1999). The microscopic observation of hyphae shows them in terms of hypha to be hyaline.

Filamentous Fungi from Animal Agricultural Farm Soil

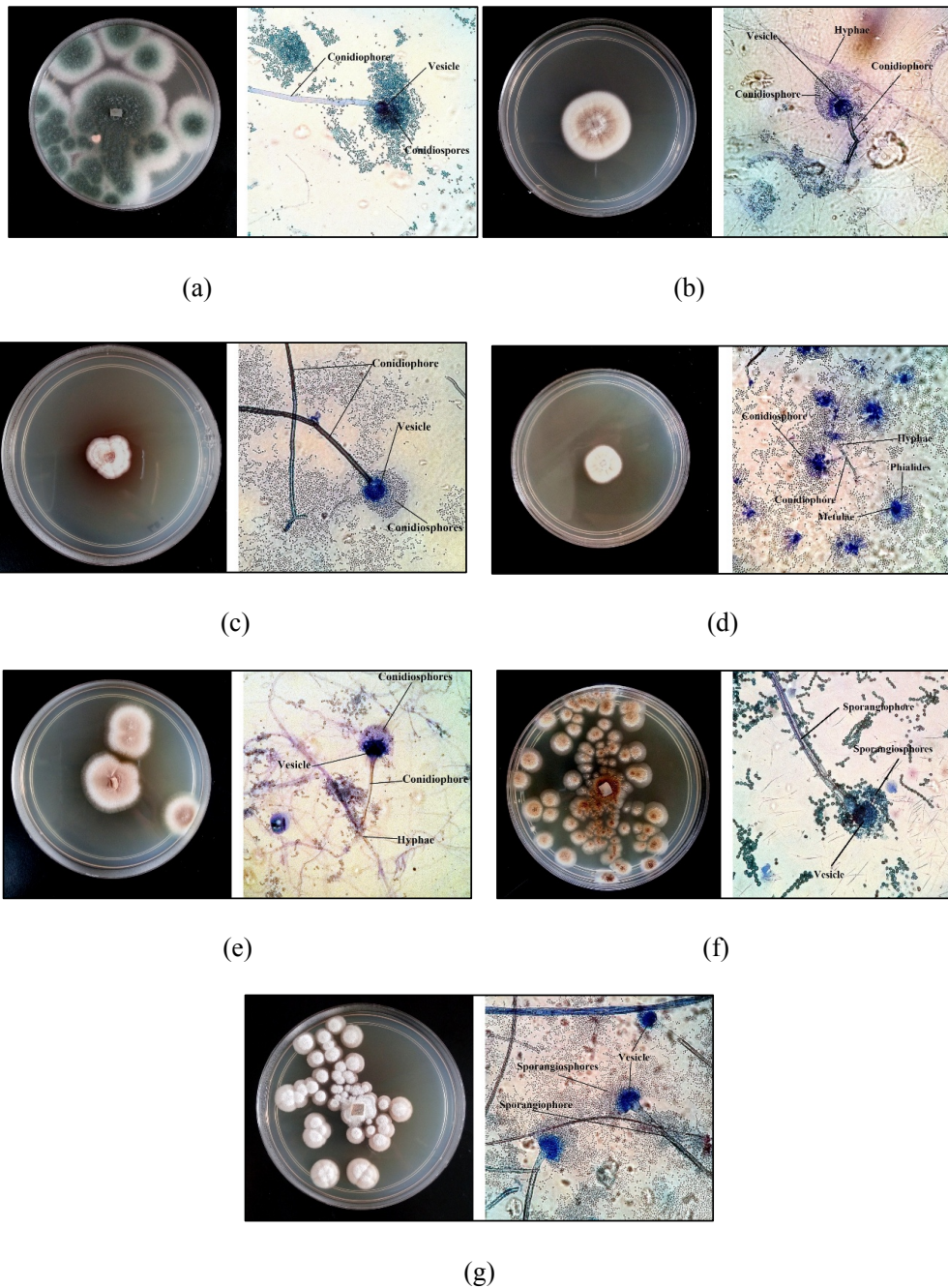


Figure 1. The macroscopic and microscopic observations of fungal isolates on the third day of incubation under 400× magnification using light microscope: (a) *A. fumigatus*; (b) *A. terreus* strain PTN 45; (c) *Aspergillus flavipes* strain ATCC1030; (d) *Eupenicillium* sp.; (e) *A. terreus* strain CO1; (f) *Aspergillus nomius* strain Tur4; and (g) *Aspergillus niveus* strain IHEM 5804

Figure 1 shows the macroscopic and microscopic views of fungal isolates. *Aspergillus fumigatus* has green coloured surface with the formation of white ring around it. The texture was flat and it did not change colour of the media even after 14<sup>th</sup> day of incubation. The vesicle and conidiospores have round shape, and no hyphae were observed. For *A. terreus* strain PTN 45, the colony colour was slightly green with the formation of white ring border. The texture was flat and the formation of segments was observed on the colony. *A. terreus* strain PTN 45 does not change the colour of the media after 14<sup>th</sup> day of incubation. For the microscopic observation, the vesicle and conidiospores are round. There were long septate hyphae observed connected to conidiophores.

The colony of *A. flavipes* strain ATCC1030 appeared white colour with a flat surface. There was also formation of segments observed on the colony. The colony changed the colour of media to brick red. From the microscopic observation, the vesicle and conidiophores were round and there was no hyphae observed connected to conidiophores.

*Eupenicillium* sp. was different from the other isolates. The colony of *Eupenicillium* sp. was observed to be white to yellow with a flat surface. No observable change in the colour of the media observed after 14<sup>th</sup> day of incubation. *Eupenicillium* sp. has round conidiospores. The aseptate hyphae is connected to conidiophores and attached to the metulae. The spread-like structure called phialides is also present. *Eupenicillium* sp. an anamorph of *Penicillium* sp. usually sporulates on the head of *Aspergillus* species (Horn & Peterson, 2008). Both *Penicillium* sp. and *Aspergillus* sp. are found abundantly in plant decaying matter, such as in the peat soil. The growth rate of *Eupenicillium* sp. was low even when cultured onto Czapek agar and it took 14 days for this fungal isolate to grow to approximately 3 cm in diameter (Stolk & Scott, 1967).

*A. terreus* strain CO1, *A. nomius* strain Tur4, and *A. niveus* strain IHEM 5804 had brown, green and white colour surfaces, respectively. The microscopic observations for these species were also found to be alike. The conidiospores and vesicle are round with flat surfaces, and septate hyphae with long conidiophores were also present. There were no colour changes in the media for all the three species observed after 14 days of incubation.

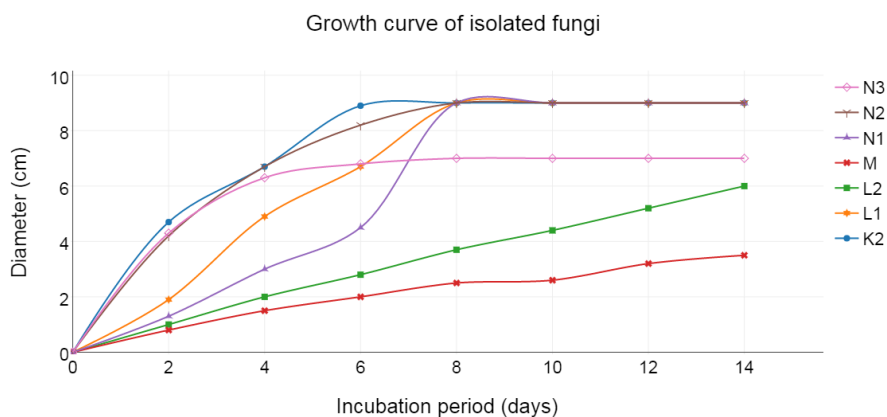


Figure 2. Growth rate of the fungal isolates from day zero to day 14. Strain K2 (*A. fumigatus*); strain L1 (*A. terreus* strain PTN 45); strain L2 (*A. flavipes* strain ATCC1030); strain M (*Eupenicillium* sp.); strain N1 (*A. terreus* strain CO1); strain N2 (*A. nomius* strain Tur4); strain N3 (*A. niveus* strain IHEM 5804)



In this study, the growth rate of each fungal isolate was measured. A colony of each fungal isolate was selected before they were measured. Figure 2 shows the growth curve of all the fungal isolates. The results show that most fungal isolates have exponential rate from day 2 to day 8. The lag phase started from day 0 to day 2 when the fungal isolates were initially introduced to the medium (PDA). At this phase, the fungal isolates took some time to adjust to their new environment and the cellular metabolism started to accelerate.

From day 2 to day 8, the growth rate increased exponentially for all the fungal isolates, except for *A. flavipes* and *Eupenicillium* sp. Both the fungal isolates' growth rates increase proportionally to the graph. During the exponential phase, the fungal isolates grew rapidly as the medium was rich in nutrients. From day 8 to day 14, the growth rates reached stationary phase where the growth started to slow down as the nutrients gradually depleted. On the other hand, the amount of toxic metabolites, waste materials and other compounds caused pH value to change. These would impair the growth of fungal isolates and result in slow growth and death.

### **Molecular Identification of the Isolated Fungi**

Filamentous fungi have high rigidity of cell wall compared to bacteria. It consists of four main components such as  $\alpha$ -glucan,  $\beta$ -glucan, chitin, and monoproprotein (Gooday, 1995). The rigidity of fungal cell wall increased due to the formation of covalent cross-link between  $\beta$ -glucan and chitin chains (Ruiz-Herrera et al., 1994). Genomic DNA extraction was conducted using the conventional method. It is the best method for Genomic DNA extraction because it is fast, easy and cost saving. By using the boiling method principle, PCR thermo cycler was used as it provides specific temperature ranges which are suitable for disruption of fungal cell wall. It also provides a longer period of incubation so that the cell wall could be completely disrupted. Genomic DNA from all the isolated fungi was successfully harvested using this method. However, this method does not enable the harvest of high quality of fungal genomic DNA due to the absence of purification steps. The high amount of genomic DNA harvested using this method was sufficient to precede for polymerase chain reaction (PCR).

Internal transcribe spacer (ITS) regions were used in molecular identification of fungi because they were closely found between other species, closely related species or even among other populations of the same species (Korabecna, Liška, & Fajfrlik, 2003). Since these regions are known for heterogeneity, *ITS1* and *ITS4* primers were used as the universal primers to identify filamentous fungi isolated. The sequence variation of ITS regions were able to distinguish between *Aspergillus* sp. from other species and a small variation between *Aspergillus* and *Penicillium* within ITS 2 region was found (Gaskell et al., 1997). Thus, ITS 1 region is sufficient for the identification of fungal isolates (Gaskell et al., 1997). In this study, *ITS1* and *ITS4* primers cover both ITS 1 and ITS 2 regions, along with 18srRNA and 5.8srRNA with amplicons size ranging from 500bp to 700bp. A BLAST search was carried out on all Genbank sequences and the sequence similarities of all the samples were 99% with a query cover of 98% for both *Aspergillus* sp. and 97% for *Eupenicillium* sp.. All the samples were identified by using the highest bit score in BLAST search.

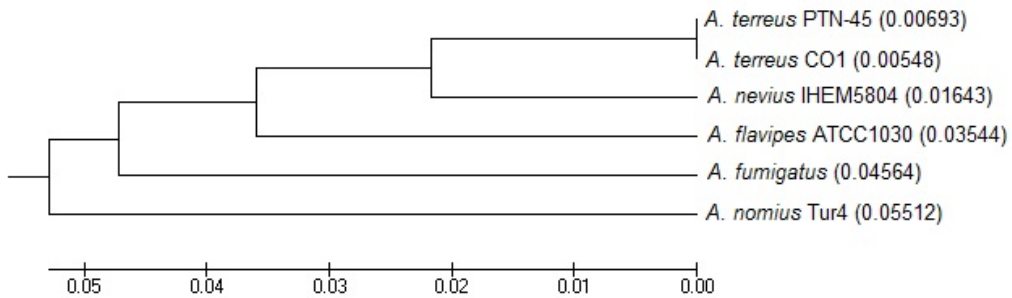


Figure 3. Neighbour-joining tree of all *Aspergillus* sp. isolated from animal agricultural farm contaminated soil which was produced using MEGA 4.1 software

Using DNA sequencing information, a phylogenetic tree was constructed from the isolated fungi, except for *Eupenicillium* sp. According to the phylogram above, a line bar represents the evolutionary lineage change over time. The longer the branch is in the horizontal dimension, the larger the amount of genetic variability. In this case, the line segment shows a genetic variability from 0.00 to 0.05. A clade was formed from *A. terreus* PTN-45, *A. terreus* CO1, *A. nevius* IHEM5804, *A. flavipes* ATCC1030 and *A. fumigatus*, indicating that they share a common ancestor. A clade or branch is defined as a group of an ancestor and all descendants. From the major clade, nested clades were formed as it is nested within one another. For example in this case, a clade of *A. terreus* PTN-45 and *A. terreus* CO1 was nested within *A. terreus* PTN-45, *A. terreus* CO1 and *A. nevius* IHEM5804 clade. Furthermore, *A. terreus* PTN-45 and *A. terreus* CO1 share a common ancestor, and thus are known as the sister group. This shows that these species have a lot of common evolutionary history but very little unique evolutionary history to either one or two sister species. Apart from that, *A. nomius* Tur4 was observed as an out group of all others *Aspergillus* sp. isolates. This is because all the members are more closely related to each other than *A. nomius* Tur4.

## CONCLUSION

A total of seven filamentous fungi were successfully isolated and identified based on the morphological observation and sequence alignment of the gene using the NCBI BLAST system. Those species were *Aspergillus fumigatus*, *A. terreus* strain PTN 45, *A. flavipes* strain ATCC1030, *Eupenicillium* sp., *A. terreus* strain CO1, *A. nomius* strain Tur4 and *A. niveus* strain IHEM 5804. From this study, it was found that peat soil from animal agricultural farm has a large quantity of *Aspergillus* sp. compared to other types of fungi. Thus, this work supports previous studies on soil micro flora which states that *Aspergillus* sp. is one of the most abundant filamentous fungi in peat soil.

## ACKNOWLEDGEMENTS

Authors would like to thank the Ministry of Higher Education, Malaysia, for funding this research under the Fundamental Research Scheme (FRGS) FRGS/2/2014/STWN10/UITM/02/1, Faculty of Applied Sciences, Universiti Teknologi MARA, Shah Alam, Selangor, Malaysia, and Atta-Ur-Rahman Institute for Natural Product Research, UiTM, Malaysia.

## REFERENCES

- Bebell, L. M., & Muiro, A. N. (2014). Antibiotic Use and emerging resistance: How can resource-limited countries turn the tide? *Global Heart*, 9(3), 347-358.
- Drenovsky, R. E., Vo, D., Graham, K. J., & Scow, K. M. (2004). Soil water content and organic carbon availability are major determinants of soil microbial community composition. *Microbial Ecology*, 48(3), 424-430. doi: 10.1007/s00248-003-1063-2
- Gaskell, G. J., Carter, D. A., Britton, W. J., Tovey, E. R., Benyon, F. H., & Løvborg, U. (1997). Analysis of the internal transcribed spacer regions of ribosomal DNA in common airborne allergenic fungi. *Electrophoresis*, 18(9), 1567-1569.
- Gavalchin, J., & Katz, S. E. (1994). The persistence of fecal-borne antibiotics in soil. *Journal of AOAC International*, 77(2), 481-485.
- Gersema, L. M., & Helling, D. K. (1986). The use of subtherapeutic antibiotics in animal feed and its implications on human health. *Drug Intell Clin Pharm*, 20(3), 214-218.
- Gooday, G. W. (1995). Cell Walls. In N. A. R. Gow & G. M. Gadd (Eds.), *The Growing Fungus* (pp. 43-62). Dordrecht: Springer Netherlands.
- Haines, J. (1995). *Aspergillus* in compost: straw man or fatal flaw? *Biocycle*, 36(4), 32-35.
- Horn, B. W., & Peterson, S. W. (2008). Host specificity of *Eupenicillium ochrosalmoneum*, *E. cinnamopurpureum* and two *Penicillium* species associated with the conidial heads of *Aspergillus*. *Mycologia*, 100(1), 12-19.
- Ruiz-Herrera, J., Mormeneo, S., Vanaclocha, P., Font-De-Mora, J. A. I. M. E., Iranzo, M., Puertes, I., & Sentandreu, R. (1994). Structural organization of the components of the cell wall from *Candida albicans*. *Microbiology*, 140(7), 1513-1523.
- Korabecna, M., Liška, V., & Fajfrlik, K. (2003). Primers ITS1, ITS2 and ITS4 detect the intraspecies variability in the internal transcribed spacers and 5.8 S rRNA gene region in clinical isolates of fungi. *Folia Microbiologica*, 48(2), 233-238.
- Krijgsheld, P., Bleichrodt, R., Van Veluw, G., Wang, F., Müller, W., Dijksterhuis, J., & Wösten, H. (2013). Development in *Aspergillus*. *Studies in Mycology*, 74, 1-29.
- Kumar, K., C. Gupta, S., Chander, Y., & Singh, A. K. (2005). Antibiotic use in agriculture and its impact on the terrestrial environment. *Advances in Agronomy*, 87, 1-54.
- Latge, J.-P. (1999). *Aspergillus fumigatus* and aspergillosis. *Clinical Microbiology Reviews*, 12(2), 310-350.
- Lees, P., & Aliabadi, F. S. (2002). Rational dosing of antimicrobial drugs: animals versus humans. *International Journal of Antimicrobial Agents*, 19(4), 269-284.

- Manshor, N., Rosli, H., Ismail, N. A., Salleh, B., & Zakaria, L. (2012). Diversity of *Fusarium* species from highland areas in Malaysia. *Tropical Life Sciences Research*, 23(2), 1.
- Moore, S., Evans, C. D., Page, S. E., Garnett, M. H., Jones, T. G., Freeman, C., & Gauci, V. (2013). Deep instability of deforested tropical peatlands revealed by fluvial organic carbon fluxes. *Nature*, 493(7434), 660-663.
- Nordenberg, T. (1998). Miracle drugs vs. superbugs. Preserving the usefulness of antibiotics. *FDA Consumer*, 32(6), 22.
- Page, S. E., Wüst, R. A. J., Weiss, D., Rieley, J. O., Shotyk, W., & Limin, S. H. (2004). A record of Late Pleistocene and Holocene carbon accumulation and climate change from an equatorial peat bog (Kalimantan, Indonesia): implications for past, present and future carbon dynamics. *Journal of Quaternary Science*, 19(7), 625-635. doi: 10.1002/jqs.884
- Pitt, J. (1994). The current role of *Aspergillus* and *Penicillium* in human and animal health. *Medical Mycology*, 32(S1), 17-32.
- Rudiyanto, M. B., & Setiawan, B. I. (2016). Further results on comparison of methods for quantifying soil carbon in tropical peats. *Geoderma*, 269, 108-111.
- Sarmah, A. K., Meyer, M. T., & Boxall, A. B. (2006). A global perspective on the use, sales, exposure pathways, occurrence, fate and effects of veterinary antibiotics (VAs) in the environment. *Chemosphere*, 65(5), 725-759.
- Song, F., Tian, X., Fan, X., & He, X. (2010). Decomposing ability of filamentous fungi on litter is involved in a subtropical mixed forest. *Mycologia*, 102(1), 20-26.
- Stolk, A. C., & Scott, D. B. (1967). Studies on the genus *Eupenicillium* Ludwig I. Taxonomy and nomenclature of *Penicillia* in relation to their sclerotoid ascocarpic states. *Persoonia-Molecular Phylogeny and Evolution of Fungi*, 4(4), 391-405.
- Shukri, S. M., Fauzi, S. M., Zainon, M. N., & Zaidah, Z. A. (2015). Morphotypic and molecular identification of filamentous fungi from animal agricultural farm contaminated peat soil. *Advances in Environmental Biology*, 9(22 S3), 1-6.
- Tamiya, H., Ochiai, E., Kikuchi, K., Yahiro, M., Toyotome, T., Watanabe, A., & Kamei, K. (2015). Secondary metabolite profiles and antifungal drug susceptibility of *Aspergillus fumigatus* and closely related species, *Aspergillus lentulus*, *Aspergillus udagawae*, and *Aspergillus viridinutans*. *Journal of Infection and Chemotherapy*, 21(5), 385-391.
- Tollefson, L., & Karp, B. E. (2004). Human health impact from antimicrobial use in food animals. *Médecine et Maladies Infectieuses*, 34(11), 514-521.

## Electrodeposition of Copper Coating on 304 Stainless Steel Substrate: Physicochemical Properties and Antibacterial Activity

Nik Norziehana Che Isa, Yusairie Mohd\*, Mohammad Hafizuddin Mohd Zaki and Sharifah Aminah Syed Mohamad

Faculty of Applied Sciences, Universiti Teknologi MARA UiTM), 40450 Shah Alam, Selangor, Malaysia

### ABSTRACT

Non antimicrobial touch surface materials such as stainless steel can act as a medium for transmitting microbes, leading to the increase of hospital-acquired infections and antibiotic-resistant microbes. Copper can be used to replace the current non-antimicrobial touch surfaces, however, the high cost of solid copper hampers copper from being the ideal choice. Therefore, stainless steel touch surfaces coated with copper can become the option for a low cost yet effective alternative. In this study, electrodeposition technique was used to coat copper on 304 stainless steel surface using 0.01 M CuSO<sub>4</sub> solution, at pH 1. The electrodeposition process was done using chronoamperometry by applying -0.25 V vs. Ag/AgCl for 15 min. Morphological observation revealed that 304 stainless steel surface was uniformly coated with compact and dense copper. EDAX analysis showed the composition of copper of 98.9 wt. %, ranging in diameter from 60-90 nm grain size. Thickness of the coating was approximately 105.8 nm. The antibacterial property of copper coating was analysed by both Gram negative *E. coli* and Gram positive *S. aureus*. Results indicated that copper coating has excellent antibacterial behaviour in destroying both bacteria. *E. coli* was more sensitive to the biocidal action of the copper coating of which 100 % reduction was observed within 5 min of exposure. As for *S. aureus*, a 100% reduction was achieved only after 10 min of exposure.

**Keywords:** Antibacterial behaviour, biofilm, copper, copper coating, electrodeposition

### ARTICLE INFO

*Article history:*

Received: 25 October 2016

Accepted: 17 March 2017

*E-mail addresses:*

niknorziehanacheisa@yahoo.com (Nik Norziehana Che Isa),

yusairie@salam.uitm.edu.my (Yusairie Mohd),

hafizuddin@yahoo.com (Mohammad Hafizuddin Mohd Zaki),

sharifah459@salam.uitm.edu.my (Sharifah Aminah Syed Mohamad)

\*Corresponding Author

### INTRODUCTION

Touch surface materials made from stainless steel are commonly found in hospitals, healthcare settings and public areas, and potentially contaminated with microbes that cause hospital-acquired infections (HAIs) (Vessey, 2013). Microbes can survive on solid surface (i.e., stainless steel), which is not an

antimicrobial active material and formed biofilm. The microbes can persist for extended periods of time, acting as microbes' reservoir, multiplying their pathways of transmission (Dancer, 2004; Page, Wilson, & Parkin, 2009). Bacteria in biofilms are drastically more resistance to antibiotics and external forces that withstand host immune response (Beech et al., 2002). One of the solutions to curb the problem is by preventing bacterial adherence onto the solid surface and inevitable stop the formation of biofilms. The use of copper in surface engineering represents an attractive solution due to the broad-spectrum biocide activity of copper towards microbes. Copper can inhibit growth of microbial biofilms by interacting with the thiol groups of bacteria proteins and enzymes (Gant et al., 2007; Sierra et al., 2013; Warnes et al., 2010).

From the literature, copper and its alloy surfaces have been thoroughly investigated for their antimicrobial activity both in laboratory and in clinical environment (Airey & Verran, 2007; Casey et al., 2010; Cassandra et al., 2013; Champagne & Helfritch, 2013; Michels, Noyce, & Keevil, 2009; Michels et al., 2005; Noyce, Michels, & Keevil, 2006; Ojeil et al., 2013; Schmidt, Attaway, & Fairey, 2013). Research shows that microbes' survival on many copper surfaces is limited to just a few hours or even minutes compared to stainless steel (Airey & Verran, 2007; Ojeil et al., 2013). The findings indicated that copper surface is a promising material to replace the contemporary use of stainless steel surfaces in the hospital and healthcare environment, since bacterial placed in contact with the dry copper surface suffered the great impact (Espirito et al., 2011). However, the use of pure solid copper is expensive (Elguindi et al., 2011; Nejad et al., 2013), and to replace the currently stainless steel touch surfaces with solid copper is very costly. Hence, one way to address the issue of material cost is by modifying the stainless steel surface with copper via coating process.

There are various techniques available for the copper-based coating process on the substrates such as vapour deposition, ion implantation, sputtering, sol-gel and electrodeposition (Alam et al., 2015; Daniel et al., 2009; Dorogov et al., 2015; Jakupi et al., 2015; Triantou et al., 2015; Zhang, An, & Chang, 2009). Recently, numerous research was found focusing on the development of processing methods for the fabrication of copper-based coating in achieving the desired structural and functional coating properties for limiting bacterial adhesion and biofilm formation (Cloutier, Mantovani, & Rosei, 2015; Palza, Delgado, & Curotto, 2015; Sharifahmadian et al., 2013; Wan et al., 2007). Despite a lot of studies revealed the available techniques to prepare good copper-based coating, only a few have discussed about the copper-based coating prepared by the electrodeposition technique for antimicrobial purpose.

Electrodeposition is a less expensive and straight-forward method with an ability to control the coating properties by effectively adjusting the experiment parameters such as applied potential or current, deposition time, source of metal ions and concentration, pH of the electrolyte solution, temperature, as well as nature of the substrate. This present work is aimed at evaluating and comparing the antimicrobial efficacy of the copper coating prepared by electrodeposition technique with stainless steel (SS304) towards *E. coli* (gram negative) and *S. aureus* (gram positive) bacteria.

## METHOD

### Substrate Preparation for Coating

The substrate used in this study is 304 stainless steel coupons (20 mm x 20 mm x 1 mm). Prior to electrodeposition process, the substrate was polished with SiC paper from P800 to P4000 grit, followed by ultrasonically cleaned in acetone, subsequently rinsed with ultrapure water and dried at room temperature. An adhesive tape was used to mask off of the substrate except for 20 mm<sup>2</sup> area on which deposition was desired.

### Electrodeposition of Copper on Stainless Steel Substrate

The electrodeposition process was performed via chronoamperometry method on the polished 304 stainless steel as a working electrode, platinum rod as a counter electrode and Ag/AgCl as a reference electrode. All the three electrodes were immersed into 0.01 M Cu<sup>2+</sup> ions (pH 1) solution. The electrodeposition process was controlled using an Autolab Potentiostat (Aut302 FRA2), and interfaced with a PC running NOVA software. The copper coating on the 304 stainless steel substrate was deposited by applying a constant potential at -0.25 V vs Ag/AgCl for 15 min.

**Characterisation of Copper Coating.** The surface morphology images of the uncoated and coated 304 stainless steel were examined using a Field Emission Scanning Electron Microscope (FESEM, Carl Zeiss SMT Supra 40VP) at various magnifications. An electron accelerating voltage of 5 kV was used to observe the morphology of the prepared samples. The elemental composition and mapping of the coated 304 stainless steel were determined by Energy Dispersive X-ray (EDAX). The control software (the Oxford INCA X-max 51-XXM 0021), equipped with FESEM, was used for EDAX analysis. Si(Li), cooled to cryogenic temperature with liquid nitrogen, was used as detector to convert X-ray energy into voltage signals. Thickness of the prepared coating was measured on at least three random areas by Surface profiler (P-6).

**Antibacterial Test.** The antibacterial activity of the prepared samples was tested using intimate contact cell suspension test but modified according to the standard method, JIZ S 2801/ ISO 22196. Two bacterial species, Gram negative (*E. coli*) and Gram positive (*S. aureus*) were selected as the test bacteria. The tested bacteria were cultured in nutrient agar overnight at 37°C, and then diluted in 10 mL of saline (0.9 % of NaCl) to become an optical density OD<sub>600</sub> nm of 0.05, which is equivalent to 10<sup>7</sup> cells/mL. Subsequently, bacterial suspension of approximately 10<sup>5</sup> cells/mL was prepared.

Copper coated stainless steel was sterilised by immersing in 95% ethanol for a few seconds, and dried at room temperature before placing it on sterile 90 mm diameter Petri dishes. The uncoated stainless steel substrate was also tested and used as a negative control. An amount of 20 µL of the diluted bacterial suspension was added onto each substrate and covered with a sterile glass cover slip in order to maintain the same contact area of suspension on each tested substrate surface during the designated contact time, to monitor the reduction rate. All

the plates were incubated at room temperature at the designated contact time (i.e., 0, 5, 10, 15, 20, 25, 30 min).

After incubation, the substrate was transferred to 10 mL of sterile phosphate-buffered saline (PBS) for 10 s to dislodge the cover slip and suspend the surviving bacteria in the PBS solution. 100 µL aliquots of the bacterial suspension was evenly spread onto nutrient agar using a sterile glass spreader and incubated overnight at 37°C. The number of colony forming units (CFUs), resulting from the growth of the viable bacteria at 37°C kept overnight, was calculated using colony counter, while reduction of exposure time of bacteria was measured. The percentage of reduction was calculated according to the following formula [1]:

$$\text{reduction, \%} \left( \frac{\text{CFU}}{\text{mL}} \right) = \frac{N_0 - N_t}{N_0} \times 100 \% \quad [1]$$

Where,  $N_0$  is the mean CFU/mL for the same substrate at 0 hour, and  $N_t$  is the mean CFU/mL from a test substrate after a designated contact time. Metal samples were removed immediately after inoculation at zero time to determine the initial number of viable bacteria.

## RESULTS AND DISCUSSION

The authors have successfully deposit the copper element onto the 304 stainless steel surface area under the laboratory set condition of,  $V = -0.25 \text{ V vs Ag/AgCl}$  and  $t = 15 \text{ min}$ , in  $0.01 \text{ M Cu}^{2+}$  ions (pH 1) solution. Figure 1 shows chronoamperometric curve of the deposition of copper onto the 304 stainless steel surface, coating the 304 stainless steel surface (inset image). From the curve, the current density shows an abrupt decrease for a short time (i.e., 5 s) at the beginning of the process. This behaviour indicates that the double layer charging of non-faradaic current has occurred. Right after, a plateau current density was observed until the end of the process indicates the nucleation growth of the copper, coating onto the stainless steel surface. The inset picture in Figure 1 exhibits the entire 304 stainless steel substrate surface that was soaked in the  $20 \text{ mm}^2$  solution during electrodeposition process, was coated with smooth and uniform red-brown colour copper.

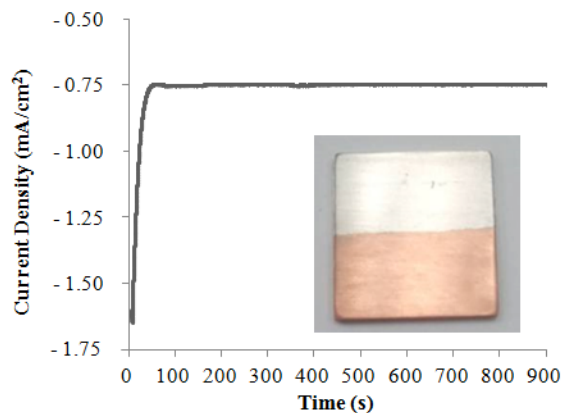


Figure 1. Chronoamperometric curve of copper coating formed on 304 stainless steel substrate at  $-0.25 \text{ V}$  for 15 min. (Inset: visual observation of the coating produced on the exposed 304 stainless steel surface)



Figure 2 shows the surface morphologies of the polished 304 stainless steel (Figure 2(a)) and copper coating produced on the 304 stainless steel surface at different magnifications (Figure 2(b) and Figure 2(c)). Polishing the stainless steel surface produced a flat surface structure with relatively minor grooves in the polishing direction. After the deposition process, the 304 stainless steel surface was coated with uniform, compact and dense copper on the entire exposed surface. At a higher magnification (Figure 2(c)), the coating with compact and homogeneous grain structure was obviously seen, ranging in 60-90 nm diameter.

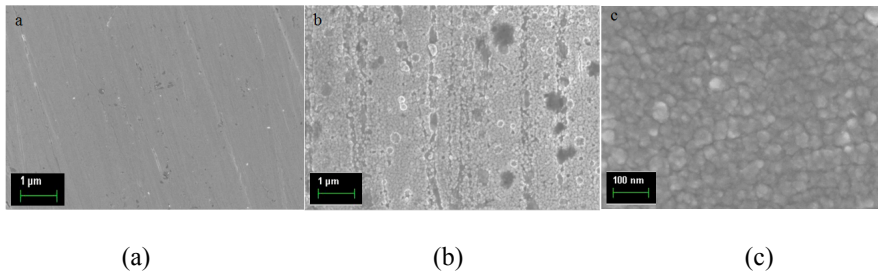


Figure 2. SEM images of: (a) 304 stainless steel; (b) copper coating prepared on 304 stainless steel substrate from 0.01 M CuSO<sub>4</sub> solution (pH 1) at -0.25 V for 15 min at magnification: (b) 5000 $\times$ ; and (c) 50000 $\times$

The EDAX analysis on the FESEM image of the copper coating (Figure 3) shows the composition of copper and oxygen is 98.9 wt.% and 1.10 wt.%, respectively. This indicates that the high percentage of copper deposited on the stainless steel surface comprises only of a minor distribution of oxide content. From the mapping images (Figure 4), it can be seen that a uniform distribution of the nano-grains copper (Figure 4(a)) on the entire exposed 304 stainless steel surface comprises only of a minor distribution of oxygen content (Figure 4(b)).

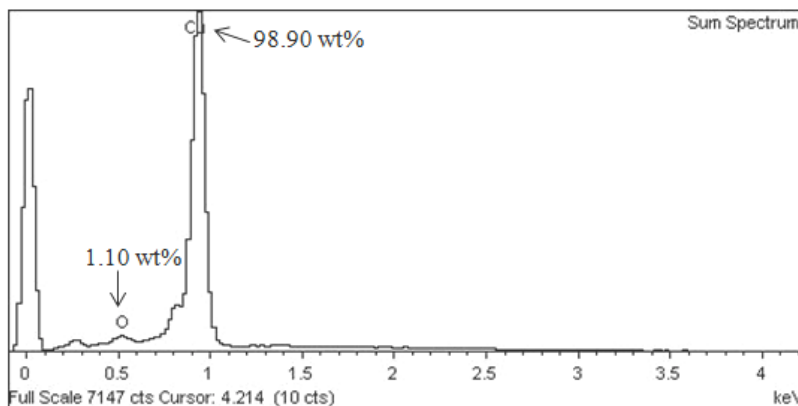


Figure 3. The elemental composition of copper coating prepared on 304 stainless steel substrate analysed by EDAX

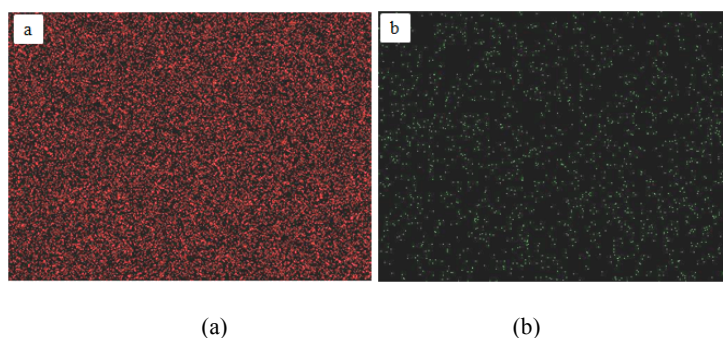


Figure 4. The EDAX elemental mapping of: (a) copper; and (b) oxygen present on the coating prepared on 304 stainless steel substrate from 0.01 M  $\text{CuSO}_4$  solution (pH 1) at  $-0.25$  V for 15 min

Proper adhesion of coating on a substrate is one of the very important factor for determining the mechanical behaviour and performance of the coated components (Okamoto, Wang, & Watanabe, 2004). Metallic films electrodeposited on the metal substrates are commonly thought to have a favourable adhesive strength since the electrodeposited films are usually bonded with substrates metallicity, without any interruption from hydrogen evolution reaction during the electrodeposition process. The adhesion quality of the copper coating on the stainless steel was observed at the cross section image by FESEM. The cross section image (Figure 5) exhibits well intact between coating and substrate. There are no voids or gaps in between the coating and substrate. In addition, nano-sized grain structures have filled-up the vacancies, of which the same condition is not possible via conventional micro-structure coating. The thickness of the coating was about 105.8 nm.

Figure 6 indicates the reduction rate of viable bacteria within the designated contact time under ambient room temperature. *E. coli* was more sensitive to the inhibitory action of the copper coating (100% reduction within 5 min of exposure), whereas 100% reduction of *S. aureus* was achieved only after 10 min of exposure. On the other hand, no obvious reduction of viable bacteria on the 304 stainless steel surface was observed even after 30 min of exposure. These findings strongly showed that copper coating has an excellent antimicrobial property than stainless steel in which there is no sign of antibacterial activity against both the tested bacteria. It is suggested that copper accumulation within the cell, cell death and DNA damage assays that copper has lethal effects towards bacteria, as stated by Ibrahim et al. (2011). Thus, stainless steel surface exerted no lethal effect.

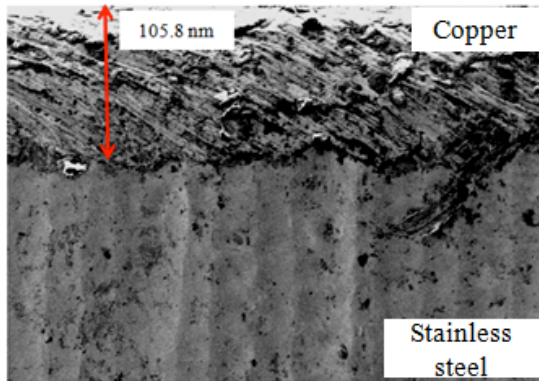


Figure 5. A cross-section image of copper deposited on 304 stainless steel substrate from 0.01 M  $\text{CuSO}_4$  solution (pH 1) at  $-0.25$  V for 15 min at  $25^\circ\text{C}$

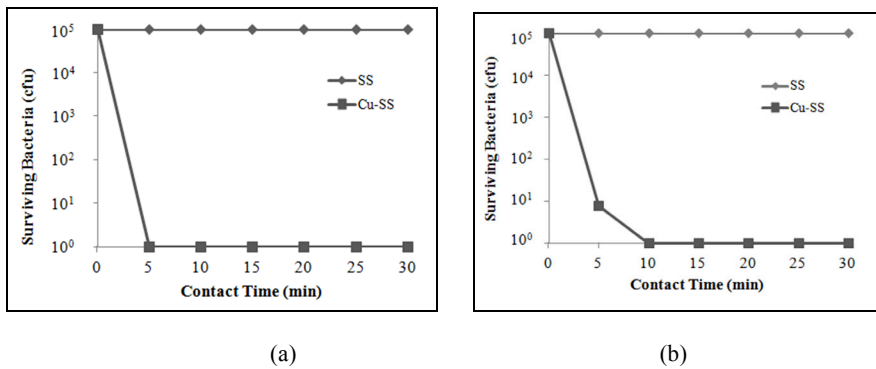


Figure 6. Viable bacterial reduction rate with contact time duration of: (a) *E. coli*; and (b) *S. aureus* (note: SS = Stainless steel; Cu-SS = Copper coated stainless steel)

Figure 7 and Figure 8 show the colony forming unit (CFU) on nutrient agar from different contact time of viable *E. coli* and *S. aureus*, respectively. On the stainless steel surface, there is no significant reduction of CFUs after 30 min of exposure. However, all the bacteria were destroyed on the copper coating surface after 5 min of exposure for *E. coli* (Figure 7). For *S. aureus* (Figure 8), fewer CFUs (which indicate more bacteria were destroyed) can be seen on the copper coating after 5 min of exposure, but after 10 min of exposure, no CFUs indicate that all the bacteria were completely perished.

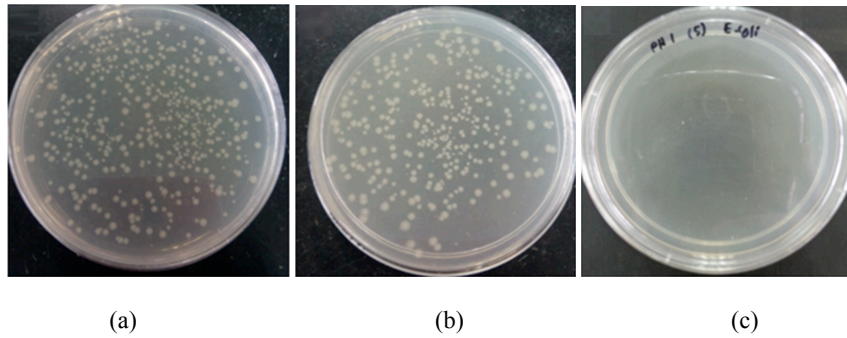


Figure 7. Colony forming unit of viable *E. coli* after being in contact with: (a) stainless steel for 0 min; (b) stainless steel for 30 min; and (c) copper coating for 5 min

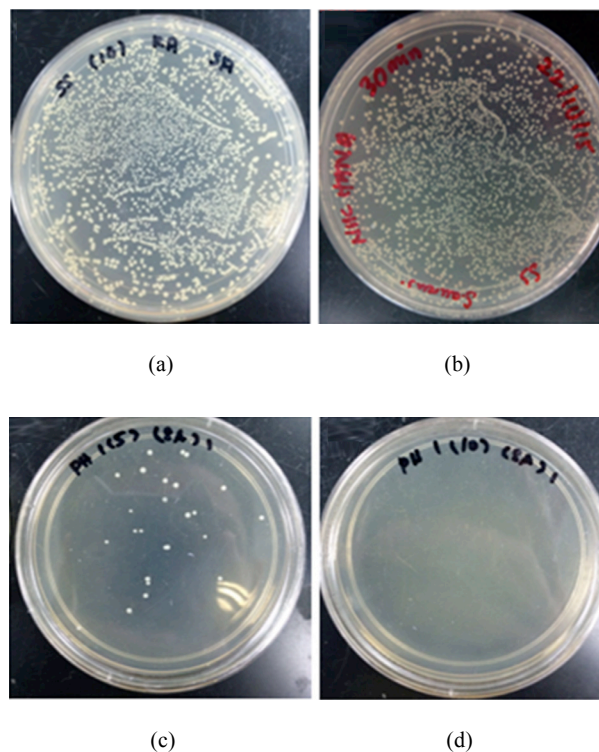


Figure 8. Colony forming unit of viable *S. aureus* after being in contact with: (a) stainless steel for 0 min; (b) stainless steel for 30 min; (c) copper coating for 5 min; and (d) copper coating for 10 min

## CONCLUSION

Copper coating was successfully deposited on the 304 stainless steel substrate through the electrodeposition technique for antibacterial applications. The copper coating showed good surface coverage with uniform distribution of copper nano-grains on the 304 stainless steel surface. In addition, the copper coating showed a very good and intact adhesion property on the 304 stainless steel based on the observation of cross section image by FESEM. Viable bacteria

on the copper coating were killed in a short period of time compared to on 304 stainless steel. *E. coli* was found to be more sensitive to the biocidal action of the copper coating (100% reduction within 5 min of exposure), whereas 10 min of exposure was required for 100% reduction of *S. aureus*. Thus, composition and grain size of copper coating play an important role in conferring the antibacterial properties, while adhesion property is an important point to ensure the durability of the coating.

## ACKNOWLEDGEMENTS

The authors wish to thank the Ministry of Higher Education (Malaysia) for the financial support through Fundamental Research Grant Scheme (FRGS) 600-RMI/FRGS 5/3 (139/2015) and Faculty of Applied Sciences, Universiti Teknologi MARA (UiTM), Shah Alam, Selangor for the facilities provided.

## REFERENCES

- Airey, P., & Verran, J. (2007). Potential use of copper as a hygienic surface; problems associated with cumulative soiling and cleaning. *Journal of Hospital Infection*, *67*, 271-277.
- Alam, M. M., Mia, M. N. H., Hasan, R., Shahinuzzaman, M., Islam, M. K., & Uddin, K. M. N. (2015). Study of structural and morphological properties of vacuum coated copper (Cu) metal thin film. *Materials Sciences and Applications*, *6*, 753-759.
- Beech, I. B., Smith, J. R., Steele, A. A., Penegar, I., & Campbell, S. A. (2002). The use of atomic microscopy for studying interactions of bacterial biofilms with surfaces. *Colloids and Surfaces B: Biointerfaces*, *23*, 231-247.
- Casey, A. L., Adams, D., Karpanen, T. J., Lambert, P. A., Cookson, B. D., Nightingale, P., Miruszenko, L., Shillam, R., & Christian, P. (2010). Role of copper in reducing hospital environment contamination. *Journal of Hospital Infection*, *74*, 72-77.
- Cassandra, D. S., Kent, A. S., Joseph, F. J., Cantey, J. R., Hubert, H. A., Katherine, D. F., Peter, A. S., Harold, T. M., & Michael, G. S. (2013). Copper surfaces reduce the rate of healthcare-acquired infections in the Intensive Care Unit. *Infection and Hospital Epidemiology*, *34*(5), 479-486.
- Champagne, V. K., & Helfritsch, D. J. (2013). A demonstration of the antimicrobial effectiveness of various copper surfaces. *Journal of Biological Engineering*, *7*, 8.
- Cloutier, M., Mantovani, D., & Rosei, F. (2015). Review: Antibacterial coatings: Challenges, perspective and opportunities. *Journal in Biotechnology*, *1295*, 1-16.
- Dancer, S. J. (2004). How do we assess hospital cleaning? A proposal for microbiological standards for surface hygiene in hospitals. *Journal of Hospital Infection*, *56*, 10-15.
- Daniel, A., Pen, C. L., Archambeau, C., & Reniers, F. (2009). Use of a PECVD-PVD process for the deposition of copper containing organosilicon thin films on steel. *Applied Surface Science*, *256S*, S82-S85.
- Dorogov, M. V., Priezzheva, A. N., Vlassov, S., Kink, I., Shulga, E., Dorogin, L. M., Lohmus, R., Tyurkov, M. N., Vikarchuk, A. A., & Romano, A. E. (2015). Phase and structural transformations in annealed copper coatings in relation to oxide whisker growth. *Applied Surface Science*, *346*, 423-427.

- Elguindi, J., Hao, X., Lin, Y., Alwathnani, H. A., Wei, G., & Rensing, C. (2011). Advantages and challenges of increased antimicrobial copper use and copper mining. *Applied Microbiology and Biotechnology*, *91*, 237-249.
- Espirito, S. C., Lam, E. W., Elowsky, C. G., Quaranta, D., Domaille, D. W., Chang, C. J., & Grass, G. (2011). Bacteria killing by dry metallic copper surfaces. *Applied Environmental Microbiology*, *77*, 794-800.
- Gant, V. A., Wren, M. W. D., Rollins, M. S. M., Jeanes, A., Hickok, S. S., & Hall, T. J. (2007). Three novel highly charged copper-based biocides: safety and efficacy against healthcare-associated organisms. *Journal of Antimicrobial Chemotherapy*, *60*, 294-299.
- Ibrahim, M., Wang, F., Lou, M., Xie, G., Li, B., Bo, Z., Zhang, G., Liu, H., & Wareth, A. (2011). Copper as an antibacterial agent for human pathogenic multidrug resistant *Burkholderia cepacia* complex bacteria. *Journal of Bioscience and Bioengineering*, *112*(6), 570-576.
- Jakupi, P., Keech, P. G., Barker, I., Ramamurthy, S., Jacklin, R. L., Shoesmith, D. W., & Moser, D. E. (2015). Characterization of commercially cold sprayed copper coatings and determination of the effects of impacting copper powder velocities. *Journal of Nuclear Materials*, *466*, 1-11.
- Michels, H. T., Wilks, S. A., Noyce, J. O., & Keevil, C. W. (2005). Copper alloys for human infectious disease control. *Materials Science and Technology Conference*, 25-28 September 2005, Pittsburgh, PA Copper for the 21<sup>st</sup> Century Symposium.
- Michels, H. T., Noyce, J. O., & Keevil, C. W. (2009). Effects of temperature and humidity on the efficacy of methicillin-resistant *Staphylococcus aureus* challenged antimicrobial materials containing silver and copper. *Letters in Applied Microbiology*, *49*, 191 – 195.
- Nejad, M., Pershin, L., Mostaghimi, J., & Ringuette, M. (2013). Evaluation of bioactivity of copper alloy coatings. *21<sup>st</sup> International Symposium on Plasma Chemistry (ISPC 21)* 4-9 August 2013, Cairns Convention Centre, Queensland, Australia.
- Noyce, J. O., Michels, H., & Keevil, C. W. (2006). Use of copper cast alloys to control *Escherichia coli* 0157 cross contamination during food processing. *Applied Environmental Microbiology*, *72*(6), 4239-4244.
- Ojeil, M., Jermann, C., Holah, J., Denyer, S. P., & Maillard, J. Y. (2013). Evaluation of new in vitro efficacy test for antimicrobial surface activity reflecting UK hospital conditions. *Journal of Hospital Infection*, *85*, 274-281.
- Okamoto, N., Wang, F., & Watanabe, T. (2004). Adhesion of electrodeposited copper, nickel, and silver films on copper, nickel and silver substrates. *Materials Transactions*, *45*(12), 3330-3333.
- Page, K., Wilson, M., & Parkin, P. (2009). Antimicrobial surfaces and their potential in reducing the role of the inanimate environment in the incidence of hospital-acquired infections. *Journal of Materials Chemistry*, *19*, 3819-3819.
- Palza, H., Delgado, K., & Curotto, N. (2015). Synthesis of copper nanostructures on silica-based particles for antimicrobial organic coatings. *Applied Surface Science*, *357*, 86-90.
- Schmidt, M. G., Attaway, H. H., & Fairey, S. E. (2013). Copper continuously limits the concentration of bacteria resident on bed rails within the intensive care unit. *Infection Control Hospital Epidemiology*, *34*(5), 530-533.

- Sharifahmadian, O., Salimijazi, H. R., Fathi, M. H., Mostaghimi, J., & Pershin, L. (2013). Study of the antibacterial behavior of wire arc sprayed copper coatings. *Journal of Thermal Spray Technology*, 22, 371-379.
- Sierra, M., Sanhueza, A., Alcantara, R., & Sanchez, G. (2013). Antimicrobial evaluation of copper sulphate (II) on strains of *Enterococcus faecalis*. In vitro study. *Journal of Oral Research*, 2(3), 114-118.
- Triantou, K. I., Pantelis, D. I., Guipont, V., & Jeandin, M. (2015). Microstructure and tribological behaviour of copper and composite copper + alumina cold sprayed coatings for various alumina contents. *Wear*, 336 – 337, 96-107.
- Vessey, A. (2013). Copper – a weapon in the war on pathogens. *Health Estate Journal*, 65-69.
- Wan, Y. Z., Raman, S., He, F., & Huang, Y. (2007). Surface modification of medical metals by ion implantation of silver and copper. *Vacuum*, 81, 1114-1118.
- Warnes, S. L., Green, S. M., Michels, H. T., & Keevil, C. W. (2010). Biocidal efficacy of copper alloys against pathogenic enterococci involves degradation of genomic and plasmid DNAs. *Applied Environmental Microbiology*, 76, 5390-5401.
- Zhang, J., An, M., & Chang, L. (2009). Study of the electrochemical deposition of Sn-Ag-Cu alloy by cyclic voltammetry and chronoamperometry. *Electrochimica Acta*, 54, 2883-2889.







## Enhancement of Oxidative DNA Damage and Alteration of p53, Bax, and Bcl-2 Protein Expressions Following Low Dose Radiation Exposure

Wan Mazlina Md Saad<sup>1\*</sup>, Mohd Khairul Amran Mohammad<sup>1</sup>,  
Muhamad Idham Mohamed<sup>1</sup> and Hairil Rashmizal Abdul Razak<sup>2</sup>

<sup>1</sup>Department of Medical Laboratory Technology, Faculty of Health Sciences,  
Universiti Teknologi MARA (UiTM) Puncak Alam, 42300, Puncak Alam, Selangor, Malaysia

<sup>2</sup>Department of Medical Imaging, Faculty of Health Sciences, Universiti Teknologi MARA (UiTM)  
Puncak Alam, 42300 Puncak Alam, Selangor, Malaysia

### ABSTRACT

This animal modelling study aimed to investigate the effects of LDR exposure on cellular ROS production, oxidative DNA damage, and alteration of cellular ultrastructure and apoptosis-related protein expressions. Ten male ICR mice were randomly divided into two groups consisting of control (Cx) and radiation (Rx) groups. On day 29 of post-acclimatisation, mice underwent total body irradiation with 100  $\mu$ Gy X-ray. Liver and lung tissues were assessed for the levels of cellular ROS production and Apurinic/Apyrimidinic sites generation. Ultrastructural alteration was detected using TEM, alteration of p53, Bax, and Bcl-2 expressions was determined by western blotting. Results showed that exposure to LDR significantly increased the levels of cellular ROS and AP sites in mice. Ultrastructure of the nucleus in Rx showed nuclear blebbing and structural changes in morphology that indicate cell death. Meanwhile, p53, Bax, and Bcl-2 proteins increased in expressions and altered the balance of Bax/Bcl-2 ratio. These findings may postulate that LDR exposure may enhance oxidative DNA damage and alter expression of apoptosis-related proteins.

*Keywords:* Bax, Bcl-2, Low Dose radiation (LDR), oxidative DNA damage, p53

### ARTICLE INFO

#### Article history:

Received: 25 October 2016

Accepted: 17 March 2017

#### E-mail addresses:

wanmaz755@salam.uitm.edu.my (Wan Mazlina Md Saad),  
arm\_meltech90@yahoo.com (Mohd Khairul Amran Mohammad),  
idham\_mlt89@yahoo.com (Muhamad Idham Mohamed),  
hairil@puncakalam.uitm.edu.my (Hairil Rashmizal Abdul Razak)

\*Corresponding Author

### INTRODUCTION

Deleterious effects of high dose radiation (HDR) exposure on human health have been widely studied compared to low dose radiation (LDR) exposure (Zielinski et al., 2009; Ponzinibbio et al., 2010). Medical radiation professions, including radiologists, dentists,

nurses and radiographers are among individuals who are mainly exposed to LDR employed in diagnostic imaging modalities, including diagnostic X-ray, computed tomography (CT), and nuclear medicine scans. These individuals are the largest occupations cohort that are exposed to ionising radiation (Zielinski et al., 2009) and thus, studies on effects of LDIR and counter mechanism are warranted. Ionising radiation (IR) has some unique characteristics as a carcinogenic and mutagenic agent which cause several impacts on human health depending on exposed and absorbed dose, duration of exposure and time interval after exposure, and susceptibility of tissues to IR (Mohamed et al., 2014; Klaunig, Kamendulis, & Hocevar, 2010).

IR can directly disrupt atomic structures as being absorbed by living cells, producing chemical and biological changes (Azzam, Jay-Gerin, & Pain, 2012) and causing damage to important macromolecules. Total body irradiation may contribute to multiple organ dysfunctions caused by oxidative stress resulting from overproduction of ROS (Gultekin et al., 2013). Thus, this results in oxidative damage as they act on biomolecules including DNA, lipids and proteins (Cardozo-Pelaez et al., 2000). A recent study by Mohamed et al. (2014) and Zakaria et al. (2014) revealed that total body irradiation of 100  $\mu$ Gy of X-ray (LDR) induced oxidative stress and inflammatory response in male ICR mice in radiation group. As IR is being absorbed by living cells, it may induce more than 100 different DNA lesions produced through direct and/or indirect effects that contribute to structural damage of DNA molecules (Martin et al., 2010; Shackelford, Kaufmann, & Paules, 2000). These lesions include single- and double-strand breaks, oxidised bases, DNA protein cross-links and abasic sites (Sudprasert, Navasumrit, & Ruchirawat, 2006). The rising levels of DNA damage as the results of radiation exposure activate several mechanisms including DNA repair mechanism and cell cycle arrest, or apoptosis. However, failure in DNA repair mechanism in preventing any potentially mutagenic and carcinogenic outcomes from DNA damage lesions may lead to activation of apoptosis mechanism (Paz-Elizur et al., 2008).

Apoptosis or programmed cell death is a prevailing cell destructive mechanism responsible in eliminating damaged cells that have been exposed to mutagenic and carcinogenic agents that are capable in contributing development of cancer (Verheij & Bartelink, 2000). The control and regulation of apoptosis mechanism are highly complex and sophisticated, which involve molecular events that occur through Bcl-2 family of proteins (Elmore, 2007). The family of Bcl-2 proteins can be either pro-apoptotic (e.g., Bax, Bcl-Xs, Bak, Bad, Bik, Bid, Blk) or anti-apoptotic (e.g., Bcl-2, Bcl-XL, Bcl-w, BAG) (Hoetelmans et al., 2000). In addition, these proteins have significant role as they may determine if the cell executes to apoptosis or aborts the process (Elmore, 2007). Apoptosis may be initiated through activation of p53-dependent mechanisms due to accumulation of DNA damage, which alters the ratio of Bax/Bcl-2 protein expressions (Verheij & Bartelink, 2000; Xu et al., 2008). The ratio of Bax/Bcl-2 protein expressions increases during the induction of apoptosis (Lee et al., 1999). Likewise, the internal vital organs were chosen as they are vulnerable to the radiation, even in lower dosage. Thus, this study aimed to investigate the effects of LDR exposure on cellular ROS production, oxidative DNA damage (AP sites), and alteration of cellular ultrastructure and apoptosis-related protein expressions.

## METHOD

### Chemicals

*In Vitro* ROS/RNS Assay Kit (Green Fluorescence) and Oxidative DNA Damage Quantification Kit (AP Sites) were procured from Cell Biolabs Inc., whereas Invisorb® Spin Tissue Mini Kit from Stratec Molecular. Polyclonal anti-mouse Bcl-2 antibodies, monoclonal anti-mouse Bax antibodies, polyclonal anti-mouse p53 antibodies, GAPDH loading control antibodies and ECL Chemiluminescence Detection Kit were from Thermo Scientific Pierce.

### Animals and Irradiation

The experimental protocols were conducted with the approval of the Committee of Animal Research and Ethics (UiTM CARE No.38/2014), Universiti Teknologi MARA. Ten four-week-old male ICR mice, each weighing 30 grams, were obtained from Laboratory Animal Facility and Management (LAFAM), UiTM Selangor. The animals underwent acclimatisation period for 28 days, and on day 29, a total of ten mice were randomly divided into two groups consisting of control (Cx) and radiation (Rx) groups. Mice from Rx were total body irradiated with single fractionated of 100  $\mu$ Gy X-ray under Philips Bucky DIAGNOST X-ray Machine. Mice were sacrificed by cervical dislocation within 12 hours following irradiation.

### Determination of Cellular ROS Production

Cellular ROS production was quantified using OxiSelect *in Vitro* ROS/RNS Assay Kit (Green Fluorescence). Lung and liver tissues were homogenised with 20mg/mL ice-cold potassium PBS prior to centrifugation at 10,000 g for 5 minutes (4°C). Tissue lysates were collected and assayed directly. The Fluorescence signal was read using fluorescence plate reader at 480 nm excitation and 530 nm emission.

### Determination of Oxidative DNA Damage (AP Sites) Production

Genomic DNA of lung and liver were isolated with Invisorb® Spin Tissue Mini Kit. Oxidative DNA Damage Quantification Kit (AP Sites) was used to quantitate AP sites. The Aldehyde Reactive Probe (ARP) that reacts specifically with an aldehyde group on the open ring form of AP sites (ARP-derived DNA) was detected with Streptavidin-Enzyme Conjugate. Quantity of the AP sites in samples was determined using POLARstar Omega Reader at 450 nm by comparing standard curve of predetermined AP sites.

### Alteration of p53, Bax, and Bcl-2 Proteins Expression

**Sample Preparation.** Frozen tissues were resuspended in Radio Immuno Precipitation Assay (RIPA) buffer. Tissues were homogenised in 20 mg/mL cold RIPA buffer containing 10  $\mu$ L EDTA-free protease inhibitor cocktail on ice, and then kept for 30 min prior to centrifugation at 10,000 g (4°C) for 20 min. Supernatant was recovered and kept in -80°C prior to electrophoresis.

**Protein Level Determination.** Protein concentration in each sample was determined using Quick Start™ Bradford Protein Assay (Bio-Rad) according to the manufacturer's protocol.

**Western Blotting Techniques.** Aliquots from supernatant containing 50 µg proteins were mixed with 5X Laemmli sample buffer at ratio of 1:5 (v/v). Samples were boiled for 5 minutes at 95°C and subjected to 10% SDS-PAGE, and transferred to a PVDF membrane. Membranes will be blocked at RT for 2 hours in blocking buffer containing 10% skimmed milk (Merck) prior to incubation with anti-p53 (1:500 dilution), anti-Bcl-2 (1:500 dilution) or anti-Bax (1:500 dilution) primary antibodies in blocking buffer for two hours in RT. Next, the membranes were washed in 1X TBST (50 mmol/L Tris-HCl, pH 7.6, 150 mmol/L NaCl, 0.1% Tween 20) three times (10 minutes each) and incubated with HRP conjugated secondary antibody (1:20 000 dilution) for 2 hours at RT. The membranes were washed three times in TBST (10 minutes each) and exposed to ECL chemiluminescence reagents for 5 minutes. Blots were then exposed to X-ray film and processed by (brand automated film processor) for radiographic detection of the bands. The autoradiograms were scanned and protein bands were quantified by densitometry using ImageJ (version 1.45 k). To verify equal protein loading and transfer, the blots were probed for GAPDH using an anti-GAPDH antibody (1:5000 dilution). Thereafter, the same protocol was followed, except that the incubation time of the primary antibody was reduced to 2 hours.

**Ultrastructural Alteration.** Freshly dissected liver tissues were washed with cold PBS, followed by fixation in 4% glutaraldehyde. Tissues were then washed with sodium cacodylate buffer and post-fixed with 1% osmium tetroxide in 0.1M cacodylate buffer, followed by dehydrating through graded alcohols and rinsing in propylene oxide before embedding in epoxy resin. Ultrathin sections were stained with uranyl acetate and then examined under FEI TECHNAI G2 TEM.

**Statistical Analysis.** Statistical analysis was performed by using Software Package for Statistical Analysis version 18.0; ANOVA, followed by Tukey test. Statistically significant was judged at 0.05.

## RESULTS

### Induction of Cellular ROS Production Following LDR Exposure

Figure 1 refers to the mean value of cellular ROS production in liver and lung tissues measured in DCF (nM). In Rx, exposure to LDR significantly increased the production of cellular ROS in liver compared to Cx ( $P = 0.01$ ). The mean value of cellular ROS production in liver tissues of Cx and Rx was  $16,243 \pm 997$  nM DCF and  $18,154 \pm 803$  nM DCF, respectively. A similar result was obtained in the lung, but there was no significant increase in Rx ( $16,594 \pm 885$  nM DCF) compared to Cx ( $15,247 \pm 760$  nM DCF) groups.

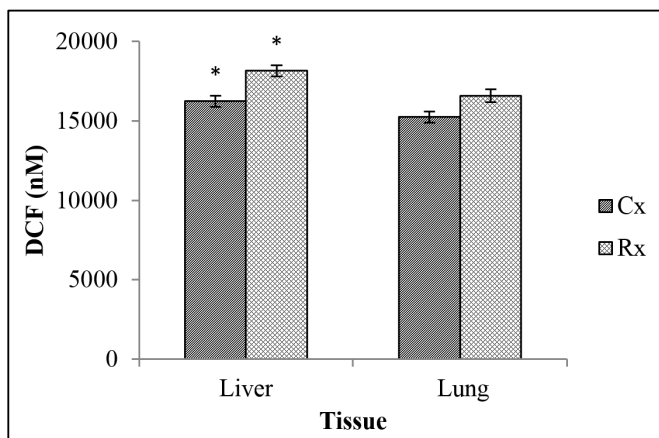


Figure 1. LDR-induced cellular ROS production. The bar chart shows the levels of cellular ROS production in liver and lung tissues of Cx and Rx. Values are expressed as mean ± SEM (n=5). \*Significant difference between Rx and Cx ( $P < 0.05$ )

### Induction of Oxidative DNA Damage (AP Sites) Generation Following LDR Exposure

The induction of oxidative DNA damage generation (AP sites) in mice tissues is shown in Figure 2. The number of AP sites generated per 105 base pairs in liver tissues of Rx showed a significant increment compared to Cx with  $P = 0.03$ . The mean numbers of noncoding AP sites per 105 base pairs generated in Rx and Cx were  $33.37 \pm 0.94$  and  $27.84 \pm 1.65$ , respectively. Meanwhile, there was a significant increment in the number of AP sites generated per 105 base pairs in the lung tissues of Rx ( $34.98 \pm 0.58$ ) compared to Cx ( $29.02 \pm 2.20$ ) with  $P = 0.001$  (Figure 2).

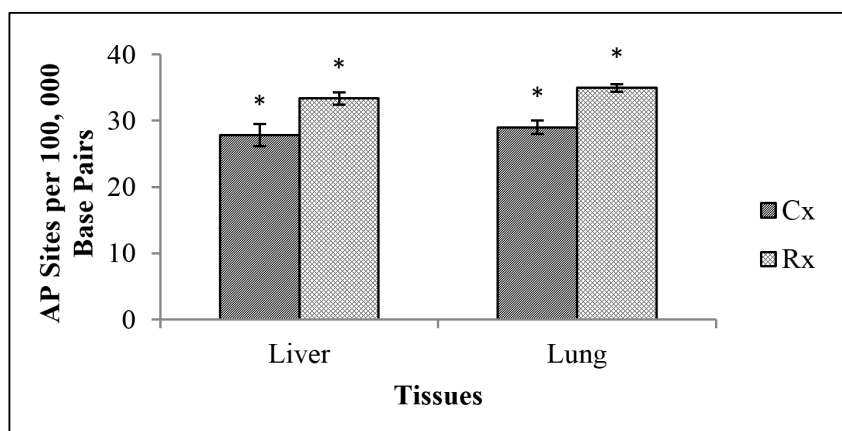


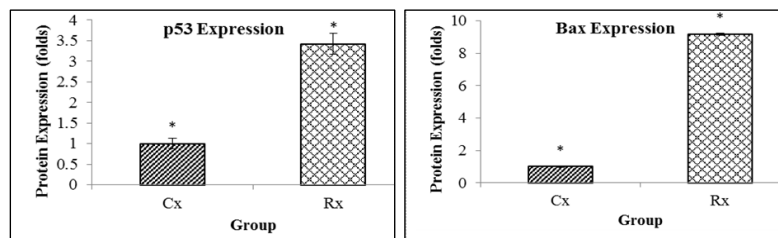
Figure 2. LDR-induced oxidative DNA damage (AP sites) production. The bar chart shows the levels of AP sites production in the liver and lung tissues of Cx and Rx. Values were expressed as mean ± SEM (n=5). \*Significant difference between Rx and Cx ( $P < 0.05$ )

### Alteration of p53, Bax, and Bcl-2 Protein Expressions Following LDR Exposure

The alteration of apoptosis-related protein expressions, p53, Bax, and Bcl-2 following LDR exposure, is shown in Figure 3(a). Figure 3(b) illustrates a significant increase in the expression of p53 in Rx compared to Cx following total body irradiation with 100  $\mu$ Gy X-ray ( $P = 0.01$ ). The expression of Bax and Bcl-2 in Rx showed significant increases compared to Cx with  $P = 0.001$  and  $P = 0.001$ , respectively, as shown in Figures 3(c) and 3(d). Densitometry analysis of these protein bands shows that p53 expression in Rx increased significantly by 3.42 folds compared to Cx. Meanwhile, Bax and Bcl-2 expressions in Rx significantly increased by 9.18 and 2.18 folds, respectively, compared to Cx. Figure 3(e) shows a significant increment in Bax/Bcl-2 ratio in Rx over Cx value by 3.30 folds ( $P = 0.001$ ), which reveals the activation of cellular apoptotic mechanism in response to LDR exposure.

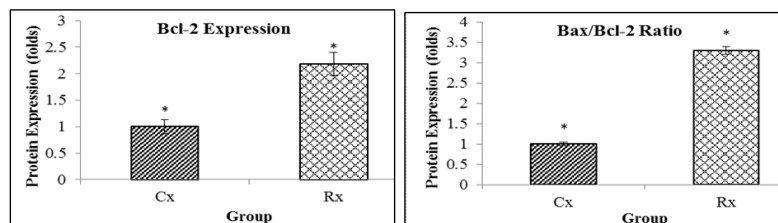
Protein	Band Intensity		Molecular Weight
	Cx	Rx	
p53			53 kDa
Bax			23 kDa
Bcl-2			26 kDa
GAPDH			36 kDa

(a)



(b)

(c)



(d)

(e)

Figure 3. Alteration of p53, Bax, and Bcl-2 protein expressions following LDR exposure: (a) representative autoradiographs of p53, Bax, and Bcl-2 protein expressions of liver tissues in Cx and Rx; and ((b) to (e)) the intensity of the bands were quantified by densitometry analysis and data were normalised using GAPDH intensity. The mean protein expression from Cx was designated as 1, and the mean protein expression from Rx was expressed as folds of optical density compared to Cx. Data are indicated as mean  $\pm$  SEM (n=5). \*Significant difference between Rx and Cx ( $P < 0.05$ ).

### Ultrastructural Alteration of Nucleus in Liver Tissues Following LDR Exposure

Severe alterations of cellular ultrastructure of nucleus were observed in the liver tissues of Rx compared to Cx (Figure 4). Figure 4(b) reveals morphologic changes of the nucleus related to apoptosis in the liver tissues of Rx. The nuclear membrane was shrunken and lost its common shape. The presence of condensed and peripheralised chromatin (X) in the nucleus of Rx is considered as a morphological characteristic of cell death through apoptotic mechanism following total body exposure to LDR.

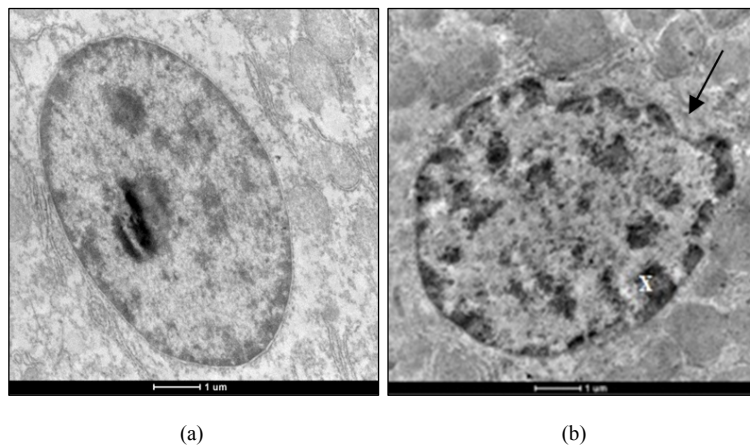


*Figure 4.* Ultrastructure alterations of nucleus in liver tissues following LDR exposure. (a) A normal ultrastructure of nucleus in liver tissues from Cx. (b) An altered ultrastructure of nucleus induced by LDR in liver tissues of Rx. This nucleus is characterised by the changes on the nuclear morphology. Nuclear membrane shrunken and lost common shape (arrow) and the present of chromatin condensation (X) in the perinuclear area (A and B: 6000×)

### DISCUSSION

Exposure to ionising radiation may lead to cellular damage through direct and/or indirect mechanisms (Cai, Koropatnick, & Cherian, 2001; Srinivasan et al., 2014). However, exposure to occupational sources of radiation frequently involves LDR (Ponzinibbio et al., 2010), which may contribute to overproduction of ROS under aerobic conditions (Cai et al., 2001). The results of this study are clinically relevance to radiation workers as they are continuously exposed to the low dose radiation from imaging modalities. As such, a single fractionated exposure was used as the baseline for a further research which is currently being conducted in assessing multiple exposures of low dose radiation in clinical setting. Results presented in Figure 1 demonstrate a significant production of ROS in the liver tissues of Rx following total body irradiation with LDR compared to Cx. This is in agreement with a study conducted by Park et al. (2001) which reveals significant increases of ROS production in lungs of male mice after a single dose of 10 Gy total-body irradiation with X-ray. It is possible to suggest that this was mainly due to the increased production in cellular ROS through radiolysis of water induced by LDR exposure, that in turn attacked cellular macromolecules including DNA through indirect mechanisms (Azzam et al., 2012).

Sites of missing bases termed as abasic sites, or apurinic/aprimidinic (AP) sites, are continuously being generated by DNA following exposure to endogenous and exogenous sources including radiation which may lead to oxidative DNA damage (Mohammad et al., 2014). Referring to Figure 2, the number of non-coding AP sites generated in the liver and lung tissues of Rx showed significant increment compared to Cx. The present study seems to be consistent with a previous *in vivo* study by Pogribny et al. (2005) which reveals the accumulation of DNA damage measured as the levels of  $\gamma$ H2AX foci in thymus tissues of mice following exposed to fractionated LDR. In addition, Ponzinibbio et al. (2010) found that CHO and MRC-5 cells treated with LDR (50 mSv) significantly induced DNA damage, as measured by alkaline comet assay compared to the control cell lines. These findings may suggest that exposure to LDR causes damage to DNA structure directly and/or indirectly through free radicals attack producing several oxidative DNA lesions including AP sites (Sudprasert et al., 2006).

p53 protein closely related to apoptosis mechanism, which remained at low state under normal condition and dramatically elevated in levels following accumulation of DNA damage (Xu et al., 2008). The present findings showed significant increment on expression of p53 in Rx by 3.42 folds compared to Cx (Figure 3(b)). Increased expression of p53 following total body irradiation with LDR in this study consistent with earlier findings by Wang et al., (1996), which revealed significant accumulation of p53 within 24 hours in adrenal glands, pancreas, thymus, skin, lungs, bone marrow and liver of C57BL/6N mice irradiated with 25 cGy and 50 cGy. An *in vitro* study conducted by Furlong et al. (2013) also supports the present findings, which demonstrates up-regulation of p53 in human keratinocyte cell line (HaCat) irradiated with a series of LDR. A possible explanation for the current finding is that LDR leads to accumulation of DNA damage, which in turn raises the expression of p53. Kastan et al. (1991), and Fei and El-deiry (2003) pointed out that the expression of p53 rises dramatically as the levels of DNA damage increase, thus activating p53 to either induce cell cycle arrest coupled with DNA damage repair or lead to cell death through apoptosis.

Damaged cells induced by ionising radiation are regulated by a complex balance in signal transduction pathways between pro-apoptotic (Bax) and anti-apoptotic (Bcl-2) proteins (Hoetelmans et al., 2000). The ratio of Bax/Bcl-2 provides important information whether cells will undergo apoptosis or not (Xu et al., 2008). In the current study, densitometry analysis of protein bands revealed significant increase of Bax and Bcl-2 expressions in Rx compared to Cx. Interestingly, the Bax/Bcl-2 ratio increased by 3.3 folds in Rx over Cx value (Figure 3(e)), which strongly suggests that total body irradiation with LDR may stimulate apoptosis when p53 protein is activated in response to DNA damage, thus altering the balance between ratio of Bax/Bcl-2. These findings are supported by a previous research by Park et al. (2008), which revealed a significant increment in the expression of pro-apoptotic proteins such as p53 and Bax within 24 hours in intestinal tissues of C57BL/6 mice after being irradiated with 2 Gy  $\gamma$ -rays. This result may explain the fact that, in apoptosis, Bax, which is a pro-apoptotic protein-containing p53-binding sites in promoter, has been shown to be regulated in response to p53 accumulation (Xu et al., 2008). Under normal physiological condition, Bax is predominantly present in the cytosol in a soluble form. However, during the activation of apoptosis, Bax becomes a membrane-bound form and cross-link as a homodimer with mitochondria (Brady & Gil-gomez, 1998). This biologically active Bax protein may form ion channels in the



mitochondria membrane that allow passive flux of mitochondria apoptogenic proteins such as cytochrome c across intracellular membrane, which leads to cells death through activation of caspases. The regulation of Bax inactivates Bcl-2 through heterodimerisation, thus increases the Bax/Bcl-2 ratio, and cells are susceptible to self-destruction (Basu & Haldar, 1998). The electron micrographs also reveal apoptosis in the nucleus of liver tissues of Rx group compared to normal ultrastructure of nucleus in Cx (Figure 4(b)). Nucleus in Rx shows shrunken and loss of common shape. Another ultrastructural changes observed in Rx after being irradiated with LDR consisting condensation of chromatin in the perinuclear area (X). The appearance of these severe alterations of the nucleus may suggest that the liver cells in Rx underwent apoptosis.

## CONCLUSION

The present study provides evidences that LDR exposure may induce oxidative DNA damage through excessive production of cellular ROS and significant increase in the production of AP sites. In addition, exposure to LDR may alter cellular ultrastructure and apoptosis-related proteins. These finding serve as important implications for estimating risks related to LDR exposure among medical radiation professions. It is perhaps best to recommend that study on cell cycle checkpoint and repair mechanisms be conducted for a better understanding of molecular mechanisms in response to LDR exposure.

## ACKNOWLEDGEMENTS

The authors gratefully acknowledge the support given by: (1) Faculty of Health Sciences UiTM Puncak Alam; and (2) UiTM Institute for Research Management & Innovation (RAGS:600-RMI/RAGS 5/3 (120/2012)) for funding the study. The authors deeply appreciate: (3) Department of Medical Laboratory Technology; and (4) Department of Medical Imaging, and Imaging Centre (IMACE), Faculty of Pharmacy, for providing the research facilities throughout this study.

## REFERENCES

- Azzam, E. I., Jay-Gerin, J.-P., & Pain, D. (2012). Ionizing radiation-induced metabolic oxidative stress and prolong cell injury. *Cancer Letters*, 327(0), 48–60.
- Basu, A., & Haldar, S. (1998). The relationship between Bcl2, Bax and p53 : consequences for cell cycle progression and cell death. *Molecular Human Reproduction*, 4(12), 1099–1109.
- Brady, H. J. M., & Gil-gomez, G. (1998). Molecules in focus Bax . The pro-apoptotic Bcl-2 family member, Bax. *The International Journal of Biochemistry and Cell Biology*, 30, 647–650.
- Cai, L., Koropatnick, J., & Cherian, M. G. (2001). Roles of vitamin C in radiation-induced DNA damage in presence and absence of copper. *Chemico-Biological Interaction*, 137, 75–88.
- Cardozo-Pelaez, F., Brooks, P. J., Stedford, T., Song, S., & Sanchez-Ramos, J. (2000). DNA damage, repair, and antioxidant systems in brain regions: a correlative study. *Free Radical Biology and Medicine*, 28(5), 779–85. Retrieved from <http://www.ncbi.nlm.nih.gov/pubmed/10754274>.
- Elmore, S. (2007). Apoptosis: a review of programmed cell death. *Toxicologic Pathology*, 35(4), 495–516.

- Fei, P., & El-deiry, W. S. (2003). P53 and radiation responses. *Oncogene*, 22, 5774–5783.
- Furlong, H., Mothersill, C., Lyng, F. M., & Howe, O. (2013). Apoptosis is signalled early by low doses of ionising radiation in a radiation-induced bystander effect. *Mutation Research*, 741-742(2013), 35–43.
- Gultekin, F. A., Bakkal, B. H., Guven, B., Tasdoven, I., Bektas, S., Can, M., & Comert, M. (2013). Effects of ozone oxidative preconditioning on radiation-induced organ damage in rats. *Journal of Radiation Research*, 54(1), 36–44.
- Hoetelmans, R., van Slooten, H. J., Keijzer, R., Erkeland, S., van de Velde, C. J., & Dierendonck, J. H. (2000). Bcl-2 and Bax proteins are present in interphase nuclei of mammalian cells. *Cell Death and Differentiation*, 7, 384–392.
- Kastan, M. B., Onyekwere, O., Sidransky, D., Vogelstein, B., & Craig, R. W. (1991). Participation of p53 Protein in the Cellular Response to DNA Damage Participation of p53 Protein in the Cellular Response to DNA Damage. *Cancer Research*, 6304–6311.
- Klaunig, J. E., Kamendulis, L. M., & Hocevar, B. A. (2010). Oxidative stress and oxidative damage in carcinogenesis. *Toxicologic Pathology*, 38(1), 96–109.
- Lee, J., Hosotani, R., Wada, M., Doi, R., Kosiba, T., Fujimoto, K., & Imamura, M. (1999). Role of Bcl-2 Family Proteins ( Bax , Bcl-2 and Bcl-X ) on Cellular Susceptibility to Radiation in Pancreatic Cancer Cells. *European Journal of Cancer*, 35(9), 1374–1380.
- Martin, L. M., Marples, B., Coffey, M., Lawler, M., Lynch, T. H., Hollywood, D., & Marignol, L. (2010). DNA mismatch repair and the DNA damage response to ionizing radiation: making sense of apparently conflicting data. *Cancer Treatment Reviews*, 36(7), 518–27.
- Mohamed, M. I., Mohammad, M. K. A., Zakaria, A. M., Ghazali, N., Mohamed Isa, M., Abdul Razak, H. R., & Md Saad, W. M. (2014). Induction of Oxidative Stress Following Low Dose Ionizing Radiation in ICR Mice. *World Journal of Medical Sciences*, 10(2), 198–203.
- Mohammad, M. K. A., Mohamed, M. I., Zakaria, A. M., Abdul Razak, H. R., & Md Saad, W. M. (2014). Watermelon (*Citrullus lanatus* (Thunb.) Matsum. and Nakai) Juice Modulates Oxidative Damage Induced by Low Dose X-Ray in Mice. *BioMed Research International*, 2014.
- Park, E., Lee, N. H., Joo, H.-G., & Jee, Y. (2008). Modulation of apoptosis of eckol against ionizing radiation in mice. *Biochemical and Biophysical Research Communications*, 372(4), 792–7.
- Park, E., Park, J., Kim, Y., Sung, J., Hwang, T., Kim, W., Park, Y. (2001). Role of Oxidative Stress in the Radiation-Induced Lung Pathogenesis in Mice. *Journal of Biochemistry and Molecular Biology*, 34(6), 544–550.
- Paz-Elizur, T., Sevilya, Z., Leitner-Dagan, Y., Elinger, D., Roisman, L. C., & Livneh, Z. (2008). DNA repair of oxidative DNA damage in human carcinogenesis: potential application for cancer risk assessment and prevention. *Cancer Letters*, 266, 60–72.
- Pogribny, I., Koturbash, I., Tryndyak, V., Hudson, D., Stevenson, S. M. L., Sedelnikova, O., Kovalchuk, O. (2005). Fractionated low-dose radiation exposure leads to accumulation of DNA damage and profound alterations in DNA and histone methylation in the murine thymus. *Molecular Cancer Research*, MCR, 3(10), 553–61.
- Ponzinibbio, M. V., Crudeli, C., Peral-García, P., & Seoane, A. (2010). Low-dose radiation employed in diagnostic imaging causes genetic effects in cultured cells. *Acta Radiologica (Stockholm, Sweden: 1987)*, 51(9), 1028–33.

- Shackelford, R. E., Kaufmann, W. K., & Paules, R. S. (2000). Oxidative stress and cell cycle checkpoint function. *Free Radical Biology and Medicine*, 28(9), 1387–1404.
- Srinivasan, M., Kalpana, K. B., Devipriya, N., & Menon, V. P. (2014). Protective effect of lycopene on whole body irradiation induced liver damage of Swiss albino mice: Pathological evaluation. *Biomedicine and Preventive Nutrition*, 4(2), 87–94.
- Sudprasert, W., Navasumrit, P., & Ruchirawat, M. (2006). Effects of low-dose gamma radiation on DNA damage, chromosomal aberration and expression of repair genes in human blood cells. *International Journal of Hygiene and Environmental Health*, 209(6), 503–11.
- Verheij, M., & Bartelink, H. (2000). Radiation-induced apoptosis. *Cell Tissue Research*, 301, 133–142.
- Wang, X., Matsumoto, H., Takahashi, A., Nakano, T., Okaichi, K., Ihara, M., & Ohnishi, T. (1996). p53 accumulation in the organs of low-dose X-ray-irradiated mice. *Cancer Letters*, 04(I 996), 79–84.
- Xu, J., Lian, L., Wu, C., Wang, X., Fu, W., & Xu, L. (2008). Lead induces oxidative stress, DNA damage and alteration of p53, Bax and Bcl-2 expressions in mice. *Food and Chemical Toxicology: An International Journal Published for the British Industrial Biological Research Association*, 46(5), 1488–94.
- Zakaria, A. M., Ghazali, N., Mohammad, M. K. A., Mohamed, M. I., Mohamed Isa, M., Abdul Razak, H. R., & Md Saad, W. M. (2014). Radioprotective Effect of Watermelon Juice Against Low Dose Ionizing Radiation-Induced Inflammatory Response in Mice. *World Journal of Medical Sciences*, 10(2), 191–197.
- Zielinski, J. M., Garner, M. J., Band, P. R., Krewski, D., Shilnikova, N. S., Jiang, H., & Semenciw, R. (2009). Health outcomes of low-dose ionizing radiation exposure among medical workers: a cohort study of the Canadian national dose registry of radiation workers. *International Journal of Occupational Medicine and Environmental Health*, 22(2), 149–156.



## Microbial Fuel Cell's Performance of Original and Deoxygenated Palm Oil Mill Effluent in 3 Different Stages of Fermentation Process

**Khairul Baqir Alkhair Khairul Amin<sup>1,3\*</sup>, Oskar Hasdinor Hassan<sup>2</sup>, Sharifah Aminah Syed Mohamed<sup>1</sup>, Yap Kian Chung Andrew<sup>3</sup>, Zulkifli Ab. Rahman<sup>3</sup>, Hazlini Mohamad Ameran<sup>4</sup>, Nurul Khamsatul Akma Kamaruzaman<sup>4</sup>, Tunku Ishak Tunku Kudin<sup>1</sup>, Ab. Malik Marwan Ali<sup>1,5</sup>, Mohd Zu Azhan Yahya<sup>6</sup> and Muhammad Haikal Zainal<sup>1</sup>**

<sup>1</sup>Faculty of Applied Science, Universiti Teknologi MARA (UiTM), 40450 Shah Alam, Selangor, Malaysia

<sup>2</sup>Faculty of Art and Design, Universiti Teknologi MARA (UiTM), 40450 Shah Alam, Selangor, Malaysia

<sup>3</sup>Milling and Processing Unit, Engineering and Processing Research Division, Malaysian Palm Oil Board (MPOB), 43000 Kajang, Selangor, Malaysia

<sup>4</sup>Centre of Foundation Studies, 42300 Bandar Puncak Alam, Selangor, Malaysia

<sup>5</sup>Institute of Science, Universiti Teknologi MARA (UiTM), 40450 Shah Alam, Selangor, Malaysia

<sup>6</sup>Faculty of Defence Science and Technology, Universiti Pertahanan Nasional Malaysia (UPNM), 57000 Sungai Besi, Kuala Lumpur, Malaysia

### ABSTRACT

Bio-electricity generation by Microbial Fuel Cell (MFC) has gained considerable attention due to its integration with wastewater treatment such as Palm Oil Mill Effluent (POME). Investigation into pH effect and determination of optimal pH value ranges growth for acidogenic, acetogenic

and methanogenic by natural mixed culture electroactive bacteria (exoelectrogens) growth in original non-Deoxygenated Mixed POME (nDMP) and Deoxygenated Mixed POME (DMP) in MFC was carried out. Current generation, power generation and maximum power were also monitored. Experimental results show that exoelectrogens in nDMP with pH 6.8 yielded the highest current generation of 61.51 mA<sup>m</sup>-<sup>2</sup> and maximum power of 17.63 mWm<sup>-2</sup>. Overall, nDMP substrates with 3 pH ranges (5.5, 6.8 and 8.0) showed equal potential to generate power that is higher than DMP substrates. Comparison carried out for inter DMP substrates demonstrated that DMP with pH 6.8 and DMP with pH 8.0 showed

### ARTICLE INFO

#### Article history:

Received: 25 October 2016

Accepted: 17 March 2017

#### E-mail addresses:

khairulbaqiralkhair@gmail.com (Khairul Baqir Alkhair),  
oskar@salam.uitm.edu.my (Oskar Hasdinor Hassan),  
sharifah459@salam.uitm.edu.my (Sharifah Aminah Syed Mohamed),  
andrew@mpob.gov.my (Yap Kian Chung Andrew),  
zai@mpob.gov.my (Zulkifli Ab. Rahman),  
hazlini@salam.uitm.edu.my (Hazlini Mohamad Ameran),  
khamsatul@salam.uitm.edu.my (Nurul Khamsatul Akma Kamaruzaman),  
tunkuishak@gmail.com (Tunku Ishak Tunku Kudin),  
ammali@salam.uitm.edu.my (Ab. Malik Marwan Ali),  
mzay@upnm.edu.my (Mohd Zu Azhan Yahya),  
muhammadhaikalzainal@gmail.com (Muhammad Haikal Zainal)

\*Corresponding Author

Khairul Baqir Alkhair Khairul Amin, Oskar Hasdinor Hassan, Sharifah Aminah Syed Mohamed,  
Yap Kian Chung Andrew, Zulkifli Ab. Rahman, Hazlini Mohamad Ameran, Nurul Khamsatul Akma Kamaruzaman,  
Tunku Ishak Tunku Kudin, Ab. Malik Marwan Ali, Mohd Zu Azhan Yahya and Muhammad Haikal Zainal

equal potential to generate power, but not for DMP with pH 5.5. Subsequently, nDMP with pH 6.8 and nDMP with pH 8.0 showed equal potential for higher maximum power compared to nDMP with pH 5.5 and DMP substrates. This finding indicates that mixed microbial communities in DMP substrate are dominant with obligate anaerobic exoelectrogens bacteria which have less capability to generate electricity compared to nDMP substrate that was dominated by the aerotolerant and/or facultative anaerobic exoelectrogens bacteria.

*Keywords:* Microbial Fuel Cell (MFC), Palm Oil Mill Effluent (POME), pH value

---

## INTRODUCTION

In Malaysia, POME is a highly polluted wastewater produced by palm oil processing mills, which was usually treated in open pond system consisting of cooling ponds, acidification ponds, anaerobic ponds and facultative ponds until its biological oxygen demand (BOD) meets the limit set by Malaysian Department of Environment (DOE) which is 5000 mg/l (Environmental quality act 1974, 1978) before discharging it into the water course (Andrew & Manaf, 2013).

POME anaerobic fermentation is a complex biochemical process in anaerobic condition, where organic matters are degraded to methane and carbon dioxide in discrete steps involving the concerted action of a myriad numbers of bacteria in several different metabolite groups of microorganism. The main pathways of anaerobic digestion are involved in 4 stages, namely hydrolysis, acidogenesis, acetogenesis and methanogenesis (Andrew & Manaf, 2013).

During hydrolysis, large polymers of carbohydrate, lipids (fat) and protein macromolecules were broken down to amino acids, long-chain fatty acids, and sugars. These hydrolysates were then further fermented during acidogenesis to produce three, four and five-carbon volatile fatty acids, where optimum pH range growth for acidogenic bacteria was between pH 5.2 to pH 6.5. These hydrolysates (products of hydrolysis process) were consumed by acetogenic bacteria and generated acetate acids, carbon dioxide and hydrogen during acetogenesis, where optimum pH growth of these bacteria was between pH 6.0 to pH 7.0. Finally, during methanogenesis, where methanogenic bacteria's pH growth environment was within the range of pH 7.5 to pH 8.5 consumed acetate, hydrogen and some of the carbon dioxide to produce methane (Rappport et al., 2008; Solera et al., 2002).

Apart from the above categorisations, bacteria may be divided into three groups according to their responses to free molecular oxygen. These groups are: (1) strictly aerobes; (2) facultative anaerobes; and (3) anaerobes which are inactive in the present of free molecular oxygen which may be divided into two subgroups; oxygen-tolerant species and oxygen-intolerant species. Anaerobic bacteria present in POME anaerobic pond could be grouped on the basis of their need for oxygen to grow. Obligate anaerobic bacteria (oxygen-intolerant species) are the bacteria that use anaerobic metabolism to grow but harmed and killed in the presence of oxygen. Meanwhile, aerotolerant anaerobic bacteria (oxygen-tolerant species) are also the bacteria that also use anaerobic metabolism to grow but could tolerate the presence of oxygen. The two subgroups mentioned above need anaerobic metabolism to grow, but not for facultative

anaerobic bacteria. Facultative anaerobic bacteria prefer to grow using aerobic metabolism processes but could switch to anaerobic metabolism in the absence of oxygen (Gerardi, 2003).

Recently, POME treatment process involving bacteria has gained some interest amongst scientists and environmentalists, and usage of bacteria together in Microbial Fuel Cell (MFC) is one of the alternatives for POME treatment. Meanwhile, the application of MFC technologies is an alternative approach to wastewater treatment that uses by-product generated electricity (Logan, 2008). In 2004, the relationship between electricity using MFCs and wastewater treatment was clearly forged when it was demonstrated that domestic wastewater could be treated to practical levels while simultaneously generating electricity (Liu & Logan, 2004). Bioelectricity generation is a new approach for generating electricity from biomass using bacteria. Therefore, bacteria were further categorised by their ability to exogenously transfer electrons called exoelectrogens that can produce power in an MFC (Logan, 2008). Other names for exoelectrogens are electrogens, anode-respiring bacteria (Torres et al., 2010) and electrochemically active bacteria/microorganism (Samir et al., 2010). Exogenously transfer electrons by bacteria are also known as e Extracellular Electron Transfer (EET) (Torres et al., 2010).

In this work, mixed POME substrates (1:1, Raw POME: Anaerobic Pond POME) were subjected into 2 factors that may influence the growth of different species of bacteria. The first factor was the pH of substrate, which was controlled into three groups of pH (pH 5.5, 6.8 and 8.0) that was the optimal pH for acidogenic, acetogenic and methanogenic bacteria (Solera, Romero, & Sales, 2002). The second factor was the dissolved oxygen (DO) in the substrate. Two types of substrates were used; one was pretreated by sparging with pure nitrogen gas (N<sub>2</sub>) (Logan, 2008) to decrease DO, while the other substrate was not pretreated. These factors were investigated in terms of the pH effect to determine the optimal pH value ranges growth for acidogenic, acetogenic and methanogenic by the exoelectrogens growth in nDMP and in MFC. In addition, the percentage of COD effective reduction was used as the indicator to determine POME treatment by the MFC. Common approaches used in most studies are entirely relying on its pH values and tend to ignore the pathways of anaerobic digestion, in which anaerobic digestion process is as important as pH values. By solving this problem, the understanding of bacteria's activity respectively to their environment, especially in acidogenesis, acetogenesis and methanogenesis stages, is enhanced.

## METHOD

In this work, the double-chambered MFC was designed and fabricated locally using acrylic fibre material with 150 mL working volume for each component. The anode (anaerobic) and cathode (aerobic) chambers were separated by a salt bridge compartment filled with molten 10% agarose of 4% potassium chloride salt (Nair et al., 2013) heated in a water bath, which was allowed to be cooled and solidified. The salt bridge assists in the proton transfer mechanism during MFC's operation. The electrode material used for anode and cathode was carbon brush (Bosch Skil Dremel PG88, German) in the sizes of 2.2 cm x 1.6 cm x 0.6 cm (used in both chambers) and 1.3 cm x 0.7 cm x 0.6 cm (used only in anode chamber) with projected area of 62.22 cm<sup>2</sup> for anode and 11.6 cm<sup>2</sup> cathode. The anode chamber is sealed to maintain its

anaerobic condition. The electrodes close circuit was connected externally through copper wires to provide the permanent connection to external resistance of 1 k $\Omega$  resistor. A schematic diagram of MFC is shown in Figure 1.

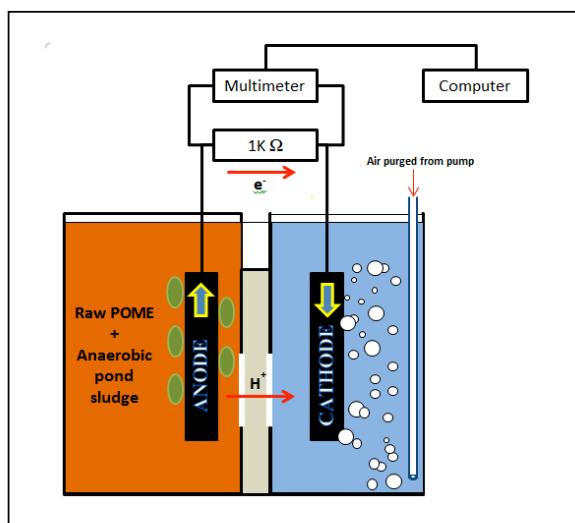


Figure 1. A schematic diagram of aqueous cathode double-chamber MFC

The substrate used is mixed POME. The substrates were prepared in 2L beakers at a mixing ratio of 1 L raw POME to 1 L of anaerobic pond POME. Gas flushing or sparging pure N<sub>2</sub> gas (Logan, 2008) through the mixed POME (Deoxygenation pretreatment) was a process to decrease DO (Japar et al., 2013; Biffinger et al., 2008; Logan et al., 2006) in the substrate. The pretreatment was applied to the first mixed POME sample mixture, DMP, while the second was not, nDMP. The two beakers were sealed with parafilm. After 24 hours, the substrates were divided into six units of 250 mL borosilicate glass reagent bottles (Bomex), where three of the bottles were filled with DMP and the rest with nDMP.

The pH of substrates were controlled by using sodium hydroxide (NaOH) that maintained pH  $5.5 \pm 0.2$ , which represented DMP pH range between 5.2 to 6.5 (DMP 5.5) and nDMP pH range between 5.2 to 6.5 (nDMP 5.5). The same procedure was done to both of the substrates, DMP and nDMP, to maintained pH  $6.8 \pm 0.2$  and pH  $8.0 \pm 0.2$  (DMP 6.8, nDMP 6.8, DMP 8.0 and nDMP 8.0). All the six controlled substrates were left for 24 hours before filling the anode chambers 125 mL of mixture. The balance of 125 mL POME batches were kept sealed in the borosilicate glass reagent bottles (Bomex) as controlled and calibrate samples.

The electrode output voltage was recorded every 15 minutes with a digital multimeter with a data logger (DM620, 50,000 Count Logger DMM and UT803, UNI-T). From these



data, power generation was calculated using power density normalised by the surface area of anode ( $P_A$ ,  $\text{Wm}^{-2}$ ) (Logan et al., 2006) using the equation [1] below:

$$P_{An} = \frac{V^2}{A_{An}R} \quad [1]$$

Where  $A$  = total area of anode electrode ( $\text{m}^2$ ),  $An$  = Anode,  $P$  = power (W),  $V$  = the potential (V) and  $R$  = external resistance ( $\Omega$ ). The polarisation curves represent the voltage as the function of the current (density) was used for the analysis and characterisation of MFC (Logan et al., 2006), whereas the power curve described the power (or power density) as the function of the current (or current density) calculated from the polarisation curve. The power increased with the current from open circuit conditions to maximum power point (MPP). From the previous works, researchers typically use the peak (top) of the power curve, which is the MPP, to report the "Maximum Power" and this maximum power occurred at the point where the internal resistance was equal to the external resistance (Logan, 2008). To obtain the maximum power data from the power curves and plot the polarisation curve, variable resistance using the resistors MODEL: ITC 8 Insulation Tester Checker (KK Instruments, Taiwan) was applied in the MFC circuit by connecting it to different resistors (0.5, 1, 2, 20, 200, 1k, 10k, 20k, 100k, 1M, 2M and 10M)  $\Omega$  and voltage reading was recorded (typically 10 to 20 min per resistor). From these data, power density and current density were calculated. The current density normalised by surface area ( $I_{An}$ ,  $\text{Am}^{-2}$ ) was calculated using equation [2] below:

$$I_{An} = \frac{V}{A_{An}R} \quad [2]$$

Where  $A$  = total area of anode electrode ( $\text{m}^2$ ),  $An$  = Anode,  $V$  = the potential (V) and  $R$  = external resistance ( $\Omega$ ) and  $I$  = current (A). From this calculation, polarisation curves and current density curves were plotted (Logan et al., 2006).

Environmental Scanning Electron Microscopy (Quanta 450 FEG ESEM, USA) was used to observe the biofilm formed on the anodic carbon brush's (ACB) surface. A cut ACB was soaked for 4 hours in 4% glutaraldehyde phosphate buffer solution for fixation process. Then, the ACB was rinsed in distilled water before the sample was observed under ESEM at 20 kV.

## RESULTS AND DISCUSSION

Voltage reading was recorded, where power and current densities were calculated by the MFC devices for DMP, and nDMP substrates with 3 different ranges of pH values showed that the power and current generation by nDMP substrates was higher compared to the DMP substrates. The voltage of nDMP 6.8 was relatively high as compared to nDMP 5.5 and nDMP 8.0, as shown in Figure 2. The same was applied to DMP, whereby DMP 6.8 recorded the highest voltage compared to the other two DMPs. The lowest power generation calculated for DMP substrate was DMP 5.5, which was almost to none after 10.5 hours of MFC's operation, and the lowest for nDMP substrates was nDMP 5.5, respectively. The highest point for the calculated power for nDMP was nDMP 6.8 at  $14.76 \text{ mWm}^{-2}$  after 102.5 hour of MFC operation, while for DMP was DMP 8.0 at  $5.04 \text{ mWm}^{-2}$  after 14.5 hour of MFC operation (Figure 2). The result shows

that pH value does affect MFC's power generation performance. The anodic pH value ranged between  $6.8 \pm 0.2$  for both DMP and nDMP substrates produced the highest power generation as compared to the other two, pH value ranges between  $5.5 \pm 0.2$  and  $8.0 \pm 0.2$ , respectively, where nDMP 6.8 substrates recorded the highest power generation. This is in agreement with Patil et al. (2011) whose previous study indicated that pH value played a crucial role for the development and current production of anodic microbial electroactive biofilm, whereby only a narrow pH window from pH 6.0 to 9.0 was demonstrated to be suitable for the growth and operation of biofilm, and that a high average of current density was achieved at pH 7.0.

nDMPs power generations are relatively higher than DMPs, as shown in Figure 2. This proves that MFC's performance is not just affected by pH value but also by the different concentrations of DO. It is possible that the capabilities of the dominant mix community's anoxic exoelectrogens in DMP to generate electricity were lower compared to dominant mix community's aerotolerant and/or facultative bacteria in nDMP. Facultative bacteria have the ability to metabolise and produce electricity in both the presence and absence of oxygen, which gives the bacteria higher survival rate than obligate bacteria. In a previous study, the experiment of *Shewanella oneidensis*'s electrical performance in MFC by exposing the bacteria in different oxygen concentration was conducted, and the researchers concluded that *S. oneidensis*'s electrical performance in aerobically condition was higher than anaerobically condition, which is similar to the bacterial behaviour against concentration of hydrogen ion (Biffinger et al., 2008).

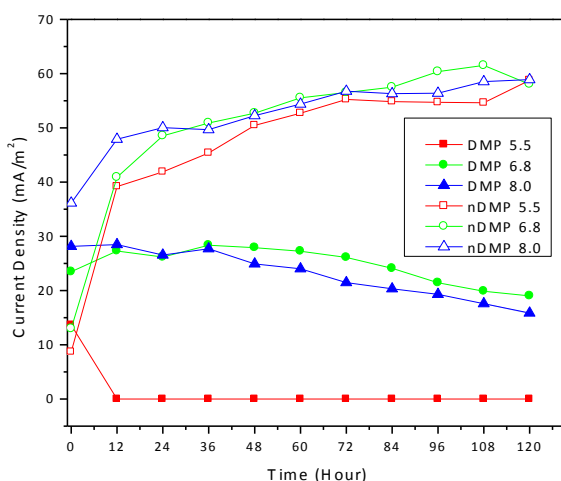


Figure 2. Power Generations with DMP and nDMP exoelectrogens bacteria by pH value

Anaerobic mix culture bacteria presence in the substrate used in this study could be divided into Obligate Anaerobic Bacteria (oxygen-intolerant species), Aerotolerant Anaerobic Bacteria (oxygen-tolerant species) and Facultative Anaerobic Bacteria that responded to the DO (Gerardi, 2003). Deoxygenation pretreatment with pure  $N_2$  gas to reduce DO content makes the environment of DMP from hypoxic to anoxic. In this condition, obligate bacteria grow and

become dominant in number compared to aerotolerant and/or facultative bacteria. Therefore, DO concentrations could determine the active species of bacteria and their populations in the mix cultured POME as shown in Figure 5, which is in agreement with Biffinger et al. (2008).

At 1k  $\Omega$  external resistance, DMP 6.8 recorded the maximum power that MFC system could generate at power density peak at 2.92 mWm<sup>-2</sup> (current density = 21.65 mA/m<sup>2</sup>) as compared to DMP 5.5 peak at 0.15 mWm<sup>-2</sup> (current density = 4.95 mA/m<sup>2</sup>) and DMP 8.0 peak at 2.09 mWm<sup>-2</sup> (current density = 18.33 mA/m<sup>2</sup>) as illustrated in Figure 3 below.

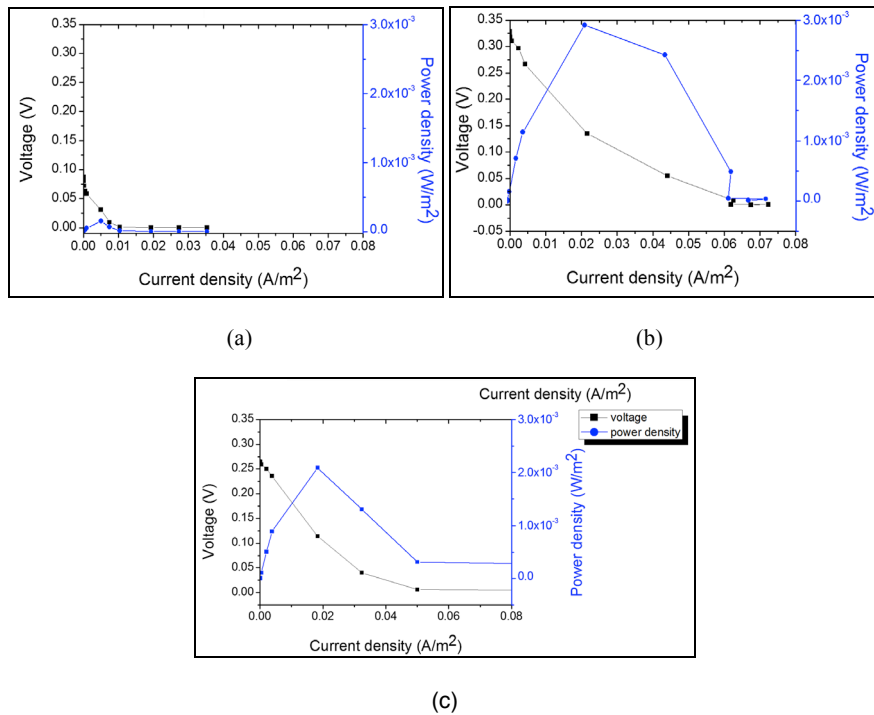


Figure 3. Polarisation and Power Curves with: (a) DMP 5.5; (b) DMP 6.8; and (c) DMP 8.0

To demonstrate the potential for greater power densities, further test was conducted with nDMP substrates. The maximum power of nDMP 5.5 was at 1K $\Omega$  external resistance, but nDMP 6.8 and nDMP 8.0 were optimum at the external resistance of 200 $\Omega$  for the other two MFC systems. At their respective external resistance, the nDMP 6.8 recorded the highest maximum power whereby the power density peak at 17.63 mWm<sup>-2</sup> (current density = 150.28 mA/m<sup>2</sup>) as compared to nDMP 5.5 which peaked at 13.84 mWm<sup>-2</sup> (current density = 59.56 mA/m<sup>2</sup>) and nDMP 8.0 peaks at 15.13 mWm<sup>-2</sup> (current density = 139.24 mA/m<sup>2</sup>), as shown Figure 4.

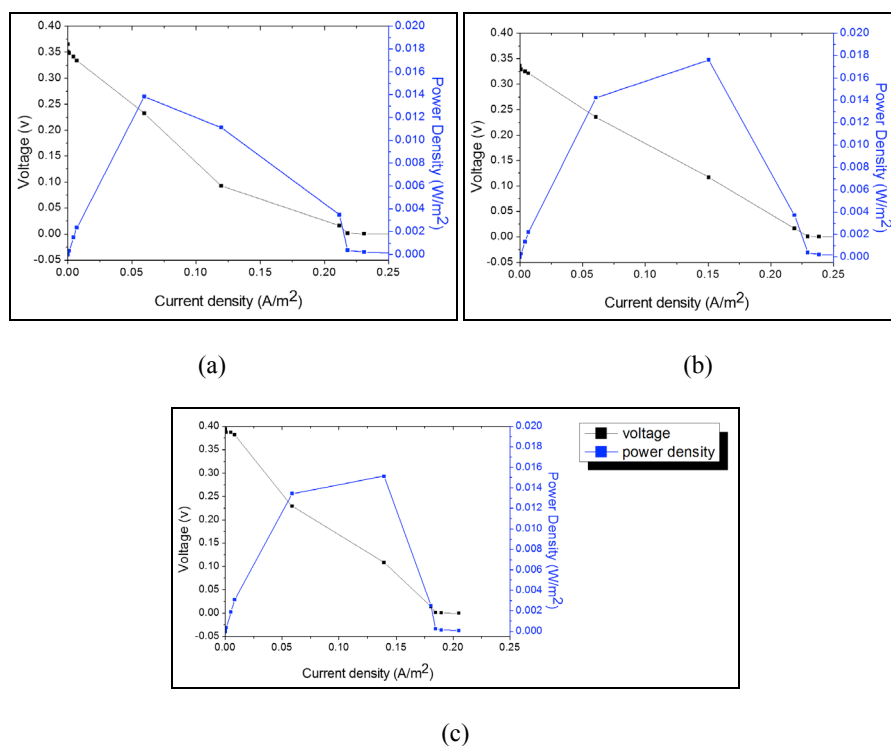


Figure 4. Polarisation and Power curves with: (a) nDMP 5.5; (b) nDMP 6.8; and (c) nDMP 8.0

Overall, the maximum power that the MFC system of nDMP substrates produced was higher than the MFC system of DMP substrates. For inter pH ranges, the maximum power of nDMP 5.5 was 92 times higher compared to DMP 5.5. Meanwhile for nDMP 6.8, the maximum power was 6 times higher compared to DMP 6.8 and nDMP 8.0, and it was 7 times higher compared to DMP 8.0. However, for intra pH ranges, nDMP 6.8 substrates recorded the highest maximum power. The maximum power of nDMP 6.8 was 1.17 times compared nDMP 8.0 and 117.5 times compared to DMP 5.5.

The anodic pH values range between  $6.8 \pm 0.2$  for both DMP and nDMP substrates which produced the highest maximum power as compared to the other two pH value ranges between  $5.5 \pm 0.2$  and  $8.0 \pm 0.2$ , respectively where nDMP 6.8 substrates recorded the highest power generation. This is in accordance with Patil et al. (2011).

Acidogenic (exoelectrogens) bacteria did not grow in Alkaliphile condition but grew in Neutrophile condition. However, the presence of acidogenic (exoelectrogens) bacteria in Neutrophile condition did not increase the maximum power demonstrated in the result above (Figure 3 and Figure 4). At this point, the acidogenic (exoelectrogens) bacteria are at the optimum, thus anodic pH ranges recorded the lowest. Although acetogenic (exoelectrogens) bacteria active in DMP 6.8 and nDMP 6.8 substrates, but this does not mean that it is exclusive for these bacteria only. Some alkaliphilic bacteria, which are methanogenic (exoelectrogens) bacteria, grow in the pH value ranges between  $6.8 \pm 0.2$ , a similar behaviour observed in Ziemiński and Frąć (2011). The fact that the conversion of fermentation product by acetogenic

(exoelectrogens) bacteria was thermodynamically possible only if the hydrogen concentration was kept sufficiently low by converting it into methane by methanogenic (exoelectrogens) bacteria. Therefore, the acetogenic and methanogenic (exoelectrogens) bacteria must cohabit in a close relationship between both classes of bacteria. This conversion of the fermentation is in agreement with Solera et al. (2002).

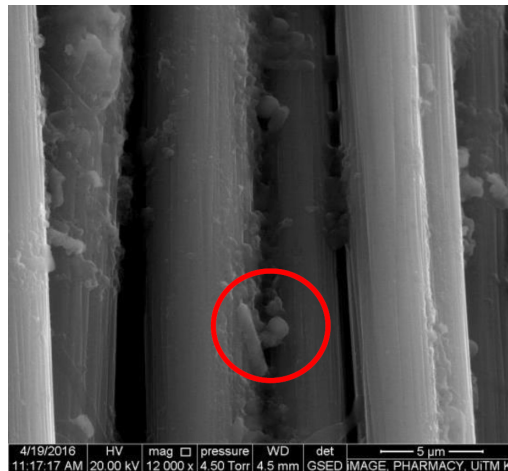


Figure 5. ESEM images of microorganisms' attachment on ACB's surface at day 5

### Environmental Scanning Electron Microscopy (ESEM)

ESEM was used to examine the ACB's surface to confirm the presence of biofilm formation. On day 5 of MFC operation, the ACB was observed under ESEM and the result is as shown in Figure 5. In Figure 5, all sorts of bacteria can be observed on the ACB's surface. The figure illustrates that the rod-shaped and round-shaped bacteria are attached (red circle) on the surface, which indicates the biofilm formed on the ACB's surface came from a mixed culture bacteria POME sample.

### CONCLUSION

The pH of  $6.8 \pm 0.2$  representing the pH range between pH 6.0 and pH 7.0 was found to be the optimal condition for acetogenic bacteria growth in both DMP and nDMP. However, nDMP produced the highest power generations and maximum power as compared to the DMP,  $17.63 \text{ mWm}^{-2}$  and  $2.92 \text{ mWm}^{-2}$ , respectively. Additionally, the nDMP substrates for all pH ranges show equal potential to generate power, and the DMP substrates for pH 6.8 and pH 8.0 also have the same potential. Nevertheless, bacteria in nDMP substrates produced relatively higher power generation and maximum power compared to bacteria in the DMP substrates.

### ACKNOWLEDGEMENTS

The authors would like to thank the Ministry of Education (MOE), Malaysia, Universiti Teknologi MARA (UiTM) and Malaysia Palm Oil Board (MPOB) for funding (RAGS and

Khairul Baqir Alkhair Khairul Amin, Oskar Hasdinor Hassan, Sharifah Aminah Syed Mohamed, Yap Kian Chung Andrew, Zulkifli Ab. Rahman, Hazlini Mohamad Ameran, Nurul Khamsatul Akma Kamaruzaman, Tunku Ishak Tunku Kudin, Ab. Malik Marwan Ali, Mohd Zu Azhan Yahya and Muhammad Haikal Zainal

GSAS) this project. Authors are also thankful to UiTM for providing the facilities, and not to forget to FECLRA Palm Oil Factory Nasaruddin in Bota, Perak, for providing the POME samples.

## REFERENCES

- Andrew, Y. K. C., & Manaf, F. Y. A. (2013). Fermentation Pathway for Palm Oil Mill Effluent. *Palm Oil Engineering Bulletin, Oct-Dec*, 109.
- Biffinger, J. C., Byrd, J. N., Dudley, B. L., & Ringeisen, B. R. (2008). Oxygen exposure promotes fuel diversity for *Shewanella oneidensis* microbial fuel cells. *Biosensors and Bioelectronics*, 23, 820–826.
- Gerardi, H. M. (2003). The microbiology of anaerobic digesters, *John Wiley & Sons, Inc*, New Jersey, USA.
- Japar, A. S., Takriff, M. S., Jahim, J. M., & Kadhum, A. A. H. (2013). Acetone–Butanol–Ethanol Fermentation from Palm Oil Mill Effluent Using *Clostridium acetobutylicum*. *Developments in Sustainable Chemical and Bioprocess Technology*, 35–41.
- Liu, H., & Logan, B. E. (2004). Electricity generation using an air-cathode single chamber microbial fuel cell in the presence and absence of a proton exchange membrane. *Environmental Science and Technology*, 38(14), 4040–4046.
- Logan, B. E. (2008). *Microbial Fuel Cells*. New Jersey, USA: John Wiley & Sons, Inc..
- Logan, B. E., Hamelers, B., Rozendal, R., Schröder, U., Keller, J., Freguia, S., & Rabaey, K. (2006). Microbial fuel cells: Methodology and Technology. *Environmental Science and Technology*, 40(17), 5181–5192.
- Malaysian Federal Subsidiary Legislation. (1978). Environmental quality act 1974.
- Nair, R., Renganathan, K., Barathi, S., & Venkatraman, K. (2013). Concentrations using hostel sewage waste as substrate. *International Journal of Advancements in Research and Technology*, 2(5), 326–330.
- Patil, S.A., Harnisch, F., Koch, C., Hübschmann, T., Fetzer, I., Carmona-Martínez, A. a., & Schröder, U. (2011). Electroactive mixed culture derived biofilms in microbial bioelectrochemical systems: The role of pH on biofilm formation, performance and composition. *Bioresource Technology*, 102(20), 9683–9690.
- Rapport, J., Zhang, R., Jenkins, B., & Williams, R. (2008). Current anaerobic digestion technologies used for treatment of municipal organic solid waste. *California Integrated Waste Management Board*, (March), 90.
- Samir, K. K., Rao, Y. S., Zhang, T. C., Buddhi, P. L., Tyagi, R. D., & Kao, C. M. (2010). Bioenergy and Biofuel from Biowastes and Biomass. *Institute of the American Society of Civil Engineers*, 6, 116–126.
- Solera, R., Romero, L. I., & Sales, D. (2002). The evolution of Biomass in a two-phase anaerobic treatment process during start-up. *Chemical and Biochemical Engineering Quarterly*, 16(1), 25–29.
- Torres, C. I., Marcus, A. K., Lee, H. S., Parameswaran, P., Krajmalnik-Brown, R., & Rittmann, B. E. (2010). A kinetic perspective on extracellular electron transfer by anode-respiring bacteria. *FEMS Microbiology Reviews*, 34, 3–17.
- Ziemiński, K., & Frąç, M. (2012). Methane fermentation process as anaerobic digestion of biomass: Transformations, stages and microorganisms. *African Journal of Biotechnology*, 11(18), 4127–4139.



## Optimising Processing Conditions of PLA Nanocomposites Using Response Surface Methodology

Norazura Ibrahim<sup>1\*</sup>, Margaret Jollands<sup>2</sup> and Rajarathinam Parthasarathy<sup>2</sup>

<sup>1</sup>Faculty of Applied Sciences, Universiti Teknologi MARA (UiTM), 40450 Shah Alam, Selangor, Malaysia

<sup>2</sup>Rheology and Materials Processing Centre, School of Civil, Environmental and Chemical Engineering, RMIT University, Melbourne VIC 3000, Australia

### ABSTRACT

Numerous studies of polylactide nanocomposites have been conducted. However, the role and importance of processing conditions is the subject of very few papers. In this work, polylactide and a constant amount (2 %w/w) of organoclay Cloisite® 30B via melt intercalation technique were produced. It is generally believed that maximum benefits are achieved when organoclay is well dispersed in PLA matrix. It might be anticipated that melt processing conditions would have an important influence on the nanocomposites formed. Experimental design was carried out based on Box-Behnken methods, a response surface methodology (RSM) well suited to the goal of process optimisation. Three levels of processing temperature, rotor speed and mixing time were chosen in this study. The response was Young's modulus. The interaction effects with the most influence on the Young's modulus of these PLA/organoclay nanocomposites are temperature and speed. The maximum Young's modulus was predicted to be 1211 MPa at a temperature, speed, and time of 175°C, 100 rpm, and 7 min, respectively. Understanding the influence of processing conditions on the mechanical properties is needed for improving nanocomposites properties. Mathematical model and optimisations plot were used to illustrate the relationship between the parameters and mechanical properties considered. Results of the data analysis using Minitab software are presented.

*Keywords:* Box-Behnken, optimizing, organoclay, polylactide, response surface methodology

### ARTICLE INFO

*Article history:*

Received: 25 October 2016

Accepted: 17 March 2017

*E-mail addresses:*

[norazura.ibrahim@gmail.com](mailto:norazura.ibrahim@gmail.com) (Norazura Ibrahim),

[margaret.jollands@rmit.edu.au](mailto:margaret.jollands@rmit.edu.au) (Margaret Jollands),

[rajarathinam.parthasarathy@rmit.edu.au](mailto:rajarathinam.parthasarathy@rmit.edu.au)

(Rajarathinam Parthasarathy)

\*Corresponding Author

### INTRODUCTION

In recent years, two major areas of study, namely nanocomposites and bio-related materials, have received much attention in industry and academia in the field of composite materials (Alexandre, Michael, & Dubois, 2000; Fischer, 2003; Ray & Okamoto,

2003). The area of nanocomposites has received considerable attention mainly because of the expectation that nanotechnology can lead to lighter and better material for engineering applications. Lately, studies based on bio-nanocomposites using clay as nano reinforcement in polylactic acid (PLA) have been a growing interest as one of the most promising materials with the brightest development prospect. PLA has attracted intensive research attention mainly because it is compostable polymer derived from renewable sources. Overall, PLA possesses the required mechanical and barrier properties desirable for a number of applications to compete with existing petroleum-based thermoplastics (Lim, Auras, & Rubino, 2008). However, PLA has inherent weaknesses in properties such as brittleness, low deflection temperature (HDT) and high price, which limit its widespread implementation (Nampoothiri, Nair, & John, 2010; Nyambo et al., 2010; Wu, 2005). On the other hand, layered silicate is naturally abundant, economic and more importantly, benign to the environment (Ray et al., 2003). Layered silicates such as organically modified montmorillonites (organoclays) appeared to be effective fillers (even at a low concentration, 1–5 wt%) for improving the overall performance of PLA/clay system (Pluta, 2006). Therefore, by producing this hybrid material, one not only obtains new biodegradable nanocomposites with improved properties in comparison with neat biodegradable polymers and enlarged application fields of biodegradable polymers, but the material would not affect the environment as well (Di et al., 2003).

Improvement of the nanocomposites properties should be dependent not only on the organoclay concentration but also on the degree of its dispersion (Pluta, 2006). Dispersion is a very important information because failure can be induced by agglomerates. In a general way, many of the properties associated with polymer clay nanocomposites are a function of the extent of exfoliation of individual clay sheets. The greatest improvement of benefits comes with exfoliated samples. This can be controlled by both the processing conditions and matching the interaction of organomodified clay to the polymer matrix (Pluta, 2006). The latter is well documented (Denault, Ton-That, & Bloch, 2006; Krishnamachari et al., 2009; Paul et al., 2003; Pluta, 2006). However, which processing factor imparts the better level of dispersion is still under discussion (Pogodina et al., 2008). Mixing is the key step in almost every polymer processing operation, affecting material properties, processability and cost (Manas-Zloczower, 1997). Therefore, its fundamental understanding is of prime importance.

PLA nanocomposites formed by melt blending have been described previously (Di et al., 2005; Pluta et al., 2002, 2006; Ray et al., 2003); however, these studies have not reported on how these conditions were chosen. Hence, this paper addresses the issue on how to predict the optimum processing condition of PLA organoclay nanocomposites using an experimental design to develop a model to obtain the desired mechanical properties. Processing temperature, rotor speed and mixing time were chosen because they were considered to have significant effects on the processing of nanocomposites in general (Hasook et al., 2008; Jollands & Gupta, 2010; Modesti et al., 2006; Pluta, 2006). Interaction between several factors greatly affects the performance of final products. Interactions cannot be determined by changing only one



variable at a time. If factors and the interactions between correlated factors are known, the optimum operating condition can be determined.

Design of Experiment (DOE) is widely used in research and development, where a large proportion of resources go towards solving optimisation problems. Statistical data and analysis can help researchers in predicting better processing conditions or better properties, leading to better outcomes of studies of materials such as nanocomposites. Process and property optimisation can save time, cost and energy. Application of DOE techniques by the engineering fraternity is limited; and research shows that when applied, they are often performed incorrectly (Antony & Kaye, 1995) because of the lack of skills in manufacturing and lack of statistical knowledge (Antony & Kaye, 1997).

The objectives of this study were to investigate the effects of temperature, speed and time on preparing nanocomposite composed of PLA with a constant amount of organoclay Cloisite® 30B (2 wt%), and construct models to predict the modulus of nanocomposite. The influence of operating conditions on the organoclay dispersion (nanostructure) on the modulus of the nanocomposites is discussed. The results of data analysis using Minitab software are presented.

## **MATERIALS AND METHOD**

### **Materials**

PLA 2002D from NatureWorks® was used as the matrix. Organically treated montmorillonite (MMT) Cloisite® 30B from Southern Clay Product was used as a filler. In order to remove water and other volatile components, PLA pellets and clays were dried in a vacuum oven at 90°C for 24 hours prior to processing.

**Preparation of the nanocomposites.** PLA pellets and a constant amount (2 %w/w) of organoclay Cloisite® 30B were melt-blended in a counter rotating Haake internal mixer. The samples were moulded by compression moulding at 190°C for 3 min before being subjected to mechanical measurements.

### **Characterisation**

An Instron model 4465 Universal Testing Frame was used to perform the tests and measure Young's modulus. The test was conducted at a constant rate of 5 mm/min at room temperature according to ASTM D638. All the samples were stored in a desiccator prior to testing.

**Experimental Design.** The experimental design was carried out based on the Box-Behnken design, a response surface methodology (RSM) well suited to the goal of process optimisation. Ferreira et al. (2007) reported that the Box-Behnken design was much more efficient than the three-level full factorial designs. Three levels of processing temperature, rotor speed and mixing

time with a constant amount (2 wt%) of organoclay Cloisite® 30B were selected for the study. The output was Young's modulus. Young's modulus was used because the mechanical function is more sensitive to changes in the microstructure of nanocomposites. The experimental data were analysed using Minitab Statistical software. The software developed a 15-run design, which included 12 combinations of the factors plus three centre points (in which all factors are at their central values), and used for fitting a second-order response surface. The three centre point runs were added to provide as a measure of process stability and inherent variability (Dong et al., 2009). A significance level of 0.05 was used for all the statistical analyses. Table 1 presents the factors and levels identified for the experiment.

Table 1  
*List of control parameters and their level for the experiment*

Control parameters	Parameter labels	Units	Low levels (-1)	High levels (+1)
Temperature	$x_1$	°C	175	195
Speed	$x_2$	rpm	60	100
Time	$x_3$	min	5	9

For predicting the optimal point, a second-order polynomial model was fitted to correlate the relationship between independent variables and response (Young's modulus). For the three factors, the equation is as follows:

$$Y = \beta_o + \sum \beta_i x_i + \sum \beta_{ii} x_i^2 + \sum \beta_{ij} x_i x_j \quad [1]$$

Where Y is the predicted response;  $\beta_o$  is model constant;  $\beta_i$  is the coefficient of  $i$ th individual factor,  $\beta_{ii}$  is the coefficient of  $i$ th factor squared,  $\beta_{ij}$  is the coefficient of interaction between the  $i$ th and  $j$ th factors, and  $x_n$  ( $n = i, j$ ) is the variable or factor value. The quality of fit of the polynomial model equation was expressed by the coefficient of determination  $R^2$ .

## RESULTS AND DISCUSSION

### Data Analysis and Interpretation

Upon obtaining the response values, the first step in the analysis involved finding the significant parameters. The results in Table 2 show the average values of four samples. The analysis was done using coded units. Use of coded units helps to eliminate any spurious statistical results due to different measurement scales of the factors, and makes them easy to interpret (Malik, Malik, Hussain, & Arain, 2011).

Table 2  
The experimental design according to Box-Behnken method

Run	x <sub>1</sub>	x <sub>2</sub>	x <sub>3</sub>	Young's Modulus (MPa)		Difference (%)
				Experimental	Predicted	
1	185	80	7	1,150	1,180	-2.2
2	175	100	7	1,210	1,210	0.3
3	195	60	7	1,190	1,190	0.0
4	175	60	7	1,140	1,150	-1.1
5	185	80	7	1,190	1,180	1.1
6	185	100	5	1,140	1,130	0.8
7	195	80	5	1,100	1,130	-2.6
8	175	80	5	1,150	1,130	1.9
9	175	80	9	1,120	1,130	-0.4
10	195	100	7	1,170	1,150	1.4
11	195	80	9	1,140	1,120	1.9
12	185	60	9	1,130	1,120	1.2
13	185	60	5	1,120	1,120	0.0
14	185	80	7	1,180	1,180	0.5
15	185	100	9	1,100	1,130	-2.6

Table 3  
Estimated regression coefficients for modulus

Term	Coef	SE Coef	T	P
Constant	1173.75	11.637	100.866	0.000
Temperature	-4.24	7.126	-0.594	0.578
Speed	4.36	7.126	0.612	0.567
Time	-2.08	7.126	-0.291	0.783
Temperature*Temperature	3.96	10.489	0.378	0.721
Speed*Speed	0.11	10.489	0.010	0.992
Time*Time	-48.66	10.489	4.639	-0.006
Temperature*Speed	-26.17	10.078	-2.597	0.048
Temperature*Time	19.10	10.078	1.895	0.117
Speed*Time	-12.90	10.078	-1.280	0.257

From the analysis and output shown in Table 3, p-values for the estimated coefficients of quadratic terms (Time\*Time) and interaction (Temp\*Speed) are 0.006 and 0.048, respectively, indicating that they are significantly related to modulus at an  $\alpha$ -level of 0.05. The adequacy of the model can be checked with R<sup>2</sup> and R<sup>2</sup><sub>adjusted</sub>. R<sup>2</sup><sub>adjusted</sub> is considered rather than solely relying on R<sup>2</sup> value because the R<sup>2</sup> value can be easily increased by adding more variables, regardless of whether these factors are statistically significant or not (Montgomery, 2009). The R<sup>2</sup> and R<sup>2</sup><sub>adjusted</sub> values for the above regression model are 88% and 65%, respectively. These values

indicated that the model fits the data well. In general, the higher the  $R^2$ , the better the model will fit our data. The polynomial model for Young's modulus ( $Y$ ) was regressed by considering only the significant terms, and this is shown below:

$$Y = -1291.8 + 10.0445x_1 + 24.4253x_2 + 170.290x_3 - 12.2377x_3^2 - 0.130850x_{12} \quad [2]$$

### Determination of the Optimal Conditions

The optimum conditions were determined using the Minitab Response Optimiser. Response optimisation is often useful in product development when determining the operating conditions, which results in desirable properties of a product. It helps to identify the combination of input variable settings that jointly optimise a single response or a set of responses. This is useful when evaluating the impacts of multiple inputs on a response.

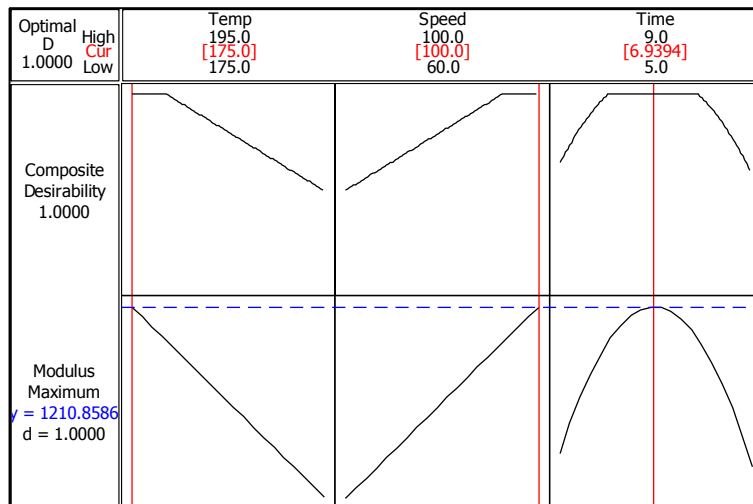


Figure 1. Optimisation plot

In Figure 1, the optimisation plot shows the effect of each factor (columns) on the response or composite desirability (rows). The vertical red lines on the graph represent the current factor settings. The numbers displayed at the top column (in red) show the current factor level settings. The horizontal blue lines and numbers represent the responses for the current factor level.

**Temperature.** Decreasing the temperature moves Young's modulus to its maximum because PLA undergoes thermal degradation at temperatures above 200°C (Garlotta, 2001). Since mixing increases the compound temperature, this suggests that it might be worthwhile to experiment with lower temperatures.

**Speed.** If we extrapolate the plots to higher values of speed, it appears that Young's modulus could be increased. This suggests that the experiment with high speed might be more desirable as it maximises the polymer–clay interactions, making the surface of layers ready for the polymer interaction. This should lead to the significant change in mechanical properties.

**Time.** In this model, Young's modulus depends on Time\*Time, indicating that as time increases, Young's modulus increases quadratically with time. Increasing the time up to middle setting moves Young's modulus to its maximum, but a further increase in time will reduce Young's modulus. This result agrees with the previous data presented by Denault et al. (2006) who suggested that longer compounding time and higher compounding temperature would lead to organoclay degradation.

According to the best fit model to the data, the maximum Young's modulus was predicted to be 1211 MPa at a temperature, speed and time of 175°C, 100 rpm, and 7 min, respectively. The model was tested for robustness by making samples at the predicted optimum mixing condition, where the measured modulus was then compared with the prediction. The modulus of a sample made at the optimum condition was 1240 MPa, which is higher by 2.4% than what was predicted by the best fit model. Hence, the agreement between the measured and predicted response is considered to be reasonable and the model is considered as robust. The optimum modulus (1240 MPa) is also 7.8% higher than the average modulus for the BBD runs (1150 MPa), so it is significant at the 99% confidence level.

Although numerical optimisation along with graphical analysis can provide useful information, it is not a substitute for subject matter expertise. Relevant background information, theoretical principles and knowledge gained through observation or previous experimentation need to be considered when applying these methods (Minitab Inc., 2007).

It is important to note that determination of the optimum conditions is specific for this nanocomposite material in this mixing configuration. When different materials or mixers are used, the optimum condition will also change. This is in good agreement with the optimum process conditions reported by Dennis et al. (2001).

## CONCLUSION

In order to optimise the processing conditions for preparing polylactide nanocomposites, the Box-Behnken design was applied to investigate three variables; processing temperature, rotor speed and mixing time, as highlighted in this study. The interaction effects with the most influence on the Young's modulus of these PLA/organoclay nanocomposites are temperature and speed. Young's modulus also increases quadratically with time.

The data were fitted with a simple mathematical model that was used to predict the condition to maximise Young's modulus. The maximum Young's modulus was predicted to be 1211 MPa at a temperature, speed and time of 175°C, 100 rpm, and 7 min, respectively. The model was found to be robust. Samples produced at the predicted optimum temperature, speed and time had a significant increase in modulus of 7.8% compared with the average readings for all the runs. Hence, making samples at optimised conditions improved the modulus significantly.

The application of Box-Behnken designs can provide answers to specific questions on the behaviour of a system using an optimum number of experimental observations. Thorough investigations into the nanocomposite morphology (transmission electron microscopy and small-angle X-ray scattering) are currently under investigation; the influence of nanoclay filler content is also being investigated. These will be the subject of a forthcoming article.

## ACKNOWLEDGEMENTS

The authors gratefully acknowledge the Ministry of Higher Education (MOHE), Malaysia, and Universiti Teknologi MARA for the scholarship support.

## REFERENCES

- Alexandre, M., & Dubois, P. (2000). Polymer-layered silicate nanocomposites: preparation, properties and uses of a new class of materials. *Materials Science and Engineering: R: Reports*, 28(1), 1-63.
- Antony, J., & Kaye, M. (1995). Experimental quality *Journal Manufacturing Engineer (UK)* 74(4), 178-181.
- Antony, J., & Kaye, M. (1997). Use your reason to understand statistics. *Quality World*, 23(10), 850-853.
- Denault, J., Ton-That, M. T., & Bloch, J. (2006). (2006). Poly(lactic acid) Nanocomposites: Fabrication Microstructure and Performance. *Design, Applications of Composites Proceedings of the Sixth Joint Canada-Japan Workshop on Composites*, 11-19.
- Dennis, H. R., Hunter, D. L., Chang, D., Kim, S., White, J. L., Cho, J. W., & Paul, D. R. (2001). Effect of melt processing conditions on the extent of exfoliation in organoclay-based nanocomposites. *Polymer*, 42(23), 9513-9522.
- Di, Y., Iannace, S., Di Maio, E., & Nicolais, L. (2003). Nanocomposites by melt intercalation based on polycaprolactone and organoclay. *Journal of Polymer Science Part B: Polymer Physics*, 41(7), 670-678. doi: 10.1002/polb.10420
- Di, Y., Iannace, S., Maio, E. D., & Nicolais, L. (2005). Poly(lactic acid)/organoclay nanocomposites: Thermal, rheological properties and foam processing. *Journal of Polymer Science Part B: Polymer Physics*, 43(6), 689-698. doi: 10.1002/polb.20366
- Dong, C. H., Xie, X. Q., Wang, X. L., Zhan, Y., & Yao, Y. J. (2009). Application of Box-Behnken design in optimisation for polysaccharides extraction from cultured mycelium of *Cordyceps sinensis*. *Food and Bioproducts Processing*, 87(2), 139-144.
- Ferreira, S. L. C., Bruns, R. E., Ferreira, H. S., Matos, G. D., David, J. M., Brandão, G. C., & Santos, W. N. L. (2007). Box-Behnken design: An alternative for the optimization of analytical methods. *Analytica Chimica Acta*, 597(2), 179-186.
- Fischer, H. (2003). Polymer nanocomposites: from fundamental research to specific applications. *Materials Science and Engineering, C*, 23, 763-772.
- Garlotta, D. (2001). A literature review of poly(lactic acid). *Journal of Polymers and the Environment*, 9(2), 63-84. doi: 10.1023/a:1020200822435

- Hasook, A., Muramatsu, H., Tanoue, S., Iemoto, Y., & Unryu, T. (2008). Preparation of nanocomposites by melt compounding polylactic acid/polyamide 12/organoclay at different screw rotating speeds using a twin screw extruder. *Polymer Composites*, 29(1), 1-8. doi: 10.1002/pc.20336
- Jollands, M., & Gupta, R. K. (2010). Effect of mixing conditions on mechanical properties of polylactide/montmorillonite clay nanocomposites. *Journal of Applied Polymer Science*, 118(3), 1489-1493. doi: 10.1002/app.32475
- Krishnamachari, P., Zhang, J., Lou, J., Yan, J., & Uitenham, L. (2009). Biodegradable Poly(Lactic Acid)/Clay Nanocomposites by Melt Intercalation: A Study of Morphological, Thermal, and Mechanical Properties. *International Journal of Polymer Analysis and Characterization*, 14(4), 336-350.
- Lim, L.-T., Auras, R., & Rubino, M. (2008). Processing technologies for poly(lactic acid). *Progress in Polymer Science*, 33, 820-852.
- Malik, Z. A., Malik, M. H., Hussain, T., & Arain, F. A. (2011). Development of Models to Predict Tensile Strength of Cotton Woven Fabrics. *Journal of Engineered Fibers and Fabrics*, 6(4).
- Manas-Zloczower, I. (1997). Analysis of mixing in polymer processing equipment. *Rheology Bulletin*, 66(1), 5-8.
- Minitab Inc. (2007). Minitab Statistical Software, Release 15 for Windows. State College, Pennsylvania: Minitab® is a registered trademark of Minitab Inc.
- Modesti, M., Lorenzetti, A., Bon, D., & Besco, S. (2006). Thermal behaviour of compatibilised polypropylene nanocomposite: Effect of processing conditions. *Polymer Degradation and Stability*, 91(4), 672-680.
- Montgomery, D. C. (2009). *Design and analysis of experiments*. Hoboken, N.J.: Wiley.
- Nampoothiri, K. M., Nair, N. R., & John, R. P. (2010). An overview of the recent developments in polylactide (PLA) research. *Bioresource Technology*, 101(22), 8493-8501.
- Nyambo, C., Mohanty, A. K., & Misra, M. (2010). Polylactide-Based Renewable Green Composites from Agricultural Residues and Their Hybrids. *Biomacromolecules*, 11(6), 1654-1660. doi: 10.1021/bm1003114
- Paul, M. A., Alexandre, M., Degée, P., Henrist, C., Rulmont, A., & Dubois, P. (2003). New nanocomposite materials based on plasticized poly(L-lactide) and organo-modified montmorillonites: thermal and morphological study. *Polymer*, 44, 443-450.
- Pluta, M. (2006). Melt compounding of polylactide/organoclay: Structure and properties of nanocomposites. *Journal of Polymer Science Part B-Polymer Physics*, 44(23), 3392-3405. doi: Doi 10.1002/Polb.20957
- Pluta, M., Galeski, A., Alexandre, M., Paul, M. A., & Dubois, P. (2002). Polylactide/montmorillonite nanocomposites and microcomposites prepared by melt blending: Structure and some physical properties. *Journal of Applied Polymer Science*, 86(6), 1497-1506. doi: 10.1002/app.11309
- Pluta, M., Paul, M. A., Alexandre, M., & Dubois, P. (2006). Plasticized polylactide/clay nanocomposites. I. The role of filler content and its surface organo-modification on the physico-chemical properties. *Journal of Polymer Science Part B-Polymer Physics*, 44(2), 299-311.

- Pogodina, N. V., Cerclé, C., Avérous, L., Thomann, R., Bouquey, M., & Muller, R. (2008). Processing and characterization of biodegradable polymer nanocomposites: detection of dispersion state *Rheologica Acta*, 47(5-6), 543-553.
- Ray, S. S., & Okamoto, M. (2003). Polymer/layered silicate nanocomposites: a review from preparation to processing. *Progress in Polymer Science*, 28, 1539-1641.
- Ray, S. S., Yamada, K., Okamoto, M., & Ueda, K. (2003). (2003). New polylactide-layered silicate nanocomposites. 2. Concurrent improvements of material properties, biodegradability and melt rheology. *Polymer*, 44, 857-866.
- Ray, S. S., Yamada, K., Okamoto, M., Fujimoto, Y., Ogami, A., & Ueda, K. (2003). New polylactide/layered silicate nanocomposites, 5. Designing of materials with desired properties. *Polymer*, 44(21), 6633-6646.
- Wu, C. S. (2005). Improving polylactide/starch biocomposites by grafting polylactide with acrylic acid - Characterization and biodegradability assessment. *Macromolecular Bioscience*, 5(4), 352-361. doi: 10.1002/mabi.200400159





## Modified Spent Tea Leaves as Bioadsorbent for Methyl Orange Dye Removal

Lim Ying Pei<sup>1</sup>, Amira Nadzirah Suhaidi<sup>1</sup>, Siti Marziya Zulkifli<sup>1</sup>,  
Syamil Hidayat Hassim<sup>1</sup>, Devagi Kanakaraju<sup>3</sup> and Lim Ying Chin<sup>2\*</sup>

<sup>1</sup>Faculty of Chemical Engineering, Universiti Teknologi MARA (UiTM), 40450 Shah Alam, Selangor, Malaysia

<sup>2</sup>Faculty of Applied Sciences, Universiti Teknologi MARA (UiTM), 40450 Shah Alam, Selangor, Malaysia

<sup>3</sup>Faculty of Resource Science and Technology, Universiti Malaysia Sarawak (UNIMAS),  
94300 Kota Samarahan, Sarawak, Malaysia

### ABSTRACT

In this work, the removal of Methyl Orange (MO) from aqueous solution was studied using a new non-conventional and eco-friendly adsorbent, spent tea leaves (STL). Untreated and acid treated STL were used as bio-adsorbent for removal of MO using batch method. Effects of different STL dosages (1 – 4 g), pH solutions (2–11) and initial dye concentrations (10 – 60 mg/L) were investigated. Adsorption experiments conducted using acid treated STL resulted in higher MO removal efficiency ranging from 79 to 92% for 1-4 g of adsorbent dosage compared to the untreated ones which resulted in only 18 to 56% of removal for the similar amount of dosage. In addition, acidic condition favours the MO removal as compared to alkaline medium. Experimental data were analysed using the Langmuir and Freundlich models of adsorption and it was found that adsorption isotherm was best described by Freundlich model and pseudo-first order equation with high correlation coefficient. Results revealed that acid treated STL, being a waste, has the greater potential to be used as adsorbent for MO removal from aqueous solution.

*Keywords:* Adsorption, bioadsorbent, biosorption, Methyl Orange (MO), Spent Tea Leave (STL)

### ARTICLE INFO

*Article history:*

Received: 25 October 2016

Accepted: 17 March 2017

*E-mail addresses:*

yingpei@salam.uitm.edu.my (Lim Ying Pei),  
amira\_nadziroxx@yahoo.com (Amira Nadzirah Suhaidi),  
sittimardziahzulkifli@gmail.com (Siti Marziya Zulkifli),  
syamil.hidayat92@yahoo.com (Syamil Hidayat Hassim),  
kdevagi@unimas.my (Devagi Kanakaraju),  
limyi613@salam.uitm.edu.my (Lim Ying Pei)

\*Corresponding Author

### INTRODUCTION

Textile dyeing and clothing is a major industry at present, globally and in Malaysia. Effluents from the textile industry are considered as one of the most problematic wastewaters and its removal has turned into a serious environmental problem. Those wastewaters are characterised by the presence of colour, high total organic carbon (TOC) levels, as well as chemical oxygen demand, mainly

due to the presence of highly coloured synthetic dyes and other organic by products. Dye effluents are usually recalcitrant to natural biological degradation or even biocides, and it is also highly toxic to aquatic organisms (Ovejero et al., 2013). Consequently, many treatment processes have been applied to remove dyes from wastewater. These processes include solar photo-Fenton degradation, photocatalysis, integrated chemical–biological degradation, and membrane filtration. However, vast applications of such processes are restricted due to technical, or economical constraint.

Biosorption, on the other hand, is an effective technology to treat dye effluents (Kaushik & Malik, 2009; Yagub et al., 2014) as it provides suitable adsorbent. Activated carbon has been widely used as an adsorbent for the removal of contaminants from wastewater. However, high operational cost hinders its commercial applications. Cheap and abundantly available adsorbents such as chitosan (Devi, Al-Hashmi, & Sekhar, 2012), fly ash (Mohan & Gandhimathi, 2009), cashew nutshell (Kumar et al., 2010), sawdust (Cheng et al., 2012) and tea leaves (Akar, Altinişik, & Seki, 2013; Zuorro, Lavecchia, Medici, & Piga, 2013) can be used as alternatives to activated carbon. Nearly 18-20 billion cups of tea are being drunk daily and tea producers are facing problem in disposing used tea leaves (STL) after tea extraction. Thus, the motivation of the present study is to utilise the waste (raw and acid treated STL) as biosorbent for the decolourisation of Methyl Orange (MO) from aqueous solution. The adsorption capacity and removal efficiency of both STLs was compared using batch method.

## **MATERIALS AND METHOD**

### **Preparation of Bio-Adsorbent**

STL were bought from nearby supermarkets and their country of origin is China. The tea leaves were washed with distilled water to remove the adhesive dirt. Then, the leaves were repeatedly boiled with distilled water until the filtrate turned into clear solution. The leaves were then dried in an oven at 100°C for 24 hours. Thereafter, the leaves were separated into two portions. The first portion of the leaves was immersed in 0.1 M HCl for 8 hrs at room temperature, while the other portion was left untreated. The leaves were then washed thoroughly with distilled water and then dried in the oven for 24 hrs. The dried STL were stored in a glass bottle until further use.

### **Biosorption Experiments**

The bio-sorption experiments were carried out in 250 ml Erlenmeyer flask containing different amounts of bio-adsorbent and 200 ml of diluted MO dye solution at desired concentration and pH. The flasks were then placed on an incubator shaker with constant agitation for 180 minutes at room temperature. The effect of adsorbent dosage (1 – 4 g), pH solution (2 – 11) and initial dye concentration (10 – 60 mg/L) were studied. Samples were collected using syringes at predetermined time intervals. The concentrations of MO were determined using

HACH spectrophotometer (Model DR2800) at 463 nm, the  $\lambda_{\max}$  for MO. The amount of MO adsorbed onto the bio-adsorbent at equilibrium was calculated using the following Equation:

$$q_{\text{eq}} = \frac{(C_0 - C_e)V}{X} \quad [1]$$

Where,  $C_0$  and  $C_e$  are the concentration at initial and equilibrium of MO in mg/L,  $V$  (L) is the volume of solution, and  $X$  (g) is the weight of adsorbent in the flask.

### Adsorption Isotherm Models

Langmuir adsorption model is based on the model of ideal monolayer adsorbed (Salleh et al., 2011). The Langmuir is adsorption isotherm model that the adsorption takes place at specific homogeneous sites of the surface of the adsorbent. The Langmuir can be expressed by the following Equation:

$$\frac{1}{q_t} = \frac{1}{q_m C_t b} + \frac{1}{q_m} \quad [2]$$

Where,  $q_t$  (mg/g) is the amount of dye adsorption at given time,  $q_m$  (mg/g) is the monolayer adsorption capacity,  $b$  is the constant related to the free energy of adsorption (L/mg), and  $C_t$  (mg/L) is the concentration of the solute in the bulk solution at given time. The Freundlich adsorption isotherm model involves a heterogeneous adsorption surface that has uneven available sites with different adsorption energies (Yagub et al., 2014). The Freundlich adsorption isotherm model is shown in the following Equation:

$$\ln q_t = \ln K_F + \frac{1}{n} \ln C_t \quad [3]$$

Where,  $K_F$  ( $\text{mg}^{1-1/n} \text{L}^{1/n} / \text{g}$ ) is roughly an indicator of the adsorption capacity, and  $1/n$  is the adsorption intensity that gives an indication of the favourability adsorption condition (Dada, Olalekan, Olatunya, & Dada 2012).

### Adsorption Surface Analysis

The surface morphology of both the untreated and acid treated STL, before and after the biosorption experiment, was characterised using Field Emission Scanning Electron Microscope (FESEM) (Carl Zeiss SUPRA 40VP FESEM) operating at 10 kV.

## RESULTS AND DISCUSSION

The surface morphologies of the untreated and acid treated STL before and after the MO adsorption analysed using FESEM are shown in Figure 1. For the untreated STL, rough surface with little voids could be seen. The surface morphology after the MO adsorption showed that most voids had been disappeared was likely due to the adsorption of MO molecules onto the pores. As for the acid treated STL, rougher surface, higher numbers of pores and void channels are visible (Figure 1(c)) compared to the micrograph of the untreated STL (Figure 1(a)).

Meanwhile, the surface became smoother and most pores have been filled with MO molecules after the adsorption experiment (Figure 1(d)).

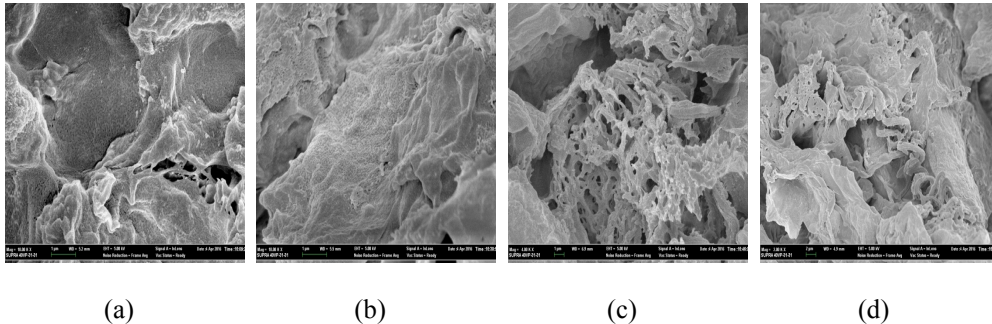


Figure 1. FESEM micrograph of the untreated STL: (a) before; (b) after the adsorption of MO and acid treated STL; (c) before; and (d) after the adsorption of MO

### Effect of Adsorbent Dosage

The effect of STL adsorbent (untreated and acid treated) dosage on the removal efficiency and adsorption capacity of MO was studied for an initial MO concentration of 20 mg/L and solid to liquid ratio was set from 5 to 20 g/L. Figure 2 and Figure 3 show the results obtained for the untreated and acid treated STL, respectively. As shown in Figure 3(a), when the dosage of the untreated STL was increased from 1 g (5 g/L) to 4 g (20 g/L), the percentage removal of MO also increased from 18% to 56%, respectively. Nonetheless, this was somehow expected as the surface area of the adsorbent and the sorption sites increased with the increasing adsorbent loading (Gong Sun, & Kong, 2013). Khosla, Kaur and Dave (2013) reported a high removal of basic yellow 2 and acid orange A from aqueous solution using the same type of adsorbent. A similar observation was also reported for the removal of MO using chitosan/alumina composite, although with much lower adsorbent dosages of 1-12 g/L (Zhang, Zhou, & Ou, 2012). The adsorption capacity decreased from 0.78 mg/g to 0.57 mg/g when the adsorbent dosage was increased from 1 g to 4 g due to the reduction in the effective surface area (Figure 3(b)).

The acid treated STL demonstrated a similar removal trend to the untreated STL. However, higher MO removal was attained when acid treated STL was used. The percentage removal obtained for 1 g, 2 g and 4 g adsorbent dosages of acid treated STL was 79%, 91% and 92%, respectively (Figure 3(a)). This result can be supported by the FESEM morphology of the acid treated STL, which showed higher surface roughness after being treated with HCl (Figure 1a) than that of the untreated STL (Figure 1(c)). A study on the adsorption of methylene blue dye onto the untreated and modified raw mango seed also revealed similar findings (Kahraman, Yalcin, & Kahraman, 2012). Based on the results obtained, the optimum dosage for acid treated STL was fixed at 2 g as the higher dosage studied, 4 g, also resulted in an almost similar percentage of MO removal after 180 min of treatment. In addition, both adsorbent dosages achieved a plateau after 80 min of contact time. This could be attributed to the saturated adsorbent surface with MO molecules. MO molecules could have fully occupied and adsorbed

onto the adsorption sites of acid treated and untreated STL within 80 min of reaction time. The adsorption capacity of the acid treated STL decreased from 2.89 mg/g to 0.73 mg/g as the dosage of STL increases, as depicted in Figure 3(b).

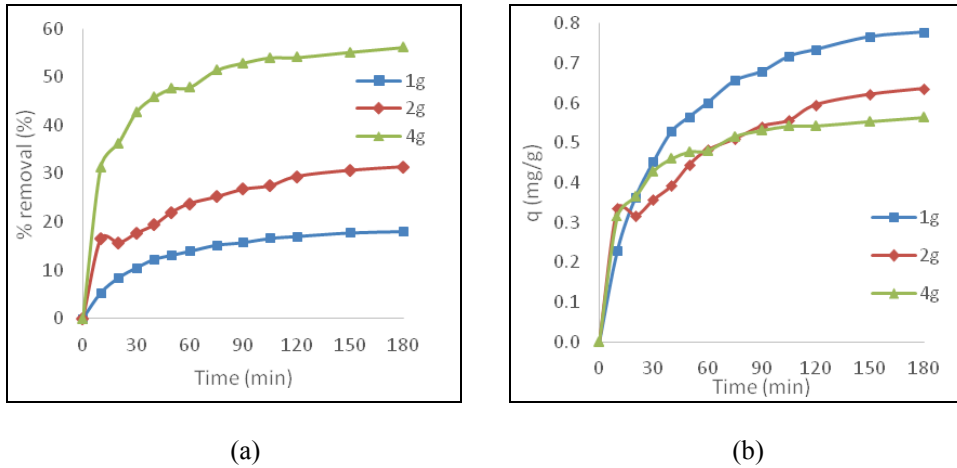


Figure 2. Effects of the untreated STL dosage on the: (a) percentage removal; and (b) adsorption capacity of MO

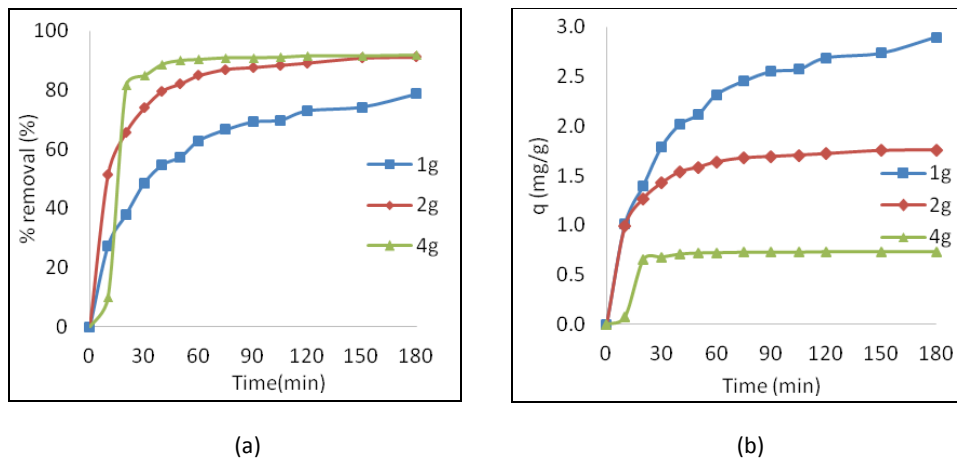
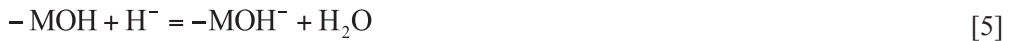


Figure 3. Effects of the acid treated STL dosage on the: (a) percentage removal; and (b) adsorption capacity of MO

### Effect of pH

To determine the effect of pH on the MO adsorption, the solution pH was varied from pH 2 to 11 for untreated STL and pH 2 to 9 for acid treated STL, while the initial concentration and adsorbent dosage were fixed as 10 mg/L and 4 g. MO is classified as an anionic dye. The

surface of MO will be positively charged at low pH and negatively charged at high pH, as shown in the equations below (Bajpai & Jain, 2010):



In general, the percentage adsorption and adsorption capacity of the acid treated STL and untreated STL decreased when pH was increased from pH 2 to 9 and pH 2 to 11, respectively (Figure 4(a) and Figure 4(b)). However, the acid treated STL yielded much higher adsorption percentage, as well as adsorption capacity, compared to the untreated STL for the studied pH ranges. About 90% of MO was adsorbed by acid treated STL at pH 2, while untreated STL only adsorbed 55% of MO at the same pH (Figure 4(b)). As for the adsorption capacity, the highest values were recorded at highly acidic condition (pH 2) for both the untreated STL (1.0 mg/g) and acid treated STL (1.9 mg/g) although the adsorption capacity of the latter was almost two folds higher (Figure 4a). The result obtained in this study corroborates with a research which reported that the highest removal of MO using modified coffee waste occurred at acidic pH, the optimum pH (Lafi & Hafiane, 2016). The low adsorption of MO at alkaline pH is due to the presence of excess OH<sup>-</sup> ions that compete with the anion, -MOH<sup>-</sup> for adsorption sites.

Based on the results obtained, pH 2 was concluded as the optimum pH for MO adsorption to take place using both acid treated STL and untreated STL under the investigated conditions.

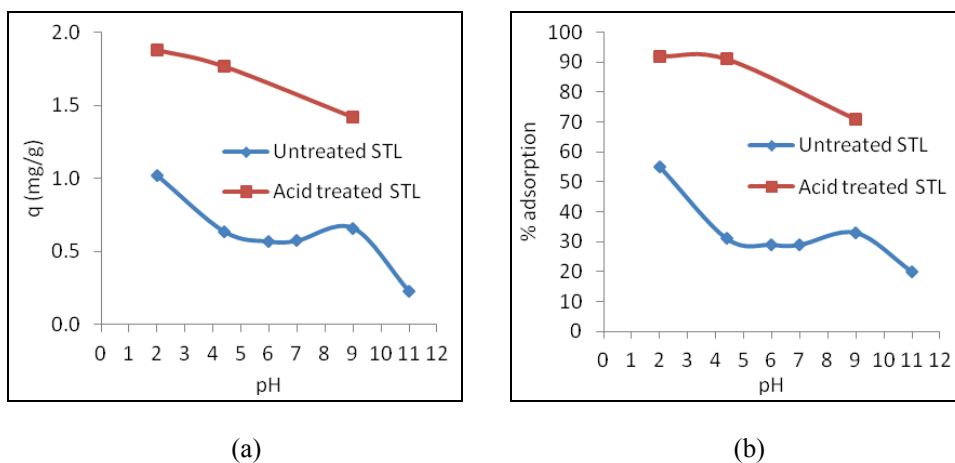


Figure 4. Effects of pH of the untreated and acid treated STL on the: (a) adsorption capacity; and (b) percentage adsorption of MO

### Effect of Initial Concentration

The concentration of MO was varied from 10 to 60 mg/L to study the effects of initial concentration on the adsorption capacity of MO. Solution pH was not adjusted while the adsorbent dosage of the untreated STL and acid treated STL was fixed as 4 g. Figure 5(a)

and Figure 5(b) show that the amount of MO adsorbed increased with the increasing initial concentration of MO. The amount of MO adsorbed at equilibrium  $q_e$  for the untreated STL increased from 0.34 to 1.40 mg/g as the initial concentration of MO increased from 10 to 60 mg/L, while for acid treated STL, the amount of MO adsorbed increased from 0.98 to 4.49 mg/g when the initial concentration of MO was increased from 10 to 60 mg/L. A similar phenomenon was also observed for the removal of MO from aqueous solution using activated carbon derived from *Phragmites australis* (Chen et al., 2010).

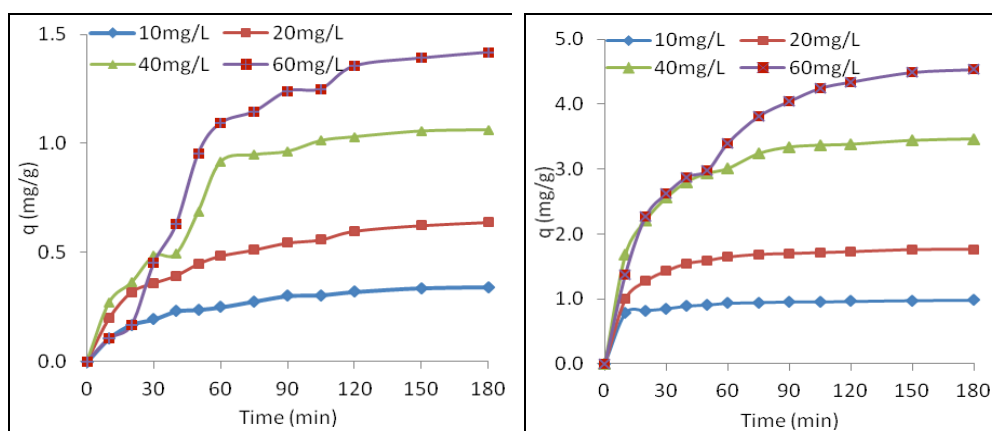


Figure 5. Effects of different initial concentrations of MO on the adsorption capacity of: (a) untreated STL; and (b) acid treated STL

All the adsorption curves, particularly the curves of high initial concentrations of MO, 20 to 60 mg/L show two zones: (i) rapid adsorption zone; and (ii) equilibrium adsorption zone. Rapid adsorption occurred for the initial 60 min of contact time for the untreated STL, whilst the initial 50 min of contact time represents this type of zone for the acid treated STL. As for the untreated STL, all initial concentrations of MO achieved equilibrium conditions at 150 min of contact time. However, the time required for acid treated STL to achieve equilibrium conditions differs with the initial concentrations of MO. For example, for the lower initial concentrations of MO, 10 and 20 mg/L, approximately 30 to 50 min was needed for attaining equilibrium while higher initial concentrations of MO, 40 and 60 mg/L consumed much longer time, about 150 min to achieve similar condition. An equilibrium adsorption time of 70 min was reported for the adsorption of MO onto banana peel and orange peel for 50 mg/L of MO (Annadurai, Juang, & Lee, 2002). The findings from this study suggest that STL is able to provide adsorption sites for MO adsorption to occur both at low and high initial concentrations of MO. This simply means that adsorption sites remained unsaturated until equilibrium was achieved.

## Adsorption Isotherms

The adsorption isotherms, Langmuir isotherm and Freundlich isotherm analyses were carried out to determine the behaviour of the adsorbate, MO over different adsorbent surfaces. The analysis was done by varying the initial MO concentrations from 10 to 60 mg/L while fixing the adsorbent dosage at 2 g. The obtained isotherm constants and correlation coefficients ( $R^2$ ) are tabulated in Table 1. The Langmuir model is represented by Equation [2] while the Freundlich adsorption model is represented by Equation [3].

Table 1

*Langmuir and Freundlich isotherm constant and correlation coefficient ( $R^2$ ) for untreated STL and acid treated STL*

Isotherm	Langmuir			Freundlich		
	Parameters	$q_m$ (mg/g)	b (mg/L)	$R^2$	KF	n
Untreated STL	2.90	0.02	0.88	0.088	1.37	0.98
Acid treated STL	3.20	2.12	0.67	1.68	2.71	0.95

Langmuir adsorption isotherm assumes monolayer coverage of adsorbate over a homogenous adsorbent surface. Within the adsorbate, the adsorption of the dyes onto the surface sites only occurs once and no further adsorption will happen once a dye molecule occupies the site. Meanwhile, the Freundlich adsorption isotherm assumes that the adsorption takes place at the heterogeneous surfaces site with the adsorption capacity directly proportional to the concentration of MO dye.

As can be seen from Table 1, judging from the  $R^2$  of both untreated STL ( $R^2 = 0.98$ ) and treated STL ( $R^2 = 0.95$ ), the adsorption data were fitted well to Freundlich isotherm than the Langmuir isotherm model. The Freundlich constant, adsorption capacity ( $K_F$ ) and n for the untreated STL were 0.088 and 1.37, respectively, whereas for acid treated STL,  $K_F$  and n were found to be 1.68 and 2.71, respectively. The greater the value of  $K_F$ , the better is the biosorption of MO. Meanwhile, adsorption intensity, n, that is greater than 1 shows the favourable adsorption. Thus, the adsorption of MO occurs on the heterogeneous surface sites.

## Adsorption Kinetic Models

The kinetics of the MO adsorption on STL was analysed using three kinetic models, namely pseudo first order, and pseudo second order and intra particle diffusion. The Pseudo-first order can be expressed in the following Equation:

$$\frac{dq}{dt} = K_1(q_e - q_t) \quad [6]$$



Where,  $K_1$  ( $\text{min}^{-1}$ ) is the rate constant of the Pseudo-first order adsorption,  $q_e$  ( $\text{mg/g}$ ) is the amount of adsorption in equilibrium and  $q_t$  ( $\text{mg/g}$ ) is the amount of dye adsorption at any given time. For the Pseudo-second order equation, the equation can be expressed in Equation [6]:

$$\frac{dq}{dt} = K_2 (q_e - q_t)^2 \tag{7}$$

Where,  $K_2$  ( $\text{g mg}^{-1} \text{min}^{-1}$ ) is the adsorption rate constant Pseudo-second order, while other parameters are those as explained for Equation [6]. The Intraparticle diffusion can be expressed as in Equation [8]:

$$q_t = K_3 t^{0.5} + C \tag{8}$$

Where,  $K_3$  ( $\text{mg g}^{-1} \text{min}^{-0.5}$ ) is the Intraparticle diffusion constant, and  $C$  is the plot intercept. The plot intercept gives an idea about the thickness boundary layer at which when the intercept value is high, the greater the thickness of the boundary layer. Among those three sorption kinetics models, the slowest rate of adsorption usually controls the whole rate of the process. For the untreated STL, the adsorption kinetic data did not follow pseudo second order and intra particle diffusion models based on the  $R^2$  values (Table 2). Data of kinetics were best discussed by pseudo-first order model for all the initial concentrations of MO. Moreover, the calculated  $q_{e(\text{calc})}$  is very close to the experimental  $q_{e(\text{exp})}$ . A similar pattern of results was also obtained for the kinetic study of acid treated STL (Table 3). The constants and  $R^2$  of three kinetic models for the adsorption of MO by the untreated and acid treated STL are tabulated in Table 2 and Table 3, respectively.

Table 2  
The rate constants and correlation coefficients ( $R^2$ ) of three different kinetic models applied for the MO adsorption by untreated STL

MO Conc, (mg/L)	$q_{e,\text{exp}}$	Pseudo-first order			Pseudo-second order			Intraparticle diffusion		
		$q_{e,\text{calc}}$	$K_1$	$R^2$	$q_{e,\text{calc}}$	$K_2$	$R^2$	$C$	$K_3$	$R^2$
10	0.34	0.29	0.02	0.98	0.28	0.37	0.81	0.04	0.025	0.95
20	0.62	0.78	0.02	0.97	0.37	0.22	0.70	0.07	0.05	0.95
40	1.05	1.12	0.03	0.96	0.19	0.26	0.76	0.03	0.09	0.92
60	1.39	1.90	0.028	0.95	3.18	0.15	0.58	0.14	0.13	0.90

Table 3  
The rate constants and correlation coefficients ( $R^2$ ) of three different kinetic models for the adsorption of MO by acid treated STL

MO Conc, (mg/L)	$q_{e,\text{exp}}$	Pseudo-first order			Pseudo-second order			Intraparticle diffusion		
		$q_{e,\text{calc}}$	$K_1$	$R^2$	$q_{e,\text{calc}}$	$K_2$	$R^2$	$C$	$K_3$	$R^2$
10	0.34	0.36	0.03	0.90	5.58	0.33	0.92	0.45	0.05	0.59
20	0.62	0.97	0.03	0.95	0.32	0.23	0.92	0.60	0.11	0.74
40	1.05	2.65	0.03	0.99	0.39	0.13	0.85	0.93	0.23	0.83
60	1.39	4.53	0.02	0.98	1.28	0.04	0.75	0.50	0.34	0.95

## CONCLUSION

In summary, acid treated STL has demonstrated higher MO removal than its untreated counterpart. Adsorption isotherm for the untreated and acid treated STL was best represented by the Freundlich isotherm model and the kinetic of adsorption process was found to follow the pseudo-first order model. The STL is an alternative substitute to activated carbon as bio-adsorbent, which is plentiful in the nature. Moreover, it has high adsorption capacity for MO. Therefore, the viewpoint of STL as adsorbent for removal of MO from aqueous dye solution is very favourable.

## ACKNOWLEDGEMENTS

This work is supported by a research grant provided by the Ministry of Higher Education through the Fundamental Research Grant Scheme (FRGS grant no. 600-RMI/FRGS 5/3 (1/2014)). The authors would also like to acknowledge the Faculty of Chemical Engineering, Universiti Teknologi MARA (UiTM), for providing the research facilities used in this work.

## REFERENCES

- Akar, E., Altinişik, A., & Seki, Y. (2013). Using of activated carbon produced from spent tea leaves for the removal of malachite green from aqueous solution. *Ecological Engineering*, 52, 19-27.
- Annadurai, G., Juang, R. S., & Lee, D. J. (2002). Use of cellulose-based wastes for adsorption of dyes from aqueous solutions. *Journal of Hazardous Materials*, 92(3), 263-274.
- Bajpai, S. K., & Jain, A. (2010). Sorptive removal of crystal violet from aqueous solution using spent tea leaves: Part I optimization of sorption conditions and kinetic studies. *Acta Chimica Slovenica*, 57(3), 751-757.
- Chen, S., Zhang, J., Zhang, C., Yue, Q., Li, Y., & Li, C. (2010). Equilibrium and kinetic studies of methyl orange and methyl violet adsorption on activated carbon derived from *Phragmites australis*. *Desalination*, 252(1), 149-156.
- Cheng, Z., Gao, Z., Ma, W., Sun, Q., Wang, B., & Wang, X. (2012). Preparation of magnetic Fe<sub>3</sub>O<sub>4</sub> particles modified sawdust as the adsorbent to remove strontium ions. *Chemical Engineering Journal*, 209, 451-457.
- Dada, A. O., Olalekan, A. P., Olatunya, A. M., & Dada, O. (2012). Langmuir, Freundlich, Temkin and Dubinin–Radushkevich isotherms studies of equilibrium sorption of Zn<sup>2+</sup> onto phosphoric acid modified rice husk. *Journal of Applied Chemistry*, 3(1), 38-45.
- Devi, M. G., Al-Hashmi, Z. S., & Sekhar, G. C. (2012). Treatment of vegetable oil mill effluent using crab shell chitosan as adsorbent. *International Journal of Environmental Science and Technology*, 9(4), 713-718.
- Gong, L., Sun, W., & Kong, L. (2013). Adsorption of Methylene Blue by NaOH-modified Dead Leaves of Plane Trees. *Computational Water, Energy, and Environmental Engineering*, 13-19.
- Kahraman, S., Yalcin, P., & Kahraman, H. (2012). The evaluation of low-cost biosorbents for removal of an azo dye from aqueous solution. *Water and Environment Journal*, 26(3), 399-404.

- Kaushik, P., & Malik, A. (2009). Fungal dye decolourization: Recent advances and future potential. *Environment International*, 127-141.
- Khosla, E., Kaur, S., & Dave, P. N. (2013). Tea waste as adsorbent for ionic dyes. *Desalination and Water Treatment*, 51(34-36), 6552-6561.
- Kumar, P. S., Ramalingam, S., Senthamarai, C., Niranjanaa, M., Vijayalakshmi, P., & Sivanesan, S. (2010). Adsorption of dye from aqueous solution by cashew nut shell: Studies on equilibrium isotherm, kinetics and thermodynamics of interactions. *Desalination*, 261(1), 52-60.
- Lafi, R., & Hafiane, A. (2016). Removal of methyl orange (MO) from aqueous solution using cationic surfactants modified coffee waste (MCWs). *Journal of the Taiwan Institute of Chemical Engineers*, 58, 424-433.
- Mohan, S., & Gandhimathi, R. (2009). Removal of heavy metal ions from municipal solid waste leachate using coal fly ash as an adsorbent. *Journal of Hazardous Materials*, 169(1), 351-359.
- Ovejero, G., Rodriguez, A., Vallet, A., & Garcia, J. (2013). Catalytic wet air oxidation of a non-azo dye with Ni/MgAlO catalyst. *Chemical Engineering Journal*, 168-173.
- Salleh, M. A. M., Mahmoud, D. K., Karim, W. A. W. A., & Idris, A. (2011). Cationic and anionic dye adsorption by agricultural solid wastes: A Comprehensive Review. *Desalination*, 280(1), 1-13.
- Yagub, M. T., Sen, T. K., Afroze, S., & Ang, H. M. (2014). Dye and its removal from aqueous solution by adsorption: a review. *Advances in Colloid and Interface Science*, 209, 172-184.
- Zhang, J., Zhou, Q., & Ou, L. (2011). Kinetic, isotherm, and thermodynamic studies of the adsorption of methyl orange from aqueous solution by chitosan/alumina composite. *Journal of Chemical and Engineering Data*, 57(2), 412-419.
- Zuorro, A., Lavecchia, R., Medici, F., & Piga, L. (2013). Spent tea leaves as a potential low-cost adsorbent for the removal of azo dyes from wastewater. *Chemical Engineering*, 32, 19-24.



## A Study on the Formation of PVA/Kenaf Nanofibres via Electrospinning

Nor Dalila Nor Affandi<sup>1\*</sup>, Mohd Rozi Ahmad<sup>1</sup>, Sabiha Hanim Saleh<sup>1</sup>,  
Muhammad Fairuz Remeli<sup>2</sup>, Nur Hayati Humairah Nur Ikhwan Teo<sup>1</sup> and  
Nurul Farihin Amran<sup>1</sup>

<sup>1</sup>Textile Research Group, Faculty of Applied Sciences, Universiti Teknologi MARA (UiTM), 40450 Shah Alam, Selangor, Malaysia

<sup>2</sup>Faculty of Mechanical Engineering, Universiti Teknologi MARA (UiTM), 40450 Shah Alam, Selangor, Malaysia

### ABSTRACT

This paper reports a study of the formation of cellulose nanofibres from kenaf waste using chemical extraction method. The extracted holocellulose was then prepared for acid hydrolysis to form the cellulose. Before mixing it with polyvinyl chloride (PVA) solution and extruded using electrospinning under different parameters to produce PVA/kenaf nanofibres. Results showed that the morphological structures of PVA/kenaf nanofibres varied at different voltages. An increase in voltage from 10 kV to 20 kV produced more beads along the fibre length. In addition, the applied voltages were found to affect the resultant fibre diameter of the PVA/kenaf nanofibres. The results also showed that the electrospinning parameters affect the shapes of the PVA/kenaf nanofibre membranes. Based on the experimental works, the optimal applied voltage was found to be at 15 kV, where the resultant fibre diameter and membrane coverage area were approximately  $43.9 \pm 3.1$  nm and  $214.2 \pm 15.8$  cm<sup>2</sup>, respectively.

*Keywords:* Cellulose, electrospinning, kenaf wastes, morphological structures, nanofibres

### ARTICLE INFO

#### Article history:

Received: 25 October 2016

Accepted: 17 March 2017

#### E-mail addresses:

[dalila@salam.uitm.edu.my](mailto:dalila@salam.uitm.edu.my) (Nor Dalila Nor Affandi),  
[rozitex@salam@uitm.edu.my](mailto:rozitex@salam@uitm.edu.my) (Mohd Rozi Ahmad),  
[sabihahanim@salam.uitm.edu.my](mailto:sabihahanim@salam.uitm.edu.my) (Sabiha Hanim Saleh),  
[fairuz1299@salam.uitm.edu.my](mailto:fairuz1299@salam.uitm.edu.my) (Muhammad Fairuz Remeli),  
[nurhayatihumairaurikhwan@yahoo.com](mailto:nurhayatihumairaurikhwan@yahoo.com)  
(Nur Hayati Humairah Nur Ikhwan Teo),  
[nurulfareyhin@gmail.com](mailto:nurulfareyhin@gmail.com) (Nurul Farihin Amran)

\*Corresponding Author

### INTRODUCTION

Kenaf (*Hibiscus cannabinus*) is a natural bast fibre from lignocellulosic source and made up of three major elements, which are the lignin, hemicellulose and cellulose (Reddy & Yang, 2005). The kenaf stem was reported to have the highest cellulose content compared to any other parts of kenaf (Akil et al., 2011). The presence of cellulose gives strength

and firmness to the plant fibres (Paster et al., 2003). Kenaf fibres have gained a great deal of attention because they are readily available, biodegradable, strong, and lightweight (Nishino et al., 2003). The fibres from kenaf can be obtained using several extraction methods such as dew retting, chemical and mechanical extraction. However, these extraction methods can only produce fibres at micron size. To enhance its potential in certain applications, there is a need to convert the microcellulose fibres into nano size cellulosic fibres.

To date, there have been a number of methods to produce nanofibres such as phase separation, template synthesis, self-assembly, drawing, and electrospinning. Electrospinning is reported to be an ideal method since it can produce nanofibres in long and continuous fibre form (Ramakrishna, 2005). There are three stages in electrospinning; which are the starting of jet and elongation of the jet in a direct course, development of bending instability and longer extension of the jet, which enable the jet turn thin and long as it pursues a looping spiral path, and jet hardening to produce nanofibres (Salem, 2001). The product of electrospinning piled up to form a nanofiber membrane (Ramakrishna, 2005).

Nanofibre membrane exhibits a number of outstanding properties such as high surface area per mass compared to bulk fibres and film (Grafe & Graham, 2003; Gopal et al., 2006) and small pore sizes (Gopal et al., 2006). Due to these properties, the membrane has the potential to be employed in liquid or gas filtration (Reneker et al., 2000; Gopal et al., 2006). In liquid filtration applications, the fine pore size of nanofibre membrane has successfully removed microparticles (Gopal et al., 2006). In addition, incorporation of nanofibre membrane with Nafion membrane has been reported to reduce methanol fuel crossover (fuel waste) from anode to cathode while maintaining proton conductivity, compared with uncoated Nafion (Ramakrishna et al., 2006). The application of nanofiber membrane was further diversified when the membrane was observed to exhibit good performance in tissue engineering (Ramakrishna et al., 2006; Gu, Ren, & Vancso, 2005; Casarano et al., 2009). Due to its high surface-to-volume ratio, electrospun membrane was reported to permit cell growth over membrane surfaces, which will generate new tissues (Ramakrishna et al., 2006).

The feasibility of electrospinning to produce fibres at nano-scale has encouraged the researchers to carry out this study. The main purpose of the study is to relate the electrospinning voltage with respect to the morphological aspects of cellulosic kenaf nanofibres.

## METHOD

In this study, kenaf wastes were extracted using chemical extraction. The ground kenaf wastes were first dried for 24 hours at 80°C. After that, the dried kenaf wastes were dewaxed using toluene:ethanol (2:1, v/v) for 6 hours. The dewaxed ground kenaf was then prepared for acid-hydrolysis by treating the wastes with 2 M sodium hydrogen chloride (HCl) at 80°C for 2 hours. Next, the kenaf wastes were treated with sodium hydroxide (NaOH) for 2 hours at 80°C and further treated with hydrogen peroxide (H<sub>2</sub>O<sub>2</sub>) at room temperature for 5 hours. Finally, the kenaf wastes were washed with distilled water and dried at 60°C to obtain cellulose.

The kenaf cellulose was then mixed with 10% w/w PVA solution to form PVA/kenaf cellulose solution. The mixing was done at room temperature under continuous agitation. The PVA solution was prepared by dissolving PVA powder (Sigma-Aldrich, Mw 125,000 g/mol)

in distilled water at 80°C for 3 hours. The preparation of the PVA/kenaf cellulose solution was adapted from a previous study (Sutka et al., 2014).

The formation of PVA/kenaf nanofibres was carried out using an electrospinning equipment (Figure 1). A single nozzle spinneret with a 23G (Ø0.65 mm) needle was used to electrospin the PVA/kenaf solution at different applied voltages ranging from 10 kV to 20 kV with an electrospinning distance of 10 cm. The solution was pumped at a constant feed rate (0.2 ml/h) using a syringe pump. The electrospinning was carried out at room temperature with relative humidity ranging from 40 to 60%. The PVA/kenaf nanofibres were deposited on grounded aluminium foil for 3 minutes with positive polarity at the needle tip. An optimal electrospinning parameter for PVA/kenaf nanofibre membranes was based on large membrane area. The resultant PVA/kenaf nanofibres were characterised for morphological structures, membrane coverage area and Fourier Transform Infrared Spectroscopy (FTIR) analysis.

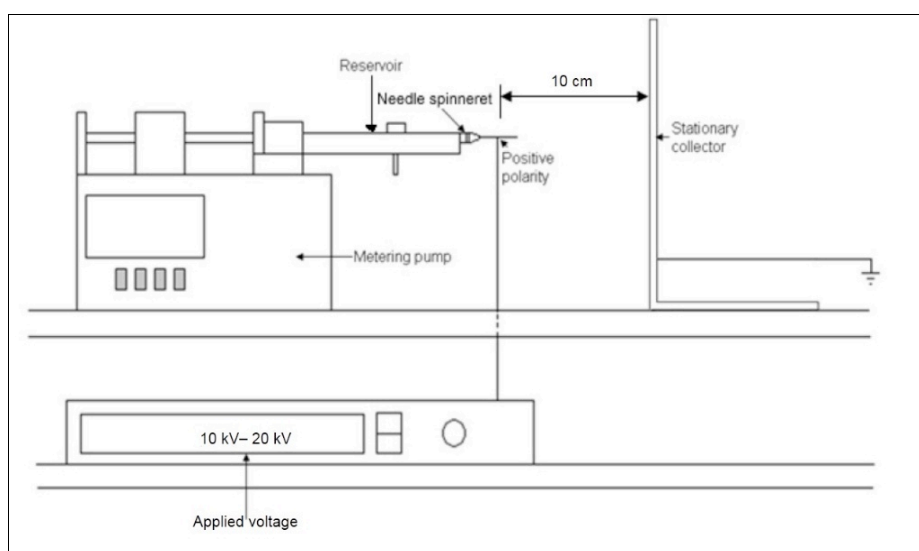


Figure 1. A schematic diagram of the electrospinning system used in the study

## RESULTS AND DISCUSSION

Figure 2(a) illustrates the morphological structures of PVA nanofibres. The PVA nanofibres have long, continuous, uniform, and cylindrical shape of fibres. The morphological structures of the PVA were found to change when kenaf cellulose was added into the PVA solution. As shown in Figures 2(b) to (d), beads are formed along the length of PVA/kenaf nanofibres. A possible reason of this is the poor chain entanglement between the PVA and cellulose. This poor chain entanglement resulted in beaded fibres rather than uniform and continuous fibres.

It was also found that more beads were formed when the voltage increased from 10kV to 20kV (Figure 2(b) to (d)). This phenomena has been described by Fong, Chun and Reneker (1999), who reported that the increase of voltage caused the electrospinning jets to hit the internal needle wall and form more beaded fibres.

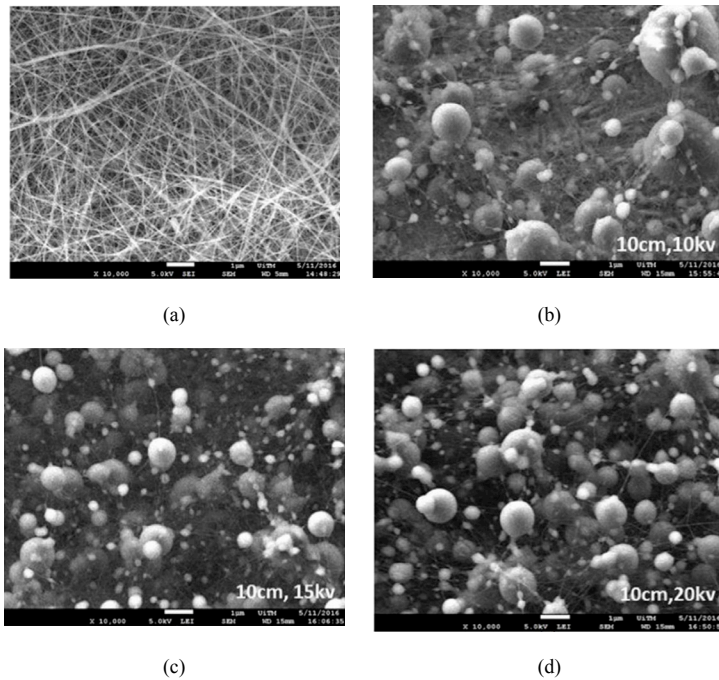


Figure 2. Typical SEM images of nanofibers: (a) PVA; (b) PVA/kenaf nanofibres at 10 kV; (c) PVA/kenaf nanofibres at 15 kV; and (d) PVA/kenaf nanofibres at 20 kV

Figure 3 shows the average fibre diameter of PVA/kenaf nanofibres at different applied voltages. The fibre diameter of nanofibres was found to increase from  $24.2 \pm 5.8$  nm to  $166.1 \pm 11.9$  nm as the applied voltage increased from 10 kV to 20 kV. By increasing the voltage, more solution was removed from the capillary tip, and this resulted in a bigger fibre diameter. The results agree with a previous study done by Ojha et al. (2008), who reported that the increase of applied voltage produced bigger fibre diameter.

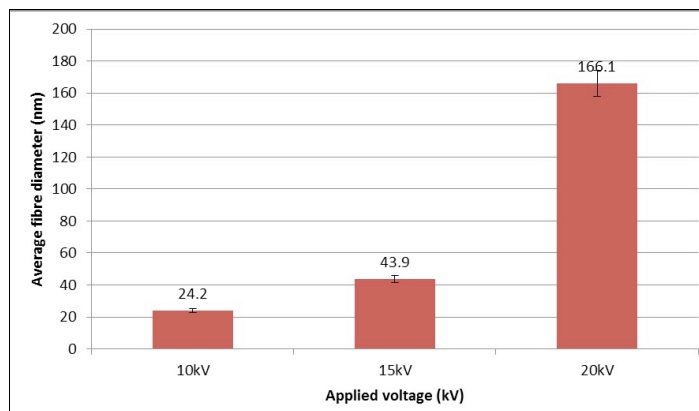


Figure 3. Fibre diameter versus applied voltage for PVA/kenaf nanofibres



Deposition of PVA/kenaf nanofibre membranes onto the collector is shown in Figures 4(a) to (c). The shapes of the membranes vary, depending on the voltages used. This could be due to the formation of unstable electrospinning jets at higher applied voltage. The average area of the membranes is presented in Figure 5. The membrane coverage areas of PVA/kenaf nanofibres increase with the increasing applied voltage. At a higher voltage, the electrospinning jets were expected to have strong electric field strength to eject fibres from the needle tip. As a result, a large membrane of PVA/kenaf nanofibres was deposited onto the collector. This result is in agreement with another study done by Affandi (2010).

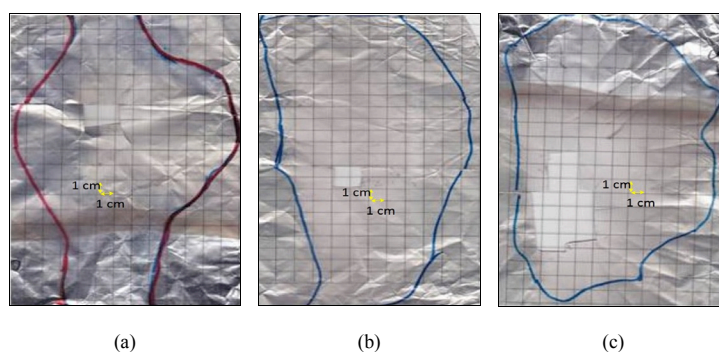


Figure 4. Photographs of the membrane coverage area at: (a) 10 kV; (b) 15 kV; and (c) 20 kV, respectively

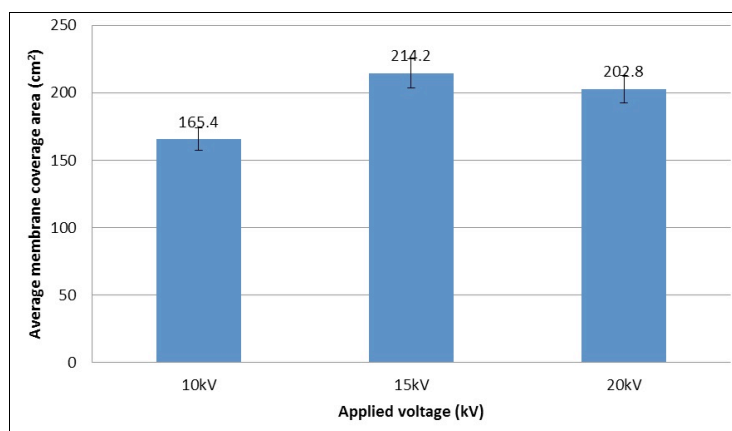


Figure 5. Membrane coverage area versus applied voltage for PVA/kenaf nanofibres

The presence of cellulose in the PVA/kenaf nanofibres was determined using FTIR. From the results shown in Figure 6, it was found that the PVA/kenaf nanofibres contain –OH (peaks from 2995 to 4000 cm<sup>-1</sup>) and fibre –OH (peak at 1638.32 cm<sup>-1</sup>). This result indicates the presence of cellulose in the nanofibres. A similar result was also observed in a previous study by Morán et al. (2008), who reported that peaks at 2995 to 4000 cm<sup>-1</sup> and 1638.32 cm<sup>-1</sup> represent the absorption bands for functional groups of cellulose.

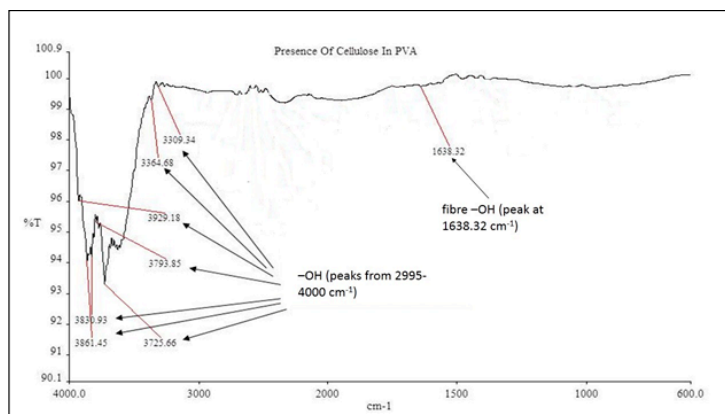


Figure 6. IR spectra for cellulose in PVA/kenaf nanofibres

## CONCLUSION

The PVA/kenaf cellulose solutions were successfully extruded using electrospinning. The results showed that the formation of beaded fibres was influenced by the voltage applied. The increase in the voltages from 10 kV to 20 kV produced more beads along the fibre length. In addition, the electrospinning parameters had significantly affected fibre diameter. The resultant fibre diameter was observed to increase from  $24.2 \pm 5.8$  nm to  $166.1 \pm 11.9$  nm when the voltage applied was increased from 10 kV to 20 kV. The results also showed that the voltage applied affected the shapes of the PVA/kenaf nanofibre membranes. Among the variation of the applied voltages used in electrospinning, the voltage of 15 kV was found to be the optimal electrospinning conditions to electrospin PVA/kenaf nanofibres. At 15 cm, the PVA/kenaf nanofibres formed a large membrane coverage area with approximately  $214.2 \pm 15.8$  cm<sup>2</sup>, respectively.

## ACKNOWLEDGEMENTS

The authors would like to acknowledge the Institute of Research Management and Innovation (IRMI), Universiti Teknologi MARA (UiTM), for providing the research funding under LESTARI Grant (Project Number: 600-RMI/DANA 5/3/LESTARI (65/2015)). The authors are also thankful to Dr. Khairunnadim Ahmad Sekak and his research team for assisting with the electrospinning setup.

## REFERENCES

- Affandi, N. D. N. (2010). *Studies on fabrication, morphology and performances of bi-layer electrospun nanofibre membranes* (Doctoral dissertation). Retrieved from RMIT University.
- Akil, H. M., Omar, M. F., Mazuki, A. A. M., Safiee, S., Ishak, Z. A. M., & Abu Bakar, A. (2011). Kenaf fiber reinforced composites: A review. *Materials and Design*, 32(8–9), 4107–4121.
- Casarano, R., Bentini, R., Bueno, V.B., Lacovella, T., Monteiro, F. B. F., Iha, F. A. S., Campa, A., Petri, D. F. S., Jaffe, M. & Catalani, L. H. (2009). Enhanced fibroblast adhesion and proliferation on electrospun fibers obtained from poly(isosorbide succinate-b-L-lactide) block copolymers. *Polymer*, 50, 6218-27.

- Fong, H., Chun, I., & Reneker, D. H. (1999). Beaded nanofibers formed during electrospinning. *Polymer*, 40(16), 4585-92.
- Grafe, T., & Graham, K. (2003). Polymeric nanofibers and nanofiber webs: a new class of nonwovens, *Nonwoven Technology Review*, 51-5.
- Gopal, R., Kaur, S., Ma, Z., Chan, C., & Ramakrishna, S. (2006). Electrospun nanofibrous filtration membrane, *Journal of Membrane Science*, 281, 581-86.
- Gu, S. Y., Ren, J., & Vancso, G. J. (2005). Process optimization and empirical modeling for electrospun polyacrylonitrile (PAN) nanofiber precursor of carbon nanofibers, *European Polymer Journal*, 41, 2559-68.
- Morán, J. I., Alvarez, V. A., Cyras, V. P., & Vázquez, A. (2008). Extraction of cellulose and preparation of nanocellulose from sisal fibers. *Cellulose*, 15(1), 149-159.
- Nishino, T., Hirao, K., Kotera, M., Nakamae, K., & Inagaki, H. (2003). Kenaf reinforced biodegradable composite. *Composites Science and Technology*, 63(9), 1281-86.
- Ojha, S. S., Afshari, M., Kotek, R., & Gorga, R. (2008) Morphology of electrospun nylon-6 nanofibers as a function of molecular weight and processing parameters. *Journal of Applied Polymer Science*, 108(1), 308-19.
- Paster, M., Pellegrino, J. L., & Carole, T. M. (2003). Industrial bioproducts; today and tomorrow. In *Industrial bioproducts; today and tomorrow*. Energetics Inc.
- Ramakrishna, S. (2005). *An Introduction to Electrospinning and Nanofibers*. World Scientific.
- Ramakrishna, S., Fujihara, K., Teo, Wee-Eong., Yong, T., Ma, Z., & Ramakrishna, R. (2006). Electrospun nanofibers: solving global issues. *Materials Today*, 9, 40-50.
- Reddy, N., & Yang, Y. (2005). Biofibers from agricultural by-products for industrial applications. *TRENDS in Biotechnology*, 23(1), 22-27.
- Reneker, D. H, Yarin, A. L., Fong, H., & Koombhongse, S. (2000). Bending instability of electrically charged liquid jets of polymer solutions in electrospinning, *Journal of Applied Physics*, 87, 4531.
- Salem, D. R. (2001). *Structure Formation in Polymeric Fibers*. Hanser.
- Sutka, A., Kukle, S., Gravitis, J., Milašius, R., & Malašauskiene, J. (2014) Electro-spinning Derived Cellulose-PVA Composite Nano-fibre Mats. *FIBRES AND TEXTILES in Eastern Europe*, 3(105), 43-46.





## Flexural Properties of Random and Unidirectional *Arenga Pinnata* Fibre Reinforced Epoxy Composite

Muhamad Faris Syafiq Khalid<sup>1</sup>, Aidah Jumahat<sup>1\*</sup>, Zuraidah Salleh<sup>1</sup> and Mohammad Jawaid<sup>2</sup>

<sup>1</sup>Faculty of Mechanical Engineering, Universiti Teknologi Mara (UiTM), 40450 Shah Alam, Selangor, Malaysia

<sup>2</sup>Institute of Tropical Forestry and Forest Products, Universiti Putra Malaysia (UPM), 43400 Serdang, Selangor, Malaysia

### ABSTRACT

This paper investigates the flexural properties of *Arenga Pinnata* fibre reinforced epoxy composite (APREC) in relation to its fibre arrangement. The composites were produced using *Arenga Pinnata* fibre as the reinforcement material and epoxy resin as the matrix. In this work, two types of *Arenga Pinnata* fibre arrangement were under-studied, randomly distributed and unidirectional distributed (UD). Samples were prepared at 10vol%, 15vol%, 20vol%, and 25vol% of fibres reinforcement to matrix ratio for both types. Three-point bending configuration flexural tests were performed for both randomly distributed APREC and UD APREC at 10vol%, 15vol%, 20vol%, and 25vol% respectively. Results indicated that UD APREC have better flexure modulus and flexure strength for all the fibre loading percentages (vol%) as compared against the randomly distributed APREC. The 25vol% UD APREC showed the highest modulus (3.783 GPa) with an increment of 31.0% as compared against the pure epoxy (2.888 GPa). It was also observed that there was no significant increment on flexure strength for both random and unidirectional APREC as compared to pure epoxy (61.125 MPa), but the flexure strength value decreased for randomly distributed fibre orientation for all fibre volume percentages (vol%).

**Keywords:** *Arenga Pinnata*, flexural properties, unidirectional fibre alignment, volume fraction

### ARTICLE INFO

#### Article history:

Received: 25 October 2016

Accepted: 17 March 2017

#### E-mail addresses:

[mfarissyafiq@yahoo.com](mailto:mfarissyafiq@yahoo.com) (Muhamad Faris Syafiq Khalid),

[aidahjumahat@salam.uitm.edu.my](mailto:aidahjumahat@salam.uitm.edu.my) (Aidah Jumahat),

[szuraidah@salam.uitm.edu.my](mailto:szuraidah@salam.uitm.edu.my) (Zuraidah Salleh),

[jawaid@upm.edu.my](mailto:jawaid@upm.edu.my) (Mohammad Jawaid)

\*Corresponding Author

### INTRODUCTION

In general, composite materials are developed to improve the properties of existing materials such as metal, ceramic, and polymer. The combination of two or more materials will create a composite material which has different properties than the original material. One of the reasons to create composite

materials is to acquire better properties which are more suitable for various applications. For example instead of using a metal hood for car bonnet, some racing cars use carbon fibre reinforced polymer (CFRP) as the hood to reduce the weight of the car. This is one of the reasons why so many researchers keep researching to improve or create new composite materials. Utilisation of natural fibres from plant sources as reinforcement to the polymer to produce natural fibre reinforced polymer composite (NFRP) is among the popular research topics today (Bakar et al., 2013; Manap, Jumahat, & Sapiai, 2015; Sapiai, Jumahat, & Mahmud, 2015). Natural fibres offer several advantages such as its natural availability, environmental friendly, abundance resources and bio-degradability (Bachtiar et al., 2012; Khalid & Abdullah, 2013).

There are varieties of plant-based natural fibres such as hemp, kenaf, flax, sisal, jute, and ramie. Pickering, Efendy and Le (2016) highlighted that selection of the type of natural fibre for the research undertaken has a strong relation to the geographical availability. For example, in Europe, the focus is on flax fibre, whereas jute, kenaf, coir and sisal mostly have gained interests in Asia (Pickering et al., 2016). In this study, the *Arenga Pinnata* fibre was chosen as the reinforcement material and the epoxy is the matrix polymer. This selection was made because of the *Arenga Pinnata* fibre is easily available in Malaysia, in addition to its high durability and resistance to sea water properties (Ishak et al., 2013). This multipurpose fibre has numerous applications such as in road constructions for soil stabilisation and also as a substitute for geotextile fibreglass reinforcement (Ishak et al., 2013). The *Arenga Pinnata* fibre is also can be found in daily items such as ropes, brushes, filters, brooms, and shelter for fish breeding (Mogea, Seibert, & Smits, 1991). Misri et al. (2010) has discovered the great potential of *Arenga Pinnata* to be used as the reinforcement fibres in polymer matrixes such as polyester and epoxy.

Natural fibre reinforced polymer (NFRP) is studied for various applications such as use in construction materials (Bachtiar et al., 2010), automotive industry (Ticoalu, Aravinthan, & Cardona, 2010), and aerospace application (Alamri, Low, & Alothman, 2012). For the structural study, emphasis must be put on the flexural property, especially on structures such as bridges and gratings (drain cover or sewer grate). One of the main factors determining the mechanical properties of NFRP is fibre orientation (Pickering et al., 2016). Siregar (2005) has studied tensile properties on woven roving, long random, and chopped random *Arenga Pinnata* fibre arrangement, where he found out woven roving have better tensile properties than long random and chopped random orientation (Bachtiar et al, 2010).

Structures such as jetty pathway and grating for drain cover have their own problems depending on the material used. The pathway made from wood plank such as in Tanjung Piai, Johor, Malaysia, needs a new coating every 6 to 12 months to avoid de-lignification of the wood caused by sea water. The wood planks also need to be replaced every 8 to 10 years. In the case of metal material for drain cover and also other grating applications, the challenges are to prevent rust that will cause the drop in mechanical properties and to avoid from being stolen. As a solution to these problems, composite materials such as glass fibre reinforced polymer (GFRP) can be used as an alternative material. However, glass fibre has some drawbacks concerning the health issues; through inhaling and touching.

This study was done to investigate the effect of the randomly distributed and unidirectional distributed *Arenga Pinnata* reinforcement fibres at 10vol%, 15vol%, 20vol%, and 25vol% on the under-studied APREC flexural properties. The under-studied specimens had gone through 3-point bending flexural load to determine their flexural properties. The specimen's surface failure characters were examined using optical microscope.

## MATERIALS AND METHOD

In this study, *Arenga Pinnata* fibre was used as the reinforcement fibres and the epoxy resins as the matrix, to produce the *Arenga Pinnata* fibre reinforced epoxy composite (APREC). The *Arenga Pinnata* fibre was harvested from Kuala Pilah, Negeri Sembilan, Malaysia. The epoxy resin (Miracast 1517) was supplied by Miracon (M) SDN. BHD, Selangor, Malaysia. The APREC was produced using 10vol%, 15vol%, 20vol%, and 25vol% *Arenga Pinnata* fibre content in two types of fibres arrangement; randomly distributed and unidirectional distributed (UD). The randomly fibre distributed APREC was prepared in 300 mm x 300 mm x 4 mm slab size and cured. The slab was then cut according to the ASTM D790-10 standard specimen size; 127 mm x 12.7 mm x 4 mm. The UD fibre APREC was prepared in 130 mm x 13 mm x 4 mm size and was later finished into the ASTM D790-10 standard specimen size of 127 mm x 12.7 mm x 4 mm, after it has been fully cured (Figure 1).

Similar method was used to prepare both randomly distributed APREC and unidirectional APREC. Firstly, the epoxy resins, hardener and *Arenga Pinnata* fibres were weighed according to the amount needed (Table 1). Subsequently, the cavity moulds were prepared by laying an aluminium plate as its base, followed by a transparent plastic sheet; to avoid the moulded APREC slabs from sticking to its base. The epoxy resin was then mixed with the hardener in a plastic cup using ratio 100 (epoxy resin): 30 (hardener), as recommended by the supplier. Half of the epoxy resin mixture in the cup was then poured into the mould and then the *Arenga Pinnata* fibres were manually laid according to the required orientation. Next, the remainder of the epoxy resin mixture in the plastic cup was poured on top of the laid fibres and was left to stand for 5 to 8 minutes. This practice is necessary to dispel the trapped air bubbles inside the matrix mixture to the surface. The solidified composite mixture was then covered with another transparent plastic sheet on its surface prior to the cold pressing process. The mould was then pressed using cold press machine for 24 hours at constant pressure of 10,000 kPa (105 kg/cm<sup>2</sup>). For the randomly APREC sample, the 300 mm x 300 mm x 4 mm slab size was then cut and finished into the standard specimen size, meanwhile for the UD APREC sample, the 130 mm x 13 mm x 4 mm slab size was just finished into the standard specimen size. Subsequently, both specimens of both qualities were ready for the flexural testing.

Table 1  
*Mass of materials to produce APREC*

No	Specimen	Mass Epoxy + Hardener (g)	Mass Fibre (g)
1	Pure Epoxy	7.7	-
2	10vol% Random APREC	369.4	45.0
3	15vol% Random APREC	348.8	67.5
4	20vol% Random APREC	328.3	90.0
5	25vol% Random APREC	307.8	112.5
6	10vol% UD APREC	6.9	0.9
7	15vol% UD APREC	6.6	1.3
8	20vol% UD APREC	6.2	1.7
9	25vol% UD APREC	5.8	2.1

Table 1 exhibits the amount of epoxy resins, hardener and fibres needed in grams for the APREC preparation. The pure epoxy sample was also prepared for comparison purposes. It is worth mentioned here that for every mixture made, 13% additional amount of epoxy resins and hardener must be added to cater for the samples preparation lost. Figure 1 shows the APREC sample was prepared using different mould sizes for both randomly distributed fibre and unidirectional fibre alignment.



Figure 1. Moulding for: (a) Randomly distributed APREC; (b) Unidirectional APREC; and (c) standard size specimen after grinding process

The 3-point bending flexure test was conducted for all the specimens using Instron Universal Testing Machine as seen in Figure 2. Specimen size of 127 mm x 12.7 mm x 4 mm was prepared according to ASTM D790-10 with a support span of 100mm. Flexure test was done for all the specimens mentioned in Table 1: Pure Epoxy; 10vol% random APREC; 15vol% random APREC; 20vol% random APREC; 25vol% random APREC; 10vol% UD APREC; 15vol% UD APREC; 20vol% UD APREC; and 25vol% UD APREC. The results were then recorded. Thus, the effects of the vol% of the *Arenga Pinnata* fibres loading and orientation on the flexural property of the APREC samples were analyzed.



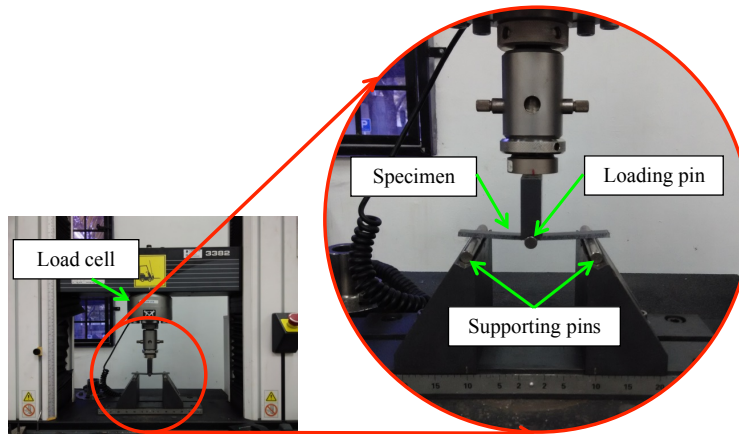


Figure 2. Flexure test setup using Instron Universal Test Machine

## RESULTS AND DISCUSSION

Figure 3 and Figure 4 show a typical stress-strain curve for 10vol%, 15vol%, 20vol%, and 25vol% for Random APREC and UD APREC respectively. Both graphs were compared against the Pure Epoxy Strain-Stress reference curve. The slope of the stress-strain curve indicates that the resistivity to deformation or the rigidity of the composite in relation to the loaded flexure stress (Ali, Sanuddin, & Ezzeddin, 2010). From the stress-strain curve below, all curves indicate brittle behaviours which are almost straight lines, with an abrupt failure end. The failure occurred without any indication; no yielding sign was observed.

Figure 3 and 4, also show that the curves for both random and UD APREC stopped earlier than pure epoxy's curve. This indicates that both fibre orientations of the APREC's prepared samples had premature break. This behavior typically caused by poor interfacial bonding between natural fibre (hydrophilic) and polymer matrix (hydrophobic) (Xie et al., 2010); it triggers failure on matrix first followed by the reinforcement fibres in the composite when under flexural load.

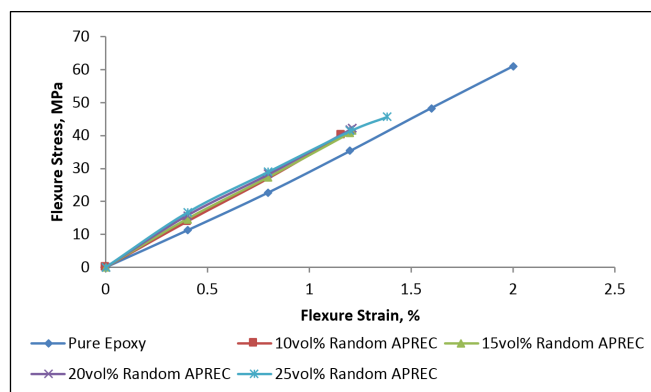


Figure 3. Typical stress-strain curve for Pure Epoxy, 10vol% random APREC, 15vol% random APREC, 20vol% random APREC, and 25vol% random APREC

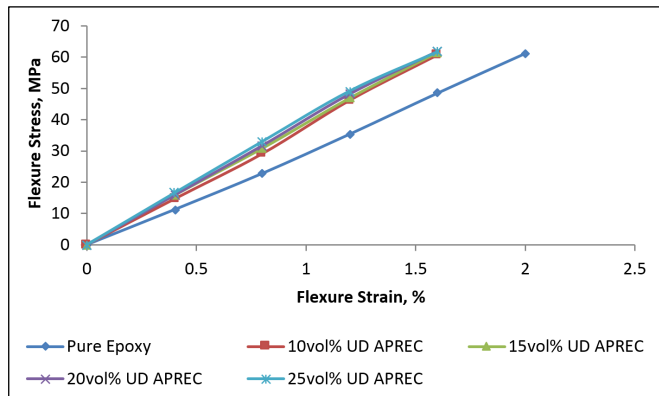


Figure 4. Typical stress-strain curve for Pure Epoxy, 10vol% UD APREC, 15vol% UD APREC, 20vol% UD APREC, and 25vol% UD APREC

Figure 5 presents bar chart for flexural modulus of Pure Epoxy and randomly distributed APREC of 10vol%, 15vol%, 20vol%, and 25vol% fibre content. As a reference, Pure Epoxy recorded modulus value of 2.888 GPa. Reinforcement of 10vol% of randomly distributed *Arenga Pinnata* increased the resistance to deformation of the epoxy by 22.7% with modulus value of 3.545 GPa. Flexural modulus showed an increase with the increment of the fibre loading volume percentages which are 3.558 GPa (23.2%) for 15vol% fibre, 3.609 GPa (25.0%) for 20vol% fibre, and 3.783 GPa (31.0%) for 25vol% random fibre content. However quite significant flexural modulus was observed for the sample APREC of randomly distributed with 25vol% fibres.

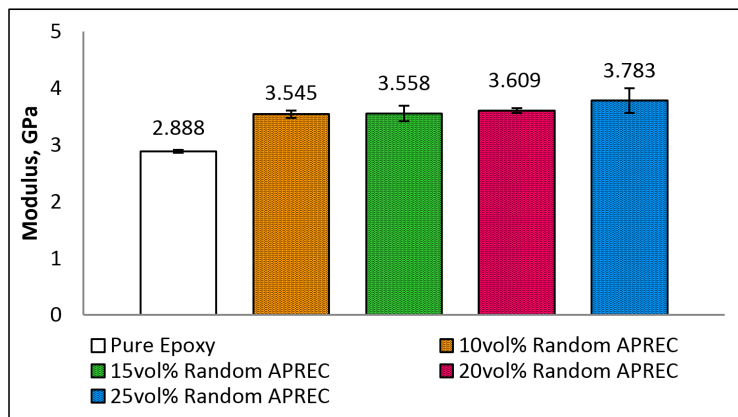


Figure 5. Flexure modulus of Pure Epoxy, 10vol% random APREC, 15vol% random APREC, 20vol% random APREC, and 25vol% random APREC

Similar modulus pattern as in Figure 5 can be seen in Figure 6 on UD APREC where flexural modulus increased with the increment of the fibre volume percentage. But, the flexural modulus readings for the UD fibres orientation are noticeably higher than the randomly distributed

fibres. The flexural modulus showed an increase with the increment of the fibre loading volume percentages which are 3.778 GPa (30.8%) for 10vol% UD APREC, 3.806 GPa (31.8%) for 15vol% UD APREC, 3.824 GPa (32.4%)for 20vol% UD APREC, and 3.984 GPa (38.0%)or 25vol% UD APREC.

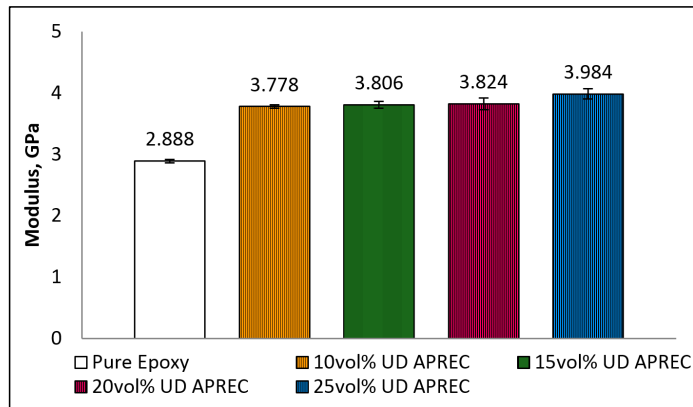


Figure 6. Flexure modulus of Pure Epoxy, 10vol% UD APREC, 15vol% UD APREC, 20vol% UD APREC, and 25vol% UD APREC

Ishak et al. (2013) reported that *Arenga Pinnata* fibre reinforced polyester composites show a significant increment of the flexural strength (at  $p \leq 0.05$ ) with the increment in fibre weight content (13%, 18%, 22%, and 29%). However, no significant improvement on flexural modulus value for woven fibre orientation was noticed in his study. In this study, a similar behaviour to Ishak et al. (2013) experiment was attained from the randomly distributed APREC, but no significant change was observed on the flexural strength of the unidirectional APREC even though their strengths were higher than the randomly distributed APREC, as shown in Table 2.

Table 2  
Flexure strength and flexure strain for different volume fraction and fibre alignment of APREC

Materials	Flexure Strength, MPa	Flexure Strain, %
Pure Epoxy	61.125 ± 2.115	2.374 ± 0.098
10vol% Random APREC	40.350 ± 2.341	1.174 ± 0.274
15vol% Random APREC	41.643 ± 0.027	1.069 ± 0.102
20vol% Random APREC	42.420 ± 0.237	1.166 ± 0.066
25vol% Random APREC	45.077 ± 2.326	1.310 ± 0.095
10vol% UD APREC	62.328 ± 2.451	1.779 ± 0.067
15vol% UD APREC	62.656 ± 2.940	1.462 ± 0.046
20vol% UD APREC	61.668 ± 3.478	1.500 ± 0.058
25vol% UD APREC	61.185 ± 0.975	1.623 ± 0.047

In the case of random APREC, the flexural strengths were 40.350 MPa, 41.643 MPa, 42.420 MPa, and 45.077 MPa for 10vol%, 15vol%, 20vol%, and 25vol% accordingly. The flexural strength values of random APREC for all fibre percentages are lower than pure epoxy strength. This situation occurred because of the premature failure of the composite where the matrix broke before fibre due to poor interfacial bonding between fibre and matrix. This condition is confirmed by examining the image captured by scanning electron microscope (SEM), in Figure 7. Ishak et al. (2013) has quoted in his review paper that flexural test was done on 10vol%, 15vol%, 20vol%, and 30vol% random short chopped sugar palm fibres (*Arenga Pinnata* fibres) reinforced epoxy composites experienced the same behaviour; the strength increased with the increased of fibre loadings of up to 20vol%, but the composite with 30vol% fibre content showed conflicting behaviour. A separate research done by Sahari, Sapuan, Ismarrubie, and Rahman (2011) on 30vol% ijuk fibres (*Arenga Pinnata* fibres) reinforced unsaturated polyester and showed that the flexural strength and modulus result obtained was 33.742 MPa and 2.424 respectively.

Fracture surface of Random APREC shown in Figure 7 indicates poor adhesion between *Arenga Pinnata* fibre and epoxy matrix where the fibre surfaces were still intact after the composite failed. Poor interfacial bonding between fibre and matrix caused a reduction in flexural strength. This is evidence with the obvious voids observed between fibre and matrix. Similar behaviour was also observed on Unidirectional APREC (Figure 8). But, the higher flexural strength performance of the UD APREC for all the fibre volume percentages were confirmed through unique shapes of the voids; slightly larger and elongated in the perpendicular direction of the loading pin.

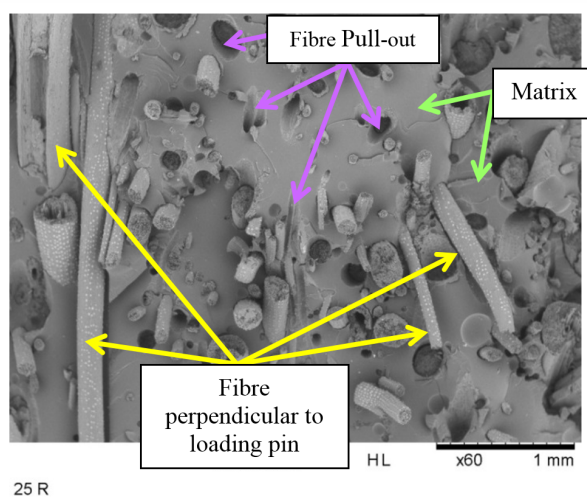


Figure 7. Fracture surface of random APREC

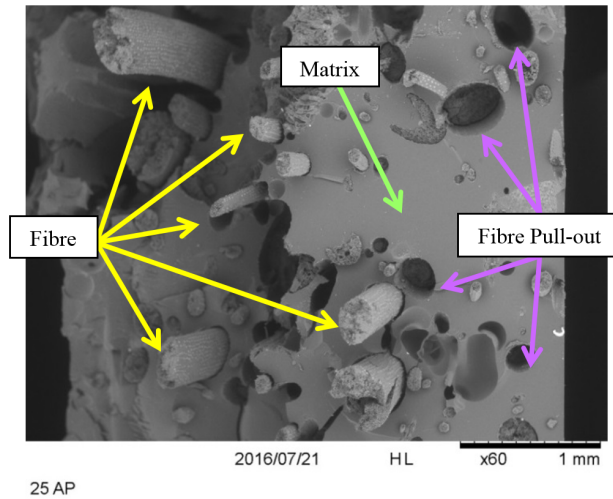


Figure 8. Fracture surface of unidirectional APREC

## CONCLUSION

The flexural test was successfully done on Pure Epoxy, random APREC with 10vol%, 15vol%, 20vol%, 25vol%, and UD APREC with 10vol%, 15vol%, 20vol%, 25vol%. The Flexural modulus indicates that both fibre orientations increased the rigidity of the composite along with the increment of vol% of fibre loading. On the other hand, the flexural strength of the Random APREC is lower than the Pure Epoxy. It can be concluded that with style of the specimens being prepared, the inclusions of *Arenga Pinnata* fibres in the unidirectional alignment did not significantly affect the flexural strength of the epoxy. For flexural strain, the Pure Epoxy sample had better flexibility as compared to both types of APREC samples. Nevertheless this study indicated that the unidirectional APREC had promising flexural properties and was able to reduce the usage of epoxy resin for intermediate strength structural application. The *Arenga Pinnata* fibre has the potential to be used as an alternative material to replace the almost extinct hardwoods such as Balau, Meranti and Cengal.

## ACKNOWLEDGEMENTS

The authors would like to thank Institute of Research Management and Innovation (IRMI), Ministry of Education Malaysia and Institute of Graduate Studies (IPSIS) UiTM for the financial supports. This research works is performed at the Faculty of Mechanical Engineering, UiTM Malaysia under the support of BESTARI GRANT 600-IRMI/DANA 5/3/BESTARI (0007/2016).

## REFERENCES

- Alamri, H., Low, I. M., & Alothman, Z. (2012). Mechanical, thermal and microstructural characteristics of cellulose fibre reinforced epoxy/organoclay nanocomposites. *Composites Part B: Engineering*, 43, 2762–2771.

- Ali, A., Sanuddin, A. B., & Ezzeddin, S. (2010). The effect of aging on *Arenga pinnata* fiber-reinforced epoxy composite. *Materials and Design*, 31, 3550–3554.
- Bachtiar, D., Sapuan, S. M., & Hamdan, M. M. (2010). Flexural properties of alkaline treated sugar palm fibre reinforced epoxy composites. *International Journal of Automotive and Mechanical Engineering*, 1, 79–90.
- Bachtiar, D., Sapuan, S. M., Khalina, A., Zainudin, E. S., & Dahlan, K. Z. M. (2012). Flexural and impact properties of chemically treated sugar palm fiber reinforced high impact polystyrene composites. *Fibers and Polymers*, 13, 894–898.
- Bachtiar, D., Sapuan, S. M., Zainudin, E. S., Khalina, A., & Dahlan, K. Z. M. (2010). The tensile properties of single sugar palm (*Arenga pinnata*) fibre. *IOP Conference Series: Materials Science and Engineering*, 11, 12012.
- Bakar, N. H., Hyie, K. M., Ramlan, A. S., Hassan, M. K., & Jumahat, A. (2013). Mechanical Properties of Kevlar Reinforcement in Kenaf Composites. *Applied Mechanics and Materials*, 465–466, 847–851.
- Ishak, M. R., Sapuan, S. M., Leman, Z., Rahman, M. Z. A., Anwar, U. M. K., & Siregar, J. P. (2013). Sugar palm (*Arenga pinnata*): Its fibres, polymers and composites. *Carbohydrate Polymers*, 91, 699–710.
- Khalid, M. F. S., & Abdullah, A. H. (2013). Storage Modulus Capacity of Untreated Aged *Arenga pinnata* Fibre-Reinforced Epoxy Composite. *Applied Mechanics and Materials*, 393, 171–176.
- Manap, N., Jumahat, A., & Sapiai, N. (2015). Effect of fibre treatment on longitudinal and transverse tensile properties of unidirectional kenaf composite. *Jurnal Teknologi*, 76, 87–95.
- Misri, S., Leman, Z., Sapuan, S. M., & Ishak, M. R. (2010). Mechanical properties and fabrication of small boat using woven glass/sugar palm fibres reinforced unsaturated polyester hybrid composite. *IOP Conference Series: Materials Science and Engineering*, 11, 12015.
- Mogea, J., Seibert, B., & Smits, W. (1991). Multipurpose palms: the sugar palm (*Arenga pinnata* (Wurmb) Merr.). *Agroforestry Systems*, 13, 111–129. JOUR.
- Pickering, K. L., Efendy, M. G. A., & Le, T. M. (2016). A review of recent developments in natural fibre composites and their mechanical performance. *Composites Part A: Applied Science and Manufacturing*, 83, 98–112.
- Sahari, J., Sapuan, S. M., Ismarrubie, Z. N., & Rahman, M. Z. A. (2011). Investigation on Bending Strength and Stiffness of Sugar Palm Fibre from Different Parts Reinforced Unsaturated Polyester Composites. *Key Engineering Materials*, 471–472, 502–506.
- Sapiai, N., Jumahat, A., & Mahmud, J. (2015). Flexural And Tensile Properties Of Kenaf/Glass Fibres Hybrid Composites Filled With Carbon Nanotubes. *Jurnal Teknologi*, 76, 115–120.
- Siregar, J. P. (2005). *Tensile and Flexural Properties of Arenga Pinnata Filament (Ijuk Filament) Reinforced Epoxy*. Universiti Putra Malaysia.
- Ticoalu, A., Aravinthan, T., & Cardona, F. (2010). A review of current development in natural fiber composites for structural and infrastructure applications. *Southern Region Engineering Conference*, 1–5.
- Xie, Y., Hill, C. A. S., Xiao, Z., Militz, H., & Mai, C. (2010). Silane coupling agents used for natural fiber/polymer composites: A review. *Composites Part A: Applied Science and Manufacturing*, 41, 806–819.



## **Advection and Dispersion of Water Quality Constituents in Batu Ferringhi Penang**

**Muhammad Ilyas Ahmad Jamalluddin<sup>1</sup> and Wei-Koon Lee<sup>2\*</sup>**

<sup>1</sup>*Jurutera Perunding Zaaba Sdn. Bhd., 50300 Kuala Lumpur, Malaysia*

<sup>2</sup>*Faculty of Civil Engineering, Universiti Teknologi MARA (UiTM), 40450 Shah Alam, Selangor, Malaysia*

### **ABSTRACT**

The incident of beach pollution in Batu Ferringhi in year 2014 has created a major concern over water quality at the tourists' haven. In order to understand advection and dispersion of pollutants in the area, a coastal hydrodynamic model of Batu Ferringhi beach was developed in this study by taking into consideration its wind, tide, coastal current and riverine runoff. The model was calibrated and validated through observations from adjacent coastal monitoring stations. Simulation was then carried out to investigate scenario of the constituent water quality which originates from the three rivers in the vicinity. Results showed high concentrations of water quality parameters observed near the headland towards the northeast of the study area, with intermittent patchy escape which may retain more than one-third the initial concentrations, weighted by the river discharge. Even more worrying is that localised trapping of up to three-quarter the initial weighted concentrations also occurs at the beach, owing to the interactions between river flow and longshore current.

*Keywords:* Advection/dispersion, Batu Ferringhi, MIKE21, water quality

### **INTRODUCTION**

In 2014, reports on beach pollution have tarnished the image of Batu Ferringhi beach,

a popular tourist destination to both the locals and international travellers. Site visits by the officials of Penang Island Municipal Council (MPPP) found that the river mouth of Batu Ferringhi was heavily contaminated with black-coloured odorous substance. The issue garnered much public attention, with complaints lodged by hotel operators, and local non-governmental organisations, such as Sahabat Alam Malaysia (SAM) and Consumers Association of Penang (CAP) voicing their concerns.

#### **ARTICLE INFO**

*Article history:*

Received: 25 October 2016

Accepted: 17 March 2017

*E-mail addresses:*

Weikoon2004@yahoo.com (Wei-Koon Lee),

ilyasaj87@gmail.com (Muhammad Ilyas Ahmad Jamalluddin)

\*Corresponding Author

Based on the tests conducted by Department of Environment (DOE), the substance is found to contain *Escherichia coli* (*E. coli*) (Shankar, 2014). It was suspected that the contamination originated from a faulty sewage system (PEG073) some 300 m upstream of the coast. Other possible sources of contamination have since been touted, from river sedimentation, failed toilet connections, illegal food outlets, laundry and car wash services, etc.

Anthropogenic sources of nitrogen and phosphorous into the marine environment have greatly modified the coastal nutrient cycling (Voss, 2011). In particular, discharge of inadequately treated wastes with significant organic contents into the coastal sea can potential cause eutrophication, red tide events, and increased fish mortality such as reported in the southwest coast of India (Babu, Das, & Vethamony, 2006). Mapping the pollutants and studying their transport and ultimate fate are thus important to monitor the well-being of marine water quality. Recently, satellite remote sensing and synthetic aperture radar (SAR) have been used to map coastal water quality (e.g., DiGiacomo et al., 2004; Su et al., 2008). However, the method is only applicable to physical qualities such as total suspended solids (TSS), oil slick, etc., and its extension to other water quality constituents is not straight forward.

Triggered by observations of high fecal coliform count in the coastal water, Babu et al. (2006) used MIKE21 to model assimilation of biological oxygen demand (BOD) from a wastewater outfall off Kochi, the west coast of India. Their study showed that region of high BOD persists in an elliptical zone near the outfall. In addition to BOD, chemical oxygen demand (COD) has also been shown to affect marine water quality and its concentration can be correlated to salinity of the receiving water (Li et al., 2015). Meanwhile, ammonical nitrogen (AN) is known to affect the acidity (pH level) of sea water (Voss, 2011).

The generally assumption which points out discharges into the sea are promptly mixed and hence their concentrations tend to reduce uniformly over time and distance is frequently flawed. Depending on the dynamical interactions between the various forcing at work such as coastal current, wave, tide, and wind, pollutant plumes may remain patchy with well-defined structure. In some cases, they may be stretched to exhibit fractal-like behaviour with localised high concentration (Zimmerman, 1986; Lee, Borthwick, & Taylor, 2014b), or washed ashore (Lee & Zaharuddin, 2015). In addition, the escape time of pollutants from the coastal domain into open sea is also highly dependent on the local geometry, bathymetry and hydrodynamics, and may further be complicated if the coastal water is stratified (Snyder 1985; Lee, Borthwick & Taylor, 2014a).

Koh, Lim and Lee (1997) evaluated the impacts of relocating the discharge outfall from Georgetown, Penang, to different locations within the strait between Penang Island and Peninsular Malaysia. Their study showed that degradation of coastal water quality is evident from raw sewage discharge. There is however a lack of similar study in the northern part of Penang Island, where Batu Ferringhi beach is located (Owens, 1978). In this paper, our purpose is to investigate the spatial and temporal changes of water quality constituents, namely BOD, COD, TSS and AN, in the coastal region of Batu Ferringhi. We present a preliminary two-dimensional model of Batu Ferringhi beach, which considers the riverine discharge from its upstream catchment, tidal fluctuation and coastal wave climate. Using observed river water quality parameters from the study area, the advection and dispersion of these pollutant



constituents were simulated over a typical tidal cycle, and the results were determined and analysed.

## METHOD

### Study Area

The study area is located in the north of Penang Island (*Pulau Pinang*), off the coast of Peninsular Malaysia in the Straits of Melaka (*Selat Melaka*) (see Figure 1). Batu Ferringhi beach is located in the Bukit Bendera district. The study area includes three rivers, namely, Sg. Batu Ferringhi River, Sg. Satu and Sg. Mas, all of which discharge into the sea in the northwest direction. Among the three rivers, Sg. Batu Ferringhi has the largest catchment area with 1135 ha. Meanwhile, Sg. Satu and Sg. Mas have less than a quarter the size, with areas of 244 ha and 211 ha, respectively.

The Penang island experiences tropical climate with the average mean daily temperature of 27°C, while the minimum and maximum temperature recorded ranges from 23.5°C and 31.4°C, respectively (Ahmad, Yahaya, & Farooqi, 2006). The humidity in the island ranges from 60.9% to 96.8%. Generally, the study area experiences uniform temperature, high humidity and heavy rainfall with two major monsoon seasons, namely, the southeast and northeast monsoons. It receives varying monthly rainfalls with an annual average of 267 cm, and up to 624 cm.

The seabed in the study area mostly consists of marine deposits of sand and clay layers, which combined can extend up to 100 m thick (DID, 2010). The geographical properties of residual soils are characterised by medium to coarse grained biotite granite layer, with predominant orthoclase and subordinate microcline (Ahmad et al., 2006). The colour of rocks along the beach vary from light grey to dark grey, depending on the amount of biotite present.



Figure 1. Location of the study (DID, 2010)

The coastline along Batu Ferringhi beach experiences semi-diurnal tidal condition. Tidal data were recorded at a jetty station (5°27'44.52"N, 100°12'27.15"E) at Teluk Bahang by Fisheries Development Authority of Malaysia (*Lembaga Kemajuan Ikan Malaysia*, LKIM), as shown in Table 1. At the worst astronomical condition, the tidal range is about 3.2m. The wave heights at the study area are generally low and seldom exceed 1.5 m (DID, 2010). During the northeast monsoon (Oct-Mar), waves are locally generated between the mainland and Penang Island with a north easterly direction and rarely exceed 0.5 m. During the southwest monsoon (Apr-Sep), wave direction is between northwest and west-north-west. These waves are influenced by the waves generated in the Andaman Sea and the largest wave height usually occurs during this period. Figure 2 shows the wave roses in the study area.

Table 1  
Tidal observations at LKIM Teluk Bahang station (DID, 2010)

Tide	Tidal level (m)	
	ACD	RL
Lowest Astronomical Tide (LAT)	+0.0	-1.42
Mean Low Water Spring (MLWS)	+0.6	-0.82
Mean Low Water Neaps (MLWN)	+1.3	-0.12
Mean Sea Level (MSL)	+1.6	+0.18
Mean High Water Neaps (MHWN)	+1.8	+0.38
Mean High Water Spring (MHWS)	+2.6	+1.18
Highest Astronomical Tide (HAT)	+3.2	+1.78

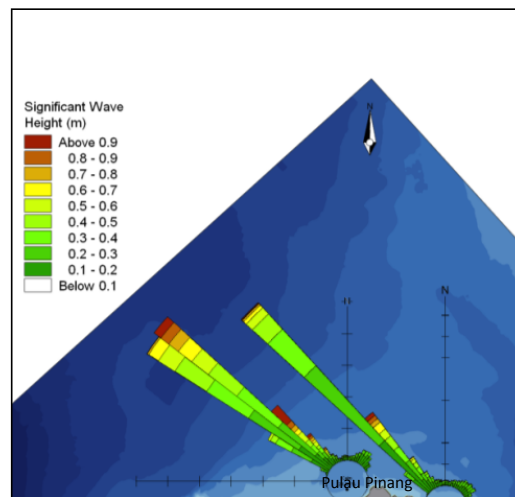


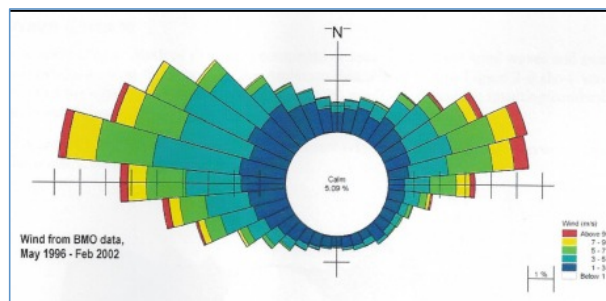
Figure 2. Wave rose in the study area (DID, 2010)

### Model Description

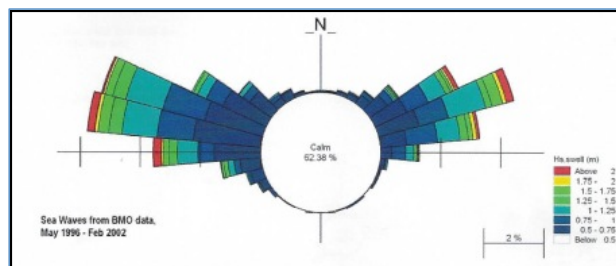
MIKE21 by Danish Hydraulic Institute (DHI) is a popular modelling software used for advanced numerical modelling for shallow water bodies, incorporating the effects of irregular coastline, complex bathymetry and open boundaries. The model solves the two-dimensional incompressible Reynolds averaged Navier-Stokes equations using Boussinesq approximation and assuming hydrostatic pressure distribution. The governing equations are discretised using Cartesian coordinates using cell-centred finite volume method. The model was vigorously tested and validated on a number of key numerical test cases with analytical solution, as well as numerous natural geophysical conditions.

The hydrodynamic (HD) module simulates water level variation, current speed, and current direction incorporating the tidal condition and river discharges. In the present study, tidal boundary condition taken from Global Tide Model (GTM) was applied along the open boundary, and then calibrated and validated against local observations. Fixed discharge boundary condition was applied at river outflow; land boundary was applied along the coastline.

Nearshore wave was analysed to assess the distribution of wave height and wave direction using MIKE21 SW (Spectral Wave). The model takes into account the effects of wave-current interaction, shoaling and refraction due to varying depth, local wind generation and energy dissipation due to bottom friction and wave breaking. Input wind data obtained from British Meteorological Office (BMO), and the wave climate data derived are as shown in Figure 3(a) and (b).



(a)



(b)

Figure 3. (a) Offshore wind rose from BMO wind data; and (b) wave rose derived using spectral analysis

The model domain chosen extends 30 km to the north, the south and the west of the study area in order to incorporate the regional circulation. Staggered flexible mesh is adopted, where the grid sizes vary from 10,000 m<sup>2</sup> (M1), to 10,000,000 m<sup>2</sup> (M4) (Figure 4). Model bathymetry was developed from secondary bathymetric survey data (Figure 5).

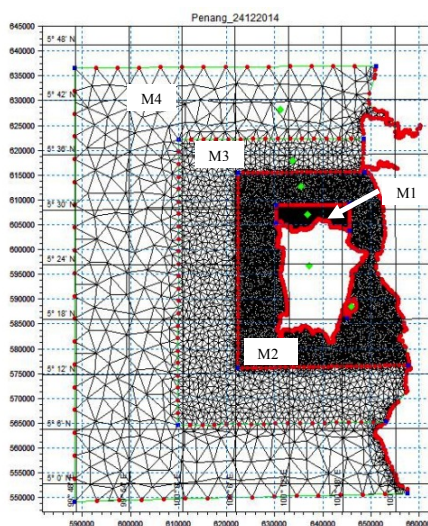


Figure 4. Staggered flexible grid system

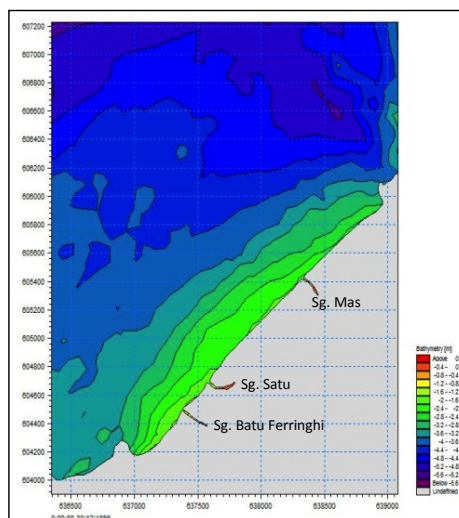


Figure 5. Bathymetry profile in the study area

MIKE21 AD (Advection/Dispersion) module models the advection and dispersion process using the simulated flow field. In this study, the basic water quality parameter, including biochemical oxygen demand (BOD), chemical oxygen demand (COD), total suspended solid (TSS), and ammonical nitrogen (AN), are considered. The inputs constitute pollutant loading rates, which are the products of the observed river discharge and the concentrations of the respective parameters at each of the river source obtained from DID.

## RESULTS AND DISCUSSION

### Calibration and Validation

Simulation was carried out from 2<sup>nd</sup> – 19<sup>th</sup> Sep 2007, which includes a 3-day ramp up period, followed by a 14-day semi-diurnal cycle. The neap and spring tidal conditions fall on 6-7<sup>th</sup> and 13-14<sup>th</sup> respectively. Average river outflow condition is considered where the magnitude for Sg. Batu Ferringhi, Sg. Satu and Sg. Mas are 1.88 m<sup>3</sup>/s, 1.15 m<sup>3</sup>/s, 0.47 m<sup>3</sup>/s respectively (DID, 2010). The dominant wind speed is 7.5 m/s coming from 288°N, and the resulting wave height ranges between 0.18 to 0.21 m above MSL.

Figures 6(a) to (c) show the calibration of the simulated results using the observation data from station LKIM in Teluk Bahang, which is located to the west of the study area. Both the water level fluctuation and current direction compared well with the observations. Meanwhile, for the current speed, the phase was well captured but the simulated troughs were generally

much higher. The values of the coefficient of determinant are shown in Table 2. Overall, the result is satisfactory.

Table 2  
*R<sup>2</sup>-values for model calibration and validation*

Location	Water level	Current speed	Current direction
Teluk Bahang	0.97	0.92	0.82
Pantai Keracut	0.97	0.99	0.99

Next, validation was carried out for the period 27-29<sup>th</sup> May 2014 by comparing the results with observations in Pantai Keracut (5°27'43.88"N, 100°10'7.21"E), which is located further west from Teluk Bahang. The water level, current speed, and current direction (Figures 7(a) to (c)) were all well captured in terms of the phase and magnitude, and *R<sup>2</sup>* values, as shown in Table 2. These suggest that the model is able to reproduce the local circulation and tidal conditions accurately.

### Simulation of Water Quality Constituents

The simulated flow field for the period 2<sup>nd</sup> – 19<sup>th</sup> Sep 2007 showed that the water levels in Batu Ferringhi beach ranged from 0.45 m to –0.45 m during neap tide, and 1.0 m to –1.1 m during spring tide. The current speed ranged from 0.04 m/s to 0.2 m/s, while current direction varied from north easterly to south westerly direction. For the advection/dispersion simulation, the observed water quality parameters in Sg Batu Ferringhi, Sg. Satu and Sg. Mas (Table 3) are used as point source input. The averaged initial concentration is weighted by the discharge in the rivers and used as a comparison to the observed concentration at sea.

Table 3  
*Initial and weighted concentration of water quality parameters (DID, 2010)*

Parameter	Initial concentration (mg/L)			Weighted concentration (mg/L)
	Sg. Batu Ferringhi	Sg. Satu	Sg. Mas	
BOD	8.32	9.00	7.09	8.38
COD	30.42	10.13	19.31	22.26
TSS	23.63	31.50	33.88	27.59
AN	1.20	0.20	0.20	0.74

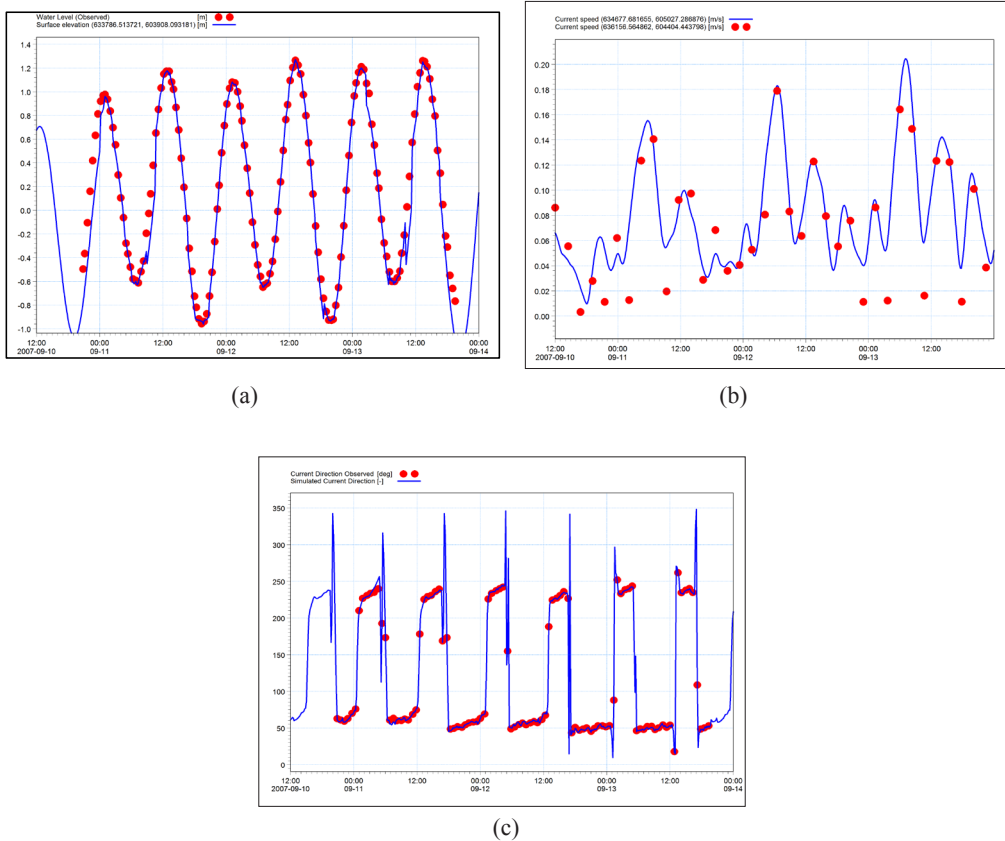


Figure 6. Model calibration using the observations from Teluk Bahang: (a) water level; (b) current speed; and (c) current direction

Figures 8(a) to (d) show the simulation results for the transport of BOD, COD, TSS and AN along Batu Ferringhi beach. The plots show the distribution scenario at noon time (12:00 p.m.) on 13 September 2007, which was during spring tide condition. In general, a net transport in the north easterly direction was observed, driven primarily by the coastal tidal current, coupled with a predominantly landward wave action.

It can be observed that high localised concentration of the four water quality constituents are trapped mainly at the headland at the northeast. Patchy escape from the headland occurs on a time scale corresponding to the tidal cycle. The highest observed concentrations for BOD, COD, TSS and AN beyond the headland were found to average at 26.8%, 33.7%, 43.5%, and 5.4%, respectively, compared to the weighted initial concentration (see Table 3). This suggests that, other than AN, the dispersion process is relatively slow along the shore in a typical tidal cycle.

## Advection and Dispersion of Water Quality Constituents

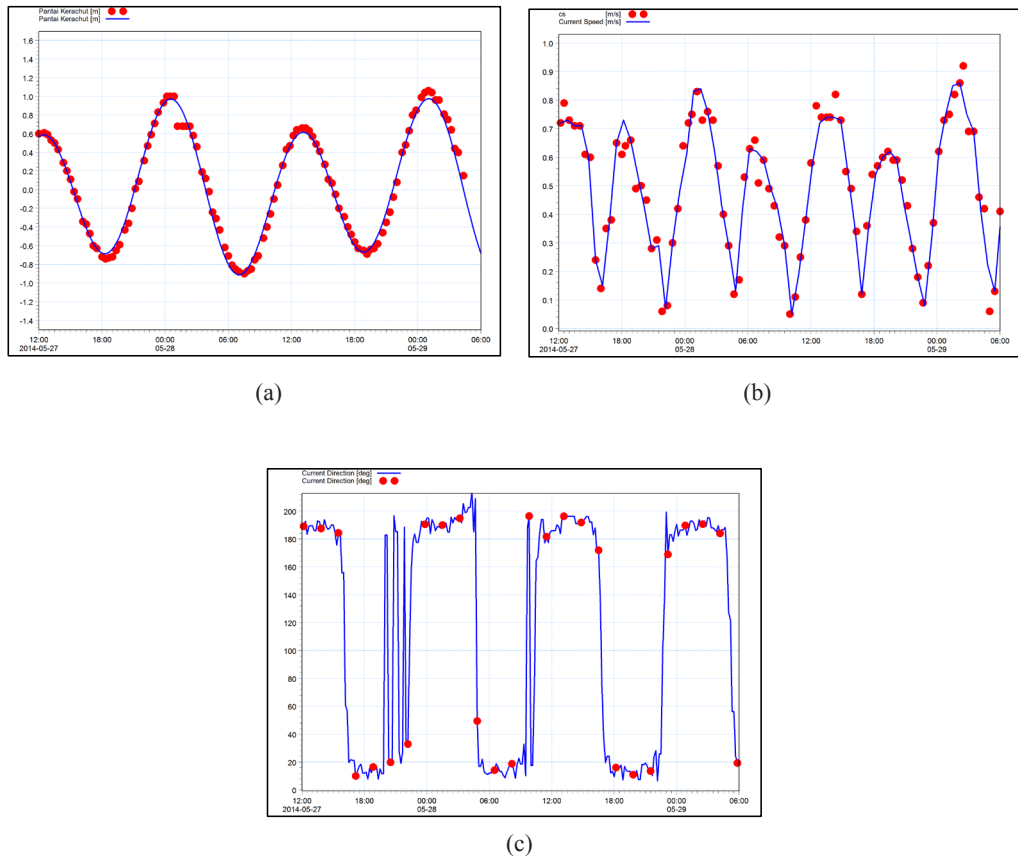


Figure 7. Model validation using the observations from Teluk Bahang: (a) water level; (b) current speed; and (c) current direction

In addition, localised trapping can also be observed towards the west of Sg. Mas. This is likely attributed to the orientation of Sg. Mas river mouth, which approaches the coastline at an oblique angle such that its discharge opposes the northeasterly longshore current, hence prohibits crossing of the constituents at the water front. More specifically, it was found that the concentrations trapped in this location is much higher, at up to 41.8%, 74.1%, 76.1% and 59.5%, respectively, compared to the weighted initial concentration from the three rivers. This suggests that both advection and dispersion are stalled at this location, and pollutants may potentially cause severe beach pollution.

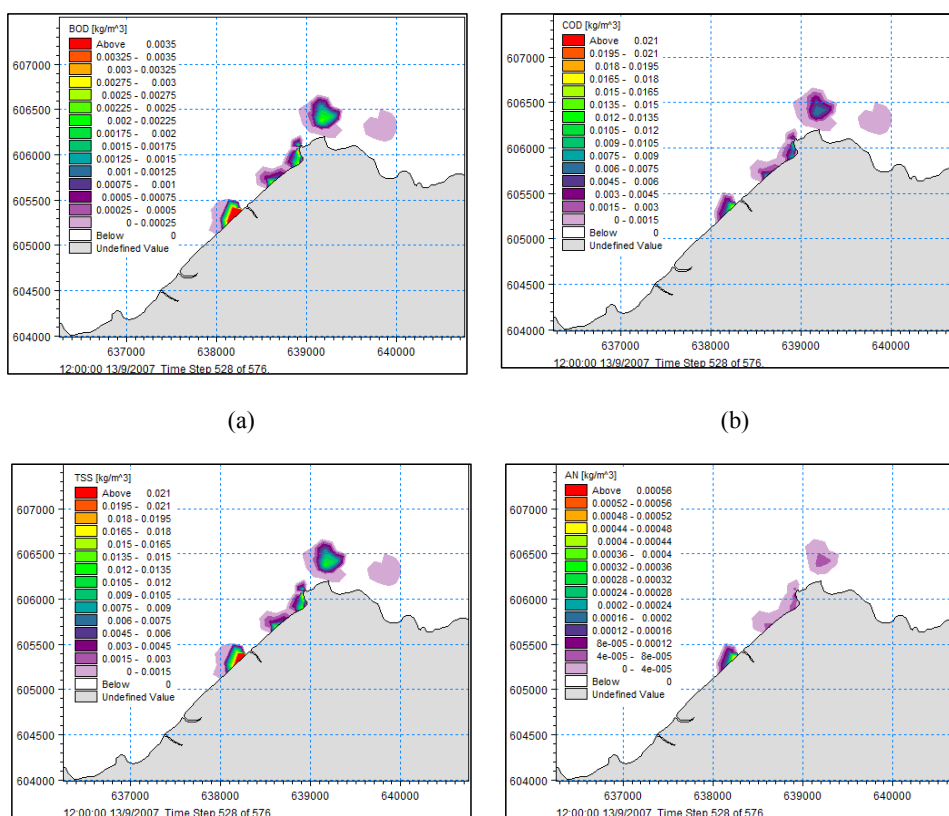


Figure 8. Distribution of: (a) BOD; (b) COD; (c) TSS; and (d) AN concentrations along Batu Ferringhi beach

## CONCLUSIONS

Hydrodynamic modelling of Batu Ferringhi beach is conducted in the present study using MIKE21 Hydrodynamic Module (HD), Spectral Wave Module (SW), and Advection/Dispersion Module (AD). Calibration and validation results show that the model is capable of reproducing the local hydrodynamics. Using water quality observations in Sg. Batu Ferringhi, Sg. Satu and Sg. Mas as the input, the transport of BOD, COD, TSS and AN in the study area was examined. The results showed that localised trapping occurred at the shoreline between Sg. Satu and Sg. Mas, as well as the headland located to the northeast of the study area, suggesting inadequate mixing, and thus dispersion, in the nearshore region.

In summary, there is a potential threat of beach pollution along Batu Ferringhi, as observed in the incident in 2014 if there is a sudden spike of pollutant discharge from the upstream catchment. Thus, proper care must be taken to monitor and regulate point and non-point sources in the upriver system of this popular beach. In the event of similar occurrences, the stretch of beach front adjacent to Sg. Mas and the headland must be closed to public access on the grounds of health and safety.



## ACKNOWLEDGEMENTS

The first author thanks Mr. Karthik, Director of Aqvaspace Sdn. Bhd., for the assistance on MIKE 21 software. The study was financed by LESTARI Grant, UiTM.

## REFERENCES

- Ahmad, F., Yahaya, A. S., & Farooqi, M. A. (2006). Characterization and Geotechnical Properties of Penang Residual Soils with Emphasis on Landslides. *Am. J. Environ. Sci.*, 2(4), 121-128.
- Babu, M. T., Das, V. K., & Vethamony, P. (2006). BOD-DO modeling and water quality analysis of a waste water outfall off Kochi, west coast of India. *Environ. Int.*, 32, 165-173.
- DiGiacomo, P. M., Washburn, L., Holt, B., & Jones, B. H. (2004). Coastal pollution hazards in southern California observed by SAR imagery: stormwater plumes, wastewater plumes, and natural hydrocarbon seeps. *Marine Pollut. Bull.*, 49, 1013-1024.
- Koh, H. L., Lim P. E., & Lee, H. L. (1997). Impact modelling of sewage discharge from Georgetown of Penang, Malaysia on coastal water quality. *Environ. Monit. Assess.*, 44, 199-209.
- Lee, W. K., Borthwick, A. G. L., & Taylor, P. H. (2014a). Tracer dynamics in two-layer density-stratified estuarine flow. *Proc. ICE - Eng. Comput. Mech.*, 167(1), 41-49, ICE, UK.
- Lee, W. K., Borthwick, A. G. L., & Taylor, P. H. (2014b). Wind-induced chaotic mixing in a two-layer density-stratified shallow flow. *J. Hydraul. Res.*, 52(2), 219-227, IAHR.
- Lee, W. K., & Zaharuddin, N. A. (2015). Lagrangian investigation on the compound effects of reclamation and proposed tidal barrage to the environmental flow. *J. Eng.*, 27, 71-80.
- Li, Z., Sheng, Y., Shi, W., Sun, Q., & Mortimer, R. J. G. (2015). Influence of salinity on COD measurements in coastal water management. *Desalination Water Treat*, 57(39), 18338-18345.
- Owens, J. D. (1978). Coliform and escherichia coli bacteria in seawater around penang island, Malaysia. *Water Res.* 2(6), 365-370.
- Shankar, A. (2014, February 4). Pollution of Batu Ferringhi: Authorities get cracking. *FMT News*.
- Snyder, W. H. (1985). Fluid modeling of pollutant transport and diffusion in stably stratified flows over complex terrain. *Ann. Rev. Fluid Mech.*, 17, 239-266.
- Su, Y. F., Liou, J. J., Hou, J. C., Hung W. C., Hsu, S. M., Lien, Y. T., Su, M. D., Cheng, K. S., & Wang, Y. F. (2008). A Multivariate Model for Coastal Water Quality Mapping Using Satellite Remote Sensing Images. *Sensors*, 8, 6321-6339.
- Voss, M. (2011). Nitrogen processes in coastal and marine ecosystems. In M.A. Sutton, C.M. Howard, J.W. Erisman, G. Billen, A. Bleeker, P. Grennfelt, H. van Grinsven, & B. Grizzetti (Eds), *The European Nitrogen Assess.*, 8, 147-176. Cambridge.
- Zimmerman, J. T. F. (1986). The tidal whirlpool: A review of horizontal dispersion by tidal and residual currents. *Neth. J. Sea Res.* 20(2-3), 133-154.





## Substituent Effect on Catalytic Activity of Palladium(II) Schiff Base Complexes for Sonogashira Reaction

Hadariah Bahron<sup>1\*</sup>, Shahrul Nizam Ahmad<sup>1</sup>, Amalina Mohd Tajuddin<sup>1</sup> and Syed Illah Al-Yahya Syed Abdul Kadir<sup>2</sup>

<sup>1</sup>Department of Chemistry, Faculty of Applied Sciences, Universiti Teknologi MARA (UiTM), 40450 Shah Alam, Selangor, Malaysia

<sup>2</sup>Centre of Foundation Studies, Universiti Teknologi MARA (UiTM), 43800 Dengkil, Selangor, Malaysia

### ABSTRACT

Chemical industries are greatly assisted by catalysts; and commonly used catalysts for C-C formation reactions are mainly phosphine-based complexes which are air and moisture sensitive. New air stable Schiff base Pd(II) complexes have been synthesised, characterised and screened for their catalytic potential. This paper reports three ONNO Schiff bases, namely, L2C [2,2'-((1E,1'E)-((2,2-dimethylpropane-1,3-diyl) bis (azanylylidene)) bis (methanylylidene)-) bis (4-chlorophenol)], L2M [2,2'-((1E,1'E)-((2,2-dimethylpropane-1,3-diyl)bis(azanylyli-dene)) bis (methanylylidene)) bis (4-methylphenol)] and L2H [2,2'-((1E,1'E) - ((2,2-dimethyl-propane-1,3-diyl) bis (azanylylidene)) bis (methanylylidene)) diphenol]. These were synthesised from 2,2-dimethyl-1,3-propanediamine and salicylaldehyde derivatives with Cl, CH<sub>3</sub> and H at the *meta* position, respectively. The compounds were reacted with palladium(II) acetate yielding three palladium(II) complexes denoted as PdL2C, PdL2M and PdL2H. The structures of all compounds were elucidated through elemental analysis, <sup>1</sup>H and <sup>13</sup>C NMR, FTIR and melting point. The complexes were screened for catalytic activities in Sonogashira coupling reaction between iodobenzene and phenylacetylene in DMSO. PdL2H was found to be the most active catalyst with 87% iodobenzene conversion after 12 hours of reaction.

**Keywords:** Catalysis, palladium(II) complexes, Schiff bases, Sonogashira, substituent

### ARTICLE INFO

#### Article history:

Received: 25 October 2016

Accepted: 17 March 2017

#### E-mail addresses:

hadariah@salam.uitm.edu.my (Hadariah Bahron),  
shahrulnizam85@gmail.com (Shahrul Nizam Ahmad),  
amalina9487@salam.uitm.edu.my (Amalina Mohd Tajuddin),  
illah.alyahya@puncakalam.uitm.edu.my  
(Syed Illah Al-Yahya Abdul Kadir)

\*Corresponding Author

### INTRODUCTION

Schiff bases have become trendy in the study of coordination compounds due to several interesting chemical and physical properties, as well as applicability in various fields. Schiff bases are able to coordinate many different metals especially transition metals and

stabilise them in multiple oxidation numbers. Schiff bases bearing O and N donors are very popular due to diverse chelating ability. The outstanding chelating ability is mainly assisted by the lone pair of electrons located in  $sp^2$  hybrid orbitals of the azomethine nitrogen. The metal complexes of Schiff bases can be air-stable and possess the ability to tolerate high temperatures which are among the key criteria of good catalysts (Keypour, Salehzadeh, & Parish, 2002).

Palladium has become an active part of coordination and organometallic chemistry related to all types of catalysis including homogeneous, heterogeneous, heterogenised and nanocatalysis. Palladium complexes are excellent and versatile catalysts in many important chemical reactions such as carbon-carbon coupling, alkylation, carbonylation and oxidation (Barder et al., 2005). They are widely employed as catalysts because Pd catalysed reactions can proceed under mild conditions, producing high yields, and bearing outstanding level of stereo-, regio-, and chemoselectivity (Ghammamy & Sedaghat, 2012).

It has been reported that in Sonogashira-Hagihara coupling reactions, palladium compounds such as  $Pd(PPh_3)_4$ ,  $PdCl_2(PPh_3)_2$ ,  $PdCl_2(CH_3CN)_2$  and  $Pd(OAc)_2$  have been commonly used as catalysts (Chinchilla & Nájera, 2011). However, phosphines have some drawbacks in that they are very sensitive to aerial oxidation and moisture and consequently demanding inert conditions which cause difficulty in handling and synthesis applications (Suzuka et al., 2010). In addition, phosphine ligands are expensive and therefore, the search for phosphine-free ligands is imperative.

Thus, this paper aims at reporting the synthesis, physicochemical and spectral characterisation of tetradentate Schiff bases and their palladium(II) complexes, as well as their catalytic activities in Sonogashira coupling reaction.

## METHOD

All chemicals and solvents purchased from commercial suppliers were used without further purification. The micro-analytical data (C, H and N) of all ligands and complexes were obtained from Thermo Scientific Flash 2000 Elemental Analyser. Melting points were determined using Stuart SMP10 and were uncorrected. Perkin-Elmer Spectrum One FTIR spectrometer using KBr pellets were employed to record Infrared (IR) spectra of ligands and complexes between  $4000 - 450\text{ cm}^{-1}$ . Meanwhile,  $^1H$  and  $^{13}C$  NMR spectra were recorded on a Bruker Varian-600MHz spectrometer using deuterated  $CDCl_3$  and expressed in a unit of parts per million ( $\delta$ , ppm). The percent conversion of iodobenzene was monitored using Gas Chromatography-Flame Ionization Detection model Agilent 6890N.

## Synthesis of L2C

A hot solution of 2,2-dimethyl-1,3-propanediamine  $C_5H_{14}N_2$  (1 mmol, 0.1022g) in absolute EtOH (10 ml) was added to a stirred solution of chlorosalicylaldehyde  $C_7H_5ClO_2$  (2 mmol, 0.3132 g) in absolute EtOH (10 ml). The solution was refluxed for 5 h, and then cooled. The yellow solid obtained was filtered off, washed with cold ethanol, and dried.

### Synthesis of L2M

A hot solution of 2,2-dimethyl-1,3-propanediamine  $C_5H_{14}N_2$  (1 mmol, 0.1022g) in absolute EtOH (10 ml) was added to a stirring solution of methylsalicylaldehyde  $C_8H_8O_2$  (2 mmol, 0.2724 g) in absolute EtOH (10 ml). The solution was refluxed for 4 h, and then cooled. The light yellow solid obtained was filtered off, washed with cold ethanol and dried.

### Synthesis of L2H

A hot solution of  $C_5H_{14}N_2$  (1 mmol, 0.1022 g) in absolute EtOH (10 ml) was added into a stirring solution of  $C_7H_6O_2$  (2 mmol, 0.2442 g) in absolute EtOH (10 ml). The solution was refluxed for 5 h before it was cooled. The yellow solid obtained was filtered off, washed with cold ethanol, and dried.

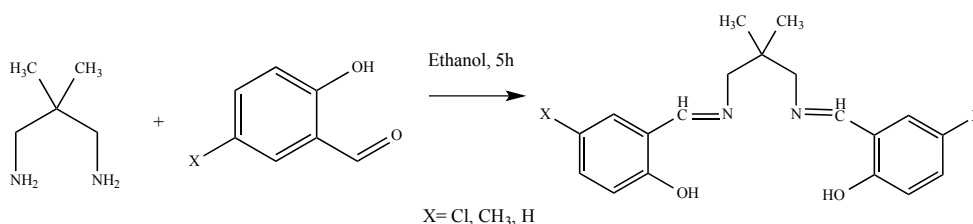


Figure 1. General synthesis of Schiff base ligands

### Synthesis of PdL2C

Palladium(II) acetate (1 mmol, 0.2248 g) was dissolved in 20 mL of acetonitrile. 1 mmol (0.3793 g) of  $C_{19}H_{20}Cl_2N_2O_2$  was dissolved separately in 20 mL of acetonitrile. The ligand solution was added dropwise into the metal salt solution, refluxed for 6 h, and cooled to room temperature. The yellow solid obtained was filtered off, washed with cold acetonitrile, and dried in air.

### Synthesis of PdL2M

The palladium(II) acetate (1 mmol, 0.2248 g) was dissolved in 20 mL of acetonitrile. 1 mmol (0.3385 g) of  $C_{21}H_{26}N_2O_2$  was dissolved separately in 20 mL of acetonitrile. The ligand solution was added dropwise into the metal salt solution, refluxed for 6 h, and cooled to room temperature. The orange solid obtained was filtered off, washed with cold acetonitrile, and dried in air.

### Synthesis of PdL2H

The palladium(II) acetate (1 mmol, 0.2248 g) was dissolved in 20 mL of acetonitrile. 1 mmol (0.3104 g) of  $C_{19}H_{22}N_2O_2$  was dissolved separately in 20 mL of acetonitrile. The ligand solution was added dropwise into the metal salt solution, refluxed for 6 h and cooled to room temperature. The dark grey solid obtained was filtered off, washed with cold acetonitrile, and dried in air.

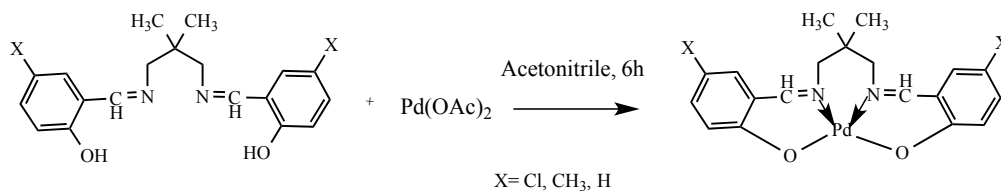


Figure 2. General synthesis of Pd(II) complexes

### Catalytic Activity Screening for Sonogashira reaction

A round-bottomed flask was charged with iodobenzene (1.0 mmol), phenylacetylene (1.5 mmol), palladium(II) Schiff base complex (0.01 mmol) and triethylamine (2.0 mmol), with stirring under aerobic condition in 7 mL of DMSO. The mixture was heated at 100°C for 12 h, monitored every 3 hours by Gas Chromatography-Flame Ionisation Detection (GC-FID) to determine the percentage conversion of iodobenzene, and calculated as follows:

$$\% \text{ Conversion} = (A_{\text{int}} - A_{\text{final}})/A_{\text{int}} \quad [1]$$

$A_{\text{int}}$  = peak area of iodobenzene before reaction

$A_{\text{final}}$  = peak area of iodobenzene after reaction

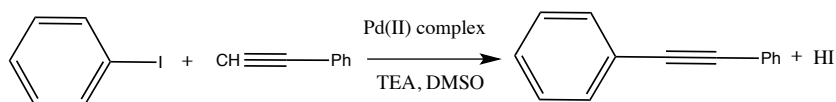


Figure 3. General procedure of Sonogashira reaction

## RESULTS AND DISCUSSION

### Elemental Analysis

The analytical data of the compounds are presented in Table 1. The experimental C, H, N percentages are in concordance with the theoretical values, indicating that the intended compounds (Figure 1 and Figure 2) have been obtained. As expected, the melting points of the parent ligands were lower than those of the complexes due to the presence of strong ionic and dative bonds in the complexes.

Table 1  
*Physicochemical data of ligands and palladium(II) complexes*

Compd.	Color	Percent Yield (%)	Chemical Formula	Melting Point (°C)	Elemental Analysis % found (calculated)		
					C	H	N
L2H	Yellow	96.6	C <sub>19</sub> H <sub>22</sub> N <sub>2</sub> O <sub>2</sub>	116	72.78 (73.52)	7.12 (7.14)	9.60 (9.03)
PdL2H	Brown	64.8	C <sub>19</sub> H <sub>20</sub> N <sub>2</sub> O <sub>2</sub> Pd	292	53.62 (55.02)	4.66 (4.86)	7.50 (6.75)
L2C	Yellow	90.9	C <sub>19</sub> H <sub>20</sub> Cl <sub>2</sub> N <sub>2</sub> O <sub>2</sub>	136	60.17 (60.17)	5.94 (5.32)	7.30 (7.39)
PdL2C	Yellow	87.8	C <sub>19</sub> H <sub>18</sub> Cl <sub>2</sub> N <sub>2</sub> O <sub>2</sub> Pd	278	47.23 (46.18)	4.10 (3.75)	5.87 (5.79)
L2M	Light Yellow	89.2	C <sub>21</sub> H <sub>26</sub> N <sub>2</sub> O <sub>2</sub>	110	74.31 (74.53)	8.70 (7.74)	8.35 (8.28)
PdL2M	Orange	85.4	C <sub>21</sub> H <sub>24</sub> N <sub>2</sub> O <sub>2</sub> Pd	254	57.55 (56.96)	5.57 (5.46)	6.81 (6.33)

### Infrared Spectroscopy

The  $\nu(\text{C}=\text{N})$  peaks of all ligands appeared in the range of 1630 to 1631  $\text{cm}^{-1}$  (Table 2 and Figure 4). These peaks shifted by about approximately 10 to 20  $\text{cm}^{-1}$  to lower frequencies of 1610 to 1620  $\text{cm}^{-1}$  in all Pd(II) complexes indicating that the  $\text{C}=\text{N}$  was experiencing a lowering in bond strength upon complexation. A possible explanation for the lowering of the  $\text{C}=\text{N}$  bond strength is the inductive effect of donation of imine lone pair of electrons to metal centres in the formation of the dative covalent bond with palladium. The lone pair of electrons on N is donated to the metal centre in the Lewis acid-base interaction, resulting in an inductive reduction of the electron density on the  $\text{C}=\text{N}$ , and making it weaker.

The peak of OH in free ligands was detected as a broad peak in the area of 3200  $\text{cm}^{-1}$ , and slightly displaced from the expected region (3300 - 3800  $\text{cm}^{-1}$ ), probably due to the formation of hydrogen bond between OH and  $\text{N}=\text{C}$ . The coordination between palladium and oxygen can be glimpsed through the disappearance of OH signal in palladium(II) complexes indicating deprotonation of the hydroxyl. The great displacement of the C-O band from 1229  $\text{cm}^{-1}$  in L2H to 1199  $\text{cm}^{-1}$ , a lower frequency in PdL2H, is also a useful evidence for the coordination of O to palladium. This is further corroborated by the shifting trend of C-N peaks, from lower to higher frequencies, indicating of a bond formation between nitrogen and metal.

There are new bands found in the range of 501 to 509  $\text{cm}^{-1}$  and 573 to 589  $\text{cm}^{-1}$  for palladium(II) complexes assignable to Pd-O and Pd-N, respectively, assenting with the values reported by Mohd Tajuddin et al. (2012). This indicates that the coordination between metal with phenolic oxygen and metal with imine nitrogen has been efficaciously attained.

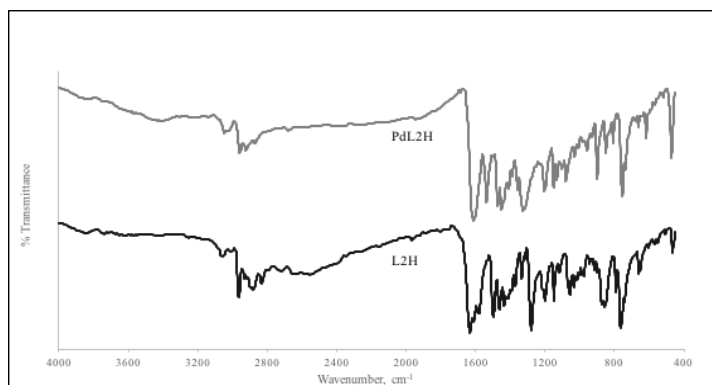


Figure 4. Representative IR spectra (L2H and PdL2H)

Table 2  
Main FTIR spectral data of ligands and their palladium(II) complexes

Compd.	Frequency, $\nu(\text{cm}^{-1})$						
	OH	C=N	C-N	C-O (phenol)	Pd-N	Pd-O	C-H $sp^3$
L2C	3249	1631	1308	1229	-	-	2971
PdL2C	-	1611	1319	1204	581	509	2963
L2M	3253	1631	1371	1228	-	-	2963
PdL2M	-	1620	1318	1207	573	518	2962
L2H	3246	1630	1333	1229	-	-	2964
PdL2H	-	1610	1328	1199	589	501	2956

### NMR Spectroscopy

From  $^1\text{H}$  NMR spectra (Table 3 and Table 4), OH signal appears as broad peak at the downfield region of 13.35 -13.60 ppm in all ligands. The phenolic protons are highly deshielded due to the presence of O and formation of hydrogen bonding (Aranha et al., 2006). The electronegativity of oxygen withdraws the density of electrons from acidic proton and causes the chemical shift to appear at the downfield region. The chemical shifts of aromatic protons appear as multiplets at 6.80-7.30 ppm. The coupling constants tabulated in Table 3 are in the range of 1 to 3 Hz and 6 to 9 Hz, suggesting the existence of *meta* and *ortho* aromatic protons, respectively. This is in agreement with the chemical shifts reported by Mohd Tajuddin et al. (2012). The protons are deshielded due to diamagnetic anisotropy that is contributed by circulating p electrons in the aromatic rings. The number of protons obtained is in concordance with the structure.

The chemical shifts for azomethine proton, H-C=N, appear as a singlet around the vicinity of 8.30 ppm for all ligands, implying that there is no pronounced effect of both electron-withdrawing and electron-donating substituents. The methyl group on the aromatic ring was detected as a singlet at 2.32 ppm in L2M, slightly downfield in comparison with the aliphatic methyl groups, owing to the resonance of electron in the aromatic environment.



Table 3  
<sup>1</sup>H NMR chemical shifts (d/ppm) of ligands

Compd.	Chemical shifts, d/ppm					
	d(O-H)	d(HC=N)	d(Ar-H)	d(Ar-CH <sub>3</sub> )	d(CH <sub>3</sub> ) aliphatic	d(CH)
L2C	13.51( <i>b</i> )	8.30( <i>s</i> )	6.91-7.35( <i>m</i> )	-	0.97( <i>s</i> )	3.50( <i>s</i> )
L2M	13.35( <i>b</i> )	8.31( <i>s</i> )	6.91-7.35( <i>m</i> )	2.32( <i>s</i> )	0.92( <i>s</i> )	3.50( <i>s</i> )
L2H	13.60( <i>b</i> )	8.37( <i>s</i> )	6.91-7.35( <i>m</i> )	-	1.11( <i>s</i> )	3.52( <i>s</i> )

Note: (*s*) = singlet; (*d*) = doublet; (*t*) = triplet; (*m*) = multiplet; (*b*) = broad; Ar = aromatic

Table 4  
<sup>1</sup>H NMR chemical shifts (d/ppm) of aromatic protons of L2H

d(Ar-H)	Multiplicity	Coupling constants, J (Hz)	Number of hydrogen
6.91	<i>td</i>	7.5, 1.1	1
7.00	<i>dd</i>	8.3, 1.1	1
7.29	<i>dd</i>	7.7, 1.7	1
7.35	<i>ddd</i>	8.6, 7.2, 1.7	1

Note: (*td*) = triplet of doublet; (*dd*) = doublet of doublet; (*ddd*) = doublet of doublet of doublet; Ar = aromatic

In the <sup>13</sup>C NMR spectra (Table 5), the peaks of carbon bonded to oxygen of the phenolic group, d(C-OH) appear in the vicinity of 165 ppm, slightly farther downfield than the azomethine carbon. This can be explained by the presence of oxygen and delocalisation of p electrons in benzene rings. The azomethine carbon appears consistently around 160 ppm with no significant influence of the substituent groups.

The presence of Cl in L2C, however, has increased the shifting of aromatic carbons by about ~2 ppm, slightly downfield as compared to the other two ligands. The electronegativity of Cl in L2C has effect on reducing the valence electron density, deshielding the carbon from the applied magnetic field. The signals of Ar-CH<sub>3</sub> and Ar-Cl were discovered at 20.33 and 123.86 ppm, respectively.

Table 5  
<sup>13</sup>C NMR chemical shifts (d/ppm) of ligands

Comp.	Chemical shifts, d (ppm)							
	C-OH	HC=N	Ar-H	Ar-CH <sub>3</sub>	Ar-Cl	CH <sub>3</sub>	CH	C(CH <sub>3</sub> ) <sub>2</sub>
L2C	164.69	160.13	118.21- 132.25	-	123.86	22.87	68.13	36.30
L2M	165.72	159.03	116.68- 133.10	20.33	-	23.47	68.01	36.26
L2H	165.75	161.22	116.97- 132.33	-	-	24.40	68.16	36.27

All palladium(II) complexes have poor solubility in all deuterated solvents, hence, no <sup>1</sup>H and <sup>13</sup>C NMR spectra were obtained.

## Sonogashira Coupling Reaction

All palladium complexes were screened as a catalyst in Sonogashira cross-coupling reaction of iodobenzene with phenylacetylene in the presence of KOH as a base in dimethylsulfoxide (DMSO) at 100°C with 1 mmol% catalyst loading.

The percentage conversion of iodobenzene was monitored using GC-FID, where sampling was done every 3 hours. Table 6 shows that the PdL2H catalysed the highest conversion of iodobenzene (87%), followed by PdL2M (73%), and PdL2C (57%). Meanwhile, control reaction was done with the absence of catalyst, where no conversion of iodobenzene after 12 h of reaction was detected.

Table 6  
*Percentage of iodobenzene conversion*

Catalyst	% Conversion of Iodobenzene			
	3h	6h	9h	12h
PdL2C	37	45	50	57
PdL2M	37	48	72	73
PdL2H	34	43	52	87

The results showed that the highest conversion of iodobenzene was attained at 12 hours, the highest reaction time. It appears that the catalytic property of these compounds was mainly controlled by the steric factor where the unsubstituted PdL2H exhibited the highest activity at 87%. With no bulky substituents at the aromatic ring, the catalytic activity was enhanced.

Comparing the catalytic activities of the substituted compounds PdL2C (57%) and PdL2M (73%), the electronic factor was also found to play an important role, albeit less significantly. The electron donating substituent, namely methyl in PdL2M, was shown to enhance the catalytic activity in comparison with the electron withdrawing Cl in PdL2C.

## CONCLUSION

Three tetradentate Schiff bases and their respective palladium(II) complexes were successfully synthesised and characterised via elemental analysis, IR spectroscopy, as well as <sup>1</sup>H and <sup>13</sup>C NMR spectroscopy.

Through infrared spectroscopy, the Schiff base ligands were observed to coordinate to palladium(II) centre through phenolic oxygen and azomethine nitrogen. PdL2H showed the highest catalytic activity in Sonogashira coupling reaction, with 87% conversion of iodobenzene after 12 h of reaction time at 100°C at 1 mmol % catalyst loading under aerobic condition.

## ACKNOWLEDGEMENTS

The authors would like to acknowledge the financial support by the Ministry of Higher Education, Malaysia through the Research Acculturation Grant Scheme (600-RMI/RAGS 5/3 (139/2014)). The authors gratefully appreciate the research facilities and scholarship provided by Universiti Teknologi MARA.

**REFERENCES**

- Aranha, P. E., Santos, M. P., Romera, S., & Dockal, E. R. (2006). Synthesis, characterization, and spectroscopic studies of tetradentate Schiff base chromium (III) complexes. *Polyhedron*, 26(7), 1373–1382. doi:10.1016/j.poly.2006.11.005.
- Barder, T. E., Walker, S. D., Martinelli, J. R., & Buchwald, S. L. (2005). Catalysts for Suzuki-Miyaura coupling processes: Scope and studies of the effect of ligand structure. *Journal of the American Chemical Society*, 127(13), 4685–4696. doi:10.1021/ja042491j
- Chinchilla, R., & Nájera, C. (2011). Recent advances in Sonogashira reactions. *Chemical Society Reviews*, 40(10), 5084. doi:10.1039/c1cs15071e.
- Ghammamy, S., & Sedaghat, S. (2012). Determination and characterization of new palladium complexes and study of their properties. *Middle-East Journal of Scientific Research*, 12(2), 264–269. doi:10.5829/idosi.mejsr.2012.12.2.63211.
- Keypour, H., Salehzadeh, S., & Parish, R. V. (2002). Synthesis of two potentially heptadentate (N4O3) Schiff-base ligands derived from condensation of tris(3-aminopropyl)-amine and salicylaldehyde or 4-hydroxysalicylaldehyde. Nickel(II) and copper(II) complexes of the former ligand. *Molecules*, 7(2), 140–144. doi:10.3390/70200140.
- Mohd Tajuddin, A., Bahron, H., Kassim, K., Ibrahim, W. N. W., & Fun, H. K. (2012). Synthesis and Characterization of Palladium(II) Schiff Base and their Catalytic Activities for Heck Reaction. *Advanced Materials Research*, 554-556(April 2016), 736–740. doi:10.4028/www.scientific.net/AMR.554-556.736.
- Mohd Tajuddin, A., Bahron, H., Kassim, K., Wan Ibrahim, W. N., & Yamin, B. M. (2012). Synthesis and Characterisation of Palladium (II) Schiff Base Complexes and Their Catalytic Activities for Suzuki Coupling Reaction. *Malaysian Journal of Analytical Sciences*, 16(1), 79–87.
- Suzuka, T., Okada, Y., Ooshiro, K., & Uozumi, Y. (2010). Copper-Free Sonogashira coupling in water with an amphiphilic resin-supported palladium complex. *Tetrahedron*, 66(5), 1064–1069. doi:10.1016/j.tet.2009.11.011.





## Syntheses, Characterisation and Application of Palladium(II) Complexes as Catalysts in Heck Cross-Coupling Reaction

Amalina Mohd Tajuddin<sup>1\*</sup> and Hadariah Bahron<sup>1,2</sup>

<sup>1</sup>Faculty of Applied Sciences, Universiti Teknologi MARA (UiTM), 40450 Shah Alam, Selangor, Malaysia

<sup>2</sup>Institute of Research Management & Innovation (IRMI), Universiti Teknologi MARA (UiTM), 40450 Shah Alam, Selangor, Malaysia

### ABSTRACT

A new series of *N,O*-bidentate ligands, L1, L2, L3 and L4, and their Pd(II) complexes, PdL1, PdL2, PdL3 and PdL4 have been synthesised and characterised using various physico-chemical techniques, namely elemental analyses, IR and <sup>1</sup>H and <sup>13</sup>C NMR spectroscopies, and conductivity analysis. The molecular geometries of PdL2 and PdL4 have been elucidated through single crystal X-ray crystallography revealing 2:1 molar equivalence of ligand: Pd with the Schiff bases that exhibited bidentate ligands behaviour, in which they coordinated through the phenolic O donor atoms and imine N. Upon complexation, the  $\nu(\text{C}=\text{N})$  around 1629-1639  $\text{cm}^{-1}$  and  $\nu(\text{C}-\text{O})$  around 1251 to 1252  $\text{cm}^{-1}$  shifted to lower frequencies by 4 to 23  $\text{cm}^{-1}$ . In this study, three parameters were chosen for the reaction conditions optimisation, which were types of bases, loadings for the catalyst, and temperatures of the reaction. Pd(II) complexes exhibited good catalytic activities for Heck coupling reaction with 100% conversion at 100°C within 12 hours of reaction time. Reducing the reaction temperature to 80°C reduced the conversion to a maximum of 80%.

**Keywords:** Bidentate Schiff base, Heck cross-coupling reaction, palladium(II), X-ray

### INTRODUCTION

Schiff bases are compounds that have been extensively studied (He & Cai, 2011) for

their selectivity and sensitivity toward various metal ions. Scientists in this field of study have put extensive work in synthesis, as well as characterisation of mono-nuclear and bi-nuclear transition metal complexes. It is reported that bidentate Schiff bases were the ligands of choice because they are known to be the most convenient and attractive ligands for metal centre complexations (Vigato & Tamburini, 2004; Drozdak et al., 2005). The metal complexes of Schiff bases especially Pd(II) and Ni(II) containing nitrogen and other

#### ARTICLE INFO

##### Article history:

Received: 25 October 2016

Accepted: 17 March 2017

##### E-mail addresses:

amalina9487@salam.uitm.edu.my (Amalina Mohd Tajuddin),

hadariah@salam.uitm.edu.my (Hadariah Bahron)

\*Corresponding Author

donor atoms have been given attention because of their stability, biological activity (Islam et al., 2013) and potential applications as catalysis (Kumar et al., 2009).

Currently, phosphines complexes are the most common catalysts applied for the cross-coupling of C—C bond formation due to the presence of strong P-donors such as tetrakis(triphenylphosphine)palladium(0) ( $\text{Pd}(\text{PPh}_3)_4$ ), which has resulted in high conversion rates catalysed by these complexes and comparative ease of modifying their properties. Nonetheless, it is also known that such low-valent, low-coordinate palladium complexes of phosphines can be extremely unstable in ambient conditions and their formation has been found to be energetically unfavourable. Furthermore, these types of compounds are not ecological friendly (Lai et al., 2005).

It is important to note that the catalysts used in Heck reaction for the formation on C—C bonds in laboratories are Pd(II) complexes with nitrogen-containing ligands (Pratihar et al., 2012). The catalytic activity of the bidentate Schiff base Pd(II) complexes not only rivals but may be better than the corresponding phosphines and sulphur equivalents. Thus, the practices of employing phosphine and sulphur-free palladium catalysts in Suzuki cross-coupling reactions are of interest to many (Lai et al., 2005).

The objective of the present work is to study the chelation behaviour of bidentate Schiff base ligands towards palladium(II) ion. Herein, some remarkable results of using several new types of *N,O*-bidentate ligands in palladium-catalysed Heck coupling reaction are presented. The efficiency of palladium(II) complexes are compared and discussed subsequently. A preliminary result of this investigation of Heck cross-coupling reaction is also reported in this paper.

## MATERIALS AND METHOD

### Materials

All operations were carried out under a dry nitrogen atmosphere. All reagents and chemical were laboratory pure grade and used without purification. A Thermo Finnigan Flash Elemental Analyser 2000 was used for microanalyses of C, H and N. The IR spectra were obtained using the Perkin Elmer 1750X FTIR spectrophotometer ( $4000\text{--}400\text{ cm}^{-1}$ ) with KBr disc samples. Prior to use, KBr of Spectroscopic grade was dried in an oven at  $110^\circ\text{C}$  overnight and then stored in a desiccator. The spectra for proton ( $^1\text{H}$ ) and carbon ( $^{13}\text{C}$ ) NMR (300 MHz) were recorded on a Bruker Varian spectrometer in  $\text{CDCl}_3$  and the results were reported in ppm ( $\delta$ ) relative to TMS, applying the residual solvent resonances as the internal references. Single-crystal x-ray diffraction investigations were carried out on Bruker SMART APEX CCD area-detector diffractometer. Analyses using gas chromatography were performed on Agilent 6890N Network GC System with a Flame Ionisation Detector (FID).

## General Procedure of the Synthesis of Schiff Base Ligands

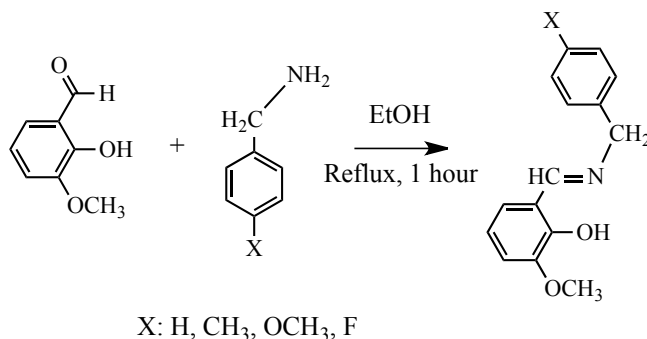


Figure 1. Synthesis of Schiff bases (L1-L4)

Schiff base ligand was synthesised by first dissolving *o*-vanillin (50 mmol, 7.6091 g) in ethanol. This was followed by adding the mixture into an ethanolic solution of benzylamine (50 mmol, 5.3869 g). The mixture was then stirred overnight to allow for it to react. Following that, the ethanol was evaporated slowly at room temperature. After a week, yellow solids appeared. The solids were collected, filtered off, and washed with ice-cold ethanol. Lastly, the sample was allowed to air-dry at room temperature and to give ligands of L1, L2, L3 and L4 (Figure 1).

### (E)-2-((benzylimino)methyl)-6-methoxyphenol (L1)

Yellow solid; yield, 37%; m.p. 62-65°C. <sup>1</sup>H NMR (300 MHz, CDCl<sub>3</sub>): δ 4.82 (s, 2H, CH<sub>2</sub>), 3.90 (s, 3H, Ar-OCH<sub>3</sub>), 6.84-7.32 (phenylic hydrogen groups), 8.42 (s, 1H, =CH), 13.85 (b, 1H, OH). <sup>13</sup>C NMR (300MHz, CDCl<sub>3</sub>): δ 56.0 (Ar-OCH<sub>3</sub>), 62.6 (CH<sub>2</sub>), 113.9, 117.9, 122.9, 127.6, 128.7 (ArC), 151.7 (C1), 127.3 (C13), 165.7 (N=CH). Anal. Calcd for C<sub>15</sub>H<sub>15</sub>NO<sub>2</sub>: C, 74.67; H, 6.27; N, 5.81%; Found: C, 74.77; H, 6.31; N, 5.91%. IR (KBr, cm<sup>-1</sup>): 3471 ν(OH), 1634 ν(C=N), 1344 ν(C-N), 1254 ν(C-O), 1054 ν(OCH<sub>3</sub>).

### (E)-2-methoxy-6-((4-methylbenzylimino)methyl)phenol (L2)

Yellow liquid at room temperature. <sup>1</sup>H NMR (300 MHz, CDCl<sub>3</sub>): δ 2.34 (s, 3H, CH<sub>3</sub>), 4.78 (s, 2H, CH<sub>2</sub>), 3.90 (s, 3H, Ar-OCH<sub>3</sub>), 6.76-7.16 (phenylic hydrogen groups), 8.39 (s, 1H, =CH), 13.97 (b, 1H, OH). <sup>13</sup>C NMR (300MHz, CDCl<sub>3</sub>): δ 21.1 (CH<sub>3</sub>), 56.1 (Ar-OCH<sub>3</sub>), 62.25 (CH<sub>2</sub>), 114.0, 117.9, 127.6, 122.9, 129.3, 127.6, 128.7 (ArC), 151.9 (C1), 134.9 (C13), 165.4 (N=CH). Anal. Calcd for C<sub>16</sub>H<sub>17</sub>NO<sub>2</sub>: C, 75.27; H, 6.71; N, 5.49%; Found: C, 74.40; H, 6.67; N, 5.38%. IR (KBr, cm<sup>-1</sup>): 3483 ν(OH), 1629 ν(C=N), 1335 ν(C-N), 1252 ν(C-O), 1039 ν(OCH<sub>3</sub>).

### (E)-2-methoxy-6-((4-methoxybenzylimino)methyl)phenol (L3)

Yellow liquid at room temperature. <sup>1</sup>H NMR (300 MHz, CDCl<sub>3</sub>): δ 3.79 (s, H, OCH<sub>3</sub>), 4.74 (s, 2H, CH<sub>2</sub>), 3.88 (s, 3H, Ar-OCH<sub>3</sub>), 6.76-7.24 (phenylic hydrogen groups), 8.38 (s, 1H, =CH).

$^{13}\text{C}$  NMR (300MHz,  $\text{CDCl}_3$ ):  $\delta$  56.03 ( $\text{OCH}_3$ ), 56.04 ( $\text{Ar-OCH}_3$ ), 61.9 ( $\text{CH}_2$ ), 114.0, 114.3, 117.9, 122.9, 129.9, 129.9 ( $\text{ArC}$ ), 151.9 ( $\text{C1}$ ), 158.8 ( $\text{C13}$ ), 165.2 ( $\text{N=CH}$ ). Anal. Calcd for  $\text{C}_{16}\text{H}_{17}\text{NO}_3$ : C, 70.83; H, 6.32; N, 5.23%; Found: C, 71.08; H, 6.32; N, 5.23%. IR (KBr,  $\text{cm}^{-1}$ ): 3467  $\nu(\text{OH})$ , 1630  $\nu(\text{C=N})$ , 1344  $\nu(\text{C-N})$ , 1251  $\nu(\text{C-O})$ , 1033  $\nu(\text{OCH}_3)$ .

### (E)-2-((4-fluorobenzylimino)methyl)-6-methoxyphenol (L4)

Yellow solid; yield, 52%; m.p. 54-56°C.  $^1\text{H}$  NMR (300 MHz,  $\text{CDCl}_3$ ):  $\delta$  4.78 (s, 2H,  $\text{CH}_2$ ), 3.89 (s, 3H,  $\text{Ar-OCH}_3$ ), 6.85-7.30 (phenylic hydrogen groups), 8.42 (s, 2H,  $=\text{CH}$ ), 13.80 (b, 1H, OH).  $^{13}\text{C}$  NMR (300 MHz,  $\text{CDCl}_3$ ):  $\delta$  56.1 ( $\text{Ar-OCH}_3$ ), 62.1 ( $\text{CH}_2$ ), 115.4, 115.6, 118.1, 122.9, 129.2, 128.7 ( $\text{ArC}$ ), 151.5 ( $\text{C1}$ ), 160.4 ( $\text{C13}$ ), 165.7 ( $\text{N=CH}$ ). Anal. Calcd for  $\text{C}_{15}\text{H}_{14}\text{FNO}_2$ : C, 69.70; H, 5.48; N, 5.41%; Found: C, 69.63; H, 5.51; N, 5.49%. IR (KBr,  $\text{cm}^{-1}$ ): 3461  $\nu(\text{OH})$ , 1636  $\nu(\text{C=N})$ , 1336  $\nu(\text{C-N})$ , 1252  $\nu(\text{C-O})$ , 1037  $\nu(\text{OCH}_3)$ .

### General Procedure of The Synthesis of Palladium(II) Complexes

In a round bottom flask, ligand, (L1) (5 mmol, 1.2064 g) was dissolved in acetonitrile (10 mL). Separately, palladium(II) acetate (2.5 mmol, 0.5612 g) was dissolved in MeCN (10 mL) and was then added into the ligand solution. The mixture was then stirred and refluxed for 4 hours to yield brown solids. The solids were filtered off followed by washing with ice-cold MeCN prior to air-drying at room temperature. The solids products were recrystallized from chloroform producing orange crystals. The recrystallization gave complexes of PdL1, PdL2, PdL3 and PdL4, respectively (Figure 2).

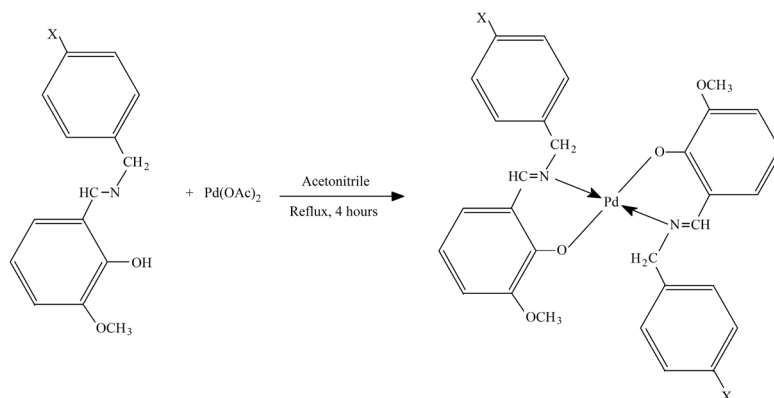


Figure 2. Synthesis of palladium(II) complexes (PdL1-PdL4)

### Bis(2-((E)-(benzylimino)methyl)-6-methoxyphenoxy)palladium(II) (PdL1)

Brown solid; yield, 91%; m.p. 256-259°C.  $^1\text{H}$  NMR (300 MHz,  $\text{CDCl}_3$ ):  $\delta$  5.12 (s, 2H,  $\text{CH}_2$ ), 3.75 (s, 3H,  $\text{Ar-OCH}_3$ ), 6.46-7.46 (phenylic hydrogen groups), 7.72 (s, 1H,  $=\text{CH}$ ).  $^{13}\text{C}$  NMR (300MHz,  $\text{CDCl}_3$ ):  $\delta$  55.9 ( $\text{Ar-OCH}_3$ ), 68.9 ( $\text{CH}_2$ ), 114.0, 120.2, 125.4, 127.4, 128.4 ( $\text{ArC}$ ), 127.2 ( $\text{C13}$ ), 162.9 ( $\text{N=CH}$ ). Anal. Calcd for  $\text{C}_{30}\text{H}_{28}\text{N}_2\text{O}_4\text{Pd}$ : C, 69.70; H, 5.48; N, 5.41%; Found: C, 61.47; H, 4.79; N, 4.72%. IR (KBr,  $\text{cm}^{-1}$ ): 1622  $\nu(\text{C=N})$ , 1316  $\nu(\text{C-N})$ , 1241  $\nu(\text{C-O})$ , 1095  $\nu(\text{OCH}_3)$ , 657  $\nu(\text{Pd-N})$ , 416  $\nu(\text{Pd-O})$ . UV-Vis ( $\text{CHCl}_3$ )  $\lambda_{\text{max}}$  (nm) = 252, 362, 473.  $\mu_{\text{eff}}$  (B.M.) (298 K): diamagnetic.



**Bis(2-methoxy-6-((E)-(4-methylbenzylimino)methyl)phenolato)palladium(II) (PdL2)**

Dark yellow; yield, 91%; m.p. 236-238°C. <sup>1</sup>H NMR (300 MHz, CDCl<sub>3</sub>): δ 2.30 (s, 3H, CH<sub>3</sub>), 5.07 (s, 2H, CH<sub>2</sub>), 3.75 (s, 3H, Ar-OCH<sub>3</sub>), 6.76-7.34 (phenylic hydrogen groups), 7.69 (s, 1H, =CH). <sup>13</sup>C NMR (300 MHz, CDCl<sub>3</sub>): 21.1 (CH<sub>3</sub>), 55.9 (Ar-OCH<sub>3</sub>), 62.25 (CH<sub>2</sub>), 114.0, 120.4, 125.4, 128.4, 129.1 (ArC), 136.1 (C13), 162.6 (N=CH). Anal. Calcd for C<sub>32</sub>H<sub>32</sub>N<sub>2</sub>O<sub>4</sub>Pd: C, 62.49; H, 5.24; N, 4.55%; Found: C, 62.47; H, 5.29; N, 4.55%. IR (KBr, cm<sup>-1</sup>): 1623 ν(C=N), 1316 ν(C-N), 1239 ν(C-O), 1092 ν(OCH<sub>3</sub>), 660 ν(Pd-N), 416 ν(Pd-O). UV-Vis (CHCl<sub>3</sub>) λ<sub>max</sub> (nm) = 246, 292, 408. μ<sub>eff</sub> (B.M.) (298 K): diamagnetic.

**Bis(2-methoxy-6-((E)-(4-methoxybenzylimino)methyl)phenolato)palladium(II) (PdL3)**

Brown solid; yield, 81%; m.p. 204-205°C. <sup>1</sup>H NMR (300 MHz, CDCl<sub>3</sub>): δ 3.77 (s, H, OCH<sub>3</sub>), 5.04 (s, 2H, CH<sub>2</sub>), 3.76 (s, 3H, Ar-OCH<sub>3</sub>), 6.47-7.39 (phenylic hydrogen groups), 7.69 (s, 1H, =CH). <sup>13</sup>C NMR (300MHz, CDCl<sub>3</sub>): 55.2 (OCH<sub>3</sub>), 55.9 (Ar-OCH<sub>3</sub>), 58.3 (CH<sub>2</sub>), 113.9, 114.0, 125.5, 129.8 (ArC), 158.8 (C13), 162.4 (N=CH). Anal. Calcd for C<sub>32</sub>H<sub>32</sub>N<sub>2</sub>O<sub>6</sub>Pd: C, 59.4; H, 4.98; N, 4.33%; Found: C, 59.12; H, 4.99; N, 4.35%. IR (KBr, cm<sup>-1</sup>): 1620 ν(C=N), 1320 ν(C-N), 1239 ν(C-O), 1032 ν(OCH<sub>3</sub>), 567 ν(Pd-N), 515 ν(Pd-O). μ<sub>eff</sub> (B.M.) (298 K): diamagnetic.

**Bis(2-((E)-(4-fluorobenzylimino)methyl)-6-methoxyphenoxy)palladium(II) (PdL4)**

Turmeric yellow solid; yield, 97%; m.p. 253-256°C. <sup>1</sup>H NMR (300 MHz, CDCl<sub>3</sub>): δ 5.06 (s, 2H, CH<sub>2</sub>), 3.36 (s, 3H, Ar-OCH<sub>3</sub>), 6.51-7.45 (phenylic hydrogen groups), 7.73 (s, 2H, =CH). <sup>13</sup>C NMR (300MHz, CDCl<sub>3</sub>): δ 55.8 (Ar-OCH<sub>3</sub>), 58.3 (CH<sub>2</sub>), 114.0, 115.1, 115.4, 125.4, 130.1 (ArC), 150.9 (C13), 162.8 (N=CH). Anal. Calcd for C<sub>30</sub>H<sub>26</sub>F<sub>2</sub>N<sub>2</sub>O<sub>4</sub>Pd: C, 57.84; H, 4.21; N, 4.50%; Found: C, 57.88; H, 4.21; N, 4.27%. IR (KBr, cm<sup>-1</sup>): 1616 ν(C=N), 1328 ν(C-N), 1248 ν(C-O), 1084 ν(OCH<sub>3</sub>), 581 ν(Pd-N), 495 ν(Pd-O). UV-Vis (CHCl<sub>3</sub>) λ<sub>max</sub> (nm) = 290, 340, 410. μ<sub>eff</sub> (B.M.) (298 K): diamagnetic.

**General Procedure for the Heck cross-coupling Reaction**

Four catalytic reactions were performed with a similar procedure using PdL1-PdL4 complexes. Optimisation was done based on the three parameters of temperatures, catalyst loadings, and bases. The palladium(II) complexes were tested as homogeneous catalysts in a series of Heck coupling reactions between iodobenzene and methyl acrylate to produce methyl cinnamate. The mixtures of iodobenzene (1 mmol), methyl acrylate (2 mmol), triethylamine, Et<sub>3</sub>N (2.4 mmol), palladium(II) Schiff base complex (0.01 mmol) and solvent *N,N*-dimethylacetamide, DMA (7 mL) were mixed in a Radley's 12-place reaction carousel and refluxed whilst being purged with nitrogen (Figure 3). The reaction was stirred for 24 hours at 100°C and monitored using gas chromatography.

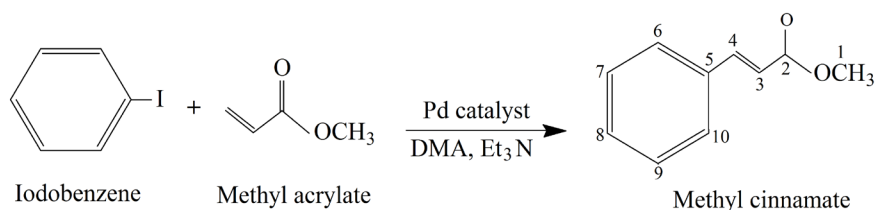


Figure 3. The Heck coupling reaction of iodobenzene with methyl acrylate

### Heck Reaction using Different Bases

The previously explained procedure was repeated using 4 different types of bases while the refluxing at 100°C. The bases used were Et<sub>3</sub>N, NaHCO<sub>3</sub>, Na<sub>2</sub>CO<sub>3</sub> and NaOAc.

### Heck Reaction using Different Catalyst Loadings

Different catalyst loadings were studied by repeating the previously explained procedures with Et<sub>3</sub>N as the base at 100°C. The palladium catalyst loadings were varied at 0.5, 1.0 and 1.5 mmol%, respectively.

### Heck Reaction at Different Temperatures

Maintaining Et<sub>3</sub>N as the base, the procedure was again repeated using palladium(II) Schiff base complex 1.0 mmol% and varying reaction temperatures at 30, 80, 100 and 120°C.

## RESULTS AND DISCUSSION

### Infrared Spectroscopy

The appearance of the C=N of azomethine in the range of 1629-1636 cm<sup>-1</sup> can be clearly observed, indicating the formation of Schiff base. The azomethine C=N bands were observed to be shifted to lower frequencies, 1612 to 1623 cm<sup>-1</sup>, in all the Pd(II) complexes. This phenomenon could be due to the withdrawal of electron density from the nitrogen atom upon coordination (Zolezzi, Decinti, & Spodine, 1999). A similar effect can also be observed in the stretching vibration of the Schiff base phenolic C–O and OCH<sub>3</sub> groups, as regard to the same group in the complexes where it can be observed to be shifted to a lower frequency, hence confirming the oxygen coordination to the metal, as reported by Gupta and Sutar (2008). The spectra also confirmed the appearance of new bands, both at 462 to 544 cm<sup>-1</sup> and 581 to 660 cm<sup>-1</sup>, which ascribed Pd–N and Pd–O vibrations, respectively. This is the evidence of the participation of nitrogen atom of the azomethine group and oxygen atom of the of OH group presents in the ligand upon complexation with Pd(II) ion (Mustafa et al., 2009; Ouf et al., 2010).

## NMR Spectroscopy

**<sup>1</sup>H NMR.** It can be observed in the <sup>1</sup>H NMR spectra of the ligands, the evidence of chemical shifts of methylene; that for the metal complexes, CH<sub>2</sub> appeared at 4.70 to 4.85 ppm as singlets and shifted to higher values of 5.00 to 6.00 ppm. Also in the spectra, ligands exhibited chemical shifts of OCH<sub>3</sub> groups at 3.80 to 3.90 ppm, whereas for Pd(II) complexes, these peaks appeared to have shifted to the values of 3.60 to 3.80 ppm. The shifting can be caused by the involvement of the adjacent imine group, which was coordinated to the Pd centre (Mohamo et al., 2012), causing the CH<sub>2</sub> groups to be more pronounced than the OCH<sub>3</sub> group. This could be due to the closer proximity of the former group to the imine group.

There was an upfield shift of azomethine protons from 8.30 to 8.50 ppm for the ligands to 7.60 to 7.75 ppm for the complexes upon complexation. This upfield shift can be linked to, that upon chelation, the conformational change that has occurred in the ligand (Mohamo et al., 2012; Tsuno, Iwabe, & Brunner, 2013). The peaks for phenolic protons of the ligands, appearing at 13.80 to 14.00 ppm, have disappeared upon complexation, which is in agreement with the work by Gupta and Sutar (2008). They explained that this might be an indication of the occurrence of complexation through deprotonation of the phenolic moiety. The spectra also shown aromatic protons appearing as multiplets in free ligands and were more clearly resolved in complexes. These complexes have JHH values of 6 to 9 Hz, which are indicative of the presence of ortho aromatic protons. Lastly, although the OH peak in the L3 was initially expected to appear in the downfield region of 10 to 14 ppm (Saheb & Sheikhshoai, 2011), no such peaks were observed. This might be due to the labile nature of phenolic protons, which had undergone rapid exchange with the deuterium present in the solvent.

**<sup>13</sup>C NMR.** The imine carbons (C=N) in the Pd(II) complexes were discovered as singlets in the region of 162.3 to 162.9 ppm, and these are similar with what have been reported by Senol et al. (2011). The peaks were shifted upfield from the equivalent peaks in the respective ligands and appeared at 165.5 to 165.8 ppm. This further supports the suggestion of imine nitrogen coordination to the Pd(II) centre. In the free ligands, C–OH signals can be observed at 151.5 to 151.9 ppm, which disappeared upon complexation. This agrees with the work by Senol et al. (2011), which provides evidence that the complexation is successfully achieved through phenol deprotonation.

Further evidence of the coordination to Pd(II) centre can be observed in the position of the peaks representing aromatic carbons succeeding complexation, where the peaks shifted downfield in the complexes.

**X-ray Crystallography.** Suitable single crystals of PdL2 and PdL4 were subjected to X-ray crystallography investigation to determine their structures. All these crystals were obtained via slow evaporation of chloroform (CHCl<sub>3</sub>) at room temperature. The ORTEP drawings of PdL2 and PdL4 are depicted in Figure 4.

The complex PdL2 (Bahron et al., 2014) was obtained as single crystals from slow evaporation of chloroform. The bond length of azomethine N1–C7 and N1–iC8 of PdL2 is 1.296(15) and 1.490(14) Å, respectively, which is consistent with the normal C=N bond lengths

observed in a similar complex, PdL4 (Bahron et al., 2011). The PdL2 crystals appeared to contain one solvated chloroform molecule used in the recrystallisation.

In the compound PdL4 (Bahron et al., 2011), the Pd<sup>II</sup> atom is tetracoordinated by two N atoms and two O atoms from the two 2-[(4-fluorobenzyl)iminomethyl]-6-methoxyphenoxy ligands, forming a square-planar geometry. The two N atoms and two O atoms around the Pd<sup>II</sup> atom are *trans* to each other. The dihedral angle between the two fluoro-substituted benzene rings is 39.03(6)°. The molecular structure is stabilised by an intramolecular C-H...O hydrogen bond. In the crystal, weak intermolecular C-H... $\pi$  interactions occur.

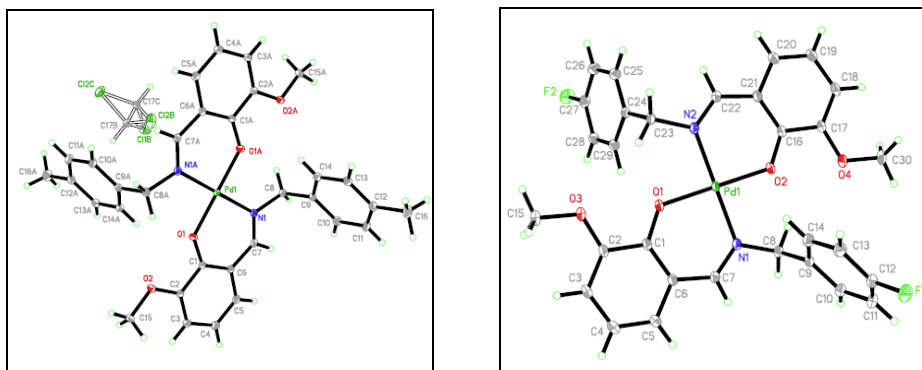


Figure 4. ORTEP diagram of: (a) PdL2; and (b) PdL4

## Catalytic Activity

**The Heck Cross-Coupling Reaction.** The coupling reactions were carried out between methyl acrylate with iodobenzene at 100°C for 24 hours in *N,N*-dimethylacetamide (DMA) solvent under nitrogen conditions. A control experiment indicated that the coupling reaction did not occur in the absence of Pd(II) complexes. The conversions were calculated based on the GC peak areas of reactants and product. From these findings, PdL1-PdL4 were found to be suitable to catalyze Heck (Table 1, entries PdL1-PdL4) up to 100% yields after 24 hours of reactions.

Table 1

Activities of Pd(II) catalysts on the Heck reaction between iodobenzene and methyl acrylate

Entry	Catalyst <sup>a</sup> (mmol%)	Conversion <sup>b</sup> (%)	TON
PdL1	1.0	100	100
PdL2	1.0	100	100
PdL3	1.0	100	100
PdL4	1.0	100	100

<sup>a</sup>Reaction conditions: 1.0 mmol of iodobenzene, 2.0 mmol of methyl acrylate, 2.4 mmol Et<sub>3</sub>N, 0.01 mmol Pd(II) complex, DMA (7 mL)

<sup>b</sup>Conversion is determined by GC. TON = mmol product/mmol catalyst used

## Optimisation

**Effect of Different Types of Bases.** Base plays a significant role in both rate and product distribution of the Heck reaction. Hence,  $\text{Et}_3\text{N}$ ,  $\text{NaHCO}_3$ ,  $\text{Na}_2\text{CO}_3$ , and  $\text{NaOAc}$  (Figure 5) were used as the bases and investigated. Base can be used to neutralise the acid (HX) ensuing from the formal exchange of a hydrogen atom with an aryl or vinyl group (Biffis, Zecca, & Basato, 2001).  $\text{Et}_3\text{N}$  was found to be the most effective base.

All the catalysts tested for the Heck reaction using  $\text{Et}_3\text{N}$  as the base showed 100% conversion.  $\text{Et}_3\text{N}$  was found to be a good base for the reaction, even though there were occasionally trace quantities of palladium metal precipitate against the walls of the glass tubes observed. In most cases,  $\text{Et}_3\text{N}$  was the base to neutralise the hydrogen iodide by-product formed by the reaction (Gupta & Sutar, 2008). This is due to the solubility of  $\text{Et}_3\text{N}$  in the reaction mixture instead of other bases. Bases solubility plays an important role in Heck reaction. Moderate yield was obtained in the reaction of PdL4 as the catalyst when  $\text{NaHCO}_3$  was used. However, longer reaction times were required to compare the reactions using other catalysts.  $\text{Na}_2\text{CO}_3$  gave lower yields compared to other bases, even after 24 hours of reaction time.

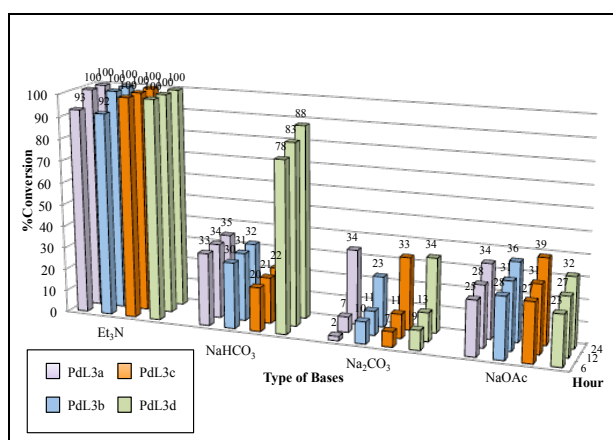


Figure 5. Effects of different types of bases on Heck reaction

## Effects of Catalyst Loadings

It is ideal to have good yields using the most minimal amount of catalysts. Hence, this study examined the effects of catalyst loadings on a convenient coupling between iodobenzene and methyl acrylate. It is of impractical interest to use huge amounts of catalyst (Parida & Rath, 2009) unnecessarily. Other than the cost of utilising the catalyst for the reaction, the cost of removal and regeneration of the catalyst at the end of its life cycle is also substantial.

It was observed that higher amount of catalysts yielded higher product conversions when the amount of catalyst was increased from 0.5 to 1.5 mmol%. This might be due to the increased availability of more basic sites, which can be linked to the dispersion of more active species. The results showed that 100% conversion of iodobenzene was reached at the catalyst loading of 1.0 mmol% as early as 6 hours of reaction time. A lower loading of 0.5 mmol% produced

100% conversion for only one sample, i.e. PdL3, after 24 hours, which is the maximum reaction time. Therefore, it was decided that a catalyst loading of 1.0 mmol% was the optimum loading for the reaction.

### Effects of Temperatures

Four different temperatures (30, 80, 100 and 120°C) were selected to study the optimum temperature for the catalysed reaction (Figure 6). By keeping other parameters fixed, the rate of conversion of iodobenzene at different temperatures was investigated through observation. Through this, a general increase in the percentage of iodobenzene conversion was observed upon increasing reaction temperature. However, at 120°C, a black precipitate of palladium metal (i.e., palladium black) was observed to have formed due to catalysts decomposition, thus inhibiting the catalytic cycle.

The lowest temperature, 30°C, yielded less than 10% conversion of iodobenzene for all the catalysts. This indicated that they were not highly active at this temperature. Upon comparing all the four catalysts, PdL1, PdL2 and PdL3 had the best performances with the highest catalytic activities recorded, even at 80°C with more than 80% conversion. On the contrary, PdL4 only produced 58% conversion at the same temperature. However, none of the catalysts managed to achieve 100% conversion even after 24 hours of reaction at 80°C. Even so, all the catalysts started to give 100% conversion of iodobenzene at only 12 hours of reaction time at 100°C. Therefore, it can be concluded that 100°C is the optimum reaction temperature for the catalysed Heck reaction.

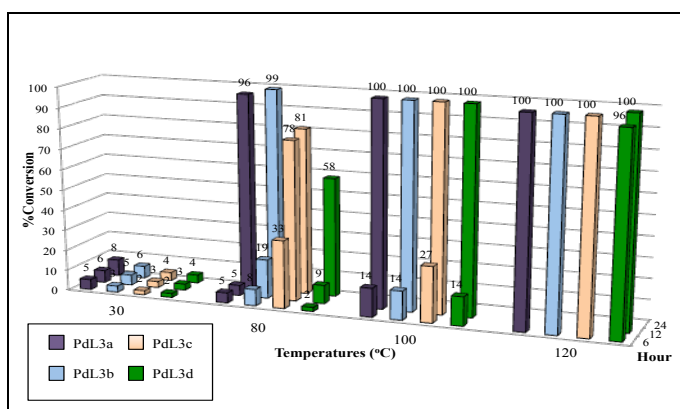


Figure 6. Effects of different reaction temperatures on the Heck reaction

### CONCLUSION

Schiff base ligands, L1, L2, L3 and L4, have been successfully synthesised and characterised. From the studies, it can be concluded that the ligands act as bidentate chelating coordinates with Pd(II) ions upon complexations to produce Pd(II) complexes, PdL1, PdL2, PdL2 and PdL4, and give square planar geometries. The ligands and complexes are thermally and air

stable. PdL1, PdL2, PdL2 and PdL4 were explored for the homogeneous catalysis of the Heck cross-coupling reaction. The yields were up to 100% after 24 hours of reactions.

## ACKNOWLEDGEMENTS

Authors would like to thank Universiti Teknologi MARA (UiTM) for the research grants no. 600-RMI/DANA 5/3/REI (13/2015) and 600-RMI/RAGS 5/3 (8/2015).

## REFERENCES

- Bahron, H. (1994). *Characterization of new metal complexes of Schiff bases and macrocyclic ligands and some mononitrosyl derivatives*. Unpublished doctoral dissertation, University of Surrey, United Kingdom.
- Bahron, H., Mohd Tajuddin, A., Wan Ibrahim, W. N., Hemamalini, M., & Fun, H-K. (2011). Bis{2-[(E)-(4-fluorobenzyl)iminomethyl]-6-methoxyphenolato}-palladium(II). *Acta Crystallographica*, *E67*, m759-m760.
- Bahron, H., Mohd Tajuddin, A., Wan Ibrahim, W. N., Chantrapromma, S., & Fun, H-K. (2014). Bis{2-methoxy-6-[(E)-(4-methylbenzyl)iminomethyl]-phenolato}palladium(II) chloroform monosolvate. *Acta Crystallographica Section E*, *E70*, m289-m290.
- Biffis, A., Zecca, M., & Basato, M. (2001). Palladium metal catalysts in Heck C-C coupling reactions. *Journal of Molecular Catalysis A: Chemical*, *173*, 249-274.
- Drozdak, R., Allaert, B., Ledoux, N., Dragutan, I., Dragutan, V., & Verpoort, F. (2005). Ruthenium complexes bearing bidentate Schiff base ligands as efficient catalysts for organic and polymer syntheses. *Coordination Chemistry Reviews*, *249*, 3055-3074.
- Gupta, K. C., & Sutar, A. K. (2008). Catalytic activities of Schiff base transition metal complexes. *Coordination Chemistry Reviews*, *252*, 1420-1450.
- He, Y., & Cai, C. (2011). Palladium tetrazole-supported complex as an efficient catalyst for the Heck reaction. *Transition Metal Chemistry*, *36*, 113-117.
- Islam, M. Al-Amin A. A., Sheikh, M. C., Alam, M. S., Zangrando, E., Alam, M. A., Tarafder, M. T. H., & Miyatake, R. (2014). Synthesis, characterization and bio-activity of a bidentate NS Schiff base of S-allyldithiocarbamate and its divalent metal complexes: X-ray crystal structures of the free ligand and its nickel(II) complex. *Transition Metal Chemistry*, *39*, 141-149.
- Kumar, A., Agarwal, M., Singh, A. K., & Butcher, R. J. (2009). Palladium(II), platinum(II), ruthenium(II) and mercury(II) complexes of potentially tridentate Schiff base ligands of (E, N, O) type (E = S, Se, Te): Synthesis, crystal structures and applications in Heck and Suzuki coupling reactions. *Inorganica Chimica Acta*, *369*, 3208-3218.
- Lai, Y. C., Chen, H. Y., Hung, W. C., Lin, C. C., & Hong, F. E. (2005). Palladium catalyzed Suzuki cross-coupling reactions using N,O-bidentate ligands. *Tetrahedron*, *61*, 9484-9489.
- Mohamo, T., Mogorosi, M. M., Moss, J. R., Mapolie, S. F., Slootweg, J. S., Lammertsma, K., & Smith, G. S. (2012). Neutral palladium(II) complexes with P,N Schiff-base ligands: Synthesis, characterization and application as Suzuki-Miyaura coupling catalysts. *Journal of Organometallic Chemistry*, *703*, 34-42.

- Mustafa, I. M., Hapipah, M. A., Abdulla, M. A., & Ward, T. R. (2009). Synthesis, structural characterization, and anti-ulcerogenic activity of schiff base ligands derived from tryptamine and 5-chloro, 5-nitro, 3, 5-ditertiarybutyl salicylaldehyde and their nickel (II), copper (II), and zinc (II) complexes. *Polyhedron*, 28(18), 3993-3998.
- Ouf, A. E., Ali, M. S., Saad, E. M., & Mostafa, S. I. (2010). pH-metric and spectroscopic properties of new 4-hydroxysalicylidene-2-aminopyrimidine Schiff-base transition metal complexes. *Journal of Molecular Structure*, 973, 69-75.
- Parida, K. M., & Rath, D. (2009). Amine functionalized MCM-41: An active and reusable catalyst for Knoevenagel condensation reaction. *Journal of Molecular Catalysis A: Chemical*, 310, 93-100.
- Pratihari, J. L., Pattanayak, P., Patra, D., Lin, C-H., & Chattopadhyay, S. (2012). Synthesis, characterization and structure of new diazoketiminato chelates of palladium(II): Potential catalyst for C-C coupling reactions. *Polyhedron*, 33, 67-73.
- Saheb, V., & Sheikshoae, I. (2011). A new Schiff base compound N,N'-(2,2-dimethylpropane)-bis(dihydroxyacetophenone): Synthesis, experimental and theoretical studies on its crystal structure, FTIR, UV-visible, <sup>1</sup>H NMR and <sup>13</sup>C NMR spectra. *Spectrochimica Acta Part A*, 81, 144-150.
- Şenol, C., Hayvali, Z., Dal, H., & Hökelek, T. (2011). Syntheses, characterizations and structures of NO donor Schiff base ligands and nickel(II) and copper(II) complexes. *Journal of Molecular Structure*, 997, 53-59.
- Tsuno, T., Iwabe, H., & Brunner, H. (2013). Synthesis and structural characterization of isomeric palladium(II) complexes with chiral N,O-bidentate ligands. *Inorganica Chimica Acta*, 400, 262-266.
- Vigato, P. A., & Tamburini, S. (2004). The challenge of cyclic and acyclic Schiff bases and related derivatives. *Coordination Chemistry Reviews*, 248, 1717-2128.
- Zolezzi, S., Decinti, A., & Spodine, E. (1999). Syntheses and characterization of copper(II) complexes with Schiff-base ligands derived from ethylenediamine, diphenylethylenediamine and nitro, bromo and methoxy salicylaldehyde. *Polyhedron*, 18, 897-904.



## **The Development of Personal Portable Wireless Range Extender for IEEE 802.11**

**Norharyati Harum\*, Nur Atikah Mohd Yusof and Nurul Azma Zakaria**

*Faculty of Information and Communication Technology, Universiti Teknikal Malaysia Melaka (UTeM), Hang Tuah Jaya, 76100 Durian Tunggal, Melaka, Malaysia*

### **ABSTRACT**

In IEEE 802.11 standard, Mobile Station (MS) such as laptop and smartphone are connected to Access Point (AP) to have a wireless connection. However, setting up AP to cover the whole area is costly and complicated. Limitation in signal capacity causes out-of-coverage area, where the MS cannot connect to the AP. In this paper, a portable wireless range extender (PWRE) is developed to assist MS that is located out of coverage area, or at the cell edge area connected to the internet. Development of PWRE involves two processes, which are connecting to existing wireless LAN (WLAN) network, and broadcasting a new WLAN network. The paper discusses development process of PWRE and analysis of its performance. PWRE was developed using a low power consumption microprocessor, known as Raspberry Pi. Performance of the developed PWRE is evaluated by comparing signal strength received by an MS located in the cell edge from an AP using two scenarios; with and without the PWRE. Results showed that the MS signal strength improved significantly with the deployment of PWRE. Other advantages offered by PWRE include being portable and energy efficient as it uses only 5V of power to operate.

*Keywords:* Access Point, IEEE 802.11, portable, Raspberry Pi, wireless range extender, WLAN

### **INTRODUCTION**

Wireless LANs are widely used for devices that support wireless connection such as

smartphone and laptop. Each device requires a better signal capacity to perform a task and get connected to the internet. Mano and James claimed that many cellular customers have increasingly desired to access good wireless signals at their premises (Mano & James, 2006).

Because of limited signal capacity and distance of coverage area from the Access Point (AP), some devices may be restricted to access the connection. For example, James

#### **ARTICLE INFO**

##### *Article history:*

Received: 25 October 2016

Accepted: 17 March 2017

##### *E-mail addresses:*

[norharyati@utem.edu.my](mailto:norharyati@utem.edu.my) (Norharyati Harum),

[ikahyusof@gmail.com](mailto:ikahyusof@gmail.com) (Nur Atikah Mohd Yusof),

[azma@utem.edu.my](mailto:azma@utem.edu.my) (Nurul Azma Zakaria)

\*Corresponding Author

and Kenneth (2011) stated that AP to client ranges are generally less than the coverage range required in a typical home, and may be lower than 10 to 15 m. Data rates of devices that operate using standard 802.11 are dependent on signal strength. As a distance in the area of coverage increases, wireless system performance may decrease (James & Kenneth, 2011). Thus, wireless signal strength degrades when Mobile Station (MS) located at the cell edge area and the signal may be too weak to be detected by MS. It also considered as a dead spot area. The service also could be unavailable and the signal could be dropped.

Besides that, John (2008) claimed that when a wireless device is positioned in a cell, the wireless device and Base Station (BS) can communicate with each other in various channels through radio frequency air interfaces. With the growth in the number of MSs that use wireless communication, it can cause problems such as a limitation of signal. The cellular wireless communication can suffer from varying levels of degradation as signals are carried over the air interface between wireless devices and MS (John, 2008). One may think that placing another AP can be a solution, but it is not the best decision because it is expensive and static, and consumes high power.

However, this problem can be solved by using a portable wireless range extender (PWRE). In this paper, a PWRE using Raspberry Pi (Rpi Repeater) is developed to enhance the signal strength and capacity. As mentioned by Severance, Raspberry Pi concepts are based on the series of Broadcom chip and supported as a machine to interact with other hardware (Severance, 2013).

In particular, a PWRE is responsible to increase wireless signal strength at locations with low signal range. As shown in Figure 1, Rpi Repeater also can create its own new signal coverage area for MS. Thus, a PWRE can be deployed easily at the dead spot areas because of the small size of Raspberry Pi. Vladimir and Mirjana (2014) stated that Raspberry Pi is an affordable, flexible, fully customisable and programmable small computer board. The physical size impacts the ease of network deployment because smaller nodes can be placed in more locations (Vladimir & Mirjana, 2014).

On the other hand, the Raspberry Pi also consumes low power to operate, making it suitable to perform as a personal devices for users. Users can just plug the portable wireless range extender to any power source such as power bank or directly from the laptop. The main goal of this study is to develop a PWRE to help MS that is located far from AP to receive a signal and also study if the tool such as Raspberry Pi can perform as a personal portable device than the current AP.

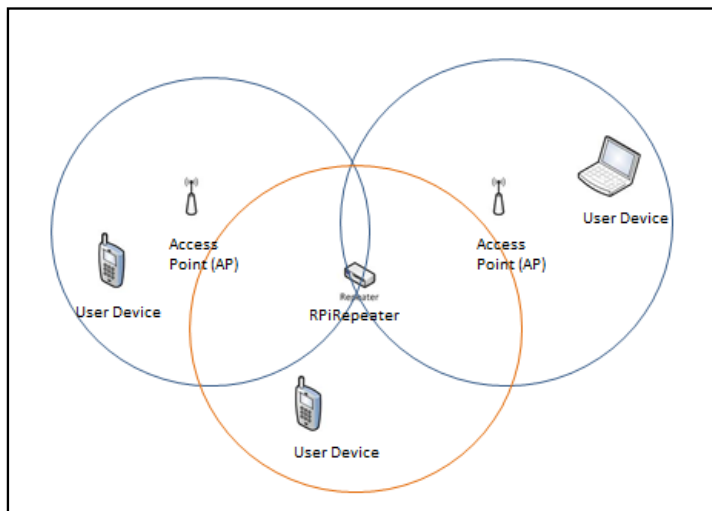


Figure 1. Access Point signal range and Portable Wireless range extender new signal coverage

## METHOD

### Design and Implementation

The purpose of this research is to build a portable wireless range extender (PWRE) using Raspberry Pi that can help to increase the wireless signal strength. This section describes the designs, lists of components, and procedures required for the research. The network interfaces are configured using two USB WiFi dongles which are known as interface wlan0 and wlan1. The system architecture illustrates the overall research diagram. Logical and physical designs determine all the information related to this research. In this paper, all the requirements to complete this project are explained below.

### Software Requirement

**Ekahau Heatmapper.** Before building the PWRE for this particular project, the data analysis was done to determine the current problem so that the PWRE would be able to solve the problem. Ekahau Heatmapper for windows is used to identify the location with AP signal and the location with a problem to access the signal. Ekahau Heatmapper provides information such as AP list, signal strength, channel, Mobile Access Control (MAC) address, and location of the AP devices.

### Hardware Requirement

**Raspberry Pi B+.** A Raspberry Pi computer looks like a PC motherboard and uses the type of microchips that are usually found in mobile phones. It uses Broadcom SoC (System on Chip) a 700MHz ARM11 processor which can handle basic computations and calculations. These processors combine processing and multimedia capability in a small shell. They do not use

too much power too quickly and keep the computer relatively cool. The model B and B+ has storage capacity for 512MB RAM, 2 USB ports and an Ethernet port (Chris, 2013).

Operating systems are mainly Linux distributions, although there are other non-Linux operating systems such as RiscOS. Linux has low memory overheads, so it is possible to run a fully functional operating system on a simple device with no permanent storage.

There are currently five Raspberry Pi models; Model A, Model B, Model A+, Model B+, and Compute Module (currently only available as part of Compute Module development kit). All the models use the same SoC, BCM2835, but other hardware features are different (*Raspberry Pi Schematics*, 2015). Models A and B use the same PCB, while the A+ and B+ are new designs that are very similar to form factor. Compute Module is an entirely different form factor and cannot be used standalone.

**USB WiFi Dongle.** In this project two USB WiFi Dongle are used as a network adapter. The purpose of using two WiFi Dongles is because this research needs to configure the PWRE to enable it to increase the strength of existing AP WiFi signal. Two WiFi Dongles are used to create two wlan interfaces, namely interfaces wlan0 and wlan1.

### Logical and Physical Design

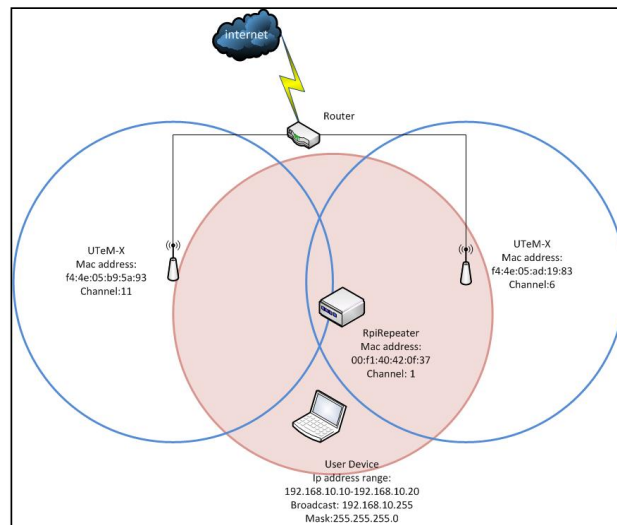


Figure 2. Physical design for product development

Figure 2 shows the physical design of the PWRE using Raspberry Pi. The blue circles represent the coverage of AP signals, and the red circle shows the new coverage signal of the PWRE produced from the existing signals. Detailed information of Figure 2 is as below:

- Access point: SSID, Mac address, channel number, wireless network 802.11n and signal strength.

- Portable wireless range extender: SSID, Mac address, channel number, wireless network 802.11n, signal strength, max speed, password and Key information.
- User Device: IPv4 dhcp address
- Wlan0 and Wlan1 interfaces.

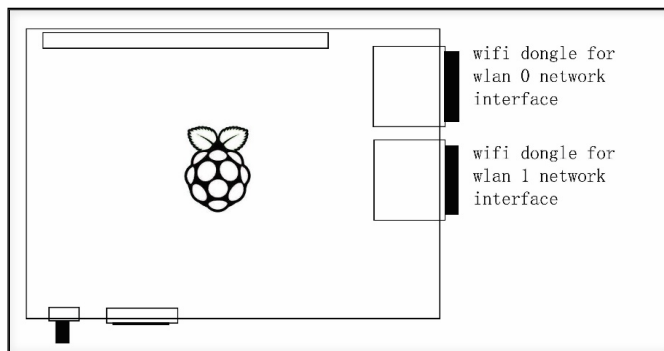


Figure 3. Logical Design for mini board structure to build this research

### Implementation

All the network services required in this work are installed using command because Raspberry Pi is a Linux core operating system. The main part of this research is to configure two USB WiFi dongles to act as the network interfaces, wlan0 and wlan1. The wlan0 interface is connected to the existing wlan network, while wlan1 broadcasts a new wlan network using a new SSID, as shown in Figure 3.

### RESULTS AND DISCUSSION

In this section, performance of the developed PWRE is discussed. The performance evaluation of signal strength is done by comparing two scenarios; when an MS located in the cell edge of AP coverage connected to AP (without the developed PWRE), and when an MS located in the cell edge of AP coverage connected to the portable wireless range extender. Figure 4 and Figure 5 show the signal strength (coverage) for both scenarios. Table 1 and Table 2 provide details of Figure 4 and Figure 5, respectively.

#### Scenario 1: An MS Located in the Cell Edge of AP Coverage Connected to AP

MS is connected to AP (without PWRE), as shown in Figure 4 and Table 1. An MS is placed within 30 meters from the AP. The reading for MS signal strength is evaluated and it shows that the signal strength degrades when the MS is placed far from the AP.

-80 dbmMS directly connected to wireless AP from 30 meters.

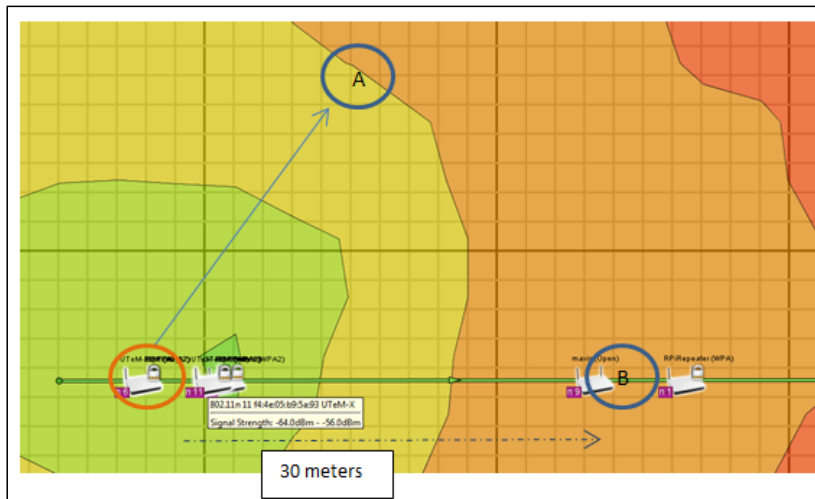


Figure 4. Test Scenario 1 where MS direct connected with AP A (without PWRE)

Table 1  
Descriptions for Figure 4

Label	Devices Info	Description
A	SSID: UTeM-X Wireless Standard: 802.11n Signal Strength: -64.0 dbm -> -56.0 dbm	AP coverage area represented with light green (medium signal), yellow (low signal), orange (lowest signal) and red (out of signal).
B	Connected to UTeM-X Signal Strength: -80 dbm	MS directly connected to wireless AP from 30 meters.

### Scenario 2: An MS Located in the Cell Edge of AP Coverage Connected to the Portable Wireless Range Extender (PWRE)

MS is connected to the PWRE (RPi Repeater), as shown in Figure 5 and Table 2. The reading for MS signal strength is collected and it shows that the signal strength increases, where the orange area (lowest signal) in Figure 4 changes to dark green area (strongest signal) in Figure 5. The dark green area is detected because the MS is connected to the PWRE. Thus, the PWRE creates its own cell and provides a strong signal to the MS. Figures 4 and 5 show that the MS located in the lowest signal area (Figure 4) can receive a strong signal when connected to the PWRE, as shown in Figure 5.

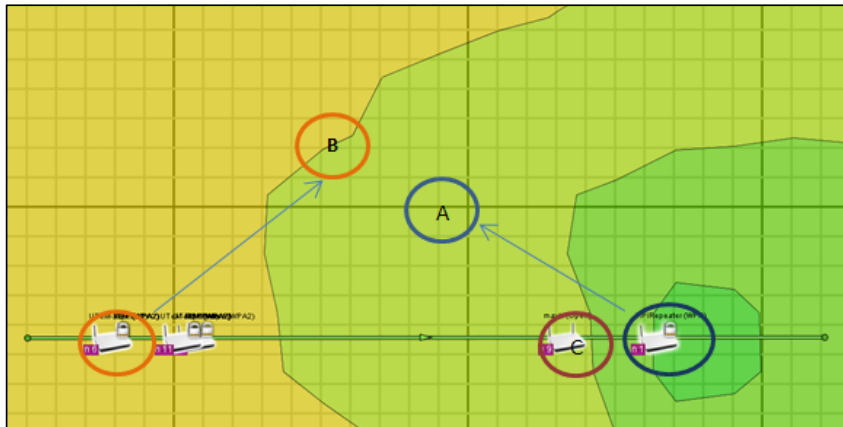


Figure 5. Test Scenario 2 where MS connected to portable wireless range extender (PWRE)

Table 2  
Description for Figure 5

Label	Devices Info	Description
A	SSID: RPiRepeater Wireless Standard: 802.11n Signal Strength: -56.0 dbm -> -48.0 dbm	Portable wireless range extender coverage area. It is represent with dark green colour (highest coverage signal), green (medium coverage signal), light green (low signal) and yellow (lowest signal).
B	SSID: UTeM-X Wireless Standard: 802.11n Signal Strength: -64.0 dbm -> -56.0 dbm	AP from the existing network for wlan0 network interface.
C	Connected to portable wireless range extender	MS connected to portable wireless range extender

Figure 6 shows a signal strength received by an MS when connected to various APs. Note that the developed PWRE (RPi Repeater) is placed near to MS during the performance evaluation. It can be seen that the developed RPi Repeater provides the strongest signal (purple line) when the MS is located far away from other APs. The PWRE will receive the signal from the existing wireless network AP and then amplify or boost it. Besides that, the PWRE not only repeats the signal, but also allows MS to connect with it in the new coverage area in case MS is unable to receive a good signal from AP.

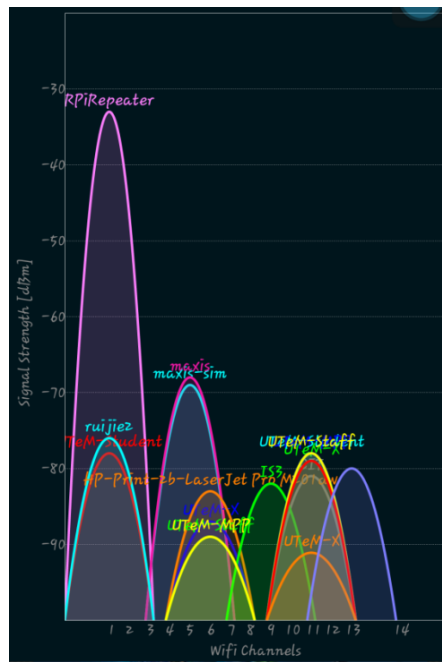


Figure 6. The graph for portable wireless range extender and AP signal strength

## CONCLUSION

In this paper, a PWRE is developed to improve signal strength received by an MS that is located at the cell edge or out of AP coverage. Based on the performance evaluation of signal strength, we found that an MS located in the cell edge, or out of the coverage area, can receive a better signal strength when using the developed PWRE known as RPi Repeater. When an MS is located in the cell edge, it can connect to both AP and PWRE in the same point but with a better signal strength when connected to the developed PWRE. From the performance evaluation discussed in the previous section, we found that the PWRE can provide the strongest signal strength compared to the signal strength of other Aps. The developed PWRE can help IEEE802.11 standard users to have wireless connection even in the cell edge and out of coverage area. Since it is operated using a small-sized microprocessor, users can bring it everywhere and have an IEEE 802.11 wireless connection everywhere and anytime. As the microprocessor is embedded in the product, it can also be developed as a multi-tasking repeater in future work since it can be attached with another system or application such as teaching tools. Besides that, the developed PWRE is also an energy efficient product because it uses only 5V to operate.

## ACKNOWLEDGEMENTS

The authors fully acknowledge Ministry of Higher Education (MOHE) and Universiti Teknikal Malaysia (UTeM), Melaka, for the approved fund (FRGS1/2014/ICT07/FTMK/02/F00227) which has made this important research viable and effective.



## REFERENCES

- Chris, E. (2013). Not-So-Humble Raspberry Pi Gets Big Ideas. *Engineering and Technology*, 8(3), 30 - 33. Retrieved from [https://documentation.meraki.com/MR/WiFi\\_Basics\\_and\\_Best\\_Practices/Wireless\\_fundamentals%3A\\_signal-to-Noise\\_Ratio\\_\(SNR\)\\_and\\_wireless\\_signal\\_strength](https://documentation.meraki.com/MR/WiFi_Basics_and_Best_Practices/Wireless_fundamentals%3A_signal-to-Noise_Ratio_(SNR)_and_wireless_signal_strength)
- James, A. P. J., & Kenneth, M. G. (2011). *Wireless Network Repeater* (U.S. Patent 7, 990, 904 B2).
- John, C. W. N. (2008). *Method and System for Proximity Detection for an In-Building Wireless Repeater* (U.S. Patent 7, 415, 242 B1).
- Mano, D. J., & James, L. A. (2006). *Repeater for Customer Premises* (U.S. Patent 7, 027, 770 B2).
- Petros, A. (2013). *Portable WiFi Signal Repeater* (U.S. Patent 2013/0242852 A1).
- Raspberry Pi Foundation. (2015). *Raspberry Pi Schematics*. Retrieved June 2015, from <https://www.raspberrypi.org/documentation/hardware/raspberrypi/schematics/>
- Severance, C. (2013). Eben Upton: Raspberry Pi. *Computer*, 46(10), 14-16.
- Vladimir, V., & Mirjana, M. (2014). Raspberry Pi as a Wireless Sensor Node: Performances and Constraints. Proceeding of 37<sup>th</sup> *International Convention on Information and Communication Technology, Electronics and Microelectronics (MIPRO 2014)*, Opatija, Croatia, 1013-1018.



## **Productivity Improvement in Automotive Component Company using Line Balancing**

**Muhammad Fikri Alif Dzulkarnain and Wan Emri Wan Abdul Rahaman\***

*Faculty of Mechanical Engineering, Universiti Teknologi MARA (UiTM), 40450 Shah Alam, Selangor Darul Ehsan, Malaysia*

---

### **ABSTRACT**

One of the issues found in small and medium industry is the poor layout design affecting its productivity and line efficiency. In automotive industries, more attention should be given in improving assembly line to increase productivity. This paper presents application of line balancing at the accelerator and brake pedal assembly line at a small and medium automotive industry. Research methodology employed in this study includes time study, visualising cycle time based on Yamazumi Chart, distribution of workload on each workstation using line balancing based on the current takt time and re-laying out the assembly line. All the proposed layouts are assessed using commercially available software, DELMIA Quest to evaluate the robustness based on parameters such as fluctuation in demand, availability of the machine, and operator capacity. Finally, the outputs presented include reduction in manpower, maximum utilisation of manpower, as well as machine and minimum total production cost. This will lead to productivity improvement of the assembly line.

*Keywords:* Automotive industry, line balancing, production efficiency

---

### **INTRODUCTION**

Today, the automotive industry is facing new challenges as a result of globalisation,

customisation and greater competition. Therefore, it is important for manufacturers to produce good quality products and meet customers' demand. In order to achieve these, the industries have applied the Lean Manufacturing (LM) System, a philosophy of production that integrates a collection of principles, tools and techniques into the business processes to improve time, workers, resources and productivity, while refining the quality level of products and services to their customers (Holweg, 2007). Due to its

---

#### **ARTICLE INFO**

*Article history:*

Received: 25 October 2016

Accepted: 17 March 2017

---

*E-mail addresses:*

fikrialiff@yahoo.com.my (Muhammad Fikri Alif Dzulkarnain),  
wanemri@salam.uitm.edu.my (Wan Emri Wan Abdul Rahaman)

\*Corresponding Author

worldwide advantage in cost, quality, flexibility and quick response, LM has become widely acceptable and adoptable best manufacturing practice across countries and industries (Womack, Jones, & Roos, 1990; Diego-Mas et al., 2009). The main objectives of LM are to reduce the cost of products and improve productivity by eliminating wastes or non-value added activities (Vaidya et al., 2013).

Plant layout design has become important in today's industry as it can positively impact the work efficiency. A good layout will maximise the overall efficiency of operations. Research on facility layout of a production line has always been a crucial research area of the industrial engineering field (Tompkins, 1996). An effective plant layout requires the ability to position employees, materials, machines, equipment, and other manufacturing supports and facilities at the right place. Designing an efficient layout will help in reducing production cycles, work-in-progress, idle times, number of bottlenecks, or material handling times, and increasing production output. A good placement of facilities contributes to the overall efficiency of operations and reduces it up to 50% the total operating expenses (Taj, & Berro, 2006).

This paper focuses on productivity improvement at an automotive assembly line for accelerator and brake pedals. The objective of this work is to study the current assembly line system using time study and Yamazumi chart. Based on these, problems in the existing layout would then be listed. Several newly proposed layouts have been presented and analysed using DELMIA Quest. The optimum layout was proposed to the manufacturer.

## METHOD

The general methodology of this study is presented in Figure 1. Initially, the time study was performed at the existing layout. Then, the Yamazumi chart analysis was constructed to evaluate the idle time of each workstation. Meanwhile, the takt time was calculated using Equation [1] (Heizer & Render, 2009), as follows:

$$\text{Takt time} = \text{Total available time in seconds} / \text{Customer demand per day} \quad [1]$$

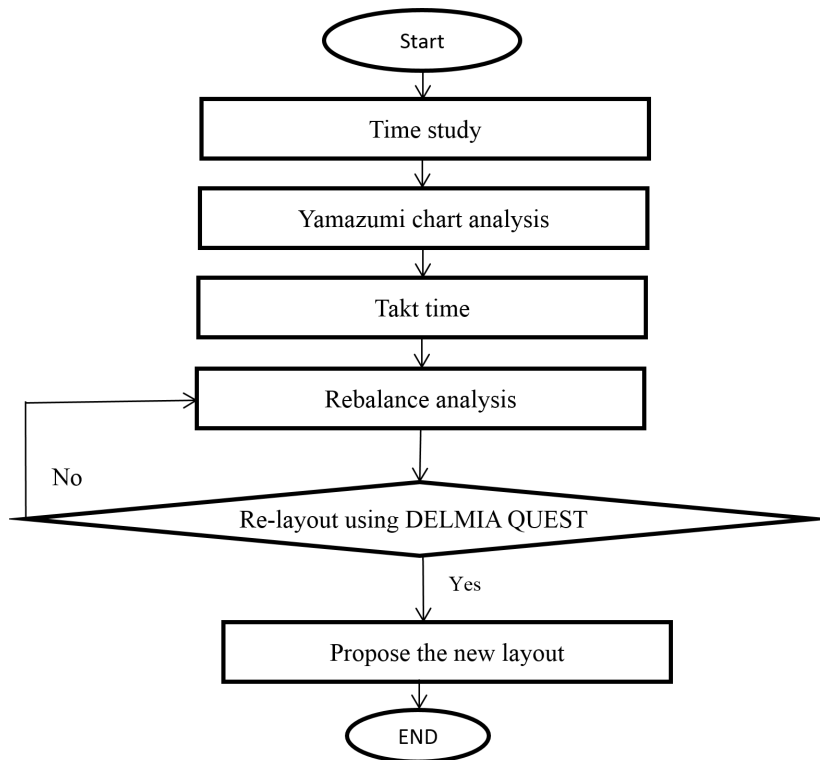


Figure 1. General method

The value of takt time was then used for rebalance analysis. However, the number of minimum workstation was calculated before conducting the rebalance analysis. The minimum number of workstation was calculated using Equation [2], as presented by Heizer and Render (2009).

$$\text{Minimum number of workstations} = \text{Total cycle time} / \text{takt time} \quad [2]$$

Total cycle time is the time required by each operator at each workstation to complete the task. After rebalance analysis was conducted, several proposed improved layouts were prepared and analysed using DELMIA Quest. The optimum layout in terms of productivity, efficiency and cost was then selected. Efficiency of the layout was calculated using Equation [3] based on the work of Heizer and Render (2009):

$$\text{Efficiency} = \text{Total task time} / (\text{No of workstations}) (\text{Largest assigned cycle time}) \quad [3]$$

### Current Layout Analysis

The study on assembly line assembling accelerator and brake pedals has been conducted to determine their efficiency. The operator motion and material movement path, from the raw

material up to the finished goods, are shown in Figure 2. The process was categorised into 4 stations consisting of assembly and welding; assembly and inspection; assembly and inspection; and final assembly, where the only machine involved in this operation was the spot welding machine.

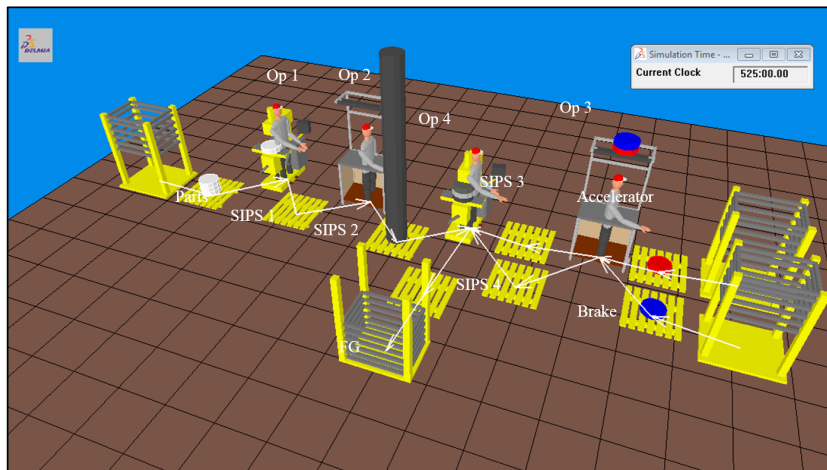


Figure 2. Current assembly line layout

Based on the current layout shown in Figure 2, Operator 1 assembled five components using a jig on the worktable and welded all the sections using the spot welding machine. Then, the base part was transferred to SIPS 1, which is also known as Standard in Process Stock, that was the hold area for the waiting parts before they went to the next process. In the simulation model, buffer acted as SIPS. Next, Operator 2 inspected and assembled the snap and fit for the mother part. Operator 3 inspected, assembled snap and fit, assembled the bushes, brake cover and parts for the accelerator and brake pedals. The finished assembled accelerator and brake pedals were put separately on SIPS 3 and SIPS 4. Operator 4 assembled the base part, tension spring, bolts and nuts, accelerator and brake pedal using jig and power tool. Finally, the finished good was put on the finished good rack.

The takt time for the current layout is 60 second per piece. This is based on the total working duration of 31,500 seconds and the demand per day is 525 pieces. Meanwhile, the efficiency of the current layout is 59.08%. Based on the time study that had been conducted, all the data from the current assembly line were visualised in a stack bar chart. Based on Figure 3, the average cycle time for Operator 1 is 42.4 seconds, Operator 2 is 19.1 seconds, Operator 3 is 44.7 seconds and Operator 4 is 35.6 seconds. The main problem with the current layout is the unbalanced workload between each workstation that leads to bottleneck and high idle time.

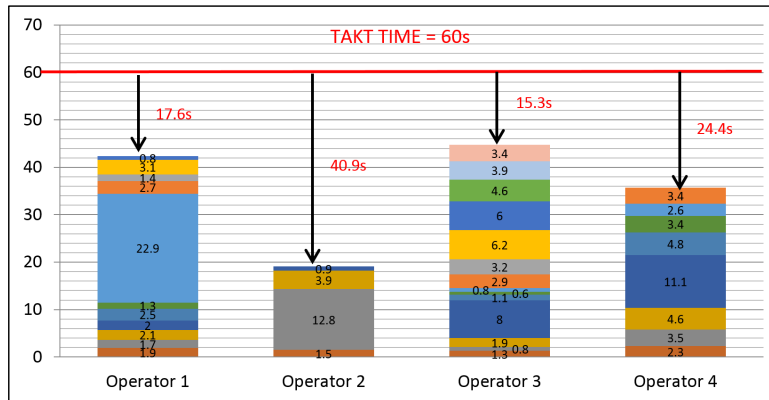


Figure 3. The Yamazumi chart for the current assembly line layout

### Proposed Layout

Rebalance is done to reduce the idle time, manpower, and total production cost. Three new layouts were proposed and analysed to evaluate their effectiveness in improving the productivity of the assembly line. The minimum number of workstation needed to be calculated. Based on the total cycle time of 141.8 s and takt time of 60 s, the minimum number of workstation required is 3.

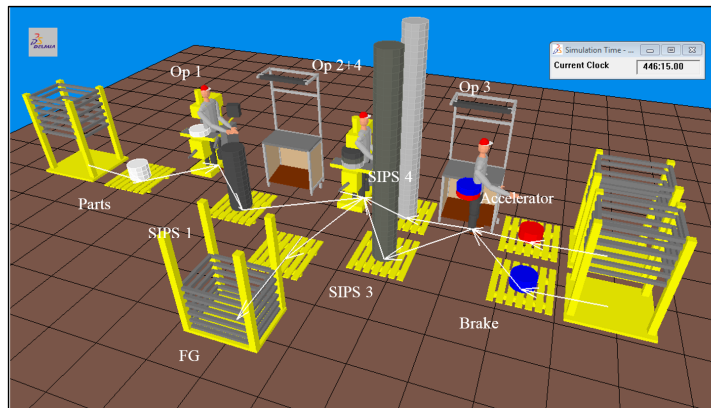


Figure 4. Propose assembly line (layout 1)

For the proposed layout 1 as shown in Figure 4, the number of workers can be reduced from four to only three operators. The operator 2 workstation could be eliminated and the task is then delegated between operator 1 and operator 4. Operator 1 would take the assembly of snap and fit for the mother part task from the previous operator 2 before the mother part is put on SIPS 1. After that, additional parts for the snap and fit are put on the worktable besides Operator 1. Operator 4 will conduct the remaining tasks from the previous Operator 2, i.e. checking the quality on the mother part by marking on the required sections. By giving the previous tasks

from Operator 2 to operator 1 and operator 4, some tasks from Operator 4 could be eliminated, i.e. taking mother part from SIPS 2. This will reduce 3.5 seconds from the overall task times. Instead of doing that, after quality check based on marking, the mother part could be put straight on the jig, which may take around 0.9 seconds. There was no proper rack for SIPS 2 as previously the completed mother part by operator 2 was either put on the worktable or put back on SIPS 1. The worktable of the previous Operator 2 was moved nearer to the worktable of Operator 4 in order to minimise the time wasted for walking and thus, ease the movement of the operator to do the tasks. As for Operator 3, all the tasks that were required to be done would remain. This could reduce a total of 3.5 seconds from the overall task time. Figure 5 shows the Yamazumi chart that summarises the time taken to complete the task at each workstation.

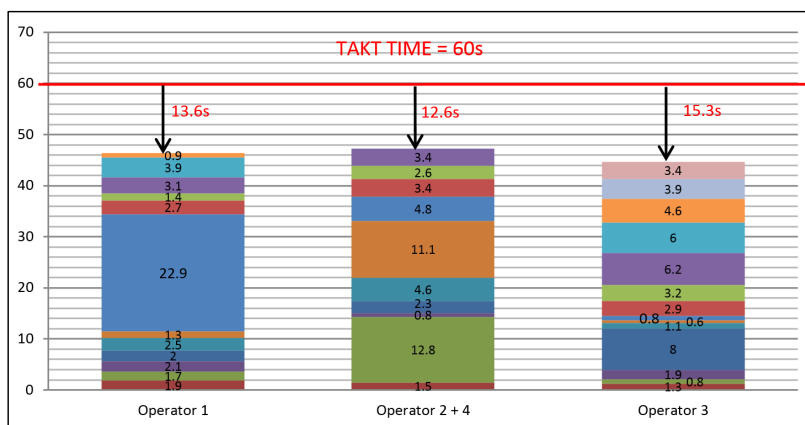


Figure 5. Yamazumi chart for the proposed assembly line (Layout 1)

For the proposed layout 2 shown in Figure 6, the number of workers can be reduced from four to three operators. This layout shows one piece flow of material, where the material flow from left to right in one direction as compared to the original layout, where the finished goods end at the centre of the layout. Based on this proposed layout, the operator who was involved in the final assembly was moved to the end position. Some of the tasks by Operator 3 previously (e.g., acquiring the accelerator pedal, checking the hole for the snap and fit, and quality checking using the marker) could be transferred to Operator 4. Additional work is given to Operator 1, where he/ she would take the assembly of snap and fit for the mother part from Operator 2 before the mother part was put on SIPS 1. Additional parts for the snap and fit are put on the working table next to Operator 1. Operator 3 would take the tasks from Operator 2 which includes checking the quality of the mother part based on marking the required sections. The worktable was moved nearer to Operator 3 in order to minimize the time waste due to walking. It was proposed that Operator 4 takes the task done by Operator 2 previously, which includes



quality checking based on marking on the mother part, other than producing the final assembly of all parts. The finished goods rack was moved to the end of the assembly line. Figure 7 shows the Yamazumi chart that summarises the time taken to complete the task at each workstation for the proposed Layout 2.

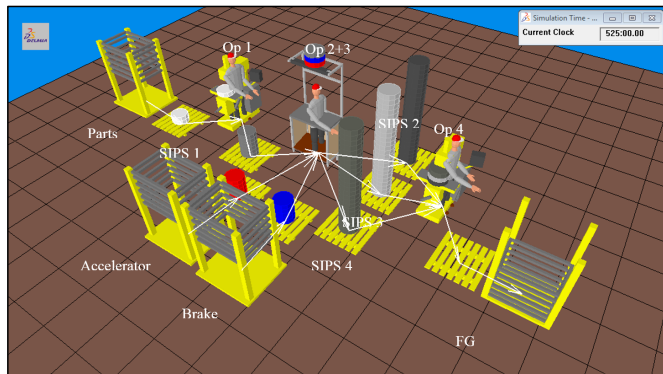


Figure 6. The proposed assembly line (Layout 2)

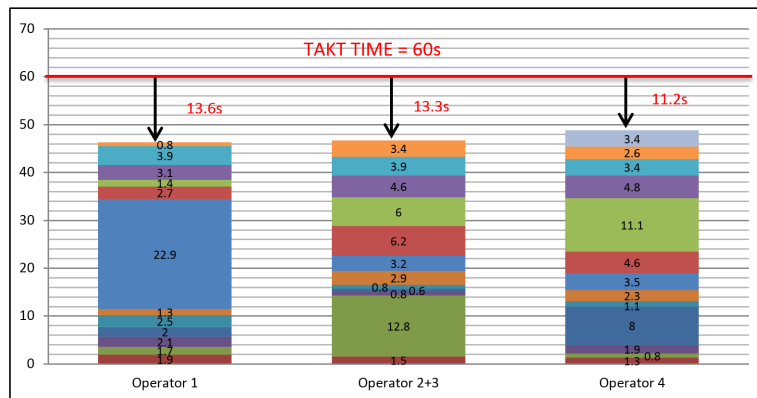


Figure 7. The Yamazumi chart for the proposed assembly line (Layout 2)

For the proposed Layout 3 (Figure 8), the number of workers can be reduced from four to three operators. Based on the original layout, Operator 4 who was involved with the final assembly is moved to the end position. All the tasks for operator 1 remain the same. Operator 3 will take all the previous tasks from Operator 2, except for checking the quality of the mother part by marking the required sections that are transferred to operator 4. The finished goods rack is moved to the end of the assembly line. A total of 1.1 second could be reduced from the overall task time, which mainly comes from the previous tasks by Operator 4. Figure 9 shows the Yamazumi chart that summarises the time taken to complete the task at each workstation.

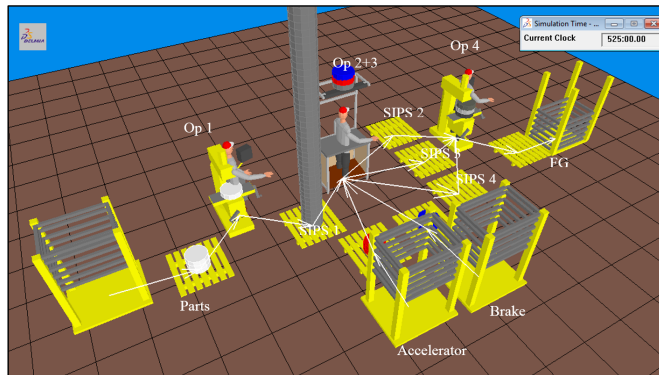


Figure 8. Proposed assembly line (Layout 3)

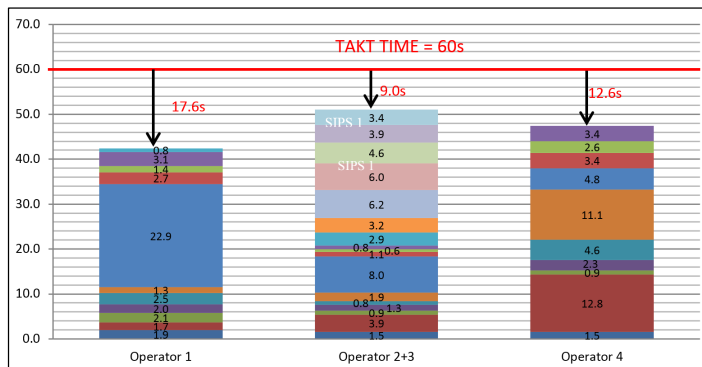


Figure 9. The Yamazumi chart for the proposed assembly line (Layout 3)

## RESULTS AND DISCUSSION

All the proposed layouts have been analysed using DELMIA Quest in order to check the effectiveness of each layout in terms of their productivity and line efficiency. The outcome was further analysed to determine the optimum layout in improving productivity. The simulation was run at 100% efficiency, or 31,500 seconds, which is the available time for the production line to run daily. However, it is impossible to run the production line at 100% efficiency due to the machine and limitation of the operator to run constantly and efficiently throughout the shift. Therefore, some allowances need to be applied to the machine availability and operator capacity. There are three types of allowance identified such as setup, breakdown and fatigue of the operators, as shown in Table 1.

Table 1  
Total machine availability and operator capacity per shift in the assembly line

Type of allowance	Percentage of allowance (%)
Setup allowance	2.5
Breakdown allowance	7.5
Operator fatigue allowance	5

Based on the information in Table 1, the new line efficiency is expected to be 85%. In order to check the overall efficiency and productivity of all the proposed layouts, simulation was performed for 26,775 seconds, which is the available time for the production line to run daily when the line is running at 85% efficiency. Table 2 and Table 3 show the comparison between the current layout and the proposed layouts when the line was running at 100% and 85% efficiency, respectively.

Table 2

*A comparison between the current layout and three proposed layouts when labours and machines worked at 100% efficiency*

Key Performance Index (KPI)	Existing layout	Proposed layout		
		1	2	3
No. of workers	4	3	3	3
Productivity (pieces/ day)	702	661	644	614
Labour productivity (pieces/ hour/ man)	20.1	25.2	24.5	23.4
Line efficiency (%)	59.08	76.94	78.78	78.17

Table 3

*A comparison between the current layout and three proposed layouts when labours and machines worked at 85% efficiency*

Key Performance Index (KPI)	Existing layout	Proposed layout		
		1	2	3
No. of workers	4	3	3	3
Productivity (pieces/ day)	594	561	547	522
Labour productivity (pieces/ hour/ man)	17	21.4	20.8	19.9
Line efficiency (%)	69.51	90.52	92.75	92.03

Based on the existing layout, the simulated results showed that it was capable to produce 702 pieces and 594 pieces per day when the line was running at 100% and 85% efficiency, respectively. The existing layout has no problem to achieve the current demand of 525 pieces per day even when the line is running at 85% efficiency. However, it requires 4 workers to assemble the component. The proposed layout requires three workers and this could result in a saving of about RM12,000 annually for eliminating one manpower.

Based on the three proposed layouts, layout 3 was eliminated because the productivity had a short of 3 pieces when the assembly line was at 85% efficiency. In reality, the production line would be expected to run at an efficiency of as low as 85% as no production line could operate at 100% efficiency when taking into account the time consumed for setup, breakdown and operator fatigue.

Meanwhile, the proposed layout 1 is preferred because it performs better in terms of production capacity, labour productivity and able to meet the daily demands of 525 pieces. Based on the data presented in Table 2 and Table 3, the results for the proposed layout 1 show that the daily production output was 661 and 561 pieces, respectively, when the line ran at

100% and 85% efficiency, where it could produce more than required. The proposed layout 1 is much better than layout 2 in terms of productivity, whereby it exceeds as much as 36 pieces based on the current demand compared 22 pieces achieved by layout 2. The one with the higher productivity is better as the efficiency might drop below 85%. The proposed layout 1 is much better in coping with the fluctuation in customers' demand and when the efficiency drops below 85%.

In addition, the proposed layout 1 incurs lower cost as compared to layout 2. The proposed layout 1 would only require the operator to move closer to the worktable compared to the original layout. Other than that, additional cost is required to produce a proper rack for SIPS 2, in which the original layout required operator 2 to just put the complete assembled part either on the worktable or on SIPS 1 again. The proposed layout 2 is costly to be implemented because it uses hydraulic system power tools for operator 4 to tighten bolts and nuts. As the worktable is to be moved to the end, a lot of adjustment is required to attach the hydraulic system to the worktable of Operator 4. Additional cost is also required to make an additional proper rack for SIPS 2.

## CONCLUSION

The objective of this study is to improve productivity in the automotive industry using line balancing technique. Performance of the existing layout is unsatisfactory due to low efficiency and high idle time. Three proposed layouts have been presented and compared in terms of their manpower requirement, line efficiency, labour productivity, production capacity and manpower utilisation. All the three proposed layouts have also been tested in terms of robustness so as to determine the optimum layout when the production line works at 100% and 85% efficiency, respectively, and when there is fluctuation in customers' demand. The effectiveness of each layout has been simulated and evaluated using DELMIA Quest. The results show that all the proposed layout presented the same results in terms of reduction in manpower. Overall, the proposed layout 1 was found to be the optimum layout in terms of line efficiency, labour productivity, production capacity and robustness when the line works at 100% and 85% efficiency, although layouts 2 and 3 were shown to be better in terms of line efficiency. Based on the calculation, the proposed layout 1 could save up to RM12,000 per year, which is a significant cost saving in the overall revenue for the company. Therefore, the proposed layout 1 is recommended for the management of a company as it will reduce one operator in the assembly line, and increase the utilisation of operators, line efficiency, and labour productivity. Thus, this could increase the company's overall productivity. This study has proven that in line balancing issue, efficiency may not be the only criterion or measurement that may be used to decide the best layout, especially in cases where options are almost equivalent to each other. In this study, the robustness of all the three proposed layouts against various important parameters, such as fluctuation in demand and production output when the workers and machine runs at 100% and 85% efficiency, had been considered. A robust layout will have the capacity to perform better in an actual live environment where change and uncertainty are common.

## ACKNOWLEDGEMENT

The authors would like to thank Suria Component Manufacturing (M) Sdn Bhd, for providing all necessary facilities and information for this research.

## REFERENCES

- Diego-Mas, J. A., Santamarina-Siurana, M. C., Alcaide-Marzal J., & Cloquell-Ballester, V. A. (2009). Solving facility layout problems with strict geometric constraints using a two-phase genetic algorithm. *International Journal of Production Research*, 47(6), 1679 – 1693.
- Heizer, J., & Render, B. (2009). *Flexible Edition Operations Management (9<sup>th</sup> Ed.)*. Pearson International Edition, 300-315.
- Holweg, M. (2007). The genealogy of lean production. *Journal of Operations Management*, 25(2), 420-437.
- Taj, S., & Berro, L. (2006). Application of constrained management and lean manufacturing in developing best practices for productivity improvement in an auto-assembly plant. *International Journal of Productivity and Performance Management*, 55(3), 332 – 340.
- Tompkins, J. A. (1996). *Facilities planning (2<sup>nd</sup> ed.)*. New York: Wiley.
- Vaidya, R. D., Shende, P. N., Ansari N. A., & Sorte S. M. (2013). Analysis plant layout for effective production. *International Journal of Engineering and Advanced Technology (IJEAT)*, 2(3), 500 - 504.
- Womack, J. P., Jones, D. T., & Roos, D. (1990). *The Machine That Change the World*. New York: Rawson Associates Scribner.





## Association between Marital Status and the Outcome of Teenage Pregnancy: A Retrospective Review in Year 2009-2012 in Hospital Ampang

Salleha Khalid\* and Muhammad Shamsir Mohd Aris

Faculty of Medicine and Health Sciences, Universiti Sains Islam Malaysia (USIM), Tingkat 13, Menara B, Persiaran MPAJ, Jalan Pandan Utama, Pandan Indah, 55100 Kuala Lumpur, Malaysia

### ABSTRACT

Teenage pregnancy is associated with maternal and neonatal morbidity. Some postulate that it is due to biological immaturity, while others postulate that it is due to inadequate antenatal care. The objective of this study is to compare the maternal and neonatal outcome between married and unmarried teenage mothers. A retrospective study was conducted from 2009 to 2012, where mothers aged below 20 year old were included. Maternal and neonatal outcome was assessed. A total of 750 patients aged below 20 year old delivered at Hospital Ampang. The trend of teenage pregnancy decreased from 3.1% in 2009 to 2.2% in 2012. A total of 578 (77.1%) mothers were married, while 172 (22.9%) were unmarried. Being unmarried was significantly associated with unbooked ( $p < 0.001$ ), preterm birth ( $p = 0.00468$ ), and lower birth weight ( $p < 0.0001$ , and unpaired T-Test with 95% CI -0.2607 to -0.0933). However there is no significant difference in the number of mothers with hypertensive disease ( $p = 0.88428$ ), diabetes in pregnancy ( $p = 0.39602$ ), mode of delivery ( $p = 0.055$  vaginal delivery,  $p = 0.4419$  caesarean section, and  $p = 0.9097$  instrumental deliveries) and NICU admission ( $p = 0.3779$ ) between the two groups. Unmarried teenage pregnancy is associated with a lack of antenatal care, preterm birth, and lower birth weight compared to their married counterpart.

*Keywords:* Marital status, pregnancy outcome, teenage pregnancy

### ARTICLE INFO

*Article history:*

Received: 25 October 2016

Accepted: 17 March 2017

*E-mail addresses:*

salleha@usim.edu.my (Salleha Khalid),

shamsir@usim.edu.my (Muhammad Shamsir Mohd Aris)

\*Corresponding Author

### INTRODUCTION

Teenage pregnancy is associated with poor maternal and perinatal outcomes (UNFPA, 2015). The increasing trend of teenage pregnancy has been attributed to several factors. Improved health and nutritional status has led to a decrease in the age of obtaining menarche (Wyshack, 1982). It has been

reported that the decline in the age of starting menarche is as much as 2 to 3 months per decade since the 19th century, making an overall decline of three years (Wyshack, 1982). Similarly, the age of sexual debut has decreased over the years as well. In the US, one half of high school students have had sexual intercourse in their lifetime, with approximately 7% reported to having sexual encounters before the age of 13 years old (Centers for Disease Control and Prevention, 2001). For most women in Asia, the onset of sexual activity coincides with marriage. However, with the increasing age one gets married at and changes in socio-cultural norms, there is an increasing number of young women commencing sexual activity before marriage (UNFPA, 2015). In China for example, 19% of unmarried women aged 15-24 years old were reported to be sexually active (Zheng et al., 2010). In Malaysia, a survey was conducted among Malaysian youth in 2009 and it was reported that 27.2% had their first sexual debut at the age of 15-17 (Low, 2009). Lee et al. found that the mean age of sexual debut was 15 (Lee, Chen, Lee, & Kaur, 2006). In another survey done in Malaysia in 2010 by Anwar et al. among 1139 students aged between 15 to 20 years, 13% were reported to have had sex (Anwar, Sulaiman, Khan, & Ahmadi, 2010). The usage of contraception has been poor among teenagers (Anwar et al., 2010). A survey on youth sexuality reported that 90% of in-school females admitted to not taking any precautions against pregnancy (Chiam, 1996). Zulkifli et al. (2000) added that only 37% of teenagers used birth control, although majority of them had knowledge regarding contraception. Meanwhile, World Health Organisation (WHO) reported that only 54% of girls and 49% of boys used a contraceptive method (WHO, 2011).

The age of marriage has been increasing over the years, while more teenagers become pregnant. Teenage pregnancy has been associated with preterm birth, low birth weight and adverse maternal outcomes (Gilbert, 2004). However, poor maternal outcomes have been suggested as not merely due to biological immaturity, but also other factors such as inadequate antenatal follow up, being unmarried, poor support, and low socioeconomic status (McAnarney, 1987). Mahfouz stated that teenage pregnancy is not a risk if there is adequate antenatal care received by the teenage mothers (Mahfouz, El Said, Erian, & Hamid, 1995). Adequate care is influenced by many factors including the presence of social support.

Although an increasing number of Malaysian women are delaying their marriage, it has been a cultural norm to be married as a teenager. This retrospective review, conducted at Hospital Ampang from 2009 to 2012, was intended to evaluate the impacts of being married compared to being single mother on the outcome of pregnancy.

## **METHOD**

Based on the annual birth census, teenage mothers were identified according to their age at the time of delivery in Hospital Ampang. Their hospital number was used to trace their history using a computer database, and this was done by medical officers who had been trained in collecting the data. Those aged below 20 years old were included in this study. Mothers aged 20 years and above at time of delivery, and those who had pre-existing medical conditions were excluded. The demographic data included the marital status, parity, and ethnicity, and



their booking status, as well as any antenatal co-morbidity diagnosed such as hypertensive disease in pregnancy and diabetes in pregnancy. The outcome can be divided into maternal and neonatal outcomes. Maternal outcome is based on the antenatal complications such as diabetes and hypertension disease in pregnancy, the mode of delivery (spontaneous vaginal delivery, instrumental vaginal delivery or caesarean section), and post-partum complications such as postpartum haemorrhage, as well as third and fourth degree vaginal wall tears, were identified. The neonatal outcomes include the week of gestation at the time of delivery, birth weight, Apgar score and NICU admission. The data were analysed using Chi-squared test and T- test with  $p < 0.05$  to be significant.

## RESULTS

### Demographic Data

For age, 5% (38/749) aged < 16, followed by 22.2% (166/749) aged 16-17, and 72.8% (545/749) aged 18-19. The youngest age was noted to be thirteen years old. The prevalence of teenage pregnancy had decreased over the years, i.e. from 3.1% in 2009 to 2.2% in 2012, as shown in Table 1.

Table 1  
*Percentage of teenage pregnancy from year 2009 to 2012*

Year	Total No. of Delivery	Teenage Mothers	Percentage (%)
2009	6485	200	3.1
2010	6832	189	2.8
2011	7449	173	2.3
2012	8302	186	2.2

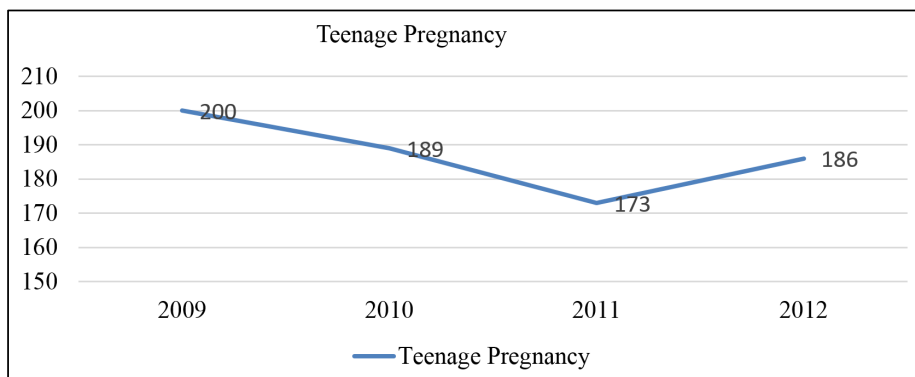


Figure 1. The trend of teenage pregnancy from 2009 to 2012

Further break-ups on the number of teenage pregnancy showed that majority of the teenage mothers aged between 18 to 19 years old (Table 2).

Table 2  
*The age group among teenage pregnancy*

Year	<16 years	16- 17	18- 19	Total
2009	9	40	151	200
2010	9	44	136	189
2011	10	25	138	173
2012	9	54	123	186
Total	37	163	548	570

Meanwhile, 83.1% (623/750) of the teenage mothers had their first pregnancy; 17% of the married teenage mothers have had their second pregnancy before the age of 20, and 5.2% of the unmarried mothers also had their second pregnancy. Out of the total number of teenage mothers, 76.8% (575/749) of them were married. The highest percentage (45.9%) of unmarried teenage mothers was among those aged below 16 years (17/37), followed by aged 16-17 years, which was 39.2% (64/163), and 18-19 years which was 16.8% (92/548). There were a total of 750 teenage deliveries during the studied period, out of which, 578/750 (77.1%) patients were married, while 172/750 (22.9%) mothers were single. The age distribution of the married and unmarried marital status is shown in Table 3.

Table 3  
*Age ethnicity and parity among married and unmarried marital status*

Age group/ Marital Status	Married	Unmarried
<16 years Old	22	17
16- 17	104	63
18- 19	452	92
Total	578	172
Ethnicity/ Marital Status		
Malays	274 (47.4%)	137 (79.65%)
Chinese	52 (8.99%)	9 (5.2%)
Indians	18 (3.1%)	6 (3.49%)
Indonesian	37 (6.4%)	7 (4.07%)
Myanmar	159 (27.5%)	5 (2.9%)
Others	38 (6.57%)	8 (4.65%)
Total	578	172
Parity		
1 <sup>st</sup> pregnancy	460 (79.6%)	163 (94.8%)
2 <sup>nd</sup> pregnancy	98 (17.0%)	9 (5.2%)
3 <sup>rd</sup> pregnancy	18 (3.1%)	-
4 <sup>th</sup> pregnancy	2 (0.3%)	-
Total	578	172

Malays made up the majority of both married and unmarried teenage mothers. There were 15 unbooked pregnancies among the married teenage mothers, and 59 unbooked pregnancies among the unmarried teenage mothers. Being unmarried is therefore significantly associated with unbooked ( $p < 0.001$ ). Table 4 shows the booking status among the teenage mothers.

Table 4  
*Booking status among teenage mothers*

Booking/ Marital Status	Married	Unmarried
Booked	563 (97.4%)	113 (65.7%)
Unbooked	15 (2.6%)	59 (34.3%)
Total	578	172
P value of unbooked pregnancy	p<0.001	

### Maternal Outcome

The mode of delivery amongst the married and unmarried teenage mothers is shown in Table 5. There is no significant difference in the mode of delivery ( $p = 0.055$  vaginal delivery,  $p = 0.4419$  caesarean section and  $p = 0.9097$  instrumental deliveries) between the two categories. However, foetal distress was the most common cause of caesarean section, followed by poor progress, and breech presentation, as shown in Table 6.

Table 7 shows the maternal outcomes between married and unmarried teenage mothers. There was no significant difference in the number of occurrences of hypertensive disease ( $p = 0.88428$ ), and diabetes in pregnancy ( $p = 0.39602$ ) among the two groups.

Table 5  
*Booking status among teenage mothers*

Mode of Delivery/Marital Status	Married	Unmarried
Vaginal Delivery	488 (84.4%)	142 (82.6%)
Caesarean Section	55 (9.5%)	20 (11.6%)
Instrumental Delivery	35 (6.1%)	10 (5.8%)
Total	578	172

Table 6  
*Indication for Caesarean section*

Indication for Caesarean Section	Married	Unmarried
Foetal distress	21 (38.2%)	5 (25%)
Poor progress	11 (2%)	1(5.0%)
Breech	91 (6.4%)	7(35%)
Others (pre-eclampsia, macrosomia, chorioamnionitis)	14 (25.4%)	7(35%)
Total	55	20

Table 7  
*Maternal outcome*

Maternal Outcome	Married	Unmarried
Hypertensive disease in pregnancy	25 (4.3%)	7 (4.1%)
Diabetes in pregnancy	8 (1.4%)	1(0.58%)
Post- partum haemorrhage	1 (0.17%)	0
3 <sup>rd</sup> degree tear	1(0.17%)	0

### Neonatal Outcome

Table 8 summarises the neonatal outcome. There was a significant difference in the number of in preterm delivery with the unmarried mothers noted to have a higher number of incidences compared to married mothers ( $p= 0.00468$ ). The unmarried mothers had a significantly lower birth weight ( $p< 0.0001$ ). However, there was no significant difference in the NICU admission between the two groups ( $p= 0.3779$ ). One neonatal death was reported among the unmarried teenage pregnancy in view of extreme prematurity at 31 week with severe intrauterine growth restrictions with a birth weight of 600 g.

Table 8  
*Neonatal outcome*

Outcome	Married	Unmarried
Preterm delivery	66/578 (11.4%)	34/172(19.8%)
P value in the difference of preterm labour	$p= 0.00468$	
NICU admission	88/578 (15.2%)	31/172 (18.0%)
P value for NICU admission	$p= 0.3779$	
Average weight	2.877g (SD 0.707)	2.7g (SD 0.513)
P value on birth weight	$p<0.0001$ unpaired (T- Test with 95% CI -0.2607 to -0.0933)	

### DISCUSSION

From 2009 to 2012, the prevalence of teenage pregnancy was found to be decreasing. This finding is in line with the earlier findings in other South Asian countries, where the greatest reduction has been documented to be as high as 40% (UNPD, 2013). This might be due to the fact that there is an increasing awareness among teenagers regarding precautions against pregnancy, either by using a barrier method such as a condom, or contraceptive pills (Zulkifli & Low, 2000). At the same time, sex education has been introduced in secondary schools in Malaysia in order to combat both sexual transmitted infections and unwanted teenage pregnancies. The National Population and Family Board, in their survey, found that although only 2.4% of school students admitted that they were having premarital sexual intercourse, 20.7% of the respondents stated that they knew friends who had had premarital sex. Meanwhile, 21.2% knew of friends who were pregnant, and 10% knew friends who had had abortions (National Population and Family Development Board, 1998). Nevertheless, one should be

cautious in interpreting such findings as the figures may not be a true reflection of the actual situation. Some teenage mothers may have opted not to disclose their pregnancy to medical professionals. They may choose to terminate their pregnancy or conceal the pregnancy, leading to infanticide and newborn abandonment.

Malays made up the majority of teenage mothers, followed by the ethnic group from Myanmar. This can be explained due to the fact that majority of the patients receiving care in the antenatal and delivery are Malays. Traditionally, it was culturally accepted for the Malays and Myanmars to get married and pregnant before the age of 20. This could be reflected by the finding that almost 77% of them were married. Moreover, the study was conducted at a public hospital, so it may not be a true reflection of the ethnicity as other races may have opted to receive their care from private healthcare professionals. Being married may indicate that the pregnancy is wanted and that the mother is well supported. This can be reflected by the finding that 97.4% of the married teenage pregnancies had their pregnancy booked. There were, in contrast, a high percentage of unbooked pregnancies among unmarried teenage mothers. From the demographic data, it can be noted that there were only 2.26% unbooked pregnancies among the married mothers, as compared to 34% of unbooked pregnancies among the unmarried teenage mothers. Booking an antenatal appointment is one of the greatest reductions and one of the most important appointments during the antenatal period. Being an unbooked pregnancy may also suggest that there is inadequate antenatal care throughout the pregnancy, and this can impact on the pregnancy outcome. Mahfouz et al. (1995) suggested that a poor outcome of pregnancy among teenage mothers may not just be due to biological immaturity, but could also be due to other environmental factors such as a lack of antenatal care as a result of poor support and a lower economic status.

Marital status is regarded as a very important status among pregnant women in Malaysia. It is still a taboo from the cultural and religious points of view for a girl or a woman to be pregnant when there are still single. Being married will determine the type of support received by the pregnant mothers, as the pregnancy will be much awaited by their partner and family members. On the other hand, unmarried teenage mothers may not be well accepted by their partner, family, school, and the society as a whole. In contrast, it will further put them in a very difficult situation, not just in the form of support they need, but also from the financial point of view. They are often ashamed with their pregnancy, causing them to stop going to school or continuing their education, and not receiving the appropriate medical attention due to embarrassment and limited financial capacity. They would only seek medical attention when emergency situations arise, i.e. bleeding or when they are in labour. Their situation may also make them liable to be taken advantage of including giving away their babies due to financial constraints and pressure by the society. Their future may be bleak, as many may not be able to continue their education and pursue their desired career.

In our study, the caesarean section rate was noted to be less than 15%. There was no significant difference between unmarried and married teenage mothers. The incidence of less than 15% is below the overall caesarean section rate in Hospital Ampang, which is around 20% to 25%. The main indication for the caesarean section among the teenage mothers was foetal distress, which is similar to the overall most common indication for the caesarean section in Hospital Ampang.

The preterm delivery was noted to be higher among unmarried compared to married teenage mothers. Similarly, the birth weight for unmarried teenage mothers was noted to be lower compared to those who were married. There were more babies admitted to NICU among the unmarried teenage mothers compared to those who were married. These neonatal outcomes could be attributed to environmental circumstances because being unmarried put teenage mother into a disadvantage condition with lack of support and financial capacity to ensure adequate nutrition and antenatal care support.

This study has some limitations. Being a retrospective study, important data may be lost. These include the social and economic background, whereby the study did not explore the economic status and kind of support the mothers had during and after their pregnancy. Thus, further studies are needed in order to determine the support needed from the healthcare point of view, as well as sources of funding. Further studies should also look into steps that need to be taken to minimise the number of unwanted pregnancies, especially those affecting young women at a tender age that could potentially affect their future.

## CONCLUSION

Being married at the age below 20 years old is still a cultural norm in Malaysia. Hence, the majority of teenage mothers were married. Nevertheless, the number of teenage pregnancy is decreasing over the years, and this is probably due to the increase in marital age and higher awareness of unprotected sexual intercourse in preventing sexually transmitted infection and unwanted pregnancy among the teenagers. Being unmarried is associated with poor antenatal care, preterm birth, lower birth weight, and higher percentage of NICU admission compared to their married counterpart.

## ACKNOWLEDGEMENTS

The authors gratefully acknowledge Universiti Sains Islam Malaysia for providing the Greenshoot Grant (Grant Number: PPP/GS/PSK/STH/30/10912) and Obstetrics & Gynaecology Department, Hospital Ampang, for making this study feasible.

## REFERENCES

- Anwar, M. S. S. (2010). Awareness of school students on sexually transmitted infections (STIs) and their sexual behavior: a cross-sectional study conducted in Pulau Pinang, Malaysia. *BMC Public Health*, 10(47).
- Centers for Disease Control and Prevention. (2001). Youth risk behavior surveillance-United States, 2001. *Morbidity and Mortality Weekly Report* 2002. *Morbidity and Mortality Weekly Report*, 51, 1–64.
- Chiam, H. K. (1996). *Report on Youth Sexuality Survey*. Selangor, Malaysia: Federation of Family Planning Association.
- Gilbert, W. J. D. (2004). Birth outcomes in teenage pregnancies. *J Matern Fetal Neonatal Med.*, 16, 265–70.

- Lee, L. K., Chen, P. C., Lee, K. K., & Kaur, J. (2006). Premarital sexual intercourse among adolescents in Malaysia: a cross-sectional Malaysian school survey. *Singapore Med. J.*, 47(6), 476-481.
- Low, W. Y. (2009). Malaysian youth sexuality: issues and challenges. *Journal of the University of Malaya Medical Centre (JUMMEC)*, 3-14.
- Mahfouz, A. A. E. S. (1995). Teenage pregnancy: are teenagers a high risk group? *Eur J Obstet Gynecol Reprod. Biol.*, 59, 17–20.
- McAnarney, E. R. (1987). Young maternal age and adverse neonatal outcome. *Am J. Dis Child*, 141, 1053–59.
- National Population and Family Development Board. (1998). *Report of the National Study on Reproductive Health and Sexuality 1994/1995*. Kuala Lumpur: National Population and Family Development Board.
- UNFPA, U. W. (2015). *Sexual and reproductive health of young people in Asia and the Pacific. A Review on Issues, Policies and Programmes*. Bangkok: United Nations Population Funds.
- UNPD. (2013). *Adolescent fertility since the International Conference on Population and Development in Cairo*. New York: UNPD.
- WHO. (2011). *Health of adolescents in Malaysia: World Health Organisation, Western Pacific Region*. WHO.
- Wyshack, G. F. R. (1982). Evidence for a secular trend in age of menarche. *New England Journal of Medicine*, 306, 1033–35.
- Zheng, X. Y., Chen, G., Han, Y. L., Chen, H., Lin, T., & Qiu, Y. (2010). Survey of youth access to reproductive health in China. *Population and Development*, 16(3), 2-16.
- Zulkifli S. N. & Low, W. Y. (2000). Sexual health education for youths – A Malaysian experience. *Asia-Pacific J. Publ. Health*, S58-S66.





## **Experimental Investigations on the Effects of Design Parameters on Single Slope Solar Still Evaporation Rate under Malaysian Conditions**

**Zainal Abidin Kamarul Baharin\* and Aishah Arinah Abdul Aziz**

*Faculty of Mechanical Engineering, Universiti Teknologi MARA (UiTM), 40450 Shah Alam, Selangor, Malaysia*

### **ABSTRACT**

Ocean offers an inexhaustible source of water which is not consumable by humans due to its high salinity. Large amounts of energy are required for desalination, and producing it from fossil fuels can cause harm to the environment. As such, solar energy can be used as an alternative energy source to provide cheap consumable water. This paper aims to investigate the effects of design parameters on single slope solar still evaporation rate under Malaysian conditions. Single sloped solar stills, with varying evaporator basin thickness and condenser plate thickness at different separator heights, were fabricated and tested. The 0.5 mm evaporator basin thickness still set has the highest evaporated volume (250 ml), with evaporation percentage of 25%, while the set with a 1 mm evaporator basin thickness has the lowest evaporation percentage (5.65%) with 56.5 ml evaporated volume. Experimental results indicate that the single slope solar still evaporation rate is very much influenced by climate parameters, namely solar intensity and ambient temperature.

*Keywords:* Desalination, evaporation rate, solar energy, solar stills

### **INTRODUCTION**

The high salinity level of seawater prevents it from being ingested by humans (Sivakumar &

Sundaram, 2013). Seawater contains around 35,000 parts per million (ppm) of dissolved salt and for fresh water, the concentration of salt has to be less than 1,000 ppm in order for it to be able to be ingested safely (US Geological Survey's Water Science School, 2016). Solar energy can be used as an alternative energy source to provide cheap potable water for remote areas where freshwater is lacking, but with an abundant amount of solar radiation and seawater (Abujazar et al., 2016).

#### **ARTICLE INFO**

*Article history:*

Received: 25 October 2016

Accepted: 17 March 2017

*E-mail address:*

[zainalkb@yahoo.com](mailto:zainalkb@yahoo.com) (Zainal Abidin Kamarul Baharin)

\*Corresponding Author

Evaporation and condensation are two main processes involved in the operation of a solar still, which is highly similar to the natural hydrological cycle (Muthu, Kalidasa, & Esakkimuthu, 2014). Utilising the greenhouse effect, a solar still consists of a basin where the seawater is placed. A transparent cover enclosing the basin will allow the sun rays to penetrate through the cover and get absorbed by the basin. This in turn will heat up the seawater and increase the vapour pressure. The transparent cover allows the resultant water vapour to condense on its inner surface and trickle down into the collector basin. The transparent cover also acts as a heat trap because it is transparent to the incoming sunlight, but is opaque to the infrared radiation which the hot water emits, creating the greenhouse effect. The roof prevents losses by enclosing the entire vapour and keeping the wind from cooling the seawater. This will allow for the temperature to rise, which will encourage evaporation (Kalogirou, 2005).

There are two modes (external and internal) in which heat transfer can occur in solar desalination (Phadatare & Verma, 2007). Heat transferring from the seawater inside the basin to the inner side of the transparent cover is the internal heat transfer that occurs within the still. This heat transfer takes place via convection, radiation and evaporation. Inside the still, the heat transfer takes place by free convection due to the actions of buoyancy force. This buoyancy force is the result of the temperature difference in the fluid that causes a variation in the density of fluid. To obtain more output, more evaporative heat transfer is needed. Radiative heat transfer has no influence whatsoever on both convective heat transfer and evaporative heat transfer which occurs simultaneously.

External heat transfers occur outside of the solar still, i.e. on the outer side of the cover, outer surface of evaporator basin and insulation. Conduction, convection and radiation are the three heat transfer modes governed by the external heat transfer and are independent of one another. The variation of water depth does not influence the external heat transfer from cover and bottom, which will remain constant and only be affected by ambient temperature and wind speed (Phadatare & Verma, 2007).

Fourier's Law of heat conduction can be expressed as:

$$\dot{Q}_{cond} = -kA \frac{dT}{dx} \quad [1]$$

Fourier's Law indicates that the rate of heat conduction through a plane wall is proportional with the average thermal conductivity, wall area, and temperature difference. However, it can also be seen from Equation 1 that the rate of heat conduction is inversely proportional to the wall thickness. This means that the wall with a greater thickness will experience lower conductivity rate, making it slower to heat the water inside the basin (UiTM, 2013).

Generally, climate and operating conditions affect the productivity of a solar still. Climate parameters include solar intensity, wind velocity, and ambient temperature. As for the operating conditions, the factors influencing productivity are the cover angle, material coated on the basin, water depth, temperature difference between the water and cover, and the insulation (Xiao et al., 2013).

Metal is usually used for evaporator basins. Copper, aluminium and steel are the common metal sheets used for this purpose (Martin & Goswami, 2005). One of the most important properties of metal application is thermal conductivity since it determines the capability of the

material to transfer heat. Meanwhile, the thermal conductivity of steel is relatively low at 48 W/m.K; however, the thermal conductivities of aluminium and copper are relatively high at 200 W/m.K and 390 W/m.K, respectively. The cost for copper and aluminium when compared to that of galvanised steel is more expensive, that is almost two times the cost of galvanised steel (Muthu, Kalidasa, & Esakkimuthu, 2014).

Depending on the duration of application, glass is usually considered more suitable for long-term applications, while plastic (such as polyethylene) is best used for short-term applications (Qiblawey & Banat, 2008). Ahsan et al. (2014) evaluated the effects of varying water depths (15, 25 and 50 mm) on productivity and concluded that as water depth increases, water productivity decreases, showing that the relationship between water depth and productivity of water is inversely proportional. The cover tilt angle is highly related to the productivity of a simple solar still. As the latitude angle of the test site becomes large, the cover tilt angle should be increased for maximum productivity (Khalifa, 2011).

Results from the experiments conducted under insulated and un-insulated conditions showed that insulated stills gave more production (Elango & Kalidasa Murugavel, 2015). In this work, single slope solar stills of different design parameters were fabricated by utilising available local materials. The experiments were conducted to study the effects of design parameters on single slope solar stills' evaporation rate under Malaysian climate.

## METHOD

### Experimental Setup

Three aluminium sheets with different thicknesses (0.5 mm, 1.0 mm and 2.0 mm) were moulded into the evaporator basin and painted black throughout to improve the radiation absorption.

Figure 1 shows that the basin of the solar still consists of two sections: evaporator basin and collector basin. The measurements are 250 mm x 250 mm and 40 mm x 250 mm for the evaporator basin and collector basin, respectively. The basin height is 55 mm and accommodates 1 litre of saline water (35,000 ppm) at a depth of 16 mm.

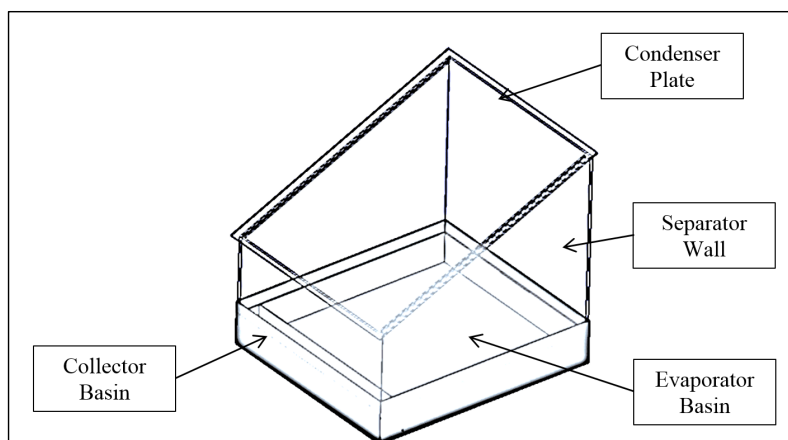


Figure 1. A schematic model of the solar still

**Nomenclature**

E05	0.5 mm evaporator basin thickness
E1	1.0 mm evaporator basin thickness
E2	2.0 mm evaporator basin thickness
W100	100 mm separator wall height
W200	200 mm separator wall height
W300	300 mm separator wall height
C2	2 mm condenser plate thickness
C3	3 mm condenser plate thickness
C4	4 mm condenser plate thickness

Condenser plates with the thicknesses of 2 mm, 3 mm and 4 mm are inclined at an angle of 30°, with the shortest height of separator wall varied into three different heights of 100 mm, 200 mm, and 300 mm. A tilt angle of 30° will increase the speed of the water droplets moving along the inner surface as compared to a lower angle which might cause it to fall back into the basin (Khalifa, 2011).

The separator walls are made of 2-mm thick glass. With three different thicknesses of evaporator basins, three different heights of separator wall, and also three different thicknesses of condenser plates, this 3 x 3 x 3 matrix totalled 27 still combinations that were tested in a three-sets-per-day manner over the course of 9 days to determine the setup that would yield the highest evaporation rate. Experiments were conducted in Shah Alam, Malaysia (3.0733° N), for a period of 24 hours (i.e., 7 a.m. to 7 a.m. the following day) and the output was measured at 2 h intervals. The stills were also positioned in the East-West direction (elevation angle) to study their effects on the evaporation process. Table 1 presents the combinations of 27 solar stills which were grouped according to the separator wall heights, while Figure 2 shows the experimental setup.

Table 1  
*Solar still set combinations*

W100	W200	W300
E05W100C2	E05W200C2	E05W300C2
E05W100C3	E05W200C3	E05W300C3
E05W100C4	E05W200C4	E05W300C4
E1W100C2	E1W200C2	E1W300C2
E1W100C3	E1W200C3	E1W300C3
E1W100C4	E1W200C4	E1W300C4
E2W100C2	E2W200C2	E2W300C2
E2W100C3	E2W200C3	E2W300C3
E2W100C4	E2W200C4	E2W300C4



Figure 2. The solar still setup

The ambient temperature and relative humidity were measured with a Sunleaves Hygro-Thermometer. Type K thermocouples (chromel-alumel) were used to measure the water, basin, and air temperatures inside the still. Water salinity values were determined using a SENSION 7 Benchtop Conductivity Meter.

### RESULTS AND DISCUSSION

Figure 3 shows the volume of water in the evaporator basin over time for all the 27 combinations.

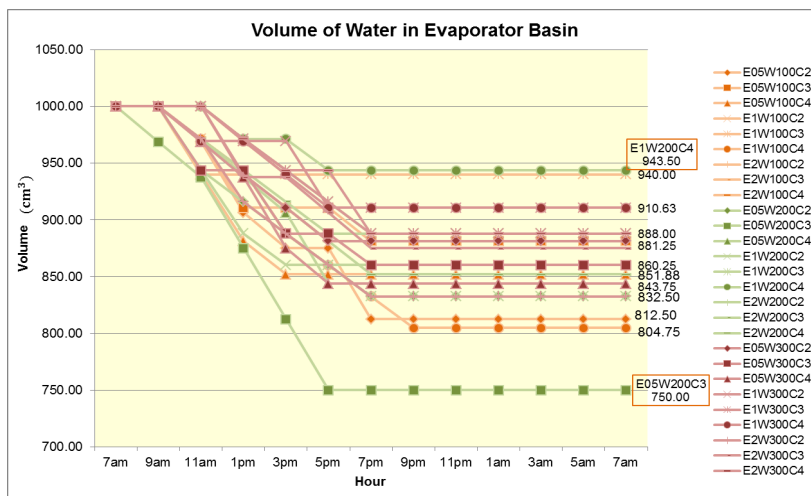


Figure 3. Volume of water in evaporator basin for all 27 combinations

Set E05W200C3 was left with the lowest volume of water (750 ml), while set E1W200C4 was left with the highest (943.5 ml). The steep decline of water volume for set E05W200C3 indicates that evaporation was occurring at a fast rate. For set E1W200C4, however, the gradual decrease of water volume means that evaporation occurred at a much slower rate.

Figure 4 shows the volume of evaporated water, which has been grouped according to the separator wall heights of W100, W200, and W300.

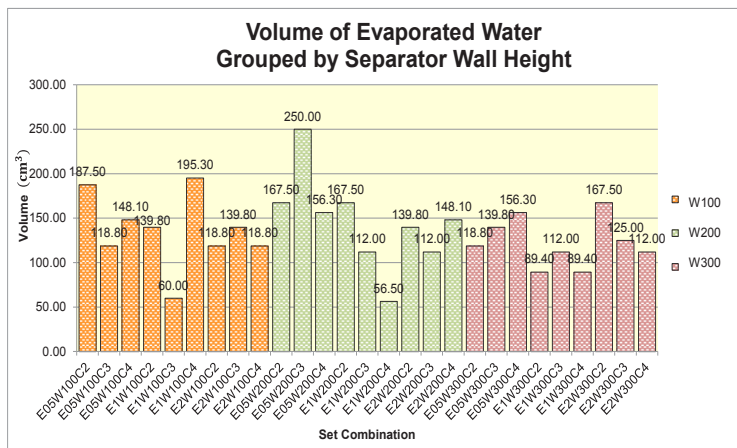


Figure 4. Volume of total evaporated water grouped by separator wall height

Set E05W200C3 has the highest evaporated volume (250 ml) at the evaporation percentage of 25%, while set E1W200C4 has the lowest evaporation percentage (5.65%) with 56.5 ml volume evaporated.

Figure 5 shows the sets with the highest and lowest evaporation rates, E1W200C4 and E05W200C3, respectively. E05W100C2 set is theoretically assumed to produce the highest evaporation rate. Figures 6, 7 and 8 show the volumes of evaporated water taken at 2 h intervals for the three sets, together with the weather conditions throughout the day.

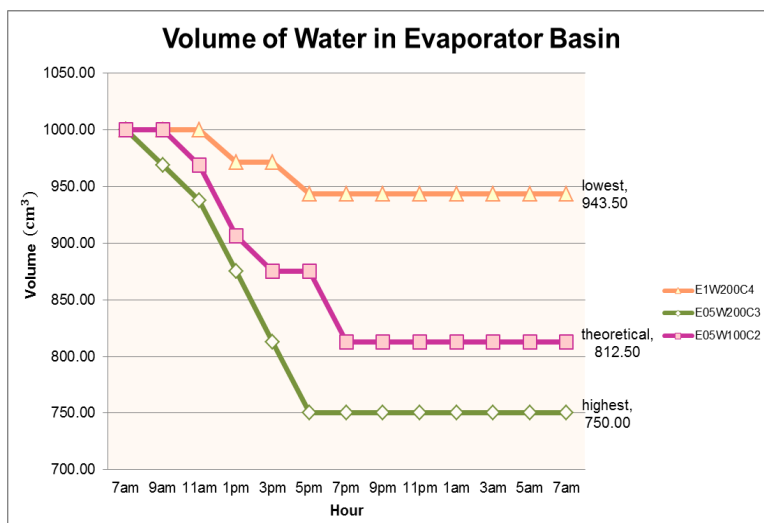


Figure 5. Volume of saltwater in evaporator basin

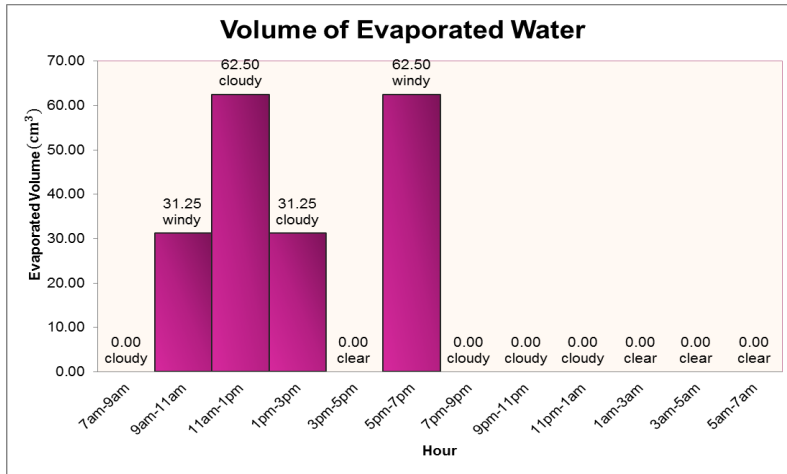


Figure 6. Volume of evaporated water for set E05W100C2

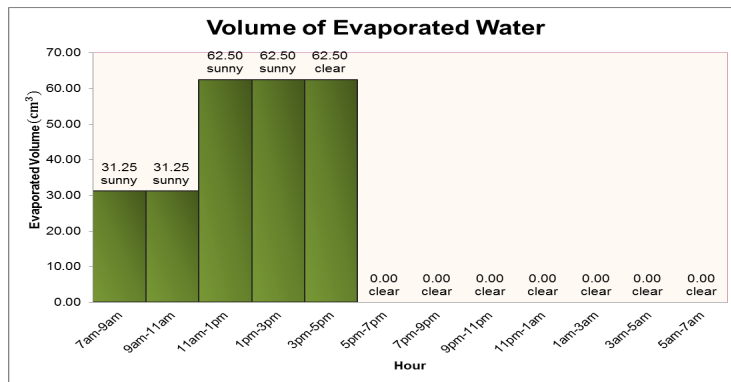


Figure 7. Volume of evaporated water for set E05W200C3

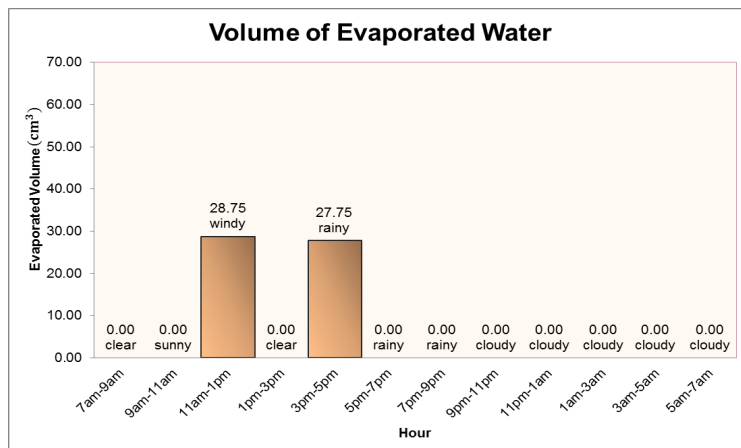


Figure 8. Volume of evaporated water for set E1W200C4

Theoretically, the productivity for set E05W100C2, which has the thinnest evaporator basin, shortest separation distance, and thinnest condenser plate, should have been the highest among all 27 sets. The thinner the evaporator basin, the greater the heat transfer from the higher ambient temperature to the lower temperature within the still, resulting in a higher evaporation rate due to the high temperature of water (UiTM, 2013). Also, the shorter separation distance results in a smaller solar still volume, concentrating more heat and causing more water evaporation in the evaporator basin (Khalifa, 2011).

However, the volume of water remaining in the evaporator basin of this set was 812.5 ml, which is more than that of set E05W100C2 (750 ml). The incompliance of the experimental results against the theoretical assumption is influenced by weather conditions. As can be seen in Figures 6 and 7, on the experiment day of set E05W100C2, the weather was mostly cloudy and this reduced the amount of solar energy available to promote evaporation. For set E05W200C3, however, it was mostly sunny and clear, resulting in a greater evaporation rate. As such, the total volume of evaporated water for set E05W200C3 (250 ml) is higher than set E05W100C2 (187.5 ml).

Set E1W200C4 has the lowest total evaporated volume (56.5 ml). This set comprises of a thicker 1 mm evaporator basin, slowing the rate of heat transfer and rise of water temperature. The weather condition on the day of the experiment for set E1W200C4 was also mostly rainy and cloudy, significantly affecting its evaporation rate. This clearly proves that climate parameters play a major role in the operation of a solar still.

Figures 9, 10 and 11 show the temperature variations for sets E05W100C2, E05W200C3 and E1W200C4, respectively.

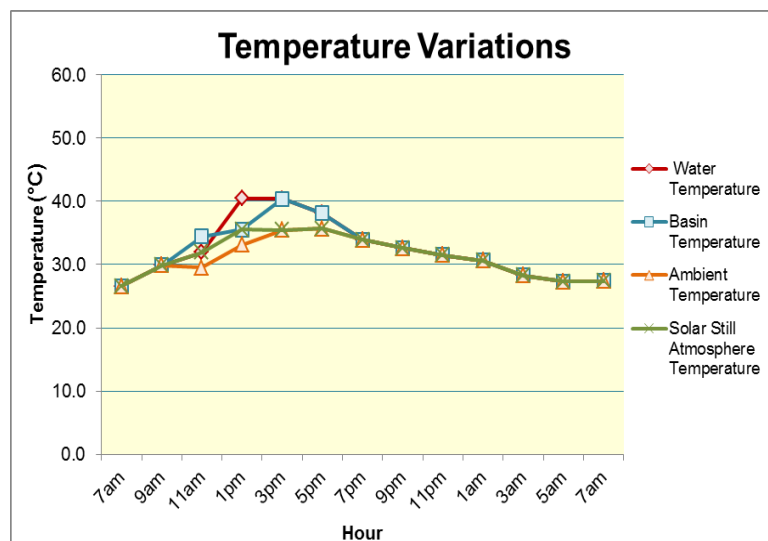


Figure 9. Temperature variations for set E05W100C2



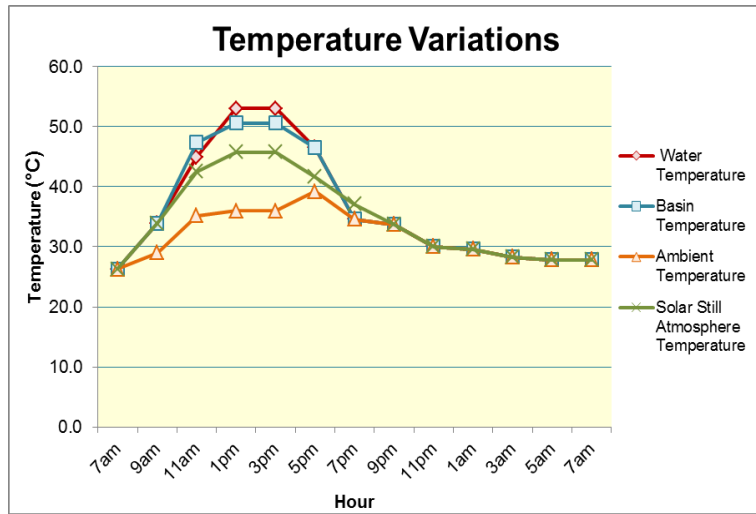


Figure 10. Temperature variations for set E05W200C3

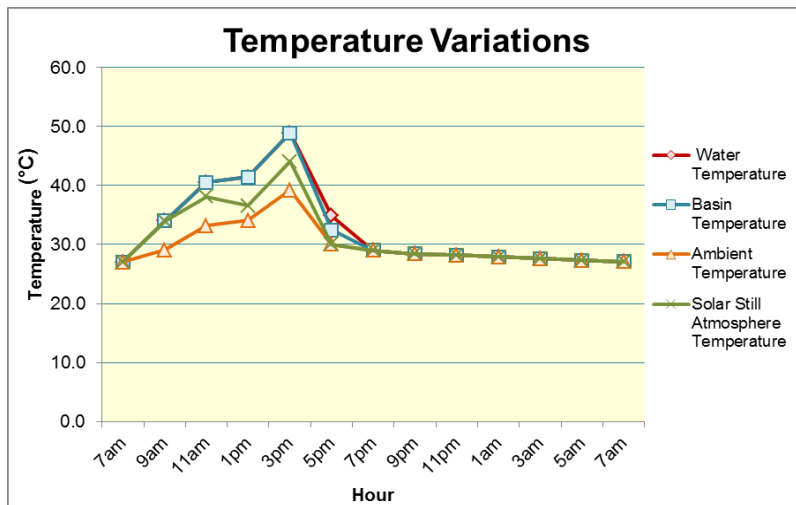


Figure 11. Temperature variations for set E1W200C4

From the graphs, all the three sets showed that during the day, water temperature, basin temperature and solar still atmosphere temperature exceeded the ambient temperature. As stated by Muthu, Kalidasa and Esakkimuthu (2014), the absorption of solar energy by the evaporator basin and heat transferred to the water enabled it to be evaporated into water vapour. Higher ambient temperature also causes the water temperature, basin temperature and the temperature within the solar still to be higher. The water temperature inside set E05W200C3 (Figure 10) is also the highest from 1 p.m. to 3 p.m., correlating with a higher rate of evaporation shown in Figure 7.

## CONCLUSION

The performance of 27 single slope solar still combinations, with different thicknesses of evaporator basins and condenser plates at different separator heights, was experimentally studied under Malaysian conditions. Thin evaporator basins allow for a higher rate of heat conduction, making it faster to heat the water inside the basin that promotes evaporation. Even so, climate parameters (solar intensity and ambient temperature) still have great influence on the still evaporation rate. Higher solar intensity and ambient temperatures will result in higher temperatures of the water and basin that will increase the evaporation rate.

## ACKNOWLEDGEMENTS

The authors would like to thank the Faculty of Mechanical Engineering and Faculty of Civil Engineering, Universiti Teknologi MARA (UiTM), for the technical assistance provided which had made this study possible.

## REFERENCES

- Abujazar, M. S. S., Fatihah, S., Rakmi, A. R., & Shahrom, M. Z. (2016). The effects of design parameters on productivity performance of a solar still for seawater desalination: A review. *Desalination*, 385, 178–193.
- Ahsan, A., Imteaz, M., Thomas, U. A., Azmi, M., Rahman, A., & Nik Daud, N. N. (2014). Parameters affecting the performance of a low cost solar still. *Applied Energy*, 114, 924–930.
- Elango, T., & Murugavel, K. K. (2015). The effect of the water depth on the productivity for single and double basin double slope glass solar stills. *Desalination*, 359, 82–91.
- Kalogirou, S. A. (2005). Seawater desalination using renewable energy sources. *Progress in Energy and Combustion Science*, 31(3), 242–281.
- Khalifa, A. J. N. (2011). On the effect of cover tilt angle of the simple solar still on its productivity in different seasons and latitudes. *Energy Conversion and Management*, 52(1), 431–436.
- Martin, C. L., & Goswami, D. Y. (2005). *Solar Energy Pocket Reference*. Earthscan.
- Muthu Manokar, A., Kalidasa Murugavel, K., & Esakkimuthu, G. (2014). Different parameters affecting the rate of evaporation and condensation on passive solar still - A review. *Renewable and Sustainable Energy Reviews*, 38, 309–322.
- Phadatare, M. K., & Verma, S. K. (2007). Influence of water depth on internal heat and mass transfer in a plastic solar still. *Desalination*, 217(1–3), 267–275.
- Qiblawey, H. M., & Banat, F. (2008). Solar thermal desalination technologies. *Desalination*, 220(1–3), 633–644.
- Sivakumar, V., & Sundaram, E. G. (2013). Improvement techniques of solar still efficiency: A review. *Renewable and Sustainable Energy Reviews*, 28, 246–264.

US Geological Survey's (USGS) Water Science School. (n.d.). Retrieved from <http://water.usgs.gov/edu/saline.html>

UiTM, Faculty of Mechanical Engineering (2013). *MEC 551 Thermal Engineering*. McGraw-Hill.

Xiao, G., Wang, X., Ni, M., Wang, F., Zhu, W., Luo, Z., & Cen, K. (2013). A review on solar stills for brine desalination. *Applied Energy*, *103*, 642–652.



## Second-hand Smoke Exposure and Psychological Distress amongst Non-Smoking Pregnant Women in Malaysia

Siti Munira Yasin<sup>1\*</sup>, Khairul Mizan Taib<sup>2</sup>, Mohd Rodi Isa<sup>1</sup>, Mohd Ariff Fadzil<sup>1</sup>, Mohd Razilan Abdul Kadir<sup>2</sup> and Saiful Farik Mat Yatim<sup>2</sup>

<sup>1</sup>Population Health and Preventive Medicine, Faculty of Medicine, Universiti Teknologi MARA (UiTM), 47000 Sungai Buloh, Selangor, Malaysia

<sup>2</sup>Faculty of Information Management, Universiti Teknologi MARA (UiTM) Puncak Perdana, 40150 Shah Alam, Selangor, Malaysia

### ABSTRACT

This study aimed to examine the association between second-hand smoke (SHS) exposure and psychological distress amongst non-smoking pregnant women. A cross-sectional study was used to obtain a representative sample of non-smoking pregnant women attending health clinics (n = 661) across six states in Malaysia. The duration of SHS exposure inside and outside the house was recorded from the participants. Psychological distress was assessed via General Health Questionnaire (GHQ-12). The analyses were conducted using a logistic regression adjusted for demographic variables and other variables. Amongst non-smoking pregnant women, the prevalence of global SHS exposure and psychological distress was 80.4% and 64.2%, respectively. In the multivariate adjusted odds ratio (OR) models for psychological distress and the duration of SHS exposures, there was an OR of 1.04 (95% CI: 0.61-1.77) for individuals with SHS exposure of 1-4 hours/week, 0.44 (95% CI: 0.23-0.81) for SHS exposure of 5-14 hours/week and 0.84 (95% CI: 0.32-2.22) for exposures of >15 hours/week compared to those with no SHS exposure outside the home. Meanwhile, SHS exposure outside the house with the duration of 5-14 hours might have temporary calming effects against psychological distress. Nonetheless, more research is needed to ascertain this.

*Keywords:* Second hand smoker, psychological distress, pregnancy

### ARTICLE INFO

*Article history:*

Received: 25 October 2016

Accepted: 17 March 2017

*E-mail addresses:*

smunira@salam.uitm.edu.my (Siti Munira Yasin),  
strategist05@gmail.com (Khairul Mizan Taib),  
marif022@hotmail.com (Mohd Ariff Fadzil),  
rodi@salam.uitm.edu.my (Mohd Rodi Isa),  
mrzilan@salam.uitm.edu.my (Mohd Razilan Abdul Kadir),  
farik@salam.uitm.edu.my (Saiful Farik Mat Yatim)

\*Corresponding Author

### INTRODUCTION

Tobacco not only kills smokers, but it also causes a major burden to those who do not smoke. Environmental tobacco smoke (ETS) or second-hand smoke (SHS) is associated with significant health risks to humans,

including heart disease, asthma, cancer and/or respiratory illnesses. Second-hand smoke exposure comprises exhaled and side-stream smoke that is released from burning cigarettes in between inhalations. The composition of SHS changes slightly when it dilutes and interacts with ambient air and other compounds in the environment (Schramm et al., 2010). Nonetheless, regardless of how the changes occur in the environment, the composition of this mixture still contains a significant level of nicotine. The concentration of nicotine in the homes of smokers ranges from 2 to 10  $\mu\text{g}/\text{m}^3$ , and there is no safe level of SHS exposure for adults (Shibuya et al., 2003).

Pregnant women are particularly vulnerable to the effects of SHS because it can have negative effects on their unborn child. Prenatal SHS exposure has been associated with risks of stillbirth, preterm delivery, low birth weight, asthma, and respiratory infections during childhood (Bachok & Salinah, 2014). Recently, increasing evidence has shown negative effects of SHS on mental health. Psychological distress has been suspected of causing reduced foetal growth and birth weight (Mehraban et al., 2013) and asthma (Turcotte-Tremblay et al., 2014) although human studies have not shown consistent results (Lukasse et al., 2014).

Psychological distress is widely used as an indicator of the mental health used in the population-based study in public health, intervention studies and clinical trials. Nonetheless, the concept is still vague for many. In terms of definition, psychological distress may be defined as a condition of emotional instability, comprised of symptoms of depression (sadness, loss of interest and a state of hopelessness) and anxiety (tensed and restlessness) (Mirowsky & Ross, 2002). The two symptoms, in addition, might be associated with somatic symptoms (e.g., insomnia, lack of energy, and headaches) which actually vary across the cultures (Kleinman, 1991; Kirmayer, 1989).

It has been suggested that there is a relationship between second-hand smoke exposures and psychological distress in adults, although further research is required (Ballbe et al., 2015; Pattanayak, Sagar, & Jain, 2012). Amongst adolescents, those with a higher duration of exposure to cigarette smoke in the home have a greater incidence of psychological distress (Padrón, Galán, & Rodríguez-Artalejo, 2012). Recently, it was reported that antenatal SHS exposure may be associated with postpartum depression (Khan et al., 2015). However, no studies have thus far evaluated the duration of SHS exposure during pregnancy and the settings that actually affect psychological distress.

In Malaysia, we have seen many advances to combat SHS since Malaysia became a signatory of the WHO Framework Convention Tobacco Control (FCTC). These advances include various campaigns (Yasin et al., 2012) and the establishment of smoke-free institutions, parks, and indoor public places. Nonetheless, we do not know how much this smoke-free law has affected smoke-free homes locally, although results have been promising in other parts of the world, where a complete smoke-free ban has been implemented (Cheng, Glantz, & Lightwood, 2011; King, Patel, & Babb, 2014). Therefore, we hope that assessing the association between mental health and SHS exposure in places not yet regulated (e.g., homes) may help enhance programmes and form future policies to combat the smoking epidemic. Accordingly, our study aims to examine the association between the duration and location of SHS exposures and its association with psychological distress amongst pregnant women.

## METHOD

A cross-sectional study was conducted from January to June 2014. Sampling was performed by multistage stratified random sampling across six states in Malaysia. The chosen states were Kelantan, Johor, Melaka, Sabah, Selangor and Pahang. Two randomly selected clinics were chosen in each state. Data collection was conducted by the researchers and a trained group of research assistants. In each clinic, the participants randomly chosen were selected by their registration number during antenatal visits on two days per week. The participants meeting the inclusion criteria included women with singleton pregnancies, without previous mental illnesses and without congenital defects. The women also needed to be able to understand and read the Malay language. The questionnaires were self-administered, and any misunderstanding in any sections was explained by the research assistants. This study was approved by the Institutional Review Board of the University and the local public health investigation board.

The questionnaire contained sociodemographic characteristics, pregnancy history, pregnancy intention, household smoking status, household smoking rules, and the General Health Questionnaire (GHQ-12). The GHQ used to measure psychological distress is widely used both locally and internationally to detect psychological distress (Afshar et al., 2015; Kutty & Sreeramareddy, 2014). However, it is just a screening tool and not a diagnostic tool. The GHQ used in this research has been validated for use in Malay (Yusoff, Rahim, & Yaacob, 2010). The GHQ comprises 12 questions that measure the general health of the population. Possible psychological distress was defined as a score of  $\geq 3$  points in the GHQ-12. In regard to SHS exposure, the respondents were asked how long they were in an enclosed area with tobacco smoke (1-4 hours/week, 5-14 hours/week, or  $>15$  hours/week), both inside and outside the home.

Data entry and analyses were conducted using IBM SPSS version 21.0. Descriptive statistics (e.g., number and percentages) were also determined. A comparison of the variables using a logistic regression served as the primary analysis. A bivariate analysis by logistic regression was used to determine the association between sociodemographic characteristics and SHS exposures in and outside the home.

The association between the duration of SHS exposure with psychological distress was done by multiple logistic models for exposure originating from inside and outside the home. Dummy terms were used to model the duration of SHS exposures. Finally, 5 sequential models were to adjust for potential confounders (Models A, B, C and D). The last model was also adjusted for inside the home if the exposure examined was outside the home and vice versa.

## RESULTS

A total of 661 pregnant women, majority of women were Malay, aged between 20-40 years old and in the second and third trimesters of pregnancy. Out of the total number, 532 (80.5%) who were exposed and 129 (19.5%) who were not exposed to any SHS were involved in this study. Three hundred and fifty-four (53.6%) women were exposed to SHS in the home, while 438 (66.3%) were exposed outside the home. Compared to the participants with no SHS

exposure, those exposed at home were significantly and more likely to work either part-time or had not worked at all and did not have any smoking rules at home (Table 1). The prevalence of psychological distress amongst the pregnant women was 64.2% (95% CI: 0.60-0.68).

**Table 1**  
*Prevalence of exposure to SHS inside the home and outside the home compared to no exposure*

Characteristics	SHS exposure at home			SHS exposure outside the home		
	N (%)	OR (95% CI)	P value <sup>a</sup>	N (%)	OR (95% CI)	P value <sup>a</sup>
<b>Ages, years</b>						
<20 years	6 (60.0)	Ref		4 (40.0)	Ref	
20-30 years	197 (40.7)	0.94 (0.28-3.15)	0.98	287 (59.3)	4.87 (1.34-17.68)	0.32
31-40 years	101 (51.3)	0.98 (0.29-3.31)	0.68	96 (48.7)	1.93 (0.53-7.06)	0.52
41 and above	6 (54.5)	1.39 (0.29-6.61)	0.76	5 (45.5)	1.69 (0.35-8.22)	0.53
<b>Ethnicity</b>						
Malay	260 (43.4)	Ref		339 (56.6)	Ref	
Chinese	37 (52.1)	1.63 (0.92-2.89)	0.38	34 (47.9)	0.65 (0.37-1.14)	0.13
Indian	3 (37.5)	0.38 (0.09-1.48)	0.94	5 (62.5)	0.44 (0.12-1.54)	0.20
Other	32 (46.4)	0.94 (0.55-1.59)	1.14	37 (53.6)	0.68 (0.39-1.17)	0.16
<b>Employment</b>						
Working full-time	155 (37.4)	Ref		259 (62.6)	Ref	
Working part-time	38 (50.7)	5.61 (2.64-11.95)	<0.001	37 (49.3)	1.46 (0.69-3.04)	0.32
Not working but worked before pregnant	77 (51.7)	2.38 (1.55-3.65)	<0.001	72 (48.3)	0.63 (0.41-0.98)	0.04
Never worked before	56 (58.3)	3.10 (1.84-5.23)	<0.001	40 (41.7)	0.38 (0.24-0.63)	<0.0
<b>Weeks of pregnancy</b>						
1 <sup>st</sup> trimester (weeks 1-12)	79 (48.8)	Ref		83 (51.2)	Ref	
2 <sup>nd</sup> trimester (weeks 13-26)	153 (42.5)	0.70 (0.46-1.07)	0.1	207 (57.5)	1.40 (0.89-2.20)	0.14
3 <sup>rd</sup> trimester (week 27 onwards)	122 (45.2)	0.67 (0.43-1.03)	0.07	148 (54.8)	0.92 (0.59-1.45)	0.73
<b>Spouse smoking status</b>						
Yes	224 (49.1)	Ref	<0.001	232 (50.9)	Ref	<0.01
No	127 (38.5)	0.18 (0.13 – 0.26)		203 (61.5)	0.37 (0.26-0.53)	
<b>Household smoking laws</b>						
No smoking is allowed	167 (37.8)	Ref		275 (62.2)	Ref	
Only special guests are allowed to smoke	14 (58.3)	2.05 (0.89-4.72)	0.09	10 (46.7)	0.38 (0.17-0.91)	0.03
Smoking permitted in certain areas in the house	107 (53.0)	5.79 (3.63-9.23)	<0.001	95 (47.0)	1.29 (0.84-1.99)	0.24
Smoking allowed everywhere	58 (55.2)	28.25 (8.71-91.66)	<0.001	47 (44.8)	2.16 (1.09-4.29)	0.03
<b>Psychological Distress (GHQ)</b>						
No psychological distress	110 (43.8)	Ref		141 (56.2)	Ref	
Psychological distress	180 (43.5)	0.84 (0.59,1.18)	0.313	234 (56.5)	0.81 (0.56, 1.18)	0.267

<sup>a</sup>Logistic regression  
Abbreviation: OR = Odds Ratio  
Ref = Reference



Table 2  
Duration of SHS exposure and the prevalence of psychological distress in pregnant mothers

	N (%)	SHS Exposure (% (95% CI))	N (%)	Prevalence of psychological distress (% (95% CI))	P value
Exposure inside the home					
None	293 (52.1)	45.3 (41.4 to 49.1)	269 (47.9)	22.7 (19.4 to 25.9)	0.008
< 1-4 hours	227 (55.8)	35.1 (31.4 to 38.7)	180 (44.2)	43.13 (39.3 to 46.7)	
5-14 hours	91 (53.5)	14.1 (11.4 to 16.8)	79 (46.5)	20.8 (17.7 to 23.9)	
15 or more hours	36 (53.7)	5.6 (3.8 to 7.3)	31 (46.3)	13.4 (10.8 to 16.1)	
Exposure outside the home					
None	207 (53.0)	32.1 (28.4 to 35.7)	183 (47.0)	66.2 (60.5 to 71.9)	<0.0001
< 1-4 hours	254 (53.2)	39.4 (35.6 to 43.1)	223 (46.8)	60.3 (55.0 to 65.6)	
5-14 hours	135 (55.1)	20.9 (17.8 to 24.1)	110 (44.9)	68.4 (64.1 to 72.7)	
15 or more hours	49 (53.8)	7.6 (5.6 to 9.7)	42 (46.2)	63.8 (59.6 to 67.9)	

Table 2 presents the relationship between the SHS exposure and prevalence of psychological distress. There was a positive relationship between duration of exposure and the prevalence of psychological distress.

Table 3  
Multivariate association between psychological distress among pregnant women by duration of exposure inside and outside home

		Duration of Exposure to SHS in the home		Duration of Exposure to SHS outside the home	
		OR (95%CI)	P value	OR (95%CI)	P value
Model A	None		Ref		Ref
	< 1-4 hours	0.90 (0.61-1.34)	0.62	1.12 (0.73-1.69)	0.62
	5-14 hours	0.68 (0.41-1.13)	0.14	0.42 (0.26-0.69)	<0.001
	15 or more hours	0.93 (0.43-2.03)	0.85	0.97 (0.48-1.99)	0.95
Model B	None		Ref		Ref
	< 1-4 hours	0.93 (0.61-1.42)	0.74	1.11 (0.70-1.75)	0.40
	5-14 hours	0.68 (0.39-1.19)	0.17	0.40 (0.24-0.67)	<0.001
	15 or more hours	0.91 (0.41-2.04)	0.82	0.87 (0.42-1.82)	0.72
Model C	None		Ref		Ref
	< 1-4 hours	1.63 (0.97-2.75)	0.06	1.11 (0.69-1.79)	0.66
	5-14 hours	1.48 (0.69-3.18)	0.31	0.42 (0.25-0.70)	0.001
	15 or more hours	1.75 (0.57-5.35)	0.33	0.79 (0.43-1.91)	0.79

Table 3 (continue)

Model D	None		Ref		Ref
	< 1-4 hours	1.39 (0.84-2.30)	0.18	1.04 (0.62-1.76)	0.58
	5-14 hours	1.26 (0.62-2.57)	0.51	0.49 (0.27-0.89)	0.02
	15 or more hours	1.45 (0.56-3.75)	0.45	1.01 (0.43-2.37)	0.98
Model E	None		Ref		Ref
	< 1-4 hours	1.64 (0.97-2.75)	0.06	1.04 (0.61-1.77)	0.88
	5-14 hours	1.48 (0.97-2.75)	0.31	0.44 (0.23-0.81)	0.01
	15 or more hours	1.75 (0.57-5.35)	0.33	0.84 (0.32-2.22)	0.72

Model A: Crude logistic regression

Model B: Adjusted for age, state, ethnicity, education level, race, employment and household income

Model C: Similar to model B with the additional adjustment for weeks of pregnancy, pregnancy planning, and spouse excitement of pregnancy

Model D: Similar to model C with the additional adjustment for spouse smoking status, household smoking laws and confidence in ability to avoid SHS exposure

Model E: Similar to model E with additional adjustment for exposure inside the home

Table 3 presents the various models, after accounting for other variables, of the relationship between psychological distress and hours of SHS exposures inside and outside the home. Exposure to SHS outside the home of between 5-14 hours showed a negative relationship with psychological distress in all adjusted models. The significance was slightly reduced in the more adjusted model. There was no significant association between hours of exposure to SHS inside the home and psychological distress.

## DISCUSSION

This study found that in non-smoking pregnant women, the prevalence of global SHS exposure and exposure to SHS at home and outside the home in Malaysia remained high. There was also a positive relationship between the duration of exposure to SHS outside the home and psychological distress.

The SHS exposure is highly prevalent amongst non-smoking pregnant women in Malaysia, and this is worrying for many reasons. First, during pregnancy, passive smokers are exposed to both mainstream and side-stream smokes, which contain the same constituents that are harmful to infant neurodevelopment. Second, toxic substances remain on surfaces and in dust, and although the smokes had disappeared after a few months, and they might react with the air to produce new toxins called the “third-hand smoke”. It is suspected that during pregnancy, foetal development is highly sensitive to this exposure (Kelishadi & Poursafa, 2014).

We found that there was a direct significant association between spouse smoking status and SHS exposure at home. This finding is consistent with other research that has also shown that the most common SHS exposures in pregnant women at home come from their spouses (Eiden et al., 2011). Additionally, our study revealed that pregnant women who were exposed to SHS at home tended not to have any smoking rules at home. We also found that establishing

particular restrictions to areas allowed for smoking at home reduced the odds of SHS exposure compared to no restrictions at all. This finding is also consistent with some previous studies that reported that husbands with higher cigarette consumption and a lack of smoke-free home rules were important factors that were significantly associated with higher levels of SHS exposure both in total and at home (Yang et al., 2010). Other parts of the world have now recommended 100% smoke-free home regulations instead of partial smoke-free rules to ensure maximum protection from SHS (King et al., 2014). Hence, it is timely that Malaysia, which has a high prevalence of adult male smokers (46.4%), evaluates the issue of smoke-free homes as mandatory for all houses.

Although substantial research has been performed on the association between smoking and mental health, only a few studies have evaluated the effects of SHS and mental health (Bandiera, 2011). A recent positive relationship between SHS and psychological distress was found in the adult population in Spain (Ballbe et al., 2015). The researchers found a direct association between home SHS exposure and psychological distress. Hence, this result is in contrast with our finding of no association between the factors. Nonetheless, our results revealed that psychological distress was associated with the duration of exposure. After adjusting for confounders in the sequential multivariate model, SHS exposure between 5-14 hours outside the home appeared to have a temporary calming effect on psychological distress. This is supported by a study among young women which revealed that cigarette smoking, or exposure to nicotine, has temporary effects on reducing stress (File, Fluck, & Leahy, 2011). Nonetheless, it contrasts with that of a relationship that has been identified in SHS exposure amongst adolescents, of no such association (Padrón, Galán, & Rodríguez-Artalejo, 2012). A reason for this relationship could be the difference in the population that was studied. To our knowledge, no studies have assessed this relationship during pregnancy. Furthermore, the difference between our results and others might be related to the differences in physiological and psychological effects that occur during pregnancy. A possible mechanism would be the role of oxytocin. Recently, oxytocin has been shown to reduce the effects of tobacco withdrawal symptoms in rats (Olf et al., 2013). It has also been suggested that oxytocin, which is high during pregnancy, can exert beneficial effects on processes thought to promote social bonding and mask the effects of mental stress (Zanos et al., 2015). This effect may explain why moderate exposure to SHS is protective to some extent compared to no exposure or excessive exposure. The association between oxytocin and mental stress, however, remains vague and requires further research.

The current study is subject to some limitations which must be interpreted with caution. First, because the study design is cross-sectional, no causal relationship can be inferred between psychological distress and SHS exposure. Second, the data were self-reports; nonetheless, self-reported results have been found to be correlated with biomarkers of exposure in many other studies. Third, we did not analyse previous exposures to SHS prior to pregnancy. Smoking at work and home may have changed over time, and previous exposure during childhood and adolescence may influence mental health once the individual reaches adulthood. In addition, it would be wise to obtain the exact hours of exposure to SHS as continuous data in order to obtain the exact relationship with psychological distress in future studies. Lastly, the GHQ

used in this research only measures short-term psychological distress, and is unable to measure mental illnesses. Hence, diagnostic tools should be used to measure mental illnesses.

This study also has some strengths which include a nationally representative sample of pregnant women. To our knowledge, this investigation is the first study to explore this association in the South East Asian region, where smoking prevalence is particularly high. In addition, we had a high participation rate, and various measures that may act as confounders were taken into consideration in the study. Hence, the factor enabled us to assess the independent association between psychological distress and SHS exposure.

## CONCLUSION

In non-smoking pregnant women, a 5-14 hour duration of exposure to SHS outside the home might have a negative relationship with the frequency of psychological distress. Hence, SHS exposure to both inside and outside home needs urgent attention.

## ACKNOWLEDGEMENTS

This project was funded by the Fundamental Research Grant (FRGS/1/ 2015/ SKK05/UITM/03/ 1). The authors would like to thank the participants and the top health facility administrators for granting permission to conduct this study.

## REFERENCES

- Afshar, H., Roohafza, H. R., Keshteli, A. H., Mazaheri, M., Feizi, A., & Adibi, P. (2015). The association of personality traits and coping styles according to stress level. *Journal of Research in Medical Sciences, 20*(4).
- Bachok, N. A., & Salinah, O. (2014). The Effect of Second-Hand Smoke Exposure during Pregnancy on the Newborn Weight in Malaysia. *The Malaysian Journal of Medical Sciences, MJMS, 21*(2), 44.
- Ballbe, M., Martinez-Sanchez, J. M., Gual, A., Martinez, C., Fu, M., Sureda, X., & Fernandez, E. (2015). Association of second-hand smoke exposure at home with psychological distress in the Spanish adult population. [Journal article]. *Addict Behav., 50*, 84-88.
- Bandiera, F. C. (2011). What are candidate biobehavioral mechanisms underlying the association between secondhand smoke exposure and mental health? *Medical Hypotheses, 77*(6), 1009-1010.
- Cheng, K.-W., Glantz, S. A., & Lightwood, J. M. (2011). Association between smokefree laws and voluntary smokefree-home rules. *American Journal of Preventive Medicine, 41*(6), 566-572.
- Eiden, R. D., Molnar, D. S., Leonard, K. E., Colder, C. R., Homish, G. G., Maiorana, N., & Connors, G. J. (2011). Sources and frequency of secondhand smoke exposure during pregnancy. [Research Support, N I H , Extramural]. *Nicotine Tob Res., 13*(8), 653-660.
- File, S. E., Fluck, E., & Leahy, A. (2001). Nicotine has calming effects on stress-induced mood changes in females, but enhances aggressive mood in males. *International Journal of Neuropsychopharmacology, 4*(4), 371-376.

- Kelishadi, R., & Poursafa, P. (2014). A review on the genetic, environmental, and lifestyle aspects of the early-life origins of cardiovascular disease. [Review]. *Curr Probl Pediatr Adolesc Health Care*, 44(3), 54-72.
- Khan, S., Arif, A. A., Laditka, J. N., & Racine, E. F. (2015). Prenatal exposure to secondhand smoke may increase the risk of postpartum depressive symptoms. [Journal article]. *J Public Health*, 14.
- King, B. A., Patel, R., & Babb, S. D. (2014). Prevalence of smokefree home rules—United States, 1992–1993 and 2010–2011. *MMWR Morb Mortal Wkly Rep*, 63(35), 765-769.
- Kirmayer, L. J. (1989). Cultural variations in the response to psychiatric disorders and psychological distress. *Social Science and Medicine*, 29, 327-339.
- Kleinman, A. (1991). *Rethinking Psychiatry. From Cultural Category to Personal Experience*. New York: The Free Press.
- Kutty, N. A., & Sreeramareddy, C. T. (2014). A cross-sectional online survey of compulsive internet use and mental health of young adults in Malaysia. *Journal of Family and Community Medicine*, 21(1), 23.
- Lukasse, M., Helbig, A., Benth, J. Š., & Eberhard-Gran, M. (2014). Antenatal maternal emotional distress and duration of pregnancy. *PloS One*, 9(7), e101682.
- Mehraban, Z., Alizadeh, L., & Narimani, M. (2013). Maternal Prenatal Pregnancy-Related Anxiety and Spontaneous Preterm Birth in Ardebil Health Centers In 2011. *Urmia Medical Journal*, 23(6), 670-675.
- Mirowsky, J., & Ross, C. E. (2002). Selecting outcomes for the sociology of mental health: Issues of measurement and dimensionality. *Journal of Health and Social Behavior*, 43, 152-170.
- Olf, M., Frijling, J. L., Kubzansky, L. D., Bradley, B., Ellenbogen, M. A., Cardoso, C., . . . , & van Zuiden, M. (2013). The role of oxytocin in social bonding, stress regulation and mental health: An update on the moderating effects of context and interindividual differences. *Psychoneuroendocrinology*, 38(9), 1883-1894. doi: <http://dx.doi.org/10.1016/j.psyneuen.2013.06.019>.
- Padrón, A., Galán, I., & Rodríguez-Artalejo, F. (2012). Second-hand smoke exposure and psychological distress in adolescents. A population-based study. *Tobacco Control*, tobaccocontrol-2012-050548.
- Pattanayak, R. D., Sagar, R., & Jain, R. (2012). Perceived health risks, attitude and readiness to quit tobacco among euthymic bipolar disorder patients in regular contact with mental health services: an exploratory study from India. *J. Ment. Health*, 21(1), 83-90.
- Schramm, S. B., Carré, V., Scheffler, J. -L., & Aubriet, F. D. R. (2010). Analysis of mainstream and sidestream cigarette smoke particulate matter by laser desorption mass spectrometry. *Analytical Chemistry*, 83(1), 133-142.
- Shibuya, K., Ciecierski, C., Guindon, E., Bettcher, D. W., Evans, D. B., & Murray, C. J. (2003). WHO Framework Convention on Tobacco Control: development of an evidence based global public health treaty. *BMJ: British Medical Journal*, 327(7407), 154.
- Turcotte-Tremblay, A. M., Lim, R., Laplante, D. P., Kobzik, L., Brunet, A., & King, S. (2014). Prenatal maternal stress predicts childhood asthma in girls: project ice storm. *Biomed Res. Int.*, 201717(10), 8.
- Yang, L., Tong, E. K., Mao, Z., & Hu, T. W. (2010). Exposure to secondhand smoke and associated factors among non-smoking pregnant women with smoking husbands in Sichuan province, China. *Acta Obstet Gynecol Scand*, 89(4), 549-557.

Siti Munira Yasin, Khairul Mizan Taib, Mohd Rodi Isa, Mohd Ariff Fadzil, Mohd Razilan Abdul Kadir and Saiful Farik Mat Yatim

- Yasin, S. M., Moy, F.-M., Retneswari, M., Isahak, M., & Koh, D. (2012). Timing and risk factors associated with relapse among smokers attempting to quit in Malaysia. *The International Journal of Tuberculosis and Lung Disease*, *16*(7), 980-985.
- Yusoff, M. S. B., Rahim, A. F. A., & Yaacob, M. J. (2010). The sensitivity, specificity and reliability of the Malay version 12-items General Health Questionnaire (GHQ-12) in detecting distressed medical students. *ASEAN Journal of Psychiatry*, *11*(1), 36-43.
- Zanos, P., Georgiou, P., Metaxas, A., Kitchen, I., Winsky-Sommerer, R., & Bailey, A. (2015). Region-specific up-regulation of oxytocin receptor binding in the brain of mice following chronic nicotine administration. *Neuroscience Letters*, *600*(0), 33-37. doi: <http://dx.doi.org/10.1016/j.neulet.2015.05.054>.



## Perspective of a Smoke-free Home among Second-hand Smokers during Pregnancy: A Qualitative Study

Izzah Amira Mohd Asri<sup>1</sup>, Nur Amirah Abd Rani<sup>1</sup>, Zulfakhri Dzulkifli<sup>1</sup>,  
Muhamad Ilmam Muhamad Jamil<sup>1</sup>, Mohd Shahril Ahmad Saman<sup>2</sup> and  
Siti Munira Yasin<sup>2\*</sup>

<sup>1</sup>Faculty of Medicine, Universiti Teknologi MARA (UiTM), 47000 Sungai Buloh, Selangor, Malaysia

<sup>2</sup>Population Health and Preventive Medicine Discipline, Faculty of Medicine,  
Universiti Teknologi MARA (UiTM), 47000 Sungai Buloh, Selangor, Malaysia

### ABSTRACT

Tobacco use is one of the largest causes of preventable diseases across the world. It is interesting to note that second-hand smoke exposure is a major public health problem in Malaysia. The objectives of this study are first, to explore the perspectives of pregnant mothers whose partners are smokers, and second, to explore barriers and facilitators to creating a smoke-free environment in their home. This study uses a qualitative method in analysing the experiences of 15 pregnant mothers taken from a specialist healthcare centre in Sungai Buloh, Malaysia. It discusses the perspectives of these pregnant mothers towards their partners' smoking habits, as well as the barriers and facilitators in creating a smoke-free home. From the interviews, it became apparent that pregnant mothers despised their partners' smoking habits due to smoke odour, lack of money, and poor health. The barriers in creating a smoke-free home include the attitude of the smoking spouse, difficulty in weaning off the habit, excessive encouragement by a spouse, difficulty in advising a smoking spouse, influences from friends, and wrong perceptions. Meanwhile, the facilitators towards creating a smoke-free home are illnesses developed through smoking, multiple reminders from family members, and nicotine replacement therapy (NRT) were perceived to work on certain smokers and habitual cues in quitting smoking. The transition process towards making homes smoke-free is complex and individualistic; healthcare professionals may need to tailor strategies

to take into account the specific contexts of each individual. More education programmes on the impacts of smoking and second-hand smoke exposures to family members and smoking cessation are needed for both pregnant mothers and their smoking partners.

### ARTICLE INFO

#### Article history:

Received: 25 October 2016

Accepted: 17 March 2017

#### E-mail addresses:

smunira@salam.uitm.edu.my (Siti Munira Yasin),  
rex\_izzah@yahoo.com (Izzah Amira Mohd Asri),  
nuramirahrani@gmail.com (Nur Amirah Abd Rani),  
zulfakhri.dzulkifli@gmail.com (Zulfakhri Dzulkifli),  
ilmamjamil2@gmail.com (Muhamad Ilmam Muhamad Jamil),  
drmsas@yahoo.co.uk (Mohd Shahril Ahmad Saman)

\*Corresponding Author

**Keywords:** Pregnancy, qualitative, second-hand smoke

## INTRODUCTION

Tobacco use is one of the largest causes of preventable diseases across the world including in Malaysia. According to the World Health Organisation (WHO), about 6 million people die each year due to tobacco; more than 5 million of the deaths are the results of direct tobacco use, while more than 600,000 are the results of non-smokers being exposed to second-hand smoke (Bilano et al., 2015). Second-hand smoke is also called environmental tobacco smoke, where people inhale the smoke exhaled by smokers.

Second-hand smoke (SHS) exposure is a major public health problem. In a retrospective study across 192 countries, about 40% of children, 35% of female non-smokers and 33% of male non-smokers were exposed to SHS in 2004 (Öberg et al., 2011). However, established public health policies have been effective in reducing exposure to SHS, the initiation of tobacco use among young people, tobacco use prevalence, tobacco related morbidity and mortality, and healthcare costs (Pierce, White, & Emery, 2012).

In addition to smoke-free policies in public spaces, these policies should also be implemented in our homes as smoke is a significant source of SHS exposure (Health & Services, 2006). Smoke-free policies in personal spaces such as in homes and cars are able to reduce the amount of people who smoke, and reduce the risks of SHS among children and non-smoking adults sharing those personal spaces with the smokers (Cartmell et al., 2011).

A report by the Institute of Medicine found that second-hand smoke can cause heart attacks. This is because tobacco contains toxic chemicals including formaldehyde, benzene, vinyl chloride and hydrogen cyanide (Pope III et al., 2011). These chemicals when inhaled by pregnant mothers will be passed to their foetus through the placenta. The chemicals passed to the foetuses can be harmful to them. For example, nicotine decreases the blood flow to a foetus while carbon monoxide will affect the baby's growth and development (Wickstrom, 2007).

In addition to this, exposure to second-hand smoke can lead to cardiovascular and respiratory diseases in adults, while it can cause sudden death in infants (Leonardi-Bee, Britton, & Venn, 2011). Reduced birth weight, risk of preterm birth, and newborn neurobehavioral deficits are the unfavourable effects of prenatal SHS exposure (Law et al., 2003). Earlier research found that the early childhood overweight mass index increases along with foetal SHS situations (Braun et al., 2010). Moreover, the effects of SHS are more prevalent among low income pregnant women. This shows how important it is for pregnant mothers to avoid SHS exposure. Sadly, most times no action is taken to prevent the exposure, such as banning smoking in cars or at home to protect the foetus and other children. There are several ways to avoid inhaling second-hand smoke; these include creating a smoke-free home and car and also avoiding places that are not smoke-free. In Malaysia, however, majority of pregnant women are exposed to tobacco smoke from their own family members, especially their husband.

There are a number of qualitative studies which have shown that some residents successfully create smoke-free homes (SFH) whereas others deal with this barrier; this indicates that a significant change in behaviour is needed (Jones et al., 2011). The main facilitator for change comprises of protecting the health of others, particularly children, while the barrier comprises of the lack of knowledge about the dangers of SHS and consequences of smoking at home (Jones et al., 2011). These prior studies focused on the smoker, whereas this research emphasised on the perspectives of non-smokers, and more specifically, the pregnant wives



of smokers. Pregnancy is the key factor that acts as a trigger for these households to create SFH as they fret about the health of their offspring. Also, the observable effects of SHS on the existing children will enhance the need for behavioural change in couples. The aims of this study are to explore the perspectives of non-smoker pregnant mothers in relation to their smoker husbands, as well as the barriers and facilitators in creating a smoke-free home. Pregnant mothers who are currently smoking were excluded from the population for this study. The study design draws from qualitative studies, in which it is more favourable than a quantitative study because it can develop hypotheses for further testing and help to understand the feelings, values and perceptions underlining and influencing the participants' behaviours. Besides this, a qualitative study may also help in generating ideas to improve the current policies in place and reduce the number of smokers.

## METHOD

This qualitative study design was conducted between July 11<sup>th</sup> and August 5<sup>th</sup>, 2016, at the Gynaecology Clinic of a public teaching hospital in Malaysia. In-depth interviews were conducted among Malay-speaking pregnant women who fulfilled the inclusion and exclusion criteria. The inclusion criteria included women attending the recruitment drive, who had been exposed to cigarette smoke from their spouses at home. We excluded the women who were currently smoking.

### Data Collection

The interviews were conducted during the patients' waiting times at the Gynaecology clinic over a period of two weeks in July 2016. Each participant was given an information sheet explaining the objectives of the study and their rights as the participants, and required to give their consent prior to the interviews. The participants' particulars were erased once the recordings had been transcribed and checked to assure confidentiality. This study was approved by UiTM Research Ethics Committee.

All the respondents were briefed on the purpose of this study before they were asked several questions based on three standardised open-ended questions. The first set covered the feelings of pregnant women towards their partner's smoking habits. The second set featured seriously unwell babies and stressed the risks vulnerable children faced from those who exposed them to smoke. The final questions explored the experience and barriers of a smoke-free environment.

1. *What do you think of your partner's smoking habit?*
2. *What are the facilitators in creating a smoke-free home?*
3. *What are your experience and the barriers in creating a smoke-free home?*

All the interviews lasted around 20 minutes and were audio-taped. The interviews were conducted by four researchers who were similarly trained in conducting qualitative interviews. As a token of appreciation for their time, the respondents were given refreshments costing around RM20 (5 USD) after the interviews. Recordings were reviewed following each interview to assess whether new ideas or elements continued to emerge. We determined that data saturation had occurred when the transcriptions revealed no new themes.

## Data Analysis

Each interview was transcribed verbatim. The transcriptions in Bahasa Malaysia were conducted by the interviewers themselves after each session. These were translated into English and reviewed by the researchers, and later checked by two independent lecturers who are fluent in both languages, both of whom are with Masters in Public Health and trained in qualitative analysis. Analysis of data consisted of a systematic thematic review of individual transcripts and notes. The research team identified primary (i.e., major topics) and secondary codes (i.e., based on recurrent themes from the major topics) of each transcript. Matrices were constructed to identify patterns and themes. The research team resolved any discrepancies through multiple discussions. The themes from the matrices and coding were identified and agreed by all the researchers. Data were stored as word documents and analysed manually by the researchers using highlighter pens, summaries and word tables. From the interview, three major themes were identified based on the objectives of the study: (a) the perspectives of mothers towards their smoker husband; and (b) the barriers and facilitators to creating a smoke-free home. As the three major themes and subthemes were identified, the focus was then placed on searching for coding from the interviews and to code them accordingly.

## RESULTS

A total of 15 interviews were conducted at the Clinical Training Centre in Sungai Buloh and Selayang. Details of all the participants can be seen in Table 1. Majority of the respondents (n=13) are Malays and the rest are Indians. Demographic details of the respondents are described in Table 1 and details of the participants' characteristics in Table 2.

Table 1  
*Respondents' sociodemographic characteristics*

Characteristics	N (%)	Characteristics	N (%)
Age		Number of Pregnancy	
20-25	1 (6.7)	1 <sup>st</sup>	10 (66.7)
26-30	10 (66.7)	2 <sup>nd</sup>	2 (13.3)
31-35	3 (20.0)	3 <sup>rd</sup>	0 (0.0)
36-40	1 (6.7)	4 <sup>th</sup> and above	3 (20.0)
Ethnicity		Employment Status	
Malay	13 (86.7)	Currently employed	4 (26.7)
Indian	2 (13.3)	Not employed/ housewives	11 (73.3)
Chinese	0 (0.0)	Monthly household salary	
Education level		<RM1000	3 (20.0)
Primary School	3 (20.0)	RM1000-RM2999	6 (40.0)
Secondary School	5 (33.3)	RM3000-RM4999	3 (20.0)
Diploma	2 (13.4)	>RM5000	3 (20.0)
Degree and above	5 (33.3)		

Table 2  
*Individual respondents' details*

Participant	Age	Which part of the house did smoking take place in	Employment	Current pregnancy
1	30	Outside	Unemployed	1
2	33	Outside	Unemployed	4
3	27	Outside	Unemployed	2
4	20	Outside	Unemployed	1
5	30	Outside	Employed	2
6	28	Outside	Employed	1
7	30	Outside	Employed	1
8	28	Outside	Unemployed	1
9	29	Outside, Inside	Unemployed	4
10	28	Outside	Unemployed	1
11	33	Outside	Employed	4
12	28	Outside, Inside	Unemployed	1
13	33	Outside	Unemployed	1
14	39	Outside	Unemployed	1
15	26	Outside	Unemployed	1

Three major themes emerged from the interviews in understanding the perspectives of pregnant mothers towards their smoker husband and exploring the barriers and facilitators in creating a smoke-free home.

### **Perceptions of Pregnant Mothers towards their Smoker Husbands**

In the first theme, through the interviews conducted, six distinct perceptions of pregnant mothers towards their smoker husband. These perceptions can be categorised as follows.

**Worsen the mother's previous health condition.** Pregnant mothers reported feeling worried that their partner's smoking habits would worsen their health conditions. This is in relation to their existing health conditions, thus making them uncomfortable in being exposed to cigarette smoke. This, in turn, is a reason for their disagreement with their partner's smoking habits, as demonstrated in the following excerpts:

*"Right now is about my allergies. Allergies cannot smell cigarette smoke. It makes me throw out."*

(Participant 1)

*"I don't like it because of its odour. Then I have sort of like sinusitis, and it really makes me uncomfortable."*

(Participant 13)

**Worried of the effects to the surroundings and unborn babies.** Pregnant mothers were well aware of the possible effects of cigarette smoke which are not limited to smokers but also to their surroundings. This inclination was due to natural pregnant maternal instincts of caring for their baby's health. No parents want their babies to be borne with a disability. This can in turn encourage couples to quit smoking for the sake of their babies.

*"We also can get diseases for example mouth cancer and lung cancer which affects breathing. Pregnancy is also affected as it may lead to prematurity."*

(Participant 10)

*"Because it will affect the baby."*

(Participant 5)

*"First, our own health and then it will affect the baby's health."*

(Participant 8)

**Long-term effects on spouse.** Cigarette smoking employs disastrous effects on the spouse who smokes in the long run. This particular habit carries a great price, not only mentally but also economically.

*"Of course it is not okay. If he continues smoking he will get sick."*

(Participant 2)

*"I am worry about his health, not good for heart. Besides, he has asthma."*

(Participant 15)

**Smell of Cigarettes.** One of the main problems that troubles pregnant mothers is the smell of cigarette smoke. Majority of the pregnant mothers cannot bear the smell of cigarette smoke. This is not particularly restricted to the period of pregnancy, but also during the time when they are not pregnant. The odour does not only present when a person smokes, but it remains in the area for some time. This creates an unhealthy environment that can affect other people as well.

*"I don't like the odour and the smoke is unpleasant."*

(Participant 15)

*"Even if I am not pregnant I still don't like the smell of smoke."*

(Participant 5)

**Financial Problems.** Financial problem is also one of the issues that emerged from the interviews. The participants felt that buying cigarettes was a waste of financial resources. Surprisingly, husbands were not embarrassed to ask for money from their wives to buy cigarettes

when they ran out of money at the end of the month. One participant revealed that her husband got emotionally aggressive if she failed to assist with his financial needs.

*“It is definitely a huge waste of money”*

(Participant 8)

*“One more thing, he uses the money for cigarettes and alcoholic beverages. RM10 per day is not enough to accommodate his habit. He will get mad if I refused to increase the amount and called me stingy.”*

(Participant 9)

**Not affected at all.** In the current situation, not all the participants agreed that their husband’s smoking habits are unhealthy. Based on the interviews, some seemed to believe that cigarette smoking is a normal trend.

*“Because of my father also smoking, so I am okay with it (laugh). Maybe I used to it.”*

(Participant 12)

### **Barriers for Creating a Smoke-Free Home**

This theme focuses on the barriers for creating a smoke-free home and the study explored the six reasons that cause these barriers.

**Attitude of the smoking spouse.** The attitude of smokers is one of the barriers to creating a smoke-free home. Thus, even though the participants kept advising their spouses, it was difficult to get through to them as the desire to quit smoking must come from oneself. The husbands gave a lot of excuses when they were advised to quit smoking.

*“I had advised him, but I am not sure if he took my words seriously”*

(Participant 1)

*“My husband is really stubborn, considering all my efforts to advise him. He told me he tried to stop, but it was not easy.”*

(Participant 7)

*“We are aware of the bad effects of cigarette smoking to secondary smoker. We have talked about this issue, but he came up with too many excuses.”*

(Participant 3)

**Difficult to wean off the habit.** Smoking cigarettes in the long run will cause smokers to be psychologically dependent to it as it contains nicotine. From the interviews, it can be seen

that majority of the smokers started to smoke at a very young age. They have been exposed to nicotine for a very long time and find it difficult to live without it.

*“But then when he have that habit, it’s hard to leave it behind. He started smoking when he was seventeen till present. He has been relying too much on smoking.”*

(Participant 12)

Even worse, there are pregnant mothers who have given up advising their husbands to stop smoking.

*“I have been asking him to quit (smoking) many times before, but nothing happened. Even my son had asked me to forget about it.”*

(Participant 14)

**Difficult to advice smoking guests.** Another barrier emerged from the cultural aspect of receiving guests. Many participants felt that it was impolite to warn smokers against smoking in their homes. They felt that doing this was a sign of disrespect to their guests. This is similar to family gatherings that involve grandparents and close family members, especially those who are older.

*“When we having guests coming, we said no smoking, but still there are still some of them who refused the rule, like when I host an open house. But then I didn’t say anything because they are guest. If they are my relatives, I will stop them.”*

(Participant 2)

*“When it come to the relatives it is okay but when it comes to relative who are older than me like my father, it is likely impossible to ask them to stop smoking. I was worried if it might hurt their feelings.”*

(Participant 4)

*“Are we supposed to say hey, do not smoke in my house to the guests? Am I right?”*

(Participant 8)

**Influence from friends.** Peer pressure is one of the main factors that attracts a person to smoke cigarettes. Some respondents claimed that they chose to smoke to ensure that their friendship remained unaffected. This gives smokers a hard time in having to choose between quitting smoking and friends. In addition, the respondents revealed that working colleagues who were active smokers would also influence their decisions to stop smoking.

*“When he hangs out with his friends, they will start smoking together.”*

(Participant 2)

*“He is a social smoker, it’s not like he smokes because he wants to smoke. Depending on the situation, if the guest is not smoking, then he knows that no one will join him smoking. So he will not smoke. If there is someone who smokes, he will join them.”*

(Participant 3)

**Perceived smoking can reduce stressors at work and in everyday life.** Stress can be defined as an emotional pressure and each individual has different ways in coping with his or her stress. From the interviews, it can be noted that some of the spouses are struggling with stress at work.

*“It’s all because of work, due to stress.”*

(Participant 10)

*“Because of work and stress, it has already becoming his habit to smoke at work with his colleagues.”*

(Participant 9)

### **Facilitators to Creating a Smoke-Free Home**

The last theme to consider as part of this study is the facilitators that can lead to creating a smoke-free home. Four facilitators were identified from the respondents’ interviews, as detailed in the following excerpts:

**Smoking spouse suffers from illness.** Based on one participant’s experience, her smoking husband was able to quit for a while when he got sick. This happened as he knew that cigarettes could worsen his condition. Sadly after recovering, he went back to his old habit. It seems like smokers will only stop smoking when they are admitted to hospital or diagnosed to have health conditions caused by smoking. There are also smokers who wanted to quit after witnessing their relatives suffering from health problems as the consequence of smoking.

*“Last time he got sick and had an operation. He has not smoked for three months. But eventually, he smokes again when he recovers.”*

(Participant 14)

**Multiple reminders from family members.** Having people to constantly remind smokers about the effects of smoking on their own health and others surrounding them helps them to stay in line. Not only does it show affection and love between family members, it also improves their health. The participants also mentioned that they had prepared a note for their guests to not smoke inside their house. The note serves as a warning to prevent them from smoking in the house.

*“No, he does not smoke in front of our children. After meals he will smoke outside. When he is done, I will ask him to wash his hand, clean his mouth, and change his clothes if there is some smell on it.”*

(Participant 3)

Sometimes, a reminder from a person who is very close to the smoker can work wonders. This can be seen from the interview, where reminders from a smoker's own mother helped him to reduce the bad habit. This shows his love for his mother and that he has tried not to hurt her feelings by obeying her order.

*"His mother told him to reduce smoking and he obeys what his mother's said."*

(Participant 15)

**Habitual cues in quitting smoking.** There was one participant who used a different approach in helping her spouse to stop smoking, i.e. by giving him a nutritious drink. She gave it to him without failing to mention that there is an improvement in his smoking habit, as the ingredients contained in the drink helps to detoxify the smoker's body.

*"Usually I gave him some nutritious drinks. There is some improvement to his habit."*

(Participant 15)

Some of the participants said that it is best to not put an ashtray in their homes. This small effort will force smokers to smoke outside the house. This practice is very good in creating a smoke-free home. It also sets a better example for the young ones in the family as they will not smoke in front of their children.

*"So far, I did not provide ashtray. So guest will not smoke in my house."*

(Participant 6)

## DISCUSSION

### Perceptions of the Pregnant Mothers

In regards to the perspectives of pregnant mothers with smoking partners, it was found that most of them have a persistent complaint towards the idea of smoking because of its impact on SHS. In Malaysia, a husband is still generally the main economic generator for a family, especially when the wife is not working. If the main generator is not functioning well due to health conditions that are caused by cigarette smoking, the whole family will be affected. Not only do they have to take care of a sick person in the family, they also have to look after the hospital bills as well. The current findings are consistent with a prior research that indicates the main concern about SHS is its health impact especially towards the surrounding and unborn babies (Leonardi-Bee, Britton, & Venn, 2011). Thus, the best way to prevent the consequences of SHS is by creating a smoke-free environment by educating the community on the impacts of smoking. The study differs from prior studies in that it shows that NRT can help in smoking cessation although it is not effective for all smokers (Bilano et al., 2015).

In addition, there are some who do not like their partner's smoking habits as it has an unpleasant odour. Most people have difficulty in adapting to their partner's smoking habits as they are not used to cigarette smoke and odour. Thus, they choose to stay away from their husbands whenever they smoke. Furthermore, lack of understanding on early life exposure towards cigarette smoking among spouses was another important factor that emerged. Therefore, it is very crucial to educate the society about the impacts of smoking in their life collectively.



Financial problems is also an emerging theme reported in the research. The price of cigarettes is quite expensive for a heavy smoker who may smoke 2 packs of cigarette a day. Therefore, it is very reasonable for the government to raise cigarette taxes so that smoking rates, especially among low income smokers, can be reduced. Raising the tax imposed on cigarettes is seen as a smart approach in controlling the demand for cigarettes in the current market.

In addition, preventing ashtrays from being put in the homes will reduce the spouse's tendency to smoke inside the house and their wife's exposure to SHS.

### **Barriers to creating a smoke-free home**

A researcher in China stated that several smokers who had tried to quit smoking failed after an abstinence for a short period of time as their friends offered cigarettes to them, which caused them to smoke again (Berg, Zheng, & Kegler, 2015). The finding from this previous study correlates with the finding in our study, as 2 out of 15 respondents reported that even though they did not buy cigarettes in an attempt to quit smoking, their spouse's friends would sometimes offer them cigarettes. Moreover, it becomes a challenge not to refuse the invitation so as to maintain a good relationship with their friends.

Furthermore, smoking can become habitual, and it can be difficult for smokers to quit. Some of our respondents stated that their husband started smoking at an early age. There are many factors that can trigger someone to smoke from an early age. We postulated that one of them is because of the early exposure to smoke by their parents. Other factors can include being influenced by friends and the curiosity to try smoking. Family and peers can influence smoking patterns as their opinions and behaviours influence individual's core cultural values and norms (Nichter, 2003). Some of our respondents stated that they had given up advising their husband to quit smoking as it was difficult to do so.

The other barrier outlined in our study is the attitude and perception of smokers themselves. One of the attitudes is the perceived reduction of stress when smoking. This issue is often used as an excuse for smokers to not stop smoking. It is very worrying as the respondents will start to believe that smoking is the only way to help their spouses in coping with stress. Prior research revealed that pregnant mothers had problems in negotiating with their husbands in order to create a smoke-free home, as there were many excuses and complaints (Bottorff et al., 2006). Thus, intervention should suggest an action that the wife and family members could take in order to create a smoke-free home such as negotiation skills. In addition, even though smokers know the bad effects of cigarette smoking, they still fail to quit as the desire to quit smoking must come from within oneself.

### **Facilitators in Creating a Smoke-Free Home**

With regards to our last theme, multiple reminders by family members act as a critical changing agent in creating a smoke-free home. The current study documented that close family members such as the smoker's mother and wife do play a role in influencing him. This finding correlates with a prior research in the United States on the interpersonal factors that facilitate in creating a smoke-free home (Kegler, Escoffery, Groff, Butler, & Foreman, 2007).

In addition, the spouses lack preventive awareness and choose to stop smoking only when their health conditions worsen. For instance, one of our respondents stated that her husband stopped smoking when he suffered from an illness and was hospitalised. This is because smoking is prohibited in hospitals to protect patients and staff from second-hand smoke exposure. Thus, smoking cessation counselling during hospitalisation by health care workers should be conducted in order to motivate patients to quit smoking. This finding is supported by a study that was published in 2012, which stated that high-intensity counselling of over 10 minutes per session and follow-up observations within at least a month for hospitalised patients were effective for successful smoking cessation, regardless of the patient's disease at admission (Rigotti, Munafo, & Stead, 2007).

About 8 participants in our study did not have a single idea on how to create a smoke-free home. Thus, educational outreach should play a role by focusing on strategies to create a smoke-free home. Moreover, efforts from community leaders, healthcare personnel, and support from the community are also needed in order to create smoke-free homes.

### **Implications of the Study**

This study has important implications for current practice and future research. Research is needed to identify measures that may facilitate the adoption of smoke-free home policy. Moreover, strategies in the form of interventions targeting to promote the adoption of smoke-free homes and addressing its challenges should be of priority. The facilitators which include good communication between the spouses, good knowledge and perception among smoking husbands and excellent family support should be taken into account when drafting the policy. In particular, it may be beneficial to address the need to provide educational aid to pregnant women in terms of communication with their spouse on the implementation of smoke-free homes. They should also be trained on how to avoid SHS exposures in public places. In practice, clinicians should promote smoke-free homes in the clinical setting, particularly among pregnant women and in household with small children.

### **Strengths and Limitations**

This study is subjected to some limitations. Firstly, this study is qualitative in nature and therefore cannot be generalised to other population groups. Although it does give some views on the issue undertaken in the study, a bigger sample size of qualitative study in the near future will give more benefits. Secondly, the sample size of this qualitative study is rather small, a bigger sample with multiple centres may be required as it may enrich the data. Lastly, the participants were heterogeneous, comprised of various backgrounds but lacked different ethnicities in Malaysia. Thus, some open-ended questions might be perceived differently by the respondents, and the participants might have responded to them differently.

The main strength of this study is that it is one of the first studies discussing on the pregnant mothers' views on exposures to second-hand smoke. This is a specific population-based study, in which their views are important for the development or enhancement of policies on smoke-free homes. Moreover, this study may also stimulate future research in this area, especially among other specific population groups.

## CONCLUSION

The study documented the perspectives of pregnant mothers about their partners' smoking habits and the barriers and facilitators in creating smoke-free homes. The findings suggest that the health of the soon-to-be delivered baby is the most important reason for mothers to disagree with their husband's smoking habits. The results also showed that many households are having social and personal problems in creating smoke-free homes. The findings of this study can be used to aid in understanding the problem and facilitating future development in increasing the number of smoke-free homes.

## ACKNOWLEDGEMENTS

This project was funded by the Fundamental Research Grant (FRGS/1/2015/SKK01/UITM/03/1). The authors would like to thank the participants for their support throughout this study.

## REFERENCES

- Berg, C. J., Zheng, P., & Kegler, M. C. (2015). Perceived benefits of smoke-free homes, the process of establishing them, and enforcement challenges in Shanghai, China: a qualitative study. *BMC Public Health, 15*(1), 1.
- Bilano, V., Gilmour, S., Moffiet, T., d'Espaignet, E. T., Stevens, G. A., Commar, A., & Shibuya, K. (2015). Global trends and projections for tobacco use, 1990–2025: an analysis of smoking indicators from the WHO Comprehensive Information Systems for Tobacco Control. *The Lancet, 385*(9972), 966-976.
- Bottorff, J. L., Kalaw, C., Johnson, J. L., Stewart, M., Greaves, L., & Carey, J. (2006). Couple dynamics during women's tobacco reduction in pregnancy and postpartum. *Nicotine and Tobacco Research, 8*(4), 499-509.
- Braun, J. M., Daniels, J. L., Poole, C., Olshan, A. F., Hornung, R., Bernert, J. T., & Lanphear, B. P. (2010). Prenatal environmental tobacco smoke exposure and early childhood body mass index. *Paediatric and Perinatal Epidemiology, 24*(6), 524-534.
- Cartmell, K. B., Miner, C., Carpenter, M. J., Vitoc, C. S., Biggers, S., Onicescu, G., . . . Alberg, A. J. (2011). Second-hand smoke exposure in young people and parental rules against smoking at home and in the car. *Public Health Reports, 575*-582.
- Health, U. D. O., & Services, H. (2006). The health consequences of involuntary exposure to tobacco smoke: a report of the Surgeon General. *Atlanta, GA: US Department of Health and Human Services, Centers for Disease Control and Prevention, Coordinating Center for Health Promotion, National Center for Chronic Disease Prevention and Health Promotion, Office on Smoking and Health, 709*.
- Jones, L. L., Atkinson, O., Longman, J., Coleman, T., McNeill, A., & Lewis, S. A. (2011). The motivators and barriers to a smoke-free home among disadvantaged caregivers: identifying the positive levers for change. *Nicotine and Tobacco Research, ntr030*.
- Kegler, M. C., Escoffery, C., Groff, A., Butler, S., & Foreman, A. (2007). A qualitative study of how families decide to adopt household smoking restrictions. *Family and Community Health, 30*(4), 328-341.

Izzah Amira Mohd Asri, Nur Amirah Abd Rani, Zulfakhri Dzulkifli, Muhamad Ilmam Muhamad Jamil,  
Mohd Shahril Ahmad Saman and Siti Munira Yasin

- Law, K. L., Stroud, L. R., LaGasse, L. L., Niaura, R., Liu, J., & Lester, B. M. (2003). Smoking during pregnancy and newborn neurobehavior. *Pediatrics*, *111*(6), 1318-1323.
- Leonardi-Bee, J., Britton, J., & Venn, A. (2011). Second-hand smoke and adverse fetal outcomes in nonsmoking pregnant women: a meta-analysis. *Pediatrics*, *127*(4), 734-741.
- Nichter, M. (2003). Smoking: what does culture have to do with it? *Addiction*, *98*(s1), 139-145.
- Öberg, M., Jaakkola, M. S., Woodward, A., Peruga, A., & Prüss-Ustün, A. (2011). Worldwide burden of disease from exposure to second-hand smoke: a retrospective analysis of data from 192 countries. *The Lancet*, *377*(9760), 139-146.
- Pierce, J. P., White, V. M., & Emery, S. L. (2012). What public health strategies are needed to reduce smoking initiation? *Tobacco Control*, *21*(2), 258-264.
- Pope III, C. A., Burnett, R. T., Turner, M. C., Cohen, A., Krewski, D., Jerrett, M., & Thun, M. J. (2011). Lung cancer and cardiovascular disease mortality associated with ambient air pollution and cigarette smoke: shape of the exposure-response relationships. *Environmental Health Perspectives*, *119*(11), 1616.
- Rigotti, N., Munafo, M. R., & Stead, L. F. (2007). Interventions for smoking cessation in hospitalised patients. *The Cochrane Library*.
- Wickstrom, R. (2007). Effects of nicotine during pregnancy: human and experimental evidence. *Current Neuropharmacology*, *5*(3), 213-222.



## Effect of the Deposited Layer, Withdrawal Speed and Coated Length on Immobilised Bromothymol Blue in Polyaniline Sol Gel towards pH Sensing Sensitivity

Norliza Othman<sup>1\*</sup>, Uzer Mohd Noor<sup>2</sup> and Sukreen Hana Herman<sup>2</sup>

<sup>1</sup>NANO-ElecTronic Centre (NET), Universiti Teknologi MARA (UiTM), 40450 Shah Alam, Selangor, Malaysia

<sup>2</sup>Faculty of Electrical Engineering, Universiti Teknologi MARA (UiTM), 40450 Shah Alam, Selangor, Malaysia

### ABSTRACT

In this work, sensors were prepared by depositing the pH sensitive indicator (bromothymol blue) entrapped in polyaniline sol-gel onto the un-cladded middle portion of optical fiber. Polyaniline is sensitive to pH. However, it is important to study ways to increase sensitivity of the indicator by improving a combination of the materials used and pH sensor fabrication method. The fabrication and characterisation of optical fiber pH sensor on absorption intensity in arbitrary unit (a.u) were evaluated and optimised. The better sensitivity of the optical pH sensor was used to identify the optimum setting for number of layers deposited, coated length, and withdrawal rate. Thickness of the membrane film depends on the number of deposited layers and withdrawal speed which mainly affects sensitivity. The sensitivity of the optical pH sensor represents the slope (a.u/pH) of the absorbance intensities in pH 4, 5, 7, 9 and 10. Results obtained herein suggest that the optimised setting for bromothymol blue sol-gel coated optical fiber with thickness of 285.4 nm is 4 deposited layers, 20mm/s withdrawal rate and 0.5 cm coated length.

*Keywords:* Bromothymol blue, plastic optical fiber, pH sensor, sol-gel

### INTRODUCTION

Indicator is important in optical pH sensing due to its capability to detect changes in absorbance intensity in the presence of hydrogen ion activity. Hydrogen ion is an important element because of its presence in almost all chemicals. It is very useful for medical applications, such as in monitoring the acidity and alkalinity of human blood which could change as little as 0.03 pH unit or less. Even small changes in pH can adversely

#### ARTICLE INFO

##### Article history:

Received: 25 October 2016

Accepted: 17 March 2017

##### E-mail addresses:

[norliza.othman87@gmail.com](mailto:norliza.othman87@gmail.com) (Norliza Othman),

[uzer@salam.uitm.edu.my](mailto:uzer@salam.uitm.edu.my) (Uzer Mohd Noor),

[hana1617@yahoo.com](mailto:hana1617@yahoo.com) (Sukreen Hana Herman)

\*Corresponding Author

affect the human body functionality. Moreover, animals and plants are also dependent on changes in the pH of their habitat (Korostynska, Arshak, Gill, & Arshak, 2008; Rovati et al., 2012; Zauner et al., 1995). Therefore, it is crucial to investigate and develop pH sensor that is able to act fast, accurate, sensitive, and stable (Hussain, 2014).

Polyaniline has been found to be the most suitable organic material to act as a matrix in aqueous medium and it is widely used in the development of pH sensor (Ayad et al., 2010; Cheng-Hsin et al., 2011; Florea et al., 2011; Patil et al., 2015; Sotomayor et al., 2001; Song & Choi, 2014; Vieira et al., 2011; Jin, Su, & Duan, 2000). Furthermore, polyaniline requires simple preparation, stable under ambient conditions and possesses high conductivity and sensitivity to detect chemical properties. This versatility makes polyaniline to be frequently used in numerous applications due its capability to act as sol-gel matrix to support pH indicator. Moreover, it has a high permeability for water and ions. The entrapment of bromothymol blue in polyaniline sol-gel films is a very important technique.

In this work, the fiber optic pH sensor was prepared with varying numbers of layers, withdrawal speeds and coated lengths of the fibers using the dip coating technique.

## METHOD

The experimental process is divided into two sections; preparation of the sensor; and instrumentation. A brief explanation on this is given below.

### Preparation of the Optical Fiber pH Sensor

The sensor membrane film is fabricated by sol-gel method. Polyaniline acts as a matrix to entrap pH indicator which was dissolved in N, N-Dimethylformamide (DMF). The mixture was magnetically stirred for 24 hours at room temperature to obtain an optimum dissolved sol-gel. 3.2 mM of bromothymol blue was mixed into 20 ml polyaniline solution and magnetically stirred under ambient temperature for 1 hour.

1000  $\mu\text{m}$  diameter optical fiber (CF01493-15) was used to fabricate the sensor. Using a knife, plastic jacket buffer at a middle portion of the fiber with 0.5 cm lengths was removed, as shown in Figure 1. These portions of fiber optic were immersed into hydrofluoric acid to remove 17.5  $\mu\text{m}$  of the cladding diameter. Prior to this, the un-cladded portion was exposed to sol-gel and the samples were then treated with Nitric Acid ( $\text{HNO}_3$ ). Finally, the un-clad portion was coated with sol-gel by a controlled dip-coating rig for 4 deposited layers and withdrawal speed was 10 mm/s. These optical fibers were kept for heat treatment at 100°C for 24 hours. The samples had to be immersed for 15 minutes in distilled water so as to allow the unbound dye to leach out prior to testing. The fabrication process was done by varying the number of deposited layers (i.e., 1, 2, 3 and 4 layers) with fixed withdrawal speed and deposited length setting of 10 mm/s and 0.5 cm, respectively. Then, the fabrication process was continued by using the optimised deposited layer but varying the withdrawal speeds at 10, 15, 20 and 25 mm/s and fixing the deposited length setting at 0.5 cm. Finally, another set of the samples was

fabricated by varying the deposited lengths to 0.5, 1.5, 2.5 and 3.5 cm against the optimised parameters for number of deposited layers and withdrawal speed. These samples were ready to be characterised.

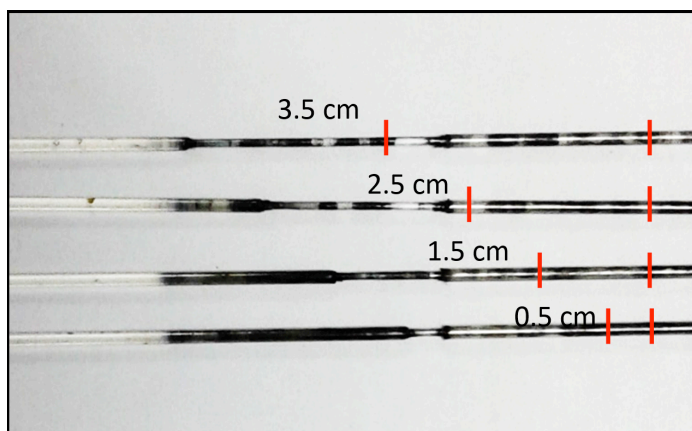


Figure 1. Plastic optical fiber with bromothymol blue sol-gel for differences re-clad region length

### Instrumentation

A schematic view of the experimental setup shown in Figure 2 was used to measure the pH sensor performance using spectroscopy of the absorption peak at 460 nm for bromothymol blue LED as the light source. A portion of re-cladded optical fiber was placed in the container filled with pH buffer solution. The optical absorption of the bromothymol blue was captured in computer with the spectrometer. Details of the pH test setup are illustrated by the flowchart in Figure 3.

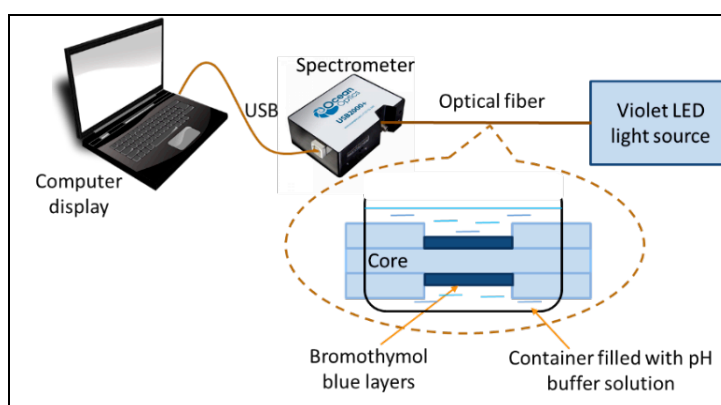


Figure 2. The experimental setup to measure the spectral response of the fiber optic pH sensor

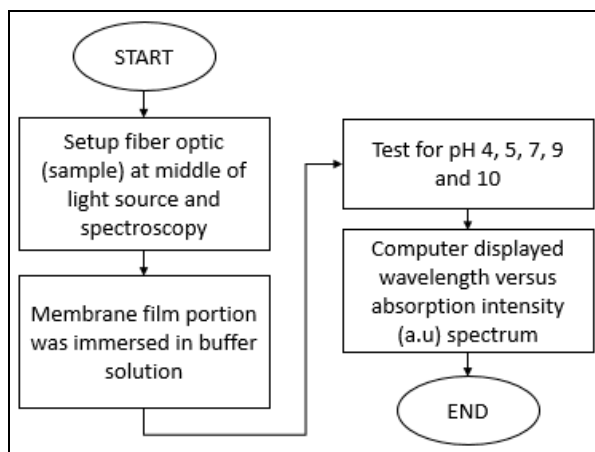


Figure 3. A flowchart of the pH test setup

## RESULTS AND DISCUSSION

### Optical Properties of Bromothymol Blue Entrapped in Polyaniline Sol-Gel

Figure 4 shows that the excitation peak for bromothymol blue in solution is strong at the wavelengths of 433 nm and 616 nm, while bromothymol blue on thin film is 430 nm. Two absorption bands were observed at 433 nm and 616 nm for the free bromothymol blue in the solution and only one absorption band was observed at 430 nm for the immobilised bromothymol blue film. This finding implies that the chemical bond between bromothymol blue and polyaniline molecules is responsible for the peak wavelength (Culshaw & Kersey, 2008; Korostynska, Arshak, Gill, & Arshak, 2007; Shastry, Abdi, & Nnanna, 2008). This shifting phenomenon of the maximum peak of wavelength could be explained as the large change in the polarity of the surrounding molecules while going from solution to film and the type of intermolecular interactions. Therefore, the blue light LED (460 nm) was selected as an appropriate wavelength for pH monitoring.

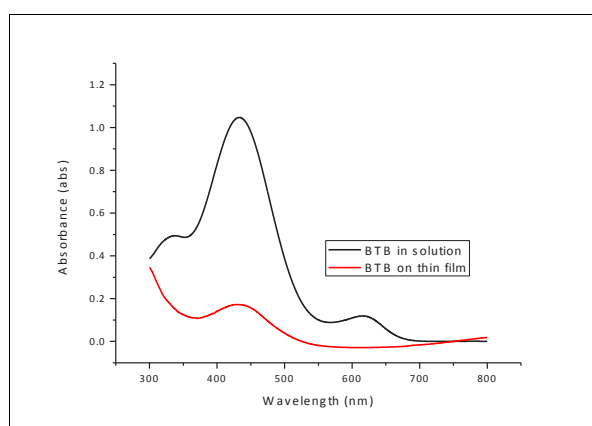
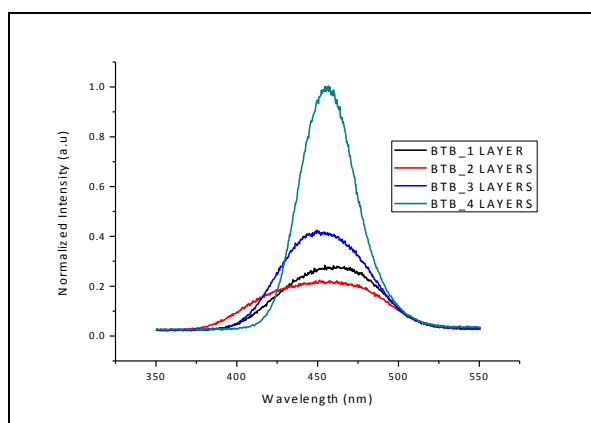


Figure 4. AUV-Vis absorption spectrum of free bromothymol blue (BTB) in DMF solvent and entrapped bromothymol blue (BTB) on the glass slide

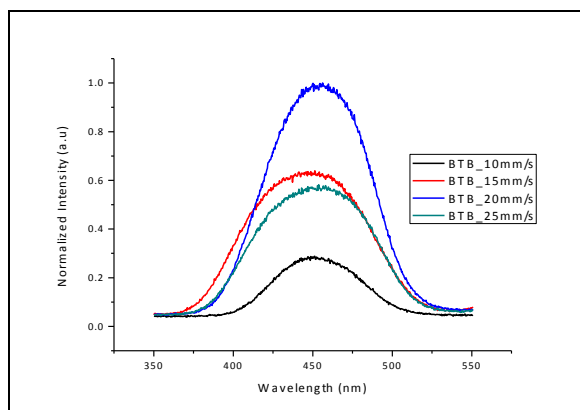


## Sensing Analysis

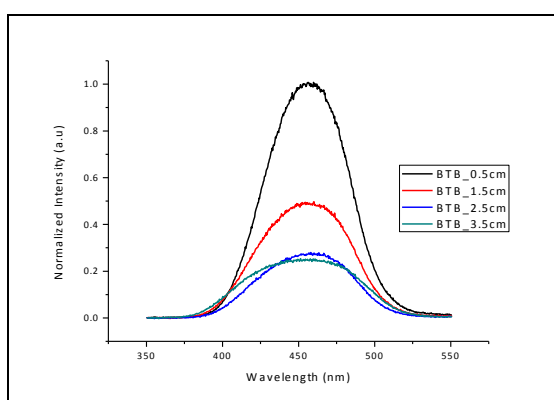
Figure 5 represents the normalised absorbance intensities of light for different number of deposited layers, withdrawal speed and coated length. Figure 5 (a) shows the normalised absorbance intensity dependence for the different multilayers deposition process that was varied for 1, 2, 3 and 4 layers. The thickness for 1, 2, 3 and 4 layers is 264.1, 268.43, 293.4 and 284.2 nm, respectively. By considering the film thickness, it is obvious that absorbance measurement increases directly proportional to the increasing number of layers (El Nahhal et al., 2012). Figure 5(b) shows the normalised absorbance intensity of the fiber optic pH sensor using immobilised bromothymol blue dye in polyaniline film deposited with different withdrawal speeds. The absorbance intensity at the maximum band increases with the increase in the withdrawal speed. However, the absorbance intensity of the optical properties decreases when the withdrawal speeds at 25 mm/s. The thickness of the samples prepared at 10, 15, 20 and 25 mm/s was 284.89, 288.52, 296.3 and 311.3 nm, respectively. It was observed that, besides the thickness, the deposited membrane film on difference un-cladded length of fiber optic is one of the important steps to produce a good sensing membrane. It is crucial to deposit the selected materials in suitable concentration, thickness of film, dried duration, and deposited length during the deposition process. Figure 5(c) shows four different deposited lengths (namely, 0.5, 1.5, 2.5 and 3.5 cm) used to investigate absorbance intensity. This measurement was to study the influence of deposited length of membrane film on the response of the optical membrane. The highest absorbance intensity of light travel in fiber optic exhibited at excitation peak of 460 nm, and the deposited length of 0.5 cm. From the graph, the output intensity of light slightly decreased when the deposited length increased from 0.5, 1.5, 2.5 and to 3.5 cm with the thickness of 285.4, 282.7, 278.4 and 279.8 nm, respectively. Initial results indicated that the highest spectral intensity of light was achieved with 4 deposited layers at 20 mm/s withdrawal rate and 0.5 cm coated length.



(a)



(b)



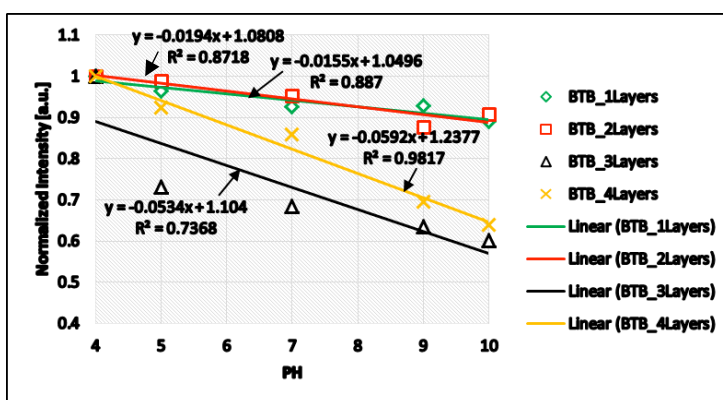
(c)

Figure 5. Entrapped bromothymol blue film normalised intensity of light spectrum for different: (a) number of deposition layers (i.e., 1, 2, 3, and 4); (b) withdrawal speeds (i.e., 10, 15, 20 and 25 mm/s); and (c) coated lengths (0.5, 1.5, 2.5 and 3.5 cm)

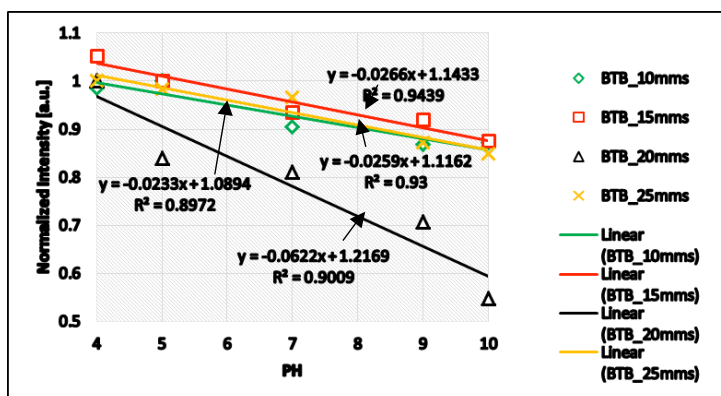
However, each parameter needs to be tested for its sensitivity to pH and to reconfirm that they are indeed optimised parameters. Hence, the sample was tested in various pH buffer solutions and the sensitivity was analysed from the slope of a linear regression line (trendline) against the calibration curve of the optical fiber pH sensor. This calibration curve was evaluated from the normalised absorbance intensity plots of light against various pH values at 460 nm. Hence, the slope and standard deviation of linear line were obtained. The slope and standard deviation of linear line represented the sensitivity and linearity of the membrane film, respectively. The sensitivity and linearity values are shown in Figure 6. Besides, the highest absorbance intensity of lights was observed at pH 4, which continued to decline as it was approaching to pH 5, 7, 9 and 10. This character shows that the highest absorbance was absorbed in the membrane film when it was treated in pH 4. Meanwhile, when the sensor exposed in the buffer solution, the hydrogen ions interacted with the molecules of pH indicators, the refractive index of sensing membrane would change, and as a result, it affected the input light absorption ability

and influenced the rate of light intensity travelling on it. The swelling and shrinkage of the polymer when pH changes are also caused by their refractive index (Chen et al., 2012; Florea, Diamond, & Benito-Lopez, 2013; Pandey & Ramontja, 2016). Thus, the optical output will be determined by the density of the hydrogen ions in the pH solution.

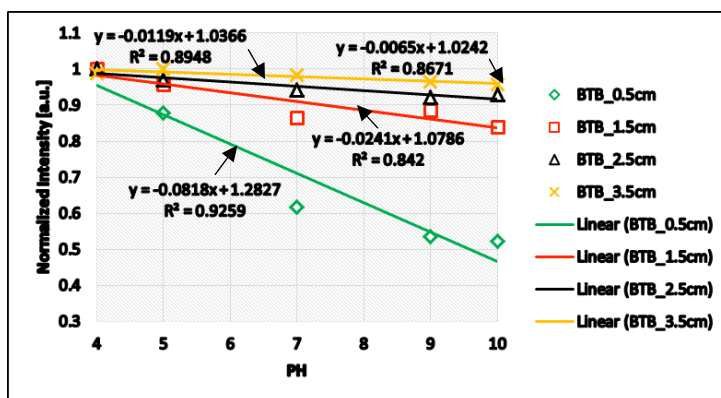
Figures 6(a), (b) and (c) show the calibration curve for the samples with different number of layers, withdrawal speeds and different coated lengths, respectively. The samples were also treated in various pH solutions, namely, pH 4, 5, 7, 9 and 10. Figure 6(a) shows that the number of deposited layers increased proportionally with the measured thickness. Membrane film thickness of the 4 deposited layers is 284.2 nm has the highest sensitivity 0.0592 a.u/pH and its linearity is 0.9817. This phenomenon is in agreement with the previous investigation by El Nahhal et al. (2012), which revealed that the presence of more polymer networks increased its surface area. In Figure 6(b), withdrawal speed continued to 20 mm/s and produced 296.3 nm thickness. This membrane film gave the highest sensitivity value of 0.0622 a.u/pH. Unfortunately, the linearity value dropped to 0.9009. According to Wu and Jun (2002), the influence of withdrawal speed depends on the thickness, porosity and refractive index of films. The researchers found that the increase in withdrawal speed would increase the thickness and refractive index of the film, as a result of the increasing number of crystalline particles per unit area and therefore decreased the porosity. This result is in agreement to the case study by Figs (2015), in which the film thickness was monitored as a function of withdrawal speed. Figs (2015) highlighted that it is important to optimise the relevant parameters at suitable withdrawal speed in order to produce good homogenous and crack-free membrane films. Figure 6(c) shows that a comparison was made between the various deposited lengths fabricated membrane sensing film; the deposited length of 0.5 cm with 285.4 nm deposited thickness exhibited the highest sensitivity toward hydrogen ions that contained in pH buffer solution, which is 0.0818 a.u/pH. This result is also supported with the linearity value of 0.9259, which is the highest compared to other deposited lengths.



(a)



(b)



(c)

Figure 6. Calibration curve plot for different: (a) coated number of layers; (b) withdrawal rate; and (c) coated length at 460 nm

Theoretically, a good sensitivity of sensor device should have a high slope (Zolkapli et al., 2016). Based on the results obtained, the highest sensitivity was achieved using 4 deposited layers, withdrawal speed of 20 mm/s, and coated length of 0.5 cm. The proposed sensor shows the sensitivity (slope) and linearity (standard deviation,  $R^2$ ) of 0.0818 a.u./pH and 0.9259 over a pH range of 4 to 10, respectively, as shown by the green line in Figure 6(c). Linearity describes how closely the straight line fits the data when  $R^2$  is nearly approaching 1 (El Nahhal et al., 2012). This linearity measurement is important to ensure the sample is reliable to be used as a sensor device.

Figure 7 shows the spectral response of bromothymol blue entrapped in polyaniline sol-gel in various pH buffer solutions. As shown in the graphs, the light intensity peak decreases as pH increases. The changes of light intensities are a measurement of how strongly a substance absorbs light. This result is in agreement with the works done by El Nahhal et al. (2012), and Shastry, Abdi and Nnanna (2008).

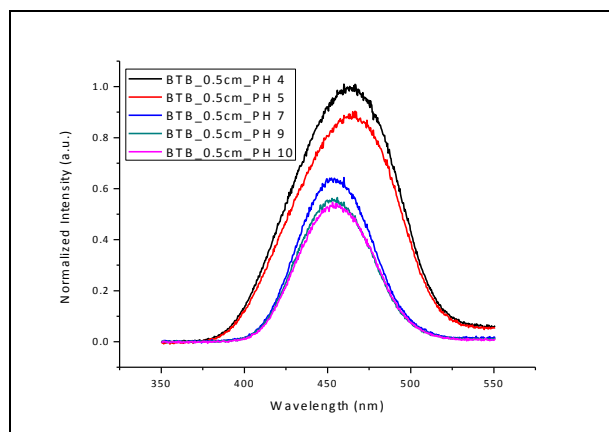


Figure 7. The normalised intensity of light spectra of optical fiber pH sensor at deposited layers is 4 layers, withdrawal speed of 20 mm/s and deposited length of 0.5 cm

## CONCLUSION

In summary, we have investigated the effects of the number deposited layers, withdrawal speed and coated length of the bromothymol blue entrapped in polyaniline sol-gel film in optical pH response. The optimised combination of parameters was found to produce the highest sensitivity with 4 deposited layers, withdrawal speed of 20 mm/s and coated length of 0.5 cm. These results will be the basis for the development of fiber optic pH sensor.

## ACKNOWLEDGEMENTS

The authors would like to acknowledge Research Management Institute (RMI), UiTM Shah Alam, and the Ministry of Higher Education (MOHE) Malaysia for the research fund. The authors also would like to acknowledge NANO-ElecTronic Centre (NET), UiTM Shah Alam, for the facilities and administrative support given.

## REFERENCES

- Ayad, M. M., Salahuddin, N. A., Alghaysh, M. O., & Issa, R. M. (2010). Phosphoric acid and pH sensors based on polyaniline films. *Current Applied Physics*, 10(1), 235-240.
- Chen, X., Yuan, C. A., Wong, C. K. Y., Ye, H., Leung, S. Y. Y., & Zhang, G. (2012). Molecular modeling of protonic acid doping of emeraldine base polyaniline for chemical sensors. *Sensors and Actuators B: Chemical*, 174, 210-216.
- Cheng-Hsin, C., Hsun-Pei, W., Cheng-Ho, C., & Peng-Rong, W. (2011). *Flexible pH sensor with polyaniline layer based on impedance measurement*. Paper presented at the Fifth International Conference on Sensing Technology (ICST), 2011.
- Culshaw, B., & Kersey, A. (2008). Fiber-optic sensing: A historical perspective. *Journal of Lightwave Technology*, 26(9), 1064-1078.
- El Nahhal, I. M., Zourab, S. M., Kodeh, F. S., & Qudaih, A. I. (2012). Thin film optical BTB pH sensors using sol-gel method in presence of surfactants. *International Nano Letters*, 2(1), 1-9.

- Figus, C. (2015). Synergic combination of the sol–gel method with dip coating for plasmonic devices. *Beilstein Journal of Nanotechnology*, 6(1), 500-507.
- Florea, L., Diamond, D., & Benito-Lopez, F. (2013). Polyaniline coated micro-capillaries for continuous flow analysis of aqueous solutions. *Anal. Chim Acta*, 759, 1-7.
- Florea, L., Lahiff, E., Diamond, D., & Benito-Lopez, F. (2011). Dynamic pH sensing in micro-fluidic devices using adaptive coatings based on polyaniline.
- Hussain M., Z. H. I., Abbasi, M. A., Nur, O., & Willander, M. (2014.). Effect of anions on the morphology of Co<sub>3</sub>O<sub>4</sub> nanostructures grown by hydrothermal method and their pH sensing application. *J. Electroanal. Chem.*, 717–718, 78–82.
- Jin, Z., Su, Y., & Duan, Y. (2000). An improved optical pH sensor based on polyaniline. *Sensors and Actuators B: Chemical*, 71(1), 118-122.
- Korostynska, O., Arshak, K., Gill, E., & Arshak, A. (2007). Review on state-of-the-art in polymer based pH sensors. *Sensors (Basel, Switzerland)*, 7(12), 3027-3042.
- Korostynska, O., Arshak, K., Gill, E., & Arshak, A. (2008). Materials and techniques for in vivo pH monitoring. *IEEE Sensors Journal*, 8(1), 20-28.
- Pandey, S., & Ramontja, J. (2016). Rapid, facile microwave-assisted synthesis of xanthan gum grafted polyaniline for chemical sensor. *International Journal of Biological Macromolecules*, 89, 89-98.
- Patil, R. B., Jatrakar, A. A., Devan, R. S., Ma, Y.-R., Puri, R. K., Puri, V., & Yadav, J. B. (2015). Effect of pH on the properties of chemical bath deposited polyaniline thin film. *Applied Surface Science*, 327(0), 201-204.
- Rovati, L., Fabbri, P., Ferrari, L., & Pilati, F. (2012). Plastic Optical Fiber pH Sensor Using a Sol-Gel Sensing Matrix. *Paola Fabbri, Luca Ferrari and Francesco Pilati, Fiber Optic Sensor*.
- Shastri, S. S., Abdi, A. M., & Nnanna, A. A. (2008, January). Investigation of fiber optic sensor for monitoring of ammonia. In *ASME 2008 International Mechanical Engineering Congress and Exposition (pp. 55-59)*. American Society of Mechanical Engineers.
- Song, E., & Choi, J. -W. (2014). Self-calibration of a polyaniline nanowire-based chemiresistive pH sensor. *Microelectronic Engineering*, 116, 26-32.
- Sotomayor, P. T., Raimundo, I. M., Zarbin, A. J., Rohwedder, J. J., Neto, G. O., & Alves, O. L. (2001). Construction and evaluation of an optical pH sensor based on polyaniline–porous Vycor glass nanocomposite. *Sensors and Actuators B: Chemical*, 74(1), 157-162.
- Vieira, N. C. S., Fernandes, E. G. R., Faceto, A. D., Zucolotto, V., & Guimarães, F. E. G. (2011). Nanostructured polyaniline thin films as pH sensing membranes in FET-based devices. *Sensors and Actuators B: Chemical*, 160(1), 312-317.
- Wu, S. A. J. W. G., & Jun S. J. (2002). Nanostructure Study of TiO<sub>2</sub> Films Prepared by Dip Coating Process. *J. Mater. Sci. Technol.*, 18(1), 31-33.
- Zauner, A., Bullock, R., Di, X., & Young, H. F. (1995). Brain oxygen, CO<sub>2</sub>, pH, and temperature monitoring: evaluation in the feline brain. *Neurosurgery*, 37(6), 1168-1177.
- Zolkapli, M., Saharudin, S., Herman, S. H., & Abdullah, W. F. H. (2016). The influence of sol-gel coated length and withdrawal rate on plastic optical fiber core towards oxygen gas sensing sensitivity. *Jurnal Teknologi*, 78(3).

## **Analysis on the OTTV of Modern-Style Apartment Facades in Bandar Sri Permaisuri, Kuala Lumpur**

**Ahmad Sanusi Hassan\* and Muhammad Hafeez Abdul Nasir**

*School of Housing Building and Planning, Universiti Sains Malaysia (USM), 11800 USM, Penang, Malaysia*

### **ABSTRACT**

The aim of this paper is to interrogate the principle of heat gain by the Overall Thermal Transfer Value (OTTV) through residential building facades. This study proposes three façade configurations as case studies to determine their capability of achieving the OTTV set by the current residential standards. Utilising the OTTV formula provided by the Malaysian Standards, the OTTV of each case study was calculated using parameters including Window-to-Wall Ratio (WWR), Shading Coefficient (SC), U-values and solar absorption ( $\alpha$ ). Results showed that each of the façade generated OTTV exceeding the regulation of  $50 \text{ Wm}^{-2}$ . The study uncovered the increase in WWR leading to the increase in OTTV. The OTTV increased alongside window areas due primarily to the high amount of heat gained through windows, a constituent component of OTTV. Simultaneously, high Shading Coefficient (SC) and U-values were found to cause the high amount of solar heat gained through windows. The result underpins the impacts of high solar heat gain particularly from windows of a building envelope on OTTV. Recommendations for improvement of OTTV of the residential façades are also discussed.

*Keywords:* Apartment facades, Green Building Index (GBI), modern style, OTTV

### **INTRODUCTION**

This study examined the impacts of façade design on the Overall Thermal Transfer

Value (OTTV) of modern-style apartment in Bandar Sri Permaisuri, Kuala Lumpur. In this study, three case studies were proposed to configure the facade option that offers the OTTV suitable to the current residential standards, in response to the tropical climate of Malaysia. Each of the case studies embodies different window configurations, while other parameters remain controlled. The repercussion of manipulating the window configurations alters the window-to-wall (WWR), a crucial parameter in measuring heat gain of windows (Zain-Ahmed et al.,

#### **ARTICLE INFO**

*Article history:*

Received: 25 October 2016

Accepted: 17 March 2017

*E-mail addresses:*

sanusi@usm.my (Ahmad Sanusi Hassan),

muhd9008@gmail.com (Muhammad Hafeez Abdul Nasir)

\*Corresponding Author

2002) in OTTV calculation. The OTTV of each façade was calculated using the OTTV equation set by Malaysian Standards and the results would be analysed to recommend a façade design that suits the residential OTTV regulation. The study undertaken will engender concerns over efficient building facade design which validates with minimum indoor heat gain issues. Heat gain from solar radiation can be regulated with the use of proper materials on the facades (Hassan et al., 2015). The outcome entails energy efficient facade design capable of reducing the cost of indoor cooling purposes (Al-Obaidi, Ismail, & Rahman, 2014). Apartment facades, Green Building Index Malaysia (GBI), and Overall Thermal Transfer Value (OTTV) are three significant keywords in this research study. They are the factors used in the research method to measure the façade performance. The definitions are as follows.

### **Apartment Facades**

One of the popular apartment styles in Malaysia is the Modern-style where multitudes can be found within decentralised city centres. Built from 1980s to 1990s, the time of rapid urban growth, the style can be physically distinguished from its apparent mass-produced façade defined by abstract and simple geometric elements (Hassan & Bakhlah, 2013). Meant to express the notion of purity of the International Style, the aftermath follows the Western patterns of design and construction, which has no basis to the Southeast Asian landscape (Hassan, 2002). In addressing mass-production, the Modern style applies modern materials like glass windows, bricks, reinforced concrete, rubbers and aluminium (Hassan & Bakhlah, 2013) in the building construction. Due to their durability to weather, these imported components are embraced as the Modern architectural styles of Malaysia which are insouciant to local values and climates (Hassan, 2002).

### **Green Building Index Malaysia (GBI)**

Concerns over energy efficiency in the built environment, which proliferated globally, resulted in the inauguration of Green Building Index in Malaysia. Designed in response to primarily addressing energy efficiency and indoor environmental quality (Rahardjati, Khamidi, & Idrus, 2010), the GBI has been widely accepted as a performance assessment tool for Malaysia's homes since its introduction in 2009. Accordingly, a growing trend towards achieving green building performance has led a shift in attitudes from conventional to green building design due to its environmental and cost benefits (Kats, 2003). The ramification witnesses more houses are designed to abide to Malaysia's tropical climate and weather conditions. Kuala Lumpur, being Malaysia's capital and the epicentre of economic and urban growth, is subjected to the local hot and humid climate. Like any tropical regions in Malaysia, the city receives high solar intensity during the day time. Therefore, construction of efficient building envelope is quintessential in Malaysia (Bakhlah & Hassan, 2012), a requisite to improve energy efficiency and indoor environmental quality.

### **Overall Thermal Transfer Value (OTTV)**

The concept of overall thermal transfer value (OTTV) was first introduced by ASHRAE Standard 90A-1980 in the United States to gauge the average heat gain through a building



envelope. In Malaysia, the OTTV concept is adopted in the Malaysian Standards 1525:2007; the standard regulates the OTTV of less than  $50 \text{ Wm}^{-2}$  for air-conditioned areas exceeding  $4000 \text{ m}^2$ . Theoretically, the OTTV measures heat transfer through building envelope by conduction through an opaque surface, conduction through glass window and solar radiation through glass window. Measuring OTTV relies on four important parameters, namely Window-to-Wall Ratio (WWR), Shading Coefficient (SC), U-values and solar absorption ( $\alpha$ ), with U-value and solar absorption having greater impact than other residential OTTV parameters (Saidur et al., 2009). For air-conditioned buildings, the amount of cooling load varies according to the heat gain of its respective building envelope. Consequently, the OTTV is a clear indicator of building envelope energy efficiency, by means of assessing the heat gain through a building envelope integral to the cooling load of air-conditioned buildings.

## METHOD

For the case study, the façade of the Cendana Apartment (Figure 1) was selected to represent a modern-style apartment to carry out the study on the OTTV of apartment façades configurations. Located at Bandar Sri Permaisuri, Cendana Apartment, a leasehold development by Tan & Tan Development is made up of a three blocks of 17-storey apartments. Comprising of 144 residential units in total, each unit is provided with 3 bedrooms and 2 bathrooms. The build-up for each unit ranges from 616 sf to 650 sf, at reasonable prices of RM65,000 to RM117,000. Temporary tenancy is also provided at the price of RM750 per month.

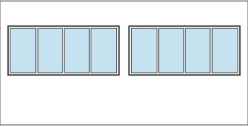
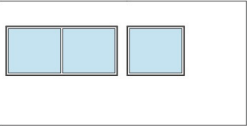
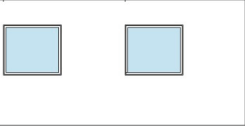
The façade style is defined as modern, embodying simple geometric elements, embellished with vertically arrayed repetitive glass windows on its brick walls. Strategically located in the heart of Bandar Sri Permaisuri, on the south-eastern corner of Kuala Lumpur, the apartment resides within an agglomeration of high-rise apartments, traffic networks, parklands, and shop houses. Subjected to tropical climate of Malaysia, the apartment receives high solar radiation, particularly on the west façade due to perennial solar radiation on west orientation in the evening (Hassan, Arab, & Bakhlah, 2015).



Figure 1. Cendana Apartment design style from 1970 – 1990 in Bandar Tun Abdul Razak, Kuala Lumpur

Referring to the façade of Cendana Apartment, two other façade configurations were generated by manipulating the area of the windows (Table 1), known as Case Study 1 and Case Study 2. While Case Study 3 mimics the original façade of the apartment. This alters the Window-to-wall ratio (WWR) of each of the case studies (Table 2).

Table 1  
Case Study and the designed façade parameters

	Case Study 1	Case Study 2	Case Study 3
			
Wall type	150 mm plastered brick wall	150 mm plastered brick wall	150 mm plastered brick wall
Window types	5 mm aluminium window single-glazing clear glass	5 mm aluminium window single-glazing clear glass	5 mm aluminium window single-glazing clear glass
Orientation	West	West	West
Facade area (m <sup>2</sup> )	18	18	18
Opaque Wall Area (m <sup>2</sup> )	11.52	13.09	14.66
Glass Area (m <sup>2</sup> )	5.24	4.08	2.72
Frame (m <sup>2</sup> )	1.24	0.83	0.62

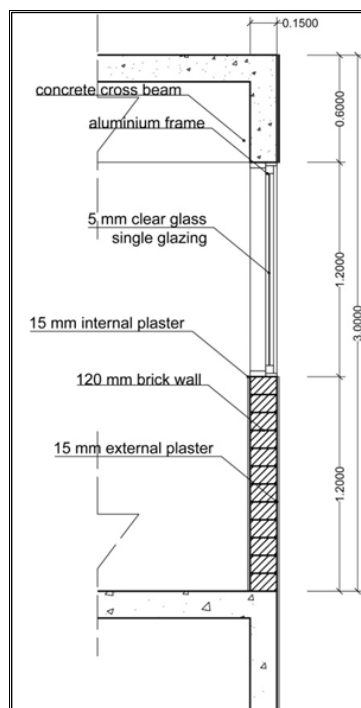


Figure 2. Floor to ceiling structural and wall detail

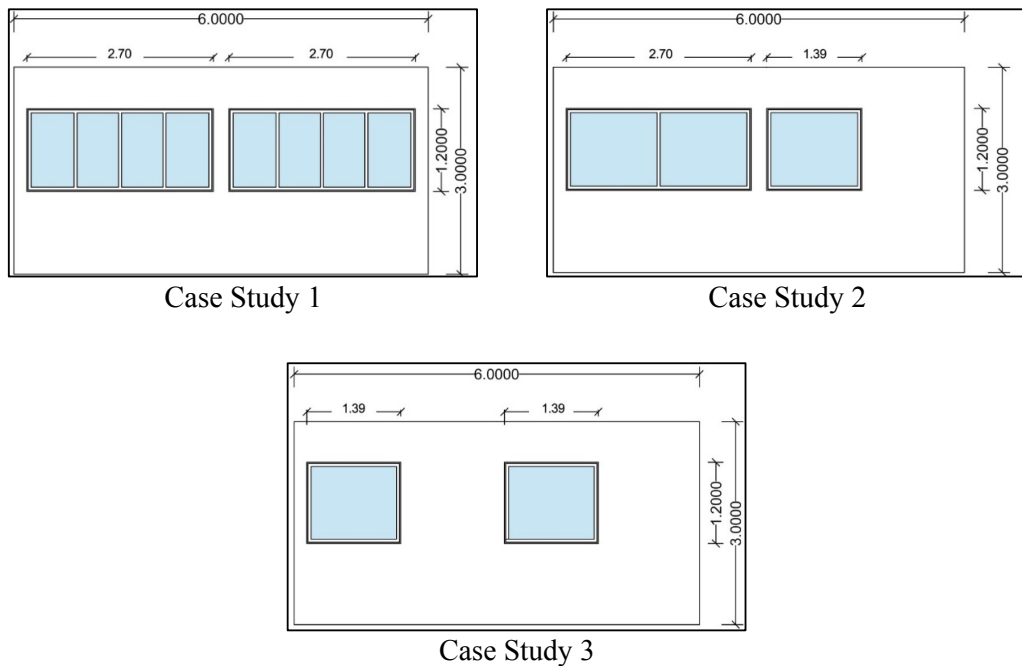


Figure 3. Apartment Façades in the Case Studies 1, 2 and 3

Table 2  
Window-to-wall ratio of the case studies

	Facade area ( $m^2$ )	Window Area ( $m^2$ )	WWR	1-WWR
Case Study 1	18	6.48	0.36	0.64
Case Study 2	18	4.91	0.27	0.73
Case Study 3	18	3.34	0.19	0.81

For this study, all the façade parameters including orientation, wall and window types, and total façade area remain similar, as shown in Table 1. For each of the case studies, the Window-to-wall ratio (WWR) is different (Table 2). According to Lam et al. (2005), WWR is the ratio of window area (glass and frame) to gross wall area. Case Study 1 accounts the highest WWR of 0.36, due to its highest area of window, followed by Case Study 2 and Case Study 3. Case Study 1 to Case Study 2 records a total reduction of 31% of the window area, while Case Study 2 to Case Study 3 records a further reduction of 41% of the window area on the west façade.

In order to study the impact of OTTV on building envelope, the OTTV for each case study, which was designed with different facades, are made up of different window and wall configurations. Each parameter of the case studies is substituted into the OTTV equation set by the Malaysian Standards 1525:2007 to quantify the OTTV of respective case studies. Results of the OTTV calculation are recorded and analysed.

According to ASHRAE 90A-1980, the general OTTV equation can be expressed as:

$$OTTV_i = \frac{Q_w + Q_g + Q_s}{A_i} \quad [1]$$

$$\frac{(A_w \times U_w \times TD_{eq}) + (A_f \times U_f \times DT) + (A_f \times SC \times SF)}{A_i} \quad [2]$$

Expressing the equation in terms of WWR results in this equation,

$$OTTV_i = [TD_{eq} \times (1 - WWR) \times U_w] + [DT \times WWR \times U_f] + [SF \times WWR \times SC \times CF] \quad [3]$$

$A_f$  = the area of fenestration ( $m^2$ )

$A_i$  = the gross area of the walls ( $m^2$ )

$A_w$  = the area of the opaque walls ( $m^2$ )

$Q_w$  = Heat Conduction through opaque walls (W)

$Q_s$  = Solar radiation through glass windows (W)

$Q_g$  = Heat Conduction through glass windows (W)

$U_w$  = U value of the opaque part of the wall ( $W/m^2 k$ )

$U_f$  = U value of the fenestration ( $W/m^2 k$ )

SC = Shading Coefficient of window

SF = Solar factor

DT = Temperature difference between exterior and interior design conditions ( $^{\circ}C$ )

$TD_{eq}$  = Equivalent temperature difference for the opaque part of the wall (K)

The OTTV concept is adopted in the Malaysian Standards 1525:2007 and the OTTV of building envelope is given by the following formula:

$$OTTV_w = 15 \times \alpha \times (1 - WWR) \times U_w + 6 WWR \times U_f + 194 \times WWR \times SC \times CF \quad [4]$$

The absorption factor of a wall  $\alpha$  indicates the degree a wall will absorb solar energy. For this study, the value of  $\alpha$  of the brick wall is 0.75 (Yao & Yan, 2011). SC is the shading coefficient of a fenestration defined as the ratio of solar heat gain through a particular glass type over the solar heat gain through a 3mm clear float glass. It measures the ability of a window to reduce solar heat gain. SC value ranges between 0 and 1. Lower SC gives lower solar heat transmission, inducing greater shading capability. For this study, the facades are made up of similar 5 mm single-glazing uncoated clear glass window, which gives the SC of 0.95. CF is the solar correction factor of different orientations in Malaysia, as shown in Table 3. For the calculation involving CF, the nearest predominant orientation is selected. For this study, only the west orientation is chosen, which gives the value of 0.94.

Table 3  
Solar correction factor of different orientations in Malaysia

Orientation	Solar Correction Factors (Malaysia)
North	0.9
North-East	1.09
East	1.23
South-East	1.13
South	0.92
South-West	0.9
West	0.94
North-West	0.9

U-value measures the rate of heat transfer through a material for every temperature difference in  $W/m^2k$ . The calculation of U-value of the component materials (Figure 2) of a structural brick wall is explained in Table 4. The U-value of materials is the reciprocal of thermal resistance  $m^2k/W$ . Therefore, the higher the U-value indicates a higher thermal transmittance of a material, thus having lower resistivity.

Table 4  
Conductivity, resistance and  $U_w$  value of structural brick wall

Structural Materials	Thickness (m)	Conductivity (W/mk)	Resistance ( $m^2k/W$ )	$U_w$ ( $W/m^2k$ )
External Finish	-	-	0.04	
Plaster (exterior)	0.015	0.57	0.026	
Brick Wall	0.1200	0.77	0.16	
Plaster (interior)	0.015	0.57	0.026	
Internal Finish	-	-	0.04	
			$\epsilon R = 0.292$	$U_w = 3.42$

Windows with coating often provide better shading than the ones without coating, thus having lower U-values, as shown in Table 5.

Table 5  
Typical U-values of different window types to measure OTTV in Malaysia (Saidur et al., 2009)

Name	Typical Values of U
Single Glazed Window with coatings	4.20
Single Glazed Window without coating	5.70

## RESULTS AND DISCUSSION

The OTTV measures heat transfer through building envelope based on three methods, namely conduction through a wall, conduction through glass window, and solar heat gain through

glass window. Tables 6-9 illustrate the results of the calculation of each constituent thermal transfer methods responsible for OTTV. The heat conduction through walls is measured using the following formula:

$$\text{Heat conduction through walls} = (1 - \text{WWR}) \times U_w \times 15 \times \alpha. \tag{5}$$

For this study, the facade with greater brick wall area (1-WWR) which is Case Study 3 generates greater thermal transfer value than the facades with smaller wall area. The results of the calculation are shown in Table 6.

Table 6  
*Heat conduction through walls*

Case Study	Façade Area $m^2$	Constant (Units)	Solar Absorption Factor( $\alpha$ )	1-WWR	$U_w$ Value	Heat Conduction Through walls / $Wm^{-2}$
1	18	15	0.75	0.64	3.42	22.90
2	18	15	0.75	0.73	3.42	26.21
3	18	15	0.75	0.81	3.42	29.08

The heat conduction through windows was measured using the following formula:

$$\text{Heat conduction through windows} = \text{WWR} \times U_f \times 6 \tag{6}$$

For this study, the facade with greater WWR, which is Case Study 1, generates a greater thermal transfer value than facades with smaller WWR. The results of the calculation are shown in Table 7. Heat conduction through windows was shown to contribute the lowest percentage of thermal transfer value with 12.6% of the OTTV. Although the values of heat conduction through wall are significantly higher than heat conduction through windows, it is also important to note that heat conduction through windows increases with facades of lower heat conduction through walls. This is partly associated with the fact that glass window has a significantly higher U-value than the brick wall material alongside increase in WWR. Appropriate selection of wall and window materials with lower U-values will result in smaller heat conduction values through walls and windows.

Table 7  
*Heat conduction through windows*

Case Study	Façade Area $m^2$	Constant (Units)	Window to Wall Ratio/ WWR	$U_f$ Value	Heat Conduction Through Windows/ $Wm^{-2}$
1	18	6	0.36	5.70	12.31
2	18	6	0.27	5.70	9.23
3	18	6	0.19	5.70	6.50

The Solar Heat Gain through Windows is measured using the following formula:

$$\text{Solar Heat Gain through Windows} = \text{WWR} \times \text{SC} \times 194 \times \text{CF} \quad [7]$$

The study highlights that higher WWR results in greater solar heat gain through windows (Table 9). From all the constituent thermal transfer methods, Solar Heat Gain through windows recorded the highest percentage of thermal transfer value, with 51% of the total OTTV for Case Study 1. The high values of heat gain through windows substantially escalate the OTTV through the building envelopes. This outcome may be due to the shading coefficient (SC) and its connection to solar heat gain as all the facades are constructed with 5 mm single-glazing uncoated clear glass window with the value of 0.95. A significant reduction in solar heat gain through windows can be induced by installing tinted or double-glazed clear low-e windows, as suggested by Hassan, Arab and Bakhlah (2015).

Table 8  
*Solar heat gain through windows*

Case Study	Façade Area $m^2$	Constant (Units)	Window to Wall Ratio	Orientation Correction Factor (CF)	SC	Solar Heat Gain Through Windows $/Wm^{-2}$
1	18	194	0.36	0.94	0.95	62.40
2	18	194	0.27	0.94	0.95	46.77
3	18	194	0.19	0.94	0.95	32.91

In order to measure the OTTV of a building envelope, all the constituent thermal transfer values were added, as shown in equation [4]. Apparently, from the calculation, Case Study 1 accounted for the highest OTTV of  $97.60 \text{ Wm}^{-2}$ , followed by Case Study 2 with  $82.21 \text{ Wm}^{-2}$  and Case Study 3, which resembles Cendana Apartment that accounted for  $68.49 \text{ Wm}^{-2}$  or the lowest amount of OTTV. Table 9 elucidates on the OTTV of each case study.

Table 9  
*Overall thermal transfer values of each of the case studies (OTTV)*

Case Study	Heat Conduction Through Walls $(Wm^{-2})$	Heat Conduction Through Windows $(Wm^{-2})$	Solar Heat Gain Through Windows $(Wm^{-2})$	OTTV $(Wm^{-2})$
1	22.90	12.31	62.40	97.60
2	26.21	9.23	46.77	82.21
3	29.08	6.50	32.91	68.49

In general, the OTTV of all the case studies exceeds the requirement of OTTV set by the Malaysian Standards which is  $50 \text{ Wm}^{-2}$ . This result does not reflect the average mean OTTV mentioned in a previous study (Saidur et al., 2009), which suggests that mean residential OTTV in Malaysia is  $41.7 \text{ Wm}^{-2}$ . This may partly be due to the higher WWR values of more than

0.19 used in this study to calibrate OTTV compared to the recommended value of 0.01 to 0.18 by the previous study. Case Study 1, with the total window area of 6.48, recorded an OTTV value of 97.60 Wm<sup>-2</sup>, while Case Study 2, which was designed to embody 31% less window area than Case Study 1, recorded an OTTV value of 82.21 Wm<sup>-2</sup>. A further reduction of 41% of the window area from case study 2 generated the OTTV of 68.49 Wm<sup>-2</sup> for Case Study 3.

The reduction value of WWR carried out by this study is insubstantial to generate the OTTV of less than 50 Wm<sup>-2</sup>. Therefore, it is proposed that further reduction in WWR must be implemented, which echoes the previous study by Fadzil, Abdullah and Harun (2009), which suggests that the value of WWR should be less than 25% for residential rooms. This study finds that the higher the WWR, the higher the OTTV will be in watt per square metre (Wm<sup>-2</sup> or W/m<sup>2</sup>). It demonstrates that the apartment design should have the optimum WWR less than 19% for the West façade for an apartment room to achieve a satisfying OTTV requirement.

## CONCLUSION

The study reveals that different façade designs generate different OTTV. An increase in the area of windows for the west façade of apartment buildings constitutes to the increase in WWR, triggering the value of Solar Heat Gain through Windows and Heat Conduction through windows. In Malaysia, all the proposed façades of the Modern style apartment exceeded the OTTV set by the residential standards of 50 Wm<sup>-2</sup>. Therefore, additional cooling load is required to substantially mitigate heat gain through the building envelope to harness energy efficient indoor environmental quality. Solar heat gain through windows contributes the highest amount of OTTV. Therefore, measures to reduce solar heat gain through windows should be implemented to reduce OTTV. For instance, since shading coefficient (SC) is one of the parameters of heat gain through windows, providing windows with lower SC could help to reduce solar heat gain and thus reducing OTTV. The residential OTTV result underscores the importance of solar heat gain reduction in windows advocating on the needs for architects to design shading elements to give shades to the window areas, alongside windows material selection (Hassan & Al-Ashwal, 2015) and self-shading strategy (Nikpour et al., 2011) for residential building façade, in accordance with energy efficiency and improvement in indoor environmental quality.

## ACKNOWLEDGEMENT

The authors would like to express their heartfelt gratitude for the financial support from Research University Grant (RU) No: 1001/PPBGN/816237 by Universiti Sains Malaysia.

## REFERENCES

- Al-Obaidi, K. M., Ismail, M., & Rahman, A. M. A. (2014). A review of the potential of attic ventilation by passive and active turbine ventilators in tropical Malaysia. *Sustainable Cities and Society*, 10, 232-240.
- Bakhlah, M. S., & Hassan, A. S. (2012). The study of air temperature when the sun path direction to Ka'abah: with a case study of Al-Malik Khalid Mosque, Malaysia. *International Transaction Journal of Engineering, Management & Applied Sciences and Technologies*, 3(2), 185-202.



- Cendana Apartment. (n.d.). Retrieved August 29, 2016, from [http://www.propwall.my/bandar\\_sri\\_permaisuri/cendana\\_apartment](http://www.propwall.my/bandar_sri_permaisuri/cendana_apartment)
- Fadzil, S. F. S., Abdullah, A., & Harun, W. M. W. (2009). The Impact of Varied Orientation and Wall Window Ratio (WWR) To Daylight Distribution in Residential Rooms. *International Symposium on Construction in Developing Economies*.
- Hassan A. S. (2002). Towards Sustainable Housing Construction in Southeast Asia. *Agenda 21 for Sustainable Construction in Developing Countries*.
- Hassan, A. S., & Al-Ashwal, N. T. (2015). Impact of Building Envelope Modification on Energy Performance of High-Rise Apartments in Kuala Lumpur, Malaysia.
- Hassan, A. S., & Bakhlah, M. S. O. (2013). Shading Analysis on Front Facade of Modern Terraced House Type in Petaling Jaya, Malaysia. *Procedia-Social and Behavioral Sciences*, 91, 13-27.
- Hassan, A. S., Arab, Y., & Bakhlah, M. S. O. (2015). Comparative study on sunlight penetration between post-modern and neo-minimalist terraced house facade in Malaysia. *Advances in Environmental Biology*, 51-55.
- Kats, G. (2003). *Green building costs and financial benefits* (p. 1). Boston, MA: Massachusetts Technology Collaborative.
- Lam, J. C., Tsang, C. L., Li, D. H., & Cheung, S. O. (2005). Residential building envelope heat gain and cooling energy requirements. *Energy*, 30(7), 933-951.
- Nikpour, M., Ghomeshi, M., Moeinzadeh, N., & Ghasemi, M. (2011). Investigating the effectiveness of self-shading strategy on overall thermal transfer value and window size in high rise buildings. *World Academy of Science, Engineering and Technology, International Journal of Civil, Environmental, Structural, Construction and Architectural Engineering*, 5(2), 103-108.
- Rahardjati, R., Khamidi, M. F., & Idrus, A. (2010). The level of importance of criteria and sub criteria in green building index Malaysia. In *International Conference on Sustainable Building and Infrastructure (ICSBI 2010)* (pp. 15-17).
- Saidur, R., Hasanuzzaman, M., Hasan, M. M., & Masjuki, H. H. (2009). Overall thermal transfer value of residential buildings in Malaysia. *Applied Sci.*, 9(213), 2.
- Yao, J., & Yan, C. (2011). Effects of solar absorption coefficient of external wall on building energy consumption. In *Proceedings of World Academy of Science, Engineering and Technology*, 76, 758-760.
- Zain-Ahmed, A., Sopian, K., Othman, M. Y. H., Sayigh, A. A. M., & Surendran, P. N. (2002). Daylighting as a passive solar design strategy in tropical buildings: a case study of Malaysia. *Energy Conversion and Management*, 43(13), 1725-1



## Synthesisation Temperature-Dependent Cytotoxicity of Bismuth Oxide Nanoparticles *in Vitro*

Nur Amirah Mohd Nor<sup>1</sup>, Zanariah Mohd<sup>2</sup>, Hairil Rashmizal Abdul Razak<sup>2</sup>, Zolkapli Eshak<sup>3</sup> and Wan Mazlina Md Saad<sup>1\*</sup>

<sup>1</sup>Department of Medical Laboratory Technology, Faculty of Health Sciences, Universiti Teknologi MARA (UiTM), 42300 Puncak Alam, Selangor, Malaysia

<sup>2</sup>Department of Medical Imaging, Faculty of Health Sciences, Universiti Teknologi MARA (UiTM), 42300 Puncak Alam, Selangor, Malaysia

<sup>3</sup>Imaging Centre (IMACE), Faculty of Pharmacy, Universiti Teknologi MARA (UiTM), 42300 Puncak Alam, Selangor, Malaysia

### ABSTRACT

Bismuth oxide nanoparticles ( $\text{Bi}_2\text{O}_3$  NPs) have gained a spot in the development of novel molecular probes for *in vivo* biomedical imaging. It exists in six polymorphic forms and each of them exerts with different stabilities according to its synthesisation temperature. The aim of this preliminary study is to determine effect of different synthesiation temperatures on cellular viability *in vitro*. One hundred  $\mu\text{g}/\text{ml}$   $\text{Bi}_2\text{O}_3$  NPs synthesised at 60, 90 and 120°C were characterised using scanning electron microscope (SEM) and their cytotoxicity was evaluated using cell viability assay (MTT assay) upon 24 hours exposure to Chang liver cells. Images captured by SEM showed an average diameter of 300 nm monoclinic-shaped with high crystalline formation of all three  $\text{Bi}_2\text{O}_3$  NPs. MTT assay revealed increase in liver cell viability as the synthesisation temperature of  $\text{Bi}_2\text{O}_3$  NPs increase. The outcomes suggested that synthesisation temperature of  $\text{Bi}_2\text{O}_3$  NPs plays a role in cellular viability, hence predictive to the biocompatibility of these nanoparticles to be applied as *in vivo* radiographic contrast medium.

**Keywords:** Bismuth oxide nanoparticles ( $\text{Bi}_2\text{O}_3$  NPs), cell viability, cytotoxicity, synthesisation temperature

### ARTICLE INFO

#### Article history:

Received: 25 October 2016

Accepted: 17 March 2017

#### E-mail addresses:

wanmaz755@salam.edu.uitm.my (Wan Mazlina Md Saad), amyramnk299@gmail.com (Nur Amirah Mohd Nor), zanariahmohd@salam.uitm.edu.my (Zanariah Mohd), rashmizal@yahoo.com.my (Hairil Rashmizal Abdul Razak), zolkapli\_eshak@puncakalam.uitm.edu.my (Zolkapli Eshak)

\*Corresponding Author

### INTRODUCTION

Fast growing nanotechnology is one of the most propitious areas in biomedical research besides other areas ranging from electronics and aerospace engineering to environmental restoration. Regardless its promising potential to improve diagnosis

and treatment of intractable diseases, its safety consideration to human health is not parallel with the growth of the nanomaterial development (Singh et al., 2009). Longer years might be needed to fully realise its potential and make it possible for clinical trial. Nanoparticles are the particles which have been technologically engineered to nanoscale dimensions ranging from 1 to 100 nm (Wilczewska et al., 2012). Due to novel physico-chemical properties contributing to its nanoscale structure, nanoparticles may exert different properties compared to its bulk counterparts and may be a causative factor to adverse biological effects in human. The impacts of nanomaterials on human health are still inadequately elucidated despite its emerging manufacturing and usage for medical purposes (Fu et al., 2014).

Nanomaterials with high atomic number ( $Z$ ) such as gold (AuNPs) and iron oxide nanoparticles (IONPs) have been discovered to induce dose and contrast enhancement in improving theranostics efficacy. However, investigations on other promising and cheaper nanoparticles with high  $Z$  number such as bismuth-based nanoparticles are still insufficient and poorly understood (Alqathami et al., 2013). Bismuth (Bi) compound is generally safe. Bi has been used in various medical settings, such as in treating syphilis, tumours, gastrointestinal disorders, eliminating *Helicobacter pylori* in peptic ulcer treatment and reduction of cisplatin-induced renal toxicity (Luo et al., 2012; Türkez, Geyikoğlu, & Keleş, 2005). Bismuth oxide nanoparticles ( $\text{Bi}_2\text{O}_3$  NPs) have recently drawn tremendous attention in bioimaging, X-ray radiosensitising and biomolecular detection. It can be possibly exploited as dose and contrast enhancement in medical imaging due to its high atomic number ( $Z = 83$ ), which is theoretically higher than gold ( $Z = 79$ ).

There are several ways in synthesizing  $\text{Bi}_2\text{O}_3$  NPs such as through co-precipitation, chemical vapour deposition, microwave-assisted and sol-gel method (Drache, Roussel, & Wignacourt, 2007). Despite these techniques, hydrothermally synthesisation has been proven as the best method in synthesising  $\text{Bi}_2\text{O}_3$  NPs powder by providing high degree of crystallinity, high purity, narrow particle size distribution and uniform morphology.  $\text{Bi}_2\text{O}_3$  NPs are known to exist in six polymorphic forms, denoted by  $\alpha$ - $\text{Bi}_2\text{O}_3$ ,  $\beta$ - $\text{Bi}_2\text{O}_3$ ,  $\gamma$ - $\text{Bi}_2\text{O}_3$ ,  $\delta$ - $\text{Bi}_2\text{O}_3$ ,  $\epsilon$ - $\text{Bi}_2\text{O}_3$  and  $\zeta$ - $\text{Bi}_2\text{O}_3$  with monoclinic, tetragonal, body-centred cubic, face-centred cubic, orthorhombic and triclinic shape respectively (Jiang et al., 2015). All of them are high-temperature metastable, except for  $\alpha$ - $\text{Bi}_2\text{O}_3$  (low-temperature stable), while  $\delta$ - $\text{Bi}_2\text{O}_3$  is high-temperature stable.  $\text{Bi}_2\text{O}_3$  NPs exerts stability distinctively at various temperatures; hence, synthesisation-temperature effect must be comprehensively evaluated to determine whether this factor plays a role in contributing cellular toxicity.

Toxicity of  $\text{Bi}_2\text{O}_3$  NPs has promoted serious concerns among researchers due to its nanoscale size, high surface area and various fabrication modification techniques (Luo et al., 2012). The aim of this study is to elucidate the viability of cells *in vitro* with  $\text{Bi}_2\text{O}_3$  NPs synthesised at different temperatures. To date, this has been no study done to find the relationship between  $\text{Bi}_2\text{O}_3$  NPs synthesised at different temperatures with possible toxicity associated. This paper focuses on *in vitro* cytotoxicity investigation of  $\text{Bi}_2\text{O}_3$  synthesised at 60, 90 and 120°C by 3-(4,5-dimethylthiazol-2-yl)-2,5-diphenyltetrazolium bromide (MTT) colorimetric assay for 24 hours.

## MATERIALS AND METHOD

### Bismuth Oxide Nanoparticles and Reagents

Bismuth oxide nanoparticles ( $\text{Bi}_2\text{O}_3$  NPs) of three different synthesis temperatures (60, 90, and  $120^\circ\text{C}$ ) were obtained in dry powder form from Nano-Biotechnology Research and Innovation (NanoBRI), Institute for Research in Molecular Medicine (INFORMM), Universiti Sains Malaysia, Pulau Pinang, Malaysia. HeLa [Chang Liver] (ATCC<sup>®</sup> CCL13<sup>™</sup>) cell lines are from American Type Culture Collection (ATCC), Minimum Essential Media (MEM), 100 X Penicillin-Streptomycin are from BioWest. Foetal Bovine Serum and 1X TrypLE express enzyme are from Gibco. Phosphate buffer saline (PBS) tablets, dimethyl sulfoxide (DMSO) and 3-(4,5-dimethylthiazol-2-yl)-2,5-diphenyltetrazolium bromide (MTT) are from Sigma-Aldrich.

### Bismuth Oxide Nanoparticles Preparation and Characterisation

All  $\text{Bi}_2\text{O}_3$  NPs in dry powder form were suspended in serum-free Minimum Essential Media (MEM) at 1 mg/ml concentration. The suspensions were vortexed at 800 rpm for 20 minutes at room temperature to form homogenous suspension before they were being filtered through a  $0.22\ \mu\text{m}$  hydrophilic polysulphonic membrane syringe bacterial filter. The stock solutions of all three  $\text{Bi}_2\text{O}_3$  NPs were then diluted to 100  $\mu\text{g}/\text{ml}$  working solution in order to perform cytotoxicity assay.

The particles size and structure of  $\text{Bi}_2\text{O}_3$  NPs were visualised using Quanta<sup>™</sup> 450 FEG (Scanning Electron Microscope) at the Microscopy Imaging Centre, Faculty of Pharmacy, Universiti Teknologi MARA, Puncak Alam.  $\text{Bi}_2\text{O}_3$  NPs powders were placed on sample holders for the images to be taken. SEM images of  $\text{Bi}_2\text{O}_3$  NPs were obtained at 5000 x magnification power, 10 kV acceleration voltage, and 2 Pa pressure.

**Cell culture.** HeLa [Chang Liver] (ATCC<sup>®</sup> CCL13<sup>™</sup>) cells were purchased from American Type Culture Collection prior to the study. The cells were maintained in Minimum Essential Media (MEM) (Gibco, USA), 10% Foetal Bovine Serum (Gibco, USA) and 1% Penicillin-Streptomycin (Gibco, USA). Cells were cultured in T-75 flask (Corning, USA) with  $37^\circ\text{C}$  humidified atmosphere of 5%  $\text{CO}_2$  and 95% air for 3 days or until reached 80% confluency prior to treatment with  $\text{Bi}_2\text{O}_3$  NPs. Confluent cells were detached from the culture flask by using 1X TrypLE (Gibco, Denmark) express enzyme for 5 minutes. Five ml of complete media was added to the flask and fairly mixed with TrypLE express enzyme and the cells were then centrifuged at 4000 rpm for 5 minutes. Cells suspension was counted using Vi-CELL<sup>™</sup> Cell Counter (Beckman Coulter, USA) and seeded at a density of  $1 \times 10^4$  cells per well in 96-well microplate (Corning, USA).

**24 hours Cell Viability Assay.**  $\text{Bi}_2\text{O}_3$  NPs synthesised at 60, 90, and  $120^\circ\text{C}$  were used to investigate *in vitro* cytotoxicity. Seeded cells in 96-well microplate were incubated for 24 hours ( $37^\circ\text{C}$ , 5%  $\text{CO}_2$  and 95% air) before exposed to 100  $\mu\text{l}$  of 100  $\mu\text{g}/\text{ml}$  of all  $\text{Bi}_2\text{O}_3$  NPs for 24 hours' treatment period ( $37^\circ\text{C}$ , 5 %  $\text{CO}_2$  and 95% air). After the incubation period, cells viability was determined using 3-(4,5-dimethylthiazol-2-yl)-2,5-diphenyltetrazolium

bromide (MTT) colorimetric assay to elucidate preliminary toxicity of  $\text{Bi}_2\text{O}_3$  NPs. 50  $\mu\text{l}$  of MTT solution was added to each well and incubated for 4 hours ( $37^\circ\text{C}$ , 5%  $\text{CO}_2$  and 95% air). MTT solution was discarded and 200  $\mu\text{l}$  of Dimethyl Sulfoxide (DMSO) was then added in each well. The fluorescence intensity was measured at 550 nm by using Tecan F200 Infinite 200-TWT Microplate Reader.

**Statistical analysis.** Statistical significance of data obtained in this study was determined by one-way analysis of variance (ANOVA) followed by Tukey's post-hoc test. Significance of data was designated as  $p < 0.05$ .

## RESULTS

Bismuth Oxide Nanoparticles Characterisation Using Scanning Electron Microscope (SEM) SEM micrographs [Figures 1(A), (B) and (C)] showed the morphology of  $\text{Bi}_2\text{O}_3$  NPs synthesised at 60, 90 and  $120^\circ\text{C}$ , respectively. The average size of  $\text{Bi}_2\text{O}_3$  NPs measured by SEM was 300 nm.

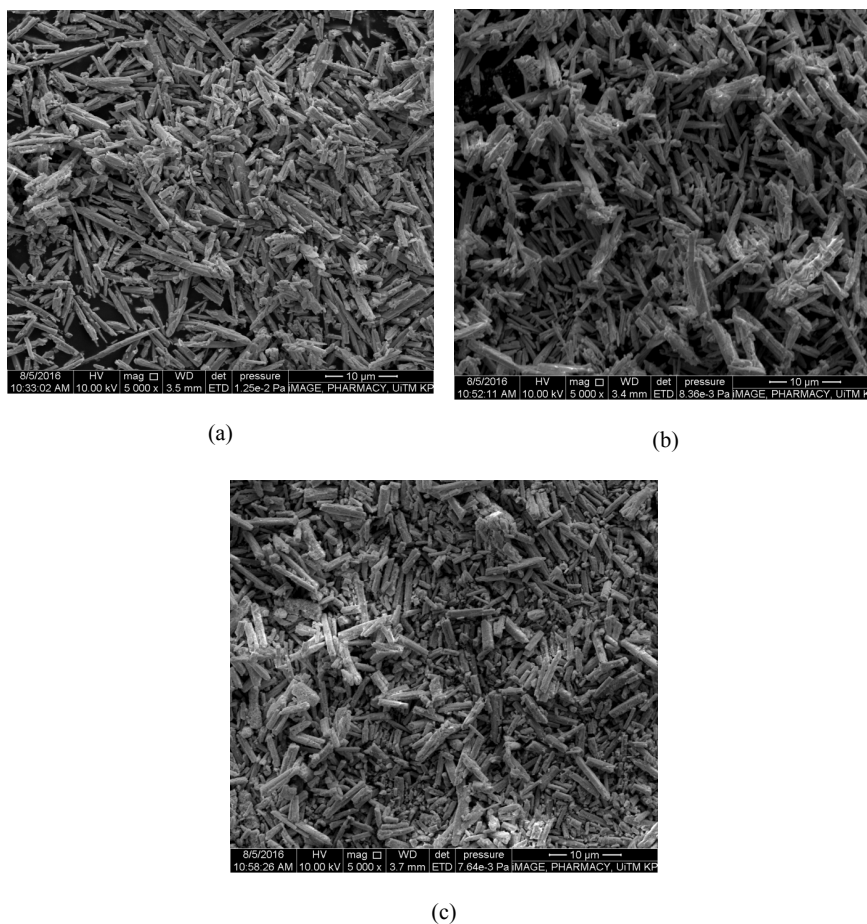


Figure 1. The SEM micrographs of  $\text{Bi}_2\text{O}_3$  NPs synthesised at: (a)  $60^\circ\text{C}$ ; (b)  $90^\circ\text{C}$ ; and (c)  $120^\circ\text{C}$ , respectively

### Cell Viability of Various Bismuth Oxide Nanoparticles *in Vitro*

Cell viability assay using MTT-based colorimetric method was used to portray the cytotoxicity profiling of 100  $\mu\text{g/ml}$   $\text{Bi}_2\text{O}_3$  NPs synthesised at 60, 90 and 120°C, respectively, in Chang liver cells following 24 hours exposure (see Figure 2). MTT results were based on the mitochondrial activity in Chang liver cells upon exposure to  $\text{Bi}_2\text{O}_3$  NPs. Non-treated cells labelled Cx was used as the negative control.

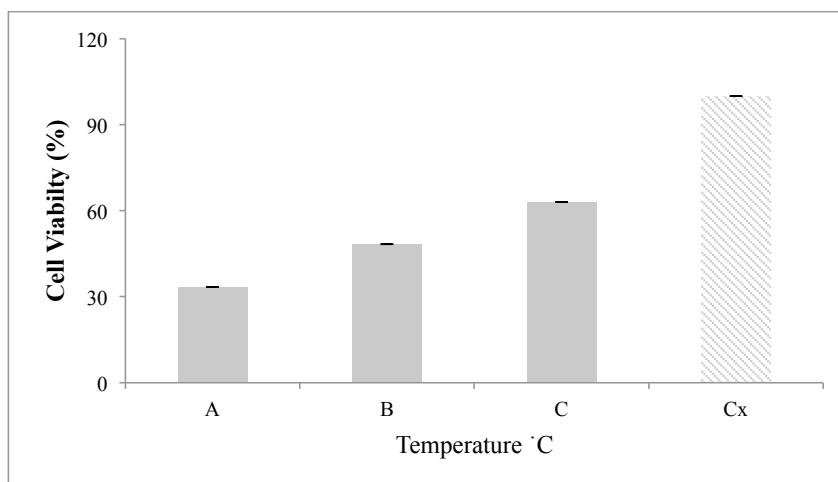


Figure 2. Cell viability percentage of Chang liver cells after 24 hours of exposure with 100  $\mu\text{g/ml}$   $\text{Bi}_2\text{O}_3$  NPs synthesized at A- 60°C, B- 90°C, and C- 120°C, respectively. Each value was expressed as means  $\pm$  SEM,  $n = 4$ . All the percentages of cell viability were statistically significant difference ( $p < 0.05$ ), as compared to control group

### DISCUSSION

Bismuth (Bi) is relatively non-toxic although it exists as one of the elements in the heavy metals group and found sparsely in the environment as co-metal in copper, lead and tin ores (Von Recklinghausen et al., 2008). Recent advancement in nanotechnology has developed several promising colloidal systems which are able to actuate as imaging contrast media with longer circulation period and less harmful excretion route. Conventional contrast media, like iodine and gadolinium, are known to have short imaging time, reduced performance and efficacy (Hainfeld et al., 2008). With further alarming concern in iodine-based contrast media regarding its toxicity which could highly danger iodine-intolerance patient, several nanoparticulated contrast media have been fabricated such as gold nanoparticles, iron oxide nanoparticles, iron-platinum alloy nanoparticles and bismuth oxide nanoparticles ( $\text{Bi}_2\text{O}_3$  NPs) as alternative contrast enhancing agents. However, among these nanoparticulated contrast media,  $\text{Bi}_2\text{O}_3$  NPs have gained special attention due to their high x-ray attenuation coefficient, high atomic number, low toxicity and are reasonably cheap.

Although Bi has been used in various medical applications, especially in treating gastrointestinal disorders, bismuth is found to be able to accumulate in various cell types including neuron, kidney and Leydig cells due to excessive ingestion and chronic use

(Stoltenberg & Danscher, 2000; Urgast et al., 2012; Stoltenberg et al., 2000). Therefore, to date, little is known about the potential cytotoxicity of Bi in human cells. The toxicity of Bi compound is associated with the release of Bi ions ( $\text{Bi}^{3+}$ ), but it is relatively low because it is the least toxic among other heavy metals (Luo et al., 2012). Unlike its bulk compound, nano-sized  $\text{Bi}_2\text{O}_3$  may induce toxicity due to its unique physicochemical properties. For example, silver nanoparticles were reported to be more toxic than silver ions (Christen, Capelle, & Fent, 2013; Johnston et al., 2010). Changes in the physicochemical properties play a major role in NPs performance. Small-sized NPs are able to penetrate into tissues and cells, hence making it easier for the detection of histopathological, cellular and molecular changes of diseases. NPs have a bigger total surface area to volume ratio, which enhances its surface activity (Hillegass et al., 2010; Mohanraj & Chen, 2007).

$\text{Bi}_2\text{O}_3$  NPs can be synthesised using multifarious methods and apparently hydrothermal method was suggested as advantageous in synthesising the nanostructures of Bi. It is known that there are six polymorphs of  $\text{Bi}_2\text{O}_3$  as described. Each exhibits wide diversity of phases, which is either stable or not stable at a moderate or high temperature (Drache, Roussel, & Wignacourt, 2007). This study was designed to characterise and investigate the preliminary toxicity of  $\text{Bi}_2\text{O}_3$  NPs synthesised at different temperatures (60, 90 and 120°C) using human Chang liver cells. Liver is the major organ for detoxification, and introduction of NPs in the body is susceptible to accumulate in this organ. Accumulation of gold nanoparticles ranging from 10 to 50 nm was found to be accumulated in the liver and spleen at 24 hours post injection (Jong, Hagens, Krystek, & Burger, 2008; Sonavane, Tomoda, & Makino, 2008). Since no study has been done to outline the  $\text{Bi}_2\text{O}_3$  NPs temperature-synthesis effect, Chang liver cells are suitable to be used as a model structure for hepatotoxicity study.

The SEM micrographs revealed that  $\text{Bi}_2\text{O}_3$  NPs synthesised at the highest temperature of 120°C showed slightly brittle looking particles with no differences of shapes and sizes observed at 60 and 90°C. This result indicates that  $\text{Bi}_2\text{O}_3$  NPs synthesised at high temperature may be less harmful to Chang liver cells. All  $\text{Bi}_2\text{O}_3$  NPs have an average diameter of 300 nm and can be ascribed as monoclinic-shaped with high crystalline formation. The transformation of bismuth polymorphic forms are highly affected by its fabrication method such as electrical conductivity or thermal expansion (Koto, 1994).

MTT colorimetric assay detects the cytotoxicity of nanoparticles by reflecting the level of damage on mitochondria function by measuring mitochondria activity enzyme and integrity of the cell membrane. From the MTT cell viability histogram, a similar trend was observed as in the SEM outcomes, where  $\text{Bi}_2\text{O}_3$  NPs synthesised at the highest temperature of 120°C have the least toxicity effects (63% cell viability, 37% cell death) in Chang liver cells, indicating biocompatibility. This result shows an indirect proportional relationship between  $\text{Bi}_2\text{O}_3$  NPs synthesis temperatures and the release of bismuth ions which induces toxicity in cells.  $\text{Bi}_2\text{O}_3$  NPs synthesised at 60°C exhibits the highest toxicity effect (33% cell viability, 67% cell death), followed by  $\text{Bi}_2\text{O}_3$  NPs synthesised at 90°C (48% cell viability, 52% cell death). However, it is difficult to weight the nanotoxicity of  $\text{Bi}_2\text{O}_3$  NPs in human cells based on only one parameter. Therefore, an extended research is warranted to further explore the actual toxicity



mechanism of Bi<sub>2</sub>O<sub>3</sub> NPs inducing damage to human cells. Previously, *in vivo* nanotoxicity studies showed exposure to 100 µg/l of colloidal bismuth subnitrate induced liver damage and cerebellar disruption (Stoltenberg et al., 2001; Türkez et al., 2005). Meanwhile, Von Recklinghausen et al. (2008) found that bismuth citrate and bismuth glutathione are not toxic to human hepatocytes and lymphocyte even at high concentrations, which contradicted with 4 µM methylbismuth compound toxicity. Ribeiro et al. (2009) reported a similar finding of non-toxic 100 µg/ml bismuth oxide via single-cell gel assay. It can be postulated that toxicity of bismuth compound may be different and highly influenced by its fabrication method.

## CONCLUSION

The preliminary cytotoxicity of Bi<sub>2</sub>O<sub>3</sub> NPs synthesised at different temperatures (60, 90 and 120°C) in Chang liver cells was evaluated using MTT assay based on the viability percentage of the cells. The outcomes of this study suggested that the biocompatibility of Bi<sub>2</sub>O<sub>3</sub> NPs increases with temperature. Therefore, this study may provide early information to biosafety of Bi<sub>2</sub>O<sub>3</sub> NPs with temperature. However, further research with extended parameters is needed to further justify Bi<sub>2</sub>O<sub>3</sub> NPs synthesis temperature effects on cellular toxicity.

## ACKNOWLEDGEMENT

The authors would like to give a special gratitude to: (1) Faculty of Health Sciences, Universiti Teknologi MARA (UiTM), Puncak Alam, and UiTM Research Management Institute with MOE RAGS: 600-RMI/RAGS 5/3 (80/2015) for funding this research; (2) Dr. Khairunisak Abdul Razak, NanoBri@INFORMM Universiti Sains Malaysia for synthesising the nanoparticles; and (3) Department of Medical Laboratory Technology and Department of Postgraduate Studies, Faculty of Health Sciences, and Imaging Centre (IMACE), Pharmacology-toxicology Research Lab, Tissue Culture Lab, Faculty of Pharmacy, UiTM Puncak Alam.

## REFERENCES

- Alqathami, M., Blencowe, A., Yeo, U. J., Franich, R., Doran, S., Qiao, G., & Geso, M. (2013). Enhancement of radiation effects by bismuth oxide nanoparticles for kilovoltage x-ray beams: A dosimetric study using a novel multi-compartment 3D radiochromic dosimeter. *Journal of Physics: Conference Series*, 444, 012025. <http://doi.org/10.1088/1742-6596/444/1/012025>.
- Christen, V., Capelle, M., & Fent, K. (2013). Silver nanoparticles induce endoplasmic reticulum stress response in zebra fish. *Toxicology and Applied Pharmacology*, 272(2), 519–528. <http://doi.org/10.1016/j.taap.2013.06.011>.
- Drache, M., Roussel, P., & Wignacourt, J. (2007). Structures and Oxide Mobility in Bi – Ln – O Materials: Heritage of Bi<sub>2</sub>O<sub>3</sub>. *Chemical Reviews*, 107(1), 80-96.
- Fu, P. P., Xia, Q., Hwang, H. -M., Ray, P. C., & Yu, H. (2014). Mechanisms of nanotoxicity: generation of reactive oxygen species. *Journal of Food and Drug Analysis*, 22(1), 64–75. <http://doi.org/10.1016/j.jfda.2014.01.005>.

- Hainfeld, J. F., Dilmanian, F. A., Slatkin, D. N., & Smilowitz, H. M. (2008). Radiotherapy enhancement with gold nanoparticles. *The Journal of Pharmacy and Pharmacology*, *60*(8), 977–85. <http://doi.org/10.1211/jpp.60.8.0005>.
- Hillegass, J. M., Shukla, A., Lathrop, S. A., MacPherson, M. B., Fukagawa, N. K., & Mossman, B. T. (2010). Assessing nanotoxicity in cells in vitro. *Wiley Interdiscip Rev Nanomed Nanobiotechnol*, *2*, 219–231. <http://doi.org/10.1002/wnan.54>.
- Jiang, Z., Wang, Y., Li, P., & Feng, C. (2015). Solvothermal Synthesis and Characterization of Bi<sub>2</sub>O<sub>3</sub> Nanoparticles, (*Icimm*), 291–296.
- Johnston, H. J., Hutchison, G., Christensen, F. M., Peters, S., Hankin, S., & Stone, V. (2010). A review of the in vivo and in vitro toxicity of silver and gold particulates: Particle attributes and biological mechanisms responsible for the observed toxicity, *40*(November 2009), 328–346. <http://doi.org/10.3109/10408440903453074>
- Jong, W. H. De, Hagens, W. I., Krystek, P., & Burger, M. C. (2008). Particle size-dependent organ distribution of gold nanoparticles after intravenous administration, *29*, 1912–1919. <http://doi.org/10.1016/j.biomaterials.2007.12.037>
- Koto, K. (1994). *SOLID STATE*, *72*, 79–85.
- Luo, Y., Wang, C., Qiao, Y., Hossain, M., Ma, L., & Su, M. (2012). In vitro cytotoxicity of surface modified bismuth nanoparticles. In *Journal of Materials Science: Materials in Medicine* (Vol. 23, pp. 2563–2573). <http://doi.org/10.1007/s10856-012-4716-1>
- Mohanraj, V. J., & Chen, Y. (2007). Nanoparticles - A review. *Tropical Journal of Pharmaceutical Research*. <http://doi.org/10.4314/tjpr.v5i1.14634>.
- Singh, N., Manshian, B., Jenkins, G. J. S., Griffiths, S. M., Williams, P. M., Maffei, T. G. G., & Doak, S. H. (2009). NanoGenotoxicology: The DNA damaging potential of engineered nanomaterials. *Biomaterials*, *30*, 3891–3914. <http://doi.org/10.1016/j.biomaterials.2009.04.009>.
- Sonavane, G., Tomoda, K., & Makino, K. (2008). Colloids and Surfaces B: Biointerfaces Biodistribution of colloidal gold nanoparticles after intravenous administration: Effect of particle size, *66*, 274–280. <http://doi.org/10.1016/j.colsurfb.2008.07.004>.
- Stoltenberg, M., & Danscher, G. (2000). Histochemical differentiation of autometallographically traceable metals (Au, Ag, Hg, Bi, Zn): Protocols for chemical removal of separate autometallographic metal clusters in Epon sections. *Histochemical Journal*, *32*, 645–652. <http://doi.org/10.1023/A:1004115130843>.
- Stoltenberg, M., Danscher, G., Pamphlett, R., Christensen, M. M., & Rungby, J. (2000). Histochemical tracing of bismuth in testis from rats exposed intraperitoneally to bismuth subnitrate. *Reproductive Toxicology*, *14*, 65–71. [http://doi.org/10.1016/S0890-6238\(99\)00060-X](http://doi.org/10.1016/S0890-6238(99)00060-X).
- Stoltenberg, M., Hogenhuis, J. A., Hauw, J. J., & Danscher, G. (2001). Autometallographic tracing of bismuth in human brain autopsies. *Journal of Neuropathology and Experimental Neurology*, *60*, 705–710.
- Türkez, H., Geyikoğlu, F., & Keleş, M. S. (2005). Biochemical response to colloidal bismuth subcitrate: dose-time effect. *Biological Trace Element Research*, *105*, 151–8. <http://doi.org/10.1385/BTER:105:1-3:151>.

- Urgast, D. S., Ellingsen, D. G., Berlinger, B., Eilertsen, E., Friisk, G., Skaug, V., & Feldmann, J. (2012). Multi-elemental bio-imaging of rat tissue from a study investigating the bioavailability of bismuth from shotgun pellets. *Analytical and Bioanalytical Chemistry*, *404*, 89–99. <http://doi.org/10.1007/s00216-012-6101-9>.
- Von Recklinghausen, U., Hartmann, L. M., Rabieh, S., Hippler, J., Hirner, A. V., Rettenmeier, A. W., & Dopp, E. (2008). Methylated bismuth, but not bismuth citrate or bismuth glutathione, induces cyto- and genotoxic effects in human cells in vitro. *Chemical Research in Toxicology*, *21*, 1219–1228. <http://doi.org/10.1021/tx700304e>.
- Wilczewska, A. Z., Niemirowicz, K., Markiewicz, K. H., & Car, H. (2012). Nanoparticles as drug delivery systems. *Pharmacological Reports*, *64*(5), 1020–1037. [http://doi.org/10.1016/S1734-1140\(12\)70901-5](http://doi.org/10.1016/S1734-1140(12)70901-5).





## Personality Prediction Based on Social Media Using Decision Tree Algorithm

**Tan Lee Chee Yoong, Nor Rahayu Ngatirin\* and Zurinahni Zainol**

*School of Computer Sciences, Universiti Sains Malaysia (USM), 11800 Minden, Pulau Pinang, Malaysia*

### ABSTRACT

Personality represents the mixture of features and qualities that built an individual's distinctive characters including thinking, feeling and behaving. Traditionally, self-assessment method via questionnaire is the most common means to identify personality. Since recommender systems and advertisement campaigns have evolved rapidly, personality computing has become a popular research field to provide personalisation to users. Currently, researchers have utilised social media data for automatically predicting personality. However, it is complex to mine the social media data as they are noisy, free-format, and of varying length and multimedia. This paper proposes a decision tree C4.5 algorithm to automatically predict personality based on Big Five model. The Big Five Inventory and ZeroR algorithm were included to be served as the baseline for performance evaluation. Experimental evaluation demonstrated that C4.5 performs better than ZeroR in terms of accuracy.

*Keywords:* Big Five, decision tree, personality, social media

### INTRODUCTION

Personality is a word derived from Latin, *persona*, which means the theatrical mask used by the actors (Ahmad, 2015). It can be

defined as a set of attributes that characterise a unique individual's behaviour, temperament, emotions and mental (Mairesse et al., 2007). Personality differentiates an individual from others in characteristic patterns of thinking, feeling and behaving. There are many different personality models used to characterise personality such as the Big Five model (Five-factor model) (John et al., 2008) and the Myers-Briggs Type Indicator (MBTI) (2016). The Big Five model conceived by Tupes and Christal (1961) consists of five traits which are the openness to experience, conscientiousness, extraversion,

#### ARTICLE INFO

##### *Article history:*

Received: 25 October 2016

Accepted: 17 March 2017

##### *E-mail addresses:*

tlyoong.ucom12@student.usm.my (Tan Lee Chee Yoong),

nrn14\_com057@student.usm.my (Nor Rahayu Ngatirin),

zuri@usm.my (Zurinahni Zainol)

\*Corresponding Author

agreeableness and neuroticism. Each of these dimensions has their own set of poles (low/high) and will be discussed further in the next section. Meanwhile, the MBTI developed by Briggs and Myers in 1950s measures the preferences on four dichotomies which are energising (introversion/extraversion), attending (sensing/intuitive), deciding (feeling/thinking) and living (judging/perceptive) (Bishop-Clark, & Wheeler, 1994). In this study, the Big Five model was selected as it is one of the most well-researched and well-regarded measures of personality structure (Golbeck, Robles, & Turner, 2011). Many psychologists have come to a consensus of it is the current definitive personality model as it is essentially correct in its representation of the structure of traits (McCrae & John, 1992).

Many studies have related personality to various real-life behaviours including Internet usage (Tan, & Yang, 2012), personality and privacy concerns (Sumner, Byers, & Shearing, 2011), movie preferences (Golbeck, & Norris, 2013) and a correlation between personality and job performance (Barrick, & Mount, 1991). These indicate that the personality model is beneficial in capturing the important aspects of an individual and its life dimension, thus triggering the interest of the computing community.

Since the last decades, social media has become a major communication tool of human beings. It consists of a group of internet-based applications which serves multiple purposes and is categorised into collaboration, social commerce, blog platforms, social networks and wikis (Kaplan, & Haenlein, 2010). It has been utilised as the platforms for creating and sharing of the users' generated contents. With hundreds of millions of people spending countless hours on social media to share, communicate, interact, and create data at an unprecedented rate, social media have become one unique source of big data (Zafarani et al., 2014). The useful knowledge extracted from big data may lead to a more confident decision making. This makes the social media mining become a popular field for research. Social media mining is the process of representing, analysing and extracting actionable patterns from social media data (Zafarani et al., 2014). However, it is complex to mine these social media data as they are noisy, free-format, of varying length and multimedia (Zafarani et al., 2014). Many different mining techniques have been proposed to mine these semi-structured data from social media including Naïve Bayes, classification trees, and association rules. Performance of each technique needs to be determined to ensure only the most accurate and meaningful data are extracted.

The aim of this paper is to develop a personality prediction model based on the Big Five model. To achieve this, 107 undergraduate students completed the Big Five Inventory (BFI) (John et al., 1991) and their profile data were extracted from Twitter. However, only 100 participants' data were qualified to be used in this research. The other seven participants' data were eliminated due to some reasons including unintentional repeated entry, missing Twitter account username, and unresponsive friend requests. Using the profile data as a feature set, we were able to train the data using implemented decision tree C4.5 algorithm to predict the students' personality traits. At this moment, our proposed model is only considering extraversion dimension due to the limitations associated to the integration with education-related decision-making system that is currently being developed by our team. Thus, each node on the decision tree represents the Twitter profile attributes and the personality dimension of extraversion. Finally, the evaluation on the precision of the proposed algorithm against other prediction algorithm is carried out.

## Personality Model

Personality indicates individual's preferences and may influence his/her decision making. Efforts were put in generating a descriptive personality model or taxonomy in which personality can be understood in a simpler way (John & Srivastava, 2008). Based on the lexical hypothesis, Allport and Odbert (1936) proposed that the most important individual differences are encoded in the language which represents the personality on a set of adjective terms. Then, Cattell (1943) used the Allport and Odbert's list and began the introduction of the Big Five model. Fiske (1949) constructed much simplified descriptions from Cattell's list of personality factors. To clarify these factors, Tupes and Christal (1961) found five relatively strong and recurrent factors, after doing an analysis of the correlation matrices from eight different samples. These factors eventually became known as the Big Five (Goldberg, 1981) which consists of five dimensions. After decades of intensive research, the psychologists reached the consensus on using the Big Five model with the five dimensions of personality trait to describe individual's personality. The Big Five personality traits are characterised by the following (John & Srivastava, 2008):

- Openness to experience: Intellectual, imaginative, and independent-minded.
- Conscientiousness: Orderly, responsible, and dependable.
- Extraversion: Talkative, assertive, and energetic.
- Agreeableness: Good-natured, cooperative, and trustful.
- Neuroticism: Moody, tense, neurotic, and, not confidence.

In the recent years, many previous works exist that infer users' personality from social media which studied the relations between individuals' personality and their interactions with the social media based on the Big Five model. Among social media sites, Twitter has become a popular social media for extracting data because it allows users to view anything about anybody even though they protect their tweets. The retweet feature in Twitter enables protected tweets to leak to the public by 'copy and paste' method of the text of protected tweets into other's own Twitter feed (Meeder et al., 2010). Due to this, even though one does not follow a specific protected tweet, he/she might somehow access the information later through the retweet feature. Literature shows that several studies extracted data from Twitter and used Twitter's feature set to study the relationship between personality and their interactions with this social site. For instance, Quercia et al. (2011) predicted the Big Five personality traits of Twitter users with the basic network properties such as followings, followers, and listed counts. Similarly, Golbeck et al. (2011a) also predicted personality using the profile data such as number of followers, number of followings, density of the social network, and number of hashtags. Lima and deCastro (2013) proposed a system to predict personality in tweets using linguistic information such as sentiment words, social processes, and family words. Celli and Rossi (2012) also correlated the Big Five personality trait of neuroticism and users' interactions in Twitter through the linguistic analysis of tweets. In addition, Sumner et al. (2012) predicted the dark triad personality from the Twitter profile attributes and the linguistic analysis of tweets. On the other hand, Gou, Zhou, and Yang (2014) automatically derived three types of personality traits from Twitter, including Big Five personality, basic human values, and fundamental needs based on individual's word choices

in written samples. Finally, Chen et al. (2015) demonstrated the Twitter's derived personality traits of openness and neuroticism for ad targeting using several features such as likelihood to click the link, follow the account, and a short written explanation for users' reported likelihoods.

Other than Twitter, researchers also employed Facebook data to infer individuals' personality. According to Quercia et al. (2011), Facebook differs from Twitter as it generally connects people who already know each other (e.g., friends, family, and co-workers); i.e. they need to be mutual friends on Facebook to fully share what they have been up to. However, they also mentioned that it is also possible to accurately predict individual's personality from information on Facebook even though the access is generally restricted. A study by Golbeck et al. (2011) predicted the Big Five personality traits of Facebook users based on several features such as structural features, personal information, activities and preferences, language features, and internal Facebook statistics. Using linguistic analysis, Sumner et al. (2011) studied the relationship between Facebook activity and personality traits, and they affirmed that there is a correlation between the two. Additionally, Alam, Stepanov and Riccardi (2013) employed bag-of-words approach and used tokens such as internet-slangs, smiles, and emoticons as features in classifying Facebook user's personality. In turn, in Celli and Polonio (2013), a Personality Recognition from Text (PRT) was presented to predict personality using the linguistic features in Mairesse et al. (2007). This work also addressed how users' personality determines their interaction and communication in Facebook. Besides Twitter and Facebook, Nie et al. (2014) used Sina Microblog and explored the unlabelled data to improve the prediction accuracy. The extracted features in their work were personal profile, social circles, social activities, and social habit.

There are several common algorithms that have been used by researchers for personality prediction. For example, M5' Rules has been used by Golbeck et al. (2011), Sumner et al. (2011), and Quercia et al. (2011), while Lima and deCastro (2013) and Sumner et al. (2012) adopted Naïve Bayes to automatically predict users' personality. Studies such as those by Golbeck et al. (2011, 2011a) and Sumner et al. (2011) applied Gaussian Processes to investigate the relationship between personality and their interactions with the social media. Golbeck et al. (2011a) also applied ZeroR in predicting Twitter users' personality. A recent work by Celli and Rossi (2012), and Celli and Polonio (2013) proposed a personality recognition algorithm from the linguistic analysis of tweets and texts to predict personality using the linguistic features in Mairesse et al. (2007). Meanwhile, Nie et al. (2014) adopted local linear semi-supervised regression algorithm for personality prediction. Chen et al. (2015) also utilised linear regression for predicting two dimensions of Big Five. Several classification methods including Sequential Minimal Optimisation (SMO), Bayesian Logistic Regression (BLR), and Multinomial Naïve Bayes (MNB) have been used by Alam et al. (2013) for automatic recognition of Big Five personality traits. Meanwhile, Gou et al. (2014) adopted lexicon-based approach for personality prediction and sharing preference of Twitter users. Finally, Sumner et al. (2012) also employed Sequential Minimal Optimisation (SMO), Random Forest, and J48 to predict the dark triad personality.

The most similar works with our current study are by Quercia et al. (2011), Golbeck et al. (2011a) and Sumner et al. (2012), but our work is focusing on predicting personality traits of Big Five model from students' social media. Additionally, in our work, we developed and



implemented C4.5 algorithm, whereas they performed classification using classifiers in WEKA (Hall, 2009). To the best of our knowledge, no study has been implementing C4.5 algorithm for personality prediction. Next, we present the process of automatic prediction of personality in the following section.

## METHOD

This paper focuses on an approach to automatically predict personality based on social media data. Decision tree C4.5 algorithm and Big Five model were used for personality classification. Data were collected from two main sources: i) Personality from BFI; and ii) Twitter. Figure 1 illustrates the overall processes involved in the students' personality prediction framework.

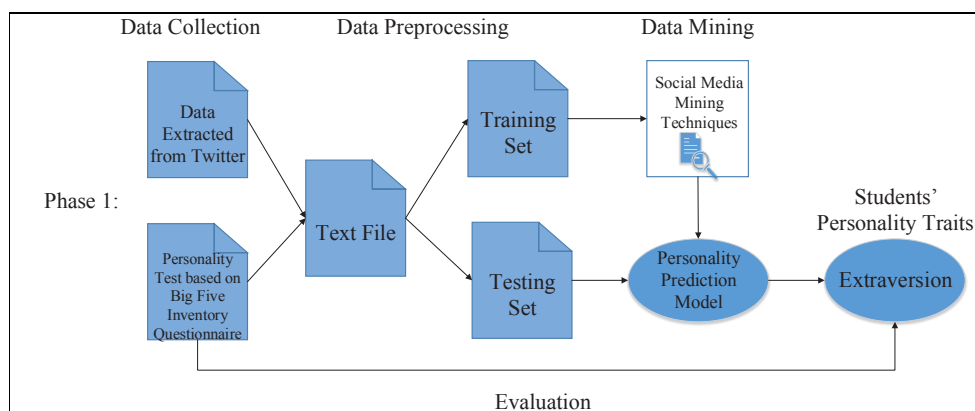


Figure 1. Framework of the student's personality prediction

A survey form was created using the Google Form and distributed online to undergraduate students through the Info Sharing Facebook Group. The survey form includes the BFI (John et al., 1991) questionnaire and their Twitter account username. As mentioned in the previous section, our research only focused on the trait of extraversion of Big Five model. Hence, only the eight questions regarding the trait of extraversion were adopted. The questionnaire begins with the statement, "I see myself as someone who...", and is followed with eight phrases representing the behaviours of respondents. The respondents rated each question on Likert scales of 1 to 5 representing the respondents' level of agreement to each phrase, where 1 indicates "Disagree Strongly" and 5 indicates "Agree Strongly". The eight phrases related to the trait of extraversion include:

- Is talkative
- Is reserved (R)
- Is full of energy
- Generates a lot of enthusiasm with
- Tends to be quiet (R)
- Has an assertive personality
- Is sometimes shy, inhibited (R)
- Is outgoing, sociable

Data extracted from Twitter consisted of Twitter profile attributes such as the number of followers, number of followings, number of tweets, number of lists and number of likes of students. These data were extracted using the Twitter Rest API, Tweepy (a Python library for accessing the Twitter API).

Data file from the survey forms were processed by filtering out those responses that did not provide Twitter account name and repeated responses were also eliminated. All the data were checked to ensure there were no missing values. If there was any, the default value was used to replace the missing value. The total score of eight questions from the BFI was summed up based on the respondents' ratings after appropriately reversing the scores of the questions that denoted with "R" (John et al., 1991), as shown above. For example, when a respondent rated the phrase "Is reserved" on scale of 5, this rating was inverted to 1 and vice versa; a respondent rated the phrase "Tends to be quiet" on the scale of 4, this rating was inverted to 2, and vice versa. The final score indicating the subject's trait of extraversion/introversion would then be manually calculated using the formula provided in John et al. (1991). The scores calculated indicate the student is extrovert if the score is above 50, and vice versa.

The Pearson correlation analysis was used to calculate the significant score between subjects' personality scores and each of the features obtained from analysing their tweets and public account data. Among the five features, the number of followers contributes the highest correlation value to the trait of extraversion (Pearson  $r = 0.422$ ,  $p < 0.05$ ), followed by the number of followings (Pearson  $r = 0.389$ ,  $p < 0.05$ ), number of lists (Pearson  $r = 0.326$ ,  $p < 0.05$ ) and number of tweets (Pearson  $r = 0.305$ ,  $p < 0.05$ ). Both number of followers and number of followings showed significant positive correlation to extraversion trait. These indicate that extraverts tend to be outgoing, sociable, and like to make more friends compared to those low in extraversion (introverts). In contrast, the number of favourites (number of likes) shows no significant linear correlation to the extraversion trait (Pearson  $r = 0.056$ ,  $p > 0.05$ ). As a result, only four features with the significant correlation (number of followers, number of followings, number of tweets and number of lists) were selected to classify the students' personality. Table 1 shows the correlation values between the profiles attribute features and the personality trait of extraversion. Correlations that are statistically significant for  $p < 0.05$  are bolded.

Out of 100 students' data, 70 of them were selected for the training set. In this training set, 37 subjects were with high level of extraversion, while 33 other subjects were with low level of extraversion (introversion). As for the testing set, there were 16 subjects with high level of extraversion and 14 subjects with low level of extraversion. The students' data were manipulated such as getting more responses and eliminating some responses to ensure the data set is relatively balanced between each class. Besides, the data for the training set were also chosen to ensure it is balanced between classes to avoid the problem of training biased toward one class which can lead to inaccurate classification.

Table 1  
*Correlation coefficient values between feature scores and trait of extraversion*

Personality Trait	Profile Attribute Sub-features	Correlation Coefficient
Extraversion	Number of followers	0.422
	Number of followings	0.389
	Number of tweets	0.305
	Number of lists	0.326
	Number of favorites	0.056

The calculated personality traits and data extracted from the Twitter were combined into a new CSV file. Next, the students' personality prediction model was constructed using the C4.5 algorithm, which was implemented in Java language using NetBeans IDE 8.1. The algorithm first read the input file and stored all the data into different variables. Table 2 shows the sample data file consisting of the training set which consists of the four aforementioned attributes and calculated poles (low/high) of extraversion dimension of each subject.

Table 2  
*Sample training set used to train students' personality prediction model*

No. of followers	No. of followings	No. of tweets	No. of lists	Class
349	173	20775	0	High
130	299	840	4	High
241	92	3172	6	High
571	327	7978	9	High
440	185	13899	2	High
155	129	633	0	High
123	123	709	1	High
36	78	1204	0	Low
19	13	133	0	Low
133	166	705	0	High

After all the data had been stored, the algorithm calculated the overall entropy of the training data set and the information gain of each and every attribute. Since the training set involved numerical data, in order to identify the information gain of an attribute, the algorithm identified all the splitting points of the attribute and then calculated the information gain for every split on each of the splitting points. Next, the splitting point with the highest information gain was selected as the splitting point and information gain of the attribute. After the splitting point and information gain of all the attributes had been identified, an attribute with the highest information gain was selected as the first node of the decision tree. These processes were then repeated for the left sub-tree of the first node followed by the right sub-tree of the first node until the decision tree was completely built. Figure 2 shows the decision tree generated from the implementation of the prediction model which represents the students' personality prediction

model. The constructed personality prediction model was then tested by the algorithm to read another file which consists of the test data set. At the end of the algorithm implementation, personality traits of the test data were successfully predicted.

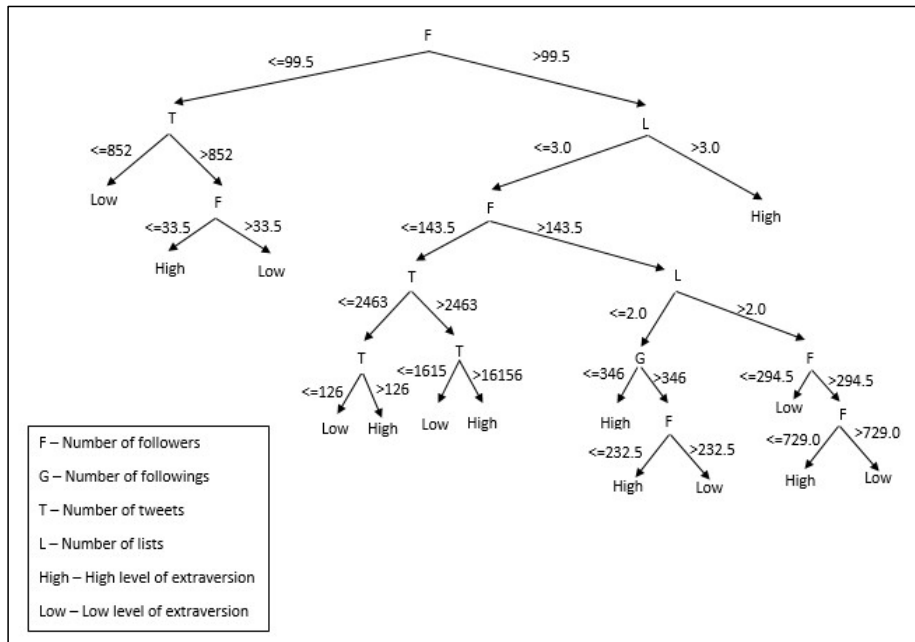


Figure 2. The decision tree generated from the students' personality prediction model

## RESULTS AND DISCUSSION

The accuracy and weighted F-measure value of various classifiers in predicting the students' personality trait of extraversion are shown in Table 3. From the table, we see that the ZeroR algorithm as the baseline produced a moderate accuracy at 53.33% with a quite low weighted average F-measure value of 0.371. Both J48 classifier implementation in WEKA and C4.5 algorithm implemented in this research produced higher accuracy and weighted average F-measure value above the baseline. The J48 classifier has better performance with higher accuracy of 86.67% with weighted average F-measure value of 0.865 as compared to the C4.5 algorithm which has generated prediction result with 73.33% of accuracy and weighted average F-measure value of 0.733.

As shown in Table 3, the implemented C4.5 algorithm achieved a lower accuracy and weighted average F-measure value than the J48 classifier implemented in WEKA machine learning toolkit. The result is due to the use of unpruning method in the implementation of C4.5 algorithm. The tree generated from the C4.5 implementation is not pruned and it causes a problem called overfitting, which may led to a less accurate personality and learning style classification. This may affect the accuracy of results (Patil et al., 2010). In contrast, tree pruning used in J48 classifier, which converts a large tree into smaller tree and has eliminated those meaningless rules, generally results in faster and more accurate classification (Patil et al., 2010).

Table 3  
*Classification results comparison in predicting personality trait of extraversion*

Algorithm	ZeroR* in WEKA	J48 in WEKA	C4.5 algorithm implemented in this research
Accuracy (%)	53.33	86.67 (v)	73.33
Weighted Average F-measure	0.371	0.865 (v)	0.733

*Remark 1.* \*. Baseline

*Remark 2.* v. Victory (Significant above baseline at  $p < 0.05$ )

Based on the results, it was found that personality trait of extraversion is positively correlated with most of the Twitter profile attributes, except the number of favorites (number of likes) with the weakest linear relationship (refer Table 1). The findings are similar to the results generated from the work by Sumner et al. (2012), which showed that followers, friends (followings), number of tweets, and number of lists are significantly correlated to extraversion, while the number of favourites did not show significant relationship. Both our study and Sumner et al.'s (2012) showed that the number of followers has the highest correlation coefficient to the extraversion trait compared to other profile features. Additionally, Quercia et al. (2011) also found that the listeners (those who follow many users) and popular (those who are followed by many) users have the strongest and significant correlations with the personality trait of extraversion. Therefore, it supports the inference that extroverts have many people following them. In the same paper, they explained that the personality trait of extraversion is the predictor for number of friends in the real world and social network. Finally, the work by Golbeck et al. (2011a) also suggested that extroverts who are outgoing and sociable tend to have more friends. Hence, the results from this research are consistent with those observed from the previous studies.

In terms of evaluation, it is difficult to compare and critically evaluate the practical performance and precision of the aforementioned studies due to the use of different evaluation methods. While Quercia et al. (2011) applied the Root Mean Square Error (RMSE) to measure the performance of their work, Golbeck et al. (2011a) employed the Mean Absolute Error (MAE) in their study. In contrast, according to Sumner et al. (2012), evaluation methods such as MAE and RMSE can mask larger errors at the extremes of a unimodal population distribution by predicting the majority of instances around the mean value. This means that, for instance, the model may predict a high extraversion as a low introversion without significantly affecting the overall MAE. Due to this reason, they adopted several evaluation criteria such as Accuracy (Acc) for both the maximum Geometric and Arithmetic means and were presented in both median split and 90th percentile split classification. In conclusion, due to the fact that each error measure has weaknesses that can produce inaccurate evaluation of the predicting results, it is impossible for the researchers to choose only one measure (Mahmoud, 1984).

## CONCLUSION AND FUTURE WORK

This study has resulted in one main insight, i.e. it is possible to predict students' personality trait from the public information they share on Twitter. The finding shows that J48 performs

better than C4.5 because of the use of unpruning method in the implementation of C4.5 algorithm. As discussed earlier, there are many previous studies working on the algorithms to automatically predict personality using social media data. Regardless of this, we have found an opportunity to explore C4.5 algorithm in the automatic personality prediction. However, the current work does not consider all the dimensions of the Big Five model. The ongoing works aim at resolving the issues with the other dimensions of the Big Five model. Other algorithms are also ventured on for personality prediction to improve accuracy. In addition, although the proposed work has been tested for a maximum of 100 students, further work must consider more participants so as to provide a more accurate representation of the entire population. With the ability to infer a student's personality trait, currently we are integrating personality with education-related decision making such as predicting students' learning styles and suggesting teaching strategies that are tailored to suit their learning styles.

## REFERENCES

- Ahmad, Z. I. (2015). *Prediction Models of Extraversion and Neuroticism of Malaysian Facebook Users*. Masters Thesis, School of Computer Sciences, Universiti Sains Malaysia, Penang, Malaysia.
- Alam, F., Stepanov, E. A., & Riccardi, G. (2013). Personality Traits Recognition on Social Network – Facebook. *Computational Personality Recognition*, 6-9.
- Allport, G. W., & Odbert, H. S. (1936). Trait-names: A psycho-lexical study. *Psychological Monographs*, 47, 1-178.
- Barrick, M. R., & Mount, M. K. (1991). The Big Five Personality Dimensions and Job Performance: A Meta-Analysis. *Personnel Psychology*, 44, 1-26.
- Bishop-Clark, C., & Wheeler, D. D. (1994). The Myers-Briggs Personality Type and Its Relationship to Computer Programming. *Journal of Research on Computing in Education*, 26(3), 358-369.
- Cattell, R. B. (1943). The description of personality: Basic traits resolved into clusters. *Journal of Abnormal and Social Psychology*, 38, 476-506.
- Celli F., & Rossi, L. (2012). The Role of Emotional Stability in Twitter Conversation. *Proceedings of the 13<sup>th</sup> Conference of the European Chapter of the Association for Computational Linguistics*. Avignon, France, 10-17.
- Celli, F., & Polonio, L. (2013). Relationships between Personality and Interactions in Facebook. *Social Networking: Recent Trends, Emerging Issues and Future Outlook*, 41-53.
- Chen, J., Haber, E., Kang, R., Hsieh, G., & Mahmud, J. (2015). Making Use of Derived Personality: The Case of Social Media Ad Targeting. *Proceedings of the Ninth International AAAI Conference on Web and Social Media*, 1-10.
- Fiske, D. W. (1949). Consistency of the factorial structures of personality ratings from different sources. *Journal of Abnormal and Social Psychology*, 44, 329-344.
- Golbeck, J., & Norris, E. (2013). Personality, Movie Preferences, and Recommendations. *Proceedings of the 2013 IEEE/ACM International Conference on Advances in Social Networks Analysis and Mining*, Niagara, Ontario, Canada, 1414-1415.

- Golbeck, J., Robles, C., & Turner, K. (2011). Predicting personality with social media. *Proceedings of the 2011 Annual Conference Extended Abstracts on Human Factors in Computing System*. Vancouver, BC, Canada, 253-262.
- Golbeck, J., Robles, C., Edmondson, M., & Turner, K. (2011a). Predicting Personality from Twitter. *Proceedings of the IEEE International Conference of Privacy, Security, Risk, and Trust, and IEEE International Conference on Social Computing*, 149-156.
- Goldberg, L. R. (1981). Language and individual differences: The search for universals in personality lexicons. In L. Wheeler (Ed.), *Review of personality and social psychology 2* (pp. 141-165). Beverly Hills, CA: Sage.
- Gou, L., Zhou, M., & Yang, H. (2014). KnowMe and ShareMe: Understanding automatically discovered personality traits from social media and user sharing preferences. *CHI 2014*. Toronto, ON, Canada, 955-964.
- Hall, M., Frank, E., Holmes, G., Pfahringer, B., Reutemann, P., & Witten, I. (2009). The WEKA data mining software: An update. *ACM SIGKDD Explorations Newsletter*, 11(1), 10–18.
- John, O. P., & Srivastava, S. (2008). The Big-Five Trait Taxonomy: History, Measurement, and Theoretical Perspectives. In L. A. Pervin & O. P. John (Eds.), *Handbook of personality: Theory and research 2* (pp. 102–138). Guilford Press, New York.
- John, O. P., Donahue, E. M., & Kentle, R. L. (1991). *The Big Five Inventory--Versions 4a and 54*. Berkeley, CA: University of California, Berkeley, Institute of Personality and Social Research.
- John, O. P., Naumann, L. P., & Soto, C. J. (2008). Paradigm shift to the integrative Big Five trait taxonomy: History, measurement, and conceptual issues. In O. P. John, R. W. Robins, & L. A. Pervin (Eds.), *Handbook of personality: Theory and research 2* (pp. 114-158). Guilford Press, New York.
- Kaplan, A. M., & Haenlein, M. (2010). Users of the world, unite! The challenges and opportunities of Social Media. *Business Horizons*, 53, 59–68.
- Lima, A. C. E. S., & deCastro, L. N. (2013). Multi-Label Semi-Supervised Classification Applied to Personality Prediction in Tweets. *Proceedings of the BRICS Congress on Computational Intelligence & 11<sup>th</sup> Brazilian Congress on Computational Intelligence*. Recife, Brazil, 195-203.
- Mahmoud, E. (1984). Accuracy in forecasting: A survey. *Journal of Forecasting*, 3(2), 139-159.
- Mairesse, F., Walker, M. A., Mehl, M. R., & Moore, R. K. (2007). Using Linguistic Cues for the Automation Recognition of Personality in Conversation and Text. *Journal of Artificial Intelligence Research*, 30, 457-500.
- McCrae, R. R., & John, O. P. (1992). An Introduction to the five-factor model and its applications. *Journal of Personality*, 60, 175-215.
- Meeder, B., Tam, J., Kelley, P., & Cranor, L. F. (2010). RT@ IWantPrivacy: Widespread Violation of Privacy Settings in the Twitter Social Network. *Proceedings of the Web 2.0 Privacy and Security Workshop co-located with IEEE Symposium on Security and Privacy*, 285-299.
- Nie, D., Guan, Z., Hao, B., Bai, S., & Zhu, T. (2014). Predicting Personality on Social Media with Semi-supervised Learning. *Proceedings of the International Joint Conferences on Web Intelligence (WI) and Intelligent Agent Technologies (IAT)*. Warsaw, Poland, 158-165.

- Patil, D. D., Wadhai, V. M., & Gokhale, J. A. (2010). Evaluation of Decision Tree Pruning Algorithms for Complexity and Classification Accuracy. *International Journal of Computer Applications*, 11(2), 23-30.
- Quercia, D., Kosinski, M., Stillwell, D., & Crowcroft, J. (2011). Our Twitter Profiles, Our Selves: Predicting Personality with Twitter. *Proceedings of the IEEE International Conference on Privacy, Security, Risk, and Trust, and IEEE International Conference on Social Computing*, 180-185, IEEE Press, Boston.
- Sumner, C., Byers, A., & Shearing, M. (2011). Determining personality traits & privacy concerns from Facebook activity. *In Black Hat Briefings*, Abu Dhabi, United Arab Emirates, 1-29.
- Sumner, C., Byers, A., Boochever, R., & Park, G. J. (2012). Predicting Dark Triad Personality Traits from Twitter usage and a linguistic analysis of Tweets. *Proceedings of the 11<sup>th</sup> IEEE International Conference on Machine Learning and Applications*, 386-393.
- Tan, W. -K., & Yang, C. -Y. (2012). Personality Trait Predictors of Usage of Internet Services. *Proceedings of the 2012 International Conference on Economics, Business Innovation*. Kuala Lumpur, Malaysia, 185-190.
- The Myers & Briggs Foundation. (2016). MBTI® Basics. Retrieved from <http://www.myersbriggs.org/my-mbti-personality-type/mbti-basics/>
- Tupes, E. C., & Christal, R. C. (1961). Recurrent personality factors based on trait ratings. Technical Report, USAF, Lackland Air Force Base, TX.
- Zafarani, R., Abbasi, M. A., & Liu, H. (2014). *Social Media Mining: An Introduction* (Draft version). Cambridge University Press. Retrieved from <http://dmml.asu.edu/smm>



## **Implementation of a Fuzzy-Based Line Follower Robot using Arduino**

**Mohammad Safwan Mohamed Alias, Ya'akob Yusof\* and Nurul Muthmainnah Mohd Noor**

*Faculty of Mechanical Engineering, Universiti Teknologi MARA (UiTM), 40450 Shah Alam, Selangor, Malaysia*

### **ABSTRACT**

Applying an intelligent system means the machine is capable of making its own unique decision. Fuzzy logic is a form of logic that acknowledges other forms of true and false values. With fuzzy logic, propositions may be diagrammatic with degrees of truthfulness and falsehood. The main aims of this study are to demonstrate the method to apply fuzzy logic in a structure that uses Arduino as its brain, and apply it in a line follower mobile robot's decision making algorithm. This mobile robot consists of two front wheels and a nub caster at the back. It uses a line follower array that consists of eight infrared (IR) sensors. The system control is based on the input from IR sensors, which measures the intensity of light reflected by the track. Data were then transmitted to the microcontroller and will then be sent the correct command to the motor driver so that the trail can be followed. The performance of the line follower robot when using the fuzzy logic algorithm was compared to the line follower algorithm, which uses simple if-else commands. Analysis is primarily on the time taken to complete the track, along with the behaviour of the robot while manoeuvring. From the results, fuzzy logic is shown to provide a better performance in terms of the time taken to complete the track compared to the other set of rules. In addition, from the video recordings, fuzzys are moving smoother as compared to the non-fuzzy logics.

*Keywords:* Arduino, Fuzzy Inference System, fuzzy logic, line follower robot, Matlab

### **ARTICLE INFO**

*Article history:*

Received: 25 October 2016

Accepted: 17 March 2017

*E-mail addresses:*

[mohdsafwan\\_mohd@yahoo.com](mailto:mohdsafwan_mohd@yahoo.com)

(Mohammad Safwan Mohamed Alias),

[yaakob2241@salam.uitm.edu.my](mailto:yaakob2241@salam.uitm.edu.my) (Ya'akob Yusof),

[muthmainnah@salam.uitm.edu.my](mailto:muthmainnah@salam.uitm.edu.my)

(Nurul Muthmainnah Mohd Noor)

\*Corresponding Author

### **INTRODUCTION**

Robots are electromechanical machines that having ability to perform tasks or actions based on electronic programming. Line follower robots are one type of mobile robots that is able to detect and follow a track drawn on the floor even when the path is altered by changing the shape of the line. The path can be a visible black line on a white background, or vice versa.

The forward movement of a line follower robot involves both motor turns on and rotates simultaneously. To move to the left, the right motor is turned on and left motor is turned off, and to move to the right, right motor is turned off and left motor is turned on. It can also move faster when one motor rotates forward while the other one rotates backward. When applying the fuzzy logic, the time to make decision whether to turn left or right is much shorter and the movement will become smoother compared to the algorithms without the fuzzy logic.

This paper discusses the design of a line follower robot operation based on fuzzy logic controller and without fuzzy logic controller. The fuzzy logic algorithm was applied in a Matlab's Toolbox, Fuzzy Inference System (FIS) software using single input, two output options. The input is the difference in the readings between eight IR sensors set in front, while the outputs are the speed for the right and left motors.

## **METHOD**

The line follower robots have few major parts, namely the microcontroller, motor driver, IR sensors, actuators and its chassis or body structure.

The microcontroller is programmed to create a mechanism for move forward, turn right or turn left based on the input returning from the sensor or comparator. When using Arduino, a comparator is not needed. The outputs of the microcontroller are fed to the motor driver.

For this study, the microcontroller used is Arduino Uno. An Arduino is one of the simplest and most easy-to-use microcontrollers available. Arduino comes with an IDE that helps to burn programming code onto the microcontroller from a computer. It is open supply and extensive documentation could be easily obtained online.

A robot needs a driver for controlling and generating power to the motor. In general, the microcontroller sends instructions to the driver after processing data from sensors and the driver transmits voltage to the motor according to the inputs (Hasan et al., 2013; Pakdaman, Sanaatiyan, & Ghahroudi, 2010). The suitable motor driver for this study is IC L298 because it is be used to control two motor (Pakdaman & Sanaatiyan, 2009).

Arduino Motor Shield which is based on the L298 was used. Two DC motors could be driven, where the speed and direction of each motor could be controlled independently. The shield is TinkerKit compatible, which means that an electronic project could be created quickly by plugging TinkerKit modules to the board.

In terms of the sensor, the most suitable type is Infrared (IR) sensor. The reasons include ease of implementation, low cost, and availability (Pakdaman, Sanaatiyan, & Ghahroudi, 2010). IR sensor is used to detect white and black surfaces. White surfaces generally reflect well, while black surfaces reflect poorly.

In the designed robot, it is decided to use an IR array that consists of eight IR sensors. The configuration of IR sensors is in-line because it gives advantage at sensing, and responding to the turns in an easy course with wide turns. It is also easy to install. Its main shortcoming is its poor in sensing capability at a greater than 90 degree turn, thus the track must avoid this.

For the movement of the line follower robot, wheels system is used. The designed mechanism used 2 DC motors because DC motors can rotate and initiate both forward and backward movement, depending on the direction of the applied current. The DC motors come with a good speed ratings and generate enough torque for the robot.

Chassis is the main supporting structure of a robot, where all the components are attached to it. Therefore, it needs sufficiently large and sturdy structure to cope with the weight of the component. There are some good materials that can be used for designing robot such as wood, plastic, aluminium and brass alloy. Thus, it was decided to use the shadow chassis, in which the chassis plates and mounts are cut from ABS plastic and the hub patterns are utilised for sensors, controllers and power. All of the components and hardware for the line follower robot are assembled, as shown in Figure 1.



Figure 1. The line follower robot

The track is shown in Figure 2. A track is a path for the line follower robot to follow. The result, which is the time taken for the robot to complete the track as well as its behaviour, is used in analysing the robot performance. An example of a simple track is either a round or rectangle shape track. While for the advanced track, there should be more intersections and corners.



Figure 2. Track

### Fuzzy Logic Controller

Figure 3 and Figure 4 show the process flowchart of the line follower robot, with and without fuzzy logic, respectively. The algorithm for this line follower robot consists of a single input and two outputs. The different value of eight IR sensors is served as the input to both algorithms. For without fuzzy, it is a simple if-else algorithm which make the robot to go left if it is too much towards the right, and vice versa. It did not have crisps value consideration and sense of motor speed. For fuzzy logic, the output of the scheme, which is acquired from the fuzzification of each input and output using the associated membership functions, will control the speed of the right and left DC motors.

For the fuzzy logic programming, Matlab's Fuzzy Logic Toolbox™ has been used to design the FIS or fuzzy logic controller, before it is embedded into the microcontroller, the Arduino UNO. The toolbox provides functions that allow the user to analyse, simulate and design the systems based on fuzzy logic.

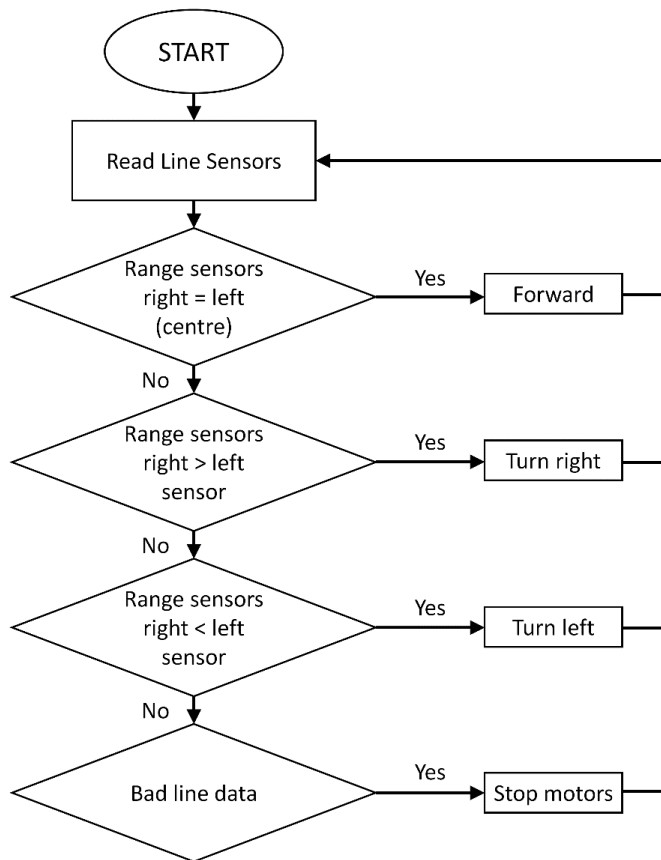


Figure 3. Flowchart for line follower robot (without fuzzy)

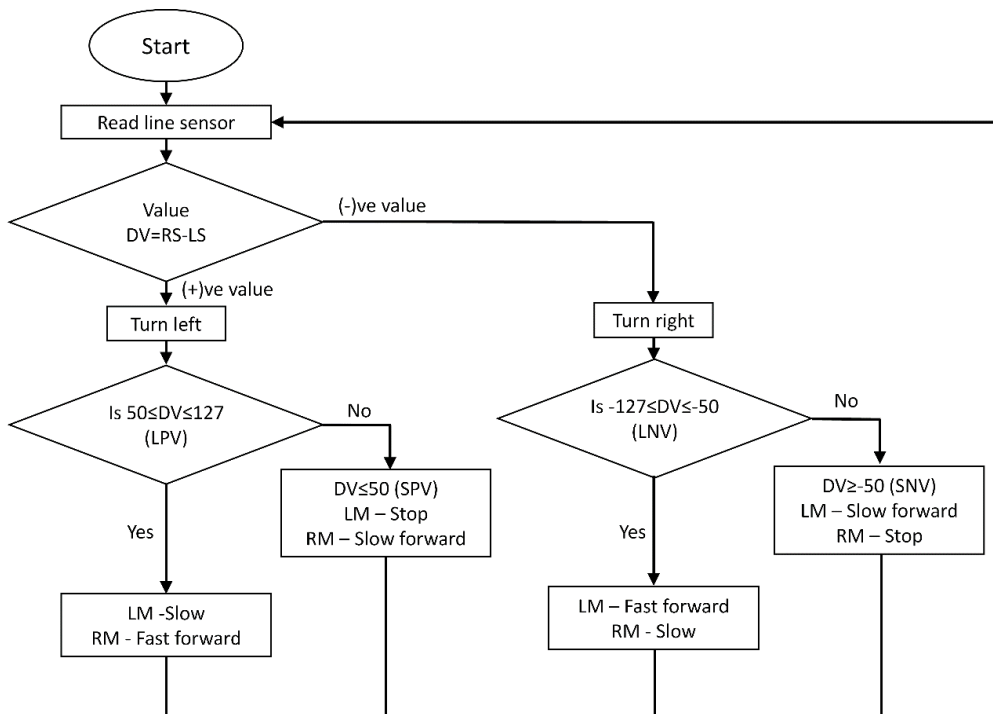


Figure 4. Flowchart for line follower robot with fuzzy logic's algorithm. The basis of this algorithm was taken from Farooq et al. (2014)

In general, a fuzzy logic controller consists of fuzzification, fuzzy rule base and defuzzification process. Fuzzification process is a process that converts crisp input value into a fuzzy value. A single input, which is the difference value between the eight IR sensors (DV), is termed by four fuzzy set. The DV ranges from -127 to +127. The terms of the fuzzy sets are presented in Table 1, while the membership functions for the input, DV, is described in Figure 3 and the following equations.

Table 1  
Fuzzy set for input of the line follower robot

Fuzzy set	Description
LPV	DV has large positive value
SPV	DV has small positive value
LNV	DV has large negative value
SNV	DV has small negative value

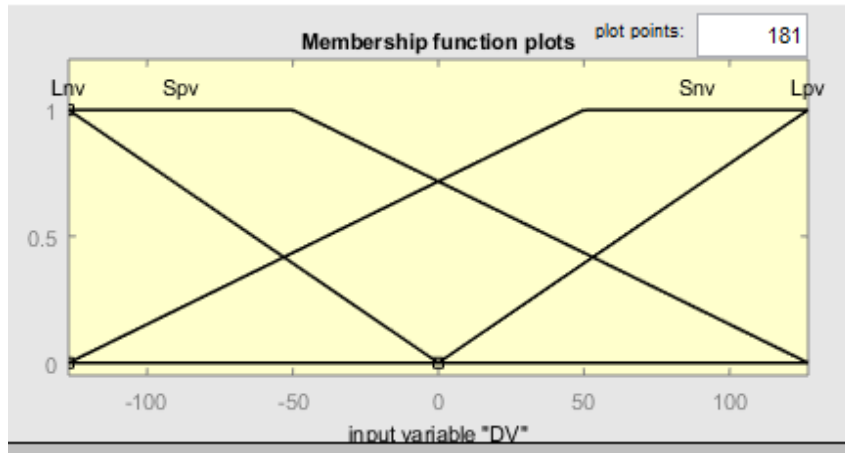


Figure 5. Membership function plot for the input (DV)

$$\mu_{DV,LPV} = \begin{cases} 0, & -127 \leq x \leq 0 \\ 0.79d_v, & 0 \leq x \leq 127 \end{cases} \quad (1)$$

$$\mu_{DV,SPV} = \begin{cases} 100, & -127 \leq x \leq -50 \\ -0.64d_v + 80.8, & -50 \leq x \leq 127 \end{cases} \quad (2)$$

$$\mu_{DV,LNV} = \begin{cases} 0.79d_v, & -127 \leq x \leq 0 \\ 0, & 0 \leq x \leq 127 \end{cases} \quad (3)$$

$$\mu_{DV,SNV} = \begin{cases} -0.64d_v + 80.8, & -127 \leq x \leq 50 \\ 0, & 50 \leq x \leq 127 \end{cases} \quad (4)$$

Over these expressions, the triangular (trimf) and trapezoidal (trapmf) membership functions were used because of their simplicity to implement and fast for computation (Farooq et al., 2014).

The output of the fuzzy controller is on the right (RM) and on the left (LM) are motor speeds, which are expressed by slow and fast fuzzy sets. Slow is the minimum (0%), while speed is the maximum (100%) speed of the DC motor. The terms of the fuzzy sets are presented in Table 2. Membership functions for both the LM and RM outputs are shown in Figure 4 and the expressions below.

Table 2  
Fuzzy set for output of a line follower robot

Fuzzy set	Description
Slow	One or both motors' speed are slow
Fast	One or both motors' speed are high

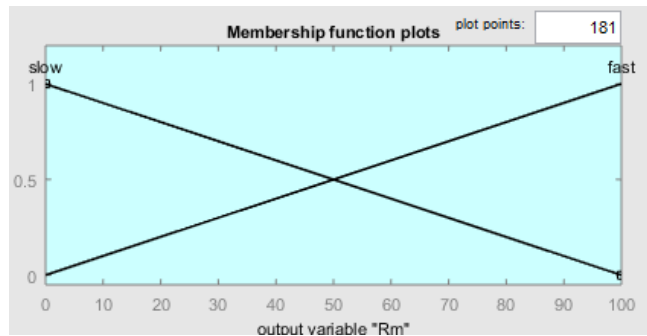


Figure 6. Membership function plot for output (RM/LM)

$$\mu_{LM,slow} = -l_m + 100, \quad 0 \leq l_m \leq 100 \quad [6]$$

In this study, the microcontroller defines the rules to control the speed of both motors to attain preferred navigation for robot. The rule-base created for the correlation between sensor values and the speed of both motors is shown in Table 3.

Table 3  
Fuzzy rule-base for the input and outputs

Output	Right Motor (RM)	Left Motor (LM)
Input		
Small negative value (SNV)	Fast	Fast
Large negative value (LNV)	Slow	Fast
Small positive value (SPV)	Fast	Fast
Large positive value (LPV)	Fast	Slow

Based on rule 1, for instance, if the sensor detects black line with small negative value, the robot will move fast forward. Rule 2 describes the situation when the robot gets diverged from the track largely in the left direction. In this situation, the robot will turn to the right to keep the robot on the track by spinning the right motor slowly and the left motor faster than the right motor.

The control output obtained from the combination of input, output membership functions, and fuzzy rules remains an imprecise or fuzzy element; and this method is known as fuzzy inference. To create fuzzy output accessible for real applications, a defuzzification method is required. The defuzzification method is supposed to convert the fuzzy output to the crisp output.

Commonly used techniques for the defuzzification method are the Mean of Maximum method, Centre of Gravity method and the Height method. The technique used in this study

is the centre of gravity method (COA). The formula for calculating the COA method can be described as:

$$Z_o = \frac{\sum_{i=1}^n Z_i \mu_{out}(Z_i)}{\sum_{i=1}^n \mu_{out}(Z_i)} \quad (7)$$

Where  $\mu_{out}(Z_i)$  is the  $i=1, 2, \dots, n$  sampled values of the gathered the output membership function and  $Z_o$  is the crisp output that described the duty cycle for PWM signal speed for the motor (Farooq et al., 2014).

### RESULTS AND DISCUSSION

The results show the performance of the line follower robot when using the fuzzy logic algorithm and the common if-else commands. Based on Figure 5, situation (a) is when the input value is large positive value, thus the output values shows RM is higher than LM. It means that the robot movement is to the left. While in situation (b), the value of LM is higher than RM. That shows, the movement robot is now in right turn.

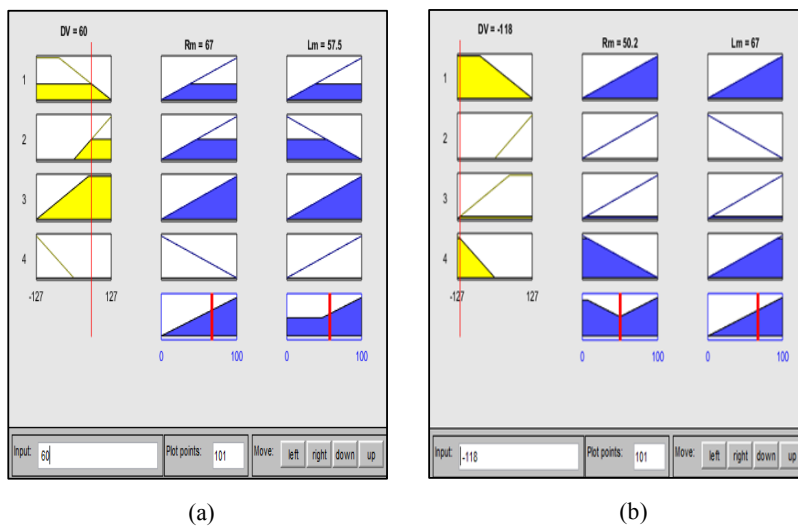


Figure 7. The rule view of the input and outputs membership function when the input was set to: (a) 60; and (b) -118 input value

Table 4  
Experimental results and observations

Criteria	Without Fuzzy Logic	With Fuzzy Logic
Average time for one complete cycle	33.8s	26.8s
Average speed for one complete cycle	4.93m/s	6.21m/s
Average time to complete five full cycles	169.1s	134.3s
Line tracking movement	Uneven, especially at corners	Smooth
Tendency to move out from track	Low	Low



The results presented are the average performance from the conducted tests. Due to the algorithm, the robot with fuzzy logic performs better than the one without fuzzy, as expected. In terms of the speed, the fuzzy's robot takes about 21% faster to complete the same track compared to the other. This is mainly due to the crisps' value considerations in the programming, as well as the speed adjustment features in the programming. It also tracks the line smoothly as compared to without fuzzy, especially when approaching corners. With the application and implementation of the fuzzy logic algorithm, it gives more advantages and benefits to the robot.

However, there are a few observations that need to be highlighted. Among other is the robot's tendency to move away far from the track, which is stated as low. This is due to the nature of the track used, which does not have sharp turns. This is because the study intends to merely demonstrate the difference between fuzzy and non-fuzzy approach. If the track consists of sharp turns, the programming will need to be improved, especially on controlling the speed of the motor.

## CONCLUSION

This paper presents an analysis of a simple line follower system, with and without fuzzy logic algorithm implemented in its brain using Arduino as its microcontroller. Both the systems were compared to illustrate which one would give a better performance in terms of the time taken to complete the track, as well as the movement of the robot. From the results, it is clear that the line follower with fuzzy logic gives a better performance compared to without fuzzy, both in terms of the time taken to complete the track and behaviour of the robot during the test.

For future experiments, it is important to improve the ability of the robot especially in taking sharp corners. In improving that ability, the algorithm will need to be improved, especially in defining the speed of the car during motion. In addition, this Matlab's FIS system is also possible to be applied in other applications such as autonomous mobile robot, autonomous vacuum cleaner and other systems.

## REFERENCES

- Farooq, U., Amar, M., Asad, M. U., Abbas, G., & Hanif, A. (2014). Fuzzy logic reasoning system for line following robot. *International Journal of Engineering and Technology*, 6(4), 244.
- Hasan, K. M., Al-Nahid, A., Reza, K. J., Khatun, S., & Basar, M. R. (2013, April). Sensor based autonomous color line follower robot with obstacle avoidance. In *Business Engineering and Industrial Applications Colloquium (BEIAC), 2013 IEEE* (pp. 598-603). IEEE.
- Pakdamani, M., & Sanaatiyan, M. M. (2009, December). Design and implementation of line follower robot. In *Computer and Electrical Engineering, 2009. ICCEE'09. Second International Conference on* (Vol. 2, pp. 585-590). IEEE.
- Pakdamani, M., Sanaatiyan, M. M., & Ghahroudi, M. R. (2010, February). A line follower robot from design to implementation: Technical issues and problems. In *Computer and Automation Engineering (ICCAE), 2010 The 2<sup>nd</sup> International Conference on* (Vol. 1, pp. 5-9). IEEE.
- Sanaatiyan, M. M. & Ghahroudi, M. R. (2010). A Line Follower Robot from design to Implementation. *Technical Issues and Problems*, 1, 5-9.



## Ziegler-Nichols First Tuning Method for Air Blower PT326

Mahanijah Md Kamal\* and Muhammad Hanihazaim Abd Halim

Faculty of Electrical Engineering, Universiti Teknologi MARA (UiTM), 40450 Shah Alam, Selangor, Malaysia

### ABSTRACT

In this work, two types of controller were designed for the nonlinear air blower system PT326 used at the Instrumentation Laboratory Faculty Electrical Engineering, UiTM, Shah Alam. This work began with collection of data from the experimental work. Once the S-shape of the system response was obtained, the procedure of getting the process dead time,  $\tau_D$  and time constant  $\tau_C$  was applied to the S-shape form. By determining these two values, the optimum values of PI and PID controllers can be calculated. From the acquired data, the simulation model was developed in MATLAB/Simulink R2013a software using the transfer function obtained from the open-loop control system. The modelling system is based on the transfer function of open-loop air blower system PT326 before the design state of finding a suitable controller can be suggested. The controller design of PI and PID was obtained using the first method Ziegler-Nichols tuning rules. The result from the simulation shows that the Ziegler-Nichols first tuning rules can be applied in designing the PI and PID controller based on S-shape response obtained in open-loop test.

*Keywords:* Air blower PT326, PI, PID, Ziegler-Nichols first method

### INTRODUCTION

Proportional-Integral-Derivative (PID) controllers are the most adopted controllers in industry due to good cost and benefit

ratio they are able to provide (Antonio, 2004). On the other hand, PID (Ziegler & Nichols, 1942; Nims, 1950; Chien, Hrones, & Reswick, 1972) control algorithm is still continued to be widely used for most industrial control systems mainly because it is simple to maintain and tune. The PID controllers are still widely used in the process industries even though control theory has been developed significantly since they were first used decades ago (Zhuang & Atherton, 1993). In the process industries, temperature control plays an important role in order to produce

#### ARTICLE INFO

##### Article history:

Received: 25 October 2016

Accepted: 17 March 2017

##### E-mail addresses:

mahanijah@jieee.org (Mahanijah Md Kamal),  
hanihazaimwork92@gmail.com

(Muhammad Hanihazaim Abd Halim)

\*Corresponding Author

good quality end products. The temperature control of different systems is required and the rates of reaction are controlled by heating and cooling the reactants. Lu and Tsai (2001) stated that in the plastic injection moulding process, the temperature in each temperature zone must be appropriately set and precisely controlled.

According to Zhuang and Atherton (1993), and Astrom and Hagglund (1994), in 1942 Ziegler-Nichols presented a tuning formula based on time response and open-loop response rate of the system. The most frequently used experimental methods the Ziegler-Nichols open-loop and closed-loop design methods. In this work, the first method of Ziegler-Nichols was used to monitor the performance of the air blower system PT326. Open-loop process identification is the most common method used to obtain the information of the process dead time and also the process response rate. Normally, the system response is in the form of S-shape by drawing a tangent line on the response curve, where the optimum values of PID controller can be attained. Nowadays, there are a lot of publications on the tangent technique and the PID controller tuning. The analysis of open-loop response using the concept of S-shape or tangent method was reformulated by Ishak and Hussain (1998) who came out with a new algorithm that offers easier and faster calculation on the process response. Further experimental study was also conducted by Ishak and Hussain (1998) who designed a PID controller to control a flow of water to verify their proposed technique. Later, the concept of open-loop response was implemented on a PID controller tuning using Ziegler-Nichols by Kamaruddin et al. (2009) for a glycerine bleaching process, whereas Hambali et al. (2012, 2013, 2014) used the Ziegler-Nichols technique for flow, temperature and also pressure based on the tangent method for various PID tuning rules. PID controller using Ziegler-Nichols and Modified Ziegler-Nichols was designed to analyse the performance of speed control of DC motor (Meshram & Kanojiya, 2012). Mathematical model of the PT326, based on harmony search algorithm and Lyapunov using adaptive fuzzy controller, was studied by Sharma, Chatterjee, and Rakshit (2014) to identify and approximate the system behaviour to a first order with a delay.

PT326 is a self-contained process and control equipment with the basic characteristics of large plant with transfer lag, system response, enable distance/velocity lag and proportional control. It models common industrial situations in which temperature control is required. The process contained in PT326 involves air that is drawn from the atmosphere by a centrifugal blower, and is heated as it passes over a heater grid before being released into the atmosphere through a duct (Alsofyani, Rahmati, & Anbaran, 2014). Figure 1 shows the methodology process of Ziegler-Nichols first tuning method proposed in this work.

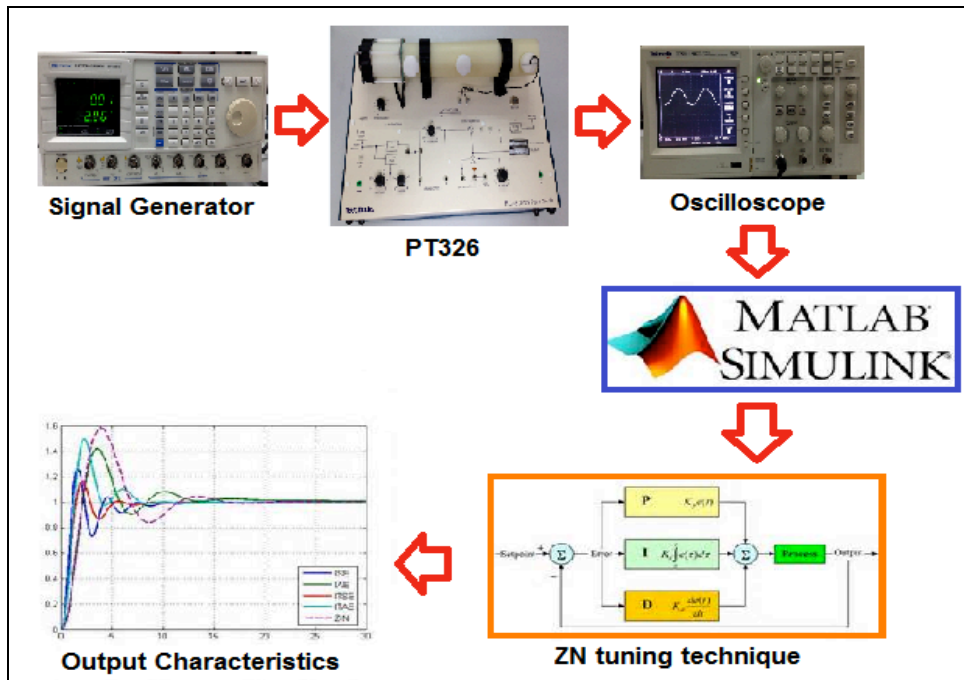


Figure 1. The methodology process

Hence, the objective of this work is to design a suitable closed-loop controller for air blower system PT326 where a model system of PT326 has been developed. The design of PI and PID controller based on Ziegler-Nichols first method was simulated in MATLAB/Simulink R2013a environment. Observation was made to monitor the response of both in order to determine the most suitable controller for air blower process PT326.

## METHOD

In this equipment, air drawn from atmosphere by a centrifugal blower is driven past a heater grid and through a length of tubing to atmosphere again. The air steam velocity may be adjusted by means of an inlet throttle attached to the blower (Rahmat, Hoe, Usman, & Wahab, 2005). Process trainer PT326 is used as an example of industrial process because of the simplicity on temperature process operation. This is a teaching aid for control system laboratories that illustrates pure time delay added to a system with first order dynamics (Dadone & Landingham, 2001). This mimics the actual industrial process that utilises the temperature parameter as the control element, where the temperature of the air blower system is maintained at a certain level.

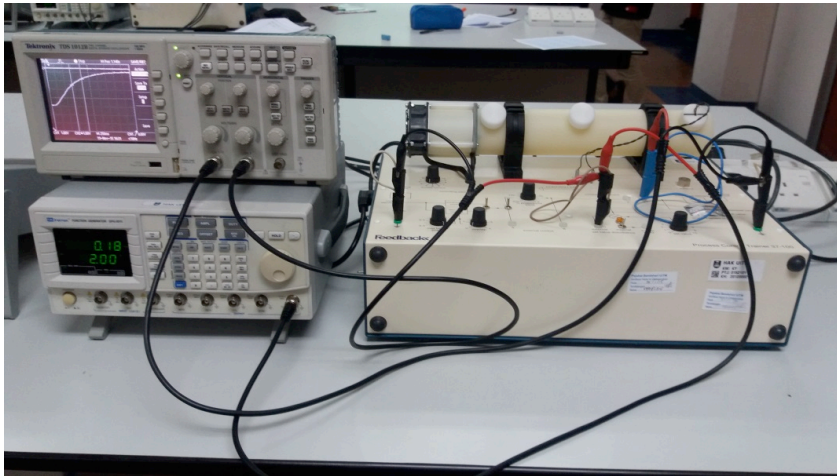


Figure 2. The experimental setup of PT326

The experimental setup of Process trainer PT326, shown in Figure 2, consists of a self-contained process and control equipment whose main function is similar to a hair dryer (Ribeiro & Cardoso, 1998), which is connected with an oscilloscope and signal generator. The process consists of heating the air flowing in the tube to the desired temperature level and the purpose of the control equipment is to measure the air temperature, compare it with a value set by the user and generate a control signal which determines the amount of electrical power supplied to a correcting element. In this case, a heater mounted adjacent to the blower, as described in Feedback Instrument Limited (1996). However, the Process trainer PT326 system only allows the gain to be adjusted in order to achieve the best characteristic outputs in terms of peak time, settling time and steady state error. This is not sufficient to control the temperature of the air blower system especially when it is operated under open-loop condition. Data measurements obtained from this experimental setup were used to design a suitable controller for temperature control of PT326.

Based on the open-loop test, a new closed-loop controller is therefore proposed using Ziegler-Nichols tuning rules in order to improve the output characteristics. The signal generator is set with an amplitude of 2V peak to peak with the temperature set at 35°C. Initially, the open loop test on frequency response with sinusoidal input signal is carried out at starting frequency of 0.01 Hz to model the process in order to obtain the transfer function of the process. The tuning of both rules was carried out to obtain the proportional constant,  $K_p$ , integral constant  $K_i$ , and derivative constant,  $K_d$ . These constants were derived from  $\tau_D$  and  $\tau_C$  obtained from the output response of an open loop test with step input using Ziegler-Nichols first method where S-shape response was obtained. The constant values were used to simulate the PI and PID controller and the output characteristics were observed.

## RESULTS AND DISCUSSION

Several methods are available for designing PID controller. The most frequently used experimental methods are the Ziegler-Nichols open-loop and closed loop design methods. In this work, however, the work focuses on Ziegler-Nichols open-loop method where the system response to a step input is in S-shape form. The experiment was conducted at the Instrumentation Laboratory Faculty of Electrical Engineering, Universiti Teknologi MARA. Figure 3 shows the response curve of process trainer PT326 of air blower system in S-shape where the design of PI and PID controller can be developed.

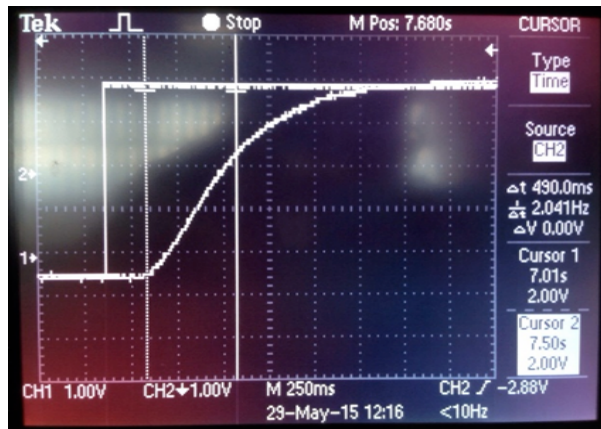


Figure 3. The S-shape response using Ziegler-Nichols first method

The design procedures are as follows:

- a) Obtain an open-loop step response from the experiment.
- b) Draw the tangent line on the response curve.
- c) Using the cross-points of the tangent with x-axis and with the steady-state output line to determine time delay,  $\tau_D$  and time constant,  $\tau_c$ .
- d) PID controller tuning design can be used using the formulae stated in Table 1.

Table 1  
Ziegler-Nichols first method open-loop tuning parameters

Controllers	$K_c$	$\tau_i$	$\tau_D$
P	$\frac{\tau_c}{\tau_D}$	$\infty$	0
PI	$0.9 \frac{\tau_c}{\tau_D}$	$\frac{\tau_D}{0.3}$	0
PID	$1.2 \frac{\tau_c}{\tau_D}$	$2\tau_D$	$0.5\tau_D$

The Ziegler-Nichols first method tuning formula is based on the value of gain  $K_c$ ,  $\tau_i$  and  $\tau_D$  to determine the output characteristics. By doing this, the Process trainer PT326 output characteristics can be improved by applying different types of controller. To illustrate the accuracy of the Ziegler-Nichols tuning formula based on Table 1, the output responses can be improved and analysed. The transfer function of the process is given as in Equation [1].

$$G(s) = \frac{K_p e^{-t_d s}}{\tau s + 1} \tag{1}$$

where

$K_p$  is steady state gain of the system

$\tau$  is time constant of the system

$t_d$  is dead time of the system

Table 2 shows the value of P controller, PI controller and PID controller design using the Ziegler-Nichols first method after obtaining the value of  $\tau_D$  and  $\tau_C$ . The air blower system PT326 only consists of P controller. Therefore, to analyse the parameters in Table 2, MATLAB/Simulink R2013a is used to model the air blower system PT326. Once the S-shape response has been obtained, the next step is to draw the tangent line on the response curve. Here, the value of time delay,  $\tau_D$  and time constant,  $\tau_C$  can be determined. The tangent line at the inflection point of S-shape curve determining the intersections of the tangent line with the time axis and the voltage axis. From the graph shown in Figure 3, the values of  $\tau_D = 0.27s$  and  $\tau_C = 0.55s$  were obtained. Once the values of  $\tau_D = 0.27s$  and  $\tau_C = 0.55s$  are known, the next step is to design the suitable controller for the air blower system PT326 using the parameters indicated in Table 1. Table 2 shows the value of P controller, PI controller and PID controller design using the Ziegler-Nichols first method. The air blower system PT326 only consists of P controller. Therefore, to analyse the parameters in Table 2, MATLAB/Simulink R2013a is used to model the air blower system PT326.

Table 2  
*Ziegler-Nichols first method open-loop tuning parameters*

Controllers	$K_c$	$\tau_i$	$\tau_D$
P	2.04	$\infty$	0
PI	1.833	0.9	0
PID	2.44	0.54	0.135

Based on the experimental results, the transfer function of air blower system PT326 was obtained. The open-loop transfer function is given in Equation [2].

$$G(s) = \frac{0.54}{(s + 0.36)(s + 1.5)} \tag{2}$$



The calculations obtained in Table 2 are used as the parameters setting in the simulation model connected with the transfer function of Process trainer PT326 as in Equation [2]. Figure 4 shows the MATLAB/Simulink model constructed where the step response is injected as the input signal.

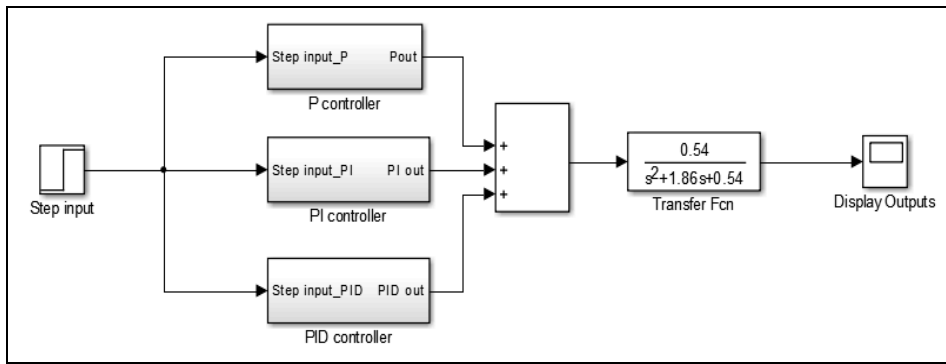


Figure 4. The model of PT326 in the Simulink model

Figure 5 shows the simulation result of three controllers: P controller, PI controller and PID controller. From the observation, with P controller, the output cannot achieve the steady-state response, whereas PI controller has the ability to improve the steady state error, and the combination of PID will improve the transient response in terms of settling time,  $t_s$ , peak time,  $t_p$  and steady state error. Based on the output response, the rise time,  $t_r$  of PID controller is faster than PI controller. However, PID controller has a higher overshoot compared with PI controller. Both controllers achieved steady state error, which indicates that the final response of Process trainer PT326 will be at a constant value at a certain length of time.

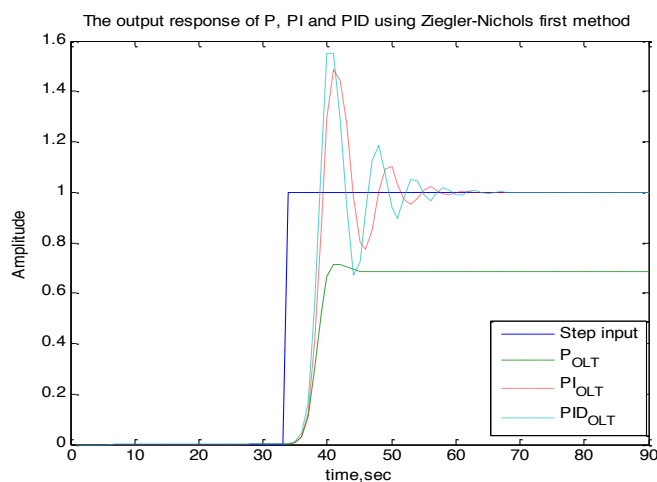


Figure 5. The controller response based on Ziegler-Nichols first method

By applying the transfer function obtained from Equation [2], the response of PI and PID controller in comparison with P controller shows that both the controllers can achieve steady-state condition. The difference between these two controllers is on the time taken to become stable. Figure 6 shows the results of output characteristics based the values obtained in Table 2, where the excitation input is a step response. Even though the output response oscillates more, the response will still achieve the steady-state condition. However, the time taken is longer from the original response, as shown in Figure 5.

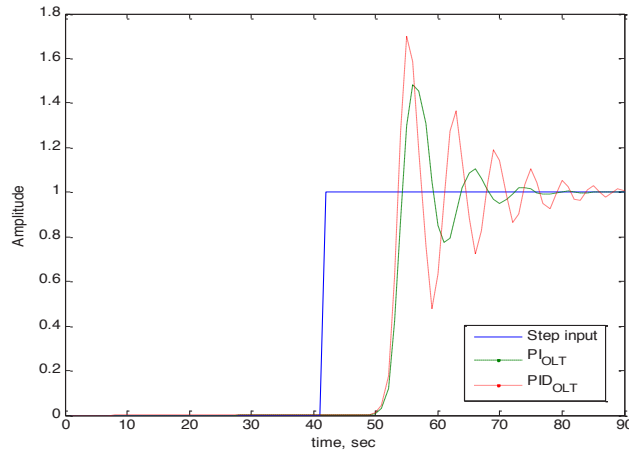


Figure 6. The effect of integrator in PID controller

In order to analyse the effect of integrator towards the process response of air blower PT326, the value of integral in the PID controller has been changed from  $\tau_i = 0.54$  to  $\tau_i = 0.48$ . As shown in Figure 7, the response of PID controller is found to be almost similar with PI controller output. If the value of integrator in PID controller is higher than the value from the open-loop test, the overshoot can be reduced and it will achieve a steady state error faster compared with the PID controller response in Figure 5 and Figure 6.

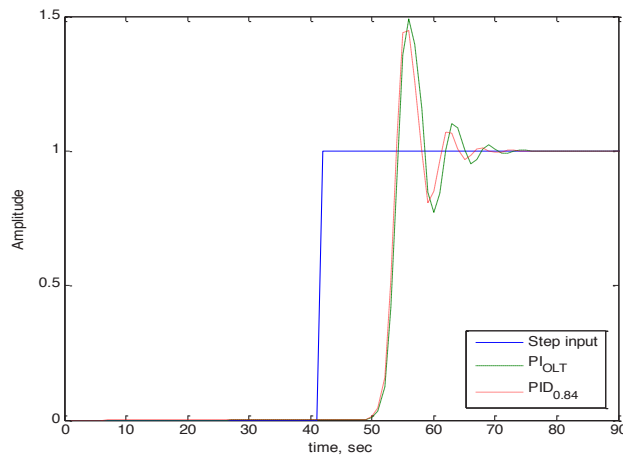


Figure 7. The effect of integrator in PID controller

## CONCLUSION

This work focuses on designing a suitable controller for air blower system PT326 in order to achieve the steady-state response. The optimum values of PID controller can be easily accessed and gained from the open-loop response. By doing the open-loop test, the design of PID controller becomes much faster. From the simulation aspect, analysis in terms of rise time, overshoot, and delay time and steady-state condition is quicker and time consuming compared with the gain adjustment. The performance of air blower system Process trainer PT326 can be further improved instead of using P controller only. The responses of both the controllers of air blower system PT326 are better in terms of response time and settling time when the Ziegler-Nichols first method is applied. It was observed that the response of PID controller depends on the type of process and requirement settings by user. However, PID controller is the most common controller used in a slow process such as temperature control. Therefore, PID controller is more suitable for air blower system Process trainer PT326.

## ACKNOWLEDGEMENT

The authors would like to acknowledge the Faculty of Electrical Engineering, Universiti Teknologi MARA for providing the financial support.

## REFERENCES

- Alsofyani, I. M., Rahmati, M. F., & Anbaran, S. A. (2014). A PID Controller Design for an Air Blower System. *IRICT 2014 Proceedings*, pp. 48-59.
- Antonio, V. (2004). A new design for a PID plus feedforward controller. *Journal of Process Control*, 14, 457-463.
- Astrom, K., & Hagglund, T. (1994). *PID controller: Theory, Design and Tuning*, Library of Congress Cataloging-in-Publication Data.
- Chien, K. L., Hrones, J. A., & Reswick, J. B. (1972). On the automatic control of generalized passive systems. *Trans ASME*, 74, 175-185.
- Dadone, P., & Landingham, H. V. (2001). Remote Control of Industrial Processes, *Mountain Workshop on Soft Computing in Industrial Applications Virginia Tech., Blacksburg. Virginia*, pp. 93-97.
- Feedback Instrument Limited. (1996). Process Trainer PT326, *User Manual, Crowborough*, 1-9.
- Hambali, N., Ang, A. A. R., Ishak, A. A. & Janin, Z. (2013). Various PID controller tuning for Air Temperature Oven System, *International Conference on Smart Instrumentation, Measurement and Applications*. KL.
- Hambali, N., Masngut, A., Ishak, A. A., & Janin, Z. (2014). Process Controllability for Flow Control System using Ziegler-Nichols (ZN), Cohen-Coon (CC) and Chien-Hrones-Reswick (CHR) Tuning Methods. *International Conference on Smart Instrumentation, Measurement and Applications*. KL.
- Hambali, N., Zaki, M. N. K., & Ishak, A. A. (2012). Reformulated Tangent Method of Various PID Controller Tuning for Air Pressure Control, *International Conference on Control System, Computing and Engineering*, pp. 17-21.

- Ishak, A. A., & Hussain, M. A. (1998). Open-loop Process Identification: Reformulation of Response Rate Calculation. *Regional Symposium on Chemical Engineering* (pp. 1-5).
- Ishak, A. A., & Hussain, M. A. (1998). Reformulation of the Tangent Method for PID Controller Tuning. *TENCON 2000*, pp. 484-488.
- Kamaruddin, N., Janin, Z., & Taib, M. N. (2009). PID controller tuning for glycerine bleaching process using well-known tuning formulas - a simulation study. *In Industrial Electronics*, pp. 1682-1686.
- Lu, C. H., & Tsai, C. C. (2001). Adaptive decoupling predictive temperature control for an extrusion barrel in a plastic injection molding process. *IEEE Transactions on Industrial Electronics*, 48(5), 968-975.
- Meshram, P. M., & Kanojiya, R. G. (2012). Tuning of PID Controller using Ziegler-Nichols Method for Speed Control of DC Motor, *IEEE International Conference on Advances in Engineering, Science and Management*, pp. 117-122.
- Nims, P. T. (1950). Some Design Criteria for Automatics Controls. *Trans AIEE* 70, 759-768.
- Rahmat, M. F., Hoe, Y. K., Usman, S., & Wahab, N. A. (2005). Modelling of PT326 Hot Air Blower Trainer Kit using PRBS signal and Cross-correlation Technique. *Jurnal Teknologi*, 42, 9-22.
- Ribeiro, B., & Cardoso, A. (1998). A Model-based Neural Network controller for a Process Trainer Laboratory Equipment. *Artificial Neural Nets and Genetic Algorithms*, Springer, 601-605.
- Sharma, K. D., Chatterjee, A., & Rakshit, A. (2014). Harmony search algorithm and Lyapunov theory based hybrid adaptive fuzzy controller for temperature control of air heater system with transport-delay. *Applied Soft Computing*, 25, 40-50.
- Zhuang, M., & Atherton, D. P. (1993). Automatic tuning of optimum PID controllers, pp. 216-224.
- Ziegler, J. G., & Nichols, N. B. (1942). Optimum settings for automatic controllers. *Trans ASME*, 64(8), 759-768.



## Synthesis and Characterisation of Silica from Palm Oil Fuel Ash (POFA) Using Alkaline Fusion Method

Nur Athirah Adam<sup>1</sup>, Alawi Sulaiman<sup>1\*</sup>, Azhari Samsu Baharuddin<sup>2</sup>,  
Mohd Noriznan Mokhtar<sup>2</sup>, Zainuri Busu<sup>3</sup> and Tengku Elida Tengku Zainal Mulok<sup>4</sup>

<sup>1</sup>Tropical Agro-Biomass Research Group, Faculty of Plantation and Agrotechnology,  
Universiti Teknologi MARA (UiTM), 40450 Shah Alam, Selangor, Malaysia

<sup>2</sup>Faculty of Engineering, Universiti Putra Malaysia (UPM), 43400 Serdang, Selangor, Malaysia

<sup>3</sup>FTJ Bio Power Sdn. Bhd., Jalan Liku, 59100 Kuala Lumpur, Malaysia

<sup>4</sup>Faculty of Applied Sciences, Universiti Teknologi MARA (UiTM), 40450 Shah Alam, Selangor, Malaysia

### ABSTRACT

Palm Oil Fuel Ash (POFA) is a biomass produced from palm oil industries. POFA is known to contain a high amount of silica and has been proven by XRF spectroscopy, in which the silicon dioxide content is 72.63%. In this study, silica was synthesised from POFA. To extract the silica, POFA was fused with alkaline agent ( $\text{Na}_2\text{CO}_3$ ) before mixing with Cethyltrimethyl Ammonium Bromide (CTAB) and Sulphuric Acid ( $\text{H}_2\text{SO}_4$ ). Sodium silicate solution from the fusion was used as silica precursor replacing conventionally used silica source, Tetraethoxilane (TEOS). XRD pattern showed that raw POFA dominantly consists of silica. Meanwhile, FTIR analysis of the synthesised silica exhibited spectra bands at  $3393\text{ cm}^{-1}$ ,  $1635\text{ cm}^{-1}$ ,  $1028\text{ cm}^{-1}$  and  $787\text{ cm}^{-1}$  that corresponded to the functional groups of Si-O and O-H. Thus, it could be concluded that silica was successfully extracted from POFA by the alkaline fusion method.

*Keywords:* Mesoporous silica, palm oil fuel ash (POFA), palm oil mill

### ARTICLE INFO

#### Article history:

Received: 25 October 2016

Accepted: 17 March 2017

#### E-mail addresses:

n.athirahadam@gmail.com (Nur Athirah Adam),  
dr\_alawi@salam.uitm.edu.my (Alawi Sulaiman),  
azharis@upm.edu.my (Azhari Samsu Baharuddin),  
noriznan@upm.edu.my (Mohd Noriznan Mokhtar),  
zainuri.b@feldaglobal.com (Zainuri Busu),  
tetzm@salam.uitm.edu.my (Tengku Elida Tengku Zainal Mulok)

\*Corresponding Author

### INTRODUCTION

Palm oil industries have been producing a variety of biomass, and are increasing annually (Yap et al., 2013). Biomass from the industry was subjected to combustion process as fuel for steam generation and yield POFA, or better known as boiler ash. POFA produced is 5% from the biomass combusted (Borhan et al., 2010). According to Yap et al. (2013), the produced POFA in Malaysia from 2007 to

2010 was 0.06 million tonnes. POFA was dumped to the open area of the palm oil mills without any beneficial returns. Furthermore, it can cause hazards to both human and environment (Tay & Show, 1995). POFA possesses pozzolanic properties due to high content of silica which is more than 50% (Hassan et al., 2015; Zarina et al., 2013). Due to the pozzolanic properties, many inventors have been conducting research utilising POFA as a replacement material to enhance the properties of cementitious composites (Noorvand et al., 2013).

Since POFA majorly consists of silica, it can be refined to produce pure silica. Thus, this study focused on extracting silica from POFA and equipped it with mesoporous characteristics. Sodium silicate from POFA acts as a precursor to yield high purity of silica. TEOS is conventionally used as silica source. TEOS is typically derived from sand as a raw material involving multi reaction pathways. These method yields silica with desired particle sizes, porosity and morphology. However, the silica precursor is expensive and has issues with sustainability (Ui et al., 2014). Thus, researchers are looking for another way to produce silica by using a greener approach with an affordable cost. Lately, researchers have come up with other source of silica such as rice husk (Wang et al., 2012), incinerator bottom ash (Liu et al., 2014) and coal fly ash (Hui et al., 2006).

There are several established methods used in order to synthesise silica. For example, silica is produced using stober method (Liu et al., 2006), hydrothermal synthesis (Wang et al., 2009), sol-gel process (Buckley & Greenblatt, 1994) and more. Mesoporous silica offers high surface areas of 500-1000 m<sup>2</sup>/g and huge pore diameters. Hence, it would make a great support material for enzyme immobilisations. For biocatalyst reactions, this allows substrate to flow through in and out of the supporting materials freely. Mesoporous silica broadly applied in various fields such as drug delivery (Wang, 2009; Slowing et al., 2008), biomedical applications (Wang et al., 2015; Maleki et al., 2016), catalysis (Liu et al., 2016; Yokoi et al., 2012), and water treatments (Paseta et al., 2016), and so on. POFA is abundant in supply, available at low cost and it is another way to utilise solid waste material that gives a new wealth to the oil palm industries.

## **MATERIALS AND METHOD**

### **Raw Materials and Chemicals**

The raw material, POFA, was collected from Felda Sungai Tengi Palm Oil Mill, Kuala Kubu Baru, Selangor, Malaysia. All chemicals, sodium carbonate (Na<sub>2</sub>CO<sub>3</sub>), Cethyltrimetyl Ammonium Bromide (CTAB) and Sulphuric acid (H<sub>2</sub>SO<sub>4</sub>) used were analytical reagent grade and purchased from R&M Malaysia. POFA was ground by using a grinder and sieved to <250µm.

### **Extraction of Silica from POFA**

Figure 1 shows the process flow diagram of silica extraction from POFA. The method was proposed by Liu et al. (2014). POFA was initially fused with Na<sub>2</sub>CO<sub>3</sub> at 900°C in a furnace for 15 minutes. Before placing them in the furnace, POFA and Na<sub>2</sub>CO<sub>3</sub> were mixed uniformly. After the fusion, the product was hydrolysed with deionised water. The solution was placed in an oven at 105°C for 24 hours. After being hydrolysed, the solution was filtered. The filtered resultant

solution contains silica, while the ash is referred to as desilicated POFA. The resultant solution is also known as sodium silicate solution and it will be further processed to yield silica powder.

Next, 1.2 g of CTAB was diluted in 20 g deionised water was added to the sodium silicate solution. Subsequently, 1M  $H_2SO_4$  was introduced into the solution until the pH became 10, and constantly stirred for 3 hours. The initial pH value of the mixture before introducing sulphuric acid was in between 11-12. The mixture was then placed in oven for 48 hours at 105oC to allow hydrothermal reaction to take place. The solid produced was later filtered and dried before calcined in furnace at 550oC for 6 hours. The calcination process completed the production of silica.

### Characterisation Study

Characterisation was carried out using Fourier Transform Infra-Red (FTIR) Spectrometer (Perkin Elmer Model 2000) in order to identify the surface functional group of the synthesized silica. The synthesised silica and POFA were also subjected to X-ray Diffraction (XRD) using Rigaku Ultima III X-ray diffractometer, with a  $2\theta$  angle ranging from  $10^\circ$ -  $90^\circ$  to get the diffraction pattern. The composition of raw POFA was determined using X-ray Fluorescence (XRF) spectroscopy.

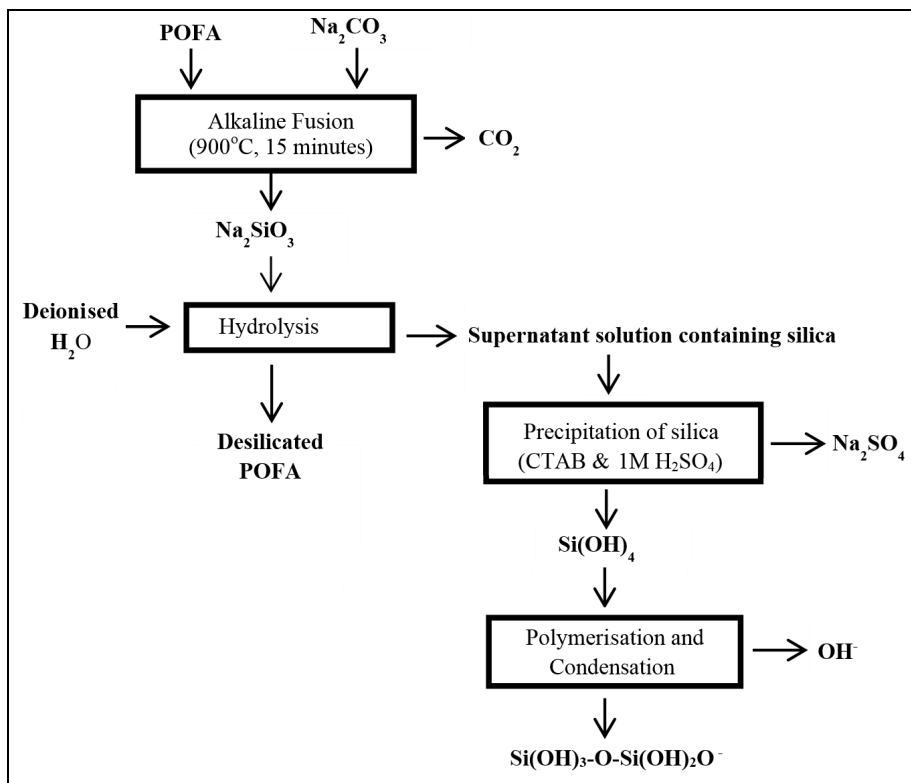


Figure 1. Silica extraction process from POFA

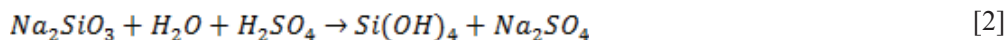
## RESULTS AND DISCUSSION

### Reaction Mechanisms

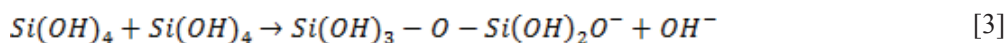
Equation 1 shows the reaction occurred when sodium carbonate was mixed with silicon dioxide at 900°C. This reaction yielded sodium silicate. As proposed by Grynberg et al. (2015), the surface of the silica was spread by the molten sodium carbonates and it led to the surface reaction generating sodium silicate.



Sodium silicate formed after the fusion was hydrolysed with deionised water, and thus allowing the leaching process of the fused sodium carbonate and silica of the POFA (Septawander et al., 2016). According to Liu et al. (2014), the silicates are readily soluble in water. The addition of sulphuric acid to the sodium silicate solution initiated the gelation of silica in the form of silicic acid, as in Equation 2. As explained in the methodology, sulphuric acid is added to sodium silicate solution until the pH reached 10. Approaching pH 10, white precipitate of silica started to appear. At this stage, the solution is stirred vigorously to promote the formation of silica. Liu's report (as cited in Mendelez-Ortiz, 2013) has stated that the required time for sodium silicate to yield silica decreases in alkaline pH.



Polymerisation of monomer silicic acid occurred results in the production of oligomeric silicic acid and water as by-product (Wilhelm & Kind, 2015). In the polymerisation process, as indicated in the Equation 3, the surface of the agglomerates is negatively charged.



In this study, CTAB acts as a template or structure directing agent to fabricate mesoporous silica materials. At the end of the process, the mesoporous silica was calcined to remove the CTAB template. As proven by the FTIR spectroscopy, no traces of CTAB were found in the synthesised silica from POFA. Figure 2 illustrates the mechanism of silica templated with CTAB to construct mesoporous structure. The agglomerates of silica after going through the polymerisation process are anionic, while the surfactant is cationic. As illustrated in Figure 2, the surfactant and anionic silica established connections through electrostatic forces.



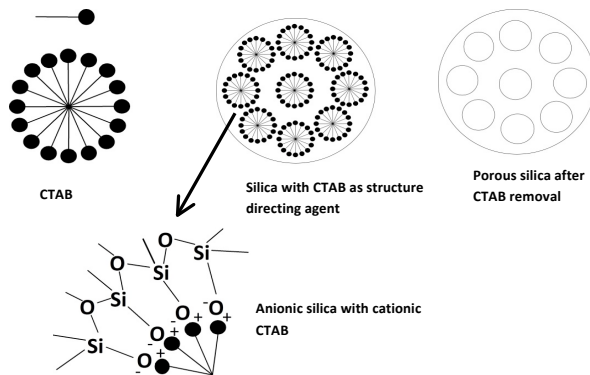


Figure 2. CTAB templated mesoporous silica

### XRF Analysis

Table 1 below shows the chemical composition of raw POFA using the XRF analysis. From the table, analysed raw POFA contains  $\text{SiO}_2$ ,  $\text{K}_2\text{O}$ ,  $\text{CaO}$ ,  $\text{Al}_2\text{O}_3$ ,  $\text{Fe}_2\text{O}_3$ ,  $\text{MgO}$  and  $\text{P}_2\text{O}_5$ . It can be observed that silica is the dominant compound in POFA, with the percentage of 72.63%. Thus, raw POFA can be used as raw materials for silica production.

Table 1  
The chemical composition of POFA

Compound	Content (%)
$\text{SiO}_2$	72.63
$\text{K}_2\text{O}$	9.77
$\text{CaO}$	5.48
$\text{Al}_2\text{O}_3$	5.03
$\text{Fe}_2\text{O}_3$	3.53
$\text{MgO}$	3.39
$\text{SO}_3$	0.18

### FTIR Spectroscopy

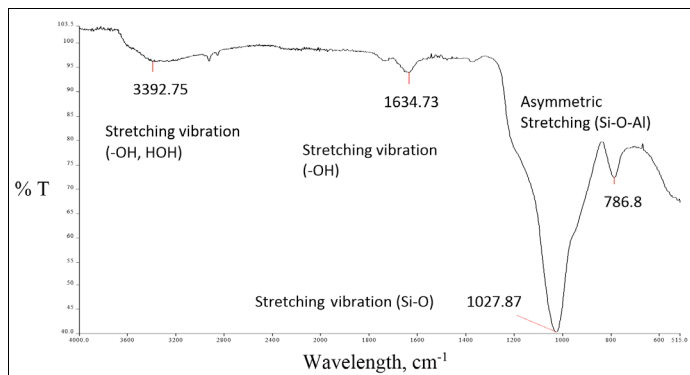


Figure 3. The FTIR spectra of silica synthesised from POFA

Figure 3 shows the spectra bands of silica extracted from POFA. Bands appearing at 3392.75 and 1634.73 attributed to the Si-OH stretching and bending and SiO-H bending, respectively. As discussed earlier, there are hydroxyl groups attached at the surface of the silica during the processes of precipitation and polymerisation. The bands appearing at 1027.87 and 786.80 show the asymmetric and symmetric stretching modes of Si-O-Si (Rahmat et al., 2016). There is no band that is corresponding to C-H vibrations observed. This shows that Cetyltrimethyl Ammonium Bromide (CTAB), which is the template material used during silica extraction, has completely been removed during calcination. These results are aligned with the previous studies by Liu et al. (2014). This also confirms that silica can be extracted effectively from POFA by using alkaline fusion method.

### XRD Analysis

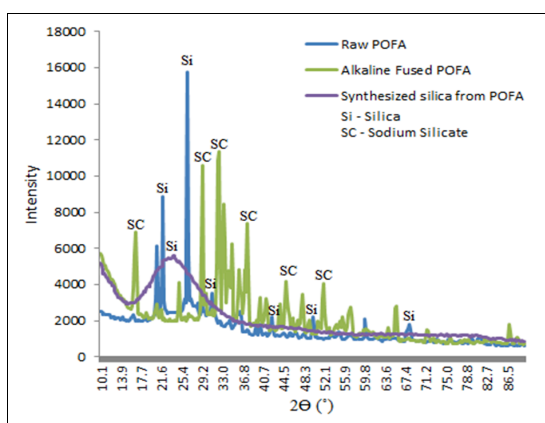


Figure 4. The XRD pattern of raw POFA, alkaline fused POFA and synthesised silica from POFA

The XRD pattern in Figure 4 shows the peaks of raw POFA, alkaline fused POFA and synthesised silica. The peaks indicate that silica is the major component in the raw POFA sample. More intense peaks appeared as POFA was fused with alkaline agent,  $\text{Na}_2\text{CO}_3$  to produce sodium silicate. The peaks corresponding to the presence of sodium silicate as the surface of POFA, which is dominated by silica particles, are being surrounded by the molten sodium carbonate during the fusion process. This indicates that the alkaline agent successfully reacted with the POFA particles to form sodium silicate. The XRD pattern of silica extracted from POFA is consistent with the report by Liu et al. (2014).

### CONCLUSION

In this study, silica was successfully extracted from POFA. The FTIR analysis results proved that silica particles extracted from POFA were of high purity and the XRD pattern of silica particles was found to be consistent with other studies. Sodium silicate solution, as the precursor silica produced from this study, can replace the expensive TEOS. On the other hand, the palm

wastes can be fully utilised for higher value-added products. Thus, this study has shown that the production of silica from POFA could be achieved using the alkaline fusion method.

## ACKNOWLEDGEMENTS

The authors would like to acknowledge the staff of Felda Palm Industries Sdn. Bhd. and Universiti Teknologi MARA (UiTM) for their assistance and guidance throughout the completion of this study. This work was financially funded by the Ministry of Education, Malaysia, through Fundamental Research Grant Scheme (FRGS) 600-RMI/FRGS 5/3 (39/2014). Special thanks also go to the organiser of the 3rd International Conference on Science and Social Research 2016 (CSSR).

## REFERENCES

- Borhan, M. N., Ismail, A. & Rahmat, R. A. (2010). Evaluation of Palm Oil Fuel Ash (POFA) on Asphalt Mixtures. *Australian Journal of Basic and Applied Sciences*, 4(10), 5456-5463.
- Buckley, A. M., & Greenblatt, M. (1994). Sol-Gel Preparation of Silica Gels. *Journal of Chemical Education*, 71(7), 599.
- Grynberg, J., Gouillart, E., Chopinet, M. -H., & Toplis, M. -J. (2015). The mechanisms and Kinetics of Reactions between Silica and Solid Sodium Carbonate. *International Journal of Applied Glass Science*, 1-8.
- Hassan, U. J. & Abdu, S. G. (2015). Characterization of a Treated Palm Oil Fuel Ash. *Science World Journal*, 10(1), 27-31.
- Hui, K. S., & Chao, C. Y. H. (2006). Synthesis of MCM-41 from Coal Fly Ash by a Green Approach: Influence of Synthesis pH. *Journal of Hazardous Materials*, B137, 1135-1148.
- Liu, S., Lu, L., Yang, Z., Cool, P., & Vansant, E. F. (2006). Further Investigations on the Modified Stober Method for Spherical MCM-41. *Materials Chemistry and Physics*, 97, 203-206.
- Liu, S., You, K., Jian, J., Zhao, F., Zhong, W., Yin, D., Liu, P., Ai, Q., & Luo, H. (2016). Mesoporous Silica Gel as an Effective and Eco-friendly Catalyst for Highly Selective Preparation of Cyclohexane Oxime by Vapor Phase Oxidation of Cyclohexylamine with air. *Journal of Catalysis*, 338, 239-249.
- Liu, Z. S., Li, W. K., & Huang, C. Y. (2014). Synthesis of Mesoporous Silica Materials from Municipal Solid Waste Incinerator Bottom Ash. *Waste Management*, 34, 893-900.
- Maleki, H., Durães, L., García-González, C. A., Gaudio, P., Portugal, A., & Mahmoudi, M. (2016). Synthesis and Biomedical Applications of Aerogels: Possibilities and Challenges. *Advances in Colloid and Interface Science*, 2-28.
- Mendez-Ortiz, H. I., Mercado-Silva, A., Garcia-Cerda, L. A., & Perera-Mercado, Y. A. (2013). Hydrothermal Synthesis of Mesoporous Silica MCM-41 Using Commercial Sodium Silicate. *Journal of the Mexican Chemical Society*, 57(2), 73-79.
- Noorvand, H., Abang Ali, A. A., Demirboga, R., Noorvand, H. & Farzadnia, N. (2013). Physical and Chemical Characteristics of Underground Palm Oil Fuel Ash Cement Mortars with Nanosilica. *Construction and Building Materials*, 48, 1104-1113.

- Paseta, L., Simón-Gaudó, E., Gracia-Gorría, F., & Coronas, J. (2016). Encapsulation of Essential Oils in Porous Silica and MOFs for Trichloroisocyanuric Acid Tablets used for Water Treatment in Swimming Pools. *Chemical Engineering Journal*, 292, 28-34.
- Rahmat, N., Hamzah, F., Sahiron, N., Mazlan, M., & Zahari, M. M. (2016). Sodium Silicate as Source of Silica for Synthesis of Mesoporous SBA-15. *IOP Conference Series: Materials Science and Engineering*, 133, 1-9.
- Septawendar, R., Sutardi, S., Karsono, U., & Sofiyarningsih, N. (2016). A Low-Cost, Facile Method on Production of Nano Zirconia and Silica from Local Zircon in a Large Scale Using a Sodium Carbonate Sintering Technology. *Journal of the Australian Ceramic Society Volume*, 52(2), 92-102.
- Slowing, I. I., Vivero-Escoto, J. L., Wu, C. W., & Lin, V. S. Y. (2008). Mesoporous Silica Nanoparticles as Controlled Release Drug Delivery and Gene Transfection Carriers. *Advanced Drug Delivery Reviews*, 60, 1278-1288.
- Tay, J. H. & Show, K. Y. (1995). Use of Ash Derived from Oil-Palm Waste Incineration as a Cement replacement material. *Resources, Conservation and Recycling*, 13, 27-36.
- Ui, S. W., Choi, I. S., & Choi, S. C. (2014). Synthesis of High Surface Area Mesoporous Silica Powder Using Anionic Surfactant. *ISRN Materials Science*, 1-6.
- Wang, L., Shan, Z., Zhang, Z., Wei, F., & Xiao, F. S. (2009). One-pot Hydrothermal Synthesis of Mesostructured Silica Nanotubes. *Journal of Colloid and Interface Science*, 335, 264-267.
- Wang, S. (2009). Ordered Mesoporous Materials for Drug Delivery. *Microporous and Mesoporous Materials*, 117, 1-9.
- Wang, W., Martin, J. C., Fan, X., Han, A., Luo, Z., & Sun, L. (2012). Silica Nanoparticles and Framework from Rice Husk Biomass. *Applied Materials and Interfaces*, 4, 977-981.
- Wang, Y., Zhao, Q., Han, N., Bai, L., Li, J., Liu, J., Che, E., Hu, L., Zhang, Q., Jiang, T., & Wang, S. (2015). Mesoporous Silica Nanoparticles in Drug Delivery and Biomedical Applications. *Nanomedicine: Nanotechnology, Biology and Medicine*, 11, 313-327.
- Wilhelm, S., & Kind, M. (2015). Influence of pH, Temperature and Sample Size on Natural and Enforced Syneresis of Precipitated Silica. *Polymers*, 7(12), 2504-2521.
- Yap, S. P., Alengaram, U. J., Jumaat, M. Z., & Foong, K. Y. (2013). Waste Materials in Malaysia for Development of Sustainable Concrete: A Review. *Electronic Journal of Structural Engineering*, 13(1), 60-64.
- Yokoi, T., Kubota, Y., & Tatsumi, T. (2012). Amino-functionalized Mesoporous Silica as Base Catalyst and Adsorbent. *Applied Catalyst A: General*, 421-422, 14-37.
- Zarina, Y., Bakri, A. M. M., Kamaruddin, H., Nizar, I. K., & Rafiza, A. R. (2013). Review on the Various Ash from Palm Oil Waste as Geopolymer Material. *Rev. Adv. Mater. Sci.*, 34, 37-43.

## Effect of Upstream Building Configurations on Mean Wind Speed Ratio at Urban Pedestrian Level Using LES

Muhd Azhar Zainol<sup>1</sup>, Azli Abd Razak<sup>1\*</sup>, Nor Merlisa Ali<sup>1</sup>, Qi Jie Kwong<sup>2</sup> and Sheikh Ahmad Zaki<sup>3</sup>

<sup>1</sup>Faculty of Mechanical Engineering, Universiti Teknologi MARA (UiTM), 40450 Shah Alam, Selangor, Malaysia

<sup>2</sup>Faculty of Architecture, Planning and Surveying, Universiti Teknologi MARA (UiTM), 40450 Shah Alam, Selangor, Malaysia

<sup>3</sup>Malaysia-Japan International Institute of Technology, Universiti Teknologi Malaysia (UTM) Kuala Lumpur, 54100 Kuala Lumpur, Malaysia

### ABSTRACT

Pedestrian level in the urban area is an important area where most of pedestrians' activities occur at this level. Therefore, the purpose of this study is to investigate effects of various building layouts on mean wind speed ratio at the pedestrian level. The mean wind speed ratio at the pedestrian level was analysed in order to determine whether the building layouts configured within this research are able to enhance outdoor ventilation and ensure good pedestrian comfort level. The simulation model consists of two main areas which are the upstream area and downstream area with a setback distance,  $d$ . The building layouts at upstream area are arranged in staggered arrangements (ST) or square arrangements (SQ), while the downstream areas are in a fixed staggered arrangement (ST). Packing density in both areas is 25% with three setback distances which are 3H, 5H and 7H. Based on the results, the mean wind speed ratio at the pedestrian level in a downstream area with longer setback distance will provide a higher mean speed ratio, and the influence of upstream building arrangements on the mean wind speed ratio of the downstream area decreases as the setback distance increases. Hence, the mean wind speed ratio of downstream area depends on the setback distance between the upstream and downstream areas.

*Keywords:* Downstream area, LES, OpenFOAM, setback distance, square (SQ), staggered (ST), upstream area

### ARTICLE INFO

#### Article history:

Received: 25 October 2016

Accepted: 17 March 2017

#### E-mail addresses:

azlirazak@salam.uitm.edu.my (Azli Abd Razak),  
muhdazharzainol@gmail.com (Muhd Azhar Zainol),  
merlisa@salam.uitm.edu.my (Nor Merlisa Ali),  
kwong.qijie@mail.com (Qi Jie Kwong),  
sheikh.ahmadzaki@gmail.com (Sheikh Ahmad Zaki)

\*Corresponding Author

### INTRODUCTION

Developments in the urban area have been occurring rapidly. This leads to constant changes in city landscapes such as the

construction of high rise buildings, roads and other infrastructures. Thus, it will reduce the percentages of open land and vegetation areas in such cities (Nilsson et al., 2014). Due to the limitation of space and high prices of land (market property) in the urban area, town planners shift city development from urban area to suburban area in order to overcome this issue (Karim, 2012). Suburban area is defined as the surrounding area of an urban area. This area consists of small buildings, terrain houses and vegetation. High rise buildings such as apartments are built to replace terrain houses whereas vegetation areas are removed in order to maximise land usage. In this study, the suburban area is known as upstream area, while the urban area as downstream area. Previous researchers mainly concentrated on the urban area parameter that influences ventilation performance such as building shape, building layout and heterogeneity of building height without considering the surrounding of suburban parameter factors. There are two methods commonly used by researchers to analyse the behaviour of wind inside the urban area, which are wind tunnel experiment and numerical simulation. Oke (1988) conducted the wind tunnel experiment to study the airflow formation of urban street canyon. He found three types of air flow patterns formed, which are isolated roughness, wake interference and skimming flow. These formation of airflows depends on the ratio of building height to the distance between buildings, which is also referred as building width. Meanwhile, Coceal et al. (2006) performed numerical simulation analysis over cubical block with different block arrays, namely staggered, square and aligned arrays. He studied the formation of turbulence structure and mean wind speed. On the other hand, Abd Razak et al. (2013) performed numerical simulation analysis over cubical block with different aspect ratios and non-uniform height. They investigated the effects of urban geometry and building height on spatially averaged pedestrian wind speed. Generally, the concept of simplified urban model is commonly applied in wind engineering studies. This concept was used to represent urban model due to the difficulties replicating the real urban model, which is required in wind tunnel experiments or numerical simulations such as in the wind tunnel experiments (Becker, Lienhart & Durst, 2002; Castro et al., 2006; Hang et al., 2012) and numerical simulations (Castro et al., 2006; Xie et al., 2006; Xie & Castro, 2008; Buccolieri, Sandberg, & Di Sabatino, 2010; Abd Razak et al., 2013b; Ikeda et al., 2014; Ikegaya et al., 2015).

## **METHOD**

The simulation analysis was carried out using OpenFOAM software, while Large Eddy Simulation (LES) was used as the turbulence model. A validation study was done to ensure the accuracy of simulation analysis. In order to verify the simulation analysis, a validation study was performed by comparing mean wind speed profiles at four locations obtained from the

measured data of Cheng and Castro (2002) as done by Abd Razak et al. (2013a) and Coceal et al. (2006). Cheng and Castro (2002) conducted wind tunnel experiment over cubical block in staggered layout with 25% of packing density ( $\lambda=25\%$ ). A similar cubical block arrangement was used and periodic boundary condition was applied in the stream-wise and span-wise direction to yield repeating model, as shown in Figure 1. Slip condition was applied at the top of the boundaries, while wall function was imposed on the bottom boundaries and the block surfaces. The grid size at pedestrian level was  $H/32$ , where  $H$  is a constant value, 25mm. To ensure a fully developed flow, the simulation initially running about  $200T$ , where  $T = H/u^*$  and statistical data were collected and averaged from  $200T$  to  $400T$ . The time step used for the simulation analysis was 0.000025. In order to develop the flow inside the computational domain, the constant pressure gradient used was obtained from the previous researcher, i.e Coceal et al. (2006), Xie, Coceal, and Castro (2008), and Abd Razak et al. (2013a). Based on the results presented in Figure 2, the mean wind speed profiles of the current study show a good agreement with mean wind speed plotted by Cheng and Castro (2002), Coceal et al. (2006), and Abd Razak et al. (2013a). Therefore, similar boundary conditions were implemented in the simulated case study.

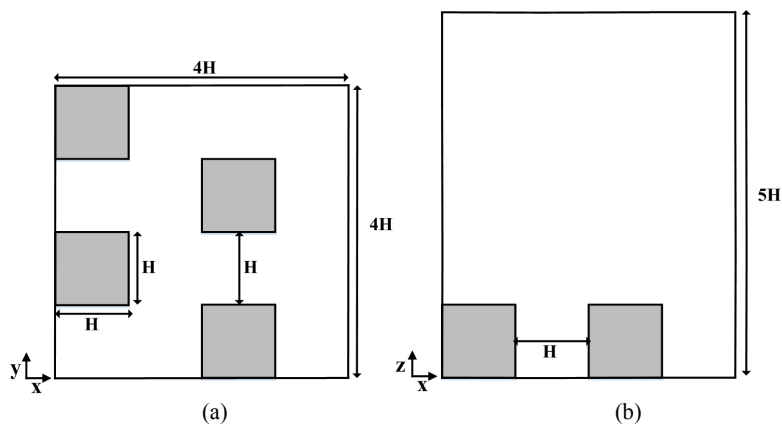


Figure 1. Simulation model of validation study on staggered arrangement with 25% packing density: (a) plan view; and (b) side view

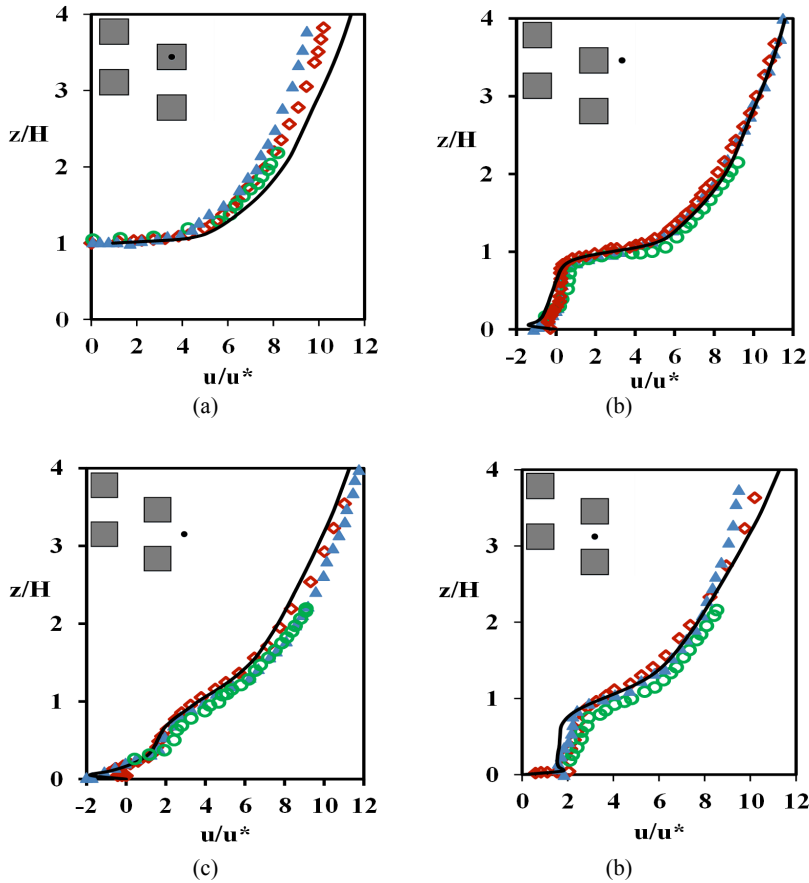


Figure 2. The profiles of mean streamwise velocity,  $u$  normalised by friction velocity  $u^*$  over four different cubical staggered arrangement locations with  $\lambda_p = 25\%$ : (a) Above the building; (b) behind the building; (c) in front of the building; and (d) in-between the gap. Black line; current study, Circle; Cheng & Castro (2002), Diamond; Coceal et al. (2006) and Triangle; Abd Razak et al. (2013)

Two types of building arrangements, which are the square arrangement (SQ) and staggered arrangement (ST) were used in these studies. The square and staggered arrangements were used in the upstream area, while only the staggered arrangement was used at downstream area. A schematic diagram of the simulation domain is shown in Figure 3. The domain was created based on three main areas, which are upstream, setback distance and downstream areas. The setback distance between the upstream and downstream areas are  $3H$  (shorter),  $5H$  (medium),  $7H$  (longest), where  $H$  is equal to  $25\text{ mm}$ . Similar building height,  $H$ , was implemented for the upstream and downstream areas. In order to reveal the effect of upstream building configuration on mean wind velocity on the downstream area, one high rise and two high rise buildings were



implemented in the upstream building area with building height  $2H$  as illustrated in Figure 4; however, a constant setback distance which is  $3H$  was used. The addition of the high rise building at upstream area would increase the frontal area ratio of the upstream area.

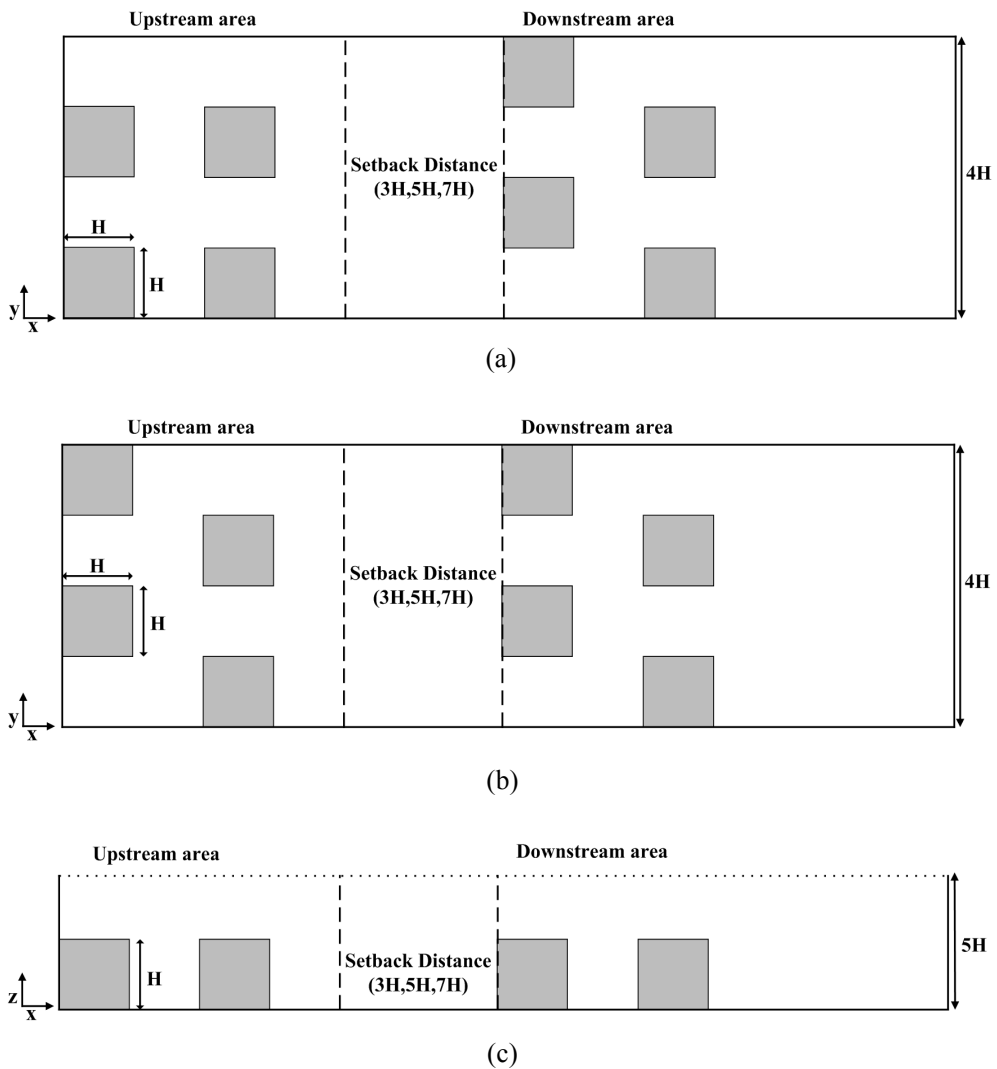


Figure 3. A schematic view of simulation domain: (a) plan view of square upstream building arrangements; (b) plan view of staggered upstream building arrangement; and (c) side view for both upstream building arrangements

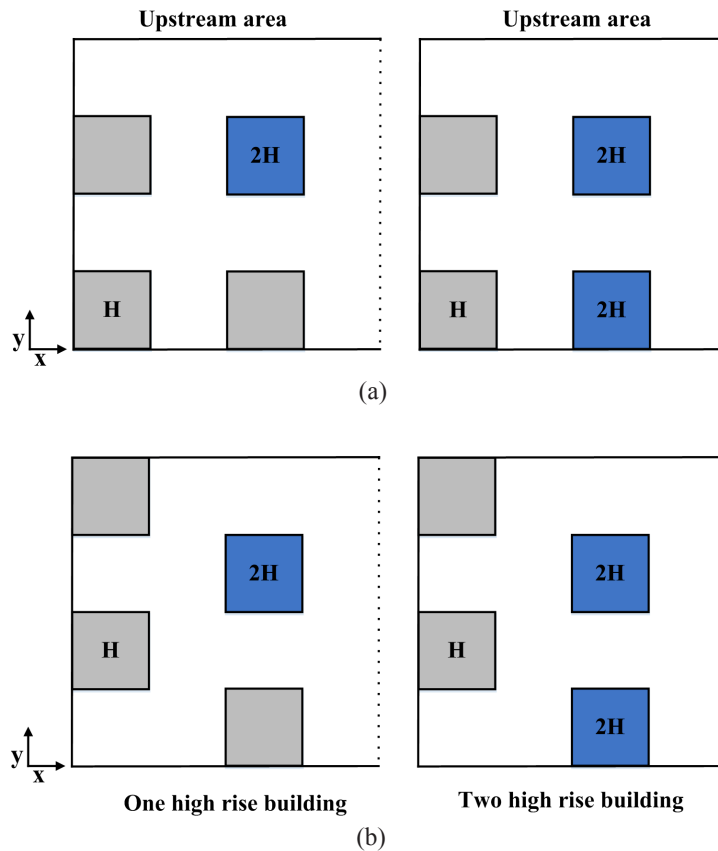
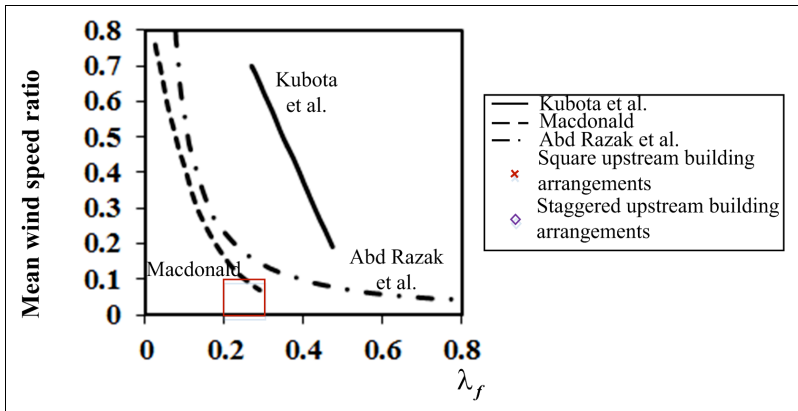


Figure 4. A schematic view of the simulation domain plan view of upstream area for non-uniform building height: (a) square upstream building arrangements; and (b) staggered upstream building arrangement

## RESULTS AND DISCUSSION

Pedestrian wind environment on an urban area is significantly affected by the urban layouts, urban building configuration and surrounding area, especially in the presence of high rise buildings. Many studies have been performed to investigate the effects of urban building arrangement, urban building packing density (*plan area ratio*), and urban building frontal area (*frontal area ratio*). For example, Kubota et al. (2008) conducted the wind tunnel experiment on several real residential districts in Japan, and revealed a strong relationship between the building coverage ratio and mean speed ratio. They also found that the mean wind speed ratio decreases linearly with the increase in the frontal area ratio. Abd Razak et al. (2013a) applied numerical analysis on the several geometric conditions with different plan area ratios, frontal area ratio, and used a constant urban building arrangement, which is staggered building arrangement as the urban layout. They found that the mean wind speed depends on the frontal area ratio and building aspect ratio, and concluded that the frontal area ratio and building aspect ratio are important parameters in determining pedestrian wind speed for ideal urban modelling conditions. Similar with Abd Razak et al. (2013a), Macdonald (2000) used simplified isolated building to analyse wind mean speed in urban canopy using the wind tunnel

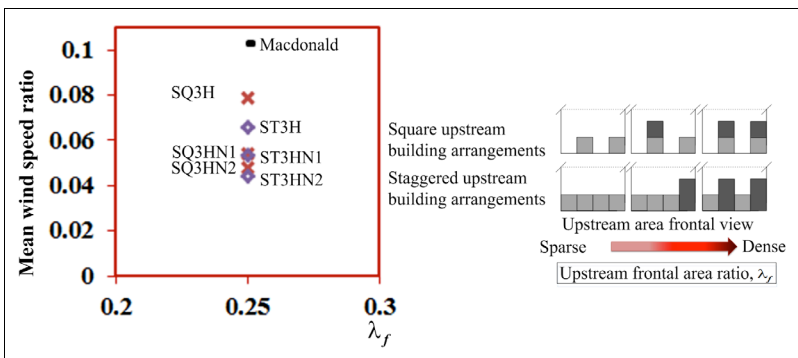
experiment. In addition, instead of using a constant urban layout as Abd Razak et al. (2013a) did, Macdonald (2000) used two types of urban layouts, which are the square and staggered arrangements. He exposed that the mean wind speed exponentially decreases as the urban packing density increases. Moreover, the turbulence length scale was affected by the increase in urban packing density.



(a)



(b)



(c)

Figure 5. Mean wind speed ratio at the pedestrian level

As mentioned above, the researchers of the urban study pointed out the contribution of urban geometry on pedestrian wind environments. They came out with different wind speed ratio equation based on their findings; however, most of the previous researchers collectively agreed that the frontal area ratio is an important parameter in determining wind speed ratio. Previous studies focused on the urban area geometry by neglecting the effects of suburban area environment. Another approach that could be done in order to investigate the pedestrian wind environment inside the urban area is by adding a suburban building geometry to analyse the contribution of this parameter on the pedestrian wind environment of the urban area. The upstream (suburban area) can be one of the important parameters that influences the mean wind speed of the pedestrian area. The mean wind speed is influenced by the setback distance between the upstream area and downstream area. The longest setback distance provides higher mean wind velocity on the downstream area. To have a thorough understanding of the mean wind velocity at pedestrian area, the result is compared with the wind speed ratio at the pedestrian level result obtained from Abd Razak et al. (2013a), Kubota et al. (2008), and Macdonald (2000).

In comparison, these researchers used different frontal area ratios on the downstream (urban area) area by neglecting the effect of upstream area (suburban area); this study used a constant frontal area ratio at the downstream area by considering the influence of upstream area in terms of setback distance and upstream building configurations. In term of setback distance, there are three setback distances used, together with a constant upstream frontal area ratio and two different upstream building arrangements. For the upstream building configuration, a constant setback distance was applied to the different upstream frontal area ratios. Figure 5(a) shows the mean wind speed obtained from the researchers mentioned above and the results obtained by these researchers are not consistent with each other due to the different normalised means of wind speed selection. Figure 5(b) and Figure 5(c) depict the mean wind speed of the effects of setback distance and upstream building configurations.

The result of mean wind speed at pedestrian level is normalised with the free stream velocity above urban canopy layer. Note that the red box in Figure 5(a) represents the mean wind speed ratio demonstrated in Figure 5(b), and Figure 5(c) is used as a comparison of the mean wind speed ratio with the previous researchers. Figure 5(b) shows the relationship of setback distance and mean wind speed ratio at the pedestrian level on downstream area. The mean wind speed ratio of the square and staggered upstream building arrangements monotonically increase with the increase of setback distance. Furthermore, the results indicate that the mean wind speed ratio of different upstream building arrangements has almost a similar value as the setback distance increases, while there are significant differences of wind speed values when the respective setback distance becomes shorter. Meanwhile, Figure 5(c) shows the relationships of the upstream frontal area ratio and mean wind speed ratio, which were the results from three upstream building configurations. According to Millward-Hopkins et al. (2011), frontal area ratio is an another important urban parameter in estimating the aerodynamics effect of the urban roughness due to the pressure drag acts on the surface roughness of the frontal area. The results obtained clearly show that the effect of the frontal area ratio at upstream area on the mean wind speed ratio at pedestrian level on downstream area was notably significant. The mean wind speed ratio at the pedestrian level decreases as the upstream frontal area ratio

increases. Furthermore, there are drastic decreases of the mean wind speed ratio between uniform upstream building and non-uniform upstream building heights. This indicates that the presence of high rise building at the upstream area will reduce the wind speed value. Apart from that, the upstream building arrangements slightly influence the wind speed at the pedestrian level on downstream area.

## CONCLUSION

This paper explains the effects of upstream building configurations in terms of setback distance and frontal area ratio of the upstream area on mean wind velocity ratio at pedestrian level on the downstream area. From the findings, these two parameters significantly influenced the mean wind velocity ratio at pedestrian level on the downstream area. The setback distance between the upstream and downstream areas influenced the mean speed value before approaching the downstream area. The mean wind speed ratio at pedestrian level of the downstream area with a longer setback distance provides a higher mean velocity ratio. Apart from that, the influence of upstream building arrangements become less on the mean wind speed ratio of the downstream area as the setback distance increases. Furthermore, the frontal area ratio of the upstream area significantly affects the mean wind value at downstream area. Inverse proportional relationship between the frontal upstream area and mean wind speed value in the downstream area is evidence.

## ACKNOWLEDGEMENTS

The authors would like to express their sincere gratitude to Universiti Teknologi MARA (UiTM) and i-Kohza Wind Engineering for (Urban, Artificial, Man-made) Environment, Malaysia-Japan International Institute of Technology (MJIT) as the Research Institutes facilitating this research. This research was financially supported by the grant-in aid for scientific research (600-RMI/FRGS 5/3 (87/2015)) from the Ministry of Higher Education, Malaysia.

## REFERENCES

- Abd Razak, A., Hagishima, A., Ikegaya, N., & Tanimoto, J. (2013a). Analysis of airflow over building arrays for assessment of urban wind environment. *Building and Environment*, 59, 56–65.
- Abd Razak, A., Hagishima, A., Ikegaya, N., Mohamad, M. F., & Zaki, S. A. (2013b). Mean Wind Flow Field around Idealized Block Arrays with Various Aspect Ratios. *Applied Mechanics and Materials*, 393, 767–773.
- Becker, S., Lienhart, H., & Durst, F. (2002). Flow around three-dimensional obstacles in boundary layers. *Journal of Wind Engineering and Industrial Aerodynamics*, 90(4-5), 265–279.
- Buccolieri, R., Sandberg, M., & Di Sabatino, S. (2010). City breathability and its link to pollutant concentration distribution within urban-like geometries. *Atmospheric Environment*, 44(15), 1894–1903.
- Castro, I. P., & Apsley, D. D. (1997). Flow and dispersion over topography: A comparison between numerical and laboratory data for two-dimensional flows. *Atmospheric Environment*, 31(96), 839–850.

- Castro, I. P., Cheng, H., & Reynolds, R. (2006). Turbulence over urban-type roughness: Deductions from wind-tunnel measurements. *Boundary-Layer Meteorology*, *118*, 109–131.
- Cheng, H., & Castro, I. P. (2002). Near-wall flow development after a step change in surface roughness, (August 2001), 411–432.
- Coceal, O., Thomas, T. G., Castro, I. P., & Belcher, S. E. (2006). Mean flow and turbulence statistics over groups of urban-like cubical obstacles. *Boundary-Layer Meteorology*, *121*, 491–519.
- Hang, J., Li, Y., Sandberg, M., Buccolieri, R., & Di Sabatino, S. (2012). The influence of building height variability on pollutant dispersion and pedestrian ventilation in idealized high-rise urban areas. *Building and Environment*, *56*, 346–360.
- Ikeda, Y., Ikegaya, N., Hagishima, A., Tanimoto, J., & Abd Razak, A. (2014). Characteristics of spatio-temporal fluctuation of urban pedestrian wind derived from Large-eddy simulation. In *6<sup>th</sup> International Symposium on Computational Wind Engineering - CWE2014, Humberg Germany*.
- Ikegaya, N., Ikeda, Y., Hagishima, A., Abd Razak, A., & Tanimoto, J. (2015). A prediction model for wind speed ratios at pedestrian level with simplified urban canopies. *Theoretical and Applied Climatology*, *127*, 655-665.
- Karim, H. A. (2012). Low Cost Housing Environment: Compromising Quality of Life. *Procedia - Social and Behavioral Sciences*, *35*(December 2011), 44–53.
- Kubota, T., Miura, M., Tominaga, Y., & Mochida, A. (2008). Wind tunnel tests on the relationship between building density and pedestrian-level wind velocity: Development of guidelines for realizing acceptable wind environment in residential neighborhoods. *Building and Environment*, *43*, 1699–1708.
- Macdonald, R. W. (2000). Modelling the mean velocity profile in the urban canopy layer. *Boundary-Layer Meteorology*, *97*(1), 25–45.
- Millward-Hopkins, J. T., Tomlin, A. S., Ma, L., Ingham, D., & Pourkashanian, M. (2011). Estimating Aerodynamic Parameters of Urban-Like Surfaces with Heterogeneous Building Heights. *Boundary-Layer Meteorology*, *141*(3), 443–465.
- Nilsson, K., Nielsen, T. S., Aalbers, C., Bell, S., Boitier, B., Chery, J. P., & Zasada, I. (2014). Strategies for Sustainable Urban Development and Urban-Rural Linkages. *European Journal of Spatial Development*, (March), 1–26.
- Xie, Z., & Castro, I. P. (2006). LES and RANS for turbulent flow over arrays of wall-mounted obstacles. *Flow, Turbulence and Combustion*, *76*, 291–312.
- Xie, Z. T., Coceal, O., & Castro, I. P. (2008). Large-Eddy simulation of flows over random urban-like obstacles. *Boundary-Layer Meteorology*, *129*(1), 1–23.



## Self-similarity Hurst Parameter Estimation with Rescaled Range Method on IP-based Campus Internet Traffic

Murizah Kassim<sup>1\*</sup>, Noor Laili Ismail<sup>1</sup>, Roslina Mohamad<sup>1</sup>, Saiful Izwan Suliman<sup>1</sup> and Mahamod Ismail<sup>2</sup>

<sup>1</sup>Faculty of Electrical Engineering, Universiti Teknologi MARA (UiTM), 40450 Shah Alam, Selangor, Malaysia

<sup>2</sup>Faculty of Engineering and Build Environment, Universiti Kebangsaan Malaysia (UKM), 43600 Bangi, Selangor, Malaysia

### ABSTRACT

Self-similarity network traffic is considered as one of stochastic process studies in telecommunications engineering. In determining self-similarity traffic, Hurst value is an important parameter to be measured. This paper presents self-similarity traffic measurement using Rescaled Range, R/S statistical method in estimating Hurst parameter value. Inbound internet traffics on an IP-based campus network in Malaysia, which implements a 16.0 Mbps speed to internet and supports 10GE bandwidth at switch level, are captured and measured. The objectives of this research are to observe and present the existence level of Hurst parameter value, type of self-similarity and overall percentage of Hurts parameter estimation. The inbound traffic is measured due to its relevancy to next development on policing and shaping algorithm traffic model. Solarwinds Net Flow machine is setup on a campus gateway to its Wide Area Network (WAN). Data of the traffic like in flow, size and speed were taken over 20 days and 14 weeks in different inter-arrival time. These traffics are analysed, which lead to the impacts of packet loss, throughput and speed in network performance. Results present the Hurst parameter value, the existence of Long Range Dependant Self-similarity traffic distribution and percentage level of Hurst parameter value for the three types of captured traffic.

*Keywords:* Analysis, Hurst Parameter Estimation, internet traffic, network performance, Self-similarity

### ARTICLE INFO

#### Article history:

Received: 25 October 2016

Accepted: 17 March 2017

#### E-mail addresses:

[murizah@salam.uitm.edu.my](mailto:murizah@salam.uitm.edu.my) (Murizah Kassim),

[lailiis@yahoo.co.uk](mailto:lailiis@yahoo.co.uk) (Noor Laili Ismail),

[roslina780@salam.uitm.edu.my](mailto:roslina780@salam.uitm.edu.my) (Roslina Mohamad),

[saiifulizwan@salam.uitm.edu.my](mailto:saiifulizwan@salam.uitm.edu.my) (Saiful Izwan Suliman)

[mahamod@ukm.edu.my](mailto:mahamod@ukm.edu.my) (Mahamod Ismail)

\*Corresponding Author

### INTRODUCTION

Analyses and measurement of network traffic are still one of ongoing studies in telecommunication data traffic. Self-similarity process modelling is taken as the main research challenges compared to traditional process (Fras, Mohorko, & Čučej, 2012).

Several studies have been carried out over the last few years on the analysis of internet network traffic on self-similarity (Arlitt & Williamson, 2005; Xiaolong, Julong, & Wanwei, 2013), traffic measurements in the high speed networks (Celeda et al., 2007; Kassim et al., 2012), as well as measurement in the next generation networks (Pezaros, 2005). A lot of studies on network traffic works have put more attention on analysing the causes and implications of network traffic problems (Kassim et al., 2012). Such problems are identified as the different applications traffic volumes, point-to-point (P2P) applications used, network games phenomena, or Voice over Internet Protocol (VoIP) application implications such as Skype and social media applications. Measured network traffic analyses help us to understand more about new behaviours in the network, realise the causes of the problems, and also forecast future network architecture maintenance and development.

Previous traditional model of communication networks has successfully been applied for analysing network traffic which is based on different methods such as Poisson (Leland et al., 1994), Markovian (Klemm, Lindemann, & Lohmann, 2003; Park & Willinger, 2000) and other various measured and fitted traffic models (Kassim, Ismail, & Yusof, 2015). Poisson processes have been used and proven that call arrivals are mutually independent; and that the call inter-arrival times are all exponentially distributed, with one and the same parameter. They have some attractive theoretical properties in which the same approaches are often used when modelling data network traffic. Packet and connection arrivals are assumed to be Poisson processes. However, several studies have shown that the distribution of packet inter-arrivals clearly differs from exponential processes (Stathis & Maglaris, 2000). Thus, the observed burst on many timescales in real traffic cannot be described with the traditional Poisson-based traffic modelling (Park & Willinger, 2000). Instead, they introduced statistically self-similar processes as a better way of modelling LAN traffic. Some research showed that certain traffics captured on a network have certain fractal-like behaviour. Self-similar or fractal processes are generally an accepted model for traffic generators which provide better models for tele-traffic analysis in modern computer networks than Poisson processes. Certain statistical parameters and results can determine the data collection is either a long-term or short-term data range (Akinci et al., 2013; Clegg, 2006). Self-similarity also has proven that data are in relation with known sequences (Faye, 2011). Meanwhile, time-to-time analyses have shown that the important requirement for conducting simulation studies of telecommunication networks is the ability to generate long synthetic stochastic self-similar sequences (Jeong & Pawlikowski, 1999). The traffic is examined on protocols and packet sizes with certain proportions. Characteristics of the client are examined closely and empirical probability distributions derived describe session lengths, and time between the user and amount of data transferred. Those probability distributions are taken to build a new model (Abrahamsson, 1999). Therefore, measurement and analysis of real traffic are important to gain knowledge of the new characteristics of the traffic. A good realistic traffic model can be used to develop new tele-traffic algorithms in controlling data packet or bandwidth to provide Quality of Services in a network (Kassim et al., 2015).

Hurst Parameter Estimation is a well-known measurement to analyse real network traffic and test on Self-similarity process properties. The Hurst measurements are important to prove self-similarities characteristics on specifies traffic properties and gather some characteristic information about the real network traffic. Analysis measurements on real traffic also are one



of the important procedures in building a new realistic theoretical traffic models. There are a few methods to estimate the Hurst parameter in identifying and proving whether data traffic is self-similarity or not. One of it is called Rescaled Adjusted Range (RS) method which is derived from a proven mathematical algorithm. The RS method is relatively simple and accurate. Analysis on the RS method has been conducted to analyse some online computing network traffics which in turn help to detect Syn-Flood DDoS attack of the network in time (Zhang et al., 2008). The RS method has also been used in other traffic analyses such as wind speed and water running so as to identify and model certain self-similarity process (Akinici et al., 2013).

This paper presents how self-similarity test is done using the mathematical measurement on Hurst parameter estimation for the inbound IP-based network internet traffic in a university campus. For this purpose, the IP-based campus traffic was captured using a Solar Winds Net Flow Traffic Analyser (NTA) which had been setup on a university IP-based campus Network in Malaysia (IPCN). Important campus IP-based campus traffic flow such as packets, bytes and packets per second (P/s) were captured and analysed. The traffic was captured from continuous streams and converted into raw numbers. Data were collected via the machine setup, which was captured at the gateway to the internet at 16.0 Mbps for the received and transmitted bandwidth interface. Three important data [namely, packets, bytes, packet per second (P/s)] were taken on 20 different days for every 15-min inter-arrival time and in 14 weeks for every one-hour inter-arrival time.

## Literature Review

Hurst effect indicates the degree of self-similarity (Gospodinov & Gospodinova, 2005). The Hurst parameter  $H$  is able to quantify the self-similarity of the accepted traffic aggregate. In a range of stochastic processes, if  $H = 0.5$ , it then corresponds to uncorrelated observation,  $H > 0.5$  to Long Range Dependents (LRD) processes and  $H < 0.5$  to Short Range Dependence (SRD) (Bianchi, Mancuso, & Neglia, 2002). Identifying whether the data are long Range Dependents or Short Range Dependents is very important when building a model. This research has proven that the design Measurement-Based Admission Controlled Traffic (MBAC) is a value-added traffic engineering tool that allows a significant increase in the network performance when offered traffic shows LRD compared to SRD. This research used two types of method to evaluate  $H$ , which are called the Aggregate Variance and Wavelet Estimator. Two graphical techniques used in the research are based on the pseudo-random self-similar sequences and fractional Gaussian noise (FGN) method. The analyses showed that the FGN method always produces self-similar sequences, with relative inaccuracy of the estimating Hurst parameter below 8% (Gospodinov & Gospodinova, 2005). This generator is recommended for practical simulation studies of high-speed telecommunication networks because of its accuracy. The two graphical techniques are called Rescaled adjusted range statistics (R/S method) and Variance Time plot technique. The R/S technique was applied to estimate the Hurst exponent, where it estimated over sections of different sizes of data. The variance-time plot is the second analysis technique that is based on property of slowly decaying variance of self-similar processes undergoing aggregation. Self-similarity is also a typical feature for fractal and chaos. In theory, regular fractals have strict self-similarity, but for irregular fractals in nature, their self-similarity could

be seen only within a certain scale-invariant region. Time series acquired by the sampling are commonly used for studying objects in nature; and they could be treated as curves on plane. Fractal analysis could be used to discuss the self-similarity of time series (Zhang & Luo, 2012). The results show that the scale in-variant extent parameter could distinguish curves with different levels of self-similarity effectively.

**METHOD**

In this study, Rescaled Range (R/S) method was used in analysing the data passed through IP-based campus traffic. The H parameter was estimated to look into the IP-based campus modelling traffic. The R/S method is one of the oldest and most well-known methods for estimating H (Abrahamsson, 1999). Equations (1)-(4) are derived as  $X_t$  denotes the number of packets that arrive at time  $t$ , i.e. the number of packets in bin  $t$ , and let,

$$Y_j = \sum_{i=1}^j X_i \quad (1) \tag{1}$$

be the cumulative inflow up to time,  $j$ . The R/S-statistic or rescaled adjusted range is defined by the ratio,

$$R/S = \frac{R(t,k)}{S(t,k)} \tag{2}$$

where (2) is the adjusted range,

$$R(t,k) = \max_{0 \leq i \leq k} [Y_{t+1} - Y_t - \frac{i}{k} (Y_{t+k} - Y_t)] - \min_{0 \leq i \leq k} [Y_{t+1} - Y_t - \frac{i}{k} (Y_{t+k} - Y_t)] \tag{3}$$

and

$$S(t,k) = \sqrt{k^{-1} \sum_{i=t+1}^{t+k} (X_i - \bar{X}_{t,k})^2} \tag{4}$$

where  $\bar{X}_{t,k} = k^{-1} \sum_{i=t+1}^{t+k} X_i$  [5]

makes it possible to study properties that are independent of scale.

The Hurst parameter  $H$  was determined through the ratio using R/S method analysis. The values of  $t$  and  $k$  were calculated for every possibility, or a sufficient number, and  $\log R/S$  was plotted against  $\log k$ . The slope of a straight line fitted to the points in the plot by the least square method was an estimation of the parameter  $H$ . As practiced, the ratio R/S was not calculated for every possible  $t$  and  $k$ . Only a number of equally spaced starting point's  $t$  and a number of intervals (lags)  $k$  were chosen. Typically, logarithmically spaced values of  $k$  are chosen because  $\log R/S$  is to be plotted versus  $\log k$ . For each starting point,  $t$  the ratio R/S is calculated for every lag  $k$  such that  $t+k \leq \text{length of } X$ . For small  $k$ , one gets many estimates of R/S, but for large  $k$ , one gets only a few, down to one, estimate of R/S. The R/S method is known to be biased towards  $H=0.7$ . It is biased upwards for small values of  $H$  and downwards for large values of  $H$ . In practice, the ratio R/S cannot be calculated for every possible starting point  $t$  and lag  $k$

(Abrahamsson, 1999). The low and high ends of the plot are usually not used when estimating  $H$  because of the influence from short-range dependence in the low end and because there are very few points to make a reliable estimate in the high end. It turns out that slight changes in the values of the cut-offs and in the number of values of  $t$  and  $k$  do not significantly affect the estimate. The values used when estimating  $H$  for the IPCN traces are described in section 4. Three types of traffic data were captured and analysed on the Hurst parameter estimation in two periods of time, which is in a day for 15 minutes time interval and a week for an hour time interval. The three types of data traffic are packet, byte and packet per second. A packet is one unit of binary data capable of being routed through a computer network. To improve communication performance and reliability, each message sent between two network devices is often subdivided into packets by the underlying hardware and software. A byte is a unit of data that are kept in a computer memory with eight binary digits. Byte for network traffic means the unit data are transferred over the network and this shows how big the data flow on the network. In data communications, packet per second (p/s) is a common measure performance for computer networks and transmission carriers. Routers and switches generally forward each packet independently which are called stateless device. Packets per second (p/s) can provide information on a more complete understanding of the device performance characteristics. Mathematical relationships can be defined, either directly or indirectly, between bandwidth with packets metrics. This is particularly important when high-touch features are configured and the device is under a high network load (Schudel, 2013). R/S algorithm method with Matlab is used to analysis the Hurst parameters estimation for the captured WAN traffic (Chen, 2008).

## RESULT AND DISCUSSION

### Hurst Parameter Estimation

Table 1 presents the estimation of Hurst parameter value in 20 days of internet traffic flow at IPCN. Most of the Hurst parameters results show that the value is above 0.5 and between 0.5 and 1. This shows that the internet flow for the packet, byte and packets per second is LRD Self-similarity. Table 2 presents the estimation of Hurst parameter in a week at most Hurst parameters results show above 0.8 and between 0.8 and 1. This shows that the all internet flow is also LRD Self-similarity.

Table 1  
*The Hurst parameter analysis in days*

Duration	RS Hurst Parameter Estimation					
	Total Packet	Hurst P	Total Byte	Hurst P	Total P/S	Hurst P
Day 1	151792300	0.9843	160925203520	0.9967	168838	0.9722
Day 2	130937122	0.7242	159090000000	0.7056	169078	0.9948
Day 3	128864305	0.8611	157370000000	0.7364	142732	0.7576
Day 4	150723974	0.6584	160960000000	0.6992	167491	0.7303
Day 5	148058779	0.9911	162092795488	0.962	165273	0.9215
Day 6	152557664	0.6688	166578041408	0.9097	169387	0.8551

Table 1 (continue)

Day 7	146582383	0.7088	160219774976	0.9342	162967	0.9131
Day 8	126617118	0.5672	127115429040	0.5685	140958	0.8149
Day 9	125034691	0.5988	119970595528	0.7218	138812	0.7707
Day 10	132756953	0.8935	130735145096	0.9151	146195	0.998
Day 11	129694083	0.7936	132889575520	0.6102	144505	0.9943
Day 12	127094554	0.5661	128450071336	0.2516	141532	0.8653
Day 13	141117938	0.4397	163497121344	0.4557	157236	0.491
Day 14	121019235	0.9056	141676542944	0.9418	133656	0.9137
Day 15	126728880	0.6822	106436874440	0.5952	144145	0.9903
Day 16	83185801	0.9205	67574123224	0.66	92023	0.8038
Day 17	86487611	0.9876	62468340562	0.974	96253	0.9544
Day 18	147269500	0.9976	119249649826	0.9794	165603	0.9926
Day 19	172414720	0.7654	157541571264	0.7468	199390	0.6576
Day 20	169870510	0.7451	158549646912	0.8294	195030	0.7654

Table 2  
The Hurst parameter analysis in weeks

Duration	RS Hurst Parameter Estimation					
	Total Packet	Hurst P	Total Byte	Hurst P	Total P/S	Hurst P
Week 1	979255535	0.8444	1082400000000	0.8353	273777	0.8309
Week 2	1006500000	0.856	1111500000000	0.9309	280427	0.8597
Week 3	995420083	0.9007	1124000000000	0.7792	277677	0.8412
Week 4	1019703808	0.9279	1024519704160	0.8387	284642	0.8953
Week 5	763712966	0.8573	803000000000	0.9308	213531	0.8514
Week 6	642292598	0.885	618685858920	0.8639	227381	0.9559
Week 7	703149766	0.8343	729440000000	0.8304	196468	0.8254
Week 8	854100229	0.8877	885130000000	0.933	237188	0.8607
Week 9	753799872	0.9362	786850000000	0.9994	250841	0.8884
Week 10	1009100000	0.9543	1122100000000	0.9388	281651	0.934
Week 11	643662676	0.9978	551387093976	0.9963	178969	0.9957
Week 12	631772322	0.8433	556010614864	0.8006	202476	0.9057
Week 13	653053453	0.9726	524477758432	0.9961	196217	0.9957
Week 14	823769800	0.999	705913040340	0.9971	246436	0.9959

**Packet R/S Analysis**

Graphs of R/S method analysis on packet internet traffic on the IPCN are taken as samples in plotting the Hurst parameters slop graph, as shown in Figures 1(a) to (e). The plotted graphs differentiate the slop of self-similarities of the captured traffic according to its Hurts parameters values results. If the plotted data are between slop 1 and slop 1/2, the Hurst parameter is LRD, i.e. its Hurst parameter is in the range of 0.5 to 1. Meanwhile, if the slop is under slop 1/2, then

it is SRD, which means that its Hurst parameter is less than 0.5. Figure 1(a) shows the self-similarity with Hurst parameter near to 0.9. Figure 1(b) shows the self-similarity with the Hurst parameter near to 0.8. Figure 1(c) shows the self-similarity with the Hurst parameter near to 0.7. Figure 1(d) shows the Self-similarity with the Hurst parameter near to 0.6. Finally, Figure 1(e) shows the self-similarity with the Hurst parameter near to 0.5. Only one day shows that the packet self-similarity Hurst parameter is equal to 0.4397. Thus, the results show that most of the traffic is LRD Self-similarity.

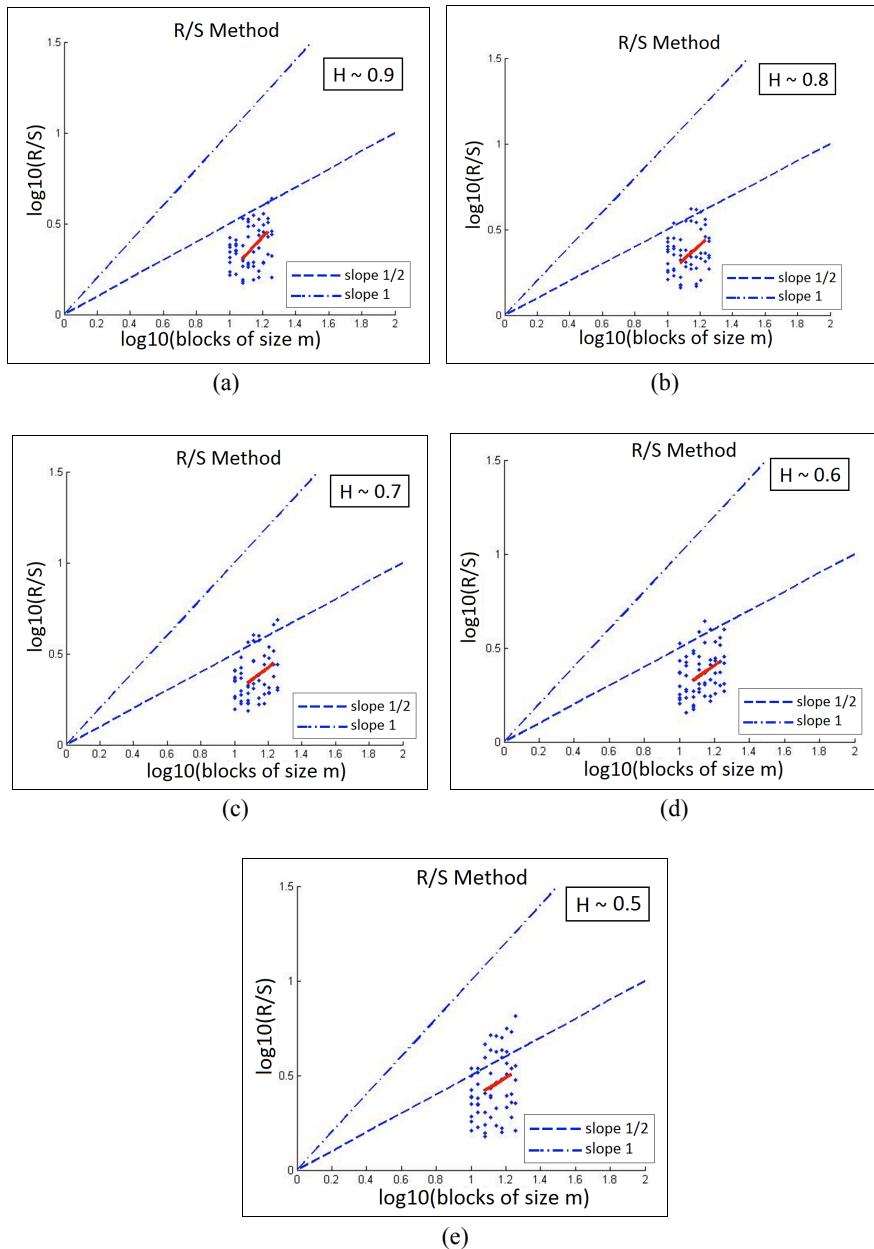


Figure 1. Daily packet Self Similar with H near to: (a) 0.9; (b) 0.8; (c) 0.7; (d) 0.6; and (e) 0.5

Figures 2(a) through (d) plotted graph of R/S method analysis on the packet internet traffic on the IPCN network. The Hurst parameters are shown in the plotted graph that differentiates the self-similarity value. The plotted graphs differentiate the slop of self-similarities of the captured traffic according to its Hurst parameters values results. If the plotted data in R/S graph are between slop 1 and slop  $\frac{1}{2}$ , the Hurst parameter is LRD, which means, its Hurst parameter is in the range of 0.5 to 1, whereas if the slop is under slop  $\frac{1}{2}$ , then it is SRD, which means that its Hurst parameter is less than 0.5. Figure 2(a) shows the highest Self-similarity value with the Hurst parameter of 0.999. Figure 2(b) shows the self-similarity with the Hurst parameter of 0.9978. Figure 2(c) shows the elf-similarity with the Hurst parameter of 0.8877 and Figure 2(d) shows the self-similarity with the Hurst parameter of 0.8343. Most of the Hurst parameter values are between 0.8 and 0.9, indicating that the Self-similarity value for LRD is very high. Thus, the results show that most of the traffic is LRD self-similarity. The one-week analysis also shows the accuracy of the self-similarity analysis, where the internet traffics is shown to be plotted nearest to slop 1 in the graph.

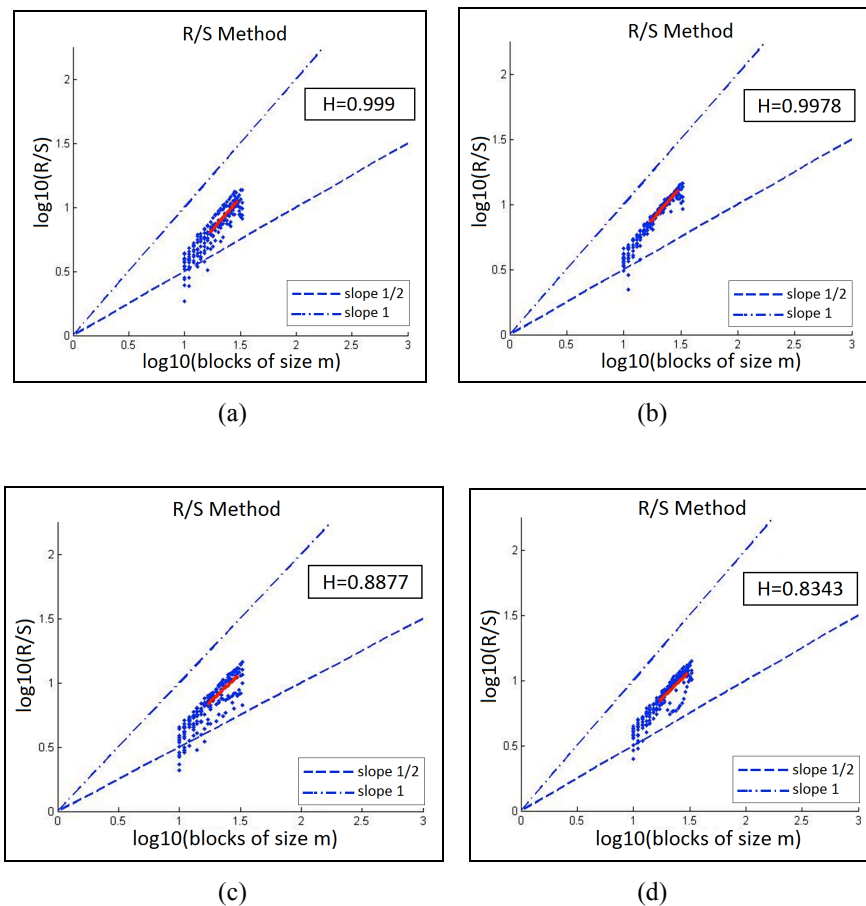


Figure 2. Weekly Packet Self Similar with: (a) H=0.999; (b) H= 0.9978; (c) H=0.8877; and (d) H=0.8343

**Byte R/S Analysis**

Figures 3(a) to (c) show the plotted graph of *R/S* method analysis on the daily byte internet traffic on the IPCN network. The highest, medium and lowest plotted graphs that differentiate the Hurst parameters value are shown. Figure 3(a) shows the Hurst parameter  $H=0.9967$ , whereas Figure 3(b) shows that the plotted  $H=0.7056$ , and Figure 3(c) shows the plotted  $H=0.2516$ .

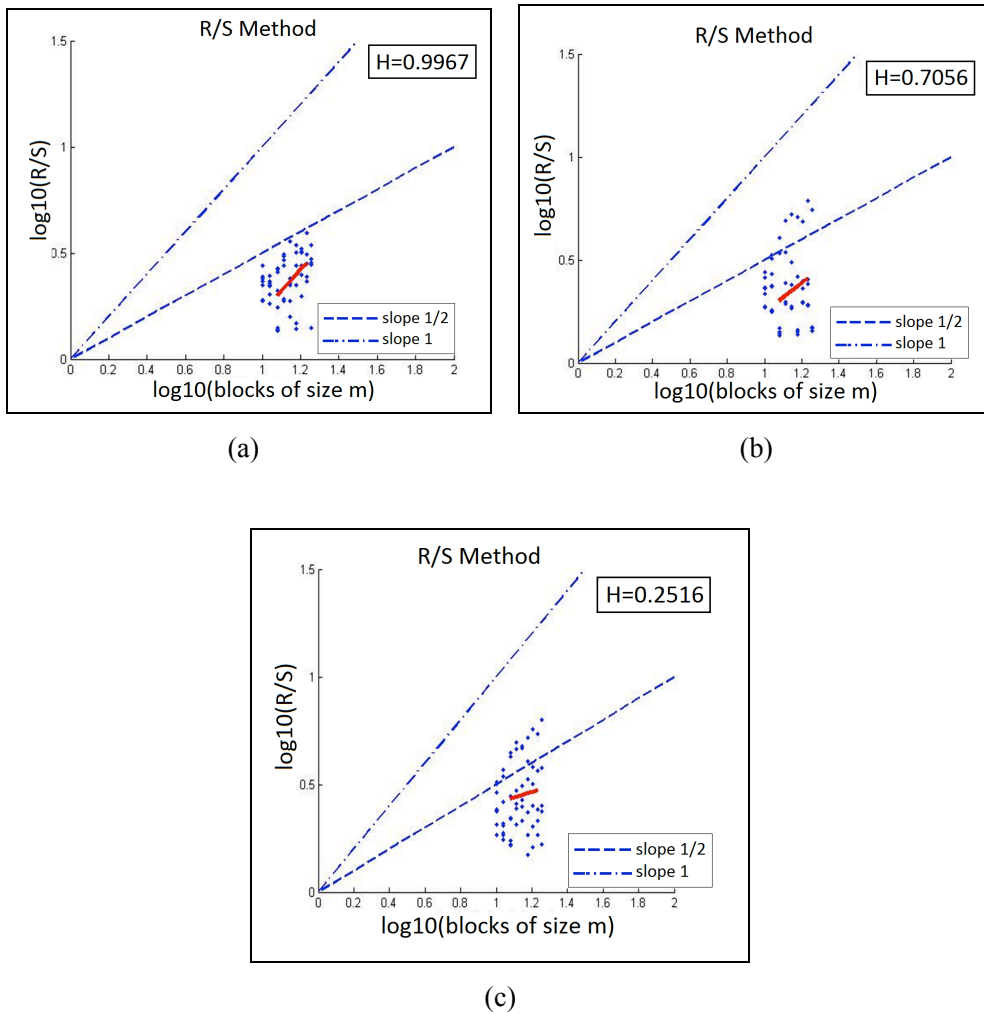


Figure 3. Daily Byte Self Similar with: (a)  $H=0.9967$ ; (b)  $H=0.7056$ ; and (c)  $H=0.2516$

Figure 4(a) to (c) show the highest, medium and lowest plotted graphs of the R/S method analysis on the weekly byte internet traffic on the IPCN network that differentiates the Hurst parameters values. Figure 4(a) shows the Hurst parameter  $H=0.9994$ , Figure 4 (b) shows the plotted  $H=0.8006$ , and Figure 4(c) shows that the plotted  $H=0.7792$ . The Hurst values which range above 0.5 shows that the self-similarity is LRD. Most of the Hurst parameter values are between 0.7 and 0.9, which mean that the self-similarity value for LRD is very high.

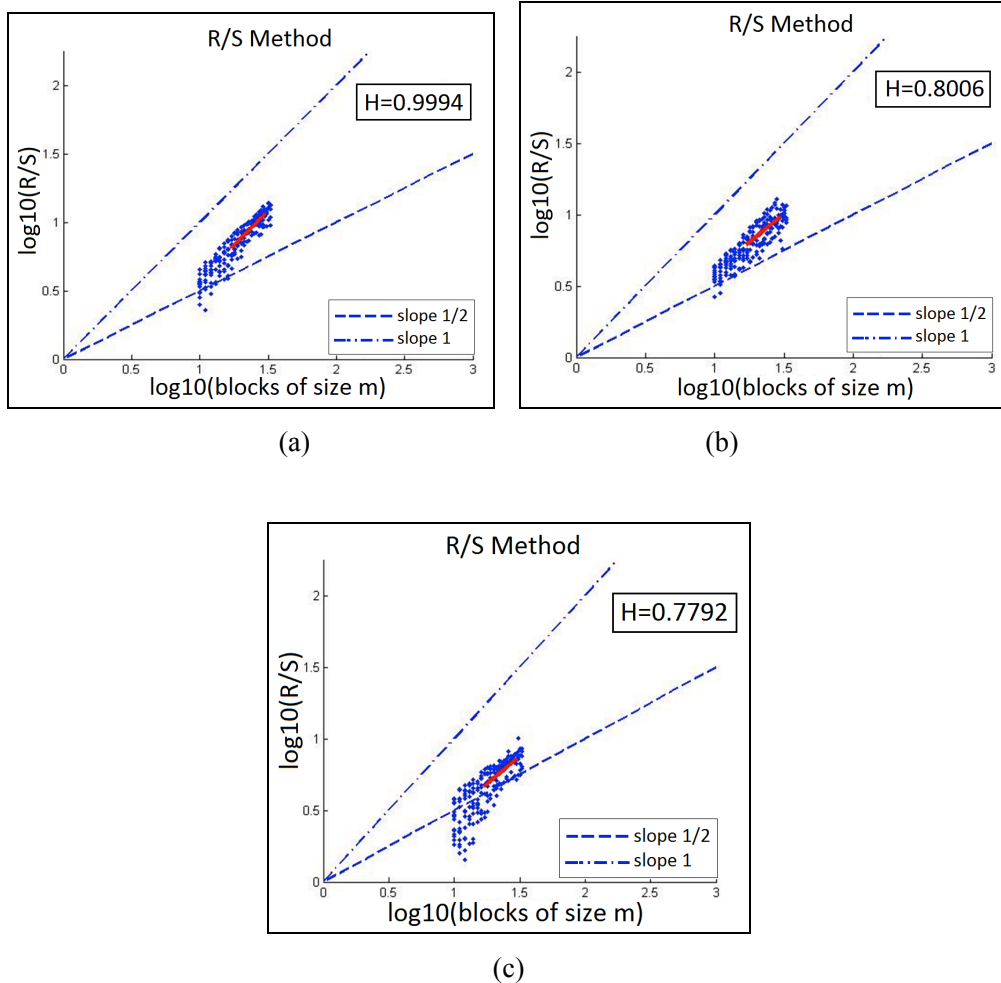


Figure 4. The Weekly Byte Self Similar with: (a)  $H=0.9994$ ; (b)  $H=0.8006$ ; and (c)  $H=0.7792$



**Packet per Second R/S Analysis**

Figures 5(a) and (b) show the highest and lowest plotted graphs of the R/S method analysis on daily packet per second (P/s) internet traffic on the IPCN network that differentiate the Hurst parameters values. Figure 5(a) shows that the Hurst parameter  $H=0.9948$ , and Figure 5 (b) shows the plotted lowest  $H=0.4910$ . Most of the Hurst values range above 0.5, which show that the self-similarity is LRD.

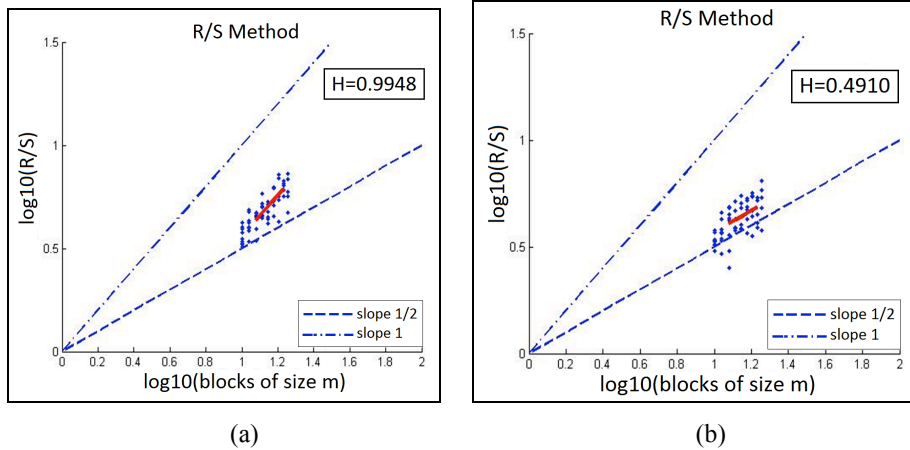


Figure 5. Daily P/S Self Similar with: (a)  $H=0.9948$ ; and (b)  $H=0.4910$

Figures 6(a) and (b) show the highest and lowest plotted graphs of the R/S method analysis on the weekly packet per second (P/s) internet traffic on the IPCN, which differentiate the Hurst parameters values. Figure 6(a) shows that the Hurst parameter  $H=0.9957$ , and Figure 6(b) shows plotted lowest  $H=0.8254$ . Most the Hurst values range above 0.5, showing that the self-similarity is LRD.

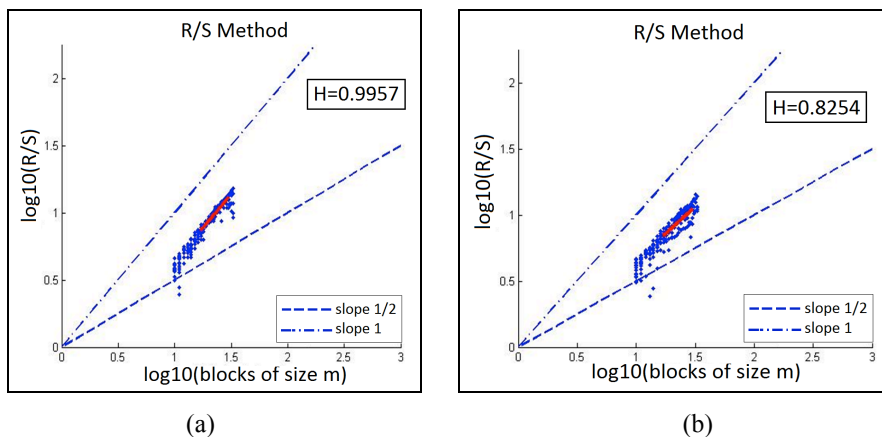


Figure 6. The weekly P/S Self Similar with: (a)  $H=0.9957$ ; and (b)  $H=0.8254$

### Long Range Dependence Analysis

Table 3 and Table 4 present the overall percentage analysis of the Hurst parameter values on the gathered internet traffic in 20 days and 14 weeks. The tabulated percentages in Table 3 show that the Hurst parameter value is above 0.9, which has the highest percentage recorded. This proves that the nearest result of the Hurst parameter to 1, or above 0.9 shows the accuracy of self-similarity. Therefore, this result can be taken as the parameter value to model the queue process for self-similarity in the simulation. Table 4 also tabulates percentage of the identified weekly Hurst parameter analysis, which shows that the percentage has the majority at 0.9 and 0.8 of the Hurst parameter value. This also proves that the weekly traffic analysis is self-similarity in LRD for packet, byte and packet per second traffic captured.

Table 3  
*The percentage of Hurst Parameter Results in 20 days*

Hurst Parameter value	Percentage		
	Packet	Byte	P/s
Hurst Parameter value $\geq 0.9$	30%	40%	50%
Hurst Parameter value $\geq 0.8$ & $>0.9$	10%	20%	20%
Hurst Parameter value $\geq 0.7$ & $>0.8$	25%	5%	20%
Hurst Parameter value $> 0.6$ & $>0.7$	15%	15%	5%
Hurst Parameter value $> 0.5$ & $>0.6$	15%	10%	0%
Hurst Parameter value $\leq 0.49$	5%	10%	5%
Total	100%	100%	100%

Table 4  
*Percentage of Hurst Parameter Results in 14 weeks*

Hurst Parameter value	Percentage		
	Packet	Byte	P/s
Hurst Parameter value $\geq 0.9$	50%	57%	43%
Hurst Parameter value $\geq 0.8$ & $>0.9$	50%	36%	57%
Hurst Parameter value $\geq 0.7$ & $>0.8$	0%	7%	0%
Hurst Parameter value $\geq 0.6$ & $>0.7$	0%	0%	0%
Hurst Parameter value $\geq 0.5$ & $>0.6$	0%	0%	0%
Hurst Parameter value $\leq 0.49$ & $>0.5$	0%	0%	0%
Total	100%	100%	100%

Figure 7 proves that the empirical distribution for the Hurst parameter value in days, which are mostly above 0.5.

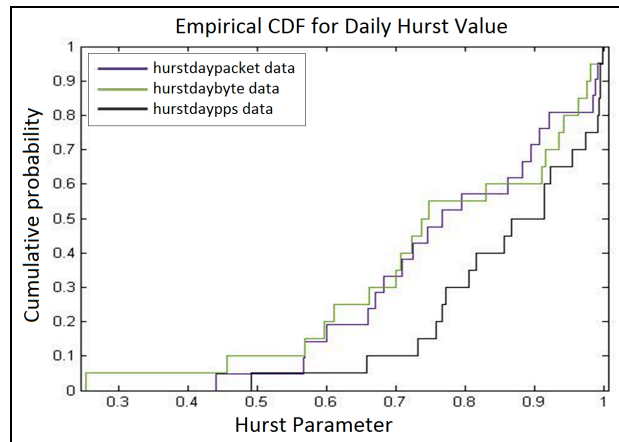


Figure 7. The empirical CDF for the Hurst parameter value in 20 days

The CDF plot shows the cumulative values for the internet traffic in flow, size and speed which relates to packet, byte and packet per second. From the graph, the parameters of median distribution are taken, which results are as derived. The Hurst parameter value shows above 0.74, which is long range dependence.

- Median value for packet traffic Hurst parameter = 0.7654
- Median value for byte traffic Hurst parameter = 0.7416
- Median value for P/s traffic Hurst parameter = 0.8892

Figure 8 proves the empirical distribution for the weekly Hurst parameter values, which are mostly above 0.7. The CDF plot shows the cumulative value for the internet traffic in flow, size and speed, which are related to packet, byte and packet per second. From the graph, parameters of median distribution are taken, from which the results are as derived. The Hurst parameter value shows above 0.89, which is long range dependence.

- Median value for packet traffic Hurst parameter = 0.8942
- Median value for byte traffic Hurst parameter = 0.9308
- Median value for P/s traffic Hurst parameter = 0.8919

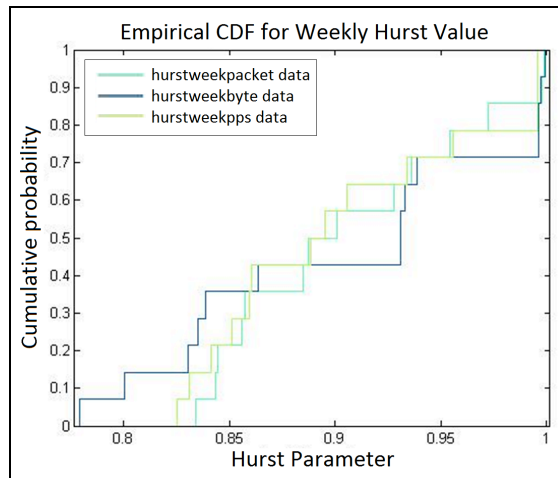


Figure 8. The empirical CDF for the Hurst parameter value in 14 weeks

## CONCLUSION

The results show that the IP-based internet traffic analysis in one of the Campus networks in Malaysia is self-similarity through estimation using the R/S method. The Hurst parameter values show that both the daily and weekly traffics are mostly between 0.5 and 1, which is LRD self-similarity. The Hurst parameter value, which is above 0.5 to 1, is identified as Long Range Dependence traffic (LRD). Only little Hurst parameter value exists in the range below than 0.5, which is above 0.2 and closest to 0.4. The nearest value, which is above 0.9 and closest to 1, is identified as most self-similar traffic. All the three types of captured traffic in flow, size and speed in days and weeks proved the estimated self-similarity values. The percentage analysis on the gathered overall Hurst parameter also proved that most values are above 0.8 and nearest to 1. Therefore, the value can be taken as a sample in running a queue model for the self-similarity traffic flow for IP-based campus network traffic in computer network. This analysis proves that the IP-based campus traffic captured at the campus university network in Malaysia is self-similar by using the R/S method.

## ACKNOWLEDGMENTS

The authors would like to thank Universiti Teknologi MARA and the Ministry of Higher Education (MOHE), Malaysia, for the financial support under the Research Acculturation Grant Scheme (Rags) No. 600-RMI/RAGS 5/3 (35/2015).

## REFERENCES

- Abrahamsson, H. (1999). Traffic measurement and analysis. *SICS Research Report*.
- Akinci, T. C., Seker, S., Guseinoviene, E., & Nayir, A. (2013). *Statistical analysis and Hurst parameter estimation for wind speed in Kizilirmak area of Turkey*. Proceedings of 2013 8<sup>th</sup> International Conference and Exhibition on Ecological Vehicles and Renewable Energies (EVER).

- Arlitt, M., & Williamson, C. (2005). An analysis of TCP reset behaviour on the internet. *ACM SIGCOMM Computer Communication Review*, 35(1), 37-44.
- Bianchi, G., Mancuso, V., & Neglia, G. (2002). *On the self-similarity of measurement-based admission controlled traffic*. Proceedings of Global Telecommunications Conference, 2002. GLOBECOM'02. IEEE.
- Celeda, P., Krmicek, V., Rehak, M., & Medvigy, D. (2007). *High-speed network traffic acquisition for agent systems*. Proceedings of Intelligent Agent Technology, 2007. IAT'07. IEEE/WIC/ACM International Conference.
- Chen, C. (2008). Hurst Parameter Estimate with RS. *Hurst Parameter Estimate with Matlab Code, Matlab Central: File Exchange*. Retrieved from <http://www.mathworks.com/matlabcentral/fileexchange/19148-hurst-parameter-estimate/content/hurst%20estimator/RS.m>.
- Clegg, R. G. (2006). A practical guide to measuring the Hurst parameter. *arXiv preprint math/0610756*.
- Faye, I. (2011). On Integer Sequences Related to a Memorization Technique. *Journal of Applied Sciences*, 11(8), 1473-1475. doi: 10.3923/jas.2011.1473.1475
- Fras, M., Mohorko, J., & Čučej, Ž. (2012). Modeling and Simulating the Self-Similar Network Traffic in Simulation Tool. *Telecommunications Networks - Current Status and Future Trends*.
- Gospodinov, M., & Gospodinova, E. (2005). *The graphical methods for estimating hurst parameter of self-similar network traffic*. Proceedings of the 2005 International Conference on Computer Systems and Technologies.
- Jeong, H. -D. J., & Pawlikowski, K. (1999). *Fast Self-Similar Teletraffic Generation Based on FGN and Wavelets*. Proceedings of IEEE International Conference on Networks (ICON).
- Kassim, M., Ismail, M., Jumari, K., & Yusof, M. I. (2012). *A Survey: Bandwidth Management in an IP Based Network*. Proceedings of International Conference on Computer, Communication and Information Sciences, and Engineering, ICCCISE 2012, World Academy of Science, Engineering and Technology (WASET).
- Kassim, M., Ismail, M., & Yusof, M. I. (2015). A new adaptive throughput policy algorithm on campus ip-based network internet traffic. *Journal of Theoretical and Applied Information Technology*, 71(2), 205-214.
- Kassim, M., Ismail, M., & Yusof, M. I. (2015). Statistical analysis and modeling of internet traffic IP-based network for tele-traffic engineering. *ARPJ Journal of Engineering and Applied Sciences*, 10(3), 1505-1512.
- Klemm, A., Lindemann, C., & Lohmann, M. (2003). Modeling IP traffic using the batch Markovian arrival process. *Performance Evaluation*, 54(2), 149-173.
- Leland, W. E., Taqqu, M. S., Willinger, W., & Wilson, D. V. (1994). On the self-similar nature of Ethernet traffic (extended version). *Networking, IEEE/ACM Transactions on*, 2(1), 1-15.
- Park, K., & Willinger, W. (2000). *Self-similar Network Traffic and Performance Evaluation*. Wiley Online Library.
- Park, K., & Willinger, W. (2000). *Self-similar Network Traffic: An Overview*. *Self-similar Network Traffic and Performance Evaluation*, 1-38.

- Pezaros, D. (2005). *Network traffic measurement for the next generation Internet*. Lancaster University.
- Schudel, G. (2013). Bandwidth, Packets Per Second, and Other Network Performance Metrics. *Cisco Security Intelligence Operations*. Retrieved from [http://www.cisco.com/web/about/security/intelligence/network\\_performance\\_metrics.html](http://www.cisco.com/web/about/security/intelligence/network_performance_metrics.html).
- Stathis, C., & Maglaris, B. (2000). Modelling the self-similar behaviour of network traffic. *Computer Networks*, 34(1), 37-47.
- Xiaolong, Y., Julong, L., & Wanwei, H. (2013). *Network traffic anomaly detection based on self-similarity using FRFT*. Proceedings of Software Engineering and Service Science (ICSESS), 2013 4<sup>th</sup> IEEE International Conference.
- Zhang, D., Liu, Y., Adi, A., & Li, H. (2008). *Improved R/S Algorithm Based on Network Traffic Self-Similarity*. Proceedings of Wireless Communications, Networking and Mobile Computing, 2008. WiCOM '08. 4th International Conference.
- Zhang, X. Y., & Luo, L. Y. (2012, 21-25 Oct. 2012). *Self-similarity analysis of time series*. Proceedings of Signal Processing (ICSP), 2012 IEEE 11th International Conference.



## **A Pre-shared Diffie-Hellman Key Exchange Scheme for a Secure TFTP Protocol**

**Nur Nabila Mohamed\*, Mohd Anuar Mat Isa, Yusnani Mohd Yusoff and Habibah Hashim**

*Faculty of Electrical Engineering, Universiti Teknologi MARA (UiTM), 40450 Shah Alam, Selangor, Malaysia*

### **ABSTRACT**

Implementation of Trivial File Transfer Protocol (TFTP) in embedded system is significant because of the speed and simplicity. However, no security service in TFTP marks its major limitations. In this work, a pre-shared Diffie Hellman Key Exchange (DHKE) technique was proposed for mutual authentication to achieve the same secret key in TFTP communication protocol. We also integrated the system with feasible compression and encryption process to significantly improve the TFTP communication performance. The DHKE proof of concept is discussed briefly to show the feasibility of the pre-shared technique on the protocol. Also, the experiment was performed on constrained embedded devices to analyse the performance of compression/encryption scheme in TFTP. From the results obtained, the combined encryption and compression process is able to reduce the time by about 30% compared to the original file transmission time. Thus, the proposed work presents both advantages to reduce file size and provide security for the data. This is a preliminary work to provide a secure TFTP communication which has benefits to be implemented in embedded system field and IoT services.

*Keywords:* Advanced encryption standard, Diffie Hellman Key Exchange (DHKE), Huffman coding, Trivial File Transfer Protocol (TFTP)

### **ARTICLE INFO**

*Article history:*

Received: 25 October 2016

Accepted: 17 March 2017

*E-mail addresses:*

nurnabilamohamed@gmail.com (Nur Nabila Mohamed),

anuarls@hotmail.com (Mohd Anuar Mat Isa),

yusna233@salam.uitm.edu.my (Yusnani Mohd Yusoff),

habib350@salam.uitm.edu.my (Habibah Hashim)

\*Corresponding Author

### **INTRODUCTION**

TFTP is a multi-purpose protocol with simple functions used in many applications such as uploading/downloading images, upgrading system, booting nodes, etc. Nevertheless, its implementation in certain situations exposes the system to risks of cyber-attacks as it provides no security mechanism. For instance, during software updates of the Access Point (AP) remote host using Trivial

File Transfer Protocol (TFTP) (Isa et al., 2012), an unauthorised user can disturb the system by installing malicious codes such as a backdoor in the boot loader, kernel, or application to hack the private information linked with the hijacked AP. Furthermore, nowadays, TFTP has been used in embedded field (IoT, embedded multi-agent system), which presents the need to solve the security problem in this protocol. Thus, in this work, we proposed integrating TFTP with a key exchange protocol for secret key exchange and implementing combined encryption and compression scheme for data protection. We believe that this proposed protocol can be a significant enhancement in pervasive computing and IoT applications for managing and upgrading embedded infrastructure.

The remainder of this paper is structured into several sections: Section 2 discusses the related work; Section 3 explains the proposed pre-shared DHKE scheme; Section 4 addresses the proposed methodology, while Section 5 presents the results and discussions of the implementation. The last section concludes the work and briefly discusses several future enhancements of secure TFTP protocol.

## Related Works

**Trivial File Transfer Protocol.** Due to insufficient storage and complexity issues in File Transfer Protocol (FTP), a faster and lightweight version (TFTP) was introduced in 1970s for configuring files and updating devices quickly and easily. However, its implementation is limited to allowing only conventional operations such as reading and writing to files. It has been noticed that in the current implementations of TFTP such as in IoT, embedded multi-agent system, etc., it might be possible for any machine to interrupt the system as TFTP does not require any authentication and directory permission checks (Bollins, 1992). In RFC 3617 (Lear, 2003), it is clearly declared that TFTP provides no mechanism for authentication within the protocol, and this protocol is vulnerable to Man-In-The-Middle (MITM) attack. Furthermore, recent research works have addressed the potential usage of this lightweight protocol for Radio Frequency (RF) (Kao et al., 2010) and remote attestation for Trusted Computing (Schiffman et al., 2011) such as Trusted Platform Modules (TPM) which have revealed the importance of security enhancements for TFTP. Hence, we believe that security integration to this protocol will bring huge advantages in the field of embedded systems.

**Diffie Hellman Key Exchange Protocol (DHKE).** DHKE algorithm was introduced by Diffie and Hellman in 1976 to securely exchange secret parameters over insecure channels. Several studies regarding the DHKE implementation method have proven that this protocol enables the communicating users to jointly establish a shared secret over the public channel (Li, 2010; Carts, 2001). However, one of its limitations is the vulnerability to MITM attack, where the unauthorised party attempts to intercept and obtain the information passing through insecure channel. For example, Alice and Bob want to share their shared secret key in a public medium.



Eve, the Man-In-The-Middle, comes to intercept by performing her own public parameters to alter their communication. The important parameters in DHKE protocol are listed below:

$A$	Alice's public value, known to Alice, Bob and Eve
$A'$	Eve's public value sent to Bob
$a$	Alice's secret value, known only to Alice
$B$	Bob's public value, known to Alice, Bob and Eve
$B'$	Eve's public value sent to Alice
$b$	Bob's secret value, known only to Bob
$g$	Primitive root modulo $p$ , known to public
$p$	Large prime numbers, known to public

MITM attack is explained based on the following steps:

- Alice and Bob agree on  $p=97$  and  $g=5$  values, in which  $p$  is a big prime number and  $g$  is the generator of  $p$ .
- Alice chooses her private value,  $a=36$  and computes her public value,  $A=50$ . She then sends  $A$  to Bob which is intercepted by Eve.
- Eve obtains the values  $97(p)$ ,  $5(g)$ , and  $A=50$  through improper means, she computes a new public value,  $A'=13$  using her secret 25. She sends  $A'=13$  to Bob.
- On the other side, Bob chooses his private value,  $b=58$ , and computes  $B = 44$ . He then sends  $B$  to Alice, which is also intercepted by Eve.
- Eve creates a new secret, 30, computes  $B'=79$ , and then sends to Alice.
- Alice believes that  $B'$  is received from Bob, so she proceeds to compute the secret key ' $K$ ' as  $K = B^a \text{ mod } p = 22$ .
- Bob understands that  $A = 13$  is received from Alice, and thus computes the secret key, ' $K$ ' as  $K = A^b \text{ mod } p = 53$ .
- Eve who has intercepted and modified the messages will compute two keys, one of which is to be shared with Alice, and the other one with Bob.
- For this, she computes the key to be shared with Alice as  $K = 5^{30} \text{ mod } 97 = 22$ , and the key to be shared with Bob as  $K = 44^{25} \text{ mod } 97 = 53$ .

Once the attack is done, Eve can decrypt the key she has exchanged between Alice and Bob and compromise the entire communication. Thus, the original DHKE protocol has no means to mitigate MITM attacks.

Therefore, we believe that the proposed pre-shared concept in DHKE is one of the simplest security solutions for securing the communication from MITM attack in the TFTP communication protocol. The pre-shared concept enables both parties to have knowledge of several parameters, and only one side needs to send the public value to the other side. The pre-shared method will be explained in Section 3. Meanwhile, the next subsection will address the need for compression and encryption in secure communication. A secure key exchange technique ensures that associated encryption and decryption keys are safely exchanged between the communicating parties.

**Compression and Encryption Approach.** In the situation when dealing with a large amount of data, compression scheme is required to reduce the size; nevertheless, the scheme alone is not sufficient as it is still accessible and open to public. Therefore, an employment of joint compression and encryption process enable faster and secured data transmission. Several related works have addressed the necessity to combine the compression and encryption approach for efficient data transmission. For instance, Singh and Manimegalai (2012) found that symmetric encryption is an efficient encryption mechanism to protect the compressed data. Also, the related work by Razzaque (2012) revealed that the execution of compression technique, followed by the encryption technique, is much more preferable as an intruder has less cleave to obtain data information when using this sequence. Meanwhile, Chaudhari (2013) proposed performing the compression technique using two types of lossless compression algorithms, followed by encrypting data using symmetric encryption (DES). Nevertheless, the author did not elaborate on the key exchange process in the system. According to the related works cited above, we believe that symmetric encryption algorithms such as AES or DES are compatible to be integrated with compression coding; thus, we integrate the proposed idea with minimal compression and encryption process to significantly reduce the computational requirements in TFTP communication.

**Related Works in Securing TFTP.** Referring to some previous works on TFTP (see Kao et al., 2010; Schiffman et al., 2011), we realised the importance of providing security mechanism in the protocol to prevent various attacks that will be used in low computational power devices. Nevertheless, there are very few studies in the field of secure TFTP protocol. So far, we have studied two recent works elaborating on the importance of securing TFTP. Horvat, Žagar and Martinović (2013) improved the security in TFTP protocol by introducing a security extension to the general TFTP using Digest Access Authentication (DAA), which was accompanied by hash function SHA1 for authentication credibility. The authors proposed two data ciphers to establish data confidentiality, XTEA and AES, because these schemes are considered secure for all known attacks. The work, however, does not explain the key exchange protocol for secret key generation, and the results on generating nonce values for TFTP protocol have also not been discussed.

In our previous works (Mohamed et al., 2013; Mohamed, Hashim & Yussoff, 2014), the framework of the proposed secure TFTP was presented, and a preliminary experiment on securing TFTP packet was done by analysing the execution and transmission time of encrypting and decrypting data. The security framework in TFTP introduced by Isa et al. (2012) provides security negotiation such as attestation before file transmission process. The author proposed a new packet header in the existing TFTP option extension using two cryptographic principles, symmetric (AES algorithm) and asymmetric encryption (DHKE concept). This work is considered as a preliminary step on securing TFTP packet but its implementation and integrity properties still have not been discussed to ensure the encrypted data payload is protected from adversary.

Based on two major related works (Isa et al., 2012; Horvat, 2013) on securing the TFTP protocol, we believe that the proposed scheme can provide considerable security requirement in TFTP communication.

**Pre-shared DHKE Scheme.** The MITM attack usually happens because DHKE does not authenticate the communicating participants. It enables the adversary to interrupt the communication by replacing his/her own public value to both communicating parties. When the client sends his public value to server, the Man-In-The-Middle intercepts it by sending its own value to either client, or server. Once they agree on the shared parameters exchange, the intruder can use the key to decrypt any messages sent out by the client, or server, and he/she is able to modify the information before transmitting it to the other side. Thus, the implementation of DHKE pre-shared public parameters has been considered as one of the reliable techniques to mitigate MITM attacks and it can be implemented in the TFTP file transmission protocol as only the server side shares the public value.

In this work, a network packet analyser called Wireshark was utilised to capture packet sent between client and server. This was done to show that if the Man-In-The-Middle tried to interrupt the communication between client and server, he/she could only get or modify the public value B, but even this would not affect the security of the whole communication system. Figure 1 shows that the intruder may read and change the server's public value, which is B, but this will not compromise the communication since both communicating parties already have knowledge of one of the public values (A). Hence, we believe that the proposed pre-shared technique is considerably secure from MITM because the adversary would have been unable to obtain the true secret value and this has become the strength in this protocol as well. Furthermore, in TFTP, the client sends the RRQ together with the server's IP address. Even after the intruder executes some modifications, the client still knows that the value received is wrong because after computing the secret key, it would fail to decrypt the data. Thus, the client would need to send another request to the server.

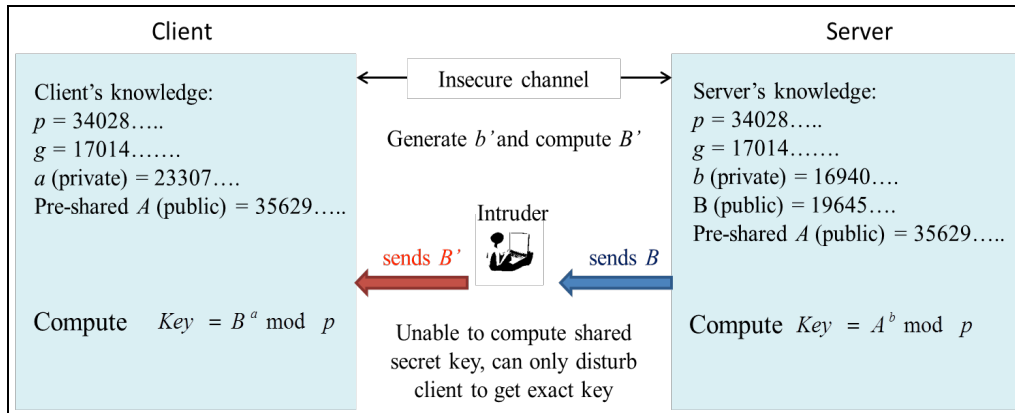


Figure 1. DHKE Pre-shared public parameters

## METHOD

### The Proposed Method

The experiment was set up using two microprocessors (Raspberry Pi) acting as both the client and server. The devices were placed in a distance about a meter connecting via wireless using Wi Pi dongle. Besides, additional software, OS Linux Raspbian 6 (Wheezy), had also been installed on each workstation. The public parameters pre-shared between the communicating devices ( $p$ ,  $g$  and  $A$ ) were established during the initial communication. The proposed key exchange concept to share the public parameters in wireless TFTP communication is illustrated in Figure 2 below. It starts with the client sending the RRQ packet to get server's public value,  $B$ . The RRQ packet sent contains opcode 1 and the filename field contains RRQ of Public Key,  $B$ . The server acknowledges the request by sending the DATA packet containing a 3 in the opcode field, the block# starts with 1 and DATA field contains the value  $B$ . The client approves by sending acknowledgment ACK packet containing opcode 4 and block# 1. The file containing payload less than 512 bytes signs the end of data transfer. In this work, the prime value for  $p$  is large and hard enough to be guessed in order to be secured against attacks. Besides, it is also important to ensure that the public value  $B$  should always be different in every transmission to prevent the adversary from computing the key easily.

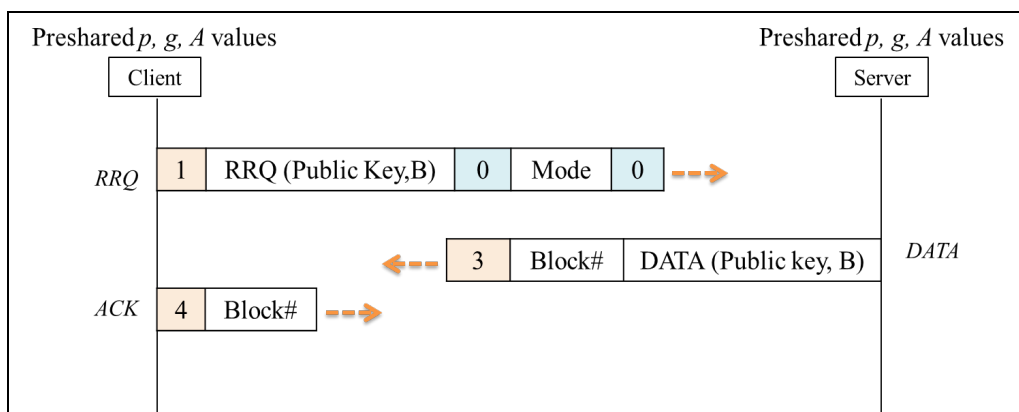


Figure 2. The proposed work in TFTP

In order to achieve time minimisation and data confidentiality in this work, Huffman coding compression algorithm and AES encryption algorithm were selected based on the related works by several researchers. A sample original file of various sizes was processed in three ways. First, it was simply encrypted using AES encryption scheme; secondly it was simply processed using the Huffman coding. Finally, the file was compressed and then encrypted, respectively. Both the results and discussions are given in the next section based on the performance of the proposed technique in TFTP communication.

## RESULTS AND DISCUSSION

### Experimental Results for Variation in File Size after Processing

Once the exchange was done and the secret key to be used in symmetric encryption and decryption process was obtained, the compression/security scheme technique was performed. The following equation was then used to compute the file size variation in kiloBytes (kB) after the compressed and encrypted process.

$$\text{Variation of File Size} = \frac{\text{Size after Compression/Encryption}}{\text{Size before Compression/Encryption}} \quad [1]$$

Table 1 shows the different variations in the file size of four file types (original file, compressed file, encrypted file, and combined compressed-encrypted file). Based on the results given below, the percentage average of compressed file is about 28.8%, which has reduced about 2/3 of the original file size. In contrast, an increase in the file size was recorded for the encrypted file due to the insertion of extra bytes of padding during encryption process. However, it can be seen that the average variation for combined scheme is about 29.3%, which is almost similar to the result obtained with independent compression thus providing good compression ratio, as the difference between them is only 1.5%. This result shows the significance of implementing the combined scheme for the proposed secure TFTP communication protocol.

Table 1  
*Variation in file sizes after processing*

Original file size (kB)	After compression		After encryption		After compression/ encryption		
	kiloByte (kB)	Percentage (%)	kiloByte (kB)	Percentage (%)	kiloByte (kB)	Percentage (%)	
9.22	2.68	0.291	9.53	1.034	2.98	0.323	
51.10	14.74	0.288	51.94	1.016	15.05	0.295	
102.21	29.45	0.288	102.50	1.003	29.75	0.291	
511.05	147.15	0.288	511.35	1.001	147.45	0.289	
1024.00	294.82	0.288	1024.29	1.000	295.13	0.288	
2047.45	289.46	0.288	2047.75	1.000	589.77	0.288	
5119.39	1473.83	0.288	5119.69	1.000	1474.13	0.288	
10239.80	2947.93	0.288	10240.10	1.000	2948.23	0.288	
20479.61	5895.83	0.288	20479.91	1.000	5896.13	0.288	
30719.41	8843.73	0.288	30719.72	1.000	8844.04	0.288	
		28.8		100.5		29.3	Average percentage (%)

### Experimental Results for File Transmission Time

The file transmission time was taken three times to ensure that the value is accurate. The transmission time for every scheme was taken to show the comparison of time difference when transmitting the original file and processed files. Based on the data given in Table 2, the transmission time increased when the file size increased. Meanwhile, transmission of the encrypted file took the longest time as the file size increased a few bytes compared to the original. The transmission was done via wireless network configuration. Therefore, it can be seen that the execution time for sending large file takes much more time. The reason is due to several connection problems such as low connection, connection lost, etc. The results were then plotted in the graph shown in Figure 3 for comparison purposes.

Based on Figure 3, the transmission time for the compressed file is the fastest compared to the other schemes. However, it can be seen it is approximately similar with the transmission time when using the combined scheme (compressed-encrypted file). It is shown that the proposed combined process is able to reduce the time by about 30% compared to the original file transmission time. Thus, this can be considered as a significant result along with the fact that it particularly presents both advantages to reduce file size and provide security for the data.

Table 2  
File transmission time

Original file transmission										
File size (kB)	9.2	51.1	102.2	511.1	1024.0	2047.5	5119.4	10239.8	20479.6	30719.4
Transmission time (s)	0.6	3.3	6.6	32.5	67.3	141.6	336.9	670.8	1017.6	1642.9
Encrypted file transmission										
File size (kB)	9.5	51.9	102.5	511.4	1024.3	2047.8	5119.7	10240.1	20479.9	30719.7
Transmission time (s)	0.7	3.4	6.8	33.1	68.1	147.1	348.5	698.8	1259.7	1820.6
Compressed file transmission										
File size (kB)	2.7	14.7	29.5	147.2	294.8	589.5	1473.8	2947.9	5895.8	8843.7
Transmission time (s)	0.24	1.6	2.7	10.5	28.7	47.5	155.1	298.9	659.3	1019.3
Compressed/encrypted file transmission										
File size (kB)	3.0	15.1	29.8	147.5	295.1	589.8	1474.1	2948.2	5896.1	8844.0
Transmission time (s)	0.2	1.9	3.1	15.8	29.3	65.9	166.3	371.0	735.4	1169.9

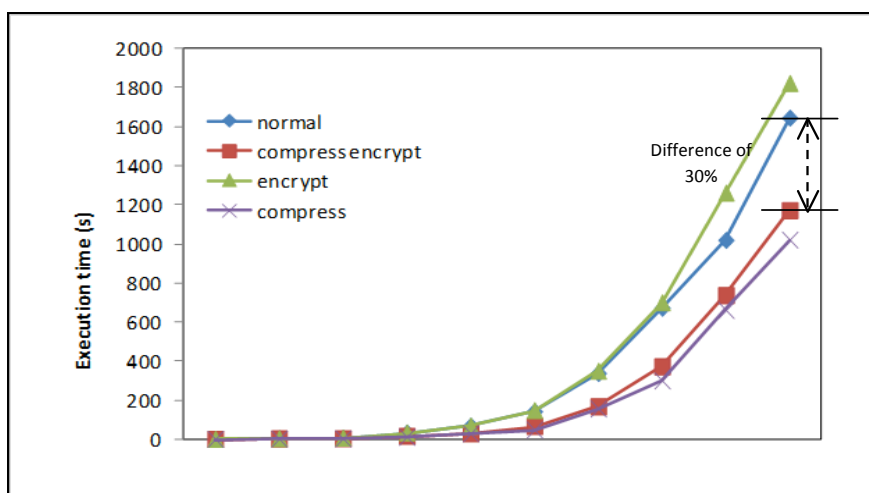


Figure 3. The TFTP file transmission time

## CONCLUSION

In conclusion, this work has introduced the key exchange concept using the pre-shared technique to secure communication in the TFTP protocol. The idea of pre-shared technique was proposed to mitigate the MITM attack, which is one of the security vulnerabilities in the DHKE protocol. It has been explained in the result and discussion section that the pre-shared

DHKE provides increased security as one of the communicating parties has already known the public value of the other and could use it to compute the secret key using DHKE.

Besides, we also have considered the implementation of file compression coding and cryptographic security mechanism in TFTP using the Huffman compression coding and AES encryption algorithm for an efficient and secure file transmission. From the results, it can be seen that the time difference when using the proposed combined process is about 30% compared to the original file transmission time. Thus, this work has presented both advantages, which are reducing file size and providing security for the data. The proposed idea of pre-shared key exchange concepts in TFTP shows a significant contribution of this work, which can enhance security while transferring data in wireless AP or IoT system to prevent any MITM attack.

## ACKNOWLEDGEMENTS

The authors would like to thank the Ministry of Higher Education (MOHE) for providing the NRGs grant 600-RMI/NRGs 5/3 (5/2013) in the project entitled, Algebraic-Structure-Based Lightweight Security Technique, Research Management Institute (RMI), UiTM, and also members of Computer Engineering research, Faculty of Electrical Engineering, UiTM Shah Alam, for supporting the research project reported in this paper.

## REFERENCES

- Bollins, K. (1992). The TFTP Protocol (Revision 2) RFC 1350. *Official Protocol Standard*, 1–11.
- Carts, D. (2001). A Review of the Diffie-Hellman Algorithm and its Use in Secure Internet Protocols. *SANS Institute Infosec Reading Room*, 1-9.
- Chaudhari, M. (2013). Fast and Secure Data Transmission using Symmetric Encryption and Lossless Compression. *International Journal of Computer Science and Information Technology*, 2(2), 58–63.
- Horvat, G., Žagar, D., & Martinović, G. (2013). STFTP: Secure TFTP protocol for embedded multi-agent systems communication. *Advanced in Electrical and Computer Engineering*, 13(2), 23–32.
- Isa, M. A. M., Mohamed, N. N., Hashim, H., S. Adnan, F. S., Manan, J. L. A., & Mahmud, R. (2012). A lightweight and secure TFTP protocol for smart environment. *IEEE Symposium on Computer Applications and Industrial Electronics*, 302–306.
- Kao, K. F., Liao, I. E., & Lyu, J. S. (2010). An indoor location-based service using access points as signal strength data collectors. *International Conference on Indoor Positioning and Indoor Navigation*, 15–17.
- Lear, E. (2003). Uniform Resource Identifier (URI) Scheme and Applicability Statement for the Trivial File Transfer Protocol (TFTP). *Request for Comment*, 3617, 1-7.
- Li, N. (2010). Research on Diffie-Hellman key exchange protocol. *2<sup>nd</sup> International Conference of Computer Engineering Technology*, 634–637.
- Mohamed, N. N., Hashim, H., & Yusoff, Y. M. (2014). Compression and Encryption Technique on Securing TFTP Packet. *IEEE Symposium on Computer Applications and Industrial Electronics (ISCAIE)*, 198–202.



- Mohamed, N. N., Hashim, H., Yussoff, Y. M. & Isa, M. A. M. (2013). Securing TFTP Packet: A Preliminary Study. *IEEE Control and System Graduate Research Colloquium*, 158–161.
- Razzaque, A. (2012). Image Compression and Encryption: An Overview. *International Journal of Engineering Research and Technology*, 1(5), 1–7.
- Schiffman, J., Moyer, T., Jaeger, T., & McDaniel, P. (2011). Network-based root of trust for installation. *IEEE Security and Privacy*, 9, 40–48.
- Singh, K. J., & Manimegalai, R. (2012). A Survey on Joint Compression and Encryption Techniques for Video Data School of Information Technology and Engineering. *Journal of Computer Science*, 8(5), 731–736.



## **Effects of the Number of Nozzles on Acoustic Signals Produced by a Ranque-Hilsch Vortex Tube**

**Khairil Muhaimin Abd Rahman\*, Wirachman Wisnoe and Valliyappan David Natarajan**

*Faculty of Mechanical Engineering, Universiti Teknologi MARA (UiTM), 40450 Shah Alam, Selangor, Malaysia*

### **ABSTRACT**

This study was carried out to investigate effects of acoustic and thermofluid performance of a Ranque-Hilsch Vortex Tube (RHVT) with different numbers of swirl generator nozzles. The number of nozzle used in the experiment was 1, 2, 3, 4, 5 and 6 nozzle(s), respectively. Sound signal produced by the device was recorded using two microphones located at hot side and cold side of the tube. The sound signal was transformed using Fast-Fourier Transform (FFT) to obtain the frequency representation. Then, the frequencies produced were related to its thermofluid performance of each configuration.

*Keywords:* Fast-Fourier Transform, nozzle, RHVT, signature frequency

### **INTRODUCTION**

RHVT (see Figure 1) is an industrial device that is able to produce hot and cold temperatures of flow from compressed air. Compressed air supplied to the inlet of the device enters the nozzles of the swirl generator to create swirl motion. This swirl flow moves close to the tube wall towards the hot end and exits through the conical valve. The central part of the flow in the tube is bounced back to create a secondary flow towards the orifice and exits through the cold end of the device. The flow of air leaving the conical valve has a higher temperature relative to the inlet temperature, while the flow leaving the orifice has a lower temperature relative to the inlet temperature.

#### **ARTICLE INFO**

*Article history:*

Received: 25 October 2016

Accepted: 17 March 2017

*E-mail addresses:*

khairil\_muhaimin90@ymail.com (Khairil Muhaimin Abd Rahman),

wira\_wisnoe@salam.uitm.edu.my (Wirachman Wisnoe),

davidfkm@salam.uitm.edu.my (Valliyappan David Natarajan)

\*Corresponding Author

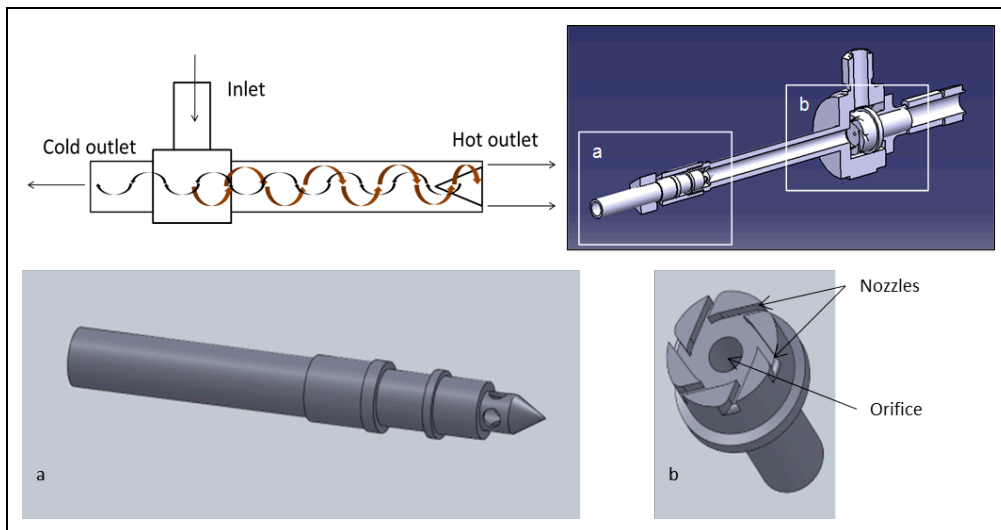


Figure 1. RHVT and its components; (a) Conical valve; and (b) Swirl generator

Despite the simplicity of its mechanism, the phenomenon is not well understood. Throughout the years, many researches have been related studies to explain the phenomenon. Universiti Teknologi MARA (UiTM), Malaysia, has started the research works on RHVT since 2011. The study covered experimental, CFD simulation, visualisation and acoustic analysis. Among other, the study by Ismail et al. (2014) showed the change of parameters influencing the performance of RHVT. They conducted experiments by changing the inlet pressure, nozzle depth and orifice diameter, and found that the increases of inlet pressure and nozzle depth would improve the performance of the device. However, the performance of the device was not in linear to the orifice diameter. Some experimental studies were also done by other researchers such as Thakera (2015) and Nimbalkar (2009). Visualisation of the device was done by Istihat et al. (2016) using transparent tube with a bigger scale from the actual RHVT. Through this visualisation, they could observe the swirl motion inside the tube. Wisnoe et al. (2016) conducted experiments to associate the effects of different nozzle depths on the acoustic signals produced by RHVT, as also suggested by Kurosaka (1982) about the acoustic streaming of the device. They observed that increasing the inlet pressure of the RHVT did not displace the frequencies significantly when the same swirl generator was used within the range of inlet pressures studied. Magnitude of the frequencies, however, changed significantly when different swirl generators were used. Different swirl generators produced different sets of frequencies. The set of frequencies-magnitudes represent a unique signature of RHVT for that specific configuration and performance of RHVT. Abd Rahman et al. (2016) further investigated the acoustic signatures produced by RHVT by studying the effects of orifice diameter on the acoustic signature at the hot tube. It was observed that the acoustic signature remained unchanged when different orifice diameters were used. In another study, Istihat et al.

(2015) presented the wavelet transformation of the acoustic signals recorded at the outlet of cold and hot tubes. The wavelet analysis allowed time-frequency representation of the signals to be obtained.

This paper focuses on effects of the number of nozzles on the acoustic signal produced at the tube and its thermofluid performances.

## METHOD

A schematic illustration of the experimental setup of the experiment is shown in Figure 2. This experimental setup is used to ensure that all thermofluid data such as mass flow rate, temperature and pressure at the inlet and two outlets are properly measured and the sounds produced at both tubes of RHVT were captured.

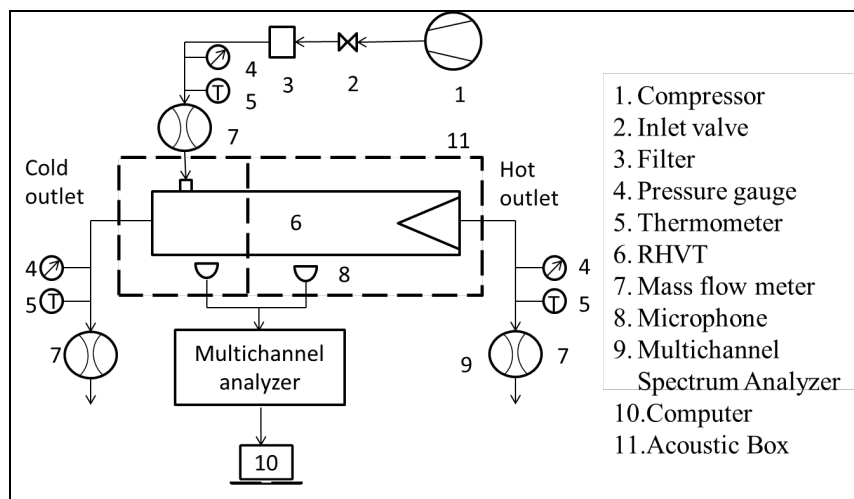


Figure 2. A schematic view of the experimental setup

The air pressure was controlled by a valve placed before the inlet. The pressures were set at 10 psi, 15 psi, 20 psi and 25 psi, respectively. This experiment was held in a thermodynamic laboratory at around 101kPa of the atmospheric pressure.

An “anechoic” box was used to isolate the sound produced at the tube from the surrounding noise. The “anechoic” box is divided into two chambers, separating the hot tube and the cold tube. This is to ensure that only the sound produced on each side is recorded. The sounds at both tubes were captured by a B&K microphone connected to a multichannel spectrum analyser.

Figure 3 shows the swirl generator used in this experiment. A total of six swirl generators were used in the experiment with different numbers of nozzles.

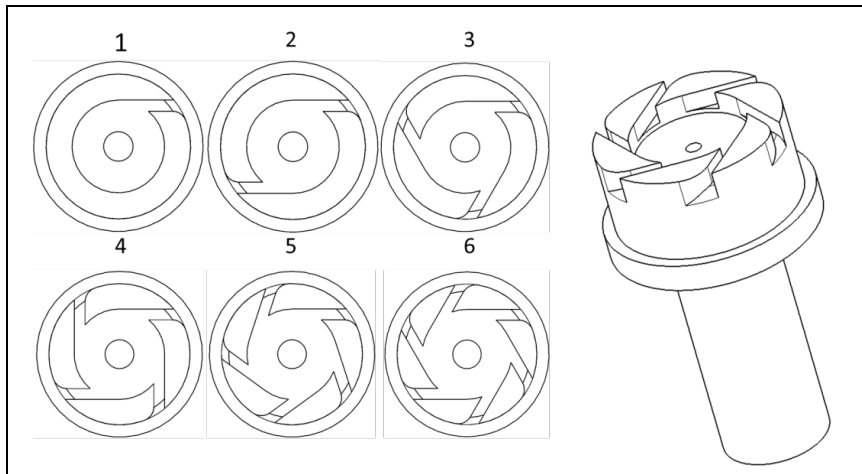


Figure 3. Drawing of the swirl generators

$\Delta T_c$  is the temperature difference between the air at the inlet ( $T_i$ ) and the cold air exiting from the cold tube ( $T_c$ ).

$$\Delta T_c = T_i - T_c \quad [1]$$

Isentropic efficiency ( $\eta_{isen}$ ) is calculated using the principle of adiabatic expansion of an ideal gas, where  $\gamma$  is the specific heat ratio (for air  $\gamma = 1.4$ ), while  $P_a$  and  $P_i$  represent the atmospheric pressure and the inlet pressure of the air, respectively (Ismail et al., 2014).

$$\eta_{isen} = \frac{T_i - T_c}{T_i \left( 1 - \left( \frac{P_a}{P_i} \right)^{\frac{\gamma-1}{\gamma}} \right)} \quad [2]$$

The recorded sounds were analysed using Fast-Fourier Transform (FFT). Main frequencies were extracted and replaced by the bars representing the frequency location and magnitude, respectively.

## RESULTS AND DISCUSSION

Figure 4 shows the variation in the different temperatures between the inlet and outlet when the number of nozzle varied. Five gage pressures were applied at the inlets. All the curves gave almost the same trend, whereby it climbed from 1 nozzle to 2 nozzles before descending at a higher number of nozzles. Higher inlet pressure gave a higher temperature difference for all number of nozzles. The maximum temperature difference was obtained when the 2 nozzles swirl generator was used (20.6°C at 30 psi inlet pressure).

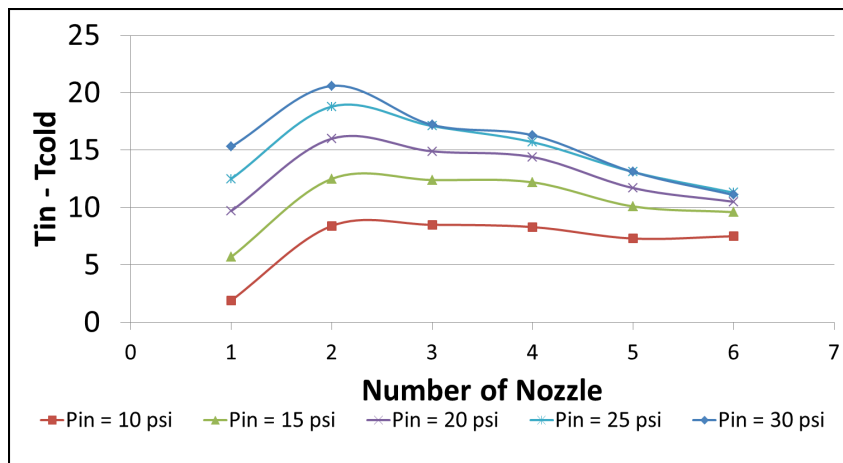


Figure 4. Cold temperature difference vs. number of nozzles

Figure 5 shows the effects of number of nozzles on the isentropic efficiency of RHVT. The isentropic efficiency gradually increased from 1 nozzle to 2 nozzles before it decreased at a higher number of nozzles. Among the six swirl generators used, the 2 nozzles generator produced the maximum efficiency (around 20% - 25%) for all the five pressures applied at the inlet. The highest isentropic efficiency achieved was 24.93% for the 2 nozzles generator at 30 psi of inlet pressure.

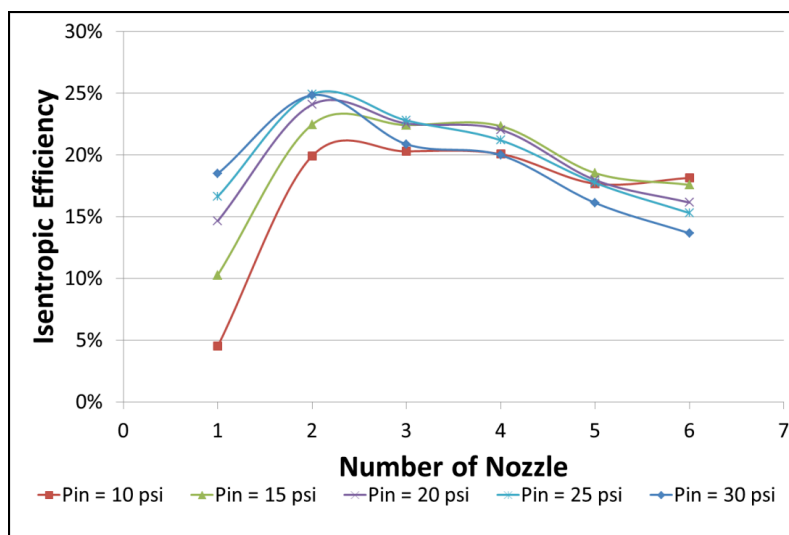


Figure 5. Isentropic efficiency vs. number of nozzle

Figures 6 and 7 represent the sound signals produced at each of the tube, respectively. The sound was recorded for 80 ms using 2 nozzles (1<sup>st</sup> column), 3 nozzles (2<sup>nd</sup> column), 4 nozzles (3<sup>rd</sup> column), 5 nozzles (4<sup>th</sup> column) and 6 nozzles (5<sup>th</sup> column) at the inlet pressures of 10 psi (1<sup>st</sup> row), 15 psi (2<sup>nd</sup> row) and 20 psi (3<sup>rd</sup> row), respectively. The signal produced by the single nozzle is not included in this acoustic analysis as the frequency produced is very weak.

The signal produced at the tube mostly contains two categories of frequencies, i.e. low and high frequencies. The low frequency is produced by the surrounding noise, such as from the air-conditioning vent (around 1200 Hz), compressor (around 2500 Hz), etc. The use of “anechoic” box eliminates the noise coming from the air-conditioning system. However, as the compressor is always connected to the device through the inlet pipe, the noise coming from the compressor (when it is running) is more difficult to eliminate. During the experiments, the compressor ran intermittently. The presence of the compressor noise can be noticed in Figure 7 below.

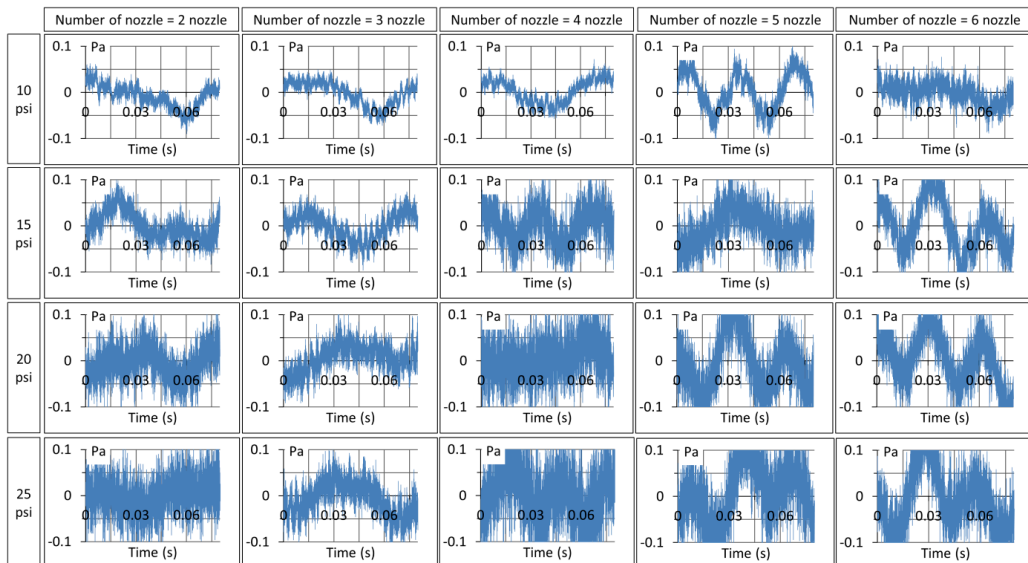


Figure 6. Signals produced by different numbers of nozzles



### Effects of the Number of Nozzles on Acoustic Signals

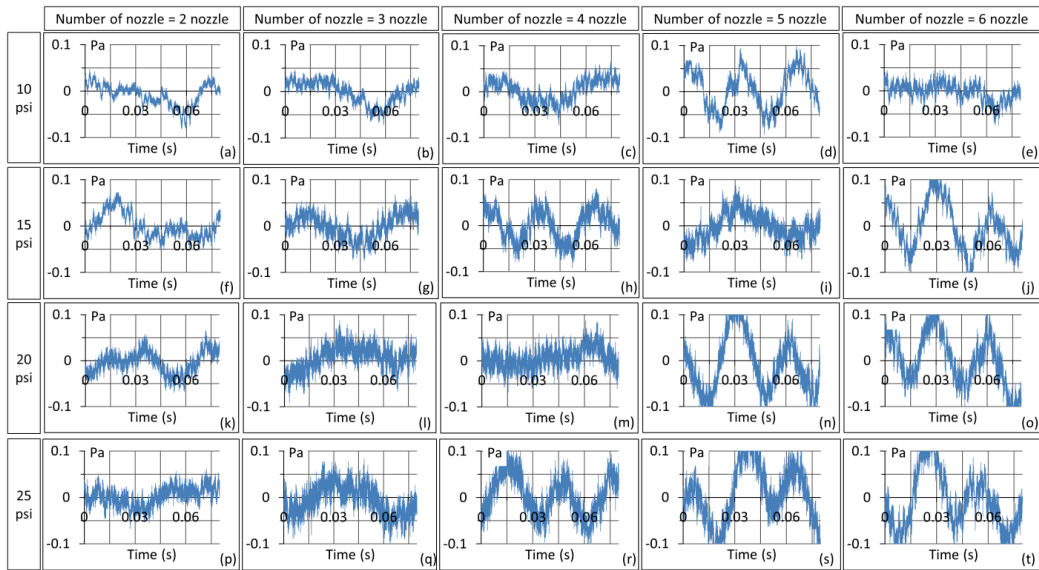


Figure 7. Signals produced by different numbers of nozzles

The magnitude of the Fourier Transform of the signals in Figures 6 and 7 is presented in Figures 8 and 9. It was obtained using FFT algorithm to show the frequency representation of the signals. The unit of vertical axis is Pa representing the sound pressure. From the FFT results, some peaks present at different locations representing significant frequencies produced by the device captured for different numbers of nozzles. It was observed that when the inlet pressure increased (from top to bottom) the magnitude of the peaks would also increase. Nonetheless, the position (the frequency) of the peaks did not seem to displace significantly when the same nozzles were used. For larger number of nozzles, more peaks appear.

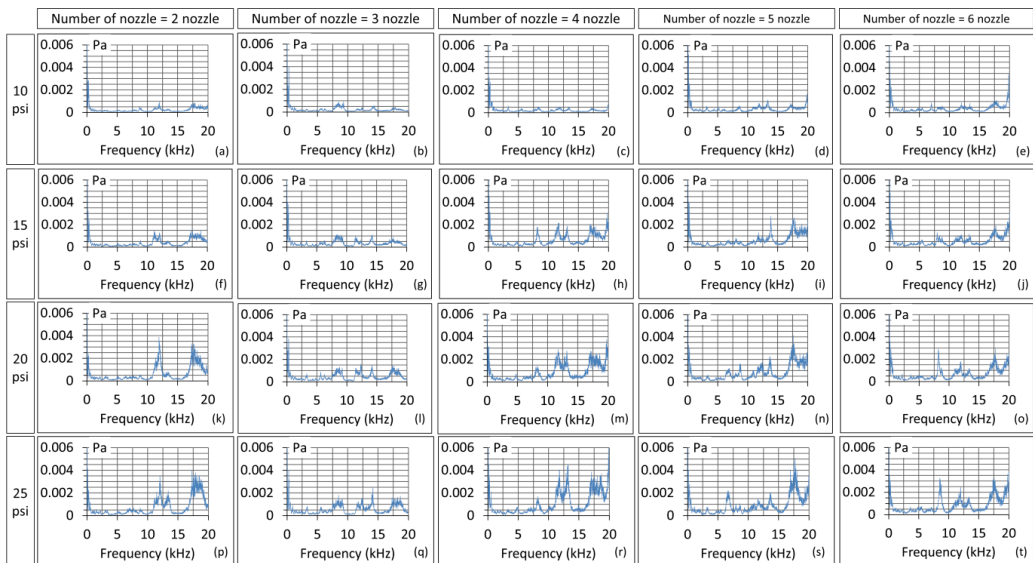


Figure 8. Frequency representation of the signals produced

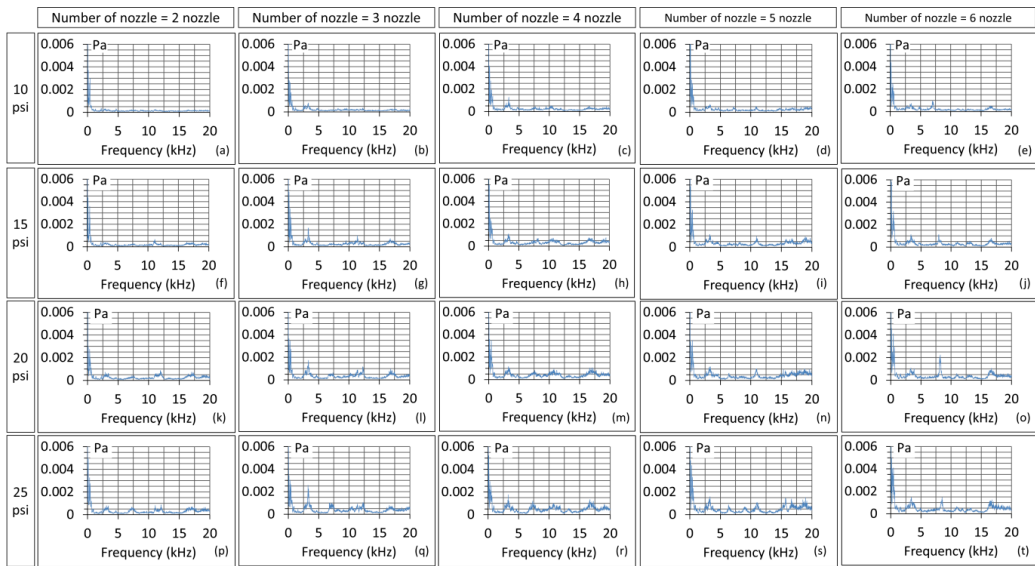


Figure 9. Frequency representation of the signals produced

In order to make the analysis clearer, the significant peaks from the FFT results were replaced by bars at the peak location with the same magnitude, producing a set of frequencies called acoustic signatures. This is shown in Figures 10 and 11. It was clearly observed that increasing the pressure at inlet did not displace the frequencies significantly when the same swirl generator was used. The magnitude was, however, getting stronger. The frequency representations shown in Figures 10 and 11 were the formed acoustic signatures of RHVT at certain configurations of the RHVT. Each set of frequencies can be correlated with the thermofluid performance of the device as shown on top of each graph. Overall, it was observed that for all the nozzle depths, the amplitude of the frequencies became more significant with the increases of efficiency and cooling temperature.

### Effects of the Number of Nozzles on Acoustic Signals

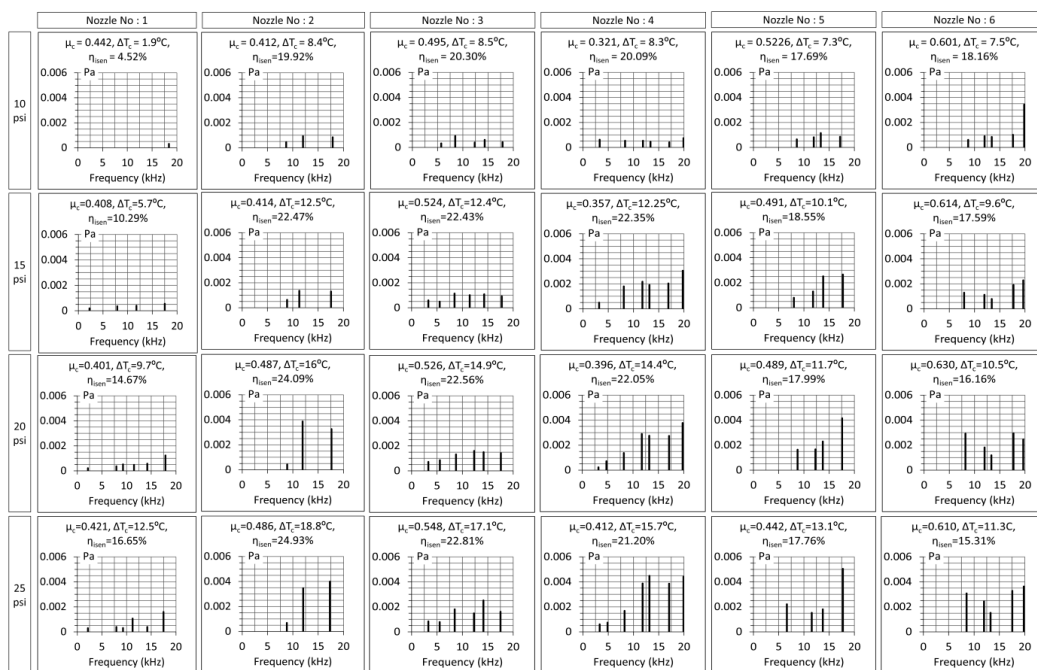


Figure 10. Acoustic signature with thermofluid data at the hot tube

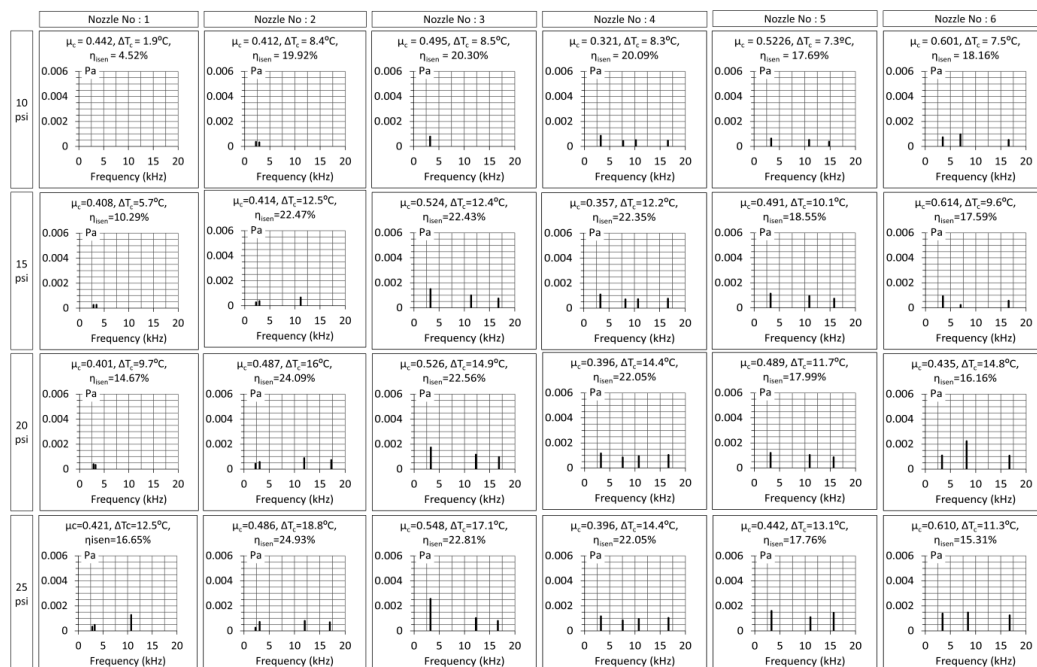


Figure 11. Acoustic signature with thermofluid data at the cold tube

## CONCLUSION

In this study, effects of the number of nozzles on the thermofluid performance of the RHVT and the acoustic signal produced on the tube were investigated. The investigation was conducted experimentally and the simple signal processing using FFT was applied. It was observed that different orifice diameters produced different sets of acoustic frequencies. This set of frequencies formed a signature of the signal that can be linked to the device's thermofluid performance. A signature frequency represents a specific configuration with a specific thermofluid performance of the device.

## ACKNOWLEDGEMENTS

The authors would like to thank the Ministry of Higher Education (MOHE), the Research Management Centre (RMC) and the Faculty of Mechanical Engineering, Universiti Teknologi MARA (UiTM), for providing the fund and support for this research under Fundamental Research Grant Scheme (FRGS), File No.: 600-RMI/FRGS 5/3 (74/2014).

## REFERENCES

- Abd Rahman, K. M., Wisnoe, W., Istihat, Y., & Natarajan, D. V. (2016). Acoustic analysis on different orifice diameter of a Ranque-Hilsch Vortex Tube (hot side). *Mechanical Engineering and Science Postgraduate International Conference, 2016*.
- Ismail, N., Wisnoe, W., & Remeli, M. F. (2014). Experimental Investigation of Orifice Diameter, Swirl Generator and Conical Valve Shape to the Cooling Performance of Ranque-Hilsch Vortex Tube. *Applied Mechanics and Materials, 510*, 174-178.
- Istihat, Y., & Wisnoe, W. (2015) Wavelet Transform of Acoustic Signal From A Ranque-Hilsch Vortex Tube. *IOP Conference Series: Materials Science and Engineering, 88*.
- Ismail N., Wisnoe W., & Remeli M. F. (2014). Experimental Investigation on the Effects of Orifice Diameter and Inlet Pressure to the Ranque-Hilsch Vortex Tube Performance. *Applied Mechanics and Materials, 465-466*, 515-519.
- Istihat, Y., Sabri, M. H., Wisnoe, W., & Abd Rahman, K. M. (2016). Flow Visualization in a Ranque-Hilsch Vortex Tube. *Journal of Mechanical Engineering*.
- Kurosaka, M. (1982). Acoustic streaming in a swirling flow and the Ranque-Hilsch (vortex tube) effect. *Journal of Fluid Mechanics, 124*, 139-172.
- Nimbalkar, S. U., & Muller, M. R. (2009). An experimental investigation of the optimum geometry for the cold end orifice of a vortex tube. *Applied Thermal Engineering, 29(2-3)*, 509-514.
- Thakare, H. R., Monde, A., & Parekh, A. D. (2015). Experimental, computational and optimization studies of temperature separation and flow physics of vortex tube: A review. *Renewable and Sustainable Energy Reviews, 52*, 1043-1071.
- Wisnoe, W., Abd Rahman, K. M., Istihat, Y., & Natarajan, D. V. (2016). Thermofluid-Acoustic Analysis of a Ranque-Hilsch Vortex Tube. *3<sup>rd</sup> International Conference on System-integrated Intelligence: New Challenges for Product and Production Engineering, SysInt, Procedia Technology*.

## **Tooth Frame Axes and Centroid for Dental Occlusal System**

**Muhammad Azmi Ayub<sup>1\*</sup>, Mohd Shafiq Azni<sup>1</sup> and Nagham Al-Jaf<sup>2</sup>**

<sup>1</sup>*Faculty of Mechanical Engineering, Universiti Teknologi MARA (UiTM), 40450 Shah Alam, Selangor, Malaysia*

<sup>2</sup>*Faculty of Dentistry, Universiti Teknologi MARA (UiTM), 47000 Sungai Buloh, Selangor, Malaysia*

### **ABSTRACT**

In dentistry, determining position and orientation parameters for each tooth mostly based on orthodontic qualitative perception. There is no quantitative method to obtain those parameters in three dimensional (3D) images, especially in some complicated cases. This study proposed a quantitative approach for locating centroid of tooth position and also its frame axes orientation. Based on Cone Beam Computed Tomography (CBCT) x-ray images, a 3D model of teeth was obtained to visualise dental features. A few dental features were used to calibrate the location of centroid and identify tooth reference axes, or frames. Two definitions of centroid and frame axes were proposed for single root and for multiple roots of teeth. Based on these two definitions, the positions and orientations of each tooth were determined and evaluated. Teeth positions and orientations were obtained with respect to a reference axis, which is the CBCT coordinate system. Having a quantitative method to obtain position and orientation of tooth, especially in 3D, will help dental rehabilitation in many ways.

*Keywords:* Centroid, orientation, position, dental occlusion, reference axes

### **INTRODUCTION**

To improve the result of dental rehabilitation, there are efforts to introduced three-

dimensional dental geometry model. Dental cast might be one of the methods to get a 3D view of a dental occlusion, but the digital models gave more advantages such as the possibility of special registration. Digital models were able to combine the collected data from different time points in one coordinate system (Grauer & Proffit, 2011). In timely manner, most of the digital models in orthodontic observation were in 2-dimensional (2D) grayscale. This causes problem when the images overlap each other and are difficult to distinguish in complicated

#### ARTICLE INFO

##### *Article history:*

Received: 25 October 2016

Accepted: 17 March 2017

##### *E-mail addresses:*

[muhdazmiayub@gmail.com](mailto:muhdazmiayub@gmail.com) (Muhammad Azmi Ayub),

[shafiqazni@gmail.com](mailto:shafiqazni@gmail.com) (Mohd Shafiq Azni),

[nagham@salam.uitm.edu.my](mailto:nagham@salam.uitm.edu.my) (Nagham Al-Jaf)

\*Corresponding Author

cases (Esa, Ayub, & Ali, 2012; Manzi et al., 2012). Later, cone-beam computed tomography (CBCT) was introduced for dental practitioners to be able to get multi-planes of dental imaging (Scarfe, Farman, & Sukovic, 2006). By using CBCT, they do not only able to have thin layer images in axial plane, but also able to view images in curved, oblique, sagittal, and coronal images plane (Aziz, Ayub, & Jaafar, 2012). Not just 2-dimensional (2D) images, CBCT is also able to provide a 3-dimensional information by reforming its data in a volume (McCoy, 2013).

To be specific, this technology is also called Cone Beam Volume Imaging/Tomography (CBVI/CBVT). This term is used to differentiate it from the connection medical computed tomography (CT). The image capture is generally a single 190° up to 360° scan sweep around the patient's head. Using "cone-beam" shaped x-ray aimed at a solid-state panel detector, the desired image volume can be covered in a single scan. Compared to medical CT, this single scan of CBVI approach is able to decrease x-ray dose from six to fifteen times during the 3D imaging examination (McCoy, 2007). However CBVI/CBVT technology does not provide analysis tools such as teeth position, teeth orientation and accurate geometry characteristics or parameters.

To determine the position and orientation of teeth, the location of centroid must first be defined. Since the definition of centroid for teeth is still not established, there are few definitions available depending on its relevance in the study. One definition is just a simple mid-point of the tooth, from the top to the bottom. The other definition is that the centroid of tooth is approximately 1/3 from the root, measured from the root to the end of the tooth crown (Burstone & Nanda, 1993). Alternatively, other researchers proposed using landmarks of the tooth to find the centroid. During molar translation, four landmarks were digitised on each molar at each time point, and then the centroid position was constructed and computed (Grauer & Proffit, 2011; Peixoto, Pinto, Garib, & Gonçalves, 2014).

The aim of this paper is to define a centroid and frame axes for each tooth in order to determine teeth position and orientation in 3D from the CBCT images. In this research, the images from CBCT scans of a patient were taken from dentistry databank in order to eliminate ethical issue. Hence, the images taken were not a real-time image data acquisition. The images can be manipulated in several views such as front, top, and side views. A user can view the x-ray images in 2D or 3D and no analysis function is available.

## **METHOD**

This study used a set of teeth from one patient to be analysed and focused on defining the centroid of the teeth and reference axis. Only seven teeth at the lower jaw on the left side of a patient were taken from x-ray image to determine the position and orientation of each tooth corresponding to the reference axis. In this study, one of the teeth with clearest view on the x-ray image was analysed using image processing algorithm to obtain more precise parameters. A 3D modelling using Computer Aided Design (CAD) software was made beforehand based on the parameters from the x-ray images to get better 3D view (Ayub, Mohamed, & Esa, 2014). Figure 1 shows the flow of the research method employed in this study. There are six stages involved in this study. The research started with thorough literature review on the subject matter, followed by modelling of dental geometry structure, defining centroid and reference

axis, image processing, data collection and analysis, and finally, the report writing. However, this paper focused only on defining centroid location (tooth position), tooth frame axes (tooth orientation), and reference axes.

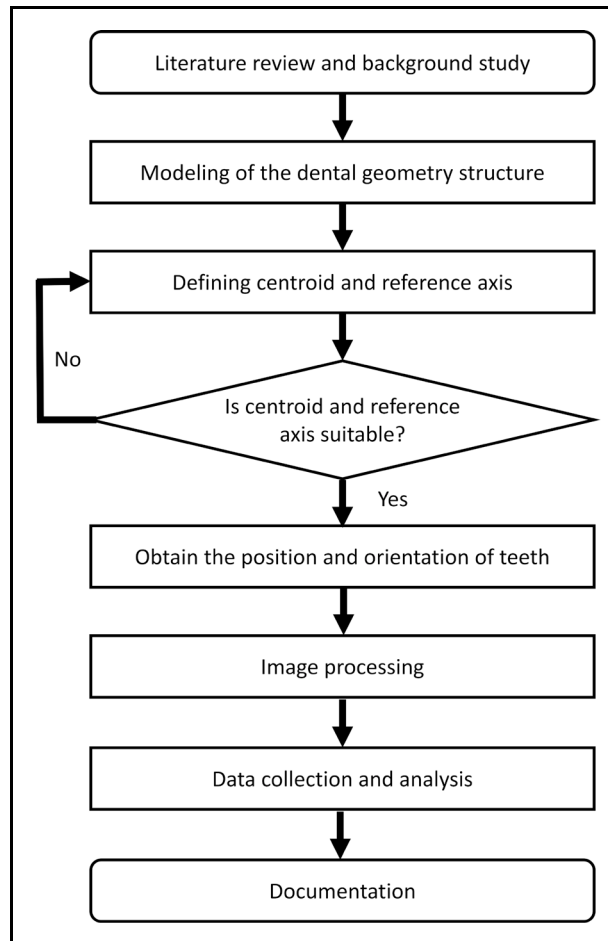


Figure 1. Overall research method

In this study, centroid is defined as  $\frac{1}{3}$  of the length ( $L$ ) measured from root to crown end, as shown in Figure 2, while for a tooth with more than one root, its centroid is defined as the bifurcation point. Bifurcation the point where tooth roots start to divide is shown in Figure 3. The x-ray images from cone beam computed tomography (CBCT) showing images slice by slice from all views but the image in two-dimensional (2D) were used in this study (Figure 4). Figure 4 shows the orthographic view of the dental occlusal, which consists of plan view (XZ reference axis), side view (YZ reference axis), and front view (YX reference axis). After several calibration processes, starting with the side view, the centroid location at the side view was determined. Then, the tooth image in side view was rotated so that the tooth is in the upright orientation parallel with vertical line of Y-axis. This approach was used in order to get

a true length of the tooth in front view. From that, the centroid from the front view is located. For the plan view, it is automatically located when both side and front view are determined.

The determination of tooth orientation is done after locating the centroid position. Using the cone beam coordinate system as reference frame, the orientations are measured from its respective axes using image processing algorithm developed in this study. For a single root tooth, a straight line that will pass through 3 points of dental features, which are the root, centroid, and peak point of a tooth are constructed and considered as the Y-axis of the tooth frame. For the tooth with multiple roots, a straight line that passes through 3 points of dental features (the root, centroid, and lowest point of the top tooth surface) are used. The Cartesian coordinate of X-axis is perpendicular to Y-axis and pass through the centroid point. Similarly, Z-axis is constructed accordingly using the right hand rule Cartesian coordinate system shown in Figure 5. The orientation of a tooth is configured as follows; rotation in X-axis is yaw ( $\Psi$ ), rotation in Y-axis is pitch ( $\theta$ ), and rotation in Z-axis is roll ( $\phi$ ).

A reference axis is needed to fix the position and orientation of a tooth in the overall Cartesian coordinate ( $x, y, z$ ) of dental occlusal system. The position of centroid is measured from the reference axes; thus, the reference axes must be fixed and remained unchanged at any circumstances. The orthographic view of CBCT was chosen since it provides all three-dimensional view and its default cone beam coordinate system was used as the reference axis. Figure 6 shows the position of the centroid and orientation of the tooth axes with respect to the reference axes of CBCT for the three adjacent teeth, LR1, LR2, and LR3.

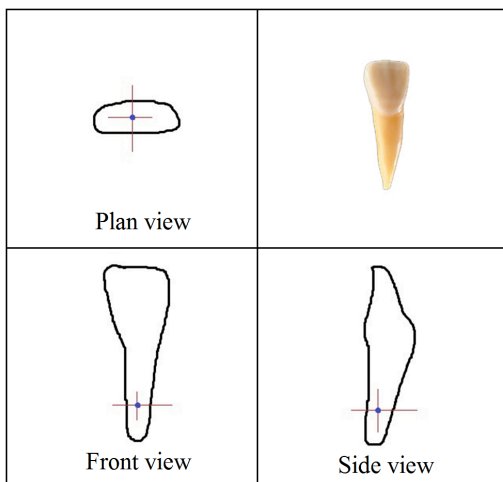


Figure 2. Centroid for single root

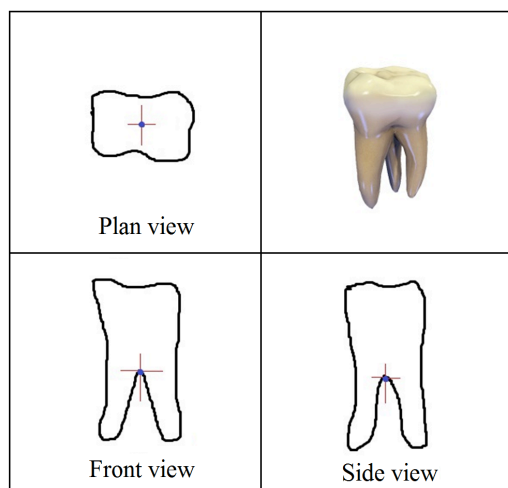


Figure 3. Centroid for multiple roots



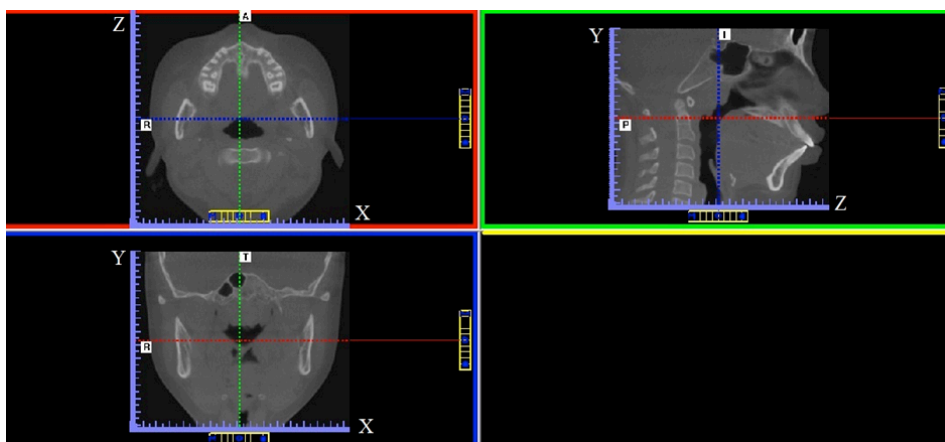


Figure 4. The orthographic view of CBCT scanner

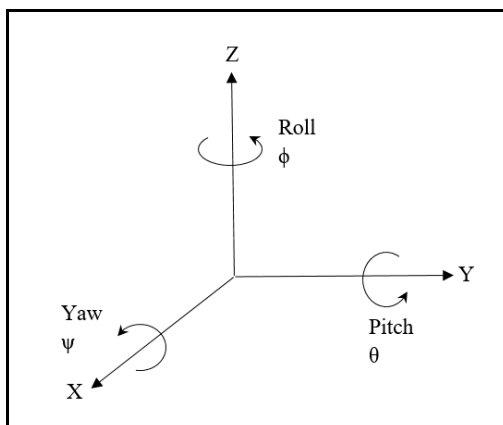


Figure 5. Orientation on axes

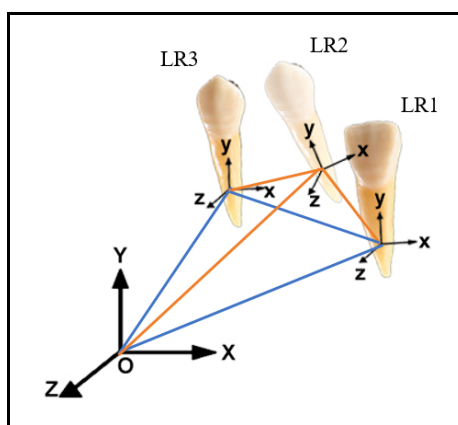


Figure 6. Position and orientation of teeth

## RESULTS AND DISCUSSION

Table 1 shows the results of the centroid position in dental configuration system. The heading of the table are as follows: tooth names, centroid position, the length of teeth, and distance of the centroid from the root. The centroid positions are the reference axes of the CBCT. In this study, the targeted teeth are the seven teeth of the lower right jaw, excluding the wisdom tooth. Those teeth are represented by LR1 until LR7 in the first column, with the names of the teeth given in the second column. LR is the acronym for “lower right”, which refers to the teeth at the lower right jaw. Numbers 1 until 7 represent the tooth from incisor until molar accordingly. The centroid position of tooth is divided into three column,  $X_c$ ,  $Y_c$ , and  $Z_c$ . Two columns on the right are the additional data gathered during the process of locating centroid.

The overall position of the dental system for the lower right jaw is shown in Figure 7. The centroid position along x-axis is  $X_c$ , which is measured from y-axis, was decreasing from LR1 to LR7. This trend indicates the position of the teeth was getting closer to the y-axis as it

measures from LR1 to LR7 accordingly.  $Z_c$  is the centroid position along the z-axis, which was measured from the x-axis. However,  $Y_c$  is the position along the y-axis and it was observed that the positions are almost the same from LR1 until LR5 with a slight decrease from LR1 to LR2. The positions start to increase for LR6 and LR7 because the locations of LR6 and LR7 centroids are quite significantly different. It is worth to highlight here that LR1 until LR5 are teeth with single root, thus their centroid are at the root. However, LR6 and LR7 are the teeth with four roots, so their centroid are according to the bifurcation point, which is above the roots. That is why LR6 and LR7 positions on the y-axis are higher than the others. If LR6 and LR7 were replaced with one root tooth, the position will still slightly increase because of the bone shape that is holding the teeth. If we look into the perspective of the frame view,  $Y_c$  is viewed from side view (YZ frame) and it also can be viewed from the front view (YX frame). However,  $X_c$  and  $Z_c$  can be viewed only from the plan view (ZX frame). Figure 4 shows the plan view of the arc of the teeth arrangement which results in such trend for  $X_c$  and  $Z_c$ .

Table 1  
Position of the centroid of teeth

Tooth	Tooth's name	Centroid position (mm)			Distance from root to top of teeth (mm)	Distance centroid from root (mm)
		$X_c$	$Y_c$	$Z_c$		
LR1	Central incisor	80.0	35.2	132.8	19.81	3.58
LR2	Lateral incisor	76.8	33.6	130.0	23.49	4.15
LR3	Canine (cuspid)	71.0	33.6	127.0	21.53	4.25
LR4	First premolar (bicuspid)	66.8	33.6	123.6	18.26	4.30
LR5	Second premolar	62.8	35.6	117.2	17.55	4.41
LR6	First molar	58.4	42.4	110.4	16.49	8.10
LR7	Second molar	55.6	46.4	98.8	14.54	5.69

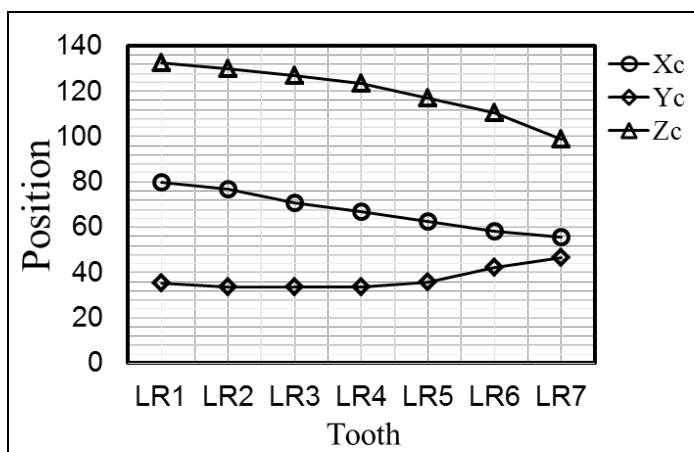


Figure 7. Centroid position of teeth

The orientation of tooth was calculated using simple trigonometric functions. The right hand rule Cartesian coordinate system was used to indicate the direction of the orientation which gave the value positive or negative. The results are shown in Table 2. The symbols  $\alpha$ ,  $\phi$ , and  $\theta$  represent the angles of tooth in x-axis, y-axis, and z-axis, respectively. The largest angle for  $\alpha$  is LR1, with an angle of  $42.10^\circ$ , while for  $\phi$  is LR7 with an angle of  $-72.92^\circ$ , and for  $\theta$  is also LR7 with an angle of  $-15.94^\circ$ .

The profiles of teeth orientations are shown in Figure 8. For the angles  $\alpha$  and  $\phi$ , the profile decreases slightly but not obviously, especially for  $\alpha$ . In general, the profile of the angle  $\phi$  is in the downward trend. For angle  $\theta$ , the graph shows a fluctuating profile. The images of teeth were taken from a patient with dental occlusal problem, so some of the orientations are not according to the normal value.

The downward trend of profile for angle  $\phi$  is significant due to the arc shape of the teeth arrangement. The difference of angle from LR1 until LR3 is small, but it starts to get bigger from LR4 until LR7. Based on this result, LR4 can be considered as the turning point of the arc shape. For the angle  $\theta$ , it is viewed from the front view, and the fluctuating profile indicates that the teeth are not in a good arrangement. Some are rotated to the left, while others are rotated to the right. From the side view, it shows the angle  $\alpha$  with a decreasing profile from LR1, which is incisor tooth, up to LR6, which is the first molar tooth. However, at the second molar tooth (LR7), the angle  $\alpha$  is slightly higher. For normal tooth occlusal, the angle  $\alpha$ ,  $\phi$ , and  $\theta$  of orientations are not necessarily at  $0^\circ$ . Each tooth has its own respective angles of orientation to meet the functionality and aesthetic appearance of the dental occlusal. The overall modelling of the teeth positions and orientations in CAD are shown in Figure 9.

Table 2  
*Orientation of the teeth*

Tooth	Tooth's name	Orientation on axis ( $^\circ$ )		
		$\alpha$	$\phi$	$\theta$
LR1	Central incisor	42.10	-28.81	4.76
LR2	Lateral incisor	39.87	-29.79	12.84
LR3	Canine (cuspid)	41.21	-31.00	14.61
LR4	First premolar (bicuspid)	30.27	-44.94	-12.68
LR5	Second premolar	26.97	-53.13	0.00
LR6	First molar	16.43	-54.18	-15.26
LR7	Second molar	22.62	-72.92	-15.94

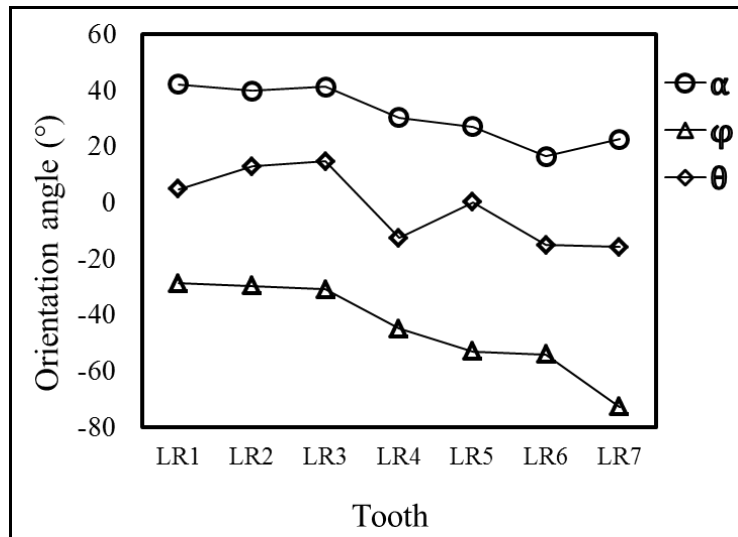


Figure 8. Orientation of teeth

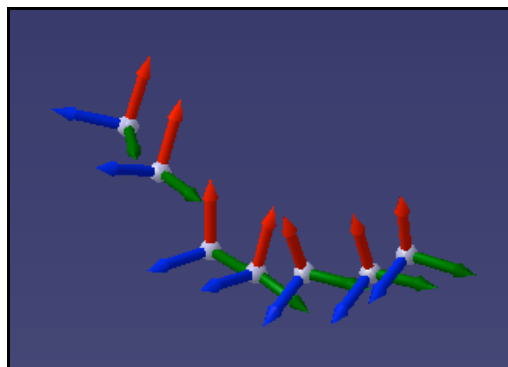


Figure 9. A 3D modelling of teeth position and orientation

## CONCLUSION

A more effective interaction between dentist and imaging machine will provide a better dental treatment to patients. One way to get this effective interaction is by developing a more comprehensive model of dental information from the imaging machine and sharing with dentists to harness human flexible and reasoning capability, coupled with the machine accuracy, repeatability and fast operation capability. A quantitative method to determine teeth positions and orientations is very important for dental rehabilitation. Currently, the positions and orientations are mostly based on orthodontic qualitative perception. This paper has successfully proposed a standard method to obtain those values in three dimensional (3D) CBCT images. A suitable definition for the centroid of tooth, orientation of tooth and also its reference axes to determine teeth position and orientation have been highlighted. The analysis of the results from this study shows that the positions and orientations of teeth are in accordance with the actual

dental occlusal. The results have been verified with the experienced orthodontic personnel. Having the quantitative method to obtain the position and orientation of tooth especially in 3D will help dentists in many ways.

## ACKNOWLEDGEMENTS

The authors gratefully acknowledge the assistance from the Ministry of Higher Education, Malaysia, in providing the FRGS Research Fund (Project Number: 600-RMI/FRGS 5/3 (75/2014)), and Universiti Teknologi MARA. The authors are also thankful to the Faculty of Mechanical Engineering and Faculty of Dentistry for providing the assistance in this research.

## REFERENCES

- Ayub, M. A., Mohamed, A. B., & Esa, A. H. (2014). In-line Inspection of Roundness Using Machine Vision. *Procedia Technology*, 15, 808–817. <http://doi.org/10.1016/j.protcy.2014.09.054>
- Aziz, M. H., Ayub, M. A., & Jaafar, R. (2012). Real-time algorithm for detection of breakthrough bone drilling. *Procedia Engineering*, 41(Iris), 352–359. <http://doi.org/10.1016/j.proeng.2012.07.184>
- Burstone, C. J., & Nanda, R. (1993). *Retention and Stability in Orthodontics*. W B Saunders Co. Retrieved from <http://www.amazon.com/Retention-Stability-Orthodontics-Charles-Burstone/dp/0721643426>
- Esa, A. H., Ayub, M. A., & Ali, B. (2012). Image analysis for deformation behavior of optical based silicone tactile sensor. *Proceedings - 2012 IEEE 8<sup>th</sup> International Colloquium on Signal Processing and Its Applications, CSPA 2012*, 23–28. <http://doi.org/10.1109/CSPA.2012.6194683>
- Grauer, D., & Proffit, W. R. (2011). Accuracy in tooth positioning with a fully customized lingual orthodontic appliance. *American Journal of Orthodontics and Dentofacial Orthopedics*, 140(3), 433–443. <http://doi.org/10.1016/j.ajodo.2011.01.020>
- Manzi, F. R., Peyneau, P. D., Piassi, F. P., De Carvalho Machado, V., & Lopes, A. C. (2012). Radiographic and imaging diagnosis of rhinolith in dental clinics: A case report. *Revista Odonto Ciencia*, 27(2), 170–173. <http://doi.org/10.1590/S1980-65232012000200015>
- McCoy, G. (2013). Occlusion confusion. *General Dentistry*, 61(1), 69–75.
- McCoy, G. D. (2007). *The Truth About Occlusion*. Boston, Massachusetts.
- Peixoto, A. P., Pinto, S., Garib, D. G., & Gonçalves, J. R. (2014). Three-dimensional dental arch changes of patients submitted to orthodontic-surgical treatment for correction of Class II malocclusion, 19(4), 71–79.
- Scarfe, W. C., Farman, A. G., & Sukovic, P. (2006). Clinical applications of cone-beam computed tomography in dental practice. *Journal-Canadian Dental Association*, 72(1), 75. Retrieved from <http://www.cda-adc.ca/JCDA/vol-72/issue-1/75.pdf>





## **An Analysis on Node Cloning Attacks Prevention Using Unique Hardware Identity in WSN**

**Norhaflyza Marbukhari\*, Yusnani Mohd Yussoff, Murizah Kassim, Mohd Anuar Mat Isa and Habibah Hashim**

*Faculty of Electrical Engineering, Universiti Teknologi MARA (UiTM), 40450 Shah Alam, Selangor, Malaysia*

### **ABSTRACT**

This paper presents a study on node impersonation attack in Wireless Sensor Networks (WSN) environment. Node cloning is a major attack among sensor where the leak of node identity is easy to clone if it is not secured. For this purpose, an analysis that explores techniques to prevent node cloning attack was done using a unique node identity. An algorithm to generate the unique identity was developed on high performance ARM hardware and programmed the data authentication together with sensor nodes. Communication among the sensor nodes and base station depends on a successful authentication using the unique identity (UID). The sensor nodes are resistant against node cloning attack when the UID identity is unequal. Results present successful generation of the UID, while execution time between two nodes is faster and low power consumption is used on the technique. The analysis has proven that the unique UID is secured by the developed node identity algorithms and against cloning attack. This outcome is significant for new development of secured WSN sensor hardware, which can be implemented in new network technology.

*Keywords:* Node cloning, node impersonation, security, Unique Hardware Identity, Wireless Sensor Network

### **ARTICLE INFO**

*Article history:*

Received: 25 October 2016

Accepted: 17 March 2017

*E-mail addresses:*

eijafly@gmail.com (Norhaflyza Marbukhari),  
ym\_yussoff@yahoo.com (Yusnani Mohd Yussoff),  
murizah@salam.uitm.edu.my (Murizah Kassim),  
anuarls@hotmail.com (Mohd Anuar Mat Isa),  
habib350@salam.uitm.edu.my (Habibah Hashim)

\*Corresponding Author

### **INTRODUCTION**

Wireless Sensor Network (WSN) is widely used in diverse applications such as defense systems, infrastructure monitoring and hospital for clinical monitoring. WSN technology, together with embedded devices and Internet of Things (IoT), has enabled collection and monitoring of real-time data at remote locations. Applications utilising the two technologies mentioned above are

currently growing at exponential rates. To collect information, sensor nodes are placed at remote area or it is far from administering involvement. Due to this nature, the sensor nodes are prone to various types of security attacks. An attacker with malicious intentions may attempt to obtain data from WSN or in the worst case scenario, it can be controlled or can cause a breakdown to the WSN infrastructure. It can be done if the attacker manages to learn the node identity, node behaviour, or by injecting false data into the sensor nodes. Therefore, possible threats must be considered prior to implementing any WSN or IoT related application.

A lot of research has been done to analyse node cloning attacks prevention to a system. Node cloning attacks can be divided into two parts: i) node replication, and ii) identity cloning, which is called node impersonation. Node replication attack is identified as one of the major attacks in WSN (Parno, Perrig, & Gligor, 2005). In this attack, an adversary seizes few sensor nodes, and then replicates them and deploys those identical replicas or cloned devices throughout the WSN. Seizing or stealing sensor nodes is not difficult due to bulk deployment of the sensor nodes in various places (Xing et al., 2008). Most of them are not protected by strong physical parameters. The unprotected sensor nodes have strong tendency to leak data in shared WSN that is interoperated by various devices and systems. Apart from that, network bandwidth is dropped due to congestions caused by floods of false network packets in WSN.

Node cloning attacks also can happen in many systems such as medical system. Cases like autonomous clinical monitoring for a patient's using digital medical sensors may incorrectly exchange data with other patients. This causes problems for medical officers to treat the patient properly due to wrong data interpretation. It also leads to an incorrect diagnosis of the patient's illness. Although the existing authentication techniques (Yang et al., 2008) provide protection from node cloning attacks, there are theoretical security gaps in their analysis. Node cloning can still occur because most of the techniques used to create an identity for a sensor node are in a communication protocol. However, their methods are lacking in special characters in a generation of node identities, which are used to prevent node cloning attacks. They used modelling techniques on the cloning attacks, and proved their security works through the simulation, but not in a real-time threat analysis. For example, in the real-time, a physical node for cloning is required and a lot of observable variables need to be controlled in order to verify the accuracy of the security protocol against the node cloning attack. This work has examined an identity node cloning attack in WSN. The proposed security protocol was designed by taking into consideration of e-health related applications. It is important to ensure security on shared information using a standard security practice. There are three common attributes of security concerns such as confidentiality, integrity, and authentication. Confidentiality guarantees data transmitted by sensor nodes are not readable or understandable to an adversary. Integrity provides confirmation on data that are not being modified by an adversary. Authentication is a process of verifying sensor node identity before joining WSN. This provides identity verification between the sensor nodes and base station. In order enhance the authentication process, a unique identity for all the sensor nodes should be generated using unique features for a given sensor. This work has addressed a method to generate the unique identity using the unique features for the given sensor.

Based on literature, a precedence works on unique identity in WSN is discussed. Several identity-based methods that introduced biometrics for identity-based signcryption are discussed.



They formalised a notion of biometric identity-based signcryption. The authors proposed an efficient biometric identity-based signcryption scheme that uses biometric information to construct a public key. The proposed method is verified by satisfying confidentiality and unforgeability in a random oracle mode (Li & Khan, 2012). Another method called zero knowledge protocol (ZKP) is for the verification of sender sensor nodes. With attachment of unique fingerprint to each node, the authors address the clone attack. In the wireless sensor network, non transmission of crucial cryptographic information is addressed by the model using ZKP. It is helpful for preventing man-in-the middle attack and replay attack. Information about different scenarios and also analysis of performance and cryptographic strength are analysed and presented in this paper (Patwekar & Kotak, 2016). From this paper, the author proved that the enhancement security for protocol can be prevented from the attacker.

A research by Li et al. (2012), presented an online or offline identity-based signature scheme for WSN. It is identified as one of the most interesting features in this scheme that provides a multi-time usage of offline storage (Li et al., 2012). The feature allows a signer to reuse the offline pre-computed information in a polynomial time, in contrast to one-time usage in previous works on the online/offline signature schemes. However, the proposed scheme is suitable only for low-power devices such as smart cards. This scheme does not use public key upon an authentication process.

A recent study also has illustrated how security in WSN can be bootstrapped by using an authenticated identity-based non-interactive protocol, namely TinyPBC. Many studies have presented those efficient security implementations for sensor nodes were found in 32-bits processors. It also discussed the ability of using IBE in WSN. Another work has claimed that the IBE is ideal for WSN. It has deliberated on how the IBE can solve a key agreement problem in WSN and also presented an approximation of the IBE performance (Kushwah & Lal, 2011). Research also showed how adversary attacks mounted on sensor nodes and stressed (Li et al., 2012). It also presented studies on other malicious users that can interfere sensor nodes communication in WSN. Another work has used a security proof to complete a model of the identity base signcryption scheme. It has demonstrated a reduced amount of implementation complexity as compared to the standard signcryption schemes. Another recent research has described one type of attack called the Sybil attack. Sybil attack is identified as an attack in which a node illegitimately takes multiple identities or claims fake IDs. The research also discussed the Sybil attack and differentiated its techniques or a mechanism that has been proposed in the previous literature on tackling the issues. The study is significant where these techniques and their limitations aided in designing novel, robust and more efficient techniques for tackling with Sybil attack on applications of sensor nodes (Singh et al., 2016).

## **METHOD**

This work generates a unique identity using a specialised hardware arrangement. The unique identity generation is imperative for all sensor nodes, which help differentiate and prevent them from various cloning attacks. There are many existing attacks that aimed to tamper a sensor node. This research presents a proposed UID technique to provide a strong unique identity generation, which is to alleviate the attacks and data threats. The UID used a hardware

code classification based on a board implementation. Integrated circuit (IC), which owns part numbers, is identified and it is used as part of the UID. The IC's part numbers is taken as inputs for the UID generation.

Figure 1 shows a flowchart that explains the generation of UID process using the generated UID technique. The generation of UID started with identifying the hardware's authentic part numbers (Part Number A and Part Number B). These two Part Numbers will be added and saved in a secured memory encrypted location. Then, the UID was generated and saved in the temporary memory; the value before were hashed.

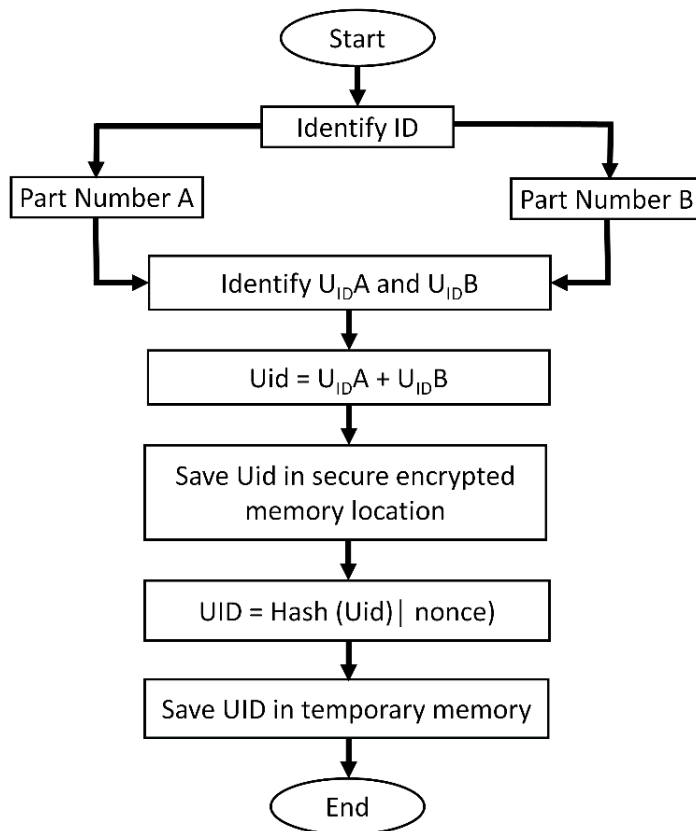


Figure 1. The UID process flow

### Image Capture Technique

Figure 2 shows the image processing method to capture the layout of IC in executing the part numbers values on the chips. A camera was used to capture the images of ICA and ICB. The captured images were sent to a PC to extract the code numbers of both ICs before they were being saved in the memory. The code numbers extracted from these ICs were saved as UidA and UidB.

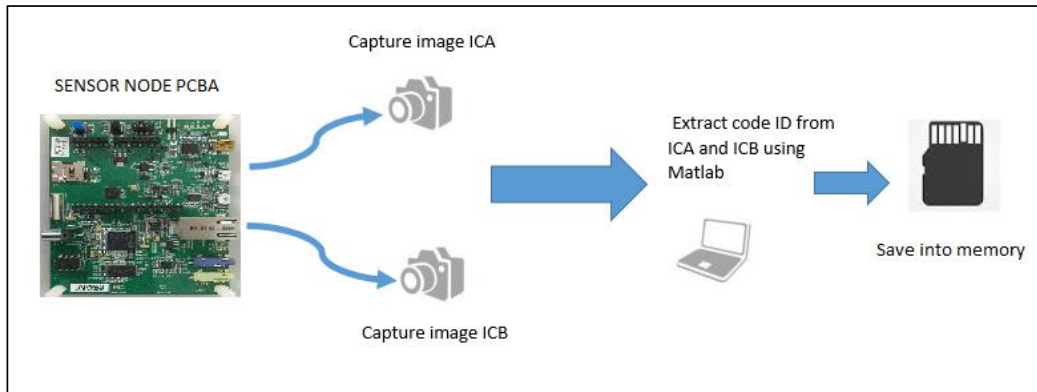


Figure 2. Block diagram for generated the ID code

### Generated ID

Figure 3 presents the ICA and ICB from which their part numbers have been identified and generated into the UID.

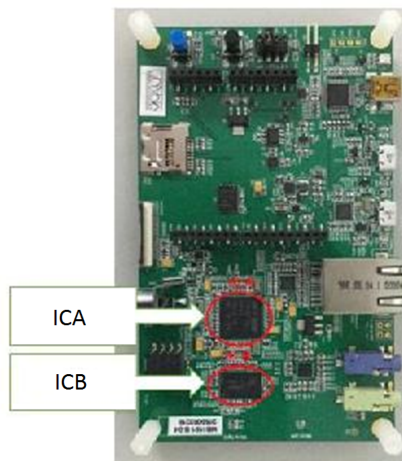


Figure 3. Integrated circuit ID Identification

**ID Combination.** ID combination is a technique where the identified two part numbers are substituted and UID is generated. The mathematical operation is programmed in ARM 34F746 using c language, as given in Equation [3.1]. The two part numbers are combined in order to hide the identity information. This task helps to hide the UID correlation therefore the probability of the UID to be cloned is low. Then the UID is saved into the secure memory encrypted location to secure the information of the sensor node identity. Technically, the addition of two part numbers is less complicated computational procedure for the device in running the algorithm.

$$UID = UidA + UidB \quad [3.1]$$

**UID Generation in secure memory.** After combining the two UIDs, the UID will be generated using Equation 3.2. After the generation of the UID has been done, it is saved in the memory inside the ARM STM34F746 as the Identity for the sensor node. The UID must be protected in a secured encrypted memory because this UID is used for implementing the method selected.

$$\text{UID} = \text{hash}(\text{UID} | \text{nonce}) \quad [3.2]$$

UID is purposely used as an identification sensor node in the WSN's system due to its unique design method that requires UID generation. This UID is applicable to be used for all the methods that demand for its Identity confirmation before proceeding with the selected method.

### RESULTS AND DISCUSSION

UID is the identification for sensor node, in lieu to the hardware used. Because of that, UID can be implemented in all the methods that demand for identity confirmation such as IBE, DHKE and others. In IBE, UID can be used as the master private key in private key generator (PKG) for sensor node. Then, the Public key is obtained to authenticate and receive the private key from the other sensor node in pairing solution. Figure 4 shows the topology for DHKE exchange public key and verify the secret key. Figure 5 shows experimental setup to implement the UID in Diffie Hellman Key Exchange (DHKE) and measure the current and time for executing the method using ARM STM34F746.

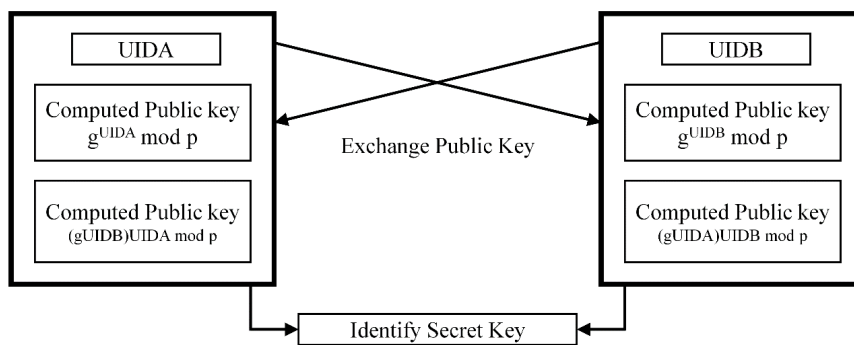


Figure 4. DHKE topology in UID implementation

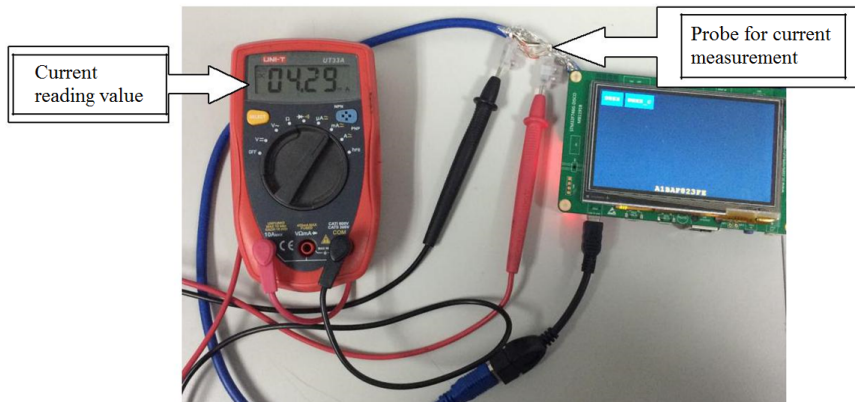


Figure 5. The experiment lab for UID Technique

The generation process of this UID method in ARM STM34F46 is using C programming language. This arithmetic calculation is written in Keil microversion5 command to create the binary file. Once the file is created, the experiment is repeated ten times for each process. The running time or the duration for executing this UID in this experiment is less. Table 1 displays the running time to complete the measurement. Figure 6 is GUI display example for ARM STM34F46 that is used for running the UID algorithm.



Figure 6. ARM STM34F746 GUI Display

In this experiment, the current usage during session is about 2.2 mA and 3.6 V voltage. In this experiment, a 7.92 mW difference power was observed during the start and loop cycle of the experiment. This character indicates that the UID uses low power for running the algorithm because of the simple algorithm used. Table 1 shows the result for the hardware. The result is based on the KA and KB values, since both the results are similar so the authentication process is passed using the UID. The measurement was replicated for ten times with different UIDs for the purpose of verifying the results, while the average running time is 0.02107628 s.

Table 1  
*Analysis results of the Unique Hardware Identity technique*

Test	Parameter	Result Parameter	Running Time (s)	Result
1	UIDA	FFFFFFFFFFFFFFFFFFFFFFFFF10	0.02097308	Pass
	UIDB	FFFFFFFFFFFFFFFFFFFFFFFFF11		
	KA	DCD09D74401A6DCE3B3D3B027236616C		
	KB	DCD09D74401A6DCE3B3D3B027236616C		
2	UIDA	FFFFFFFFFFFFFFFFFFFFFFFFF12	0.02098238	Pass
	UIDB	FFFFFFFFFFFFFFFFFFFFFFFFF13		
	KA	2F6F81F7E4279CB334CF5FD588D28CBB		
	KB	2F6F81F7E4279CB334CF5FD588D28CBB		
3	UIDA	FFFFFFFFFFFFFFFFFFFFFFFFF14	0.02105921	Pass
	UIDB	FFFFFFFFFFFFFFFFFFFFFFFFF15		
	KA	9C657758E86D56026E777D0616C779AC		
	KB	9C657758E86D56026E777D0616C779AC		
4	UIDA	FFFFFFFFFFFFFFFFFFFFFFFFF16	0.02107283	Pass
	UIDB	FFFFFFFFFFFFFFFFFFFFFFFFF17		
5	KA	78FDFD1D1E154E076C1940C781A71AB2	0.02098701	Pass
	KB	78FDFD1D1E154E076C1940C781A71AB2		
	UIDA	FFFFFFFFFFFFFFFFFFFFFFFFF18		
	UIDB	FFFFFFFFFFFFFFFFFFFFFFFFF19		
	KA	7CAB725EABE99FB95161D89B672BD18F		
	KB	7CAB725EABE99FB95161D89B672BD18F		
6	UIDA	FFFFFFFFFFFFFFFFFFFFFFFFF1A	0.02106648	Pass
	UIDB	FFFFFFFFFFFFFFFFFFFFFFFFF1B		
	KA	CE5555EAB34E92B4E0FF0DF1D3713B9C		
	KB	CE5555EAB34E92B4E0FF0DF1D3713B9C		
7	UIDA	FFFFFFFFFFFFFFFFFFFFFFFFF1C	0.02113299	Pass
	UIDB	FFFFFFFFFFFFFFFFFFFFFFFFF1D		
	KA	6F458F3994D86DB7A2A44CCEFC3311A3		
	KB	6F458F3994D86DB7A2A44CCEFC3311A3		
8	UIDA	FFFFFFFFFFFFFFFFFFFFFFFFF1E	0.02115109	Pass
	UIDB	FFFFFFFFFFFFFFFFFFFFFFFFF1F		
	KA	6D158702E63581D6B5129E0D7E4E16EA		
	KB	6D158702E63581D6B5129E0D7E4E16EA		
9	UIDA	FFFFFFFFFFFFFFFFFFFFFFFFF2E	0.02118097	Pass
	UIDB	FFFFFFFFFFFFFFFFFFFFFFFFF3F		
	KA	8A8FAA60F537DCF40413FBA8B54CB55F		
	KB	8A8FAA60F537DCF40413FBA8B54CB55F		
10	UIDA	FFFFFFFFFFFFFFFFFFFFFFFFF4E	0.02115679	Pass
	UIDB	FFFFFFFFFFFFFFFFFFFFFFFFF5F		
	KA	172422583416C40000000000000000		
	KB	172422583416C40000000000000000		

## CONCLUSION

A unique identity based on hardware in preventing node cloning attack in wireless sensor network was successfully developed with cryptographic computation capability. The security analysis indicates that the UDI can be deployed in small devices with constrain CPU and memory to secure the node and uses less power in running the Algorithm. An algorithm to generate the unique identity is developed on high performance ARM hardware and programmed the data authentication together with sensor nodes. The study proved that the UID was successfully generated with faster execution time between two nodes in WSN. It is also confirmed that the unique UID is secured by the developed node identity algorithms. This research is valuable for the new development of secured WSN sensor hardware's which can be implemented in new network technology.

## ACKNOWLEDGMENTS

The authors would like to acknowledge the Ministry of Education (MOE), Malaysia, for providing the grant 600-RMI/FRGS 5/3 (141/2015), and Universiti Teknologi MARA (UiTM), for supporting this research work.

## REFERENCES

- Kushwah, P., & Lal, S. (2011). An efficient identity based generalized signcryption scheme. *Theoretical Computer Science*, 412(45), 6382-6389. doi: 10.1016/j.tcs.2011.08.009
- Li, F., & Khan, M. K. (2012). A biometric identity-based signcryption scheme. *Future Generation Computer Systems*, 28(1), 306-310. doi: 10.1016/j.future.2010.11.004
- Li, F., Khurram Khan, M., Alghathbar, K., & Takagi, T. (2012). Identity-based online/offline signcryption for low power devices. *Journal of Network and Computer Applications*, 35(1), 340-347. doi: 10.1016/j.jnca.2011.08.001
- Parno, B., Perrig, A., & Gligor, V. (2005). *Distributed detection of node replication attacks in sensor networks*. Paper presented at the 2005 IEEE Symposium on Security and Privacy (S&P'05).
- Patwekar, I. A., & Kotak, V. (2016). Implementation of Zero Knowledge Protocol in Wireless Security.
- Singh, R., Singh, J., & Singh, R. (2016). Sybil Attack Countermeasures in Wireless Sensor Networks. *Sybil*, 6(3).
- Xing, K., Liu, F., Cheng, X., & Du, D. H. C. (2008). Real-Time Detection of Clone Attacks in Wireless Sensor Networks, 3-10. doi: 10.1109/icdcs.2008.55
- Yang, Y., Deng, R. H., Bao, F., & Zhou, J. (2008). *Using Trusted Computing Technology to Facilitate Security Enforcement in Wireless Sensor Networks*, 43-52. doi: 10.1109/aptc.2008.13







## Effects of Environment and Fibre Architecture on Wear Properties of Nano-Filled Epoxy Polymer Composite

Aidah Jumahat\*, Anis Adilah Abu Talib, Eliya Farah Hana Mohd Kamal, Muhammad Tarmizi Sulaiman and Ahmad Syahrul Mohd Roslan

*Faculty of Mechanical Engineering, Universiti Teknologi MARA (UiTM), 40450 Shah Alam, Selangor, Malaysia*

### ABSTRACT

In this paper, the wear properties of nano-filled Glass Fibre Reinforced Polymer (GFRP) composite are studied based on the effects of the architecture of the glass fibre and test environment. Wear tests were done under two different conditions; dry environment test and wet environment test. The dry and wet environment tests were conducted using the abrasion resistance tester (TR600) and slurry erosion tester, respectively; the slurry mixture of sand and water were used in the wet environment test. Two types of glass fibres architecture were understudied; unidirectional and woven. It was found that 3 wt.% filler content is the optimum amount to be used for the GFRP composite. Unidirectional nano-filled GFRP composites exhibited the lowest wear rates due to their closely aligned glass fibre arrangement. The unidirectional fibre alignment provided less empty spots for the interlocking process to take place, thus reducing the ploughing action of wearing. However, when tested in the wet environment, effects of other testing parameters such as the architecture of fibre and filler contents became less significant. The composites, which were tested in wet environment, showed the lowest wear rates compared to the ones tested in the dry environment. This is due to the presence of water that helps to wash away the pulverised glass fibre, thus reducing the friction and the three-body wear effect.

*Keywords:* Abrasive wear, dry sliding, glass fibre, polymer composite, slurry erosion test

### ARTICLE INFO

#### *Article history:*

Received: 25 October 2016

Accepted: 17 March 2017

#### *E-mail addresses:*

[aidahjumahat@gmail.com](mailto:aidahjumahat@gmail.com) (Aidah Jumahat),

[anisadilah86@gmail.com](mailto:anisadilah86@gmail.com) (Anis Adilah),

[eliya.kamal@gmail.com](mailto:eliya.kamal@gmail.com) (Eliya Farah Hana Mohd Kamal),

[mizisulaiman90@gmail.com](mailto:mizisulaiman90@gmail.com) (Muhammad Tarmizi Sulaiman),

[syahrulroslan92@gmail.com](mailto:syahrulroslan92@gmail.com) (Ahmad Syahrul Mohd Roslan)

\*Corresponding Author

### INTRODUCTION

Abrasive wear is described as when a material experiences loss in its mass due to continuous contact made with an abraded surface of a moving counter body. There are basically four main mechanisms associated with abrasive wear, namely micro-fatigue, micro-cutting, micro-cracking, and micro-ploughing (Morioka, Tsuchiya, & Shioya, 2015). Micro-

fatigue is described when a rough worn surface could be observed on the material after abrasion. On the other hand, micro-cracking usually occurs to brittle materials due to high-stress concentration applied onto the material's surface by an abrasive surface. Micro-cutting is defined when there is detachment of particles from the material's surface. Lastly, micro-ploughing is when particles are being detached or swept sideways by an abrasive counter face, together with the presence of ridges and grooves (Morioka et al., 2015). There is another common wear behaviour that is always being associated with abrasive wear, i.e. the three-body abrasive wear. This behaviour occurs due to the debris, or removal of particles, are quite large in size, and consequently act as the third counter body which aids in abrading the material further, aside from the material and counter face (Hrabě & Müller, 2016).

Glass Fibre is a well-known fibre which is commonly used in composites in order to enhance the mechanical properties of polymer matrix composites. Albeit having a profound effect in improving the mechanical strength of the composite, it does not happen to have the same kind of effects in improving the wear properties of the composites due to the nature of the glass fibre which could be easily pulverised, as highlighted by Sumer, Unal, and Mimaroglu (2008). Therefore, in an extensive effort to improve the properties of Glass Fibre Reinforced Polymer composite (GFRP), nanofillers are incorporated into the polymer (Jumahat, Talib, & Abdullah, 2016; Jumahat, Kasolang, & Bahari, 2015; Basavarajappa & Ellangovan, 2012). Nano-fillers have been proven to improve the wear properties of the GFRP composite due to the ability of the fillers to form a tribo-protective layer where the layer protects the surface of the material from being further worn out by the counter body. On the other hand, the fillers are also said to have a cushioning effect on the asperities presence in the composite, thus helping in absorbing shock from the imposing and abrading counter body, as well as filling up the voids that may be present in the composite (Basavarajappa & Ellangovan, 2012). The optimum filler content being reported are between 1 wt.% and 4 wt.%. When the filler content is more than 5 wt.%, the fillers tend to agglomerate. This reduces the wear properties of the composites since the agglomerated nano-fillers will end up digging out in larger chunks affecting higher mass loss (Friedrich, Zhang, & Schlarb, 2015).

The load applied and speed used during the wear test are also said to affect the wear rate of the composite. Higher load and speed applied will contribute in higher friction built up. This induces softening of the matrix, as well as separation of the matrix from the reinforcement, thus higher mass loss will be experienced by the composite (Basavarajappa & Ellangovan, 2012; Sumer, Ugnal, & Mimaroglu, 2008; Agrawal, Singh, & Sarkar, 2016). However, there is another testing parameter which has a more significant effect on the wear rate compared to the speed and load which is environment test. Dhieb et al. (2016) highlighted that wear test conducted in water or lubricated environment diminished the speed and load effects on the wearing rate of the composite. This is because in a wet environment, the flowing fluid will wash away the debris produced from wearing motion. This will have either a positive or negative effect on the wear rate of the composite. If the debris produced by the materials is intended to be formed into a tribo-protective layer, then washing away the debris will not have a significant effect in improving wear as it has been expected to have. Meanwhile, if the debris produced

was unwanted and could possibly cause the occurrence of three-body abrasive wearing, then washing it away would result in a better wear performance (Dhieb et al., 2016; Sumer, Unal, & Mimaroglu, 2008).

Wearing of material also could be affected by the surface topography of the material. Higher surface roughness would incur a higher material loss as the increase in asperities' height and the number would provide a good interlocking spot between the material and counter body. Better interlocking will end up in higher mass loss of the material. Increment in surface topography, i.e. surface roughness, or difference in the homogeneity of the surface will also provide a good interlocking motion that will result in higher wear rate (Ruckdäschel, Sandler, & Altstadt, 2013; Chauhan, & Thakur, 2013). Therefore, this paper investigates the effects of different environments, dry sliding and slurry wear test, as well as the architecture of glass fibre, unidirectional and woven on the wear rate of the nano-filled epoxy polymer composite.

## METHOD

### Fabrication of Composite

Commercial epoxy (Miracast 1517 A/B), supplied by Miracon (M) Sdn. Bhd., Malaysia, was used for this study. Miracast 1517 epoxy was cured by Miracast 1517 hardener with the ratio of 100:30. The nano-clay I.30E, used as the filler, was supplied by Sigma-Aldrich (M) Sdn Bhd. 1 wt.%, 3 wt.% and 5 wt.% of nano-clay in the epoxy samples were fabricated using high shear mixing process. The mixtures were milled at 12 m/s speed and 60°C. Then, the nano-modified resin was applied onto the woven and unidirectional mat of glass fibres and the composite samples were produced using the vacuum bagging system.

### Abrasive Wear and Slurry Erosion Test

The specimens were subjected to two types of tests, which are the abrasive wear and slurry erosion tests. The test parameters used are indicated in Table 1 and Table 2 for the abrasive wear and slurry erosion test, respectively.

Table 1  
*Test condition for abrasive wear test*

Testing Parameters	Experimental Condition
Test Standard	ASTM D 3389
Contact Geometry	Cylinder on flat
Type of motion	Unidirectional sliding
Applied Load	20 N
Sliding Speed	267 rpm
Sliding distance	10,000 m (2000 m Interval)
Specimen Shape (Dimensions)	Disc ( $\phi = 123$ mm, $t = 5-6$ mm)

Table 2  
Test condition for slurry erosion test

Testing Parameters	Experimental Condition
Slurry Material	Mixture of sand and water
Type of sand	Medium size ( $\phi$ = 0.2- 0.63 mm)
Type of motion	Unidirectional sliding
Sliding Speed	267 rpm
Sliding distance	10,000 m (2000 m interval)
Specimen Shape (Dimensions)	Bar (L= 75 mm, W= 25 mm, t= 6 mm)

For every 2000 mm interval, the machine was stopped and the mass of the specimen was weighed. The specific wear rate of the composite was calculated using formula 1, by substituting the recorded mass loss into the formulae:

$$W_s = \frac{\Delta m (g)}{L (m) \times \rho \left( \frac{g}{mm^3} \right) \times F (N)} \quad [1]$$

Where the specific wear rate ( $W_s$ ) was described as the function of mass loss ( $\Delta m$ ) over the multiplication of the sliding distance ( $L$ ), density ( $\rho$ ), and applied load ( $F$ ). The specific wear rate is expressed in  $mm^3/Nm$  unit (Nordin et al., 2013).

## RESULTS AND DISCUSSION

First of all, the optimum filler content that is the most suitable to be used in GFRP composite needs to be determined. From Figure 1, it could be observed that when unidirectional glass fibre was used to reinforce the epoxy matrix, the specific wear rate increased significantly compared to pure epoxy. This is due to the nature of the glass fibre being easily pulverised, as highlighted by Sumer et al. (2016). When nano-clay filler was incorporated into the GFRP composite, the wear shows a different effect depending on the amount of nano-clay used in the composite. When 1 wt. % of nano-clay was used in the UniGFRP composite, the wear rate seemed to be improving. However, after 6000 m of sliding distance, it was observed that the wear rate started to worsen. This might be due to the amount of filler incorporated which was too little; therefore, after 6000 m, the filler had all been dug out by the abrasive counter body. When there was no filler left in the epoxy, the surface topography of the composite started to increase, therefore, exposing the surface to easier ploughing and cutting of the surface by the abrasive counter body, as previously explained by Ruckdäschel et al. (2013), Morioka et al. (2015), and Friedrich et al. (2005).

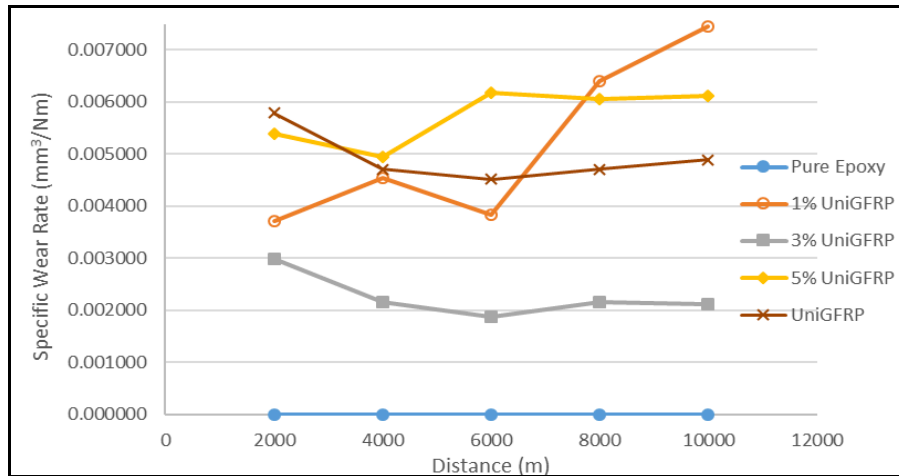


Figure 1. Specific wear rate of nano-modified unidirectional GFRP composite

When 3 wt.% of nano-clay was incorporated into the epoxy, the specific wear rate showed promising improvement. However, when 5 wt.% of nano-clay was used, the wear rate seemed to be increasing. As it was highlighted beforehand by Friedrich et al. (2005), the optimum filler content to be incorporated into the matrix is usually around 1% to 4%. When the filler amount exceeds 5%, the filler will have a high possibility to agglomerate. Agglomerated fillers will enable larger chunks of material to be dug out during abrasion. Hence, it could be stipulated that 3 wt.% of nano-clay is the optimum filler content that should be incorporated into the epoxy matrix in GFRP composite, and henceforth, this type of composite will be used for the wear rate study on the test environment and architecture of glass fibre.

When comparing the two architectures of the glass fibre tested in the dry environment from Figure 2, it could also be observed that the unidirectional GFRP (UniGFRP) significantly exhibited lesser and better specific wear rate compared to Woven GFRP (WGFRP). This is because the woven glass fibre provides more spots for the interlocking motion to take place. The empty space between each weave will provide an access for the interlocking between the surface and abraded counter body to take place, hence, better ploughing and cutting of the materials' surface took place, as described by Ruckdäschel et al. (2013), and Chauhan and Thakur (2013). As for the unidirectional GFRP, the fibres are aligned closely together and the spot for the interlocking process to take place is limited, and thus, avoiding the pulverisation and ploughing of the glass fibre which consequently result in lesser specific wear rate.

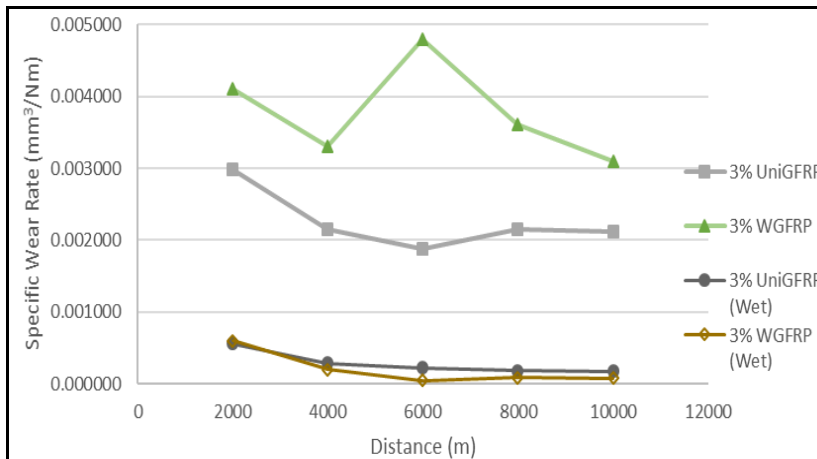


Figure 2. Specific Wear Rate of 3 wt. % Nano-modified Unidirectional and Woven GFRP Composite under dry and wet environment

Based on Figure 2, the specific wear rate of 3 wt.% nano-modified unidirectional and woven GFRP composite under dry and wet environment were observed. Compared to the dry environment, the wear rates exhibited by the composites tested in the wet environment are much lower. This result supports the claimed made by Sumer, Unal, and Mimaroglu (2008) and Dhieb et al. (2016), which stated that the wet condition would result in the best wear rate of the composite. When the composites were tested in wet condition, other testing parameters and the structure of the fibre did not have as much significant effect as the ones tested in the dry environment. This is because in wet condition, the water helps to wash away the debris made by the pulverised glass fibre. Washing away the debris will then reduce the three-body abrasive wear. Water also provides a lubricating layer which aids in a smoother sliding motion, hence reduces the friction and wear rate. Albeit insignificant, in the wet environment, the woven GFRP composite seems to have displayed better wear performance compared to unidirectional GFRP. This may be because in the wet environment, not only the pulverised glass fibres are being washed away by the water, but the sand helps in filling in the voids between each weave thus reducing exposed spots for interlocking activity. Reduction in interlocking spots will reduce the ploughing and cutting action of the WGFRP composite, thus resulting in reduced specific wear rates. The wear rates for the composites tested in the wet environment also seemed to exhibit wear rate almost similar to the pure epoxy in Figure 1.

Based on Figure 3, it could be observed that the results for specific wear rates obtained for 1, 3, and 5 wt.% nano-clay filled UniGFRP composites tested under the wet environment were different from the results which had been observed earlier in Figure 1. When being tested under the dry condition, it was found that 3 wt % of nano-clay was the most optimum amount of fillers to be added to the GFRP composites since it exhibited the least wear rates amongst other nano-filled unidirectional GFRP composites. However, for the tests which had been done under the wet environment, the amount of nano-fillers incorporated into the GFRP composite seemed to be less significant. The specific wear rates of these composites appeared to be almost

similar, especially after 6000 m of sliding distance. Not only the wear rates are lesser than the ones tested under dry condition, but the specific wear rates for these composites exhibited wear rates almost comparable to pure epoxy, which is notable. This is because, when the repeating abrasive motion happens with the presence of water or fluid, the water serves as a lubricating layer which will aid in lessening the friction by reducing the effect of load and speed between the material surface and abrasive counterpart. As highlighted by Sumer, Unal, and Mimaroglu (2008) and Dhieb et al. (2016), the effects of filler content and testing parameters on the wear rates would be diminished when tested under a wet condition. Therefore, it could be concluded that nano-modified GFRP composites are highly potential to be used in a wet environment which also requires excellent mechanical strength and wear properties.

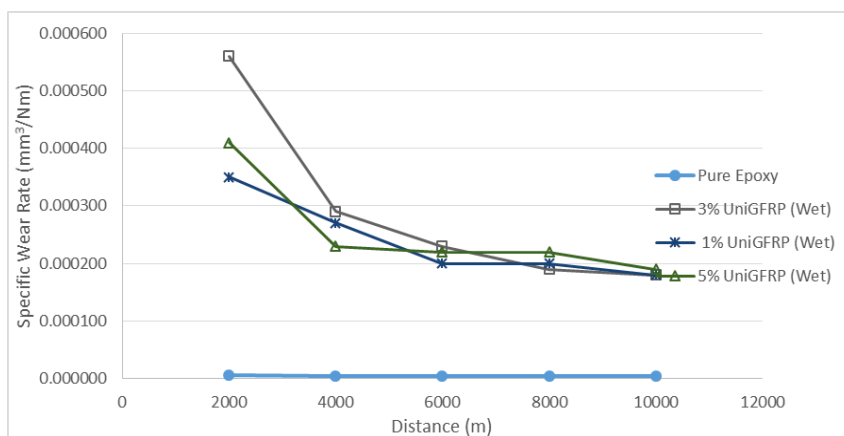


Figure 3. Specific wear rate of nano-modified unidirectional GFRP Composite tested in wet environment

## CONCLUSION

Effects of the environments, as well as architecture of nano-clay modified composites, have been thoroughly studied. The optimum filler content for this composite in the dry condition was determined to be 3 wt. % since it showed the lowest wear rates compared to 1 wt.% and 5 wt.%. The wear rate for 3 wt.% nano-filled GFRP composites was also lower compared to the unmodified GFRP composite. Similarly, the architecture of the glass fibres also appeared to have some effects on the wear rates of the composites. The unidirectional GFRP displayed improved wear rate compared to the woven GFRP composite. This is because the unidirectional glass fibres are aligned closely together, which provide fewer voids or empty spots for the interlocking process to take place, therefore inhibiting the ploughing and cutting of the material. On the other hand, the wet environment demonstrates to have the most significant effect on the wear rate of composite and the best wear rates compared to the ones tested in the dry environment. In the wet environment, the effects of the architecture of the glass fibre and the amount of nano-fillers incorporated into the GFRP composites seemed to have been diminished. This is because in the slurry erosion test, water in the slurry mixture helped to wash away the debris produced during abrasion, thus reducing the three-body abrasive wear effect. The water also

served as the lubricant, which helped to reduce the friction by reducing the effects of load and speed on the surface material when abraded. The sand in the mixture was also stipulated to help in filling in the voids between each fibre weave, thus reducing the spots for interlocking action to take place. The nano-modified GFRP composites were also postulated to be best applied in applications which operate under the wet environment that also requires excellent mechanical strength on top of good wear properties.

## ACKNOWLEDGEMENTS

The authors would like to thank Institute of Research Management and Innovation (IRMI), the Ministry of Education, Malaysia, and Institute of Graduate Studies (IPSIS), UiTM, for the financial support. This research work was performed at the Faculty of Mechanical Engineering, UiTM, Malaysia, under the support of BESTARI GRANT 6600-IRMI/MyRA 5/3/BESTARI (019/2017).

## REFERENCES

- Agrawal, S., Singh, K. K., & Sarkar, P. K. (2016). A comparative study of wear and friction characteristics of glass fibre reinforced epoxy resin, sliding under dry, oil-lubricated and inert gas environments. *Tribology International*, *96*, 217-224.
- Basavarajappa, S., & Ellangovan, S. (2012). Dry sliding wear characteristics of glass-epoxy composite filled with silicon carbide and graphite particles. *Wear*, *296*, 491-496.
- Chauhan, S. R., & Thakur, S. (2013). Effects of particle size, particle loading and sliding distance on the friction and wear properties of cenosphere particulate filled vinylester composites. *Materials and Design*, *51*, 398-408.
- Dhieb, H., Bujinsters, J. G., Elleuch, K., & Celis, J. (2016). Effect of relative humidity and full immersion in water on friction, wear and debonding of unidirectional carbon fiber reinforced epoxy under reciprocating sliding. *Composites Part B*, *88*, 240-252.
- Friedrich, K., Zhang, Z., & Schlarb, A. K. (2005). Effects of various fillers on the sliding wear of polymer composites. *Composites Science and Technology*, *65*, 2329-2343.
- Hrabě, P., & Müller, M. (2016). Three-body abrasive wear of polymer matrix composites filled with *Jatropha Curcas L.* *Procedia Engineering*, *136*, 169-174.
- Jumahat, A., Kasolang, S., & Bahari, M. T. (2015). Wear properties of nanosilica filled epoxy polymers and FRP composites. *Jurnal Tribologi*, *6*, 24-36.
- Jumahat, A., Talib, A. A. A., & Abdullah, A. (2016). Wear Properties of Nanoclay Filled Epoxy Polymers and Fiber Reinforced Hybrid Composites. *Nanoclay Reinforced Polymer Composites: Nanocomposites and Bionanocomposites* Singapore: Springer, 247-260.
- Morioka, Y., Tsuchiya, Y., & Shioya, M. (2015). Correlations between the abrasive wear, fatigue, and tensile properties of filler-dispersed polyamide 6. *Wear*, *338-339*, 297-306.
- Nordin, N. A., Yussof, F. M., Kasolang, S., Salleh, Z., & Ahmad, M. A. (2013). Wear Rate of Natural Fibre: Long Kenaf Composite. *Procedia Engineering*, *68*, 145-151.



- Ruckdäschel, H., Sandler, J. K. W., & Altstädt, V. (2013). On the friction and wear of carbon nano fiber reinforced PEEK-based polymer composites. *Tribology of Polymeric Nanocomposites*. Retrieved from doi.org/10.1016/B978-0-444-59455-6.00008-8.
- Sumer, M., Unal, H., & Mimaroglu, A. (2008). Evaluation of tribological behaviour of PEEK and glass fibre reinforced PEEK composite under dry sliding and water lubricated conditions. *Wear*, 265, 1061-1065.



**REFEREES FOR THE PERTANIKA  
JOURNAL OF SCIENCE AND TECHNOLOGY**

**VOL. 25 (S) APR. 2017**  
*Special Edition*

**Advances in Science & Technology**

The Editorial Board of the Journal of Science and Technology wishes to thank the following:

Abdullah Mohamed  
*(UPM, Malaysia)*

Agus Arsad  
*(UiTM, Malaysia)*

Ahmad Nasser Mohd Rose  
*(UMP, Malaysia)*

Ahmad Rostam Md Zin  
*(HKL, Malaysia)*

Akmal Zulayla Mohd Zahid  
*(UiTM, Malaysia)*

Anizah Kalam  
*(UiTM, Malaysia)*

Aryani Ahmad Latiffi  
*(UTHM, Malaysia)*

Azriny S. Khalid  
*(Dublin, Republic of Ireland)*

Baljit Singh Bhathal Singh  
*(UiTM, Malaysia)*

Famiza Abd Latif  
*(UiTM, Malaysia)*

Gabriele Anisah Froemming  
*(UiTM, Malaysia)*

Hairul Azman  
*(UNIMAS, Malaysia)*

Hassimi Abu Hasan  
*(UKM, Malaysia)*

Husna Zainol Abidin  
*(UiTM, Malaysia)*

Jamaluddin Mahmud  
*(UiTM, Malaysia)*

Khaled Ali Al-Attab  
*(USM, Malaysia)*

Mohamad Ali Ahmad  
*(UiTM, Malaysia)*

Mohammad Isa Mohamadin  
*(UiTM, Malaysia)*

Mohammad Johari Ibahim  
*(UiTM, Malaysia)*

Mohd Amran Md Ali  
*(UTeM, Malaysia)*

Mohd Faizul Md Idros  
*(UiTM, Malaysia)*

Mohd Nazri Ismail  
*(UPNM, Malaysia)*

Muhammad Jamaluddin  
*(University Avenue Edmonton, Canada)*

Musalmah Mazlan  
*(UiTM, Malaysia)*

Nafisah Mohd Isa@Osman  
*(UiTM, Malaysia)*

Nazarudin Safian  
*(UKM, Malaysia)*

Noordini Mohamad Salleh  
*(UM, Malaysia)*

Noraini Wahab  
*(UiTM, Malaysia)*

Norhati Ibrahim  
*(UiTM, Malaysia)*

Nurin Wahidah Mohd Zulkifli  
*(UM, Malaysia)*

Nursuriati Jamil  
*(UiTM, Malaysia)*

Ooi Lu Ean  
*(USM, Malaysia)*

Puteri Sarah  
(UiTM, Malaysia)

Rapiaah Mustaffa  
(USM, Malaysia)

Rohana Ahmad  
(UiTM, Malaysia)

Rozaimi Ghazali  
(UTeM, Malaysia)

Rui Neves Madeira  
(Campus do IPS, Portugal)

Salmi Razali  
(UiTM, Malaysia)

Sarina Sulaiman  
(IIUM, Malaysia)

Siti Amira Othman  
(UTHM, Malaysia)

Siti Halimah Sarijo  
(UiTM, Malaysia)

Suhaimi Abdul Latif  
(IIUM, Malaysia)

Syahrullail Samion  
(UTM, Malaysia)

Tay Chia Chay  
(UiTM, Malaysia)

Tengku Ahmad Damitri Al-Astani Tengku Di  
(USM, Malaysia)

Tomasz Rak  
(Rzeszow University of Technology, Poland)

Wan Mazlina Wan Mohamed  
(UiTM, Malaysia)

Wan Razarinah W. Abd. Razak  
(UiTM, Malaysia)

Weitao Xu  
(The University of New South Wales, Australia)

Woi Pei Meng  
(UM, Malaysia)

Zulkiflee Abd Latif  
(UiTM, Malaysia)

---

HKL - Hospital Kuala Lumpur  
IIUM - International Islamic University of Malaysia  
SIRIM - Scientific and Industrial Research Institute of Malaysia  
UiTM - Universiti Teknologi MARA  
UKM - Universiti Kebangsaan Malaysia  
UM - Universiti Malaya  
UMP - Universiti Malaysia Pahang

UNIMAS - Universiti Malaysia Sarawak  
UPNM - Universiti Pertahanan Nasional Malaysia  
UPM - Universiti Putra Malaysia  
USM - Universiti Sains Malaysia  
UTeM - Universiti Teknikal Malaysia Melaka  
UTHM - Universiti Tun Hussein Onn Malaysia

---

While every effort has been made to include a complete list of referees for the period stated above, however if any name(s) have been omitted unintentionally or spelt incorrectly, please notify the Chief Executive Editor, *Pertanika* Journals at [nayan@upm.my](mailto:nayan@upm.my).

Any inclusion or exclusion of name(s) on this page does not commit the *Pertanika* Editorial Office, nor the UPM Press or the University to provide any liability for whatsoever reason.

# *Pertanika Journals*

*Our goal is to bring high quality research to the widest possible audience*

## **INSTRUCTIONS TO AUTHORS** (Manuscript Preparation & Submission Guide)

Revised: June 2016

Please read the Pertanika guidelines and follow these instructions carefully. Manuscripts not adhering to the instructions will be returned for revision without review. The Chief Executive Editor reserves the right to return manuscripts that are not prepared in accordance with these guidelines.

### **MANUSCRIPT PREPARATION**

#### **Manuscript Types**

*Pertanika* accepts submission of mainly **four** types of manuscripts for peer-review.

##### **1. REGULAR ARTICLE**

Regular articles are full-length original empirical investigations, consisting of introduction, materials and methods, results and discussion, conclusions. Original work must provide references and an explanation on research findings that contain new and significant findings.

*Size:* Generally, these are expected to be between 6 and 12 journal pages (excluding the abstract, references, tables and/or figures), a maximum of 80 references, and an abstract of 100–200 words.

##### **2. REVIEW ARTICLE**

These report critical evaluation of materials about current research that has already been published by organizing, integrating, and evaluating previously published materials. It summarizes the status of knowledge and outline future directions of research within the journal scope. Review articles should aim to provide systemic overviews, evaluations and interpretations of research in a given field. Re-analyses as meta-analysis and systemic reviews are encouraged. The manuscript title must start with "Review Article:".

*Size:* These articles do not have an expected page limit or maximum number of references, should include appropriate figures and/or tables, and an abstract of 100–200 words. Ideally, a review article should be of 7 to 8 printed pages.

##### **3. SHORT COMMUNICATIONS**

They are timely, peer-reviewed and brief. These are suitable for the publication of significant technical advances and may be used to:

- (a) report new developments, significant advances and novel aspects of experimental and theoretical methods and techniques which are relevant for scientific investigations within the journal scope;
- (b) report/discuss on significant matters of policy and perspective related to the science of the journal, including 'personal' commentary;
- (c) disseminate information and data on topical events of significant scientific and/or social interest within the scope of the journal.

The manuscript title must start with "*Brief Communication:*".

*Size:* These are usually between 2 and 4 journal pages and have a maximum of three figures and/or tables, from 8 to 20 references, and an abstract length not exceeding 100 words. Information must be in short but complete form and it is not intended to publish preliminary results or to be a reduced version of Regular or Rapid Papers.

#### 4. OTHERS

Brief reports, case studies, comments, concept papers, Letters to the Editor, and replies on previously published articles may be considered.

**PLEASE NOTE: NO EXCEPTIONS WILL BE MADE FOR PAGE LENGTH.**

#### Language Accuracy

Pertanika **emphasizes** on the linguistic accuracy of every manuscript published. Articles must be in **English** and they must be competently written and argued in clear and concise grammatical English. Contributors are strongly advised to have the manuscript checked by a colleague with ample experience in writing English manuscripts or a competent English language editor.

Author(s) **must provide a certificate** confirming that their manuscripts have been adequately edited. A proof from a recognised editing service should be submitted together with the cover letter at the time of submitting a manuscript to Pertanika. **All editing costs must be borne by the author(s)**. This step, taken by authors before submission, will greatly facilitate reviewing, and thus publication if the content is acceptable.

Linguistically hopeless manuscripts will be rejected straightaway (e.g., when the language is so poor that one cannot be sure of what the authors really mean). This process, taken by authors before submission, will greatly facilitate reviewing, and thus publication if the content is acceptable.

#### MANUSCRIPT FORMAT

The paper should be submitted in one column format with at least 4cm margins and 1.5 line spacing throughout. Authors are advised to use Times New Roman 12-point font and *MS Word* format.

##### 1. Manuscript Structure

Manuscripts in general should be organised in the following order:

##### Page 1: Running title

This page should **only** contain the running title of your paper. The running title is an abbreviated title used as the running head on every page of the manuscript. The running title should not exceed 60 characters, counting letters and spaces.

##### Page 2: Author(s) and Corresponding author information.

This page should contain the **full title** of your paper not exceeding 25 words, with name(s) of all the authors, institutions and corresponding author's name, institution and full address (Street address, telephone number (including extension), hand phone number, and e-mail address) for editorial correspondence. First and corresponding authors must be clearly indicated.

The names of the authors may be abbreviated following the international naming convention. e.g. Salleh, A.B.<sup>1</sup>, Tan, S.G<sup>2\*</sup>., and Sapuan, S.M<sup>3</sup>.

**Authors' addresses.** Multiple authors with different addresses must indicate their respective addresses separately by superscript numbers:

George Swan<sup>1</sup> and Nayan Kanwal<sup>2</sup>

<sup>1</sup>Department of Biology, Faculty of Science, Duke University, Durham, North Carolina, USA.,

<sup>2</sup>Office of the Deputy Vice Chancellor (R&I), Universiti Putra Malaysia, Serdang, Malaysia.

A **list** of number of **black and white / colour figures and tables** should also be indicated on this page. Figures submitted in color will be printed in colour. See "5. Figures & Photographs" for details.

##### Page 3: Abstract

This page should **repeat** the **full title** of your paper with only the **Abstract** (the abstract should be less than 250 words for a Regular Paper and up to 100 words for a Short Communication), and **Keywords**.

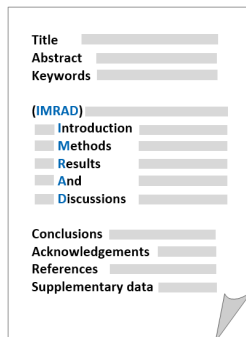
**Keywords:** Not more than eight keywords in alphabetical order must be provided to describe the contents of the manuscript.

#### Page 4: Introduction

This page should begin with the **Introduction** of your article and followed by the rest of your paper.

#### 2. Text

Regular Papers should be prepared with the headings *Introduction, Materials and Methods, Results and Discussion, Conclusions, Acknowledgements, References, and Supplementary data* (if available) in this order.



Title \_\_\_\_\_  
 Abstract \_\_\_\_\_  
 Keywords \_\_\_\_\_  
 (IMRAD)  
 Introduction \_\_\_\_\_  
 Methods \_\_\_\_\_  
 Results \_\_\_\_\_  
 And \_\_\_\_\_  
 Discussions \_\_\_\_\_  
 Conclusions \_\_\_\_\_  
 Acknowledgements \_\_\_\_\_  
 References \_\_\_\_\_  
 Supplementary data \_\_\_\_\_

#### MAKE YOUR ARTICLES AS CONCISE AS POSSIBLE

Most scientific papers are prepared according to a format called IMRAD. The term represents the first letters of the words Introduction, Materials and Methods, Results, And, Discussion. It indicates a pattern or format rather than a complete list of headings or components of research papers; the missing parts of a paper are: Title, Authors, Keywords, Abstract, Conclusions, and References. Additionally, some papers include Acknowledgments and Appendices.

The Introduction explains the scope and objective of the study in the light of current knowledge on the subject; the Materials and Methods describes how the study was conducted; the Results section reports what was found in the study; and the Discussion section explains meaning and significance of the results and provides suggestions for future directions of research. The manuscript must be prepared according to the Journal's instructions to authors.

#### 3. Equations and Formulae

These must be set up clearly and should be typed double spaced. Numbers identifying equations should be in square brackets and placed on the right margin of the text.

#### 4. Tables

All tables should be prepared in a form consistent with recent issues of Pertanika and should be numbered consecutively with Roman numerals. Explanatory material should be given in the table legends and footnotes. Each table should be prepared on a new page, embedded in the manuscript.

*When a manuscript is submitted for publication, tables must also be submitted separately as data - .doc, .rtf, Excel or PowerPoint files- because tables submitted as image data cannot be edited for publication and are usually in low-resolution.*

#### 5. Figures & Photographs

Submit an **original** figure or photograph. Line drawings must be clear, with high black and white contrast. Each figure or photograph should be prepared on a new page, embedded in the manuscript for reviewing to keep the file of the manuscript under 5 MB. These should be numbered consecutively with Roman numerals.

Figures or photographs must also be submitted separately as TIFF, JPEG, or Excel files- because figures or photographs submitted in low-resolution embedded in the manuscript cannot be accepted for publication. For electronic figures, create your figures using applications that are capable of preparing high resolution TIFF files. In general, we require **300 dpi** or higher resolution for **coloured and half-tone artwork**, and **1200 dpi or higher** for **line drawings** are required.

Failure to comply with these specifications will require new figures and delay in publication.

**NOTE:** Illustrations may be produced in colour at no extra cost at the discretion of the Publisher; the author could be charged Malaysian Ringgit 50 for each colour page.

#### 6. References

References begin on their own page and are listed in alphabetical order by the first author's last name. Only references cited within the text should be included. All references should be in 12-point font and double-spaced.

**NOTE:** When formatting your references, please follow the **APA reference style** (6th Edition). Ensure that the references are strictly in the journal's prescribed style, failing which your article will **not be accepted for peer-review**. You may refer to the *Publication Manual of the American Psychological Association* for further details (<http://www.apastyle.org/>).

## 7. General Guidelines

**Abbreviations:** Define alphabetically, other than abbreviations that can be used without definition. Words or phrases that are abbreviated in the introduction and following text should be written out in full the first time that they appear in the text, with each abbreviated form in parenthesis. Include the common name or scientific name, or both, of animal and plant materials.

**Acknowledgements:** Individuals and entities that have provided essential support such as research grants and fellowships and other sources of funding should be acknowledged. Contributions that do not involve researching (clerical assistance or personal acknowledgements) should **not** appear in acknowledgements.

**Authors' Affiliation:** The primary affiliation for each author should be the institution where the majority of their work was done. If an author has subsequently moved to another institution, the current address may also be stated in the footer.

**Co-Authors:** The commonly accepted guideline for authorship is that one must have substantially contributed to the development of the paper and share accountability for the results. Researchers should decide who will be an author and what order they will be listed depending upon their order of importance to the study. Other contributions should be cited in the manuscript's Acknowledgements.

**Copyright Permissions:** Authors should seek necessary permissions for quotations, artwork, boxes or tables taken from other publications or from other freely available sources on the Internet before submission to Pertanika. Acknowledgement must be given to the original source in the illustration legend, in a table footnote, or at the end of the quotation.

**Footnotes:** Current addresses of authors if different from heading may be inserted here.

**Page Numbering:** Every page of the manuscript, including the title page, references, tables, etc. should be numbered.

**Spelling:** The journal uses American or British spelling and authors may follow the latest edition of the Oxford Advanced Learner's Dictionary for British spellings.

## SUBMISSION OF MANUSCRIPTS

Owing to the volume of manuscripts we receive, we must insist that all submissions be made electronically using the **online submission system ScholarOne™**, a web-based portal by Thomson Reuters. For more information, go to our web page and [click "Online Submission"](#).

### Submission Checklist

1. **MANUSCRIPT:** Ensure your MS has followed the Pertanika style particularly the first four pages as explained earlier. The article should be written in a good academic style and provide an accurate and succinct description of the contents ensuring that grammar and spelling errors have been corrected before submission. It should also not exceed the suggested length.

**COVER LETTER:** All submissions must be accompanied by a cover letter detailing what you are submitting. Papers are accepted for publication in the journal on the understanding that the article is **original** and the content has **not been published** either **in English** or **any other language(s)** or **submitted for publication elsewhere**. The letter should also briefly describe the research you are reporting, why it is important, and why you think the readers of the journal would be interested in it. The cover letter must also contain an acknowledgement that all authors have contributed significantly, and that all authors have approved the paper for release and are in agreement with its content.

The cover letter of the paper should contain (i) the title; (ii) the full names of the authors; (iii) the addresses of the institutions at which the work was carried out together with (iv) the full postal and email address, plus telephone numbers and emails of all the authors. The current address of any author, if different from that where the work was carried out, should be supplied in a footnote.

The above must be stated in the cover letter. Submission of your manuscript will not be accepted until a cover letter has been received



2. **COPYRIGHT:** Authors publishing the Journal will be asked to sign a copyright form. In signing the form, it is assumed that authors have obtained permission to use any copyrighted or previously published material. All authors must read and agree to the conditions outlined in the form, and must sign the form or agree that the corresponding author can sign on their behalf. Articles cannot be published until a signed form (*original pen-to-paper signature*) has been received.

Please do **not** submit manuscripts to the editor-in-chief or to any other office directly. Any queries must be directed to the **Chief Executive Editor's** office via email to [nayan@upm.my](mailto:nayan@upm.my).

Visit our Journal's website for more details at <http://www.pertanika.upm.edu.my/home.php>.

### **HARDCOPIES OF THE JOURNALS AND OFF PRINTS**

Under the Journal's open access initiative, authors can choose to download free material (via PDF link) from any of the journal issues from Pertanika's website. Under "**Browse Journals**" you will see a link, "*Current Issues*" or "*Archives*". Here you will get access to all current and back-issues from 1978 onwards.

The **corresponding author** for all articles will receive one complimentary hardcopy of the journal in which his/her articles is published. In addition, 20 off prints of the full text of their article will also be provided. Additional copies of the journals may be purchased by writing to the Chief Executive Editor.



## Why should you publish in

# Pertanika?

### BENEFITS TO AUTHORS

**PROFILE:** Our journals are circulated in large numbers all over Malaysia, and beyond in Southeast Asia. Our circulation covers other overseas countries as well. We ensure that your work reaches the widest possible audience in print and online, through our wide publicity campaigns held frequently, and through our constantly developing electronic initiatives such as Web of Science Author Connect backed by Thomson Reuters.

**QUALITY:** Our journals' reputation for quality is unsurpassed ensuring that the originality, authority and accuracy of your work are fully recognised. Each manuscript submitted to Pertanika undergoes a rigid originality check. Our double-blind peer refereeing procedures are fair and open, and we aim to help authors develop and improve their scientific work. Pertanika is now over 38 years old; this accumulated knowledge has resulted in our journals being indexed in SCOPUS (Elsevier), Thomson (ISI) Web of Science™ Core Collection, Emerging Sources Citation Index (ESCI), Web of Knowledge [BIOSIS & CAB Abstracts], EBSCO, DOAJ, ERA, AGRICOLA, Google Scholar, ISC, TIB, Journal Guide, Citefactor, Cabell's Directories and MyCite.

**AUTHOR SERVICES:** We provide a rapid response service to all our authors, with dedicated support staff for each journal, and a point of contact throughout the refereeing and production processes. Our aim is to ensure that the production process is as smooth as possible, is borne out by the high number of authors who prefer to publish with us.

**CODE OF ETHICS:** Our Journal has adopted a Code of Ethics to ensure that its commitment to integrity is recognized and adhered to by contributors, editors and reviewers. It warns against plagiarism and self-plagiarism, and provides guidelines on authorship, copyright and submission, among others.

**PRESS RELEASES:** Landmark academic papers that are published in Pertanika journals are converted into press-releases as a unique strategy for increasing visibility of the journal as well as to make major findings accessible to non-specialist readers. These press releases are then featured in the university's UK and Australian based research portal, ResearchSEA, for the perusal of journalists all over the world.

**LAG TIME:** The elapsed time from submission to publication for the articles averages 3 to 4 months. A decision on acceptance of a manuscript is reached in 3 to 4 months (average 14 weeks).



Address your submissions to:  
The Chief Executive Editor  
Tel: +603 8947 1622  
[nayan@upm.my](mailto:nayan@upm.my)

Journal's Profile: [www.pertanika.upm.edu.my/](http://www.pertanika.upm.edu.my/)

## Call for Papers 2017-18

now accepting submissions...

*Pertanika* invites you to explore frontiers from all key areas of agriculture, science and technology to social sciences and humanities.

Original research and review articles are invited from scholars, scientists, professors, post-docs, and university students who are seeking publishing opportunities for their research papers through the Journal's three titles; JTAS, JST & JSSH. Preference is given to the work on leading and innovative research approaches.

*Pertanika* is a fast track peer-reviewed and open-access academic journal published by Universiti Putra Malaysia. To date, Pertanika Journals have been indexed by many important databases. Authors may contribute their scientific work by publishing in UPM's hallmark SCOPUS & ISI indexed journals.

Our journals are open access - international journals. Researchers worldwide will have full access to all the articles published online and be able to download them with zero subscription fee.

*Pertanika* uses online article submission, review and tracking system for quality and quick review processing backed by Thomson Reuter's ScholarOne™. Journals provide rapid publication of research articles through this system.

For details on the Guide to Online Submissions, please visit [http://www.pertanika.upm.edu.my/guide\\_online\\_submission.php](http://www.pertanika.upm.edu.my/guide_online_submission.php)

## About the Journal

*Pertanika* is an international multidisciplinary peer-reviewed leading journal in Malaysia which began publication in 1978. The journal publishes in three different areas — Journal of Tropical Agricultural Science (JTAS); Journal of Science and Technology (JST); and Journal of Social Sciences and Humanities (JSSH). All journals are published in English.

**JTAS** is devoted to the publication of original papers that serves as a forum for practical approaches to improving quality in issues pertaining to tropical agricultural research- or related fields of study. It is published four times a year in *February, May, August* and *November*.

**JST** caters for science and engineering research- or related fields of study. It is published twice a year in *January* and *July*.

**JSSH** deals in research or theories in social sciences and humanities research. It aims to develop as a flagship journal with a focus on emerging issues pertaining to the social and behavioural sciences as well as the humanities, particularly in the Asia Pacific region. It is published four times a year in *March, June, September* and *December*.



An Award-winning  
International-Malaysian Journal  
— CREAM AWARD, MoHE  
—Sept 2015



A Pre-shared Diffie-Hellman Key Exchange Scheme for a Secure TFTP Protocol <i>Nur Nabila Mohamed, Mohd Anuar Mat Isa, Yusnani Mohd Yussoff and Habibah Hashim</i>	303
Effects of the Number of Nozzles on Acoustic Signals Produced by a Ranque-Hilsch Vortex Tube <i>Khairil Muhaimin Abd Rahman, Wirachman Wisnoe and Valliyappan David Natarajan</i>	315
Tooth Frame Axes and Centroid for Dental Occlusal System <i>Muhammad Azmi Ayub, Mohd Shafiq Azni and Nagham Al-Jaf</i>	325
An Analysis on Node Cloning Attacks Prevention Using Unique Hardware Identity in WSN <i>Norhafyza Marbukhari, Yusnani Mohd Yussoff, Murizah Kassim, Mohd Anuar Mat Isa and Habibah Hashim</i>	335
Effects of Environment and Fibre Architecture on Wear Properties of Nano-Filled Epoxy Polymer Composite <i>Aidah Jumahat, Anis Adilah Abu Talib, Eliya Farah Hana Mohd Kamal, Muhammad Tarmizi Sulaiman and Ahmad Syahrul Mohd Roslan</i>	345

Perspective of a Smoke-free Home among Second-hand Smokers during Pregnancy: A Qualitative Study <i>Izzah Amira Mohd Asri, Nur Amirah Abd Rani, Zulfakhri Dzulkifli, Muhamad Ilmam Muhamad Jamil, Mohd Shahril Ahmad Saman and Siti Munira Yasin</i>	191
Effect of the Deposited Layer, Withdrawal Speed and Coated Length on Immobilised Bromothymol Blue in Polyaniline Sol Gel towards pH Sensing Sensitivity <i>Norliza Othman, Uzer Mohd Noor and Sukreen Hana Herman</i>	205
Analysis on the OTTV of Modern-Style Apartment Facades in Bandar Sri Permaisuri, Kuala Lumpur <i>Ahmad Sanusi Hassan and Muhammad Hafeez Abdul Nasir</i>	215
Synthetisation Temperature-Dependent Cytotoxicity of Bismuth Oxide Nanoparticles in Vitro <i>Nur Amirah Mohd Nor, Zanariah Mohd, Hairil Rashmizal Abdul Razak, Zolkapli Eshak and Wan Mazlina Md Saad</i>	227
Personality Prediction Based on Social Media Using Decision Tree Algorithm <i>Tan Lee Chee Yoong, Nor Rahayu Ngatirin and Zurinahni Zainol</i>	237
Implementation of a Fuzzy-Based Line Follower Robot using Arduino <i>Mohammad Safwan Mohamed Alias, Ya'akob Yusof and Nurul Muthmainnah Mohd Noor</i>	249
Ziegler-Nichols First Tuning Method for Air Blower PT326 <i>Mahanijah Md Kamal and Muhammad Hanihazaim Abd Halim</i>	259
Synthesis and Characterisation of Silica from Palm Oil Fuel Ash (POFA) Using Alkaline Fusion Method <i>Nur Athirah Adam, Alawi Sulaiman, Azhari Samsu Baharuddin, Mohd Noriznan Mokhtar, Zainuri Busu and Tengku Elida Tengku Zainal Mulok</i>	269
Effect of Upstream Building Configurations on Mean Wind Speed Ratio at Urban Pedestrian Level Using LES <i>Muhd Azhar Zainol, Azli Abd Razak, Nor Merlisa Ali, Qi Jie Kwong and Sheikh Ahmad Zaki</i>	277
Self-similarity Hurst Parameter Estimation with Rescaled Range Method on IP-based Campus Internet Traffic <i>Murizah Kassim, Noor Laili Ismail, Roslina Mohamad, Saiful Izwan Suliman and Mahamod Ismail</i>	287

A Study on the Formation of PVA/Kenaf Nanofibres via Electrospinning <i>Nor Dalila Nor Affandi, Mohd Rozi Ahmad, Sabiha Hanim Saleh, Muhammad Fairuz Remeli, Nur Hayati Humairah Nur Ikhwan Teo and Nurul Farihin Amran</i>	85
Flexural Properties of Random and Unidirectional Arenga Pinnata Fibre Reinforced Epoxy Composite <i>Muhamad Faris Syafiq Khalid, Aidah Jumahat, Zuraidah Salleh and Mohammad Jawaid</i>	93
Advection and Dispersion of Water Quality Constituents in Batu Ferringhi Penang <i>Muhammad Ilyas Ahmad Jamalluddin and Wei-Koon Lee</i>	103
Substituent Effect on Catalytic Activity of Palladium(II) Schiff Base Complexes for Sonogashira Reaction <i>Hadariah Bahron, Shahrul Nizam Ahmad, Amalina Mohd Tajuddin and Syed Illah Al-Yahya Syed Abdul Kadir</i>	115
Syntheses, Characterisation and Application of Palladium(II) Complexes as Catalysts in Heck Cross-Coupling Reaction <i>Amalina Mohd Tajuddin and Hadariah Bahron</i>	125
The Development of Personal Portable Wireless Range Extender for IEEE 802.11 <i>Norharyati Harum, Nur Atikah Mohd Yusof and Nurul Azma Zakaria</i>	137
Productivity Improvement in Automotive Component Company using Line Balancing <i>Muhammad Fikri Alif Dzulkarnain and Wan Emri Wan Abdul Rahaman</i>	147
Association between Marital Status and the Outcome of Teenage Pregnancy: A Retrospective Review in Year 2009-2012 in Hospital Ampang <i>Salleha Khalid and Muhammad Shamsir Mohd Aris</i>	159
Experimental Investigations on the Effects of Design Parameters on Single Slope Solar Still Evaporation Rate under Malaysian Conditions <i>Zainal Abidin Kamarul Baharin and Aishah Arinah Abdul Aziz</i>	169
Second-hand Smoke Exposure and Psychological Distress amongst Non- Smoking Pregnant Women in Malaysia <i>Siti Munira Yasin, Khairul Mizan Taib, Mohd Rodi Isa, Mohd Ariff Fadzil, Mohd Razilan Abdul Kadir and Saiful Farik Mat Yatim</i>	181

**Contents**

**Advances in Science and Technology Research**

- Serological and Molecular Detection of RhD DEL Phenotype in National Blood Centre, Malaysia 1  
*Safura Ramli, Evana Kamarudin and Mazura Bahari*
- Seasonal Temporal Distribution of Forecasted Wind Speed Data in Langkawi, Malaysia 7  
*Siti Noratiqah Mohamad Deros, Arnis Asmat and Shattri Mansor*
- Isolation and Characterisation of Filamentous Fungi from Animal Agricultural Farm Soil 19  
*Muhammad Shukri Senwan, Muhd Fauzi Safian, Zainon Mohd Noor and Zaidah Zainal Ariffin*
- Electrodeposition of Copper Coating on 304 Stainless Steel Substrate: Physicochemical Properties and Antibacterial Activity 29  
*Nik Norziehana Che Isa, Yusairie Mohd, Mohammad Hafizuddin Mohd Zaki and Sharifah Aminah Syed Mohamad*
- Enhancement of Oxidative DNA Damage and Alteration of p53, Bax, and Bcl-2 Protein Expressions Following Low Dose Radiation Exposure 41  
*Wan Mazlina Md Saad, Mohd Khairul Amran Mohammad, Muhamad Idham Mohamed and Hairil Rashmizal Abdul Razak*
- Microbial Fuel Cell's Performance of Original and Deoxygenated Palm Oil Mill Effluent in 3 Different Stages of Fermentation Process 53  
*Khairul Baqir Alkhair Khairul Amin, Oskar Hasdinor Hassan, Sharifah Aminah Syed Mohamed, Yap Kian Chung Andrew, Zulkifli Ab. Rahman, Hazlini Mohmad Ameran, Nurul Khamsatul Akma Kamaruzaman, Tunku Ishak Tunku Kudin, Ab. Malik Marwan Ali, Mohd Zu Azhan Yahya and Muhammad Haikal Zainal*
- Optimising Processing Conditions of PLA Nanocomposites Using Response Surface Methodology 63  
*Norazura Ibrahim, Margaret Jollands and Rajarathinam Parthasarathy*
- Modified Spent Tea Leaves as Bioadsorbent for Methyl Orange Dye Removal 73  
*Lim Ying Pei, Amira Nadzirah Suhaidi, Siti Marziya Zulkifli, Syamil Hidayat Hassim, Devagi Kanakaraju and Lim Ying Chin*



**Pertanika Editorial Office, Journal Division**  
Office of the Deputy Vice Chancellor (R&I),  
1st Floor, IDEA Tower II,  
UPM-MTDC Technology Centre  
Universiti Putra Malaysia  
43400 UPM Serdang  
Selangor Darul Ehsan  
Malaysia

<http://www.pertanika.upm.edu.my/>  
E-mail: [executive\\_editor.pertanika@upm.my](mailto:executive_editor.pertanika@upm.my)  
Tel: +603 8947 1622/1620

**PENERBIT**  
**UPM**  
UNIVERSITI PUTRA MALAYSIA  
**PRESS**

<http://penerbit.upm.edu.my>  
E-mail : [penerbit@putra.upm.edu.my](mailto:penerbit@putra.upm.edu.my)  
Tel : +603 8946 8855/8854  
Fax : +603 8941 6172

